AD A121367

Illinois Institute of Technology, Chicago, Illinois 60616

INSTABILITIES IN NEAR FIELD OF TURBULENT JETS AND THEIR
DEPENDENCE ON INITIAL CONDITIONS AND REYNOLDS NUMBER

by

R. E. Drubka and H. M. Nagib

IIT Fluids & Heat Transfer Report R81-2

December, 1981

DTIC
ELECTE
NOV 1 2 1982

IIT

REPORT DOCUMENTATION PAGE	READ INSTRUCTIONS BEFORE COMPLETING FORM	
1. REPORT NUMBER **AFOSR-TR- 82-0962**	2. GOVT ACCESSION NO. $AD\text{-}A121\ 367$	3. RECIPIENT'S CATALOG NUMBER
4. TITLE *(and Subtitle)* INSTABILITIES IN NEAR FIELD OF TURBULENT JETS AND THEIR DEPENDENCE ON INITIAL CONDITIONS AND REYNOLDS NUMBER	5. TYPE OF REPORT & PERIOD COVERED **INTERIM**	
	6. PERFORMING ORG. REPORT NUMBER	
7. AUTHOR(s) Robert E. Drubka and Hassan M. Nagib	8. CONTRACT OR GRANT NUMBER(s) F49620-80-C-0053	
9. PERFORMING ORGANIZATION NAME AND ADDRESS Illinois Institute of Technology Department of Mechanical Engineering Chicago, Illinois 60616	10. PROGRAM ELEMENT, PROJECT, TASK AREA & WORK UNIT NUMBERS 61102F 2307/A2	
11. CONTROLLING OFFICE NAME AND ADDRESS Air Force Office of Scientific Research/NA	12. REPORT DATE December 1981	
Bolling Air Force Base, D.C. 20332	13. NUMBER OF PAGES 400	
14. MONITORING AGENCY NAME & ADDRESS(if different from Controlling Office)	15. SECURITY CLASS. (of this report) UNCLASSIFIED	
	15a. DECLASSIFICATION/DOWNGRADING SCHEDULE	

16. DISTRIBUTION STATEMENT *(of this Report)*

Approved for public release, distribution unlimited

17. DISTRIBUTION STATEMENT *(of the abstract entered in Block 20, if different from Report)*

18. SUPPLEMENTARY NOTES

19. KEY WORDS *(Continue on reverse side if necessary and identify by block number)*

Turbulent Jets; Jet Instabilities; Axisymmetric Instability; Helical Instability; Pairing; Subharmonic Resonance; Nozzle-lip Influence; Nonlinear Interaction; Initial Conditions; Non-parallel Flow Effects; Self Excitation; Feedback Mechanism;

20. ABSTRACT *(Continue on reverse side if necessary and identify by block number)*

Near-field pressure and velocity measurements, along with multiple flow visualization techniques, were obtained at several azimuthal positions to establish the effect of initial conditions and Reynolds number on the development and nature of instabilities in the initial region of axisymmetric free jets. In cases where the exit boundary layer is laminar, the natural jet is found to be unstable alternately to axisymmetric and helical modes having Strouhal numbers of 0.013 and 0.016, respectively. The scaling of these modes is independent of Reynolds number and initial jet disturbance level. (CONTINUED)

DD FORM 1 JAN 73 1473   EDITION OF 1 NOV 65 IS OBSOLETE

However, the disturbance level does determine the sensitivity of the initial region to the helical mode. When the initial axisymmetric mode grows to a finite amplitude, a subharmonic resonance mechanism that leads to pairing develops two fundamental wavelengths from the jet exit. The axisymmetric and helical modes interact nonlinearly, generating numerous sum and difference modes. With the strong growth of the subharmonic mode, a secondary set of nonlinear interactions develops between the subharmonic mode and the above modes.

A strong near-field pressure is associated with each of these instability modes and is coherent with the velocity fluctuations in the jet over the entire growth and decay regions of each mode. The details of this field reveal that pairing is not responsible for a feedback mechanism. This strong near-field pressure acts as a natural excitation to the jet. When the background disturbance is sufficiently low, a natural coupling is observed at special operating conditions where the initial modes are coupled to the mode observed near the end of the potential core of the jet.

When the exit boundary layer is turbulent, a linear instability mechanism which scales with $St_\theta = 0.024$ is documented near the exit. By locally applying linear spatial theories to account for the flow divergence, the development of the jet is adequately described from the initial region to the end of the core.

ACKNOWLEDGEMENT

TABLE OF CONTENTS

LIST OF TABLES

LIST OF FIGURES

x

xii

xvii

xxi

LIST OF SYMBOLS

Symbol	Definition
a	Speed of Sound
c_r	Wave phase speed normalized by the mean jet velocity
$C_{up}(f)$	Velocity-pressure coincident spectral density function
D	Jet exit diameter
D_i	Inlet diameter of contraction
f	Frequency
f_f	External forcing frequency
f_i	Initial instability frequency of jet with turbulent exit boundary layers
$f_{i,o}$	Initial axisymmetric eigenfrequency of jet with laminar exit boundary layers
$f_{i,1}$	Initial helical eigenfrequency of jet with laminar exit boundary layers
f_r	Response frequency of jet due to external excitation at frequency f_f
$Q_{up}(f)$	Velocity-pressure single sided cross spectral density function
K	Kurtosis
L	Length of extension tube used in generating a turbulent boundary layer
L_u	Streamwise integral length scale
m	Azimuthal mode number
p	Time dependent pressure fluctuations
p'	RMS of pressure fluctuations

Symbol	Definition
$Q_{up}(f)$	Velocity-pressure quadrature spectral density function
$R_{up}(\tau)$	Velocity-pressure cross correlation
Re	Reynolds number = $U_j D/\nu$
S	Skewness
$S_{up}(f)$	Velocity-pressure cross spectral density function
St	Strouhal frequency = fD/D_j
St_f	Final Strouhal frequency observed in jet near and of potential core
St_i	Strouhal frequency based on f_i
$St_{i,o}$	Strouhal frequency based on $f_{i,o}$
St_θ	Strouhal number = $f\theta/U_j$
U	Streamwise local mean velocity
U_j	Streamwise mean velocity in potential core
U_{max}	Maximum streamwise mean velocity
u'	RMS of streamwise velocity fluctuations u
x	Streamwise coordinate
x_L	Streamwise extent of nozzle lip influence region
x_m	Streamwise location of structure interaction
x_o	Virtual origin of jet
x_r	Streamwise position of initiation of subharmonic resonance
Y	Radial coordinate
$Y_{0.5}$	Radial coordinate where $U/U_j = 0.5$

Symbol	Definition
α_r	Spatial wave number
$-\alpha_i$	Spatial growth rate in the streamwise direction
Γ_{up}	Coherence between velocity and pressure fluctuations
γ	Azimuthal angle in a plane perpendicular to the streamwise axis
λ_a	Acoustic wavelength
$\lambda_{i,o}$	Wavelength of initial axisymmetric eigenmode
σ	Standard deviation obtained from a least squares curve fit
θ	Local momentum thickness $$\equiv \int_0^\infty (U/U_j)\,(1-U/U_j)\,dY$$
θ_i	Initial momentum thickness of exit boundary layer
$\theta_{0.1}$	Measure of momentum thickness based on integration over the streamwise velocity interval $(0.1\,U_j,\ U_j)$
ν	Kinematic viscosity
ϕ_{up}	Relative phase angle between velocity and pressure fluctuations of a given frequency

ABSTRACT

Near-field pressure and velocity measurements, along
with multiple flow visualization techniques, were
obtained at several azimuthal positions to establish the
effect of initial conditions and Reynolds number on the
development and nature of instabilities in the initial
region of axisymmetric free jets. In cases where the
exit boundary layer is laminar, the natural jet is found
to be unstable alternately to axisymmetric and helical
modes having Strouhal numbers of 0.013 and 0.016,
respectively. With proper normalization, the scaling of
these modes is independent of Reynolds number and initial
jet disturbance level. However, the disturbance level
does determine the sensitivity of the initial region to
the helical mode. When the initial axisymmetric mode
grows to a finite amplitude, a subharmonic resonance
mechanism that leads to pairing develops two fundamental
wavelengths from the jet exit. This position corresponds
to where strong entrainment into the jet is first
observed. Because of the alternating instability of the
jet, the axisymmetric and helical modes interact
nonlinearly, generating numerous sum and difference
modes. With the strong growth of the subharmonic mode, a
secondary set of nonlinear interactions develops between
the subharmonic mode and the above modes.

A strong near-field pressure is associated with each
of these instablity modes and is coherent with the
velocity fluctuations in the jet over the entire growth
and decay regions of each mode. The details of this
field, along with the scaling of the resonant position,
reveal that pairing is not responsible for a feedback
mechanism. This strong near-field pressure acts as a
natural excitation to the jet. When the initial
background disturbance level in the exit boundary layer
for a given mode is lower than the velocity fluctuations
generated through the functional relationship with the
pressure field, that mode initially grows exponentially
in the jet with a phase speed determined by its Strouhal
number. The initial amplitude of these modes is
determined by the acoustic efficiency of the downstream
source, with the lower frequency modes being more
efficient. When the background disturbance is
sufficiently low, a natural coupling is observed at
special operating conditions where the initial modes are
coupled to the mode observed near the end of the
potential core of the jet.

When the exit boundary layer is turbulent, a linear
instability mechanism which scales with $St_\theta = 0.024$ is
documented near the exit. By locally applying linear
spatial theories to account for the flow divergence, the
development of the jet is adequately described from the
initial region to the end of the core. In general, if

the shear-region divergence and subharmonic resonance of the jet are incorporated, the behavior of the near region of the jet can be explained by such a linear theory coupled with locally parallel flow assumptions.

CHAPTER I

INTRODUCTION

Over the past few years, the Fluids group at IIT has been interested in the relationship between large scales in fully turbulent flows and basic instability mechanisms. This interest stems from the attractiveness of potential applications of various types of passive and active devices to control, manage or manipulate these flows. In the two latest works, Wlezien (1981) examined the evolution of the low wavenumber structure in a turbulent wake and Corke (1981) examined the role, origin and manipulation of large scales in a turbulent boundary layer. These investigations examined two classical flows with new conceptual ideas and state of the art signal processing. The outcome of this led to the clarification of much of the confusion which had existed in the previous literature. It is with this same spirit that another classical flow is examined here.

Research on turbulent free jets has been actively carried out for the past twenty-five years. Traditionally, this work either examines the nature and characteristics of the acoustic far field or the development of the hydrodynamic field of the jet. Ideally, one of the end results is to determine the link between these two fields with the eventual prospect of reducing jet noise. Unless the dynamics of the

developing jet are properly understood, the link between these two fields cannot be properly described and the prospects for reducing jet noise are marginal at best.

Measurements in the acoustic far field cannot describe the dynamics of the jet nor can they identify the major sources, due to the compact appearance of a jet from large distances. For this reason, a large effort has been consentrated into examining the details of the jet flowfield. It will be seen though, that some of these results are confusing, not well understood, or quite often contradictory.

Background and Motivation

In the mid 1960's and early 1970's, important discoveries were made by examining the development of axisymmetric jets and two dimensional shear layers, in particular with flow visualization. Work by Crow and Champagne (1971) in an axisymmetric jet proved that there was an orderly structure to the, previously believed, random turbulence in the jet. These large scale structures are an integral part of the jet development and can even be enhanced under certain conditions when a slight surging of the jet is introduced. These large scales develop from turbulent exit boundary layers and can be tied to the instability of the developing jet. Prior to this, Bradshaw (1965) recognized that when the exit boundary layer is laminar, the initial jet

development could be thought of as a series of vortex rings, which Wille (1963) observed to pair or coalesce as they traveled downstream. They believed that this pairing gave rise to a characteristic frequency which was one half of that associated with the initial structures.

Brown and Roshko (1974) in a two dimensional shear layer also observed the emergence of large scales that merged with their neighbors as the shear layer developed downstream. These phenomena persisted even at high Reynolds numbers. Similar observations were made by Winant and Browand (1971) in a low Reynolds number experiment in a two dimensional shear layer. In this case the initial boundary layer was laminar and the authors concluded that the pairing of structures was the mechanism for the growth of the shear layer.

From these observations, it became clear that turbulence is not as purely stochastic as previously believed. Two different points of view arose during this era. One group viewed these large scale structures as dominating the growth and evolution of the developing flow in both axisymmetric jets and two dimensional shear layers. It was even believed that their evolution and interaction played a major role in the noise generation mechanism. As a consequence, flow visualization, acoustic excitation and conditionally sampled techniques became widely used in an attempt to extract statistical properties of the structures themselves and of their

interactions. Others continue to view these as remnants of the instability and transition process that are not likely to persist at the technologically important Reynolds numbers. In either case, the understanding of these large scales can only be approached from an instability point of view. In our view, the growth of the large scales is most likely related to the evolution of unstable modes of the mean shear.

Theoretical works have dealt with strictly two-dimensional shear layers and axisymmetric jets. A shear layer depends only on one length scale, e.g., the axial distance or length describing the width of the shear layer. An axisymmetric jet though, has an extra added dimension, that being the radius or a length representing the azimuthal variation. No matter how thin the axisymmetric shear layer is, this azimuthal dependence still exists. Keeping this distinction in mind, a survey of the relevant literature is presented.

Theoretical work on strictly two dimensional shear layers is examined first. Michalke (1964) first examined the initial growth of disturbances on a hyperbolic tangent velocity profile using a temporal formulation of the problem. For this case, modes having a Strouhal number between 0 and 0.04 were amplified and the maximum amplified mode occurred at a Strouhal number based on momentum thickness of 0.017. Since the problem was formulated in a temporal frame, the phase speed of the

disturbance has a constant value of 0.5 and independent of St_θ . In 1965, Michalke reformulated the problem in a spatial sense where the disturbances grow in the streamwise direction. The amplification curves calculated using the same mean velocity profile exhibited similar behavior, although the amplification rates near its maximum value were approximately 20% higher than in the temporal case. The main difference between these two formulations was in the phase speed of the disturbance. In the spatial case, disturbances below the maximum amplified St_θ were found to be dispersive while those above the maximum amplified St_θ were found to be non-dispersive. The basic assumptions utilized in these formulations were those of parallel flow and linear instability.

Freymuth (1966) experimentally examined the initial instability characteristics of an axisymmetric jet with a laminar exit boundary layer using external accustic forcing. Amplification rates and phase speeds of the forced modes were determined. The main findings were that the phase speed measurements are dispersive in nature for forcing frequencies below the maximum amplified mode. From this point on there should have been no doubt that spatial amplification was the only proper formulation. However, amplification rates measured by Freymuth were approximately 20% below those calculated from the linear spatial theory of Michalke

(1965). The unfortunate aspect of this was that the experimentally measured amplification rates happened to lie near the temporal theory. This caused much confusion over the proper formulation. Even though the experiments of Freymuth (1966) were carried out in an axisymmetric jet, the results are compared to shear layer analyses here just to show that the spatial theory properly described the non-dispersive nature. The difference in amplification rates were probably due to a difference in profile shape.

Recent work by Monkewitz and Huerre (1981) examined the effect on the mode amplification of velocity ratio across a two dimensional shear layer and also the effect of slightly changing the mean velocity profile. When the mean velocity profile in the shear layer was calculated using laminar boundary layer assumptions, it was found that the maximum amplification is approximately 20% lower than that for the hyperbolic tangent profile. This difference accounted for the discrepancy of Freymuth's (1966) measurements. Although the profiles look extremely similar, the difference lies in the maximum slope of the profile; in this case the hyperbolic tangent profile has an initially larger slope. This change in slope modifies the initial vorticity distribution in the inviscid Rayleigh equation. Once again parallel flow assumptions were used.

The basic linear theories just described consider

the initial exponential growth of an unstable mode in a parallel flow. Kelly (1967) has determined that when this linear instability reaches a finite value, another instability based on subharmonic resonance can arise. In this case the frequency of the new instability is exactly one-half of the original linear instability. The subharmonic resonance is weakly non-linear and described by the Mathieu equation. This formulation is temporal but it does give insight into the mechanism for the emergence of the subharmonic mode.

As the initial linear instability grows in amplitude toward a value of about 1%, the shear layer begins to roll-up and form discrete vortices. The formulation proposed by Kelly (1967) does not account for this, since by the time the discrete vortices are observable the problem is fully nonlinear. Pierrehumbert (1980) examined the effect of this nonlinearity on the subharmonic resonance. His results, formulated again in a temporal sense, indicate that the growth rate of the subharmonic mode which evolves from this parametric instability is approximately 30% higher than that which would exist just based on simple exponential growth according to Michalke's (1965) spatial theory. In this case the nonlinearity of the rolled-up vortices enhances the growth rate of the subharmonic mode. In recent work by Ho and Huang (1981) in a two dimensional shear layer, pairing of vortices is shown to be a product of this

subharmonic instability. In fact, the pairing occurs where the energy of the subharmonic saturates.

We now turn our attention to the instability theories for axisymmetric jets. The first major paper on the theoretical analysis of axisymmetric jets was presented by Batchelor and Gill (1962). Linear inviscid stability theory, assuming parallel flow and temporal development was used to analyze both the near and far regions of the jet. Even though a top hat profile was used for the near region, so that its usefulness is limited, the far downstream jet profile, corresponding to the region past the potential core, was found to be unstable to helical disturbances and stable to axisymmetric disturbances. To explain the work of Crow and Champagne (1971), Michalke (1971), in a paper which did not receive adequate attention, reformulated a spatial instability theory for axisymmetric jets to account for a finite momentum thickness of the initial region. A family of axisymmetric hyperbolic tangent profiles were considered, each having a different momentum thickness associated with it. Even though parallel flow assumptions were used, the family of profiles could be used to describe a locally parallel flow condition at any axial distance up to the end of the potential core. The family of profiles are described as a function of R/θ , where R is the radius where the local mean velocity is 50% the jet velocity and θ is the

momentum thickness. For large values of R/θ, the amplification curves are nearly identical to those of a strictly two-dimensional shear layer. However, a significant difference lies in the behavior of the phase speed. For a two-dimensional shear layer, the phase speed is always less than one. For an axisymmetric jet with a large R/θ though, phase speeds larger than one are predicted at low Strouhal numbers. This is not surprising because of the additional length scale, i.e., the jet radius. This was experimentally confirmed by Bechert and Pfizenmaier (1974). These differences continue in the limit as R/θ approaches infinity. Only when the jet radius is infinite does the difference disappear, i.e., when the flow reduces to a one length scale problem. In addition to these differences, non-axisymmetric modes can be amplified. Michalke (1971) found that the first helical mode has amplification characteristics nearly identical to the axisymmetric mode. In this case maximum amplification for both axisymmetric and helical modes occurred at the same Strouhal number. No region where the phase speed is larger than one was found for the helical mode.

In a similar work, Mattingly and Chang (1974) emloyed the same formulation as Batchelor and Gill (1962) and Michalke (1971) but used an axisymmetric gaussian distribution to describe the downstream development of the jet. The measured velocity profiles were obtained in

a water jet where the Reynolds number was only 300. Even
though these measurements were obtained at these low
values, the above authors' theory showed that near the
nozzle the amplification of the axisymmetric and helical
modes differed by only 12%, with that of the axisymmetric
mode being larger. The frequency of the maximum
amplified helical mode was 20% higher than that for the
axisymmetric mode. To date, this result has not yet been
verified by experiments. Similar work was also presented
by Chan (1974). In his experiments, it was observed that
the maximum amplified mode is a function of the radial
position. This result could not be predicted from
parallel flow assumptions, however.

Crighton and Gaster (1976) used a multiple-scales
expansion to take into account the slow divergence of the
developing jet and examined the evolution of the
axisymmetric mode. The main findings of this study
indicate that when the instability characteristics for
the diverging flow are compared to the theory using
locally parallel flow assumptions, the characteristics of
the most unstable mode along the centerline are nearly
identical. The results also indicate that the maximum
amplified mode was a function of radial position, with
that in the mean shear region being larger than on the
centerline, agreeing with Chan (1974). Even though no
radial information on amplification rates or phase speeds
can be obtained from the locally parallel flow, the

determination of the most unstable mode on the centerline is consistent with the weakly non-parallel theory. This analysis was extended by Plaschko (1979) to incorporate the first two helical modes. The results once again resembled those predicted by Michalke (1971), when locally parallel flow assumptions are used.

Based on Michalke's (1971) spatial theory, the initially most amplified disturbence frequency for a hyperbolic tangent mean velocity profile corresponds to a Strouhal number of 0.017. This value was not found to be sensitive to the shape of the profile as determined by Monkewitz and Huerre (1981). This value was confirmed by Freymuth (1966) and by Zaman and Hussain (1981) for an acoustically excited jet with a laminar exit boundary layer. However, in a naturally developing jet Hussain and Zaman (1978), among others, show that the initial frequency in a jet occurs at a $St_{\theta} = 0.012$. A survey of the literature reveals that this value varies from 0.009 to 0.017. No rational explanation has been offered for this peculiar behavior. When the jet is acoustically forced, an axisymmetric field is imposed on the jet. However, in the naturally developing jet it has been assumed that the initial instability is axisymmetric. Upon examination of the shear layer velocity spectrum of Husain and Hussain (1979), a multiplicity of spectral peaks are noted in the range of Strouhal numbers 0.01 to 0.016. However, there is no way to identify the spectral

peaks without determining the azimuthal characteristics of these modes. Part of the reason for the multiple peaks may be due to the nearly equal amplification for non-axisymmetric modes as predicted by linear theories. It is quite surprising that axisymmetry of naturally developing jets is usualy assumed without documentation of the initial azimuthal dependence.

From the experiments of Bruun (1977), Hussain and Clark (1981), Davis and Davies (1979), Yule (1978), and Peterson (1978) among a long list of others, pairing or large scale interactions have been found to contribute to the growth of the jet when the initial exit boundary layer is laminar. The number of observed pairings between the initial instability and final Strouhal mode near the end of the core varies between 1 and 3 among different authors. The question remains though, how important is pairing in different operating condition and in particular to the far field noise. To properly answer this, the role of nonaxisymmetric disturbances must be examined. This has not yet been addressed. Axisymmetry has normally been assumed. Using this assumption, Acton (1980) modelled an axisymmetric jet using a series of vortex rings. In this case the development of the jet can only proceed through the pairing process. It is on this assumption that Ho (1981) bases his subharmonic evolution model.

In recent years it has been observed that a

disturbance field generated by the pairing process may affect the subsequent evolution of large scales. This was first noted by Dimotakis and Brown (1976). Work in an impinging jet by Ho and Nosier (1980) shows that at certain high values of Reynolds number a resonance mechanism occurs when the sum of the number of downstream wavelengths and the number of wavelengths in the upstream acoustic field is an integer. This is the so-called feedback mechanism. In a naturally developing jet, Laufer and Monkewitz (1980) suggest that the initial region of a jet is modulated by a frequency corresponding to that developed near the end of the potential core. With this, Laufer (1980) and Ho (1981) attempt to interpret the initial evolution of jets by a natural feedback mechanism. They state that the pairing sends back a pertubation which synchronizes the next pairing. As proof of this model, Gutmark and Ho (1981) reported that the initial instability frequency of the jet varies in a stepwise fashion with Reynolds number. Recently Ho (1981) discovered that the stepwise nature was due to a low level acoustic disturbance in the facility which coupled to the initial instability of the jet in a manner similar to that introduced artificially by Kibens (1980). A closer examination of the feedback model needs to be undertaken to determine its applicability.

All of the above experimental research is based on an axisymmetric view of the jet. Moore(1977) found that

the "final" Strouhal mode varied between axisymmetric and helical modes. Once the non-axisymmetric nature is introduced, the simple pairing model would not correctly or completely describe the development of the jet. If there are non-axisymmetric modes developing in the initial region of the jet then forcing the jet and imposing axisymmetry cannot be representative of its natural development. The existance and importance of these modes however has not been explored.

Work in a forced jet by Kibens (1979) showed that when the initial instability is related to the "final" jet frequency by an integral multiple of two, the jet became extremely organized, pairings were localized and the development of initial frequency to final frequency occurred through a number of pairings. Under this condition it was also noted that discrete peaks in the acoustic field were at frequencies corresponding to the pairing generated frequencies. When the ratio of the frequencies was not a simple multiple of two, this behavior was not as dramatic, based on a private communication with Kibens. It was clear then that some type of coupling mechanism was involved. Hints at this same coupling were also observed by Zaman and Hussain (1980). It is not clear if the coupling is a natural phenomenon or if it is due to the imposed axisymmetry, be it controlled or incidental.

Pui and Gartshore (1979) have examined the effect of

free stream turbulence on the development of a
two-dimensional shear layer. Their results indicated
that the disturbance level increased the mean growth rate
of the shear layer. Chandrsuda et al. (1978) examined
the effect of free stream turbulence on the large scales
in turbulent mixing layers and concluded that the initial
three dimensionality in a free jet appears via a vortex
ring instability. They also suggest that if the exit
boundary layer is turbulent a Brown-Roshko type of
structure will not appear. Hussain and Zedan (1978) show
that the initial growth of the jet is unaffected by
changes in the initial momentum thickness but increases
as the peak intensity in the exit boundary layer
increases. In this case a jet with turbulent exit
boundary layer grew faster than initially laminar ones, a
result contradicted by the work of Browand and Latigo
(1979). The results of Hussain and Zedan (1978) did
show, however, that the mean characteristics and hence
the large scale evolution were dramatically affected by
the initial disturbance level in the boundary layer.
This recent research indicates that the initial
conditions play an important role in the development of
the jet. However, it is unclear whether the initial
conditions change the characteristics of the developing
instabilities.

From the literature review of some of the more
relevant works, it is clear that the initial development

of a natural jet has not been well examined. In particular, the role of the various identified mechanisms in the developement of the jet noise field remains contradictory and unclear. If one is to control the jet and manage its noise field, one must understand the generating flow field and, in particular, its energetic large structures. With this in mind the objectives of this work emerged.

Objectives

1) To examine the initial instability characteristics of a natural "axisymmetric" free jet and to determine if other than axisymmetric instabilities and large scale structures play an important role in the development of the jet. If so, to find out how do they affect the simple axisymmetric thinking about jet development. In addition, to assess the importance of the non-parallel flow or divergence of the jet in regard to its instabilities.

2) To investigate the effect of initial conditions and Reynolds number on the nature of the developing instabilities. The initial conditions can be altered by changing the state of the exit boundary layer, increasing the Reynolds number with a constant core intensity

or by fixing the Reynolds number and altering
the disturbance level at the exit by utilizing
suitable upstream grids. A close relation
between initial conditions and jet evolution
can then be derived.

3)   To closely examine the evolution of the
     subharmonic mode. Utilizing near field
     pressure measurements and velocity measurements
     in the jet, conduct experiments to prove or
     disprove the feedback mechanism as well as
     establish the degree of importance of pairing
     in natural jets. Also, to closely examine the
     upstream influence of downstream evolving
     modes, constantly keeping initial conditions
     in mind.

4)   To determine if a natural coupling exists
     between the initial instability of the jet and
     the "final" Strouhal mode and, if so, how is it
     affected by the initial conditions. In
     addition, find out whether the coupling is
     natural and simply enhanced by forcing or
     whether forcing imposes this condition on the
     flow. The "final Strouhal mode appears to be
     the dominant frequency in the far field jet
     noise.

Near the end of the potential core, the jet maintains its maximum characteristic velocity with the most mass flux, because of entrainment. The large scales at the end of the near region of the jet may very well be the most energetic of the noise generating eddies. If we are to understand the relation between the jet flow and its noise field in depth, we need the above information well documented and understood.

CHAPTER II

EXPERIMENTAL FACILITIES AND INSTRUMENTATION

Wind Tunnel Characteristics

The present experiment was conducted in an open circuit wind tunnel having a 15.4 cm diameter circular test section and powered by compressed air. During the preliminary portion of this experiment several modifications were made to this facility. These modifications and some of their effects on the initial jet shear layer instability are discussed in Appendix A.

In its final configuration, compressed air enters an acoustically treated upstream duct after passing through a control valve, as well as particulate, and oil filters all of which are acoustically treated externally. The air then enters a large internally acoustically lined settling chamber and encounters a series of flow manipulators of different types and shapes before passing through a 25:1 axisymmetric contraction having a 15.4 cm exit diameter. The maximum flow rate through this contraction exit was found to be approximately 16 m/s. The flow manipulators were designed according to Loehrke and Nagib (1972) for flow uniformization and turbulence reduction. Information concerning the design and construction of this facility can be found in the reports by Ahmed, et al (1976) and Tan-atichat, et al.(1980). With the above arrangement, a flow with extremely low

disturbance level and internal acoustic noise is available.

The schematic of Figure 1 shows the test section and nozzle configuration for the various test flow conditions which were utilized. A detailed examination of the characteristics of these flow conditions is described in the following chapter. The various lengths of the test sections were formed by bolting together smaller sections of precision machined plexiglass tubing. Two meters above the exit of this test section, a 3m x 2m fabric canopy was constructed to eliminate the effect of external drafts in the room originating from the air conditioning system. Laboratory traffic was also controlled to further minimize any external influences on the jet.

Nozzle Characteristics

Based on preliminary results and on the results of Tan-atichat (1980) a nozzle with a fifth order polynomial contour (FO) was chosen for the bulk of the current investigation. As shown in Figure 1 the ratio of the length of nozzle to its inlet diameter is equal to 1 and the nozzle has a contraction ratio of 9:1. The fifth order contour accomodates a zero slope and curvature at both the inlet and exit of the nozzle. Tan-atichat (1980) found that this aids in reducing both the mean streamwise velocity overshoot and the radially inward

velocity component at the outer edge of the jet, near the nozzle exit, as compared to a matched cubic (MC) type of the same dimensions. The 5.14 cm exit diameter also provides a large enough dimension compared to the exit boundary layer thickness so that curvature effects on the initial shear layer are small.

The exit face of the nozzle is shown full scale in Figure 2. The lip thickness is 2.57 cm or one-half the exit diameter. In addition, eight azimuthal pressure taps were installed to examine the fluctuating pressure field near the boundary layer separation point. Each pressure tap is 1.2 mm in diameter and located 3.8 mm away from the diameter of the nozzle exit. These pressure taps extend approximately 2 cm into the face of the nozzle before exiting through its side. Pressure fittings of length 1.27 cm, and 1.6 mm O.D. (1.1 mm I.D.), made from bulged stainless steel tubing, were then glued into the side of the nozzle and extended out approximately 6.5 mm.

Two other nozzles, both of which were of the matched cubic type, were also utilized during the experiment. In this case the profile curvature is non-zero at both the inlet and exit. Both had the same contraction length as the FO. One MC nozzle had a 5.14 cm exit diameter including an identical face geometry as that of the FO. The other MC nozzle had a 2.57 cm exit diameter and a face lip thickness of 3.81 cm.

All of the above nozzles were designed and fabricated during the thesis of Tan-atichat (1980). Further information about them can be found in this reference.

Instrumentation

Both analog and digital acquisition were utilized in this study. Digital acquisition and processing was used exclusively in the determination of the statistical characteristics of the developing jet for each test flow condition. Analog processing along with a two channel real time spectrum analyzer was found to be quite adequate for the remainder of the study.

A single sensor hot-wire probe was utilized throughout this experiment. The sensor diameter was 3.8 μm and had an active sensor length of 1.2 mm. The probe body was made from 2.5 mm brass tubing. Prong tips were made from 76 μm jewelers broaches, 2.5 cm in length. The prong separation at the tips was 2.5 mm. Another set of broaches 1.2 cm in length were attached directly behind the prongs at their base in the streamwise direction. This improved prong rigidity without increasing the projected prong size in the flow direction. A single glass fiber was also attached to the prongs near their top to reduce any prong vibration. When off axis data was taken, the probe was oriented at approximately a 45° angle to the streamwise direction so that the probe body was outside the shear layer and only

the prongs were immersed in the flow. For centerline
data, the probe was oriented in the streamwise direction
and the probe support was located approximately 70 probe
body diameters downstream of the sensor. The above probe
dimensions and sensor orientation were experimentally
determined to eliminate shear layer probe interference
problems, described by Hussain and Zaman (1978), and also
to minimize any probe vibration effects for the higher
Reynolds number cases. This if further discussed in
Appendix A.

A triaxial traversing mechanism was used to hold and
position the probe. Equipped with a digital position
indicator, it was capable of positioning the probe to
within 0.2 mm of a desired location.

Analog Signal Processing. Pressure measurements
were made using a B&K type 2209 Precision Sound Level
Meter with a 1/2 in. condensor microphone. A B&K probe
microphone kit was utilized to fit a 2 mm diameter tube,
1 cm in length, to the 1/2 inch microphone. This
arrangement was dynamically tested and found to have a
flat amplitude response over 4000 Hz which was past the
limit of the frequency range of interest. Either a
3 cm or 15 cm length of hypodermic tubing was used to
connect the calibrated sound level meter to any of the
pressure taps on the nozzle. The sound level meter was
always located at the rear side of the nozzle when using

this configuration to ensure minimum interference. The 3 cm length of tubing was used for axial phase and coherence measurements while the 15 cm length was utilized for determining the azimuthal phase and coherence. Both systems were dynamically calibrated and peaks were observed in the amplitude spectrum corresponding to frequencies associated with standing waves in the pressure tap system. A small amount of steel wool was then inserted in the hypodermic tubing to act as damping. With the system properly damped, the amplitude spectrum was flat to within 3db re. 2×10^{-5} N/m^2 up to 4000 Hz. Since only streamwise gradients of phase difference at a given frequency were to be examined, not the absolute value, the phase transfer function due to the pressure tap system was not accounted for in the final results. For cases where greater amplitude accuracy was required, the sound level meter with the 2 mm tubing was placed with minimum disturbance so that the end of the 2 mm tubing was at the pressure tap opening at the nozzle face thereby bypassing the pressure tap system in the nozzle. The use of all three systems verified the consistency of the results.

A schematic of the instrumentation used for the analog processing is shown in Figure 3. The hot-wire was powered by a DISA 55M01 constant temperature anemometer at an over-heat ratio of 1.7 and linearized with a TSI model 1072 Signal Linearizer. To obtain a true mean

velocity reading, the output of the linearizer was passed
through a voltage to frequency converter and then the
frequency modulated wave train was counted over a 10 sec.
interval. The output of both the linearizer and the
sound level meter were input to a two channel real time
spectrum analyzer (HP3582A), which computes single and
cross power spectrum along with two channel coherence and
phase functions. The outputs were also connected to a
PAR correlator.

Digital Signal Processing. As described previously,
all off axis velocity profiles and spectral
characteristics at the jet exit were acquired digitally.
A schematic of this arrangement is shown in Figure 4. A
pressure transducer monitored a pressure tap upstream of
the nozzle which was calibrated with the mean jet
velocity. Both signals were biased and amplified to
cover as much of a ±10v range as possible to minimize
quantization error. Only lower order statistics were
required for the shear layer profiles, namely mean and
rms velocities. For this reason, the signals were
sampled at a low rate of 100 Hz and a single record of
length 1700/channel was taken at each position. For
spectral surveys, the output of the anemometer was low
passed at 5 kHz and sampled at a rate of 10 kHz. One
hundred records, each of length 2052/channel, were taken
at each position. For further information about the

digital acquisition and processing system at IIT (DAPS)
the reader is referred to Wlezien (1981).

Digitally recorded wire output voltages were then
linearized via a squared forth order polynomial as
described by Drubka and Wlezien (1979). All processing
on the digitally acquired data was performed on a
Univac-1100/81 mainframe computer.

Flow Visualization Techniques

In addition to the measurements described in the
previous section, extensive flow visualization was taken
in the Reynolds number range of 20,000 to 100,000.
Numerous smoke visualization techniques were examined
including the "smoke-wire" technique utilized at IIT
(Corke et al., 1977). It became quite apparent that two
separate non-intrusive techniques were required. The
first was to examine the evolution and three
dimensionality of the organized structures, and the
second to examine the entrainment of the surrounding
ambient air into the jet.

The first technique that was developed was the
"round" smoke wire which is a modification of the simple
"smoke-wire" technique. A schematic of this is shown in
Figure 5. A 0.13 mm Dia. stainless steel wire is placed
azimuthally around half the circumference of the nozzle
just outside the separation point. Oil is wiped on the
wire and a D.C. voltage applied across the two leads.

The vaporized smoke is entrained near the nozzle lip and marks the subsequent evolution of the jet. Mean velocity profiles and shear layer velocity spectra indicated that the developing shear layers were not affected by the presence of this smoke wire arrangement. The second technique, used either in conjunction with the round smoke wire or separately, utilized an entrainment wire. One end of this wire was attached approximately 1 mm from the end of the round smoke wire at the upper portion of the nozzle. This wire was then aligned to be in a plane passing through the jet centerline and perpendicular to the viewing direction. It was held taut 6 nozzle diameters downstream and inclined at an angle larger than the jet spreading rate. Oil was wiped on and vaporized, marking a two-dimensional view of the entrainment into the jet. This latter method is similar to that utilized by Moallemi and Goldschmidt (1981).

In order to extract maximum information from these visual techniques, two separate means of recording them were utilized. Photographic records were either taken using a 35 mm SLR camera or using a Beckman & Whitley high speed camera. The latter was used to examine the cyclic evolution and interaction of the coherent structures while the former was used to relate the large scale structures to the dynamics of instability processes.

<u>Conditioned</u> <u>Visualization</u>. In order to relate the observed coherent structures to the instability process in the jet, it was necessary to trigger a photograph when a certain event was taking place. For example, this event could be a large amplitude deviation away from the long time variance, or perhaps a certain phase of a given frequency. Conditioning schemes were designed based on these requirements and are shown in Figure 6.

The hot-wire probe, described earlier, was utilized as the event detector. Its position was always aligned so that the local mean streamwise velocity was 60% of the jet velocity. The linearized signal from the probe was A-C coupled and amplified. At this point a choice had to be made as to whether some characteristic of the entire signal was to be used or whether a narrow band analysis of the signal was needed. If a narrow band analysis was deemed necessary, the signal was band-passed at a given frequency which was determined from a real time spectrum analysis. The signal was next simultaneously sent through a variable threshold detector and also a positive slope zero crossing detector which were constructed from LM 322 timing chips as described by Jung (1977). Either one of these signals could then be used as a condition for the photographic record to be taken.

As previously discussed by Laufer (1981), the velocity fluctuations in the initial shear layer are amplitude modulated. In attempting to use a simple

amplitude threshold on this type of signal, the phase information is lost. To regain this phase information a multiple conditioning scheme was utilized. The output of the amplitude detector set an RS type flip-flop. Its output went to an AND gate along with the output of the zero crossing detector. Thus, if the amplitude of the signal was larger than the threshold, the subsequent positive slope zero crossing would give the condition. If the signal amplitude was not large enough, the flip-flop was reset by the original zero crossing signal after a short time delay. In this manner the same relative phase is maintained between selected events. The condition pulse train could also be time delayed to change its phase relative to the zero crossing. The accuracy of this method for examining different phases of the instability process is solely dependant on the bandwidth of the signal. This accuracy decreased with increasing streamwise position due to the increased phase modulation. Either condition could then be used as a condition input in the associated smoke wire electronics.

A typical example of this conditioned visualization is shown in Figure 7 for a Reynolds number of 20,000. The conditioning probe is located at $x/D = 1.5$ at a radial position where $U/U_j = 0.6$. These photographs were triggered on a positive zero crossing after a large amplitude event. In this case the large amplitude event was the merging of two structures which is observed

downstream of the prong tips. This particular
conditioning captures the initial structures one quarter
of the initial instability wavelength before they
interact. As can be seen from a comparison between these
two realizations, the flow field upstream of the
conditioning probe is quite similar indicating a
consistent conditioning scheme. The evolution of the
flow downstream of the probe though is at a different
phase for each realization. Since the conditioning probe
triggers the photograph on a relative phase of zero
degrees, only phase modulation of the signal can account
for this downstream phase variation between realizations.
Inserting a time delay after the condition pulse, the
interaction could also be observed at different stages of
its development.

To properly interpret any flow visualization, an
ensemble of realizations must be examined. An unbiased
method to determine statistical information about the
visualization is to use two dimensional image processing
techniques as Corke (1981) presents. At the time of this
study, this system was not yet available. The only means
available to examine an "average" structure was to use a
multiple exposure photographic technique in a similar
manner to the flash schlieren system Moore (1976) used in
a high speed jet. This method, even though being a
biased estimator of the ensemble average, due to the
nonlinear response of the film to light intensity, yields

the average characteristics of the visualization when a consistent triggering scheme is used.

The number of realizations needed for a suitable ensemble, for the present technique was determined through the following test. The number of realization on a frame of film was varied from 1 through 16 for case 1L at a Reynolds number of 39,000. For this case the probe was located at an $x/D = 0.5$ and the event was triggered on the next positive zero crossing after the amplitude of the signal was larger than a preset threshold level of $2u'$, where u' is the long time averaged rms of the signal. These results are shown in Figure 8. As the number of realizations is increased, the large scale structures downstream of the first interaction become smeared due in part to the random position of the already diffusely marked structures. The structures before the interaction position however, remain clearly defined for 4 or more realizations. To minimize the nonlinear effect on the ensemble average yet maximize the number of realizations, it was decided to use 8 as the standard.

With the number of realizations determined, it was necessary to find a suitable amplitude threshold value using the same conditioning scheme as in the previous figure. These results are illustrated in Figure 9. The ensemble in Figure 9(a) was triggered on a random positive zero crossing. As can be seen, the structures are also randomly positioned and no average structure is

evident. As the threshold level is increased, the average structure emerges from the ensemble. The large scale structures become better defined as the amplitude threshold is increased up to a value of 2 u'. Increasing this value further seems to have minimal effect on the ensemble averaged structure. For this reason the value of 2u' was chosen to be the amplitude threshold. A similar threshold level dependence was found by Bruun (1977) using a two probe education technique in a jet with a Reynolds number of 10,000. In this case it was determined that the amplitude threshold level was of second order when it was between u' and 3u', and a value of 2u' was chosen in the study.

Using the same conditioning scheme as in Figure 7, with the conditioning probe farther upstream, a multiple exposure photograph was compared to a single realization for Re = 20,000 in Figure 10. In this case, the initial threshold and number of exposures were set to the values previously determined. With this conditioning scheme, the first two structures are frozen in space indicating the regularity of the event. Downstream of these structures, where other structures have paired, one observes a smearing of the structures due to the phase variation as indicated by Figure 7. This smearing is not due to a lack of coherent structures but to a random phase variation in their position. This figure serves as a reminder that education techniques in natural jets are

only as good as the conditioning scheme and that the evolution of the jet downstream of the conditioning signal need not be phase locked to the upstream event.

To examine the cyclic behavior of the growth and evolution of the large scale structures, high speed movies were taken using a Beckman & Whitley model 350 high speed camera along with a model 358 electronic flash. The electronic flash, fitted with a parabolic reflector, gave a 11 ms flash of 3 million peak beam candlepower output. The smoke was illuminated from above in a plane perpendicular to the line of sight. The film used was Kodak Recording film having an ASA of 1000 and then further pushed to 6000.

The framing rates were dependent on the jet Reynolds number and also the exit boundary layer state. The flash duration and jet velocity determined the number of cycles of the initial jet instability for the laminar boundary layer cases. This curve is shown in Figure 11. The framing rate utilized was a compromise between the maximum framing rate which could be operated under the lighting conditions and the lowest framing rate which yielded adequate cyclic resolution of the developing structures. This upper limit on the framing speed was found to be roughly 4200 frames/sec at low Reynolds numbers and decreased by 10% at a Reynolds number of 70,000. The lower limit on the framing rate was determined by the cyclic resolution of the structures.

This limit was determined by setting the framing speed at least three times the initial jet instability frequency. This gave a resolution of 3 frames/initial instability cycle or 6 frames/subharmonic cycle. The actual framing rates which were used are summarized in Figure 11. For the turbulent exit boundary layer cases, the maximum framing rate was determined to be 7000 frames/sec. Results from the flow visualization study will be presented throughout the remaining chapters.

CHAPTER III

TEST FLOW CONDITIONS

Grid Characteristics

The experimental facilities, discussed in the previous chapter, were originally designed with a modular concept by Tan-atichat (1980) to examine the effect of axisymmetric straining on turbulence of different scales. Using various grids sufficiently upstream of the contraction he was able to develop homogeneous turbulence before the contraction inlet. The streamwise development of these initial conditions was carefully documented along with the exit plane characteristics.

In the present investigation it was decided to alter the exit plane disturbance characteristics by using various grids while keeping the same contraction. The cases of Tan-atichat (1980) were carefully examined and two different grids were chosen. These correspond to test flow conditions 2L and 3L as illustrated in Figure 1 . The characteristics of these grids are shown below in Table 1. Here M is the mesh of the grid, σ the solidity, t the thickness and x/M the normalized distance between the grid and the inlet of the contraction. For all cases examined the grids were sufficiently upstream so that the turbulence was homogeneous at the inlet of the contraction.

Table 1. Grid Characteristics

Flow Condition	M (cm.)	σ	t (mm.)	x/M
2	0.635	0.34	1.19	36
3	2.54	0.35	2.10	26

The grid used in flow condition 2 was a punched steel plate with square holes arranged in a square array. The grid for flow condition 3 was a punched steel plate with round holes arranged in a triangular array. Both of these grids have a low enough solidity so that their is no danger of them exhibiting anomalous behavior (Tan-atichat, Nagib and Loehrke, 1981). As observed in Figure 1, no upstream grid is used in flow condition 1.

Laminar Exit Boundary Layer

To obtain a qualitative feeling for the effect of these grids on the initial development of the jet, flow visualization for Cases 1L, 2L and 3L is presented in Figure 12 at a Reynolds number of 39,000. The case designations are described in Figure 1. The number refers to the test flow configuration while the latter refers to the state of the exiting boundary layer. Thus as one goes from 1L to 3L at a constant Re, the

disturbance level in the core is increased. From Figure 12 it is observed that as the upstream flow is changed from 1L to 3L, the initial three dimensionality of the developing jet is increased. Before examining these effects in detail, the jet exit characteristics must be established for the above test flow cases.

The normalized mean streamwise velocity profiles at the jet exit for cases 1L, 2L and 3L are shown in Figure 13. These profiles are identical. Thus the test flow condition has no appreciable effect on the mean profile at the jet exit. The shape of this profile agrees with the results of Tan-atichat (1980) for a fifth order nozzle. At 80% of the jet radius there is approximately a 4% velocity overshoot. By $x/D = 0.1$ for this Reynolds number, this overshoot is no longer observed.

The effect of the test flow condition on the core disturbance level is shown in Figure 14. The disturbance level in the core of the jet is a definite function of flow condition as one expects. The core intensity for case 1L is found to be 0.05% and independent of Reynolds number. At a Reynolds number of 42,000 this value is increased to roughly 0.1% for case 2L and further increased to 0.16% for case 3L. The intensity for the latter two cases were found to vary slightly with Reynolds number. Associated with an increased core intensity is an apparent increase in fluctuation level in the exit boundary layer. As the core disturbance level

increases, these fluctuations massage the developing boundary layer and subsequently they become internalized in the boundary layer. The variation of the peak fluctuation intensity in the exit boundary layer for all laminar boundary layer flow conditions tested is shown below in Table 2.

Table 2. Peak Fluctuation Level in Laminar Exit Boundary Layer Cases

			$Re \times 10^{-3}$		
Case	39	42	52	80
1L	0.014	0.011	0.012	0.054
2L	0.019	–	0.024	–
3L	0.051	–	–	–

These results indicate that at a constant value of Re, the peak fluctuation level increase with increasing flow condition designation number. The results for case 1L show that the peak intensity in the boundary layer is invariant between Reynolds numbers of 39,000 and 52,000. Above this value the intensity increases with Reynolds number.

From these few observations, the main effect on the developing jet of introducing a grid is to alter the disturbance level in the exit boundary layer. The mean

exit profiles are unchanged and it is believed that the effect of the core disturbance level is of second order over the range indicated in Figure 14.

The spectral characteristics and higher order statistics of the streamwise fluctuations across the jet exit were also examined. The velocity spectrum for each case exhibited a smooth behavior and was void of any spurious peaks. This was checked across the jet exit for each flow condition. The variation of the skewness and Kurtosis across the exit plane is shown in Figure 15. The fluctuations for case 1L exhibit zero skewness for a wide radial range across the jet indicating its Gaussion nature. As the flow condition is changed to 2L and 3L, the skewness becomes slightly negative. Near the outer edge of the jet, i.e. approaching the boundary layer, the skewness becomes more negative as the disturbance level is increased. This change in skewness indicates that large positive values of the velocity fluctuations are not as frequent as large negative values. The Kurtosis for all of the cases has a value of approximately 3, once again indicative of nearly Gaussion behavior in the core.

The streamwise velocity spectra were inverse Fourier transformed to obtain the auto correlation. The integral time scale was computed and normalized by the jet velocity to obtain an indication of the streamwise length scale. The radial variation of this at the jet exit for the three flow conditions is shown in Figure 16. These

results are consistent with those of Tan-atichat (1980).
What is interesting to note is that over 70% of the jet
diameter the length scales have a constant value. There
are only minimal differences between cases 2L and 3L.
The values for case 1L are also indicated on the figure.
It is not surprising that this case does not agree with
cases 2L and 3L since at this low core disturbance level
the fluctuations are not representative of true
turbulence, and the length scale measured is not of any
significance.

For all of the cases listed in Table 2, the
normalized mean velocity profile of the exit boundary
layer was Blasius, having a shape factor of approximately
2.2. The momentum thickness of the exit boundary layer
was determined and is shown in Table 3.

Table 3. Variation of Momentum Thickness of Laminar
    Exit Boundary Layer, in cm., with Reynolds Number
    and Flow Condition

Case	34	42	52	80
		$\text{Re} \times 10^{-3}$		
1L	0.022	0.020	0.0176	0.0145
2L	–	0.0193	0.0172	–
3L	–	0.0186	–	–

Considering the data for case 1L, it is observed that the momentum thickness varies inversely as the square root of the Reynolds Number. This once again confirms the Blasius nature of these boundary layers. As the disturbance level increases, the momentum thickness decreases by 7% while the Reynolds number is kept constant at 42,000. Even though additional data were not taken for cases 2L and 3L, the same Reynolds number behavior is expected since the exit boundary layer profile is still Blasius.

The streamwise variation of the growth of the momentum thickness of the jet near the nozzle lip region is documented in Figure 17 for case 1L at a Reynolds number of 42,000. Within the first 80 initial momentum thicknesses, or approximately 0.3D, the momentum thickness increases by 40%. This variation of the initial momentum thickness is different than that observed by Freymuth (1966). The development of the normalized mean velocity profiles over this region is shown in Figure 18. Within this region the velocity profiles are self-similar. The data lie between the curves for a hyperbolic tangent profile and that for a Blasius type profile for a free shear flow. It is not clear from these measurements which of these curves, if either, the data actually represents. Even though the two analytic profiles are nearly identical, they yield vastly different amplification rates of the most unstable

eigenmode. This is due to a small difference in the maximum slope of the curves which subsequently alters the vorticity distribution across the layer for the stability analysis. The normalized profiles for cases 2L and 3L are shown in Figure 19 over this same axial range and a similar behavior is observed.

It is very interesting to examine the deviation of the data away from one of the analytic functions with increasing downstream distance. For simplicity, the deviation of the data away from the hyperbolic tangent function is examined in Figure 20. Here, σ is simply an indication of the average error in fitting the data with a hyperbolic tangent function. Within the first 0.3 diameters, the value of $\sigma/2\theta$ remains essentially constant for Case 1L. This is the same region over which the similarity in profiles was observed in Figure 18. Between 0.3D and 0.7D, a large deviation away from the hyperbolic tangent profile is observed. Beyond this region, however, the mean profiles return to nearly the same normalized profiles as was observed near the nozzle exit. A similar behavior is also shown for case 2L. Data were taken for case 3L only near the nozzle lip. In this region, it is observed that the test flow condition has no influence on the normalized mean velocity profile. It will be shown in later chapter that the region of large deviation is associated with the region of pairing in the jet.

Lastly, the effect of the test flow condition on the shear layer velocity spectrum near the nozzle exit is examined in Figure 21 for a Reynolds number of 40,000 along U/U_j = 0.6. The region below 200 Hz is first focused on. As the core disturbances are increased, there is an increase in low frequency spectral energy by a factor of 10 from case 1L to 3L. Above 200 Hz, the observed peaks in the spectra for cases 1L and 2L are related to observed instability modes and hence will not be discussed until later. What is important in this figure is that the initial spectral characterisitcs of the separated boundary layer are significantly altered by the various test flow conditions. In fact, by changing the flow condition from 1L to 3L, there is a broad band increase in the spectral content of the separated layer.

Turbulent Exit Boundary Layer

In addition to the laminar exit boundary layer cases, measurements were also carried out using fully turbulent boundary layers. This part of the investigation was only carried out using core flow condition 1. In order to obtain fully developed, zero pressure gradient, turbulent boundary layers, one of two small straight ducts was connec'.ed to the nozzle face as indicated in Figure 1. A 5 mm wide strip of low roughness height sandpaper was installed at the nozzle-duct junction. This method fixed the transition

point at this location. By the end of either duct, fully
turbulent boundary layers were established. Mean
velocity and turbulence intensity profiles along with
velocity spectra proved that the exit boundary layer was
indeed fully turbulent. A summary of the exit boundary
layer characteristics at two Reynolds numbers is
presented in Table 4.

Table 4. Variation of Exit Momentum Thickness ond Peak
Turbulence Intensity with Reynolds Number for Turbulent
Exit Boundary Layers

| L/D | Re = 39,000 | | Re = 80,000 | |
	θ (cm.)	$(u'/U_j)_{max}$	θ (cm.)	$(u'/U_j)_{max}$
0.75	0.054	0.124	0.056	0.120
1.50	0.064	0.122	0.070	0.119

Due to the method of producing these boundary layers, the
exit momentum thickness was a weak function of Reynolds
number. For this reason two different lengths of duct
were utilized to vary the initial momentum thickness. At
a Reynolds number of 80,000, there exist a 25% variation
inbetween the boundary layers generated along the two
ducts.

The initial development of the jet for the case with
the short duct is shown in the visualization of Figure 22

over a range of Reynolds numbers. Due to the highly
dispersive nature of this boundary layer, no discrete
streaklines are observed near the jet as in Figure 12.
However the development of large scale coherent
structures is clearly evident. It becomes quite apparent
from viewing these photos that a simple two dimensional
view, which would consist of examining only the upper and
lower portion of the photograph, as presented by Hussain
and Clark (1981) does not give enough information
concerning the structural behavior of the jet. A three
dimensional view is a necessity.

Finally, the mean streamwise velocity profile at the
jet exit for the short duct at a Reynolds number of
42,000 is shown in Figure 23. The velocity profile is
flat across the jet and a typical boundary layer profile
is observed at the outer edges. Properly normalized the
velocity profile for the longer duct was nearly
identical. All normalized profiles were found to be
independent of Reynolds number.

CHAPTER IV

JET DEVELOPMENT - MEAN FLOW

The basic test flow conditions have been described in the previous chapter. From the visualization in Figures 12 and 22, it is clear that both the initial core conditions and the exit boundary layer conditions affect the initial structural development of the jet. The question is to what extent are these changes manifested in the time-mean characteristics of the jet. This chapter examines this question by considering the evolution of the time averaged streamwise velocity field both along and off the jet centerline. The measurements presented in this chapter were acquired digitally as described in Chapter II and utilized the 5.14 cm fifth order nozzle.

On Centerline

The Reynolds number dependence of the streamwise velocity component along the jet centerline is first examined for test flow condition 1L. The mean and RMS evolutions are shown in Figures 24 and 25 respectively, along with the data from Crow and Champagne (1971) for a similar exit diameter nozzle but having an initially turbulent exit boundary layer. The centerline variation of U/U_j , Figure 24, shows that the potential core of the jet extends to a value between 4 and 4.5 diameters for the range of exit Reynolds numbers examined. This value

agrees well with the results of previous investigations.
Over the Reynolds number range 39,000 - 52,000 the decay
of the mean velocity downstream of the potential core is
essentially unchanged. As the Reynolds number is raised
to 79,000, the centerline velocity decays at a slower
rate and is nearly identical to that measured by Crow and
Champagne. The general behavior that the decay rate
decreases with increasing Reynolds number has been
observed by Hussain and Clark (1977) in a two dimensional
jet and by Hill, Jenkins and Gilbert (1975) in an
axisymmetric jet. As demonstrated by this figure, the
sensitivity of the decay rate to Reynolds number is not
constant. It would appear then that another parameter
which maybe an implicit function of Reynolds number could
be controlling the decay rate. One such parameter is the
fluctuation intensity in the exiting boundary layer.
Referring back to Table 2 in Chapter III, it was noted
that over the Reynolds number range of 39,000 to 52,000
the peak streamwise fluctuation level in the exit
boundary layer remained between 1.1% and 1.4%. Over this
same range, the mean centerline velocity decay rate is
observed to be nearly invariant. At a Reynolds number of
79,000 though, the exit fluctuation level has increased
to approximately 5%. Correspondingly, the mean
centerline velocity decays at a slower rate. With just
the Reynolds number behavior for one test flow condition
it is not possible to speculate on the nature of the

asymptotic approach of the high Reynolds number case to the decay rate found by Crow and Champagne (1971). This will be focused on once the remainder of the test flow conditions have been examined. It is a rather interesting concept however, to think that a simple single parameter measured at the jet exit may dictate the downstream evolution. If this concept is found to have a solid foundation then the growth rate of the jet would most likely scale with this same parameter.

The centerline variation of u' for case 1L is shown in Figure 25. The magnitude of the streamwise turbulence intensity decreases with increasing Reynolds number. Once again, as in the previous figure, this dependency is not uniform. The values of u'/U_j in the Reynolds number range 39,000 to 52,000 appear to be invariant. At Re = 79,000, the centerline rms level drops, once again corresponding to an increase in the peak fluctuation level in the exit boundary layer.

These results appear to suggest that for a given core disturbance condition the mean centerline statistics are related to the fluctuation level in the exiting boundary layer. As this level increases, the mean centerline velocity decays at a slower rate, and the streamwise turbulence intensity decreases.

If the above hypothesis is correct then by changing the disturbance level at a constant Reynolds number, a similar phenomenon should be observed. This is shown in

Figures 26 and 27 where the initial boundary layer
fluctuation level is altered by changing the test flow
condition at a constant Reynolds number. The variation
of U/U_j for each test flow condition at a Reynolds number
of 39,000 is shown in Figure 26. The length of the
potential core is unaffected by the disturbance level.
The decay rate, however, decreases with increasing
disturbance level. This decrease has an asymptotic value
similar to that achieved when the exit boundary layers
are fully turbulent as in test flow condition 1T, with
$L/D = 0.75$. As the flow condition is changed from 1L to
3L, the peak intensity in the exit boundary layer changes
from 1% to 5.3% and the core disturbance level increases
from 0.05% to 0.16%. The peak intensity in the boundary
layer for case 3L at Re = 39,000 is nearly equal to that
for case 1L at Re = 79,000. Comparing Figures 24 and 26
and also 25 and 27, the mean and rms characteristics for
both cases are identical. Thus, it appears that the
centerline characteristics are highly dependent upon the
conditions of the exit boundary layer. From this data it
would appear that the influence of the core disturbance
level is of second order when it is below 0.2% for
laminar exit boundary layers.

In both figures, the asympototic values lie on the
results of Crow and Champagne (1971). The results of
Crow and Champagne were obtained in a 5.1 cm jet over the
Reynolds number range 63,000 to 124,000 and were found to

be invariant. The results for case 1T at a Reynolds
number of 39,000 are identical to those. Similar results
were also found for case 1T, with L/D = 0.75, at Re =
79,000. When the centerline characteristics were
compared to those obtained by Hussain and Zaman (1980)
using different sizes of nozzles, the asymptotic levels
did not agree. These results indicate that first and
second order statistics along the jet centerline are
Reynolds number invariant, at least up to the first nine
diameters, when the exit boundary layers are fully
turbulent and similar sized jets are examined. When the
exit boundary layer is laminar, this ceases to be true.
The centerline statistics in this case are a function of
the fluctuation level of the exit boundary layer and also
probably depend on the nozzle diameter. The mean
velocity decays at a slower rate and the streamwise
turbulence intensity decreases with increasing
fluctuation level in the exit boundary layer. Above
levels of 5%, these characteristics reach an asymptotic
behavior which coincide with the fully turbulent boundary
layer.

Off Centerline

Having examined the centerline characteristics of
the jet, the mean characteristics off axis are now
investigated. To describe the developing axisymmetric
mixing layer, a suitable length scale must be utilized.

A number of investigators have utilized various length
scales in the study of two-dimensional mixing layers.
Some involve the use of the downstream distance from the
virtual origin while others use a length scale which
characterizes the local velocity profile. The only
detailed measurements in an axisymmetric shear layer,
however, were carried out by Hussain and Husain (1980)
and by Husain and Hussain (1979). The local vorticity
thickness and also a measure of the momentum thickness,
$\theta_{0.1}$, where

$$\theta_{0.1} = \int_{0}^{Y_{0.1}} [U/U_j] \ [1-U/U_j] \ dY$$

were both used in their investigation. In this case the
integration was terminated at $Y_{0.1}$, the radial position
where the local velocity is 10% of the jet velocity, in
order to reduce hot-wire rectification errors on the low
speed side of the jet. It was decided to use this   .
variable as the length scale for this investigation in
order to compare the present results to those of the
above authors.

In order to most accurately evaluate this parameter,
the measured jet profile at any downstream location was
fit with a cubic spline with a small amount of damping to
give a smooth analytic profile. The data were always
compared to the analytic profile to ensure that the
profile accurately described the data. With this

analytic function the upper limit in the integral could be determined exactly. The analytic profile was then numerically integrated.

The variation in the maximum streamwise turbulence intensity with downstream distance is first examined in Figure 28 for the four test flow conditions at Re = 39,000. When the initial boundary layer is laminar, the initial intensity peaks near x/D = 1.5 due to a large amplitude growth which is associated with an instability mechanism as will be shown in later chapters. This intensity reaches a maximum value and then decreases to an asymptotic value. The growth of the shear layer can be considered self-similar in terms of streamwise turbulence intensity when this value is reached. In the case of the turbulent exit boundary layer the shear layer is not able to sustain the same level of instability mechanisms under natural conditions. In this case the magnitude of $(u'/U_j)_{max}$ increases monotonically to an asymptotic value. As shown in this figure, the maximum intensity for case 1T, with L/D = .75, has just begun to reach an asymptotic value by 5 diameters. However, by this axial distance the mixing region can no longer be considered a single axisymmetric shear layer but rather a mixing layer interacting with itself as seen by the disappearance of the true potential core in Figure 26. This behavior for initially laminar and turbulent boundary layers has also been observed by Husain and

Hussain (1979), Yule (1978) and Bradshaw (1966), among others.

From Figure 28 it is noted that the asymptotic value of the maximum streamwise turbulence intensity is a function of the initial flow condition. When the initial boundary layer is laminar, this value decreases from a value of 0.173 for an exit boundary layer peak fluctuation level of 1.2% to a value of 0.157 at an exit boundary layer level of 5.1%. For this case, the final asymptotic value is identical to that when the initial boundary layer is turbulent. Similar results were found for case 1L as the exit Reynolds number was increased. At Re = 79,000, the asymptotic value was found to be 0.157, which is identical to that observed in case 3L at Re = 39,000. The asymptotic value of $(u'/U_j)_{max}$ over the Reynolds number range of 39,000 to 52,000 was found to vary from 0.173 to 0.168. Over this range the peak intensity in the boundary layer changed by less than 1%. The centerline characteristics were found to be independent over this range and the asymptotic peak intensity was also found to be essentially constant. These results are in complete agreement with the centerline characteristics and once again indicate that the condition of the exit boundary layer is firmly linked to the downstream mean jet evolution.

The above dependence on exit intensity is contradictory to those of Hussain and Zedan (1978). In

their work they showed that the asymptotic peak
turbulence intensity increased monotonically with maximum
intensity of the exit boundary layer, and that this
maximum asymptotic value was limited to value of about
0.18. It was also determined that this asymptotic value
was independent of initial momentum thickness. For their
operating conditions, the peak exit boundary layer
intensity varied between 8% and 17%. In the present
case, the intensity of the exit boundary layer was
changed by either changing the jet Reynolds number or by
changing the core disturbance level characteristics. It
was shown that both methods yielded consistent results.
Values of maximum intensity in the exit boundary layer
varied from 1% to 5%, much lower than those used by the
above authors. However, it is not believed that this
difference in exit fluctuation level would cause the
difference in trends due to the asymptotic behavior
between cases 3L and 1T. This point will be examined in
further detail in the latter part of this chapter.

The normalized mean and RMS velocity profiles for
the four test flow conditions at Re = 39,000 are shown in
Figures 29 through 36. In Figure 29, the mean velocity
profile attains a self similar form by approximately 1.5
diameters downstream of the exit. Based on the results
of Figures 28 and 30, the streamwise intensity reaches
self similar form by 2 diameters. In this case the mean
and RMS velocities become self similar at approximately

the same position. This was also observed by Hussain and Zedan (1978) as long as the exit boundary layers remain laminar.

The development of the velocity profiles for case 2L is shown in Figures 31 and 32. As in the previous case, the mean velocity profile becomes similar by two diameters. This is also borne out in the similarity of the streamwise intensity in Figure 32. The same is true for case 3L shown in Figures 33 and 34.

The shapes of the normalized velocity profiles for cases 1L, 2L and 3L are identical when Figures 29, 31 and 33 are examined closely. When Figures 30, 32 and 34 are examined, the profiles for the streamwise intensity are also nearly identical. There are two differences clearly visible in this case however. First, the maximum intensity in the self preserving region decreases with increasing disturbance level and secondly, the shape of the peak in the profile flattens and becomes broader as the disturbance level increases.

The normalized velocity profiles for case 1T are illustrated in Figures 35 and 36. In this case the mean velocity has already reached self similarity by one diameter. The streamwise intensity profiles however appear to be reaching self similarity by 4 to 5 diameters as described earlier. When these profiles are compared to those of the three test cases which had laminar exit boundary layers it is observed that all cases exhibit

nearly identical self similar profiles for the mean velocity when scaled with a thickness parameter based on the local mean velocity profile. The shape and width of the streamwise intensity profiles are also identical between the four test cases. The differences here lie in the value of the maximum amplitude and also the curvature of the profile at the maximum amplitude. This observation was also made by Browand and Latigo (1979) in a two-dimensional mixing layer.

Hussain and Zedan (1978) show a distinct difference in these profiles however, with the most differences arising between the turbulence intensity profiles.

In the previous series of figures, the radial coordinate was normalized by a thickness parameter, $\theta_{0.1}$, which was a characteristic of the local mean profile. The downstream growth of this parameter, indicating the entrained flow into the jet, is examined next. The growth of this parameter for the four test flow conditions at Re = 39,000 is shown in Figure 37. At one diameter, the shear layer is initially thickest for the turbulent boundary layer and thinnest for the low disturbance level case. This is due to the difference in the initial momentum thickness. As the shear layer develops downstream, $\theta_{0.1}$ increases linearly with axial distance. The low disturbance level case corresponds to the largest growth rate. When the free-stream disturbance level is increased, leading to an increase in

the boundary layer fluctuations, the corresponding growth of the shear layer decreases. The lowest growth observed in Figure 37 corresponds to the case when the exit boundary layer is fully turbulent.

The question is what structural characteristics of the developing shear layer are responsible for the change in growth observed in Figure 37. To examine this question, flow visualization of the entrainment process was carried out and a few of the results are displayed in Figure 38. The first observation that can be made is that for cases 1L, 2L and 3L, there is no significant visible entrainment into the jet until the vorticity wave, as marked by the smoke from the round smoke wire, becomes nonlinear and rolls up. After this region, smoke is quickly entrained into the jet through the induced velocity field of these structures. One would expect therefore that the growth of the layer would sharply increase here. This will be quantitatively documented in a later chapter. Another observation from this figure and Figure 12 is that as the disturbance level is increased, the initial structures become more three dimensional and weaker. This weakening is observed by the decrease in the penetration of the entrained air into the mixing layer. Consequently, if the dynamics of the large scale structures are responsible for ingesting a large fraction of the total entrained air, as is certainly evident in the near region, any alteration of

its coherence or strength will alter the entrainment and hence the shear layer growth.

In the case of 1T, there is no structure visible having any azimuthal coherence within the first two diameters as indicated by the smoke density from the round wire or from the trajectory of the smoke streaks from the entrainment wire. From the previous figure the growth rate is observed to be approximately 40% larger for case 1L than for case 1T. The difference in the growth of the shear layer must then be partly due to the lack cf the strong entrainment process from the large scale structures observed in case 1L. It is evident that the method of entrainment into the jet in the first few diameters is substantially different between the initially laminar and turbulent exit boundary layers.

The growth rate for these cases as a function of jet Reynolds number was calculated using a linear least squares technique and is displayed in Figure 39. The behavior of the growth rate at Re = 39,000 was just described. These values vary from 0.024 for case 1T to 0.038 for case 1L. For case 1L, the growth rate decreases as the Reynolds number increases until an asymptotic value of approximately 0.03 is reached. The variation for case 2L is less, in this case reaching an asymptotic value of 0.028. Upon examination of case 1T, the growth rate is found to be independent of Reynolds number and have a value of 0.024. This similarity in

growth rate for this case was also observed in the similarity of the centerline profiles as well as the shear layer profiles as described earlier.

As Re increases, the difference in growth rate for the four test cases diminishes. The conditions depicting this trend for case 1L are visualized in Figure 40. At lower values of Re, the initial large scale structures are a dominant feature of the flow. When this structure is responsible for entraining ambient air, the streak lines from the entrainment wire will have regions where they converge. Examination of the highest Re case shows that this type of entrainment is visible only near the nozzle lip. Farther downstream the streaks become reminiscent of case 1T where the streaks are more uniformly entrained into the flow. Even when the large scale structures are observed farther downstream, where the bulges into the entrained smoke are noticed, the streak paths are fairly linear indicating that only weak entrainment by these structures is present. The structural characteristics of the developing shear layer is clearly Reynolds number dependent unless the exit boundary layers are turbulent or unless a sufficient free stream disturbance level is added, which acts mainly through the boundary layer, to weaken these initially laminar structures.

Earlier in the chapter, it was observed that the asymptotic peak intensity in the shear layer decreased

with an increase in the peak fluctuation level in the exit boundary layer. The centerline mean velocity was also found to decay slower with increasing fluctuation level in the boundary layer and to be independent of the initial momentum thickness. The dependence of $\theta_{0.1}$, on this disturbance level is replotted in Figure 41 for all test flow conditions and Reynolds numbers tested. The growth rate decreases monotonically with increasing fluctuation level in the exit boundary layer. This single curve includes a wide range of Reynolds numbers, initial boundary layer momentum thicknesses, laminar and turbulent exit boundary layers, different core disturbance levels, and also different disturbance scales. Amazingly, the growth rate of the jet appears to be represented by a single parameter, that being the boundary layer fluctuation level. This result is consistent with the mean and rms centerline characteristics described earlier.

Work by Browand and Latigo (1979) in a two dimensional mixing layer show the growth rate of an initially turbulent boundary layer to be 40% lower than that of an initially laminar boundary layer. Even though their experiment was strictly two-dimensional and operated at a velocity ratio of 0.7, the qualitative nature of the results are still valid and agree with the present results. These results though are contradictory to those of Hussain and Zedan (1978) who show that the

growth rate of an initially turbulent boundary layer is larger than that of an initially laminar boundary layer. This is shown in Figure 41 where their data has been included. At a boundary layer fluctuation level of 0.06 both sets of data are in good agreement. Hussain and Zedan (1978) show no data below this level though. Above this level, both sets of data diverge.

With the computation of the growth rates in Figures 39, the virtual origin of the initial shear layer, x_o, was determined and is shown in Figure 42. For all cases except Case 1L at Re = 39,000 the virtual origin is located upstream of the nozzle exit. Similar results were found by Hussain and Zedan (1978). However, the nature of the trend of x_o is once again contradictory. Wygnanski and Fiedler (1970) and Batt (1975) also show that the virtual origin is upstream of the nozzle exit when the initial boundary layers are turbulent, agreeing with the present results.

CHAPTER V

JET DEVELOPMENT - UNSTEADY FLOW AND INSTABILITIES

In the previous chapter the time mean characteristics of the developing jet were examined for different initial core and exit boundary layer conditions. Before considering a detailed examination of the instability mechanisms involved in each of the above cases, a few general observations will first be made concerning the nature of the instabilities found in the initial jet region both on and off the jet centerline. These developing instabilities are vortical in nature. As these vorticity waves develop spatially, there is a definite pressure field associated with this growing vorticity field. This pressure field may be an efficient radiator so that it is felt back at the boundary layer separation point. If so, then depending on the strength of this field and on the internal disturbance level of the exiting boundary layer, this irrotational pressure field may act as a natural excitation to the jet. Velocity fluctuations associated with this disturbance field would subsequently grow exponentially, superimposed on the naturally developing eigenmode. General observations will be made about the nature and identification of the instability modes along with their relation to the near-field pressure.

Laminar Exit Boundary Layer

In Chapter III, three test flow conditions were described which had laminar exit boundary layers. For a given value of Re, the fluctuation level in these boundary layers could be altered through the use of suitable grids located upstream of the contraction which also altered the core disturbance characteristics. In this chapter the Reynolds number is typically fixed at 42,000 and the effect of changing the initial jet characteristics on the spectral development of the jet is examined.

The characteristics of test flow condition 3L which corresponds to the highest flow disturbance case is first examined in Figures 43 and 44. In each figure, the axial development of the streamwise velocity spectrum, shown in an arbitrary scale, is displayed along with the coherence between that velocity signature and the irrotational pressure field outside the nozzle lip taken at a relative angle of $\gamma = o$ (see Figure 2). The off axis development is first examined in Figure 43. In this case the radial location is adjusted at each streamwise position so that the local mean velocity is 60% of the core velocity. This radial position is at the peak turbulence intensity as observed in Figures 33 and 34.

Initially, the u velocity, shown here in log amplitude, is characterized by a uniformly decreasing spectrum which is reminiscent of a typical turbulent

signal. The initial boundary layer is however laminar. With these initial conditions, there is virtually no coherence between the initial velocity fluctuations in the shear layer and the pressure field near the separation point. The only significant coherence which is observed at this location is found at frequencies of approximately 730 Hz and 880 Hz. By an axial position of 0.5 diameters, a large broadband increase in the streamwise velocity spectrum, shown here in linear scale, is observed between 600 Hz and 1000 Hz in which four distinct spectral peaks are observed. Two peaks occur at frequencies of 730 Hz and 880 Hz, which are the frequencies at which a weak coherence was observed at x/d = 0.2. A third peak is observed near 1000 Hz. For each of these peaks, a coherence is observed between the velocity fluctuations at this axial position and the pressure field just outside the nozzle lip separation point. Clearly, these instability modes are radiating a pressure field which is felt at the separation point. At this same axial position a small spectral bump is incipient near 370 Hz. This is more clearly observed in the peak coherence around this frequency. This corresponds to the subharmonic mode of the 730 Hz peak. It should be noted that the subharmonic mode does not appear until the fundamental reaches a finite amplitude for this particular test flow condition. This is what has been typically observed in the literature.

By a value of x/d = 0.6, the peaks at 730 and 880 Hz remain and the first subharmonic of 730 Hz becomes more distinct along with a strong increase in the value of its coherence. This peak then continues to grow while the two high frequency peaks decay. By one diameter, the spectral peaks have vanished and the shape of the spectrum is slowly returning to its random nature as previously observed at x/D = 0.2. At one diameter there is still a weak coherence between the subharmonic mode and the nozzle lip pressure field even though the spectral peak has been smeared out by the background fluctuations.

The spectral characteristics along the jet centerline are shown in Figure 44. The first streamwise position here corresponds to the last position examined in the off axis case. At x/D = 1 the subharmonic mode is clearly evident along with its high coherence. With an increase in streamwise distance, both the spectral peak and high coherence decay. At x/D =1, another broad band spectral peak which has significant coherence is observed near 140 Hz. As the streamwise distance is increased, the coherence of this mode slowly diminishes and a broad band spectral peak emerges near 100 Hz. This mode does not appear to be related to the initial peak near 140 Hz since the coherence at this frequency is away from the new spectral peak at this axial position.

The nature of the off axis spectrum is extremely

similar to that observed by Husain and Hussain (1979) in their naturally developing jet. Similar multiple peaks were observed but were not focused on in their study. The asymptotic value of u'/U_j which they found off axis was 0.159, nearly identical to the value that was determined in Chapter IV for Case 3L. The measured jet growth rate was also nearly identical to that measured for this case. It seems that the experimental test flow condition of theirs (exit core intensity = 0.34%) is extremely similar to the present highly disturbed test flow.

A single realization of the structure of the flow for test flow 3L was shown in Figure 12. For this initially high disturbance level flow condition, the initial roll up is highly three dimensional. From this single realization it is unclear as to whether there is any further organized motion present. To examine this in greater detail, a high speed visualization sequence taken at a Reynolds number of 42,000 is shown in Figure 45. The outer region of the initial jet rolls up near a value of $x/D = 0.5$ and is highly three dimensional. Corresponding to this position, a broad band increase in spectral energy from 600 Hz to 1000 Hz was observed in Figure 43. This frequency range is clearly related to the initial jet instability. As these structures move downstream, pairing is clearly observed. From Figure 43, it is noted that this sequence is related to the spectral

development of the 360 Hz mode.

From the visualization it is evident that the pairing mechanism takes place even in this highly disturbed flow condition. This would account for two of the spectral peaks in Figure 43, i.e., 730 Hz and its first subharmonic. There still remain numerous peaks which must be examined. Before examining these in greater detail, let us focus our attention on the nature of the peaks at 730 Hz and 880 Hz. With the hot-wire at $x/D = 0.5$ and at the same radial position as in Figure 43, the phase spectrum was determined between the velocity at this position and the pressure field at the nozzle lip as a function of azimuthal separation angle γ. The hot-wire remained stationary while the pressure readings were obtained circumferentially around the jet. The variation of the azimuthal phase difference of these two modes is shown in Figure 46. The top curve represents the 730 Hz mode. In this case the phase difference is essentially constant, indicative of an axisymmetric mode as described by the ideal m=0 curve. Here m is the azimuthal wave number. This result is not too surprising in light of the observed subharmonic for this mode. Since the subharmonic generation is related to the pairing activity and ideally the pairing in a jet is an axisymmetric phenomenon, the axisymmetry of the fundamental mode is not unexpected. This axisymmetric mode is referred to as $f_{1,0}$.

The bottom curve examines the azimuthal structure of the 880 Hz mode. In this case the phase difference varies around the jet reaching a value of 180° at a value of γ of 180°. Included in this figure is the ideal phase variation for the first helical mode, m = 1. It is quite evident that this peak at 880 Hz is the first helical mode. This mode is denoted by $f_{i,0}$. The azimuthal variation will be examined further in Chapter VIII.

Even though the measurements unquestionably show the appearance of the first helical mode, it was not observed in the flow visualization sequence in Figure 45. Indeed, further visualization showed that the axisymmetry of the flow was non-stationary. The flow alternated between initially axisymmetric and helical disturbances. Unfortunately, long enough observation times were not recorded to obtain a convergent estimate of the percentage of occurance of each flow state. From this initial observation that both axisymmetric and helical modes are present for this flow condition, it becomes quite evident that the initial instabilities in a jet cannot be thought of in terms of developing from a quasi-two dimensional shear layer.

From this figure and Figure 43, both the axisymmetric and helical modes for this flow condition appear to have similar growth rates; a result predicted by Michalke (1971) and by Mattingly and Chang (1974). What is important though is that these modes develop at

different frequencies. In fact, this difference is nearly identical to that predicted by Mattingly and Chang (1974). Based on Figure 43, the helical mode develops at a frequency which is approximately 20% larger than that for the axisymmetric mode. Because of this frequency difference and the nearly equal amplitude growth, the possibility of encountering a nonlinear interaction between these modes exists, particularly in the switch over from the m=o mode to the m=1 mode. This conjecture is examined in further detail in Figure 47 where a detailed streamwise velocity spectrum, taken at $x/D = 0.5$ and at a radial position of $U/U_j = 0.6$ is presented for a Reynolds number of 50,000. Four sharp spectral peaks are observed at this position: the initial axisymmetric mode, the initial helical mode, the first subharmonic of the axisymmetric mode and also a mode which exactly corresponds to the difference between the axisymmetric and helical modes. In addition to these, other modes are observed which are the multiple sum and difference modes between $f_{i,0}$ and $f_{i,1}$ and also between $1/2f_{i,0}$ and $(f_{i,1} - f_{i,0})$. Based on the results of Miksad (1973), it is clear that there is a nonlinear interaction between the axisymmetric mode and the helical mode. It also appears that there may also be a nonlinear interaction between the subharmonic mode and a low frequency mode which has evolved from the initial nonlinear interaction between the axisymmetric and helical modes. This point

will be taken up later.

There are a few differences which exist between the present case and that of Miksad (1973) so that a direct comparison is not rigorously possible. In this naturally developing case the interaction is between planar and nonplanar waves. The effect of different azimuthal modes interacting to produce nonlinear modes has not been previously addressed. It is expected however, that their features are not grossly different from those of the strictly two dimensional case. The second difference is that in this unforced case, the m=0 and m=1 modes do not usually coexist. Mode switching is observed and its effect on the development of the nonlinear modes is unclear.

Having examined test flow 3L and identified the major spectral peaks, a few general observations will next be made about the influence of the disturbance level on the instability characteristics of the jet. Test flow condition 2L is presented in Figures 48 and 49. The off axis characteristics are first examined for a Reynolds number of 42,000 at a radial position where $U/U_j = 0.6$. Initially at x/D = 0.2 the axisymmetric, helical and subharmonic modes are observed in the coherence along with all of the nonlinear interactions previously described. At this early station the velocity fluctuations in the shear layer for the above modes are strongly correlated to the pressure field at the nozzle

lip. The modes which are already observed as discrete spectral peaks are $f_{i,0}$ and its subharmonic. Here the subharmonic mode has a slightly higher amplitude. This early occurance of the subharmonic mode before the jet develops was not seen in case 3L. Due to the high coherence it must be related to the sensitivity of the exiting boundary layer to the near field pressure. By $x/D = 0.5$, the initial axisymmetric mode has grown to a value much larger than its subharmonic. This is a result which is expected based on the simple linear spatial theory of Michalke (1971). In this case the helical mode does not amplify to as large a level as was observed in case 3L. This mode however is there and is clearly observed in the coherence and the indicated difference modes. At $x/D = 0.75$ the subharmonic mode has grown and has over taken the amplitude of the initial instabilities. By one diameter the spectrum becomes quite random. Even at this downstream position there remains a strong coherence in the difference mode and weak coherence at the subharmonic mode.

The centerline characteristics are next considered in Figure 49. At one diameter, which was the last off axis position discussed, there exists spectral peaks and high coherence in the subharmonic mode and the $(f_{i,1} - f_{i,0})$ mode. As the axial distance is increased, there is spectral broadening of the modes along with a decrease in the coherence. Even at five diameters there

is still a non zero coherence. The $(f_{i,1} - f_{i,0})$ mode is clearly identified in the velocity spectrum and is coherent with the near field pressure even at five diameters. As the axial position is increased from one to five diameters, a gradual growth in spectral energy is observed near 100 Hz, reaching a maximum value at five diameters. Normalizing this frequency with the diameter of the jet and the jet velocity, it is found that the nondimensional Strouhal frequency has a value of 0.42. It is more evident here than in the previous case that this mode develops independently of the nonlinear mode $(f_{i,1} - f_{i,0})$. This is the final jet-core Strouhal frequency, sometimes called the preferred mode, Crow and Champagne (1971) and Hussain and Zaman (1981) or column instability, Kibens (1978). Its characteristics are discussed further in a subsequent chapter.

Having examined cases 2L and 3L, we next consider the lowest disturbance level case, flow condition 1L. The measurements presented here are at the same Reynolds number and radial position as for the results for cases 2L and 3L. The off axis characteristics are shown in Figure 50 and the centerline characteristics are shown in Figure 51. The off axis development is similar to that of case 2L with a few exceptions. Below 300 Hz there is a large increase in the observed coherence due to a decrease in background fluctuations in the boundary layer. At $x/D = 0.2$, strong coherence is observed for

all modes. In this case the highest spectral amplitude occurs at the difference mode of $(f_{i,1} - f_{i,0})$. The amplitude of the subharmonic mode is lower and the amplitude of the fundamental is lower yet. The drastic difference between the behavior here and that for case 3L at the same axial position is due only to a slight difference in the core intensity and more important, in the spectral content of the initial boundary layer. Test case 3L is probably typical of many of the flow conditions existing in jet research facilities. By reducing this level slightly, a clearer picture of the instability characteristics can be examined without being masked by the background fluctuations.

The second difference between the three test cases lies in the absence of a large amplitude peak corresponding to the helical mode for case 1L. However, if the coherence function is carefully examined at a frequency 20% higher than $f_{i,0}$, a strong peak exists. This is the helical mode. This is also noted by the occurance of the nonlinear interaction modes.

As the disturbance level decreased, the amplitude of the helical mode also decreased perhaps indicating less time in this state. It is quite possible then that even though both the axisymetric and helical modes are initially present, the selection and early amplification of the helical mode is dependent on the initial disturbance characteristics.

The centerline characteristics, described in Figure 51 clearly show the same phenomena as in case 2L. The interesting point in this figure is to examine the spectral development near 100Hz. At $x/D = 1$ no discrete spectral peak is observed at this frequency although a coherence of approximately 0.2 is observed. By two diameters a large amplification has been observed relative to the 170 Hz peak. This mode finally evolves to a distinct peak at $x/D = 5$. The Strouhal number of this mode is 0.42. This is the evolution of the long wave jet instability, discussed in Chapter I, and it is quite apparent that it develops as the other jet instabilities are forming. What is surprising is that even at five diameters there exists a significant non-zero coherence between these velocity fluctuations and the pressure field at the nozzle lip. This low frequency pressure field could lead to the low frequency modulation of the initial shear layer that Laufer (1981) discusses.

Both axisymmetric and helical modes are present in this flow as demonstrated by visualization records such as those of Figure 52. These photos were taken at a Reynolds number of 42,000. The top photo was conditioned on the subharmonic spectral peak. As can be seen, this corresponds to an axisymmetric mode. The bottom photo was taken randomly in time and clearly illustrates both the helical nature and its change back to an axisymmetric

mode. This occurance is rare as was represented by the low amplitude of the helical mode in the velocity spectrum.

Turbulent Exit Boundary Layer

Having examined the general characteristics of the instability process when the boundary layer is initially laminar, we next focus on the case when the exit boundary layers are fully turbulent. Results for this are shown in Figures 53 and 54. The off axis streamwise velocity spectrum for Case 1T, with $L/D = 0.75$, at $Re = 42,000$ is shown in Figure 53. Initially the boundary layer is fully turbulent as observed by its monotonically decreasing spectrum along with the documentation in Chapter III. A short distance from the lip, at $x/D = 0.1$, a broad spectral peak is observed to form near 600 Hz. This peak was observed at all radial positions outside of the core. The location of this peak will be shown in Chapter VI to correspond identically to the peak value obtained from the pressure measurements at the nozzle lip. The frequency of this peak decreases inversely as the axial distance is increased until by one diameter, a peak at the longwave jet Strouhal frequency is observed. The development of the centerline streamwise velocity spectrum is shown in Figure 54. In this case, only one spectral peak is observed at any axial position, and that one peak corresponds to the

downstream jet Strouhal frequency. Even at x/D = 0.1,
this mode is observed on the centerline.

The development of this mode is similar to that
observed when the initial boundary layer is laminar. In
that case it was also determined that the evolution of
that mode was separate from the initial instabilities of
the jet. The emergence of this longwave instability is
independant of the state of the initial boundary layer.
The value of its Strouhal frequency though is probably
dependent on the initial momentum thickness of the jet.
The observation of the independence of the state of the
initial boundary layer was recently recorded by Hussain
and Zaman (1981) and is further confirmed here.

When the jet has initially laminar boundary layers,
both axisymmetric and helical modes are present. The
question which now must be asked is what is the azimuthal
nature of this long wave instability. The development of
this mode is visually observed in Figure 55. This figure
shows two realizations of the jet having initially
turbulent boundary layers at a Reynolds number of 75,000.
In both cases the initial development of this mode is
axisymmetric. By two diameters the mode changes to a
helical nature. This behavior was predicted by Mattingly
and Chang (1974). Close to the jet the dominant
instability mode is axisymmetric. As the jet grows, the
momentum thickness increases and the helical mode emerges
as having the largest growth rate. This behavior is

clearly demonstrated in this figure. Such a comparison between the theory, which uses an initial laminar boundary layer, and the turbulent boundary case is valid only because of the nearly identical self preserving mean profiles as indicated in Figures 29 and 35. Once this helical mode has developed, it remains the dominate instability, perhaps even past the end of the potential core.

CHAPTER VI

NEAR-FIELD PRESSURE OF INITIAL JET

In the previous chapter the general characteristics of the jet instabilities were examined. In all cases there was a definite, and in some cases strong, coherence between the velocity fluctuations in the jet and the near field pressure. Thus the pressure field associated with the evolving vorticity field of the instability modes in the jet must be felt back at the nozzle lip. Depending on the characteristics of this pressure field and the nature of the disturbances in the exiting jet, this field may act as a natural small amplitude external excitation to the jet, i.e., a self-excited jet.

A subharmonic feedback mechanism in naturally evolving jets has been speculated by Gutmark and Ho (1980) and by Laufer (1981) to be a phase bearer and the mechanism for vortex pairing. Before considering how these speculations fit into the overall picture developed from the present results, a detailed examination of the pressure field at the nozzle lip is first undertaken. Once this has been presented, the interaction between the pressure field and the developing instabilities in the jet are explored in the following chapter.

Scaling of Initial Axisymmetric Mode

If it is assumed that the generation of the initial free eigenmode of the jet is unaltered by the downstream

developing vorticity field through an unsteady pressure field at the nozzle lip, then for cases where the exit boundary layer thickness is small compared to the jet diameter, i.e. $D/\theta > 50$, (Michalke, 1971), linear stability theory, using parallel flow assumptions, would predict that the instability mode would scale with the momentum thickness of the exit boundary layer at a constant Strouhal number, St . This result is applicable to laminar boundary layers and perhaps also to turbulent boundary layers. As Crighton (1981) states, "if the scale of the turbulence is small compared to the wavelength of the initial instability mode", this condition may be satisfied.

In cases where the boundary layer is laminar, the exit boundary layer momentum thickness is inversely proportional to Re. This was confirmed in Chapter III. Since

$$St_\theta = CONST. \tag{VI-1}$$

then

$$St_\theta * D/\theta \; \alpha \; \theta^{-1}$$

or

$$St \; \alpha \; \sqrt{Re} \tag{VI-2}$$

This result shows that in cases where the exit boundary layer is laminar, and when a linear instability mechanism is acting to select the most unstable mode, the initial Strouhal frequency is proportional to the square root of the jet Reynolds number.

Mattingly and Chang's work (1974) examining the linear stability of axisymmetric jets brings out a number of enlightening points. Using a family of measured profiles to describe the mean velociy distribution of the jet, it was determined that for initial boundary layers which were thin compared to the jet diameter, both the axisymmetric and first helical modes had nearly the same amplification rate and occurred at frequencies that differed by 17%. It was documented in the previous chapter that the helical mode developed at a frequency approximately 20% higher than that of the axisymmetric mode. This result clearly showed that the initial jet is equally sensitive to both axisymmetric and helical disturbances. Since both modes were found to have nearly equal growth rates, extra information is necessary to determine the conditions under which one mode may dominate. It was also observed that the growth of the helical mode was tied into the disturbance characteristics in the jet initially. In the lowest disturbance level case, the helical mode was only observed through the coherence measurement. No large discrete spectral peak was measured. Thus, single channel spectra may not always be sufficient to determine these modes.

In much of the literature on axisymmetric jets neither the initial conditions across the jet nor the initial off-axis characteristics are well documented.

Recently Kibens (1981) documented the initial instability frequency characteristics for a 2.54 cm and a 6.33 cm jet, using hot-wire measurements, and found that in both cases the initial jet instability scaled with Equation (IV-2).

On the other hand, Gutmark and Ho (1980) in an axisymmetric jet showed that the initial instability frequency (and not the Strouhal frequency) does not increase monotonically with increasing Reynolds numbers, but rather was found to be stepwise. Ho (1981) determined that the occurrence of the steps was due to a low level spatially coherent acoustic excitation which was developed within the settling chamber. The original speculation was that the stepwise increase was a result of satisfying the feedback condition described in Chapter I. It will be first shown that the original speculation had no grounds and the observed steps had to be related to an acoustic disturbance as Ho found. To do this the characteristics of the feedback condition are first examined.

If the restriction that only axisymmetric modes are allowed, then according to Ho and Huang (1981), the number of waves in a feedback loop should be an integer.

$$\frac{1}{2} f_{i,o} \left[\frac{x_m}{\overline{c}_r} + \frac{x_m}{a} \right] = N \qquad \text{(VI-3)}$$

where x_m is the position of the first vortex merging, $\overline{c}_r$

is the dimensional phase speed of the subharmonic, a is the speed of sound and $\frac{1}{2}f_{i,0}$ the subharmonic frequency. For typical experiments in the moderate Reynolds number range, $a \gg \bar{c}_r$ so that Equation (IV-3) simplifies to

$$\frac{x_m}{D} = \frac{2N\bar{c}_r}{f_{i,o}D}$$

In a jet, Gutmark & Ho (19080) found N to have a value of one. The effect of dropping the second term on the concept of a feedback loop is considered in Chapter XI. It will be shown in Chapter VII that

$$\bar{C}_r = 0.5 \ U_j$$

With this, Equation (IV-4) becomes

$$\frac{x_m}{D} \doteq \frac{N}{St_{i,o}} \qquad\qquad (VI-4)$$

This shows that the pairing location is inversely proportional to the initial Strouhal frequency.

The original speculation about the stepwise behavior of the initial instability frequency centered about the idea of the location of the pairing fixed in space. If this was the case, from Equation (VI-5) it is observed that the initial Strouhal frequency would be stepwise and not the initial instability frequency. In fact the results of Peterson (1978) show that the completed pairing position was indeed inversely proportional to the

initial Strouhal frequency as described above. Kibens
(1980) showed that if one allowed resonant modes upstream
of the jet exit then when the initial jet eigenfrequency
is near the resonant frequency, the jet would lock onto
this mode and discrete steps in frequency would appear.
A similar type of behavior was observed with wide band
external excitation in Appendix A. Thus, the stepwise
behavior of the initial eigenfrequency must be due to an
external acoustic forcing.

To further clarify these views, the variation of the
initial axisymmetric instability frequency with Reynolds
number was examined for the test cases described in
Chapter III. Results for test flow condition 1L using a
FO nozzle is shown in Figure 56. Two separate sets of
data were taken. One set corresponds to data taken
off-axis with the hot-wire probe described in Chapter II,
while the other set corresponds to data taken from one of
the pressure taps around the circumference of the jet.
As described in Chapter V, multiple peaks in the
streamwise velocity spectrum were observed. Based on the
phase measurements around the jet and the off-axis
development, the mode which developed a distinct
subharmonic frequency was determined to be the initial
axisymmetric instability mode. It was carefully checked
that the frequency of this mode did not vary in either
the downstream or cross-stream direction. To ensure that
the probe did not influence the measurements of this

mode, the amplitude spectrum of the pressure fluctuations, using one of the pressure taps, was taken with the probe removed from the flow. Details of the form of the pressure spectrum will be discussed later. However, a distinct peak corresponding to this frequency as determined from the velocity spectra was observed. When this data were plotted in non-dimensional form, it was noted that the variation of the initial Strouhal frequency is linear with the square root of the jet Reynolds number according to Equation (VI-2). This variation is substantially different from that observed in Appendix A where the jet was developing in an acoustically noisy environment.

In Chapter III the value of the initial momentum thickness of the jet was determined along with its near field development. The initial momentum thickness (i.e., the exit boundary layer momentum thickness) is not a suitable parameter to scale the initial jet instability frequency. This is so because this parameter can not take into account the spectral characteristics of the exit boundary layer. For example, in Table 2 the initial exit momentum thickness decreased from case 1L to 3L. However, the jet required a longer spatial distance for the initial jet instability to develop (Chapter V). This is opposite of what one would expect if the initial momentum thickness was utilized as a scaling parameter. The proper parameter then is one which describes a

particular feature of the initially growing eigenmode.
For this reason, the momentum thickness at the position
where a peak in the streamwise velocity spectrum at the
initial axisymmetric instability frequency was first
detectable was utilized to normalize all cases. In this
manner the same relative starting point in the growth of
this instability mode can be maintained between test flow
conditions. Normalizing the data of Figure 56 with this
parameter, it is observed that the initial axisymmetric
mode scales as

$$St_\theta = 0.013$$

It should be noted here that for this initially low
disturbance level condition, $\theta=\theta_{0.1}$ since the first peak
is observed very near the jet exit. This value of St_θ
agrees with the results of Zaman and Hussain (1981). In
this case they found that the natural instability occurs
at $St_\theta = 0.012$. Here, they normalized by the initial
momentum thickness of the jet. Surprisingly, this value
does not correspond to the maximum amplified mode
according to linear theory, $St_\theta = 0.017$, which has been
documented by the above authors under external forcing.
Thus, the initial axisymmetric mode is not the most
amplified. Similar observations were made by Pfizenmaier
(1971) and by Michalke (1972). Since no azimuthal phase
information has been presented in the above work, it is
presumed that the modes which are described are indeed
axisymmetric.

A mechanism to clarify this mode selection has been proposed by Zaman and Hussain (1981). In this case they suggest that the shear layer naturally responds to disturbances which have maximum growth rather than maximum growth rate. Here the maximum growth rate was experimentally determined to occur at $St_\theta = 0.017$. These views however, are based solely on the dominance of an axisymmetric mode. Much of the recent literature has been biased toward axisymmetric modes because of the attractiveness of the pairing process to describe the jet growth. Helical modes have been ignored. A discussion on the influence of the helical modes on this selection mechanism is deferred, however, until all of the relevant data has been presented.

The experiments carried out by Gutmark and Ho (1980) utilized a matched cubic nozzle. In a private communication with Ho (1981) it was suggested that perhaps it was some characteristic associated with matched cubic design which led to the stepwise behavior of $f_{i,0}$. To clarify this, measurements were conducted utilizing both a 5.14 cm MC nozzle and also a 2.54 cm MC nozzle. These cases are shown in Figures 57 and 58. In both cases, the initial axisymmetric Strouhal frequency is lineary related to the 0.5 power of the jet Reynolds number and in neither case is any stepwise behavior observed. Unfortunately, the initial momentum thickness of this shear layer was not measured so that it is

uncertain if the initial jet still scales at $St_\theta = 0.013$.
It is believed however, that the nozzle shape will not
influence this value. Since the nozzle design of Zaman
and Hussain (1981) is radically different from the fifth
order design used here and no difference in the scaling
of the Strouhal frequency was observed, it is plausible
to believe that matched cubic also scales in the same
manner.

As the disturbance level in the core of the jet, and
hence in the boundary layer, is increased, it is
important to determine the effect on the scaling of the
initial jet instability. The core disturbance level can
be characterized by its fluctuation intensity and also
its spectral characteristics. The core disturbance
becomes internalized in the boundary layer. If the
disturbance level in the boundary layer is low then one
would expect that the disturbance would have no influence
on the selection of the initial instability frequency
since a linear instability mechanism is acting. To
examine this, the variation of the initial axisymmetric
instability frequency was documented for test flow
conditions 2L and 3L. The disturbance characteristics
for these cases were described in Chapter III. Results
of this study are shown in Figures 59 and 60. In each
case the variation of St with the square root of Re is
linear. In addition, when normalized by the measured
momentum thickness using the same criterion as in case

1L, the scaling of the initial Strouhal number is
unchanged from that case. Even though the initial
boundary layer disturbance characteristics and the
downstream evolution of the jet are vastly different for
test flow conditions 1L, 2L and 3L as observed in Figure
12, and Chapter V, the selection of the initial
axisymmetric instability mode remains the same when
properly scaled. Referring back to Table II in Chapter
III, if the initial momentum thickness was used to scale
cases 2L and 3L, there would have been no similarity in
the normalized eigenfrequency.

Scaling of Other Instability Modes.

In the previous section the initial axisymmetric
instability frequency was determined in some instances
using the near field pressure, measured at the nozzle
exit. A typical pressure spectrum is shown in Figure 61
for cases 1L, 2L and 3L at a Reynolds number of 42,000.
Also included is a spectrum of the background noise in
the laboratory measured 0.3 m behind the nozzle at the
same value of exit velocity. The background noise
exhibits a uniformly decreasing behavior and contains no
discrete spectral peaks for the jet to possibly lock
onto. The background pressure spectrum was measured over
the entire operating range of exit velocities, flow
configuration and nozzle geometries to ensure that no
external peaks were present. Coherence measurements

between this pressure signal and the velocity signal in the initial jet near the nozzle lip indicated that the two signals were uncorrelated at all frequencies.

The pressure spectrum corresponding to test flow condition 1L is first considered. A number of distinct spectral peaks are clearly evident and indicated in the figure. The initial axisymmetric and helical modes are both observed with the axisymmetric mode being about 8 db larger than the helical mode. These two frequencies correspond to the smallest amplitude spectral peaks observed. A large amplitude subharmonic peak, approximately 20 db greater than the axisymmetric mode, is also observed. The magnitude of this mode indicates the strength of its upstream radiation field. Two other spectral peaks, both of nearly equal magnitude as the subharmonic mode, are identified as the difference mode generated by the non-linear interaction between the initial axisymmetric and helical modes and also a mode which is the difference mode generated by the non-linear interaction between the above mentioned difference mode and the subharmonic mode. The sum mode for the above interaction is also observed lending further support for the idea of this second non-linear interaction.

The pressure spectrum for case 2L shows the same spectral trends as for case 1L with the exception of a broadband decrease in the magnitude of the pressure field. As the disturbance level is increased further to

case 3L, clear spectral peaks for the low frequency modes
are not apparent with the exception perhaps of the
subharmonic mode. It should be noted here that the shift
in frequency from case 1L to 3L is due to a small
increase in the scaling momentum thickness even though
the initial thickness decreases slightly. This
frequency, however, when normalized by the proper
momentum thickness does not change between cases as
observed in Figures 56 through 60 for the initial
axisymmetric mode.

A few basic conclusions can already be made. First,
the effect of the internal disturbance level of the jet
and in particular the exit boundary layer has a distinct
effect on the near field pressure outside the boundary
layer separation point. For low disturbance levels,
peaks exist in the pressure spectrum corresponding to the
initial instability modes, the subharmonic mode, and
modes which are generated through non-linear
interactions. As the disturbance level increases, there
is a broadband decrease in this pressure field. In
addition to this, the peaks corresponding to the
subharmonic mode and the lower frequency non-linear modes
are no longer distinct, indicating an increase in the
randomization due to the increased three dimensionality.
This randomization is observed in the flow structure
between cases 1L and 3L in Figure 12. As was previously
noted, the growth rate of the jet also decreased with

increasing disturbance level. This was partially
attributed to the weakening of the initial developing
coherent structures as observed in the entrainment
visualization in Figure 38. This weakening due to the
increase of background disturbances is now also observed
in the broadband decrease of the pressure field.

Having identified the peaks in the pressure
spectrum, the nature of the scaling of these modes is
examined next. For each of the test flow conditions,
spectra similar to those in Figure 61 were taken over
small increments of Reynolds number. The frequency of
each peak was normalized by the jet diameter and jet
velocity. The variation of this non-dimensional Strouhal
frequency with Reynolds number is shown in Figures 62
through 65. The results for test flow condition 1L are
shown in Figure 62. It is observed that all of the modes
in the pressure spectrum vary linearly with the square
root of Re. This indicates that all of these modes scale
at constant value of St_θ. Even though data were not
taken for the initial helical mode for this case, except
for that from Figure 61, the linear behavior of the
non-linear developing modes implies the linear behavior
of this mode also.

To ensure that this behavior was uninfluenced by the
nozzle shape, a similar set of measurements was taken
using a 5.14 cm MC nozzle. These results are summarized
in Figure 63. As in the previous figure, the observed

modes scale in an identical manner. It would thus appear
that the basic behavior of these modes is independent of
the two nozzle contours examined.

The variation of the Strouhal frequency modes for
cases 2L and 3L is shown in figures 64 and 65
respectfully. The behavior of case 2L is identical to
that of case 1L. The measurements of the initial helical
mode in Case 3L were taken in the shear layer using the
hot-wire probe previously described. Since no distinct
spectral peaks were visible in the pressure spectrum
below the subharmonic mode for this case, none are
presented here even though they are clearly evident in
the off-axis spectra of Figure 47. The behavior of these
modes is identical to the previous cases. This indicates
that even though the downstream development of the jet is
dependent on the initial disturbance level, the scaling
of the evolving instability modes is not. This ensures
the linearity of the problem initially.

The nozzle lip pressure field is next examined for
the case when the exit boundary layer is turbulent.
Using test flow condition 1T with the short duct having
L/D = 0.75, a single pressure tap was installed just
outside the separation point at the same radial position
as the taps on the face of the FO nozzle. Typical
pressure spectra at two Reynolds numbers are shown in
Figure 66 for this condition. The pressure spectra in
this case show a distinct difference between those from a

laminar boundary layer as described in Figure 61. In
this case there is a single broad-band peak of spectral
energy, the magnitude and center frequency of which
increases with Re. Based on the differences between the
two types of spectra, one would expect a drastic
difference in the evolution of the jet in the near
region.

Examples of the structure of the jet when the
boundary layers are fully turbulent were displayed in
Figure 22 for the Reynolds number range from 39,000 to
100,000. The initial jet consists mainly of fine grain
scales which eventually roll up into a well defined
coherent structure.

Noting the center frequency in the pressure spectra
as described above, the Strouhal frequency based on the
nozzle diameter was determined as a function of Re.
These results are shown in Figure 67. Included in this
figure are the two different length of ducts for case 1T.
In each case, the Strouhal frequency appears to be
independent of Re. However, the values for each case are
different. Remembering that the momentum thickness for
each case was essentially independent of Re, as described
in Chapter III, the Strouhal frequencies were
recalculated based on the exit momentum thickness. These
results are shown in Figure 68 and indicate that the
pressure field at the nozzle lip which is associated with
the initial instability of the jet, scales at a constant

value of Strouhal number. This value is found to be equal to 0.024. A similar observation was also made by Hussain and Zaman (1981) in a two-dimensional mixing layer with an initial turbulent boundary layer. It would thus appear that initially a linear instability mechanism is also acting on a jet with turbulent boundary layers as proposed at the beginning of this chapter. A peak in the velocity spectrum at this frequency was observed in Figure 53. This is a further indication of the weak linear instability that develops naturally.

The value of this Strouhal number for the turbulent boundary layer though is approximately twice that found when the exit boundary layers were laminar. The exit boundary layer profiles for cases 1L, 2L and 3L remain Blasius over the range examined while the profiles for case 1T are fully turbulent. Clearly, the shape of the exit profile will have a large effect on the non-dimensional frequency of the initial eigenfrequency. The magnitude of this difference has not been numerically determined yet.

A summary of the results for the scaling of the modes observed in the pressure spectra and in the velocity spectra of the initial jet for all cases is presented in Figure 69. In this plot the instability frequencies are normalized by the momentum thickness near the nozzle lip. Each mode develops at a constant value of Strouhal number, St_θ . The results of Michalke (1971)

for the initially most amplified axisymmetric and helical modes are also indicated. The initial helical mode nearly matches this frequency. With the degree of uncertainty in the momentum thickness measurements and in the proper choice for the momentum thickness, the value of St_θ of this mode is certainly within the error bounds for agreeing with the theory of Michalke. It should be remembered that the theory by Michalke utilized a family of hyperbolic tangent profiles. With the profiles examined in Chapter III, the initial off-axis are only approximately hyperbolic by the time the initial instability mode is first observed in the velocity spectrum.

The initial axisymmetric mode occurs at a value 20% lower than the initial helical mode. Its subharmonic mode also scales at a constant Strouhal number. Also observed are the modes which arise through non-linear interactions. The results for the initial turbulent boundary layers are also shown. This result can not be compared to the calculations by Michalke (1971) though because of the substantial difference in mean velocity profile.

These results show that independent of the initial state of the boundary layer, an initial linear instability is always observed. The scaling of this frequency depends on the initial time-mean velocity profile of the jet. When the initial boundary layer is

laminar, both initially axisymmetric and helical modes are observed. The frequency of the helical mode observed is almost identical to that predicted by the linear theory of Michalke (1971). The initial axisymmetric mode occurs at a frequency of 20% lower than the helical mode, a fact which agrees quite well with the results of Mattingly and Chang (1974). Modes which are generated by non-linear interactions of these modes are also observed to occur at a constant value of St_θ. The scaling of the instability modes for the laminar boundary layer were independent of the background disturbance level when the proper scaling was used.

Coupling Between Long and Short Waves

In the previous sections the characteristics of the initial jet instabilities, which scale with the momentum thickness near the exit boundary layer, have been examined. In addition to these instabilities, it is well known that a long wave instability which scales on the jet diameter is also observed. The value of this Strouhal frequency typically has been found to vary between 0.3 and 0.6 depending which test facility was used and is essentially independent of Reynolds number. This instability is identified on the jet centerline typically 2-5 diameters downstream of the jet exit. The emergence of this mode was identified in Figures 44, 49, 51 and 54.

Recent work by Kibens (1980) showed that when the exit boundary layer was laminar and the initial axisymmetric Strouhal frequency was an integral power of 2 of the long wave jet frequency, a small amount of axisymmetric excitation at the initial jet eigenfrequency had a tremendous effect on the organization of the jet in such a manner that a large fraction of the energy was associated with the coherent structures. Axisymmetric vortex pairings were clearly observed and found to be stationary. This mechanism was observed to be the coupling between the initial axisymmetric mode and the long wave jet instability.

The applicability of this to naturally evolving jets will next be examined. Based on the above results, a necessary condition for this to occur is that the initial axisymmetric Strouhal frequency of the jet be an integral power of two of the long wave jet instability,

$$St_{i,o} = 2^n St_f$$

The Reynolds numbers at which this coupling would occur would then be given by

$$Re^* = C (2^n St_f)^2$$

In the above equations, n is identified as the number of vortex pairings. It must be assumed that the vortex

interactions are all axisymmetric for these relations to hold.

The jet Strouhal numbers were first determined for the five test cases along the jet centerline at $x/D = 5$. At this downstream location, the peak in the velocity spectrum was well defined for all cases. The results from this study are shown in Figure 70. In each case, St is found to be independent of Reynolds number. The value of St , however, is a function of the test flow condition, varying from 0.42 to 0.485. For test flow conditions 1L and 2L, St has a constant value of 0.42 and only marginally increases to 0.43 for test flow condition 3L. When the fully turbulent boundary layer using the short duct was tested, St had a value of 0.47. When a thicker turbulent boundary layer was utilized, the value of St increased to 0.485.

The value of this Strouhal number is a definite function of the initial momentum thickness of the jet. For case 1T, using the long duct, the value of $D/2\theta$ is approximately equal to 40 and independent of Reynolds number. As this ratio is increased to 50, the value of St drops to 0.47. The initial laminar boundary layers all have a value of $D/2\theta$ larger than 110. For this case the Strouhal frequency reaches an asymptotic value of 0.42.

With the information provided in Figure 56, the value of C in Equation (VI-4) was calculated for test

flow condition 1L as:

$$C = 3720$$

Knowing this value and the value of St from Figure 70, the Reynolds numbers at which this coupling might take place were calculated from Equation (VI-4).

The results are

$$Re^* = \begin{array}{ll} 2600 & n=1 \\ 10,500 & n=2 \\ 42,000 & n=3 \\ 168,000 & n=4 \end{array} \qquad (VI-5)$$

This result indicates that this coupling occurs predominately at low and moderate Reynolds numbers. As Re increases this coupling becomes less frequent.

Operation of the present 5.14 cm jet was limited to Reynolds numbers larger than 30,000. Below this value the pressure field at the nozzle lip was not much larger than the background level and the jet could have been susceptable to external disturbances. The facility could not be continuously run at an exit Reynolds number of 168,000. Therefore, if any indication of the coupling mechanism is present in the naturally evolving jet, it would be observed at Re = 42,000.

If this coupling is to occur, then the jet would become more organized in an axisymmetric sense. This increase in organization would lead to an increase in the observed coherent energy. Some of this energy would be visible in the subharmonic mode but would probably

unalter the growth of the initial linear axisymmetric

instability. This increase in the subharmonic energy

would then be associated with a stronger pressure field

for this mode, which would then be felt at the nozzle

lip. To examine this, pressure spectra at the nozzle lip

were taken at various Reynolds numbers using the

alternate pressure measuring system which bypassed the

pressure taps for higher accuracy. For each Reynolds

number the amplitude of the subharmonic pressure peak was

normalized by the magnitude of the peak of the initial

axisymmetric mode, $f_{i,0}$. These results are displayed in

Figure 71 for test cases 1L, 2L and 3L.

For case 1L there is a sharp maxima in the curve

which occurs at the exact Reynolds number predicted by

Equation (VI-5). A closer examination of the pressure

spectra indicated that the magnitude of the peak at f

continuously increased with Re. The peak at the coupling

position thus corresponded to an increase in the pressure

field at $f_{i,0}/2$. This coupling is weak though since the

increase in the ratio of the pressure amplitudes is only

about two. Another indication of the weak coupling is

the observance of only one subharmonic mode in the

pressure spectrum. This coupling mechanism was based on

the idea of continual vortex pairing until the downstream

jet Strouhal frequency was reached. This continual

pairing would then lead to the development of modes $1/2f_{i,0}$

and $1/4f_{i,0}$. The second pairing mode is clearly not

observed. A third indication of the relatively weak coupling is the lack of effect this coupling has on the growth rate for the jet presented in Figure 39 for this Reynolds number.

Once the background disturbance level is increased as in cases 2L and 3L, this natural coupling disappears, i.e., the jet is no longer capable of self-excitation. In these cases, the emergence of an initial helical mode was clearly noted. With the competition between this mode and the initial axisymmetric mode, it is not surprising that an axisymmetric coupling is not observed. If initial axisymmetric perturbations of sufficient intensity were added at the proper frequency so that the axisymmetric mode completely dominated the initial helical mode development, then this coupling between long and short waves would be observed at the indicated coupling position. These results suggest that continual pairing is not the coupling mechanism between long and short waves as Kibens (1980) found. By externally exciting the jet in the manner of Kibens, it is possible to overide the effect of the helical disturbances. The continual pairing then is a result of the externally imposed axisymmetric forcing and not a result of the coupling mechanism.

To observe the effect of the helical mode on the natural coupling, consider the variation of the following ratio: the magnitude of the peak corresponding to the

mode developing from the nonlinear interaction between
the subharmonic mode and the mode which developed through
a nonlinear interaction between the initial axisymmetric
and helical modes normalized by the magnitude of the peak
of the subharmonic mode in the pressure spectrum. This
amplitude ratio is an indication of the relative
importance of the helical to axisymmetric modes. This
complex form using radiation from the interaction modes
rather than the original modes has been selected since
the former ones have lower frequencies and are more
efficient radiators at a fixed distance from the jet.
This ratio behaves in the manner shown in Figure 72 as a
function of Reynolds number. The results for case 1L are
considered first. At the coupling position this ratio
has a minimum value. This minimum corresponds to the
increased axisymmetric field described above. As the
Reynolds number increases, the relative importance of the
helical mode grows as observed by the trend of the data
toward values of this ratio larger than one. In case 2L,
no natural coupling was observed. This is further shown
here by the importance of the helical mode as indicated
by this ratio being larger than one. The level of the
data for case 2L is equal to that at the higher Reynolds
numbers for case 1L. This further shows that as the
disturbance level increases, the helical mode is quite
distinct and the flowfield can no longer be thought of as
being fully axisymmetric.

To ensure that this coupling behavior was not influenced by the shape of the nozzle, a similar study performed using a 5.14 MC nozzle. These results are displayed in Figures 73 and 74. The coupling Reynolds number for this case is essentially the same value as for the FO nozzle since the exit boundary layers are nearly identicle. The coupling phenomenon is once again displayed in Figure 73 for test case 1L. The only difference in the behavior of the two nozzles is the larger value of $p'(0.5f_{i,0})/p'(f_{i,0})$ for the matched cubic nozzle. Upon examination of the values of the peaks in the spectra, it was determined that the increase in this value was due to a decrease in the value of $p'(f_{i,0})$.

The variation of the rms pressure of the subharmonic nonlinear interactive mode is shown in Figure 74. In this case the behavior of both nozzles is nearly identical and once again demonstrates the natural coupling position and the emergence of the helical mode as the disturbance level in the boundary layer is increased as a result of increasing the jet Reynolds number. These results are consistent with those of the previous figures. It thus appears that the only difference between the two nozzles is the magnitude of the pressure field at the nozzle lip due to the initial development of the axisymmetric instability mode.

CHAPTER VII

INSTABILITY EVOLUTION OF INITIAL JET

In Chapter V general observations were made about the instability modes found in the jet and their relationship to the pressure field near the nozzle lip. In Chapter VI the details of this pressure field were closely examined. In that chapter it was noted that large peaks existed in the nozzle lip pressure spectra which corresponded to the instability modes observed in the jet. In fact, a high coherence was measured between this near field pressure and the downstream velocity fluctuations which indicated a strong relationship between the downstream evolution of the jet and its initial development through an unsteady irrotational pressure field at the nozzle lip. This relationship and the actual development of the instability modes in the initial jet are examined in detail in this chapter. Both amplitude and phase measurements were made to examine the different characteristics of the evolutionary process. In order to relate this instability process to the pressure field at the nozzle lip, detailed two point coherence measurements were also made.

For all cases examined in this chapter, a single hot-wire was traversed along the jet at a constant azimuthal angle of $\gamma = 0°$;see Figure 2. The pressure tap in the nozzle face at this same azimuthal position was

simultaneously monitoring the pressure field. Using this
signal as a reference, the coherence and phase spectra
were computed with the signal from the hot-wire as
described in Chapter II. Single channel velocity spectra
were also computed to obtain the RMS amplitude of each
instability mode.

Amplitude Development

The growth of the instability modes are first
considered for the low disturbance level condition of
case 1L. The behavior at the natural coupling condition,
corresponding to Re = 42,000 as described in Chapter VI,
is shown in Figures 75-78 for two different radial
positions in the jet. The first position which is
considered is at a radial location where the local mean
velocity is 60% of the jet velocity. This position, as
noted in Chapter IV, corresponds to the ray along which
the maximum turbulence intensity is found. The behavior
of the initial axisymmetric instability and its
subharmonic is described in Figure 75. The first
measuring position near the nozzle lip for which a large
enough signal-to-noise ratio existed in the hot-wire
output, so that non-random spectral content was
measurable for the initial axisymmetric mode, was x/D =
0.03. This corresponded to a value of x/θ_i of
approximately 8. At this position, the amplitude of the
subharmonic mode is an order of magnitude larger than the

corresponding value for the initial axisymmetric mode.
This is a result which has not been previously reported
in the literature. In fact, the subharmonic mode was
never observed until the amplitude of the fundamental
mode reached a finite level. This initially large
subharmonic amplitude is a result of the self-excitation
of the jet, i.e., from the natural forcing by the
downstream evolving subharmonic mode through an upstream
pressure field which is felt at the nozzle lip, or
separating point.

Both modes initially grow exponentially with the
growth rate of the initial axisymmetric mode being larger
as one would expect from linear theory. Because of the
difference in growth rates, both modes attain the same
relative amplitude by $x/D = 0.2$. The initial
axisymmetric mode subsequently reaches a finite
amplitude, at which point the growth of the mode deviates
from exponential growth. At that location, the growth
rate of the subharmonic suddenly increases by 46%. The
subharmonic mode then appears to once again grow
exponentially, overtaking the initial instability mode in
amplitude and reaching a peak value of 5%. Just before
this maximum is reached the amplitude of the initial
axisymmetric mode decreases to a local minimum before
increasing to approximately the same value as that for
the subharmonic mode by $x/D = 0.8$. From the flow
visualization taken at this Reynolds number, it is noted

the peak in the subharmonic amplitude corresponds to the average pairing position, an observation first made by Ho and Huang (1981), in a two dimensional shear layer.

We now return to the nature of the initially large amplitude of the subharmonic mode with respect to its fundamental. Freymuth (1966) showed that when the separated layer of an axisymmetric jet was excited by a low level external sound source, the growth of this instability mode in the initial jet was linearly related to the pressure field at the nozzle lip by

$$\frac{u'}{U_j} = B(St) \frac{p}{\frac{1}{2}\rho U_j^2} \exp(-\alpha_i x) \qquad \text{(VII-1)}$$

where the function B actually describes the receptivity of the separated layer to the imposed pressure field (Morkovin and Paranjape, 1971). It is hypothesized here that the naturally existing near field pressure acts in the same manner.

The initial growth rates for these two modes were determined to be

$$-\alpha_i \theta(f_{i,o}) = 0.092$$

$$-\alpha_i \theta(\tfrac{1}{2} f_{i,o}) = 0.040$$

These two values are nearly identical to those predicted by Monkewitz and Hueere (1981) for a Blasius profile at these frequencies. This result indicates that the initial subharmonic development is due to a linear instability. It is observed that initially

$$\frac{u'(1/2f_{i,o})}{u'(f_{i,o})} = \frac{p'(1/2f_{i,o})}{p'(f_{i,o})}$$

Here the ratio of the pressures was determined from Figure 71. This agrees with the external forcing case of Freymuth (1966) assuming that $B(\frac{1}{2}f_{i,0})/B(f_{i,0})$ is nearly unity, an assumption which is consistent with his results.

These results indicate that for this ultra low disturbance condition, the initial separating layer is receptive to the naturally existing pressure field of the subharmonic mode. Both modes initially develop independently since a linear mechanism is acting. From only the amplitude development though it is not possible to determine the phase relationship between the two waves. This linearity persists until the initial axisymmetric mode reaches a finite amplitude. At this point, denoted x_r/D, it was observed that the subharmonic mode growth rate changed. Referring back to Figure 20, it is observed that at this position the mean velocity profile begins to change substantially. In fact it is not until both modes have attained nearly equal amplitudes by $x/D = 0.8$ does the shape of the profile return to a nearly hyperbolic tangent profile. Clearly, this secondary growth region of the subharmonic mode is associated with a different type of instability mechanism than in the initial region. This secondary region is due to a subharmonic resonance mechanism as presented by

Kelly (1967), as will be detailed later. However this
work cannot completely describe the phenomena since x_r/D
flow visualization indicates that the initial jet has
already rolled up into a finite vortex element. The
effect of this finite size must also be included. Some
information on this effect can be obtained from the work
by Pierrehumbert and Widnall (1981). This secondary
instability is the driving force which leads to the
pairing process.

If the natural pressure field is acting as a small
excitation to the jet, then based on the nature of the
pressure spectrum in Figure 61 one would expect to
observe all of the nonlinearly developing modes growing
exponentially near the nozzle lip and all having
initially larger amplitudes than the initial axisymmetric
mode. The relative amplitude of each mode would then be
determined by the ratio of the magnitude of the pressure
peaks in Figure 61. The near field development of these
modes is shown in Figure 76. The initial behavior is
exactly as expected. The ratio of the initial amplitudes
of any two modes is simply determined by the ratio of the
associated peak values in Figure 61. This is clearly a
self-excited naturally developing jet. Once again, the
initial growth rates of each of these modes are well
predicted by the theory of Monkewitz and Hueere (1981).

Examining Figures 75 and 76 closer, it is observed
that the initial exponential growth of each mode ceases

at the resonant position. This change in instability

behavior is also observed in the growth of the momentum

thickness of the jet in Figure 77. Up to the resonant

position, it was previously pointed out that the initial

momentum thickness changed by 40%. Strong entrainment

into the jet only is observed after the resonant

position. In fact the growth of the jet is linear after

this point except for an additional 25% increase in the

growth rate at the average pairing location. These

results are an indication that simple linear theories

cannot predict this secondary instability even using

quasi-parallel or slowly diverging flow assumptions.

The behavior of these instability modes for this

Reynolds number along $U/U_j = 0.9$ is shown in Figures 78

and 79. These figures should show a consistent behavior

with the previous two figures. The subharmonic mode is

initially higher in amplitude, exhibits exponential

growth to $x/D = 0.3$ where the growth rate increases by

40% and a new region of exponential growth is observed.

In this case, once the amplitude of the subharmonic

reaches a value of 2%, a plateau is formed where the

amplitude remains constant with axial distance. Even

though the magnitude of the initial fundamental mode is

lower in the inner region of the jet than in Figure 76,

the subharmonic growth rate changes when the amplitude of

the subharmonic is 50% that of the fundamental. This was

also observed in Figure 76. The behavior of the

nonlinearly developed modes is shown in Figure 79. Once again the initial exponential growth of these modes is observed up to the resonant position. After this position all of the modes with the exception of the fundamental grow to an equilibrated value of 2% past $x/D = 0.6$.

The previous figures referred to the Reynolds number case where a natural coupling between long wave and short wave instabilities was observed. It is important to determine if the initial behavior of the jet is due to this special operating condition or if it is independent of Reynolds number. Examination of Figure 69 revealed that all of the observed modes scaled at a constant Strouhal number, based on a properly chosen momentum thickness, and was independent of Reynolds number. One may therefore expect the characteristics of the initial jet to also be Reynolds number invariant with respect to the nature of the development, although the initial amplitude levels of the pressure peaks were found to be dependent on Re. This is examined in Figures 80 though 86, where the evolution of these modes have been documented over the Reynolds number range from 34,000 to 80,000.

For each of the cases shown, the relative amplitude of the subharmonic mode with respect to its fundamental is given by the results in Figure 71. Since the nature of this phenomenon is independent of Reynolds number, it

must be naturally occurring. If it is naturally

occurring, why hasn't this phenomenon been reported in

the literature? This question will be answered shortly.

From these figures, the basic behavior of both the

initial axisymmetric mode and its subharmonic mode

emerge. A strong pressure field associated with the

subharmonic mode is radiated back to the nozzle lip.

This pressure field forces the initial jet and this mode

subsequently grows exponentially. The initial amplitude

of the subharmonic is a linear functional of this

pressure field. At the same time, the initial

axisymmetric eigenmode of the jet develops and amplifies

from its original background level amplitude. When this

instability reaches a finite amplitude of approximately

O(1%), the growth rate of the subharmonic changes,

increasing by approximately 40%, and a new exponential

growth region is observed. This change in growth rate is

the emergence of a secondary instability, not associated

with a hyperbolic tangent profile, and is also linear.

The behavior of these modes after this axial position is

much more dependent on the radial position. Along $U/U_j =$

0.6, which is at the peak intensity in the jet shear

layer, a clear pattern emerges. The exponential growth

of the secondary instability of the subharmonic mode

continues until the initial jet instability reaches a

maximum value. This saturation of the initial mode is

associated with the deviation of the exponential growth

of the subharmonic mode. The subharmonic continues growing to a maximum value at the expense of the energy in the initial axisymmetric mode until this mode decays to a minimum value. It is at this position that initial structures are in the process of merging, as observed by the earlier visualization. The subharmonic then decays after the completion of pairing and the initial instability mode gains energy to its final equilibrated position.

Along the radial position $U/U_j = 0.9$, such a discrete behavior is not observed. The exponential growth of the initial mode along with the exponential growth of the subharmonic mode and its secondary instability are all observed. However, the discrete difference between these modes at the pairing position is not observed. Both modes appear to grow to a maximum value and then slowly decay. The subharmonic mode still appears to deviate from exponential growth at the maximum amplitude of the initial axisymmetric instability. In all cases, the subharmonic mode reaches a higher amplitude than its fundamental.

Much of the recent work on instability in two dimensional shear layers considers the evolution of the total energy of a given mode integrated across the shear layer and not the local RMS fluctuations. This integrated quantity is a spatially averaged variable which will indicate the gross features of the

instability. It cannot, however, detect some of the more important details of the instability evolution. For example, the sharp dip in amplitude of the initial axisymmetric mode at the pairing position would be averaged out. This is not to say that the use of the total energy is without merit but rather that it cannot isolate the fine points of the instability process.

The variation of the nonlinearly developed modes also has a consistent Reynolds number behavior. These modes must initially develop past the resonant position. The pressure field associated with these developing modes radiates back to the nozzle lip. This in turn linearly forces the jet and these modes subsequently grow exponentially prior to the resonant position. The amplitude development of these modes changes at the resonant position and the modes continue to grow until all reach equilibrated values.

When the core disturbance is low enough, it was noted that the characteristics of the instability evolution are independent of Reynolds number. The effect of background disturbance levels on these instability characteristics is examined next. The evolution of the initial axisymmetric mode and its subharmonic for test flow condition 2L at Re = 42,000 along $U/U_j = 0.6$ is shown in Figure 87. For this case, the initial subharmonic amplitude is approximately a factor of 5 larger than the amplitude of the initial axisymmetric

eigenmode. This ratio is once again predicted in Figure 71. In this case, as well as with case 1L, there is an initial exponential growth followed by a secondary instability of the subharmonic mode. For case 2L, the subharmonic growth rate also changes slope when $u'(f_{i,0}) = 2u'(\frac{1}{2}f_{i,0})$. The fundamental reaches a peak amplitude in both cases and at this position the growth of the subharmonic mode is no longer exponential. In case 2L, the magnitude of the initial instability mode then decreases but a sharp drop is not observed as in case 1L. The subharmonic amplitude reaches a peak value equal to that of the fundamental. This peak has a much broader axial extent than that of case 1L. This is associated with the randomization of the pairing position as observed in visualization.

When the background disturbance level is increased by usage of test flow condition 3L, a different behavior of the initial instability process is observed in Figure 88. There is no initial growth of the subharmonic mode. From Figure 61, a spectral peak at the subharmonic frequency is evident. However, the background disturbance level in the initial separating boundary layer is large enough so that the shear layer is not receptive to the level of forcing provided by the nozzle lip pressure field. Not until the fundamental has grown to a finite level, where it begins to deviate from exponential growth, does the subharmonic emerge. The behavior past this point is

nearly identical to case 2L. In fact, it is this
behavior which has been documented in the literature both
in axisymmetric jets and also in two dimensional shear
layers. This is a result which is extremely important.
The basic nature of the initial evolution of the
instability modes is highly dependent on the background
disturbance level both in the jet core and also in the
nozzle exit boundary layer. Above a certain disturbance
level, the initial separated layer is not receptive to
the external pressure field at the nozzle lip. It seems
as though many of the experimental facilities which have
been used in the literature are of this high disturbance
level condition. Once the disturbance level is reduced,
as in the present experiment, more details of the
instability process are revealed. Also included in
Figure 88 is the initial amplitude development of the
helical mode. For this flow condition the amplification
is nearly identical to that observed for the initial
axisymmetric mode as was previously discussed in
Chapter V.

Phase Development

Any description of an instability process by its
amplitude development alone is incomplete unless its
phase variation is also considered. The phase
development for each of the modes and case presented in
Figures 75 through 88 was determined. The pressure field

at the nozzle lip was used as a phase reference so that the downstream phase variation of the instability mode could be determined. No attempt was made to correct the absolute value of the reference phase due to the transfer function of the pressure tap measuring system. The initial value of the phase difference between the velocity fluctuations and the nozzle lip pressure field is not important here. It is only the phase differences with respect to this initial value that are relevant. As in the previous set of figures, the low disturbance level condition, case 1L, is first examined at a Reynolds number of 42,000. The phase development for the initial axisymmetric instability and subharmonic modes is shown in Figure 89.

From this figure, the phase difference varies linearly with axial distance for the initial axisymmetric mode. The dashed line passing through the data represents a constant phase speed of 0.5 indicating the non-dispersive nature of this mode. This phase speed is determined using the method presented by Knisely and Rockwell (1980). The normalized phase speed, C_r, is defined by

$$C_r = \frac{f\lambda}{U_j}$$

or

$$C_r = \frac{St}{[d\phi_{up}/d(x/D)]}$$

An initially different behavior is observed for the subharmonic mode. In this case there is an initial region near the nozzle lip where ϕ_{up} is independent of axial position. This region extends up to an axial position of x_L/D. By the resonant position the subharmonic is traveling at the same phase speed as its fundamental. This is a necessary condition for the definition of a resonant mechanism and also allows for efficient energy transfer from the fundamental wave to the subharmonic.

From the initial amplitude development of the subharmonic mode, it was determined that this was a linear instability. If this was a simple linear instability, the phase speed of this mode should have a value of 0.81 as predicted by Monkewitz and Hueere (1981). Upon examination of the phase variation, this is not observed. Instead, a constant phase is initially observed and then the wave becomes non-dispersive. This clearly is not indicative of a simple linear mechanism. This behavior can be due to one or two effects. First, there may be a region near the nozzle lip where the pressure field interacts with the trailing edge of the nozzle. If this is the mechanism, then this region of lip influence should scale with the Strouhal frequency of the instability mode. If the data does not scale in this manner, then this constant phase may be due to probe interference.

The downstream phase variation of the nonlinearly developed modes for the same conditions is shown in Figure 90. Again, each mode is characterized by a region near the nozzle lip where the phase is constant. Upon examination of these two figures, one finds that this position, x_I/D, is frequency dependent, moving downstream at lower frequencies. This lends support to the first speculation above. The scaling of this will be further examined once all of the phase data have been presented. It is interesting to note that the difference mode has a phase speed of 0.6 past the nozzle lip influence region. What is surprising is that for this low frequency mode, the nozzle lip influence region extends beyond the resonant position. Clearly, there is an interaction between the radiated pressure field and the nozzle lip.

The phase variation for case 1L over the Reynolds number range from 34,000 to 60,000 is shown in Figures 91 through 95. In each case, the fundamental mode has a phase speed of approximately 0.5. The subharmonic mode along with the other modes have an initial region where the phase is constant before becoming a traveling wave. The subharmonic mode in all cases becomes non-dispersive near or at the resonant position.

Once the Reynolds number is increased to 80,000, an interesting phenomenon occurs. The character of the phase variation of the subharmonic mode changes. This is shown in Figures 96 and 97. Initially there is a small

region near the nozzle lip where the phase is constant, $x < x_L$. Past it, the subharmonic has a phase speed of 0.81. This is the phase speed that Monkewitz and Hueere (1981) predicted. At an x/D value of 0.16, the phase speed suddenly changes to a non-dispersive wave speed of 0.5. In this case, this change occurs exactly at the position where the amplitude growth rate changes slope. The change between primary to secondary instabilities for the subharmonic modes takes place over a very small distance.

From these phase measurements, the variation of the initial axisymmetric wavelength was determined. The downstream phase variation was first fit to a linear function. From this, the wavelength was determined from the calculated slope. These results are shown in Figure 98. This figure shows that the initial axisymmetric wave length varies inversely proportional to the square root of Reynolds number as predicted by linear theory. These results give an indication of the accuracy of this method for determining the downstream phase variation.

From the previous figures showing the downstream phase development, every mode was observed to have a finite region near the nozzle where the phase difference was constant. When this region is plotted versus the Strouhal frequency of the instability mode based on the jet diameter, for all cases between Reynolds numbers 34,000 and 80,000, the behavior in Figure 99 is obtained.

The data taken over this wide range of conditions collapse to a single curve. This nozzle lip region is found to be an exponentially decreasing function of the mode Strouhal frequency. These results are somewhat consistent with the results discussed by Crighton (1981) in his review paper showing that there is a region near the nozzle lip which is affected by the requirements of the Kutta condition. They also show that this region decreases with increasing frequency.

Having examined the characteristics of case 1L, the effect of changing the flow condition on the downstream phase variation is observed in Figures 100 and 101. The phase variation in Figure 100, which corresponds to test flow condition 2L, shows only minimal differences from that exhibited in Figure 89 for case 1L. The subharmonic behavior is quite similar. There is an initial region where the phase is constant. Between this region and the position of the subharmonic resonance, the phase velocity appears to be different than 0.5 and closer to the value of 0.81 previously observed in the case 1L at Re = 80,000 data. The accuracy of the phase variation within this region is not sufficient to determine an accurate phase speed. At the resonant position, however, there is little doubt that the wave has a phase speed of 0.5, matching that of the fundamental.

The phase variation for case 3L is shown in Figure 101. Both the initial axisymmetric and helical modes

have nearly identical phase speeds of 0.5. As was previously discussed, no peaks were observed in the velocity spectrum for the subharmonic mode until the fundamental reached a finite amplitude. This is further reflected in this figure by a lack of non-random phase information in the subharmonic mode until a streamwise distance where the initial axisymmetric mode reaches a finite amplitude. After this point the subharmonic wave travels at a phase speed nearly equal to that of its fundamental.

Relationship to Near-Field Pressure

The characteristics of the initial instability evolution have just been examined. The relationship between these characteristics and the near-field pressure is now investigated through the coherence function, Γ_{up}, between the velocity fluctuations in the initial jet and the pressure field outside the nozzle lip at the same relative azimuthal angle. The axial variation of the coherence for case 1L at Re = 42,000 is first examined in Figures 102 through 105 for a radial positions of U/U_j = 0.9.

The variation of the initial axisymmetric instability mode is considered first in Figure 102. For both positions in the jet, the coherence initially has a value of approximately 0.4. This initial value remains nearly constant until an axial distance of about 0.6,

where pairing was observed in the flow visualization, and then gradually decays. This behavior is quite different from that observed for the subharmonic mode which is shown in Figure 103. Similar trends are observed at both radial positions. Initially, a high coherence of 0.6 is measured up to an axial position of 0.2D. The region of this constant coherence corresponds to the region of nozzle lip influence. Once this region is past, the coherence drops and reaches a minimum value of 0.3. This minimum value occurs at the resonant position. Associated with the growth of the subharmonic secondary instability is an increase in the level of coherence. The coherence increases and reaches a maximum value at the axial location where the peak subharmonic amplitude was observed. From this point on, the coherence gradually decays.

This result indicates that the subharmonic pressure field is generated during the growth and decay of the subharmonic secondary instability with its strength being a function of its velocity amplitude. It is over this same region that the pairing activity is observed. However, this pressure field is associated with the growth and decay of an instability mode and not due to the pairing as previously believed by Laufer (1981). This pressure field propogates away from this region with the speed of sound and is felt back at the nozzle exit. The pressure field acts as an external excitation to the

jet and a subharmonic mode emerges at the nozzle lip and grows exponentially. Since the pressure field and the growing velocity field are related by a linear functional, the initial coherence is high and remains at that level throughout the region where the pressure field interacts with the nozzle. After this point the coherence drops. This drop in coherence will be discussed once the azimuthal variations have been presented in the next chapter. The coherence variation of the nonlinearly developing modes is described in Figures 104 and 105. The interactive mode between the subharmonic and difference mode is first examined in Figure 104. As in the previous figure, the coherence initially has a constant value throughout the nozzle lip influence region. Beyond this region, the coherence decays. The behavior of the difference mode, shown in Figure 105, is substantially different from the modes just described. In this case, the peak coherence along $U/U_j = 0.6$ occurs where the amplitude of initial axisymmetric mode attains a minimum value as shown in Figure 75. This is also the position where the amplitude of the difference mode, Figure 76, reaches its maximum value. Along $U/U_j = 0.9$ the difference mode first reaches its maximum amplitude farther downstream than along $U/U_j = 0.6$ as indicated in Figure 78. This position is consistent with the location of the peak in the coherence.

The Reynolds number behavior was examined next for Case 1L. Results corresponding to Reynolds numbers of 52,000 and 60,000 are presented in Figures 106 through 109. These figures show that the coherence development associated with all of the observed modes is essentially independent of Reynolds number when viewed in terms of the position of the nozzle lip influence region, the resonant position and the peak energy in the associated mode.

The behavior of the coherence for the initial and subharmonic modes for Re = 80,000 is shown in Figures 110 and 111, respectively. Initially, a very high coherence exists for the initial instability mode. In fact, as Re increase the coherence of this mode increases. This is due to the increased vorticity in the initially separated layer which leads to a stronger pressure field at the nozzle lip. Beside the initially higher coherence, the behavior of this mode is independent of Reynolds number. The evolution is quite different from the previous subharmonic evolutions in that the sharp drop in coherence is not observed at the resonant position. A small drop in coherence at this point is observed along $U/U_j = 0.9$ but is not as drastic of an effect as before. From the phase speed measurements it was noted that after the nozzle lip influence region the subharmonic wave behaved both in amplitude and phase speed as a linear eigenmode. It is unclear if the change in the behavior

of the coherence in this region is due to this observed difference.

Finally, the effect of background disturbance level on the coherence variation is examined in Figures 112 through 114 at a Reynolds number of 42,000. When Case 2L is compared to Case 1L, the variation of the coherence for the initial axisymmetric instability is nearly identical. The basic shape of the coherence variation for the subharmonic mode is also identical to that of Case 1L along $U/U_j = 0.6$. The difference lies in the magnitude of the coherence. Case 2L is characterized by higher background disturbances which reduces the magnitude of the initial coherence from 0.6 in case 1L to 0.3 in case 2L. This drop in coherence is simply due to the effect of extraneous background noise at this frequency as described in Appendix B. The subharmonic secondary instability occurs at the resonant position and a high degree of coherence with the pressure field at the nozzle lip is still observed. The shape of the coherence variation for the nonlinearly developing modes is described in Figure 113. The basic nature of this variation is consistent with the previous results. The behavior of the initial region however is not as clear because of the initial background disturbance level.

The results for case 3L are displayed in Figure 114. Due to the much higher level of background disturbances there is no coherence between the pressure field and any

velocity fluctuations in the initial jet shear layer. A
strong coherence in the subharmonic mode appears when the
subharmonic resonance begins. This resonant or secondary
instability is still highly coherent with the near field
pressure. In fact a subharmonic peak in the pressure
spectrum was observed in Figure 61 for this case. The
zero coherence prior to the resonant position is
certainly due to the high background noise for this case.
The question which cannot be answered yet is whether the
shear layer is receptive to this pressure field initially
so that a low amplitude wave would grow spatially and
have a coherent phase relation to the nozzle lip. The
amplitude of this mode would be buried in the background
noise so that a simple velocity spectrum could not reveal
it. If the answer to this question is yes then a closed
feedback loop exists for the entire subharmonic
evolution, including the phase information. If the
answer to the question is no, then in general there is no
feedback loop, and the observed feedback loop for cases
1L and 2L is only a result of the ultra low disturbance
levels. This subject is discussed further in Chapter XI.

CHAPTER VIII

AZIMUTHAL DEPENDENCE OF
INITIAL JET INSTABILITIES

In Chapter V, information on the azimuthal phase variation was required to identify the initial axisymmetric and helical modes. Once the nature of these modes was known, all of the observed peaks in the near field pressure spectrum and also in the velocity spectrum were identified. The axial development of these modes was subsequently examined in Chapter VII. A complete discussion of these modes would be incomplete though without also describing their azimuthal dependence in detail.

The measurement techniques were discussed in Chapter II. At every axial location, the hot-wire was placed at a radial position such that the local mean velocity was 90% of the core velocity. Phase and coherence measurements were then made between this signal and the pressure field at the nozzle. The azimuthal dependence was obtained by varying the relative angle between the pressure tap and the velocity sensor. A consistency check on this data was obtained by repositioning the velocity sensor at a different azimuthal angle and once again checking the azimuthal variations in both the phase and coherence. The measurements presented in this chapter were found to be dependent on only the relative separation angle between the velocity sensor and the

pressure port. The uncertainty in the measured values of the coherence appeared to be approximately 0.07.

The results for test flow condition 1L are presented first for a Reynolds number of 42,000. After discussing these results, the Reynolds number dependence is examined. Finally, selected cases from flow conditions 2L and 3L are presented and compared to those of flow condition 1L.

The downstream behavior of Case 1L at a Reynolds number of 42,000 is shown in Figures 115 through 120. The azimuthal variation of the coherence and normalized phase difference for the initial axisymmetric mode is shown in Figures 115 and 116 respectively. The axial locations listed are representative of different regions of amplitude behavior as indicated in Figure 75 through 79. At $x/D = 0.2$ both the subharmonic and fundamental have nearly equal amplitudes. By $x/D = 0.4$, the secondary instability of the subharmonic mode has developed and the growth of the fundamental mode is non exponential. The peak intensity in the subharmonic mode was observed at $x/D = 0.6$ along with a local minimum in the initial axisymmetric mode. The pairing process is fully completed by $x/D = 0.8$ and near $x/D = 1$ the flow is approaching self similarity.

The azimuthal variation of the coherence for the initial axisymmetric mode is examined in Figure 115. Within the experimental uncertainty, the coherence is

initially independent of azimuthal angle. With

increasing axial distance the level of the coherence

drops but still remains nearly constant around the jet.

The phase variation for this case is illustrated in

Figure 116. Within the initial exponential growth region

there is a nearly zero phase shift around the jet. This

indicates the axisymmetry of the initially developing

mode. This axisymmetry is observed to persist even when

the secondary instability of the subharmonic mode is

growing. Near and after the pairing process location,

the axisymmetry of the mode is lost. Over this region

the maximum averaged phase difference is observed to be

near 90 degrees.

The behavior of the subharmonic mode is displayed in

Figures 117 and 118. The coherence, shown in Figure 117,

is initially uniform around the jet in the initial

exponential growth region of this mode. This indicates

that the early spectral development of the subharmonic

mode is independent of azimuthal angle. In the region

where the subharmonic resonance has begun, the coherence

at a relative separation angle of 0 degrees is a minimum,

agreeing with the results of Figure 103. As the

separation angle is increased, the coherence increases to

a maximum value when the pressure port and velocity

sensor are on diametrically opposite sides of the jet.

This result was independent of initial azimuthal angle of

the velocity sensor. The nature of this behavior will be

examined when all of the subharmonic data has been presented. At the axial location of the peak intensity of the subharmonic mode and also farther downstream, the nature of the coherence distribution changes. Maximum coherence is observed at a relative separation angle of zero degrees. The coherence decreases with increasing separation angle and it has a minimum value at a separation angle of 180 degrees. This behavior is not surprising. Over this region there is an increase in the background disturbance level. Once the separation angle is increased, the uncorrelated background disturbance adds more noise to the system and hence the coherence drops. Minimum coherence is observed at the maximum separation angle. The phase variation of this mode is shown in Figure 118. This mode initially develops axisymmetrically and continues to remain axisymmetric even at one diameter downstream. It is clear that the subharmonic resonance is an axisymmetric mode. What is surprising is that even after the pairing has occurred and the mean shear region becomes transitional, the axisymmetry of the subharmonic mode persists.

The dependence for two of the nonlinearly developing modes is considered next in Figures 119 and 120. In these figures, the difference mode arising from interaction between the initial axisymmetric and helical modes and with the mode developed through the interaction between the subharmonic mode and the aforementioned

difference mode are examined. The coherence for the
difference mode remains independent of separation angle
up to the location of the peak subharmonic intensity.
After this region, the coherence decays with increasing
separation angle for the same reasons as those for the
subharmonic mode. For the subharmonic difference mode
the coherence is constant around the jet in the region
before the peak subharmonic intensity. More information
about these modes is revealed in the phase measurements,
presented in Figure 120.

The difference mode is considered first. At x/D =
0.2, which is in the initial exponential growth region of
this mode, the phase measurements indicate that this mode
is nearly axisymmetric. This is due to the dominance of
the initial axisymmetric mode for this low disturbance
level condition. The downstream variation along with the
variation for the subharmonic difference mode is not as
clear. If a mode is strictly axisymmetric, helical or
some other higher mode, its azimuthal wave number is
clearly defined. When axisymmetric and non axisymmetric
modes interact nonlinearly, the azimuthal wave number may
switch back and forth between modes. If this type of
switch over is occurring, then the averaged phase
measurements are not a clear indication of the azimuthal
development.

The effect of Reynolds number on this development is
shown in Figures 121 through 134. This is first examined

for the initial axisymmetric mode. The coherence
measurements for this case are shown in Figures 115, 121,
and 129. Below Reynolds numbers of 52,000, the exit
boundary layer was observed to have a nearly constant
maximum fluctuation level of 1%. Over this same range,
the downstream behavior of the azimuthal variation of the
coherence for the initial axisymmetric mode is the same.
When the Reynolds number is increased to 60,000, the peak
intensity in the exit boundary layer is approximately 3%.
This increase in the background disturbance level is
reflected in the coherence variation in Figure 129. The
reader is referred to Appendix B for additional
discussion on the coherence function. Similar
observations are made with respect to the phase
measurements in Figures 116, 122 and 130. Below Re =
52,000 the initial axisymmetry of the mode is reflected
by the measurements. At Re = 60,000 this is not readily
apparent. However, over the region of high deviation
from axisymmetry, the value of the coherence drops to
near zero levels. As the coherence drops, the phase
measurements become less accurate.

Over this same Reynolds number range, the azimuthal
development of the subharmonic mode is invariant. For
all axial positions the strong axisymmetry of the mode is
clearly evident. This is observed in Figures 117, 118,
123, 124, 131 and 132. The axisymmetry of this mode is
indicative of the axisymmetry of $f_{i,0}$. The large phase

variation of this mode is due to the lack of correlation rather than actual phenomena. Upon examination of the nonlinearly developed modes in Figures 119, 120, 125, 126, 127, 128, 133 and 134, no unusual behavior is detected as a result of increasing the Reynolds number.

These results show that the azimuthal behavior of these modes, for a given region in its amplitude development, is independent of Reynolds number. Since the phase and coherence are being measured under natural conditions, the increase in background disturbance level in the exiting boundary layer, due to an associated increase in the Reynolds number, can severely reduce the signal to noise ratio. Increasing the noise decreases the measured coherence, see Appendix B. In Chapter VI, it was carefully shown that the scaling of these modes was Reynolds number invariant. One would also expect their development to be similar. This was already hinted at in Chapter VII and this was also shown here in cases were an increase in the natural disturbance level did not contaminate the results.

Azimuthal phase measurements were presented in Figure 46 at one streamwise location for case 3L for a Reynolds number of 42,000 to illustrate the initial existence of both axisymmetric and helical modes. More information about these modes are now presented. The azimuthal variation for the coherence for this same condition is shown in Figure 135. The initial

axisymmetric mode is characterized by a constant value of coherence which is independent of separation angle. The behavior for the helical mode is also shown. A local minimum is observed at a 90° separation angle. This behavior was established for any absolute angle the velocity sensor was at as long as the separation angle was at 90 degrees with respect to the pressure port. The downstream development of the coherence for these modes is shown in Figure 136. Up to an axial distance of 0.6D the coherence for the axisymmetric mode is independent of the relative azimuthal separation angle. At this streamwise location, the maximum amplitude of this mode was observed in Figure 88. Once this mode starts to decay, the coherence is no longer a constant value and smooth variation is observed. The form of the coherence for the helical mode at these downstream positions indicates a similar behavior to that observed in the previous figure. By x/D = 0.75, the coherence at zero degree separation angle has dropped sufficiently but the same basic shape is still maintained. The phase variation of these modes for the same downstream locations are shown in Figure 137. Irrespective of what downstream location was examined, both the axisymmetric mode and the helical mode remain clearly identifiable.

The variation of the coherence for the subharmonic mode for cases 2L and 3L are displayed in Figure 138. These results show the effect of increased background

disturbance levels on the coherence distribution. This is due in part to the randomization which was observed in the pressure field with increasing disturbance levels in Figure 61. The near field pressure does not remain as coherent as in the ultra low disturbance level cases.

CHAPTER IX

SIGNATURE OF INSTABILITIES ON JET CENTERLINE

In the previous chapters the axial and azimuthal development of the various instability modes were examined along two positions in the mean shear region of the jet. In an initial cursory examination of the axial dependence, presented in Chapter V, it was observed that the development of these instability modes is strongly imprinted on the jet centerline. In fact, past an axial distance of one diameter, these modes could only be tracked in the core region because the velocity fluctuations, due to the transitioning flow in the mean shear region, masked those of the instability modes. The signature of these modes on the jet centerline is examined in this chapter along the entire core region. The dependence of the evolution of these modes on the initial flow conditions is also examined.

The axial variation of the coherence between the streamwise velocity fluctuations on the jet centerline and the near field pressure for case 1L at a Reynolds number of 42,000 is first shown in Figure 139. The coherence for the observed modes grows and then decays in a manner similar to that observed for their amplitude development. The weakest coherence is associated with the initial axisymmetric eigenmode. The coherence of this mode peaks at $x/D = 0.4$ before decaying. This axial

position corresponds to the position of the peak
intensity of the mode as was observed in the mean shear
region in Figures 75 and 78. The subharmonic mode
initially exhibits a high coherence near the nozzle lip.
This coherence grows to a peak value in the subharmonic
resonant region where maximum energy was observed in the
subharmonic mode. After this point the subharmonic
coherence gradually decays. The nonlinearly arising
difference mode develops a peak coherence near the same
position. The coherence of this mode decays at a much
slower rate. It is quite surprising that even after four
diameters, a strong coherence exists between the velocity
field here and the near field pressure. It is quite
clear that the pressure field at the nozzle lip for all
of the modes is associated with the vorticity development
throughout the entire axial region bounded by the
potential core. This pressure field is not generated
within a localized region. The notion that only the
pairing process produces a pressure signal which is then
radiated back to the nozzle lip is simply not consistent
with the coherence behavior of the observed modes.

A similar behavior is observed for a slightly higher
Reynolds number of 52,000 as is shown in Figure 140. In
addition to the observed modes which scale with the jet
momentum thickness, the coherence variation for the
potential-core final Strouhal mode is also established.
It is observed that this mode has a coherence of about

0.2 from 1 to 4 diameters downstream. The influence of this mode at the nozzle lip has been speculated about in the literature for quite sometime. It is shown here that the velocity fluctuations of this mode over the entire core are correlated to the near field pressure. This once again indicates that the peak in the near field pressure spectrum is due to the spatial vorticity evolution of its associated mode. The spatial growth for a few of the observed modes in this case is shown in Figure 141. Here the amplitude development is dominated by the low frequency nonlinearly developing modes.

The axial variation of the coherence for various modes for test flow condition 2L at a Reynolds number of 42,000 is shown in Figure 142. Comparing the nature of this with the results for test flow condition 1L, presented in Figures 139 and 140, one finds no substantial differences. This was expected based on the results of Chapter VII where similar conclusions were drawn. The amplitude development of the lower frequency modes for this case is shown in Figure 143. Each of these modes initially grows nearly exponentially. The non-exponential behavior is probably due to non parallel aspects of the flow over this region. As in the previous cases, the subharmonic amplitude reaches a peak value at the same axial position as was observed in Figure 87. This position is where the maximum amplitude was observed in the mean shear region. The nonlinearly developed

modes continue growing until a value of x/D of about 1.5 diameters. After this position the amplitude of these modes grows at a much slower rate. Near the same axial position of 1.5 diameters, Figures 28 and 32 show that the mean and turbulence intensity profiles across the jet shear region have attained self similarity. This may be related to the change in the observed instability behavior. At this point though it is unclear what mechanisms are involved.

The centerline characteristics are next examined for test flow condition 3L. These results are shown in Figure 144. Included in this figure are the initial axisymmetric mode, its subharmonic and the core final Strouhal frequency. Upon examination of the downstream variation of the coherence along with Figures 140 and 142, one notes no differences are found in the nature of development between the three test flow conditions. The only effect that the introduction of background disturbance level has on the centerline characteristics is to reduce the overall level of the measured coherence. This effect is discussed in more detail in Appendix B.

In Figures 140 and 144 the potential-core final Strouhal mode was found to be correlated to the near field pressure along the entire axial extent of the potential core. The emergence of this mode was most clearly noted in the ultra low disturbance level condition of flow 1L. The centerline amplitude

development of this mode for this case at Re = 42,000 is shown in Figure 145. Also included in this figure are the results of Crighton and Gaster (1976) who calculated the centerline spatial amplification rates for an axisymmetric disturbance in a slowly diverging jet flow. Excellent agreement is observed within the first 2.5 diameters even though the measured divergence rate is approximately 25% greater than that used in the theoretical predictions. As the divergence rate increases, the local amplification rate should decrease. This is probably part of the discrepancy between predictions and the measurements beyond 2.5 diameters. This result seems to indicate that over the region of agreement, the amplification should also be obtainable using locally parallel flow assumptions.

CHAPTER X

INSTABILITY EVOLUTION OF INITIAL JET
UNDER EXTERNAL FORCING

The natural evolution of an axisymmetric jet has
been presented in details in the previous chapters. In
this chapter, some of the characteristics of the initial
jet are examined under external forcing. In recent work
by Ho and Huang (1981), they report that the response
frequency of a two dimensional shear layer is not
necessarily that of the excitation input. Steps were
observed in the response frequency which corresponded to
merging of two and three vortices at a time. This type
behavior is not indicative of a linear response of the
forced eigenmode. A similar behavior was found in
Appendix A when the background room disturbance level was
high and forcing was applied. Unlike this behavior, this
chapter deals with pure tone low level forcing for the
various test flow conditions so that the initial response
is linear. Local growth rates and phase speeds are then
determined for the various test conditions and compared
to linear spatial theories.

Documentation of Forcing Conditions

The jet was forced through excitation from a
loudspeaker positioned 2m away from the jet at an angle
of 60 degrees with respect to the jet centerline. A
pressure tap in the nozzle face at $\gamma = 0°$ was used to

monitor this excitation field while a single hot-wire probe was used to measure the streamwise growth of the disturbance in the shear layer at the same relative azimuthal angle. From visualization results and azimuthal investigations of the initially developing flow, the forced disturbance field was axisymmetric. The sensitivity to the forcing occured at the separation line of the jet nozzle through its receptivity to the far field of the loudspeaker. This mechanism assured the axisymmetry of the forced initial instability.

The typical response of the shear layer with external excitation is shown in Figure 146. In this case, the response frequency of the initial jet is plotted versus the forcing frequency. Both variables are then normalized by the frequency of the naturally developing axisymmetric eigenmode. The case shown is for test flow condition 1L at two different Reynolds numbers. Identical behavior is observed in all other test flow conditions having laminar exit boundary layers. In each case, the response frequency of the shear layer is identical to the forcing frequency. For any case tested, the shear layer could only be excited 2.4 times the initial natural axisymmetric eigen-frequency. This value was approximately 25% below the frequency of the neutral mode.

In all of the measurements, the amplitude of the disturbance pressure field was carefully adjusted so that

a unity coherence was obtained between the near field pressure and the velocity fluctuations of the disturbance in the near jet region. This ensured that the forced response of the initial jet was linear. However, unity coherence could not be obtained for forcing frequencies above approximately $2f_{i,0}$. This meant that at high forcing frequencies the pressure field did not induce a linear response of the jet. The effect of this on the growth characteristics of the mode will be discussed shortly.

Typical flow visualization results for test flow condition 1L are shown in Figures 147 and 148. The effect of the Strouhal forcing frequency on the initial jet development is illustrated in Figure 147. Photograph (a) shows the typical development of the jet under natural conditions. When a pressure field at the initial axisymmetric eigen-frequency is applied, (c), the initial development becomes much more organized as expected. The axisymmetry of the disturbance field is also observed in the initial jet structures. When forced at the subharmonic mode frequency, the initial development is described by Figure 147(b). Photograph (d) illustrates the development of the jet when the forcing frequency is 2.3 times the natural axisymmetric eigen-frequency. It is in this region of excitation frequency that a non unity coherence was observed.

The entrainment into the jet under these excitation

conditions is depicted in Figure 148. The excitation

causes an initial axisymmetric perturbation which

subsequently grows to a finite level and rolls up.

Induction by these large structures entrains the

surrounding air into the jet. Similar observations were

also made in cases 2L and 3L. Visualization of this type

of behavior was carried out by Bouchard (1981) in a water

jet. Results of his work also point out the importance

of the initial large structures and their forcing

frequency in the initial entrainment into the jet.

Measurements of the mean velocity profiles across

the jet at different axial positions were shown in

Figures 18 and 19 for all test flow conditions with

laminar exit boundary layers. Also plotted on these

figures were the hyperbolic tangent velocity profile and

a two dimensional shear layer profile assuming a Blasius

boundary layer at the separation point or exit. The

results are inconclusive as to which velocity profile the

data reflects. The main difference in the velocity

profiles from a stability point of view is the maximum

slope the profile attains. The difference in slope

changes the initial vorticity distribution across the

layer. This small difference, as Monkewitz and Huerre

(1981) point out, leads to changes in the maximum

amplification rate of approximately 20%. The region of

maximum slope corresponds to the region of the data that

is least accurate due to the resolution limitations of

the traversing mechanism.

For a number of streamwise locations, the mean velocity profiles were fit to a hyperbolic tangent profile. The average error in curve fitting this profile was denoted σ. The variation of this error, normalized by twice the momentum thickness, with axial position was shown in Figure 20 for all three test flow conditions at Reynolds number of 42,000 without external forcing. Independent of flow condition, the initial mean velocity profiles fit the hyperbolic tangent functions with the same accuracy up to $x/D = 0.3$, where a strong deviation began to appear. For this reason, the measurements at this value of Re were limited to axial positions less than 0.3D. In fact, when excitation frequencies less than $2f_{i,0}$ were applied, a unity coherence was observed throughout this region.

The amplitude and phase development for case 1L at Re = 42,000 for different forcing frequencies is described in Figures 149 and 150. The phase measurements were carried out in the same manner as those described in Chapter VII. Regions of exponential growth of the amplitude are clearly evident in Figure 149 for all modes with the exception of the mode having a Strouhal frequency of 0.03. This mode is in the region where unity coherence was not observed. This lack of linearity is quite evident from the amplitude development of the mode. A simple model for the behavior at high

frequencies was proposed by Bechert (1974). Here the upstream travelling disturbance field interacts with the downstream developing instability wave. The amplitude behavior of this high frequency mode agrees with his model. In this respect, the coherence function properly predicts when this type of instability process is truly linear. Growth rates of the modes were calculated both locally and by a linear regression over the exponential growth region. From the phase variations with downstream distance, the average phase speed was also calculated locally and over the entire region using the method described in Chapter VII. All of these results were normalized with the momentum thickness at the axial position where the first peak in the velocity spectrum of the initial axisymmetric instability frequency was observed. The reasons behind choosing this particular parameter were given in Chapter VI.

Comparison to Theoretical Results

From the results of Figure 17 it is observed that over the region of measurements the divergence of the jet, $d\theta/dx$, is 1.7%. Because of the nearly parallel nature of the flow in this region, it is not surprising that the growth of the disturbances is exponential over the entire region as indicated in Figure 149. This fact is also borne out in the observation of a constant phase speed over the same region as shown in Figure 150. As long as

the measured coherence had a unity value, it was observed
that the locally calculated growth rates and phase speeds
were nearly indentical to those obtained using a least
squares technique to fit the data over the entire
measuring range.

These results along with the results obtained in the
initial exponential region of the naturally developing
jet are summarized in Figures 151 through 155. The
calculated amplification rates for case 1L are shown in
Figure 151. Included in this figure is the amplification
curve determined by Michalke (1971) for an axisymmetric
jet having a hyperbolic tangent profile. In addition,
the amplification curve presented by Monkewitz and Huerre
(1981) for a two dimensional shear layer is shown. The
data for both natural and excited conditions follow the
results of latter authors' work quite well. Even though
their analysis is for a strictly two dimensional case,
the previous results of Michalke (1971) indicate that for
a jet with initially thin boundary layers there is no
difference in the amplification rates from that obtained
for a two dimensional shear layer. The difference
between the axisymmetric and plane cases however should
be evident in the phase speed of the mode, particularly
at low frequencies.

This result is shown in Figure 152. In this case
the phase speed clearly follows the trend of Michalke's
(1971) analysis for the jet. At low frequencies, ultra

fast waves are observed just as in the case of Bechert and Pfizenmaier (1975) and predicted by Michalke (1971). These results indicate that the developing instability is a jet instability and viewing the initial shear layer as locally two dimensional because of an initially thin boundary layer assumption is not completely correct.

The results for cases 2L and 3L are shown in Figures 153 through 155. These results are consistent with the previous case. They once again show that the disturbance levels introduced by changing the flow conditions are sufficiently low so that a linear mechanism still dominates.

A summary of all of the amplification rates for all of the cases is shown in Figure 156 along with the data of Freymuth (1966). Remarkable agreement is observed between all of the indicated data and the theory of Monkewitz and Huerre (1981). It is expected that this comparison is valid only for initially thin boundary layers. As the thickness increases, the deviation from their theory should increase. These results are however, encouraging. To obtain maximum quantitative information from these locally parallel theories, the results of Michalke's (1971) paper should be recomputed using an axisymmetric version of the Monkewitz and Huerre (1981) profile. It is also clear that the non-parallel effects over the measuring region are of second order, i.e., in the very near region of the jet.

CHAPTER XI

DISCUSSION

In the previous chapters a number of different aspects concerning the natural development of turbulent jets have been examined. This investigation, for the most part, concerned itself with the initial region of the jet, extending to approximately five diameters downstream. The effects of Reynolds number and initial conditions on the mean development of the jet and also on the characteristics of the developing instability modes were established. The purpose of this chapter is to summarize the above results so that a complete picture of the dynamic development of the jet is presented..

Axisymmetric, Helical and Subharmonic Resonance Instabilities and Their Interaction

The instability mechanisms, which were observed to develop in a turbulent jet, were found to be dependent on the initial state of the boundary layer. Cases for which the exit boundary layer was laminar and initially thin are discussed first. For the sake of this discussion, a boundary layer is assumed to be thin when $D/2\theta > 50$. From a careful mapping of the azimuthal phase variation of the observed spectral peaks in the initial region of the jet, it was determined that the jet is initially unstable to both axisymmetric and helical modes. The helical mode was observed to occur at a frequency 20%

higher than that of the initial axisymmetric mode. The initial instability of the jet alternates between these two modes. The percentage of time that the jet initially exhibited either m=0 or m=1 behavior strongly depended on the initial disturbance characteristics in the exit boundary layer.

When the disturbance level in the exit boundary layer was on the order of 1%, the initial jet was dominated by the axisymmetric mode. As this disturbance level was increased, either by increasing the Reynolds number or by artificially introducing varying levels of background turbulence at a constant Reynolds number, the percentage of time the helical mode was observed also increased. At the highest disturbance level conditions, the probability of finding either mode was approximately 0.5. This perhaps is an asymptotic limit for laminar exit boundary layers. This behavior was also observed in the one dimensional velocity spectrum in the mean shear region of the jet. For initial disturbance levels of about 5%, the nearly equal amplitude development of both modes was documented. Corresponding to a decrease in the percentage of time the m=1 mode was observed, due to a decrease in disturbance level, there was a decrease in the magnitude of this peak in the time averaged velocity spectrum. At very low disturbance levels, only coherence measurements between the near-field pressure and the velocity fluctuation in the mean shear region could

identify the initial helical mode.

Due to the influence of the background disturbance level on the initial mode selection, experiments carried out in some of the cleaner test facilities that exist would not be able to identify the helical mode unless one is specifically looking for it by utilizing multiple channel techniques in the frequency domain. The observation of the dual nature of the initial jet instability was unknowingly detected by Husain and Hussain (1980). These experiments were carried out at a high Reynolds number and the initial disturbance level in the exit laminar boundary layer was 3%. The dual nature of the spectral peaks separated by 20% are clearly observed. Some of their results were correctly described in terms of probe interference effects. However, even when taking this into account, the side band peak they observed is at the proper frequency of the helical mode as determined by the present investigation. Even the magnitude of this peak compared to the axisymmetric mode agrees with the ratio found here for a similar exit core intensity case.

The present results also agree with the predictions of Michalke (1971) and of Mattingly and Chang (1974). Both papers described the nearly equal sensitivity of the jet to axisymmetric and helical modes initially. It was only in the work of the latter authors that the difference in the most amplified frequencies of these

modes is described. This was due to a slightly different mean velocity profile compared to Michalke's (1971).

Before considering the possible interactions of these modes, the development of the jet from an initial axisymmetric state is considered. The initial axisymmetric mode grows exponentially until a finite amplitude of approximately 1% of the jet velocity is reached. The reason for the observed exponential growth, even though the jet is non-parallel in this region, is discussed in a later section of this chapter. A subharmonic resonance mechanism, as proposed by Kelly (1967), then takes place and the growth of this new subharmonic instability leads to the pairing process. The concept that pairing is a result of a subharmonic resonance mechanism was pointed out by Ho and Huang (1981). The growth of this subharmonic mode reaches a maximum value at the pairing location, and this amplitude is larger than the value for the initial axisymmetric mode. It was also shown that at the resonant position both the fundamental and subharmonic waves have the same phase speed of 0.5 the jet velocity, a necessary requirement for a resonance mechanism. In addition to the equal phase speeds, the fundamental and subharmonic modes must be out of phase for the pairing to occur, as demonstrated by Riley and Metcalfe (1980).

An attempt to illustrate the out of phase nature of the modes during resonance is shown in the conditioned

visualization of Figures 157 and 158. In both cases the conditioning probe is located just downstream of the resonant position. The photographs in Figure 157 were triggered on the fundamental mode. The structures just downstream of the initial roll up of the jet have approached each other and are just beginning to pair. If one examines the visualization for the subharmonic mode trigger in Figure 158, the same structures have already merged. These results are consistent for all three cases. Since the visualization was taken at the same relative phase of zero degrees for each mode, this shows that the two modes are indeed out of phase during resonance.

In addition to the subharmonic resonance, another set of instabilities was observed. The initial axisymmetric and helical modes, which originally developed through a linear instability, interact nonlinearly. This nonlinearity is depicted in the generation of sum and difference modes along with higher order modes. The modes which were generated through this interaction agreed with those observed by Miksad (1973) in a forced two-dimensional shear layer. What is very much different in the present case though is that this develops naturally and the interaction is between axisymmetric and non-axisymmetric modes. Of these nonlinearly generated modes, the one which exhibited a maximum amplitude was the difference mode. Miksad (1973)

also found this to be an energetic mode. It appears that this nonlinear interaction takes place in the change over between the axisymmetric and helical modes, during their alternating performance.

In addition to this nonlinear interaction, a second nonlinear interaction was observed. In this case an interaction was observed between the subharmonic mode and the difference mode which originally developed through a nonlinear interaction between the axisymmetric and helical modes. Generation of modes at the sum and difference of these frequencies was also evident.

When the frequencies of all of the above modes were properly normalized, it was determined that the Strouhal number of these modes are independent of Reynolds number and initial background disturbance level. A consistant normalization was obtained when the momentum thickness at the location where a spectral peak was first observed for the initial axisymmetric mode was used.

With this, one finds that the development of a turbulent jet with a laminar exit boundary layer is determined by a series of linear and nonlinear instabilities involving axisymmetric, subharmonic and helical modes. Even though these modes scale at a constant Strouhal number, the degree of nonlinearity and three dimensionality is dependent on the initial background disturbance characteristics in the exit boundary layer. If this jet was externally forced at the

initial instability frequency at low levels just sufficient to eliminate the natural amplitude and phase modulation of this mode, an axisymmetric flow field would be established which would inhibit the development of the helical mode initially and hence the other nonlinear interactions. If various eduction techniques were used to examine the development of the large scales in the near region of the jet under these conditions, the educed flowfield will not represent the naturally developing flow, particularly when the initial disturbance is sufficient so that both m=o and m=1 modes are equally important. This is one of the major pitfalls of conditional sampling; see Wlezien (1981) for additional comments on this.

In cases where the initial boundary layer was turbulent, an instability mechanism was also identified. This mode initially scaled at a constant Strouhal number of 0.024. This same value was also found by Hussain and Zaman (1981) in a two dimensional shear layer. The initial boundary layer in this case was marginally thin and the instability frequency varied inversely with the local momentum thickness until the jet was thick enough to support the $St = 0.47$ mode. The nature of this instability was found to be independent of Reynolds number and initial exit boundary layer thickness.

In addition to these instabilities, the long wave instability which scaled with the jet diameter was also

documented. This scaling of the mode was found to be weakly dependent on the initial conditions. As the disturbance levels in the exit boundary layer increased, the growth of the jet decreased. Thus at any downstream position, the jet was thinner, which corresponded to larger values of D/θ for the higher disturbance level conditions. According to Michalke (1971), even though the jet is sufficiently thick, slightly larger values of D/θ lead to higher frequencies. This increase in final Strouhal frequency with increasing disturbance levels was reported in Chapter VI.

This long wave mode is the same one that has been called the jet Strouhal frequency or jet-column instability, e.g., see Kibens (1979). Based on the volume of measurements presented here, it is conjectured that this mode reflects the local instability of the jet near the end of the potential core. As pointed out earlier, one should not be surprised that this mode is quite energetic. Since modes developed earlier in the jet scale with smaller lengths and since lower frequency have a farther reaching noise radiation field, the dominance of this frequency in the far field pressure is not necessarily that surprising. However one must recognize the existence of a cascade of instabilities of decreasing frequencies along the jet, even past the end of its core. The farther downstream, the more important is the helical mode.

Relation Between Instabilities and Near Field Pressure

Once the various instability mechanisms were established, the characteristics of the near field pressure were examined. Pressure spectra taken just outside the boundary layer separation point revealed numerous discrete peaks when the exit boundary layer was laminar. These peaks correspond to the different instability modes observed in the jet. In low disturbance level conditions, small amplitude peaks were observed at frequencies corresponding to the initial axisymmetric and helical modes. Large amplitude peaks were observed for the subharmonic mode and the difference mode generated through the nonlinear interaction between the initial $m=o$ and $m=1$ modes. Strong peaks were also observed at the sum and diffference modes generated through the nonlinear interaction between the subharmonic mode and the previously discussed difference mode. These results indicate that the low frequency downstream developing modes are more acoustically efficient than the higher frequency modes.

As was pointed out in Chapter V, the amplitude development of the other modes, which were generated through the nonlinear interactions, was weak compared to the modes described above. These weak modes were not clearly defined in the pressure spectrum. The characteristics of the pressure spectrum were also

influenced by the background disturbance level. In cases where the mean vorticity across the separated layer was kept constant, increasing the peak disturbance level in the exit boundary layer caused a broad band decrease in the amplitude of the measured pressure spectrum along with spectral broadening of the observed peaks. Associated with these changes in near-field pressure characteristics was an increase in three dimensionality in the initially developing flow along with lower peak amplitude of the developing instabilities as the disturbance level was increased.

This pressure field in turn acted as a small amplitude natural excitation to the jet. For cases 1L and 2L it was shown in earlier results, agreeing with those of Freymuth (1966), Morkovin and Paranjape (1971) and Mungur (1977) for forced conditions, that the external pressure field and the responding velocity field developing in the jet were related by a linear functional. Thus the magnitude of a peak in the pressure spectrum determines the initial amplitude of that mode in the jet. Due to the linear nature of this, the mode initially grows exponentially with an amplification rate determined by its Strouhal number. In case where the background disturbance level in the exit boundary layer was lower than the initial amplitude of the naturally forced mode, peaks corresponding to those in the pressure spectrum were observed in the velocity spectrum near the

nozzle. These modes were then observed to initially grow exponentially as described above. This was monitored over the entire Reynolds number range examined for cases 1L and 2L. Due to the characteristics of the near field pressure, all of the observed modes had an initially larger amplitude than either the initial axisymmetric or helical modes. In fact, the naturally developing eigenmodes radiated a distinct pressure field which in turn altered the naturally developing eigenmodes into a partially forced response in particular, at Reynolds numbers providing match conditions.

From extensive coherence measurements it was determined that for any observed mode, the pressure field at the nozzle lip was highly correlated to the velocity fluctuations over the entire growth and decay of that mode, with a peak coherence observed at the peak amplitude. In the case of the subharmonic mode it was determined that the evolution of the resonant instability was the source of the large pressure amplitude observed at the nozzle lip.

One can easily show that the source region of the subharmonic mode is roughly $\lambda_a/10$ long. In terms of the radiated far field this can be considered an acoustically compact source. It can not however be considered as compact in the near field sense. Because of this, if the pairing process was responsible for the generated pressure field, then the coherence between the velocity

and pressure fluctuations would have been non-zero only where they paired. This is clearly not the case. The simplistic model suggested by Laufer (1980) is clearly not correct. The pairing of two structures does not send back a signal to synchronize the next pairing. Rather, it is the entire subharmonic instability which is responsible for the pressure field and the pairing is simply the result of the resonant instability. A similar type of result was obtained by Heavens (1980) who tried to show that the pairing of two structures radiated a pressure field. His results indicated that there was no direct relationship.

While pairing is one of the mechanisms for large scale intraction in the jet, no evidence of its regularity in naturally developing jets can be found. In particular, the higher the disturbance level in the initial conditions, the more irregular is the pairing, i.e., it is modulated in space and time. Ample evidence is provided here for this conclusion, e.g, see Figures 157 and 158.

Scaling of Initial Axisymmetric Instability and its Subharmonic Resonance

In the previous chapters it was shown that in cases where the exit boundary layers were laminar, the frequency scaling of both the initial axisymmetric mode and its subharmonic mode were independent of Reynolds number and background disturbance level conditions. It

will be shown in this section that the downstream characteristic of these modes are also identical when the proper normalization is used in the streamwise direction. From the phase measurements presented in Chapter VII, the wavelength of the initial axisymmetric mode was determined. It was also found that past the resonant location, the wavelength of the subharmonic mode is twice that of the fundamental. Phase measurements of the subharmonic mode between the nozzle lip influence region and the resonant position were inconclusive for Re < 80,000. For this reason, this data is normalized by the wavelength of the subharmonic mode during resonance. Upon normalizing the streamwise distance by the mode wavelength, the development of the axisymmetric and subharmonic modes is shown in Figures 159 and 160 for case 1L.

Initially the amplitude of the subharmonic mode is an order of magnitude larger than that of the fundamental. This was shown to be due to the natural forcing of the flow due to its downstream development. The subharmonic mode initially grows exponentially. At one subharmonic wavelength downstream, the subharmonic resonance takes over and the amplification of this mode increases by 40%. Even though the initial amplitude of the subharmonic mode is larger at Re = 42,000 then at 52,000 or 60,000, due to the natural coupling condition discussed in Chapter VI, the amplitude development of

these modes past the resonant position is nearly
identical. These results indicate that at the coupling
condition the development of the initial axisymmetric
mode is not changed. In fact, only the initial amplitude
of the subharmonic mode is increased, due to a stronger
pressure field. However, as the resonant mechanism
progresses, nearly equal maximum amplitudes are observed.

In these figures the subharmonic resonance was
observed to occur at one subharmonic wavelength. This
value however is misleading. The proper interpretation
of this position is not one subharmonic wavelength but
rather two initial wavelengths. The reasoning behind
this is clearly evident. For the subharmonic mode there
is an initial region where the phase is constant. After
this region the subharmonic has a phase speed of 0.81
which was clearly evident in the high Reynolds number
case. Associated with this difference in phase speed
between fundamental and subharmonic modes is a difference
in wavelength such that $2 \lambda_{i,0}$ is greater than the actual
wavelength of the subharmonic in this region. This is
simply because the two waves develop initially from
linear mechanisms. It is only after the resonance that
the subharmonic mode changes phase speed so that the
wavelengths are related by a factor of two. The
subharmonic wavelength thus changes as it develops.
Since the resonance is actually triggered by the finite
amplitude state of the fundamental, the true

interpretation of the resonant position is that it occurs
at two fundamental wavelengths downstream.

The downstream growth of the jet for case 1L at a
Reynolds number of 42,000 is next shown in Figure 161.
At the resonant position of two fundamental wavelengths,
the jet begins its linear growth. From the visualization
it is observed that the initial roll up of the jet
occured at this position. The average pairing position,
as determined from the visualization, is also indicated.
Near this position there is approximately a 10% increase
in the jet thickness as compared to the linear growth.
The case illustrated in Figure 161 is for the natural
coupling condition of Case 1L. where energy in the
subharmonic mode was greatest. In this case pairing has
only a small influence on the linear growth region. For
all other cases the effect will be even less. For
natural developing flows the momentum thickness of the
jet does not remain constant until pairing occurs, after
which it doubles. This is only true in certain forced
conditions as presented by Ho and Haung (1981).

The nature of the subharmonic resonance is also
shown in Figure 162. In this case, Figure 20 has been
replotted in a normalized streamwise coordinate. Prior
to resonance, the mean velocity profile remains nearly
hyperbolic tangent in nature, indicative of the initial
linear instability. As resonance begins, the mean
velocity profile develops a large deviation from this

profile. This is associated with an instability of a new base flow, that being the initial rolled up structure. The deviation arises from the relative movements of these structures leading to pairing. This deviation was originally observed in the conditionally ensembled mean velocity profiles obtained by Hussain and Zaman (1980). This large deviation is indicative that the instability of this new base flow, the subharmonic resonance, is different from the initial instability which originally developed this structure.

The effect of changing the background disturbance characteristics on the amplitude development for these modes in shown in Figure 163 for a Reynolds number of ·42,000. The initial amplitude of the subharmonic mode is lower for case 2L than for case 1L due to the decreased magnitude in the pressure field as observed in Figure 61. Case 3L, as reported earlier, showed no initial subharmonic growth. In all three cases though, the subharmonic resonance is found to occur at two initial instability wavelengths. Once past the resonant position, the amplitude development for cases 2L and 3L are nearly identical. The resonant position is found to be independent of Reynolds number and background disturbance level as long as the exit boundary layers remained laminar.

A summary of the measured amplification rates for the initial axisymmetric mode, the initial subharmonic

mode and the subharmonic resonant mode are shown in
Figure 164 for case 1L over the Reynolds number range
examined in Chapter VII. This shows that the initial
amplification of the axisymmetric and subharmonic modes,
normalized by the proper momentum thickness, is
independent of Reynolds number and the values agree well
with those predicted by Monkewitz and Huerre (1981).
More scatter is observed in the data for the measured
amplification rates of the resonant mode but it appears
that the amplification rates do not scale with the
momentum thickness near the jet exit. This is gratifying
to see since it is expected that this mode should scale
with the momentum thickness at the resonant position. If
this is true then the local momentum thickness of the jet
at the resonant position will not scale with the inverse
square root of the Reynolds number. This is indicated by
the deviation away from the dashed line. There is
insufficient data on the momentum thickness at the
resonant position to comment further on this conjecture.

The effect of Reynolds number and background
disturbance level on the downstream variation of the
coherence between the velocity fluctuations in the jet
and the near field pressure at a relative angle of zero
degrees is examined next in Figure 165. In both cases
the downstream location is normalized by twice the
initial axisymmetric wavelength. This figure illustrates
the Reynolds number independence of the coherence

behavior for Case 1L. The quality of the collapse in
this case is also an indication of the high confidence
level in the data. The variation between test flow
conditions at a constant Reynolds number is shown in
Figure 166. The initial development of the coherence
function up to the resonant position was clearly shown to
be a function of the initial background disturbance
level. It was very surprising to find that the shape of
the coherence distribution past the resonant position is
essentially unaffected by the initial conditions. These
three test flow conditions were vastly different in terms
of jet development. The jet growth rate decreased and a
substantial increase in three dimensionality was observed
as one proceeded from case 1L to case 3L. In fact, the
pairing process was more randomized and non-axisymmetric
in the higher disturbance level cases. Still, the nature
of the coherence between the radiated pressure field and
the velocity fluctuations in the jet for the subharmonic
mode appear to be unaffected. This further illustrates
that the resonance mechanism is independent of
disturbance level.

Coupling Between Long and Short Waves

In Chapter VI it was observed that when the initial
instability frequency was an integral multiple of two of
the final Strouhal frequency and the background
disturbance level low enough, a natural coupling was

observed which led to an increase in the magnitude of the subharmonic pressure field. This criterion for coupling was first presented by Kibens (1979) for a forced jet where the initial Strouhal frequency cascaded down to the final Strouhal frequency through a number of vortex pairings. In the present case, a natural coupling is observed using the same criterion even though after the first pairing the axisymmetry of the flow is quickly destroyed due to the strong nonlinear modes so that this simple cascading is not observed.

This conflict seems to indicate that even though there is coupling, the simple cascading model proposed by Kibens (1979) is not the mechanism. However the model predicts the coupling conditions exactly. Examination of Figures 159 and 160 reveals that when this coupling condition is met only the subharmonic mode is affected; the initial axisymmetric mode is unaffected. The initially larger amplitude of the subharmonic is due to an initially stronger pressure field. During resonance the coupling and non coupling positions have nearly equal amplitude behavior. This is also observed in Figure 165 where the coherence is essentially unaffected during resonance. The only difference lies in the higher coherence observed between the nozzle lip region and the resonance region along $U/U_j = 0.6$. This appears to be the only significant difference between coupling and non coupling conditions. Perhaps the coupling takes place

before the subharmonic resonance.

This coupling was only observed under low
disturbance levels. Under higher disturbance levels the
emergence of the helical mode disrupted the natural
coupling conditions. When the jet is properly forced
though, as in Kibens (1979,1980) experiment, this latent
coupling emerges and can be quite dominant. Clearly the
axisymmetry of the flow is a necessary condition.
However, more work is required to determine the exact
nature of this mechanism.

The Jet: A Non-Parallel Flow

Based on Figures 17, 37 and 161 it becomes quite
evident that the development of the jet is that of a
non-parallel flow. This is true for jets having
initially laminar or turbulent exit boundary layers.
When the exit boundary layer is laminar, there are two
distinct regions where non-parallel affects enter: the
region before the subharmonic resonance, and the region
after the resonance where the linear growth of the jet
has begun. The divergence in the early region is roughly
one-half that after the resonance position. From this
and the nature of the observed instabilities in this
case, a correct formulation of the stability problem
would have to include the non-parallel aspects of the
flow, the unsteadiness or time dependency of the initial
modes, nonlinear interaction effects, the initial

disturbance level characteristics and also the
interaction of the downstream flow with the boundary
layer separation region through an acoustic near field.

This type of formulation is not available nor is one
expected in the near future due to its complexity. The
only available theories are linear and assume that
either the flow is locally parallel or that there is a
slow spreading of the jet. The nature of these theories
were discussed in Chapter I. It is the intention of this
section to show that the linear parallel flow theories
can be utilized locally to determine the qualitative
nature of the developing jet when the subharmonic
resonance mechanism is also included. Since these
theories are linear, there is no hope of accounting for
the nonlinear interactions which develop between the m=0
and m=1 modes. However, some could be introduced as
additional linear modes into the analysis.

The results of Michalke (1971) and those of
Mattingly and Chang (1974) show characteristics which are
similar in nature. However, due to the amount of
information available in the former authors paper, his
results will be used here for discussion purposes.

From Michalke's theory (1971), the Strouhal
frequency of the most amplified mode can be found as a
function of the local momentum thickness. This curve is
shown in Figure 167. It indicates that as the local
thickness increases the frequency of the maximum

amplified mode decreases. This behavior is identical for the m=o and m=1 modes for Strouhal frequencies above 0.5. This close similarity is presumably due to the shape of the profile utilized. Mattingly and Chang's (1974) results would be about 17% apart. Also included in this figure is the initial Strouhal frequencies for Cases 1L, 2L and 1T at Re = 42,000. In each case the value of was that used in the normalization described in Chapter VI. The trend of the data is similar to the predicted results. The main difference is in the initial mean velocity profiles between 1L, 2L and 1T. From earlier results (see Figure 69) the Case 1T behavior was expected to fall above this curve and cases 1L and 2L below this curve.

Crighton and Gaster (1976) have found that there is little difference when considering the linear stability of a slowly diverging jet as compared to the analysis using linear theory assuming locally parallel conditions, as far as the determination of the most amplified wavelength and phase speed is concerned. One however can not obtain radial information concerning the amplification rate using locally parallel flow assumptions. To qualitatively describe the basic development of the jet, the use of the locally parallel flow assumption is a reasonable first order approach.

This assumption is first used in describing the development of the jet when the initial boundary layer is

turbulent. This is illustrated in Figures 168 and 169.

In the case examined, the initial exit boundary layers
can still be considered thin. It was observed that the
turbulent boundary layer became unstable at a certain
frequency near the nozzle. This corresponds to the data
for case 1T in Figure 167. As the downstream distance
was increased, the shear region of the jet increased as a
ratio of the jet width, and the frequency of this peak
decreased in the manner shown in Figure 168. Michalke's
results show that for these thin jets the Strouhal number
of the mode should remain constant along with the
amplification rate based on the local momentum thickness.
This prediction was recently confirmed by Hussain and
Zaman (1981) for a two dimensional shear layer. Similar
scaling should be observed here due to the thin nature of
the exit boundary layers and the similarity between
amplification curves for two dimensional shear layers and
thin axisymmetric jets. It is only after the jet has
developed to a sufficiently thick layer with a smaller
potential part that the final Strouhal mode becomes
dominant. This is also observed in Figure 168.

Based on the results of the previous chapters,
pairing can be characterized by an instability of
azimuthally coherent structures triggered by a
subharmonic resonance mechanism. In cases where the exit
boundary layer was laminar, two distinct regions of
non-parallel effects were observed. The first

corresponds to the region where the initial modes grew
exponentially. The second corresponds to the region
after the subharmonic resonant position. The divergence
in the second region was nearly three times that of the
first region. From flow visualization it was concluded
that very little smoke was entrained into the jet until
after the resonant position. Thus in the first region
the divergence is probably due to viscous diffusion in
the radial direction of the initially separated region.
Because of this much lower divergence rate and the
thinness of the exit boundary layer, the flow can be
assumed as parallel over this entire region. Exponential
growth up to the resonant position would then be
expected. This is precisely what was observed.

In Kibens' (1979) work, the vortex pairing was
localized in a jet by low level azimuthal excitation. It
was observed that the frequencies found along the jet
centerline decreased in a stepwise manner, with the steps
occuring at the pairing position. Even though the simple
linear theory outlined above cannot describe the pairing
process due to the nonlinearity involved and the
deviation away from the hyperbolic tangent profile during
the subharmonic resonance, a similar staircase behavior
can be predicted from Michalke's theory (1971) by
assuming that the subharmonic mode remains spatially
coherent during the resonance even though the flow is
diverging. This is a rather wishful assumption but the

basic behavior in Figure 169 is similar to that observed by Kibens (1979). Along the first horizontal line the amplification of the initial axisymmetric mode decreases. The vertical line corresponds to the position where the first subharmonic mode has an equal amplification rate as the fundamental. The amplification of this subharmonic grows and then decays until the amplification of its subharmonic increases to a value equal to its fundamental and so on.

Prospects for Controllability of Jets

It has been demonstrated that the jet is dominated by the growth and decay of various instability mechanisms. A radiated pressure field was found to be associated with each of these instability characteristics. Because of the linearity between this radiated pressure field and the developing modes in the jet, it should be possible to utilize the natural pressure field at the nozzle to actively introduce disturbances with the amplitude and azimuthal distribution determined from the near field pressure. This disturbance field could be delayed to be out of phase with the pressure field. The out of phase nature of this excitation would effectively cancel the early linear instabilities in the jet. This method may work with either laminar or turbulent exit boundary layers. If the early instability development of the jet is

altered, the "final" Strouhal frequency may also be controllable. This type of imposed disturbances which are controlled by the naturally developing flow field itself seems quite attractive. In fact, this type of active control may lead to substantial noise reduction.

CHAPTER XII

CONCLUSION

Utilizing simultaneous near-field pressure and velocity measurements, along with multiple flow visualization techniques, the effect of initial conditions and Reynolds number on the development and nature of instabilities in the initial region of axisymmetric turbulent free jets has been examined. Based on the results which were graphically presented and the arguments which were discussed in the previous chapters, a number of conclusion can be drawn. These are presented below.

Conclusions

When the exit boundary layer is laminar, the natural jet is initially unstable alternately to axisymmetric and helical modes. The axisymmetric mode scales at a constant Strouhal number of 0.013 while the helical mode scales at a constant Strouhal number which is 20% higher than this value. This behavior is independent of Reynolds number and initial conditions when properly scaled. The relative occurence of these modes is highly dependent on the initial disturbance characteristics at the jet exit. It is only at low Reynolds number and for low initial disturbance levels that the axisymmetric mode dominates initially. As either of these variables increase both modes become equally important.

When the initial axisymmetric mode grows in
amplitude to about 1% of the jet velocity, a secondary
instability, the subharmonic resonance, develops and
leads to the pairing of axisymmetric vortical structures.
The downstream position of this resonant interaction
occurs after two wavelengths of the initial axistymmetric
mode. At this position the subharmonic wave has obtained
the same phase speed as the fundamental and the two waves
are out of phase. This point is also associated with the
initial roll up of the jet and the first downstream
position where strong entrainment into the jet is
observed.

Due to the alternating nature of the initial
instability of the jet, the axisymmetric and helical
modes interact nonlinearly to develop numerous sum and
difference modes, typical of a two wave nonlinear
interaction. As these modes develop downstream, the
subharmonic mode also interacts nonlinearly with these
modes. Just downstream of the peak amplitude of these
latter nonlinear interactions, strong three-
dimensionality and transition to fully turbulent flow are
observed.

Due to the multiplicity of spectral peaks recorded,
the true identification of these modes cannot be
determined without azimuthal information. Lack of proper
identification of these modes, coupled with low level
incidental disturbances in a number of facilities, has

lead to the previously reported non-ideal behavior of steps in the initial instability frequency as a function of Reynolds number. These steps are not related to a feedback mechanism or pairing.

Each of these instability modes generates a pressure field which is coherent with the velocity fluctuations in the jet over the entire growth and decay range of that mode and not just at the pairing position. This and the scaling of the resonant position reveal that pairing is not responsible for a feedback mechanism. This strong near-field pressure acts as a natural excitation to the jet. When the initial background disturbance level in the exit boundary layer is lower than the amplitude of the velocity fluctuations generated through the functional relationship with the pressure field for a given mode, that mode initially grows exponentially in the jet with a phase speed determined by its Strouhal number. The initial amplitude of these modes is dependent on the acoustic efficiency of the source. As expected, the lower frequency modes are more efficient.

Under extremely low disturbance levels a natural coupling is observed between the initial instability of the jet and the Strouhal mode associated with the final stages of the potential core. This was observed when the two frequencies are related by integral multiples of two. This coupling is not related to the pairing process as previously believed. At this coupling position,

subharmonic pressure radiation is increased leading to a reinforcement of the axisymmetry of the flow.

When the exit boundary layer is turbulent, a linear instability based on the mean profile is observed near the nozzle where the frequency scales at a constant Strouhal number of 0.024. The development of the jet from the nozzle lip to the end of the potential core is found to be adequately described by locally applying linear spatial theories to account for the slow divergence of the jet. The instability-generated large scales develop initially in an axisymmetric form and then change over to a helical mode before the end of the potential core. This mode probably persists past the end of the core.

In general, it is concluded that for these turbulent jets, with laminar or turbulent initial conditions, a great deal of appreciation of the flowfield can be gained by viewing the jet as a non-parallel shear flow which is always susceptible to instabilities. Viewing the jet as a shear layer first and then as a jet near the end of the potential core, may have led to many misleading perceptions. In any case, the instability of turbulent layers and the role of subharmonic resonance appear to be key mechanisms in our findings.

Recommendations

Based on the results of this investigation a number of recommendations for future work can be made. The azimuthal characteristics of the instantaneous pressure field at the nozzle should be examined for each instability mode. Careful manipulation of this natural field to drive a low level disturbance field may lead to the controllability of the jet and a decreased far field noise radiation with only minimal additional power input. A more comprehensive examination of the nonlinear interaction between axisymmetric and helical modes need to be investigated. The azimuthal behavior of the near field pressure radiated from the nonlinearly generated modes needs to be clarified. Further work must be carried out to examine the basic mechanisms involved in the natural coupling that occurs under low disturbance conditions between the initial axisymmetric mode and Strouhal mode near the end of the core. The documented nature of the subharmonic resonance and nonlinear instabilities as well as the importance of the flowfield interacting with itself through an acoustic field should give an impetus to future theoretical work in this area.

APPENDIX A

EFFECT OF BACKGROUND ENVIRONMENT
ON INITIAL JET INSTABILITY

During the initial phase of this investigation the
components in the compressed air supply system were not
acoustically treated. A flow condition which was similar
in nature to case 1L was set up and the characteristics
of the initial jet instability frequency were examined as
a function of Reynolds number. The miniature hot-wire
probe discussed in Chapter II was not yet constructed so
a stock laboratory probe whose prong thickness was of the
order of the exit boundary layer thickness was utilizaed.
The variation of the initial Strouhal frequency with the
square root of Reynolds number is shown in Figure 169.
As was discussed in Chapter VI, this variation should be
linear if the acting instability mechanism is also
linear. The observed behavior is clearly not linear.

At first it was thought that this variation was due
to a characteristic associated with the nozzle. A
different shape nozzle was tried and the same trends were
observed. What was interesting was that the steps that
were observed occured at constant values of Strouhal
frequency. In fact the values of these steps occured at
the long wave-short wave coupling conditions, discussed
in Chapter VI, and also at multiples of 1.5 times these
coupling frequencies. When the jet was excited with the
speaker discribed in Chapter X, different responses
resulted depending if the operating Reynolds number was

in the step or non step region. When the operating
conditions were in a nonstep region, the excitation
frequency and response frequency were identical as the
frequency was reduced until a particular step was
reached. Further reduction in excitation frequency was
associated with an increase in the jet response frequency
as indicated. This non continuous nature between
excitation frequency and jet response frequency was
similar to the type of results Ho and Huang (1981)
observed in a forced two dimensional shear layer.

It was observed that in the natural developing case
the shear layer frequency changed slightly with
increasing streamwise position. Even though the prong
size was below that suggested by Hussain and Zaman (1978)
to minimize probe interference effects, this possiblity
was not ruled out. To determine if this was true, the
miniature probe discussed in Chapter II was constructed.
This reduced the prong dimensions by an order of
magnitude. With this new probe the frequency did not
vary in the streamwise direction. The steps however
still remained, as indicated in Figure 170. The pressure
spectrum was then measured away from the nozzle to
examine the background disturbance field. This is shown
in Figure 171. Strong distinct pressure fluctuations
from the supply system were observed. The magnitude of
these peaks was dependent on the exit Reynolds number but
the frequencies were not. Upon examination of this in

greater detail, it was determined that the steps occurred in regions where the peaks occured. The jet did not lock on to the peak frequency but rather it chose that frequency which coupled it to the long wave instability. This is why a constant Strouhal frequency was observed in the step region and not a constant frequency. Only when the initial jet instability frequency was near 4000 Hz did it lock onto this valve. When the supply system was acoustically treated, the background pressure spectrum exhibited no distinct peaks. This is observed in Figure 61. With the system properly treated acoustically, the variation of the initial instability frequency with the square root of Reynolds number was represented by the ideal linear behavior as in Figure 56.

To test the susceptability of this clean jet to acoustical disturbances, low level wide band excitation which was barely audible was beamed at the jet. The pressure spectrum characteristics which were observed at the nozzle are shown in Figure 172. The two broadband peaks observed are simply characteristics of the speaker which was utilized. From Figures 173 and 174, the initial jet response is completely altered. The two plateau regions correspond to the area of the broad band spectral peaks observed in the excitation pressure spectra.

This excercise was designed to show the high sensitivity of the jet to low level acoustic

disturbances. In fact, when any visualization was taken,
the fan from the strobe had to be disconnected. The jet
was indeed sensitive to any low level acoustic field in
the laboratory.

APPENDIX B

DISCUSSION ON COHERENCE FUNCTION

Let $u(t)$ and $p(t)$ be time series of stationary random processes. If it is further assumed that each series is also ergodic for the sake of simplicity then a Fourier transform pair can be constructed as

$$S_{up}(f) = \int_{-\infty}^{\infty} R_{up}(\tau) \exp(-i2\Pi f \tau)\, d\tau$$

$R_{up}(\tau)$ is defined as the cross correlation between the two signals and $S_{up}(f)$ is defined as the cross-spectral density function. This cross spectral density function is described over both positive and negative frequencies. Typically, a new function is introduced which is only defined over positive frequencies.

$$G_{up}(f) = 2\, S_{up}(f) \quad f \geq o$$

$$o \qquad f < o$$

This function is defined as the single sided cross spectral density function. This function is in general complex. The real and imaginary parts are defined as

$$G_{up}(f) \equiv C_{up}(f) - i\, Q_{up}(f)$$

Here $C_{up}(f)$ is defined as the coincident spectral density function and $Q_{up}(f)$ is defined as the quadrature spectral density function. Since the single sided cross spectrum

is complex, it can be represented by a phasor. Thus

$$G_{up}(f) = |G_{up}(f)| \exp[-i\phi_{up}(f)]$$

The function $\phi_{up}(f)$ is defined to be the phase spectrum. The magnitude of the single sided cross spectrum is usually normalized by the magnitude of the auto spectrum of each signal. This normalized value is called the coherence function.

$$\Gamma_{up}(f) \equiv \frac{|G_{up}(f)|^2}{|G_{uu}(f)| \; |G_{pp}(f)|}$$

Bendat and Piersol (1980) discuss in detail a number of characteristics of this function. First, if the coherence has a vlaue of one, u(t) and p(t) are linearly related. If the coherence is between zero and one, either extraneous noise is in the system, u(t) and p(t) are not linearly related, or the output u(t) is due to other inputs besides p(t).

The above authors also show that when noise is present in the output u(t), the measured coherence is given by

$$\Gamma_{up}(f) = 1 - \frac{|G_{nn}(f)|}{|G_{uu}(f)|}$$

A similar experession can be derived for the case when noise is present only in the input p(t). These results show that the addition of extraneous noise reduces the

level of the coherence by the inverse square of the rms

signal to noise ratio.

APPENDIX C
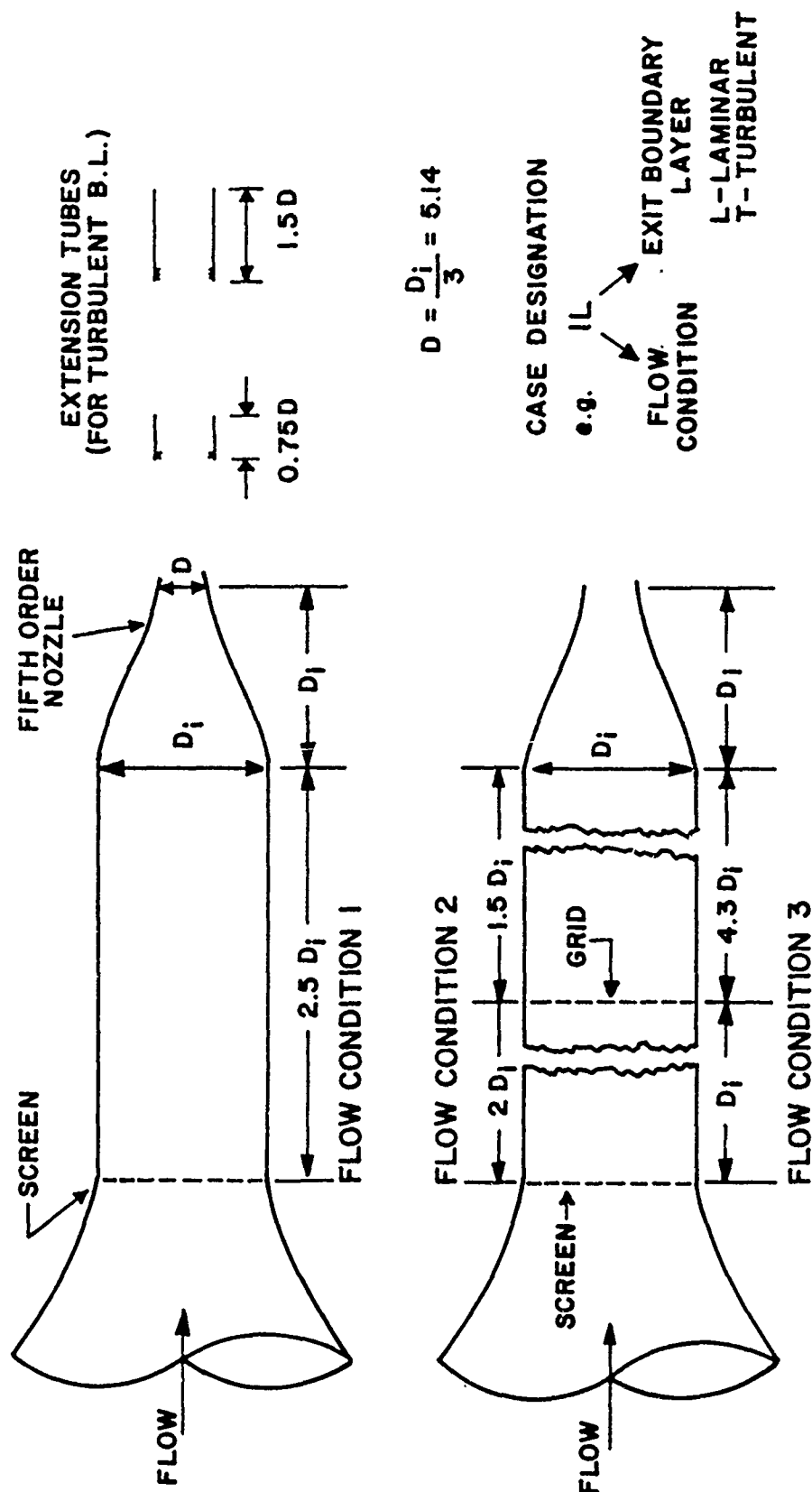
Figure 1. Schematic of Settling Chamber and Nozzle Configurations Used to Generate Different Initial Conditions of Jet
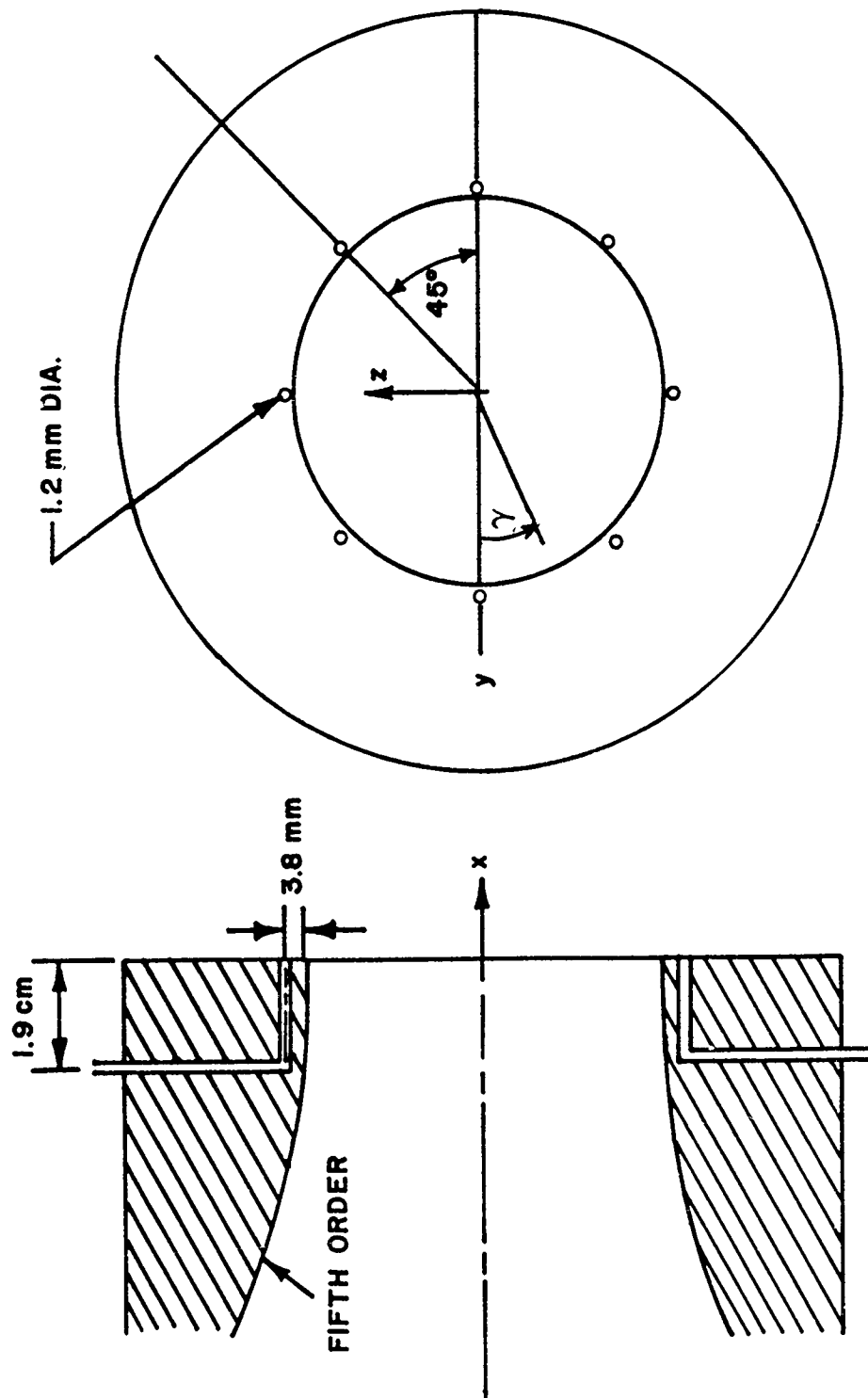
Figure 2. Schematic of Fifth-Order Nozzle Face Showing Azimuthal Pressure Taps
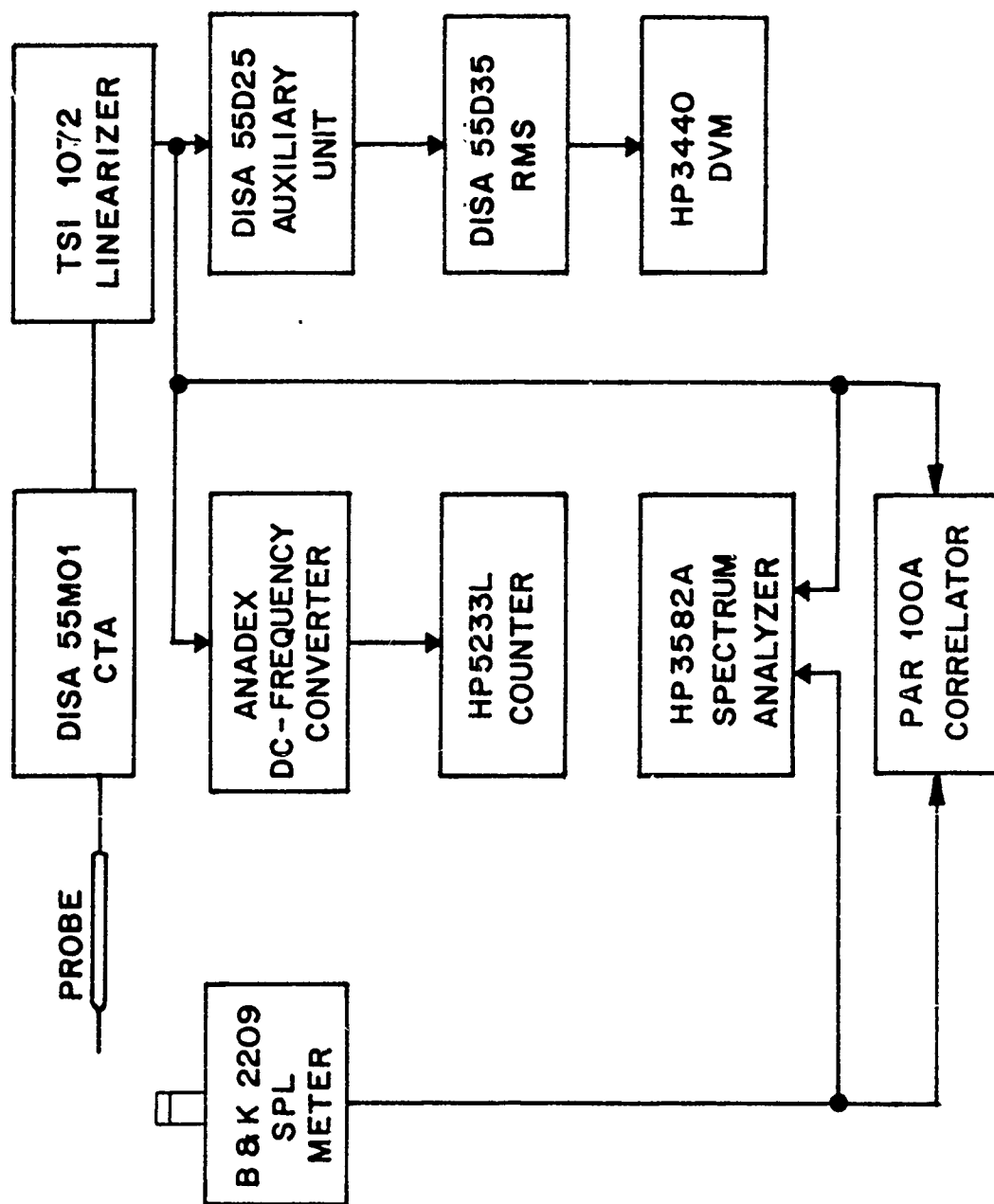
Figure 3. Instrumentation for Analog Measurements of Velocity and Pressure Signal
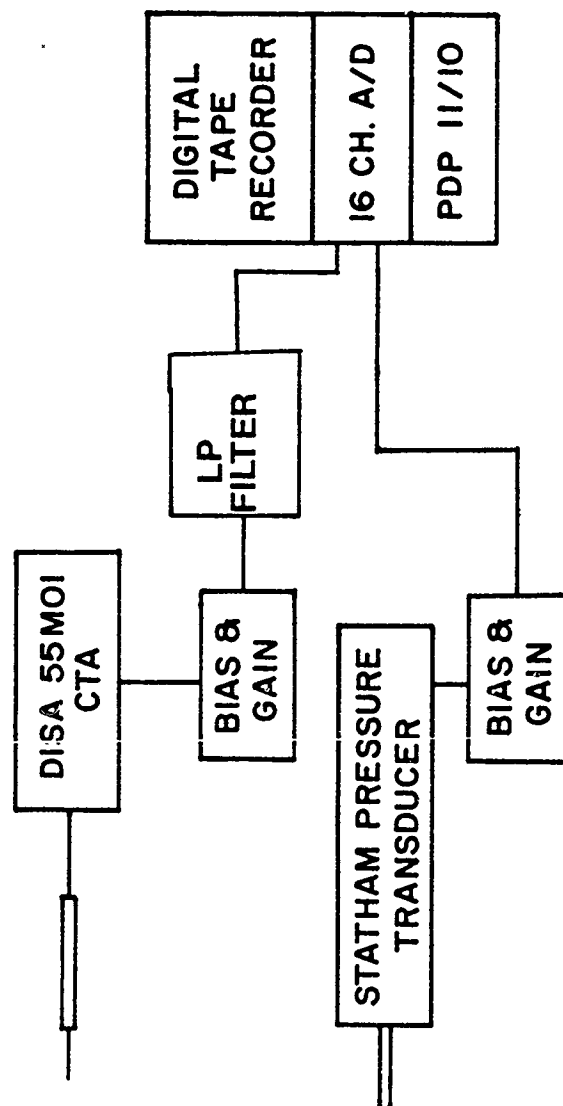
Figure 4. Instrumentation Used for Digital Acquisition of Velocity and Pressure Signals

4 mm

1.3 mm NEEDLE

4 mm

VIEWING DIRECTION

0.13 mm DIAMETER STAINLESS STEEL WIRE

3 mm
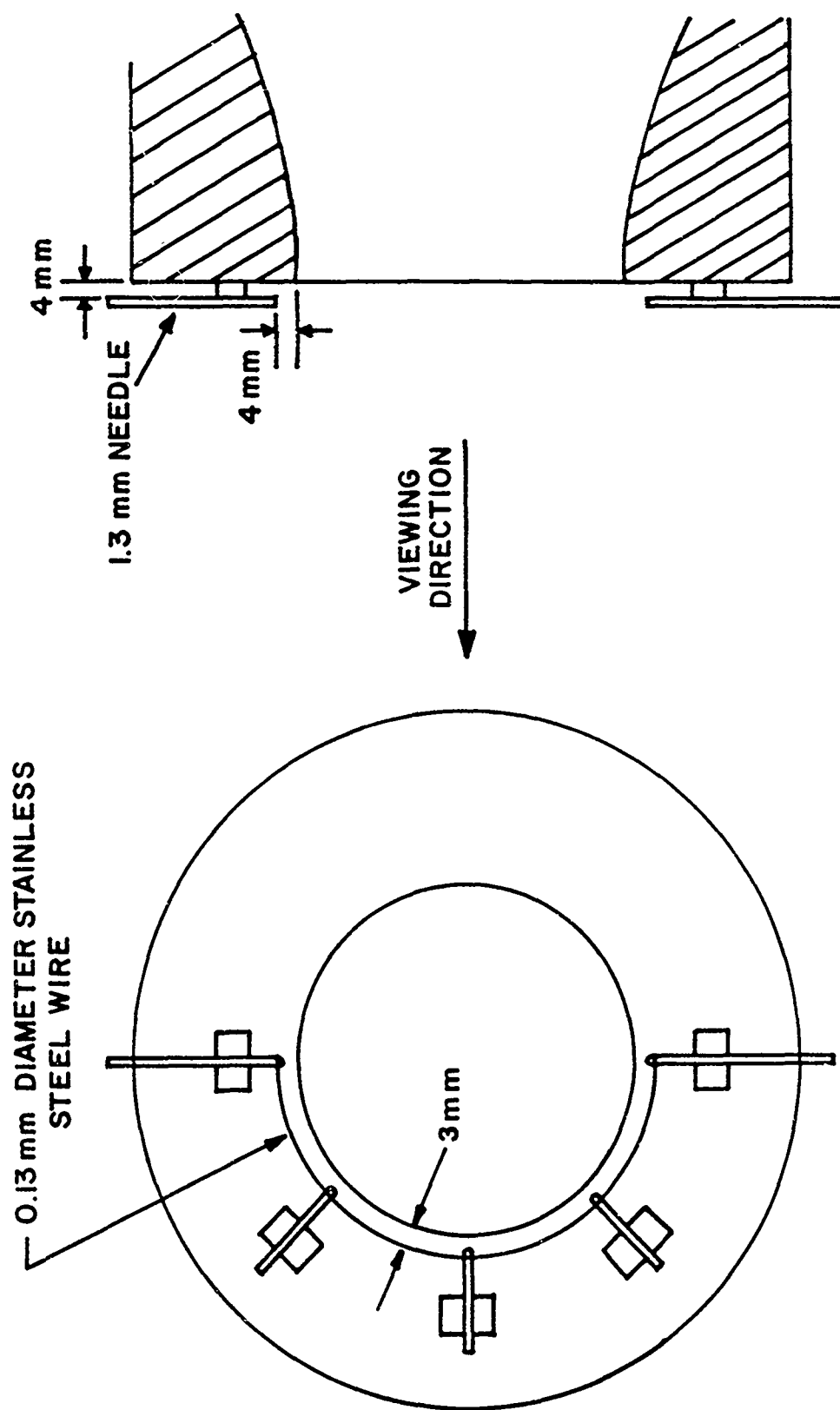
Figure 5. Schematic of Semi-circular Smoke Wire Used for Flow Visualization
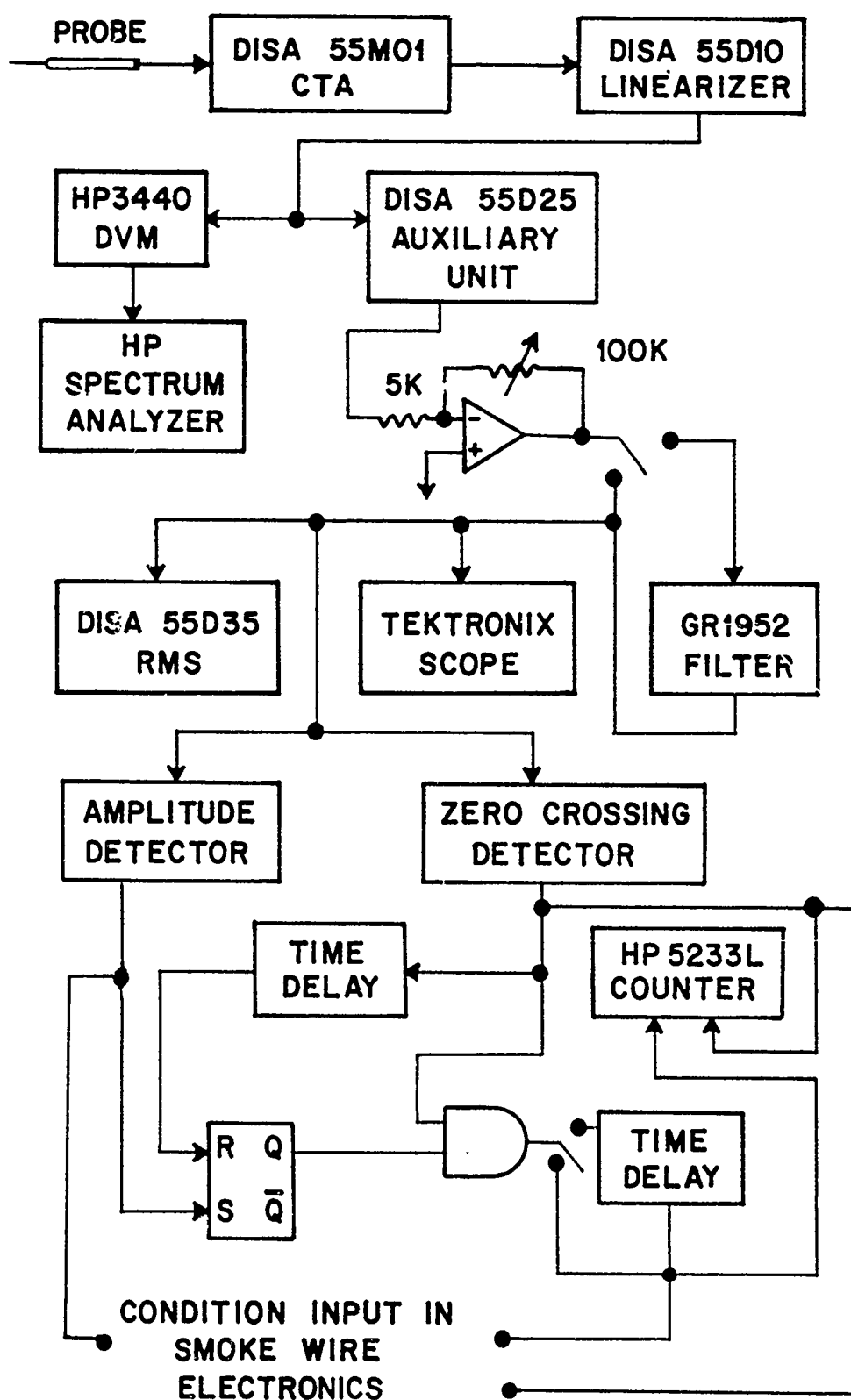
Figure 6. Instrumentation for Conditioned Flow
Visualization
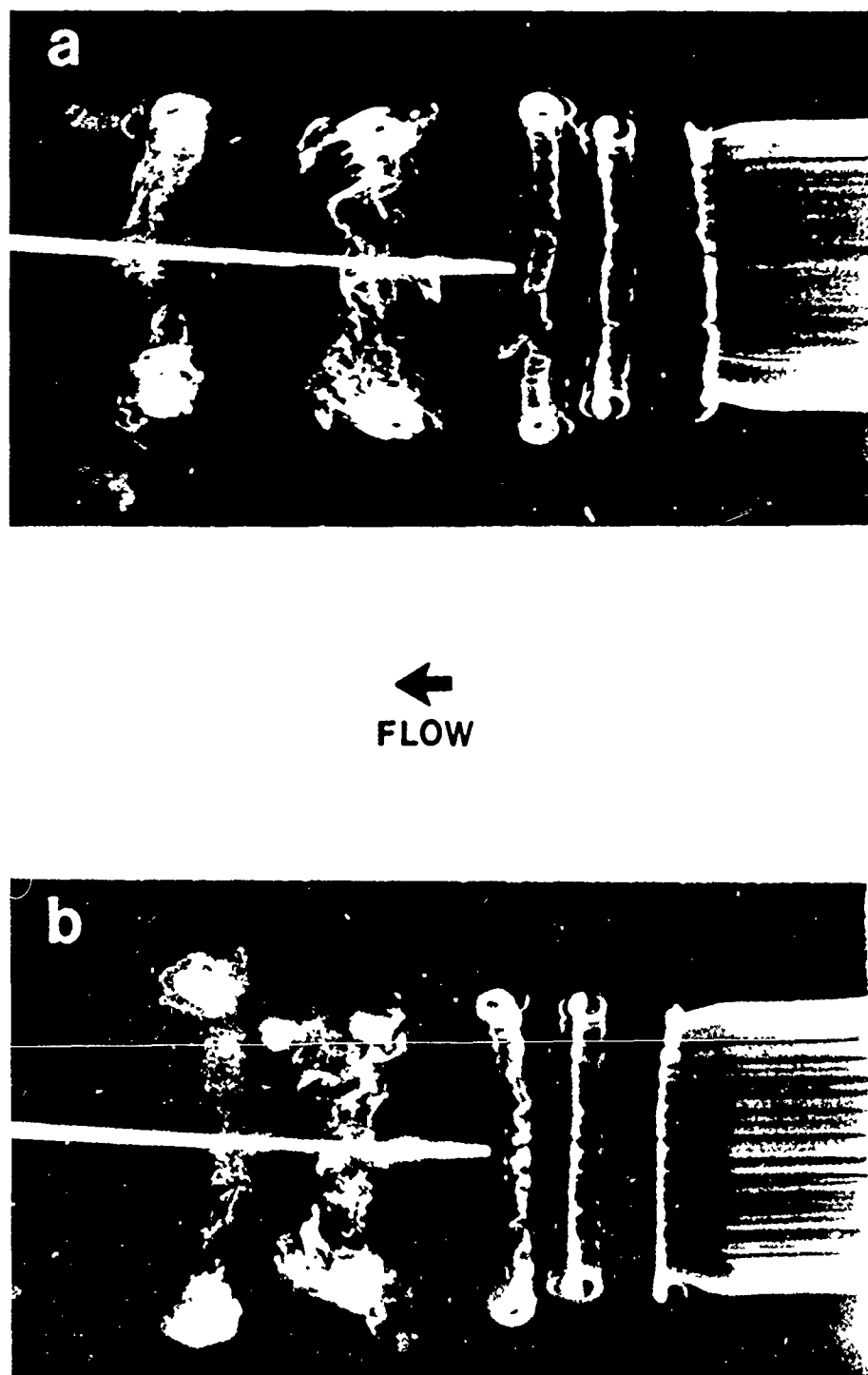
FLOW

Figure 7. Flow Visualization at Re = 20,000 Conditioned on
a Positive Slope Zero Crossing After a Large Amplitude
Event: Conditioning Probe at x/D = 1.5, U/U_j= 0.6
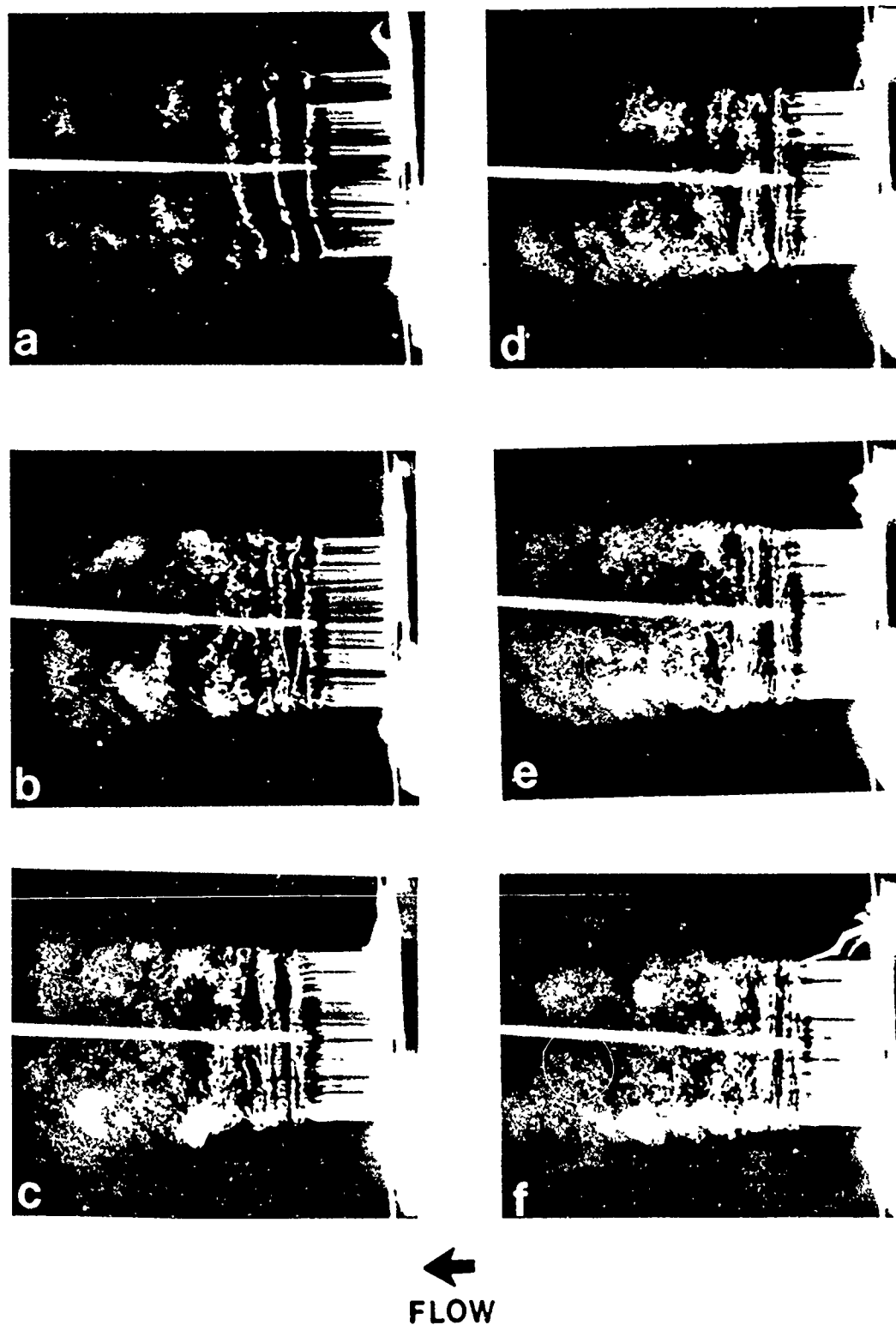
FLOW

Figure 8. Determination of Number of Realizations Necessary for a Suitable Ensemble: (a) 1, (b) 2, (c) 4, (d) 8, (e) 12, (f) 16
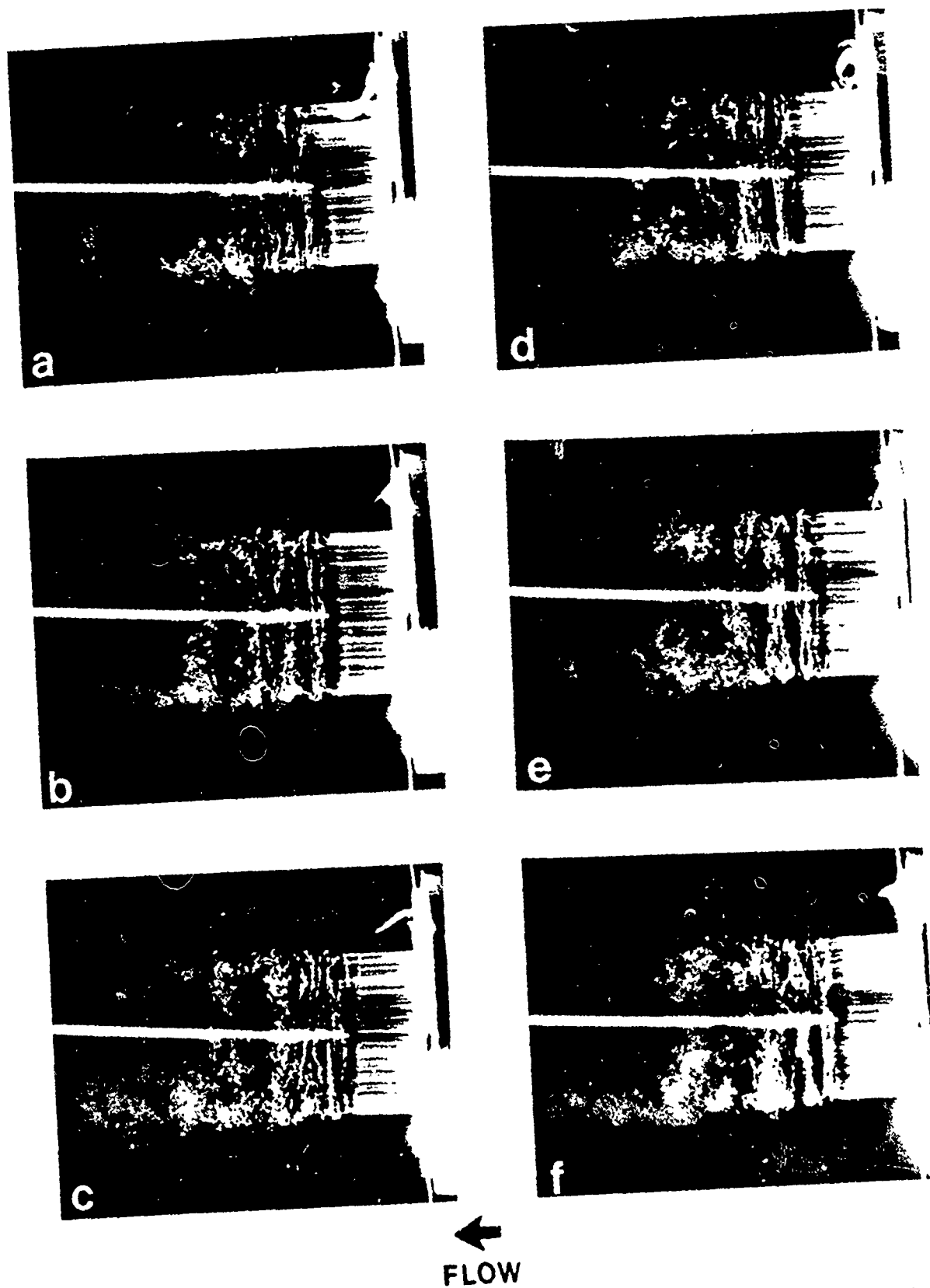
FLOW

Figure 9.   Determination of Suitable Amplitude Threshold for an Eight Realization Ensemble: (a) 0, (b) 0.5 u' , (c) u' , (d) 1.5 u' , (e) 2 u' , (f) 2.5 u'
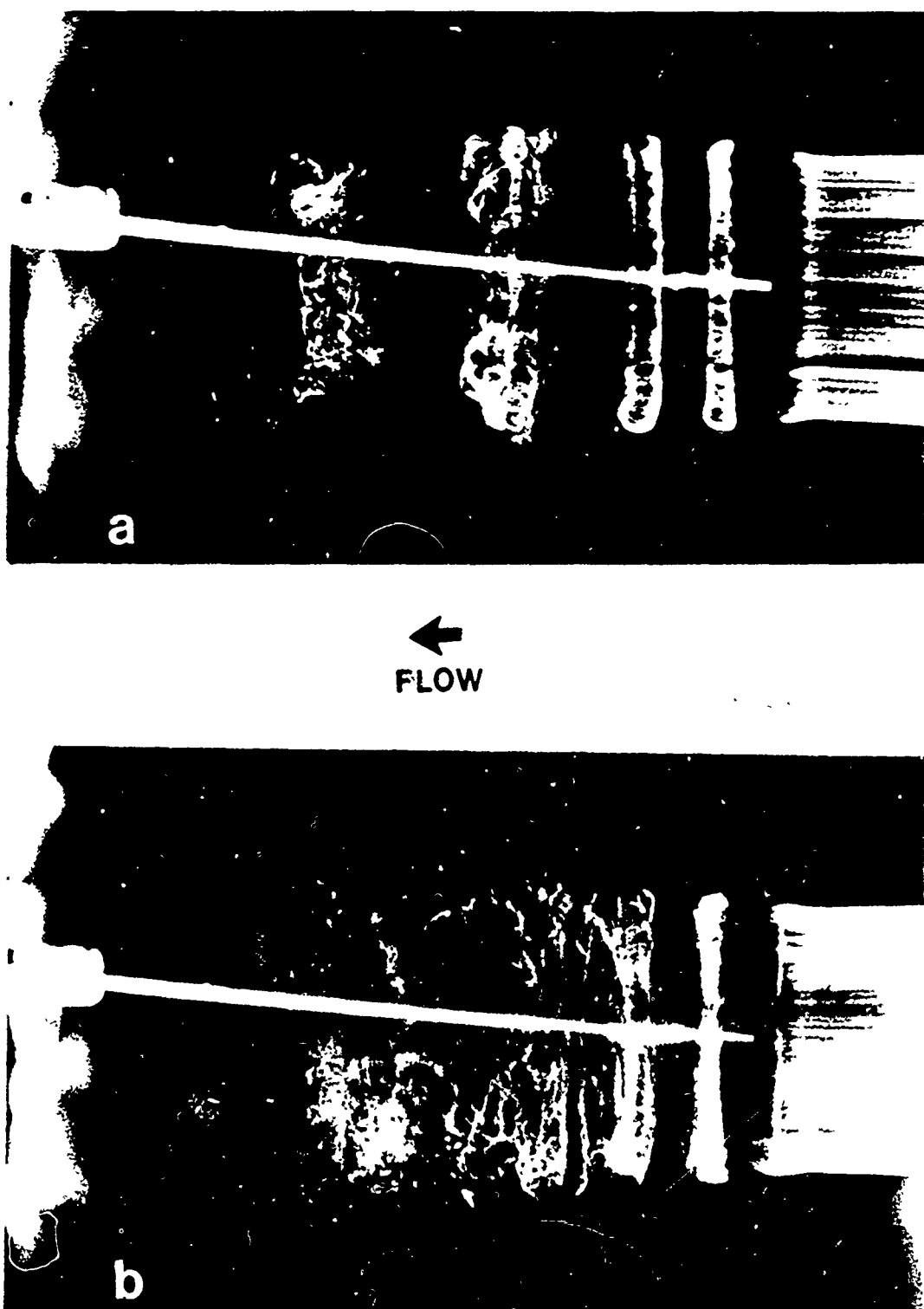
FLOW

Figure 10. Flow Visualization at Re = 20,000 Conditioned
on a Positive Slope Zero Crossing After a Large
Amplitude Event: (a) Single Exposure, (b) Eight
Realization Multiple Exposure
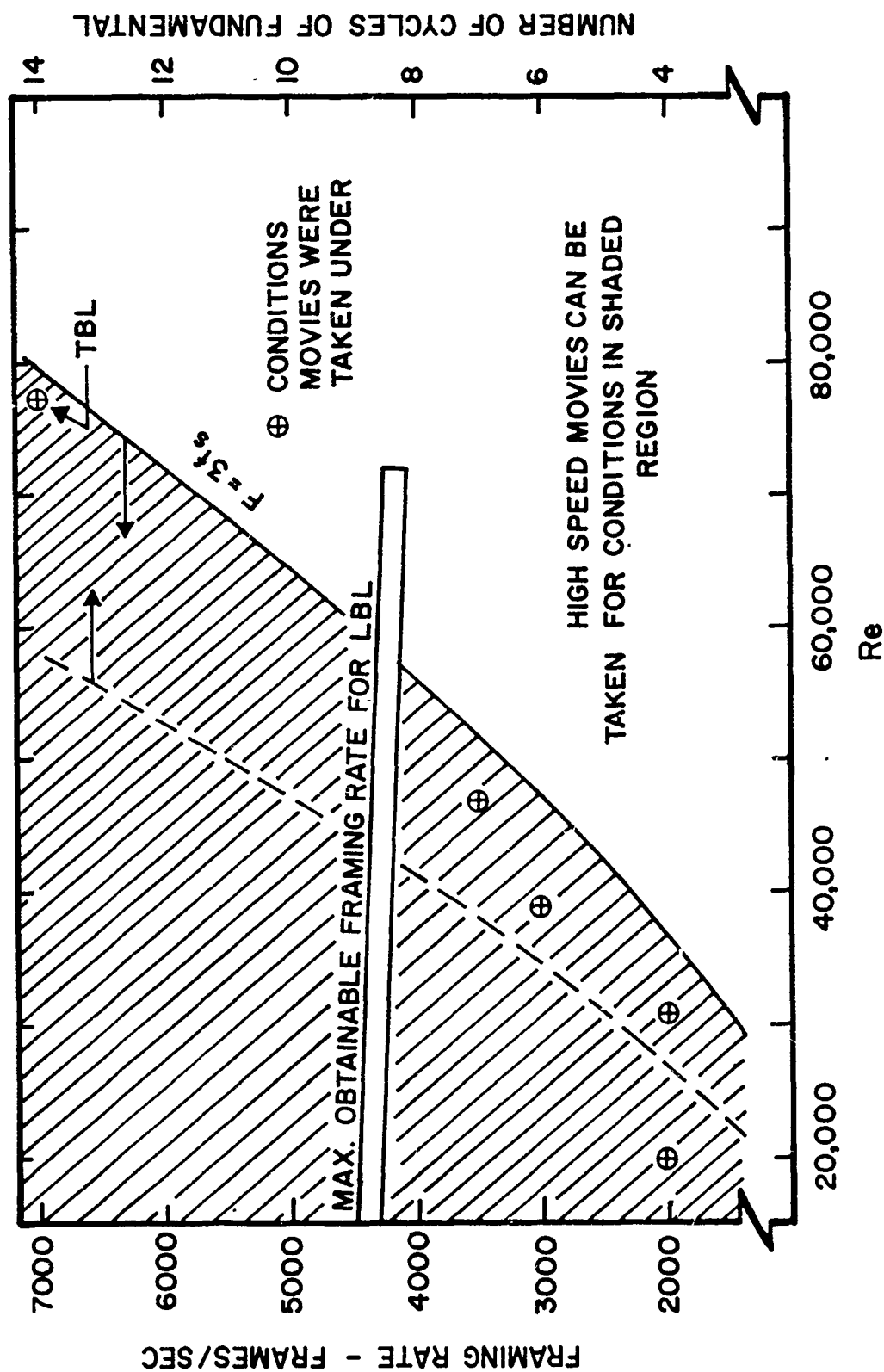
Figure 11. Framing Rate as a Function of Reynolds Number for High Speed Flow
Visualization Movies
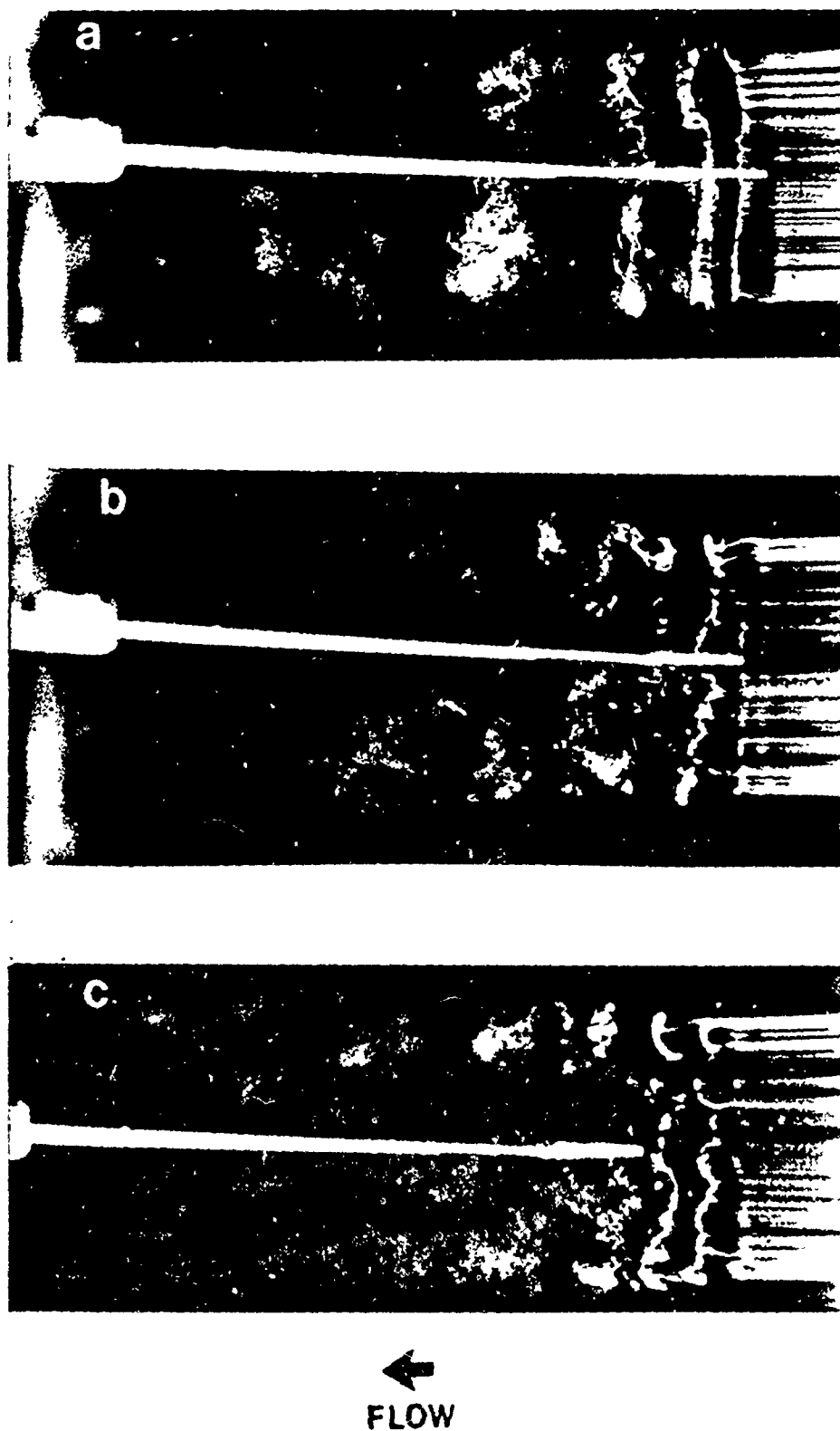
FLOW

Figure 12. Flow Visualization at Re = 39,000 Illustrating
the Effect of Disturbance Level on Initial Jet
Development: (a) Case 1L, (b) Case 2L, (c) Case 3L
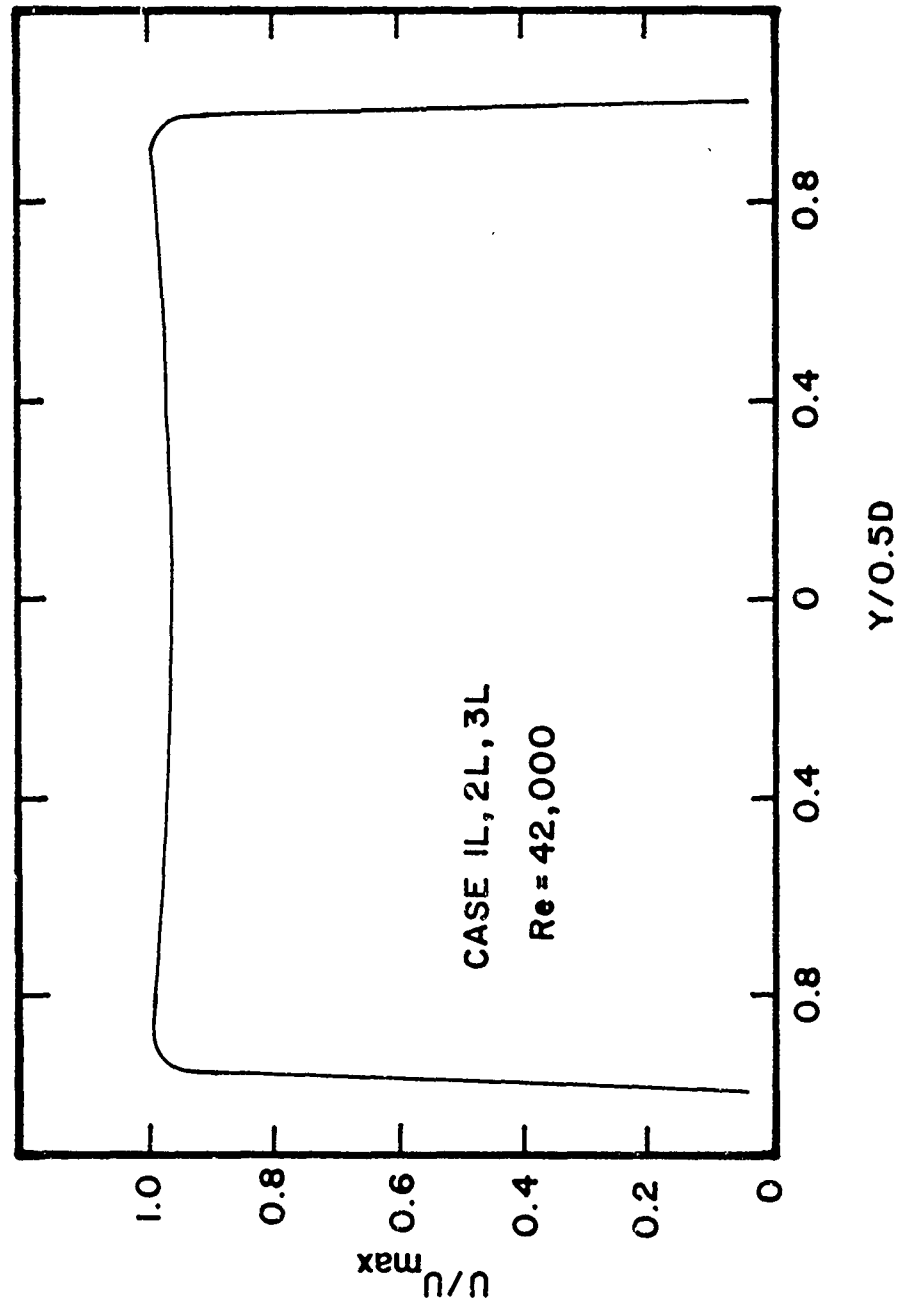
Figure 13. Normalized Mean Streamwise Velocity Profiles for Initial Laminar
Boundary Layer Cases; Re = 42,000, x/D = 0.05
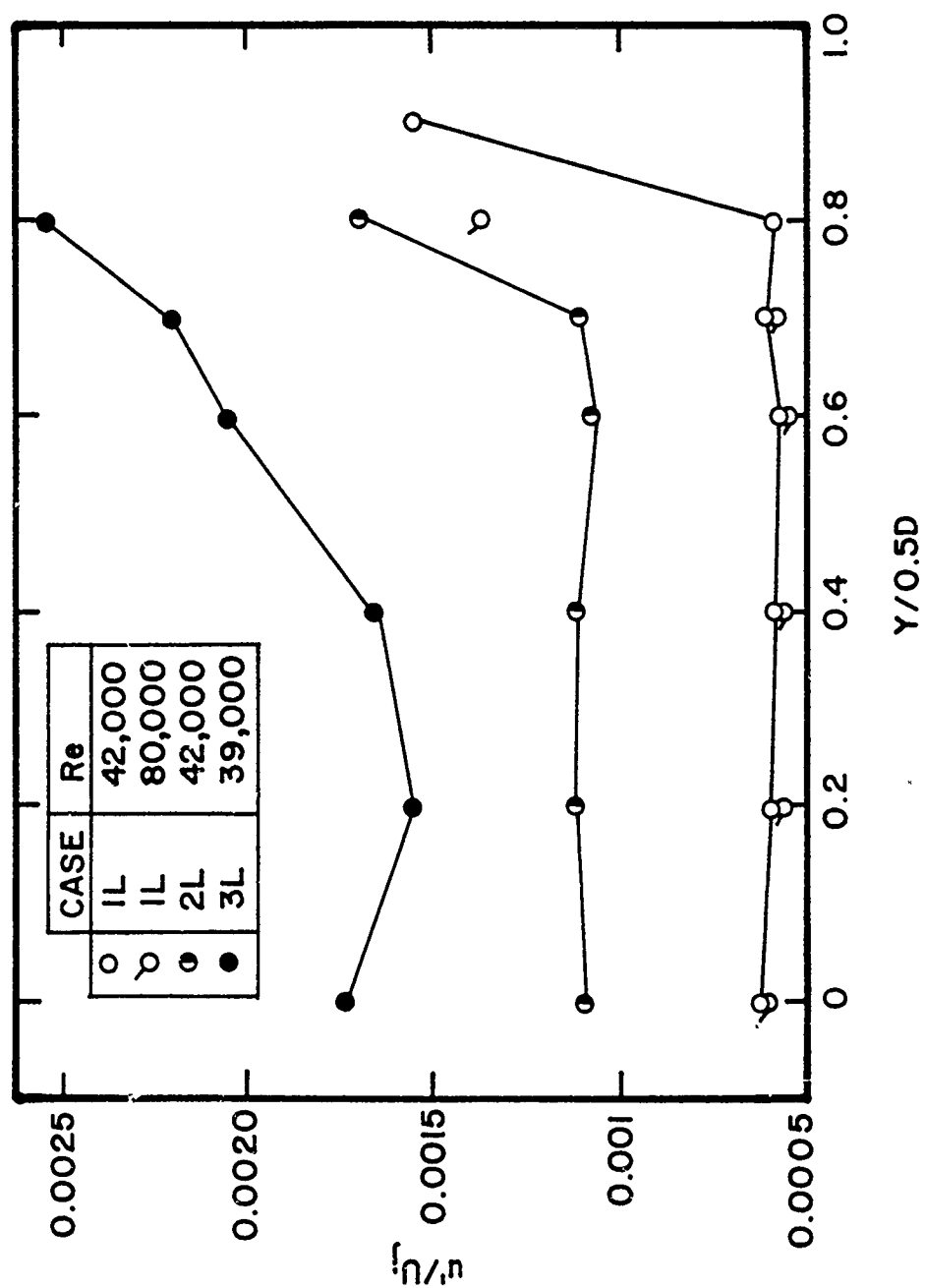
Figure 14. Streamwise Turbulence Intensity Distribution Across Jet Exit for
Cases 1L, 2L and 3L
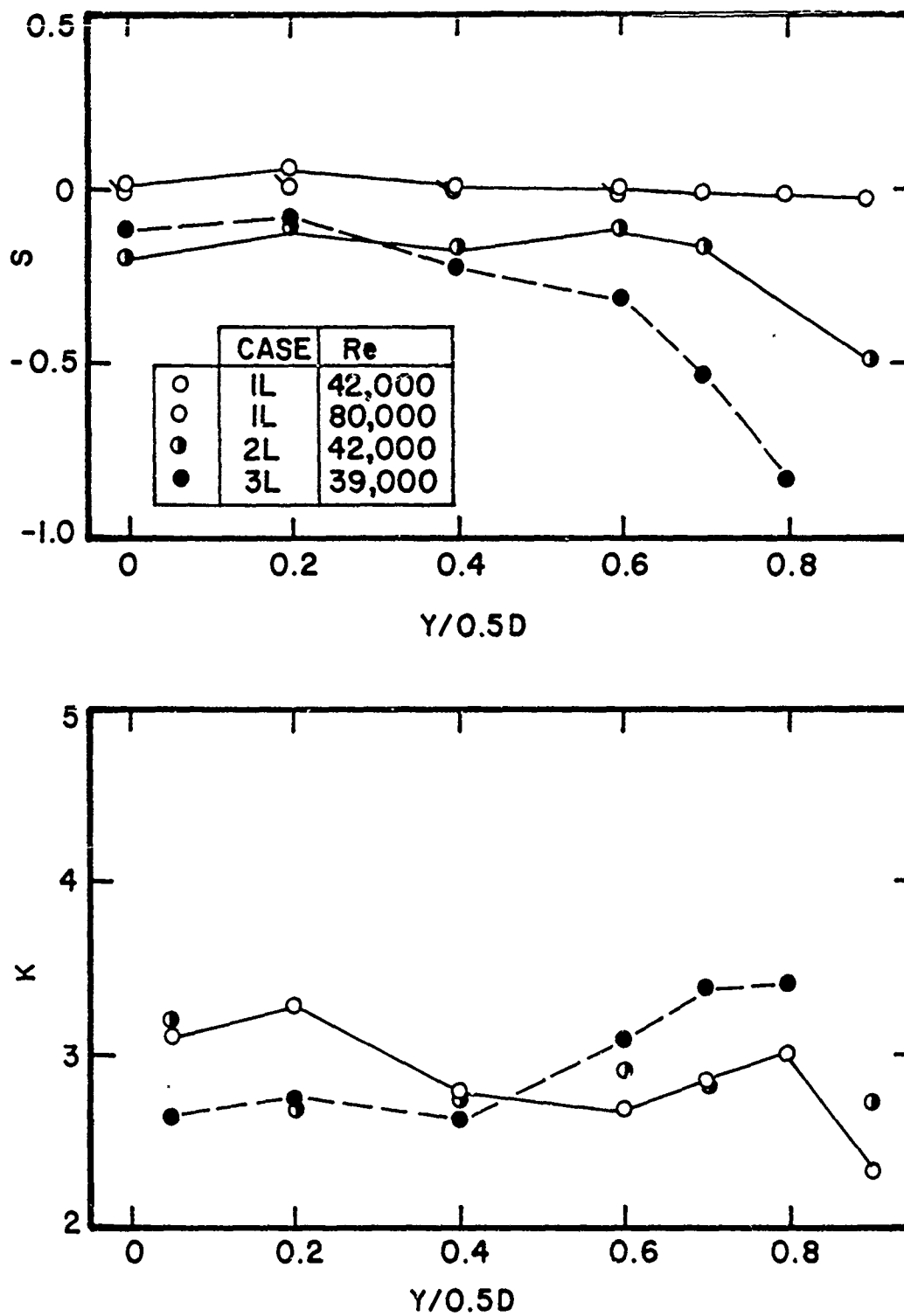
Figure 15. Distribution of Skewness and Kurtosis of Streamwise Velocity Across Jet Exit for Cases 1L, 2L and 3L
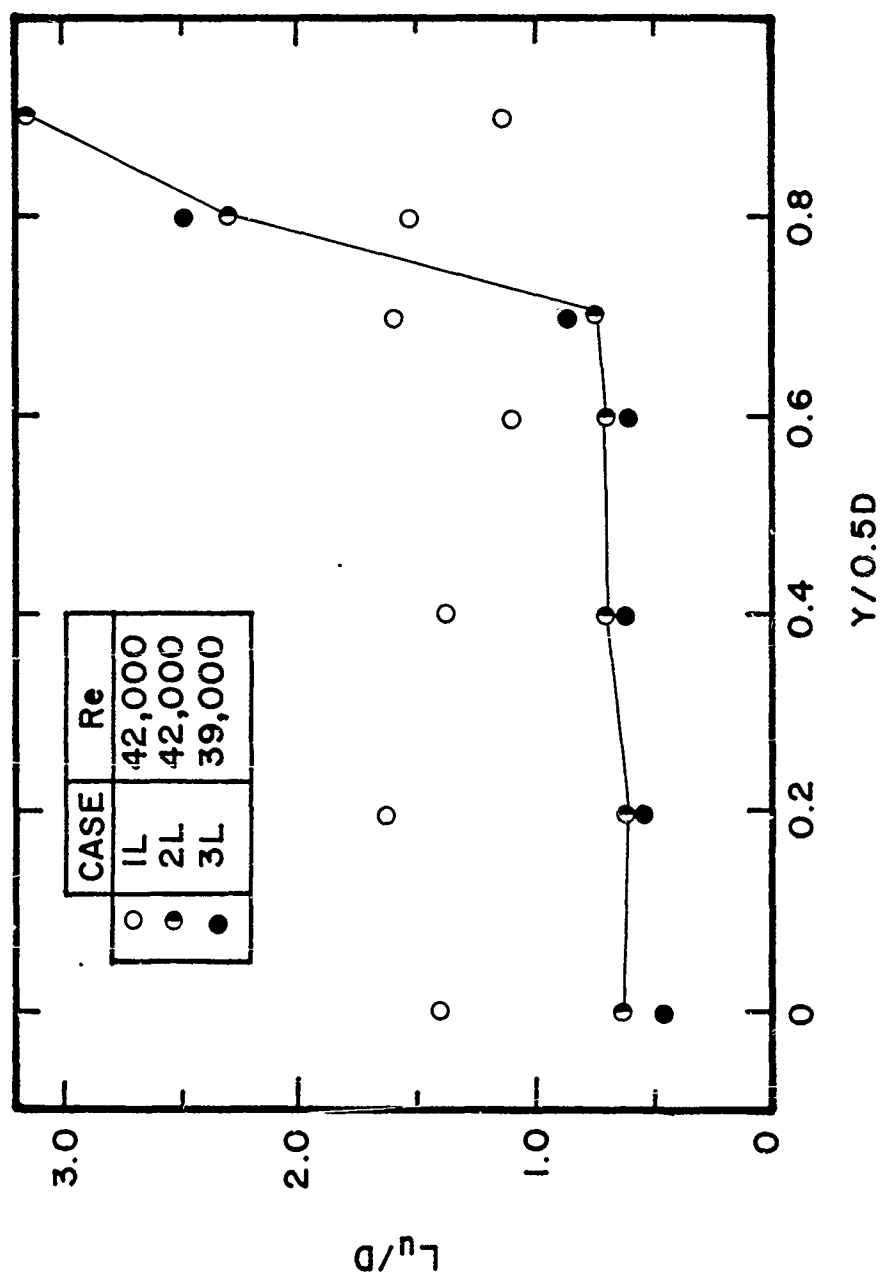
Figure 16. Variation of Streamwise Integral Length Scale Across Jet Exit for Cases 1L, 2L and 3L
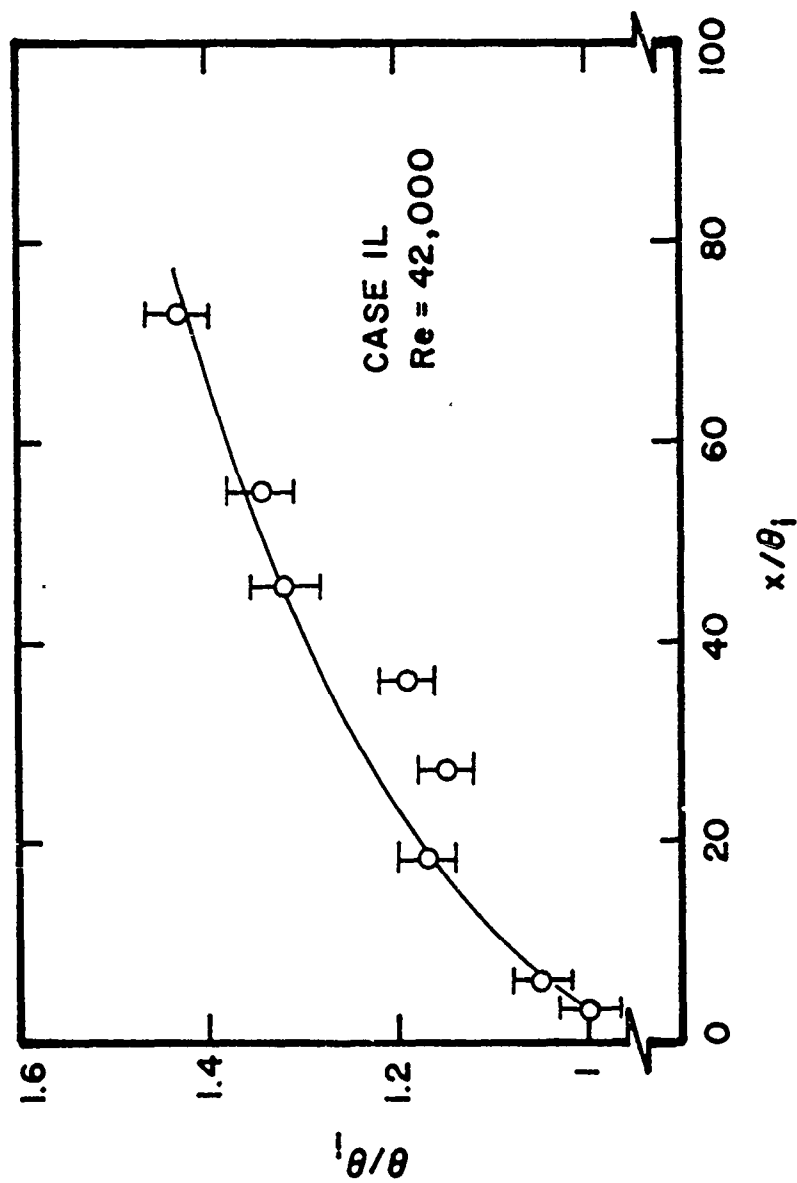
Figure 17. Growth of Initial Jet Momentum Thickness for Case 1L at Re = 42,000
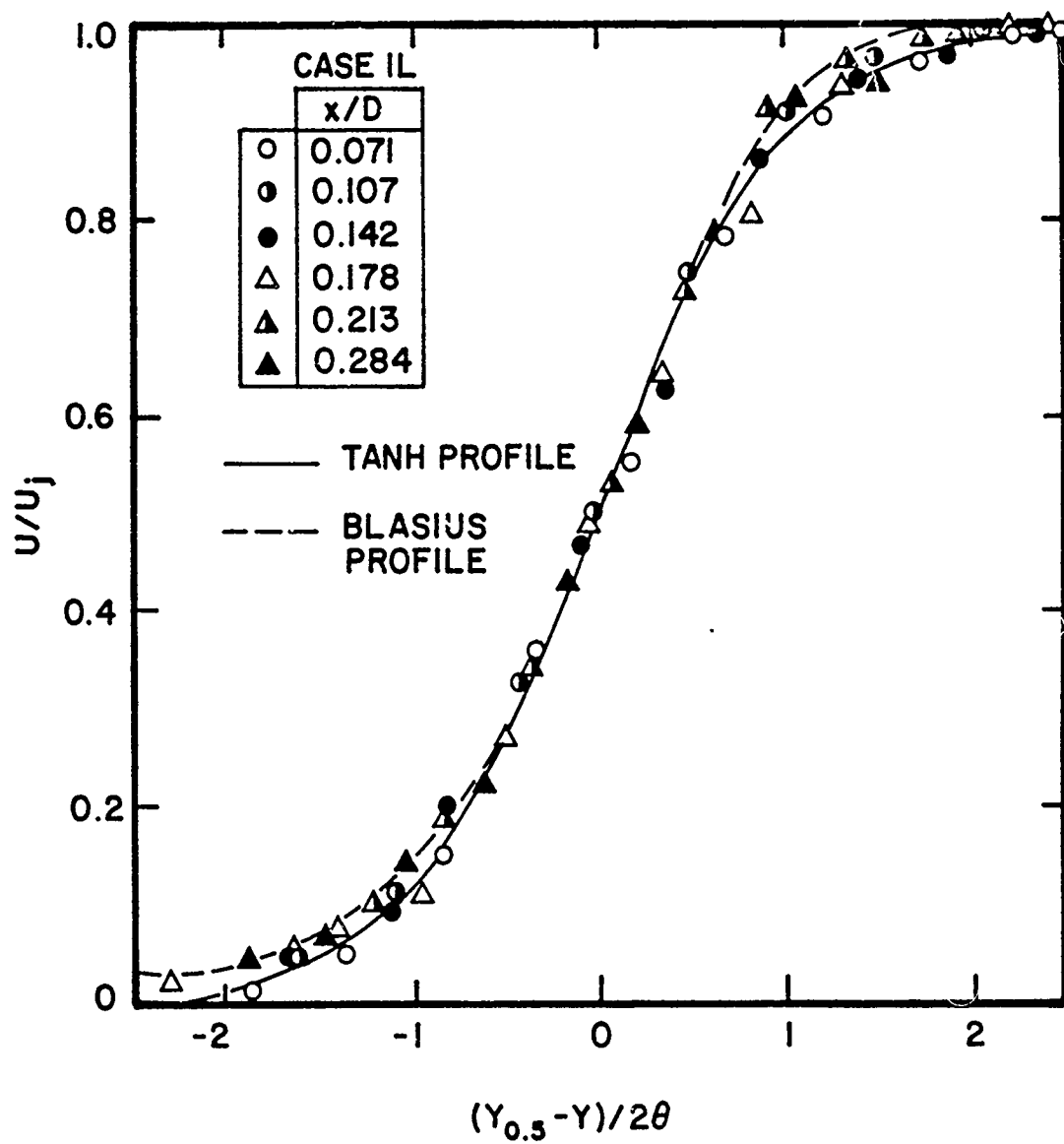
Figure 18. Normalized Streamwise Velocity Profiles in Near Region of Jet for Case 1L.
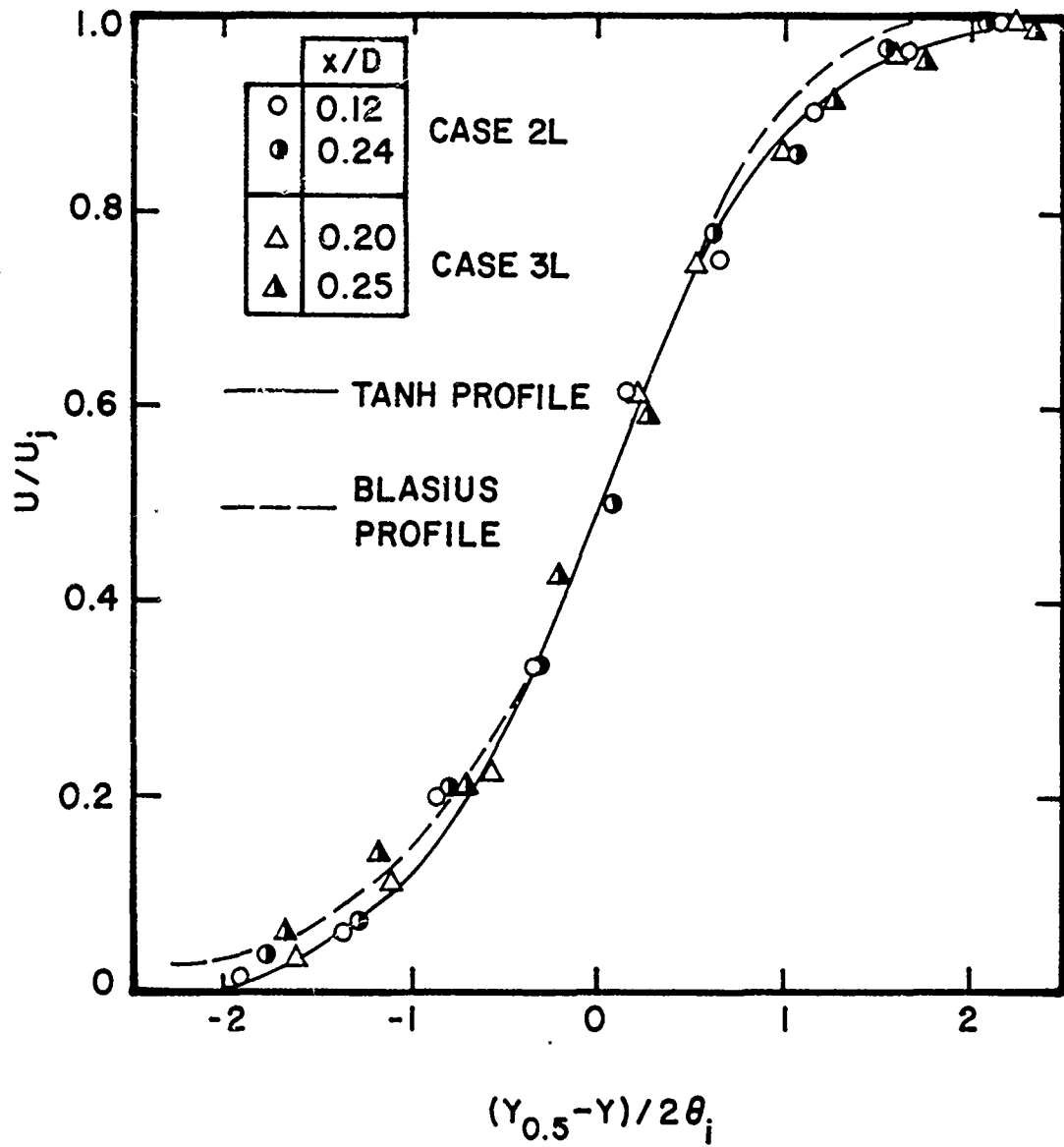
Figure 19. Normalized Streamwise Velocity Profiles in Near
Region of Jet for Cases 2L and 3L
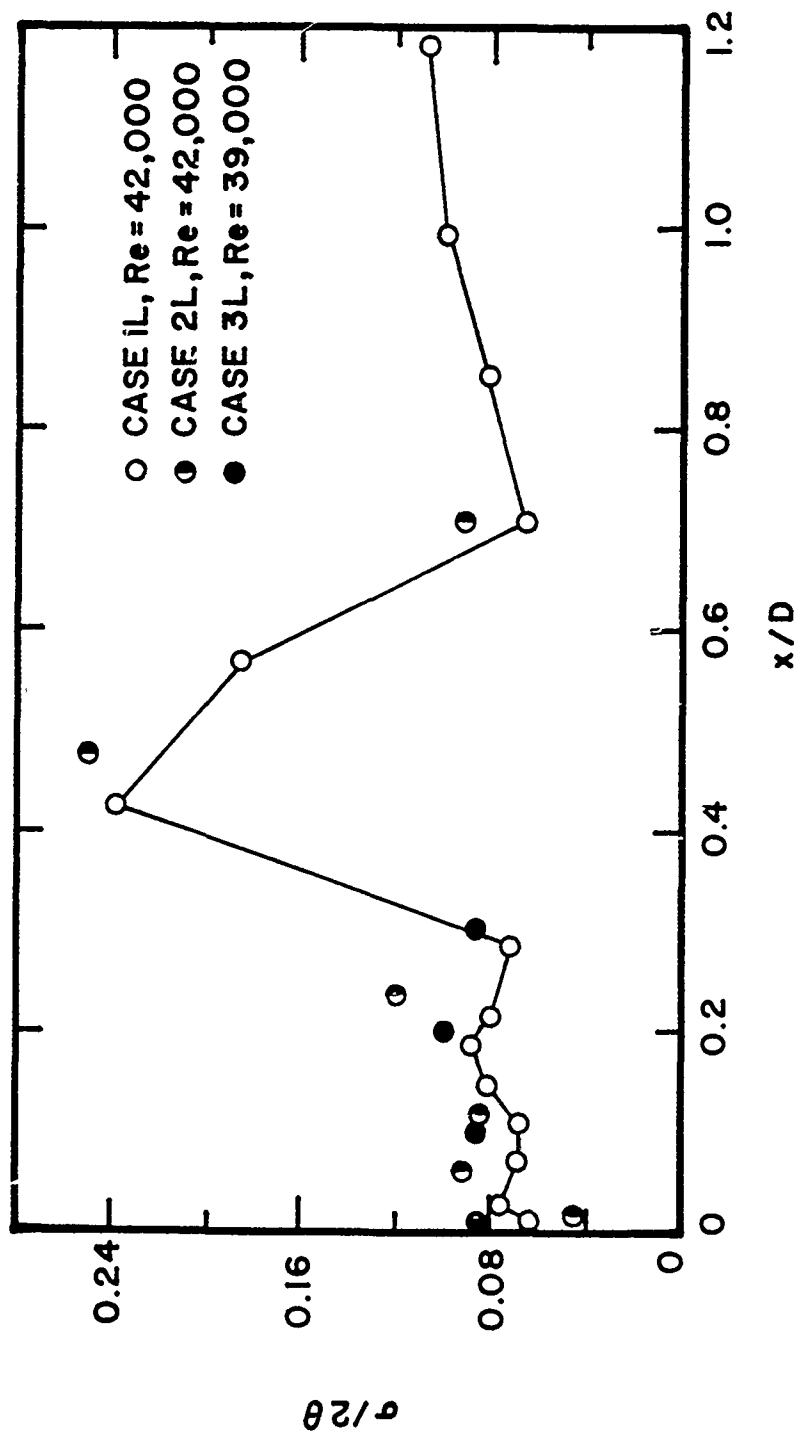
Figure 20. Deviation of Measured Jet Velocity Profiles from Hyperbolic Tangent Function with Downstream Position
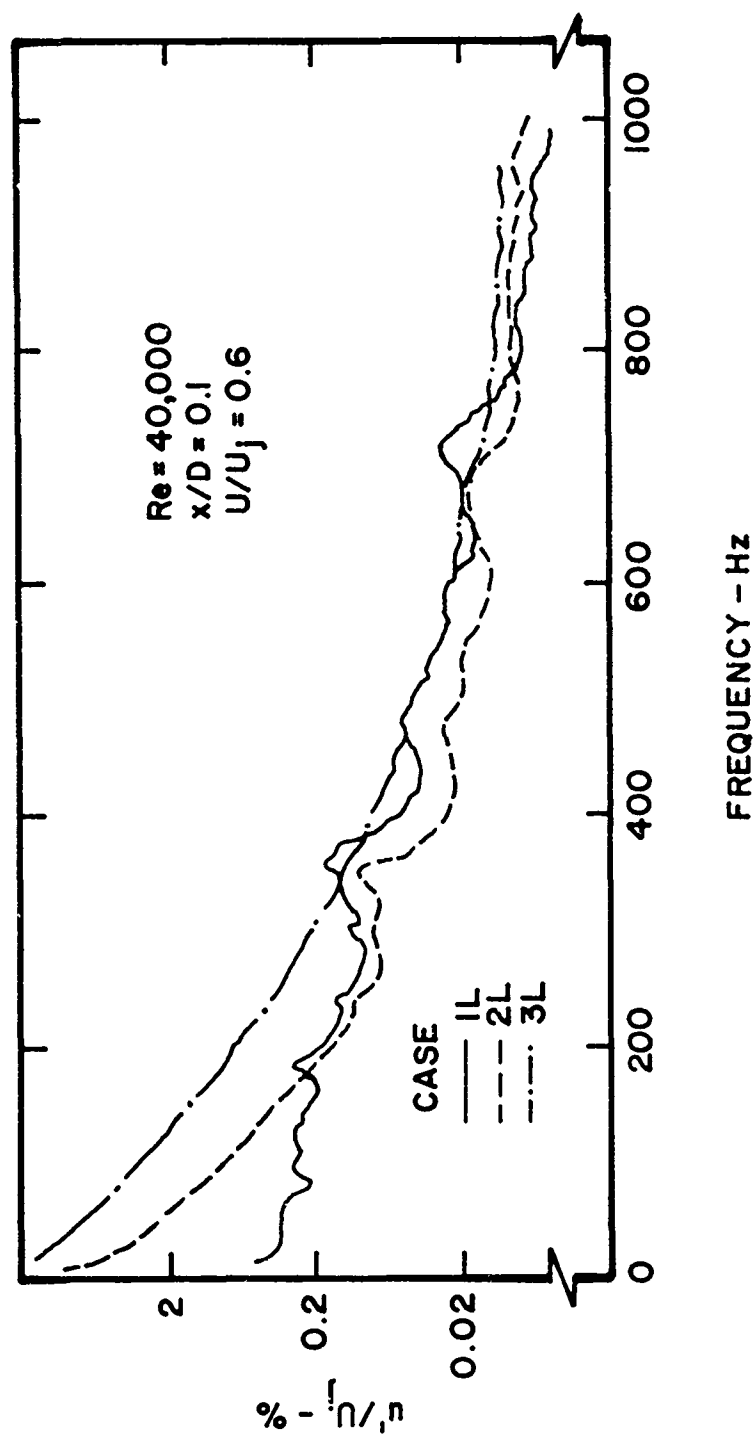
Figure 21. Influence of Initial Disturbance Level on Streamwise Velocity Spectra Near Jet Exit

FLOW
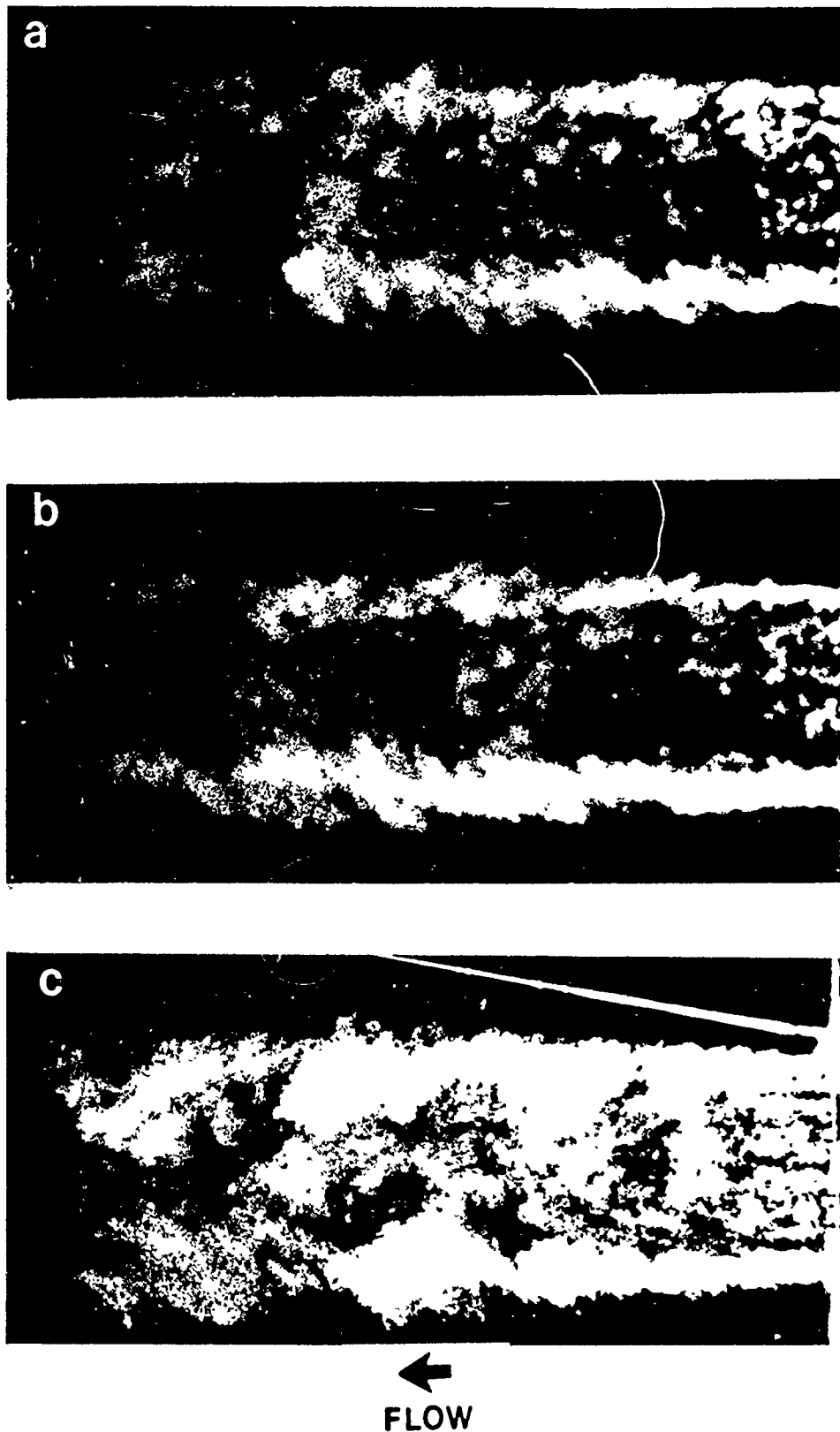
Figure 22. Visualization of Jet Development from Initial
Turbulent Boundary Layers; Case 1T with L/D = 0.75:
(a) Re = 42,000, (b) Re = 65,000, (c) Re = 100,000
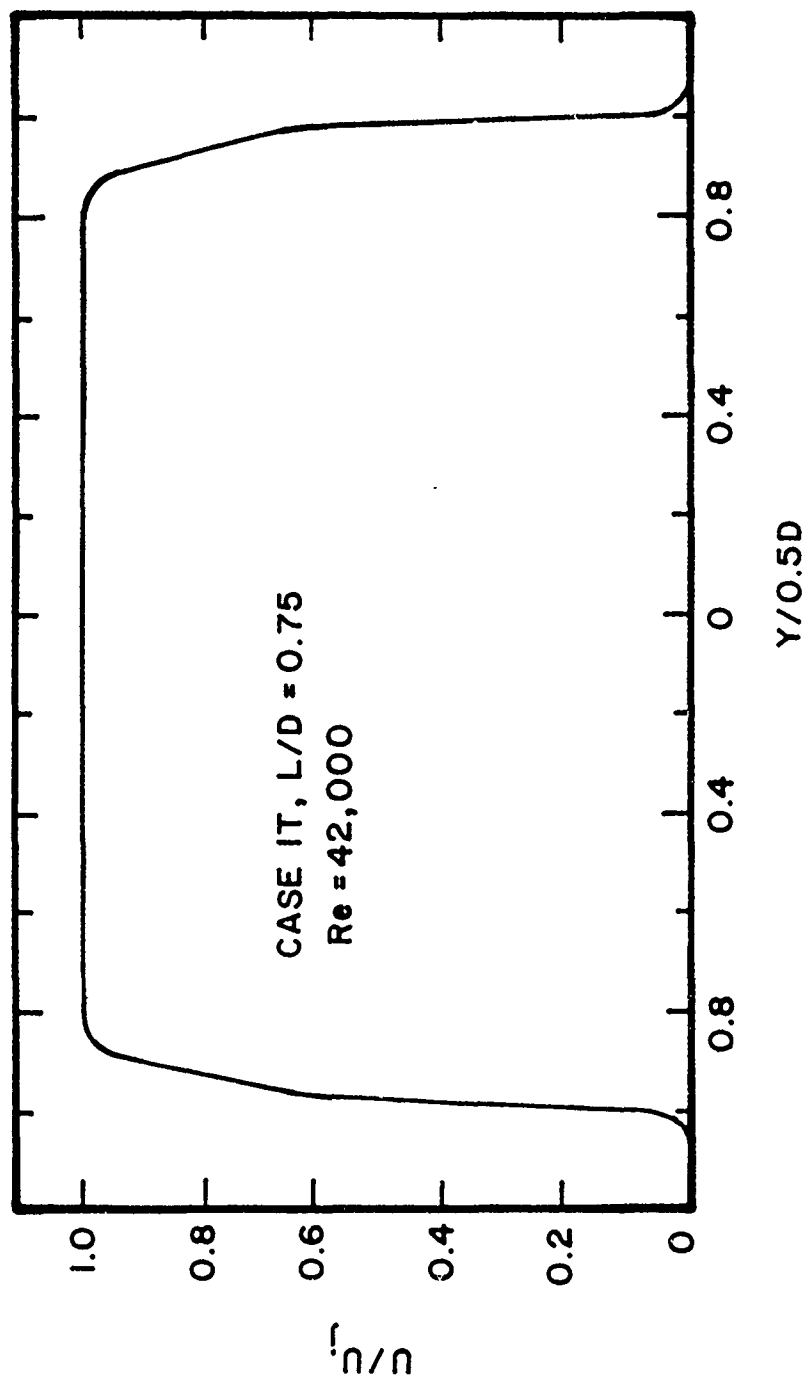
Figure 23. Normalized Mean Velocity Profile for Initial Turbulent Boundary Layer;
Case 1T with L/D = 0.75, Re = 42,000, x/D = 0.05
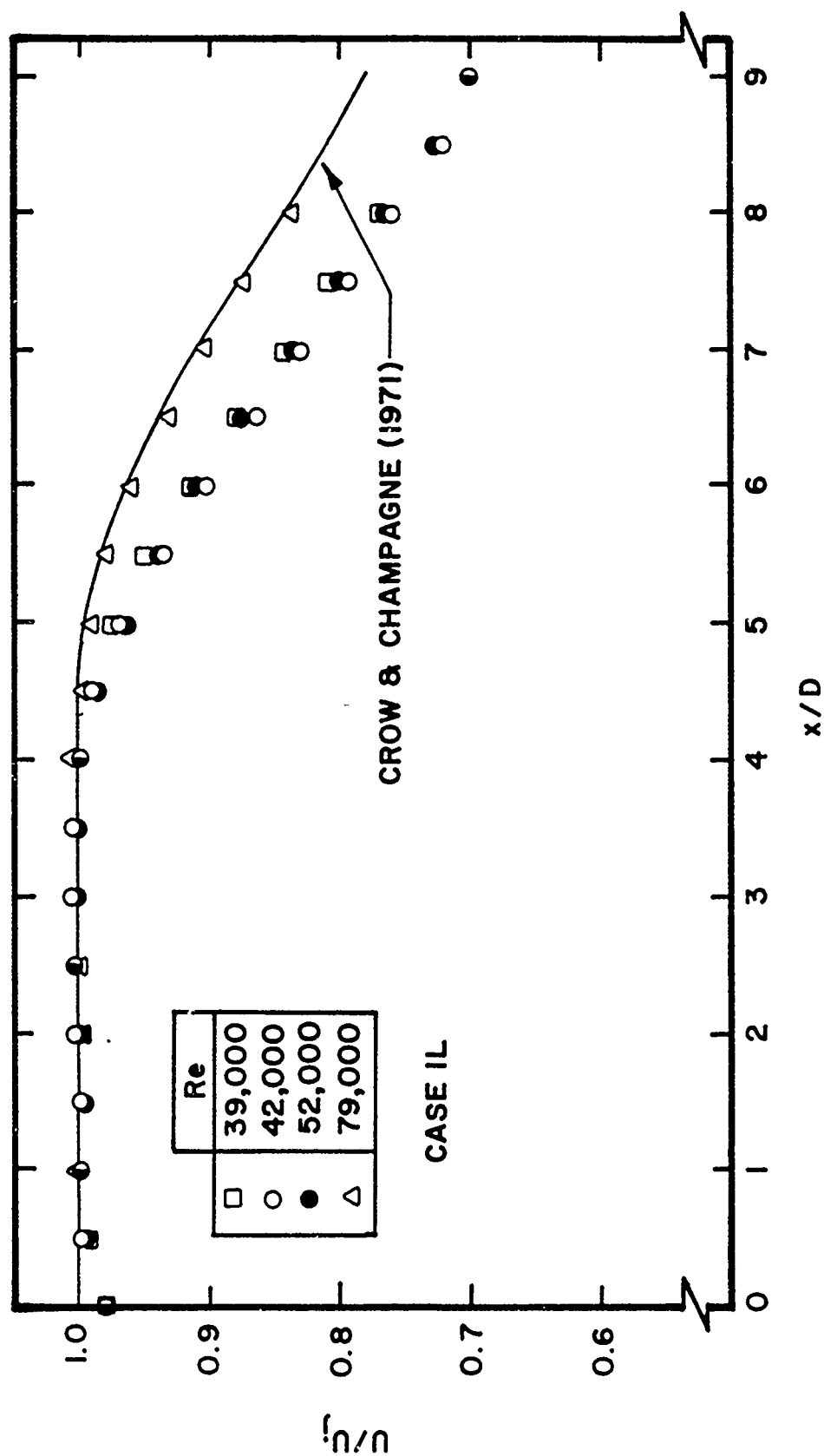
Figure 24. Effect of Reynolds Number on Mean Streamwise Velocity Decay along Jet Centerline for Case 1L
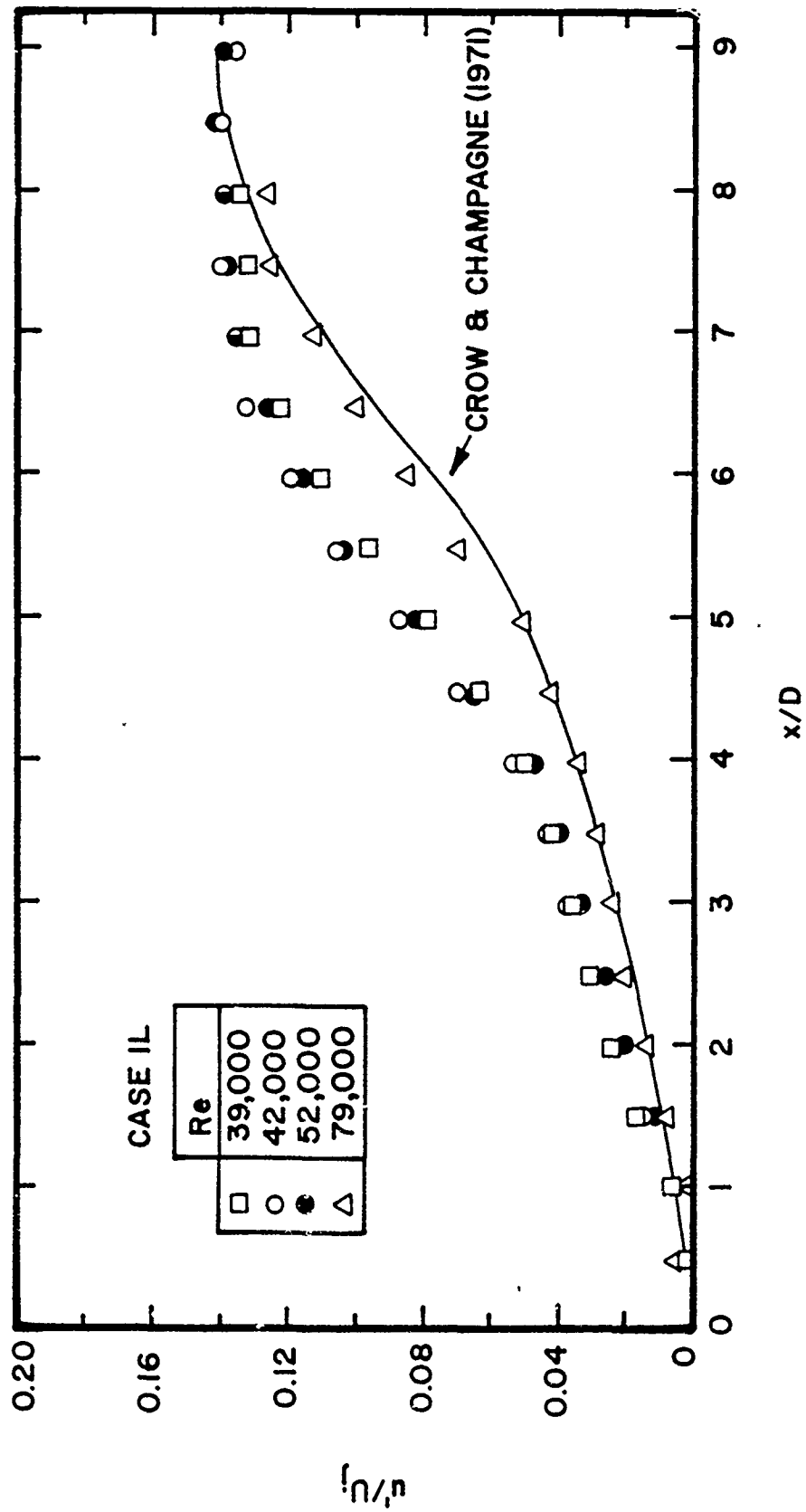
Figure 25. Effect of Reynolds Number on Development of Streamwise Turbulence
Intensity along Jet Centerline for Case 1L

216
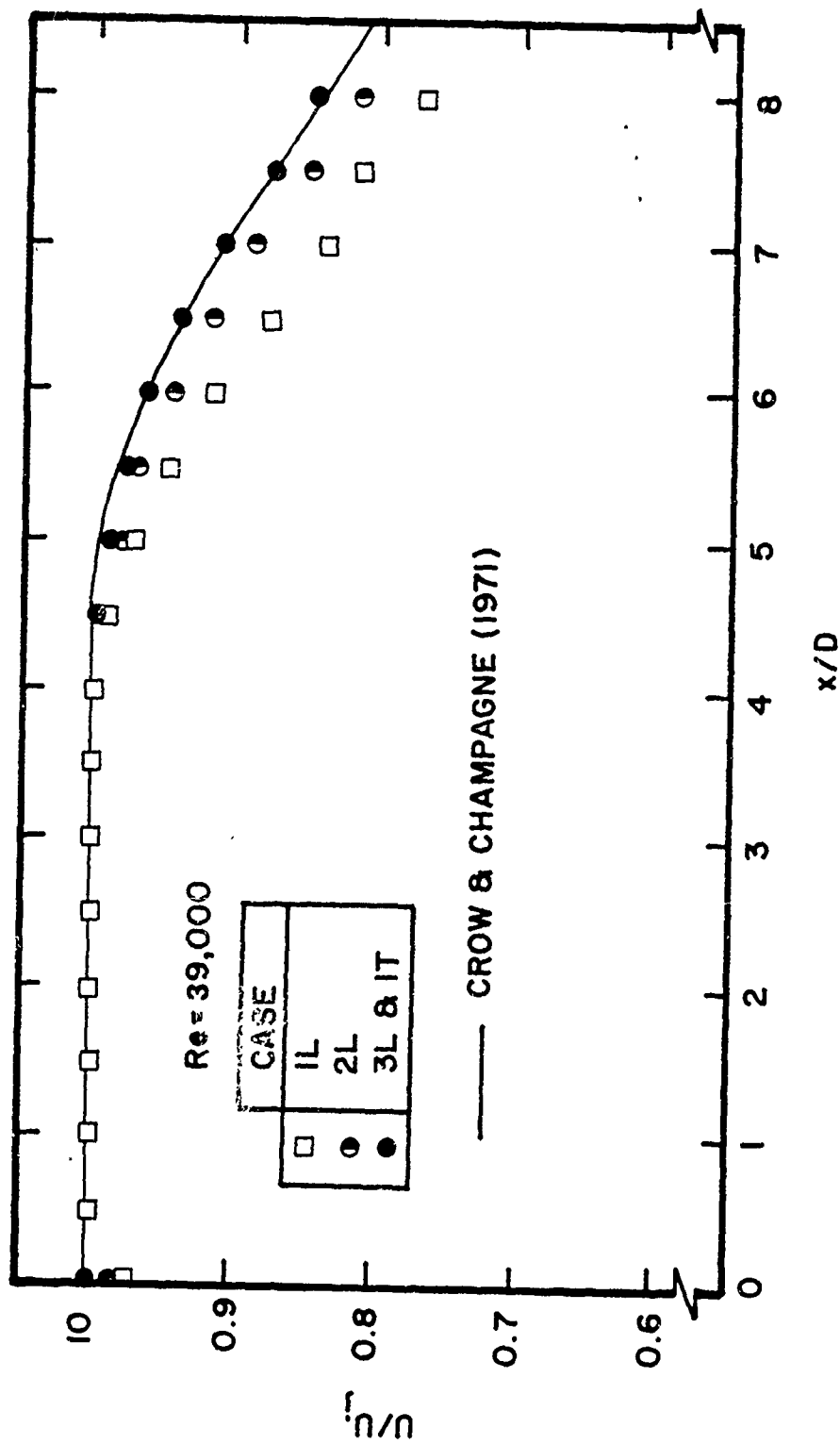
Figure 26. Effect of Initial Disturbance Level on Decay of Mean Streamwise Velocity along Jet Centerline; Re = 39,000
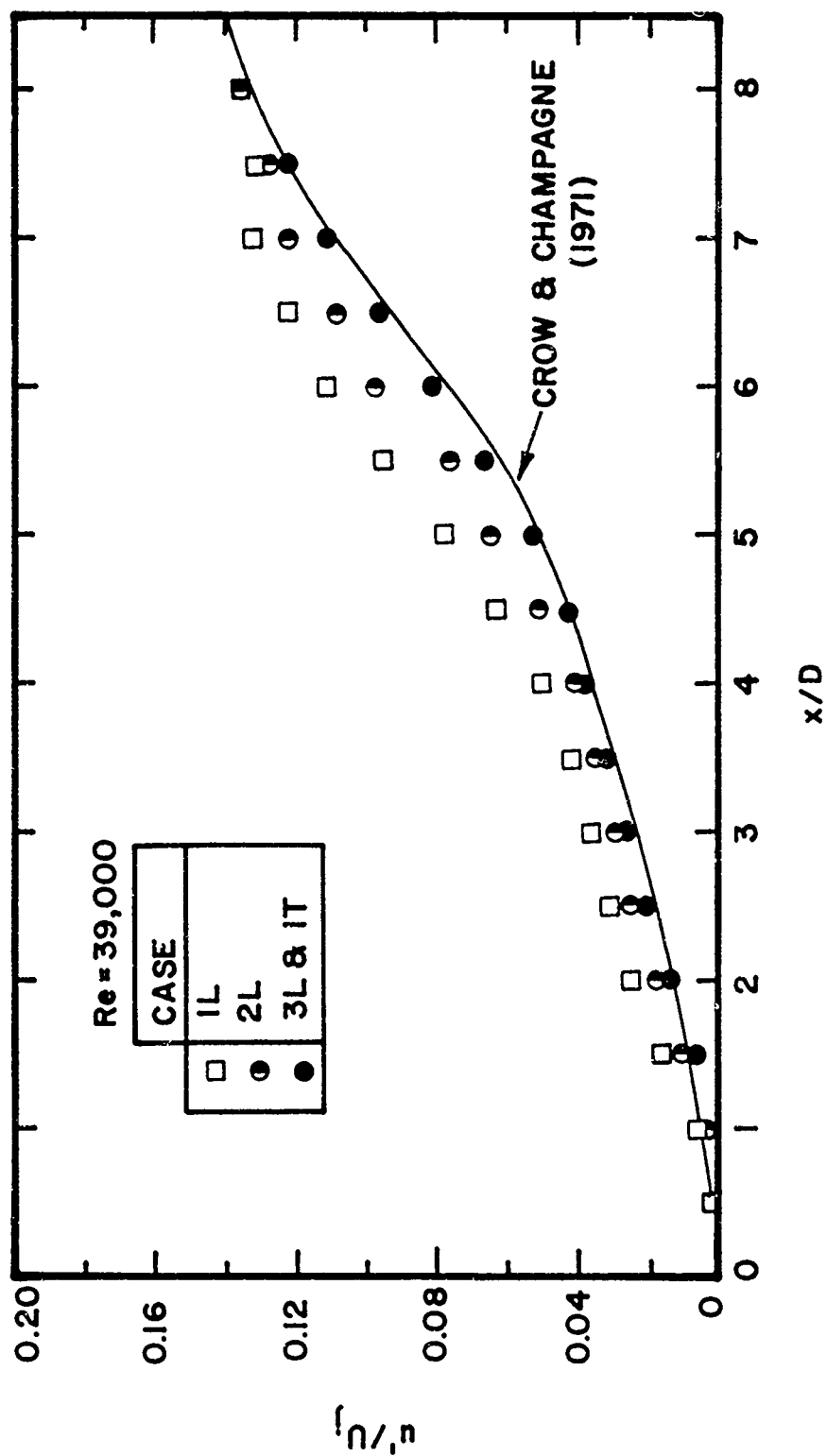
Figure 27. Effect of Initial Disturbance Level on Development of Streamwise Turbulence Intensity along Jet Centerline; Re = 39,000
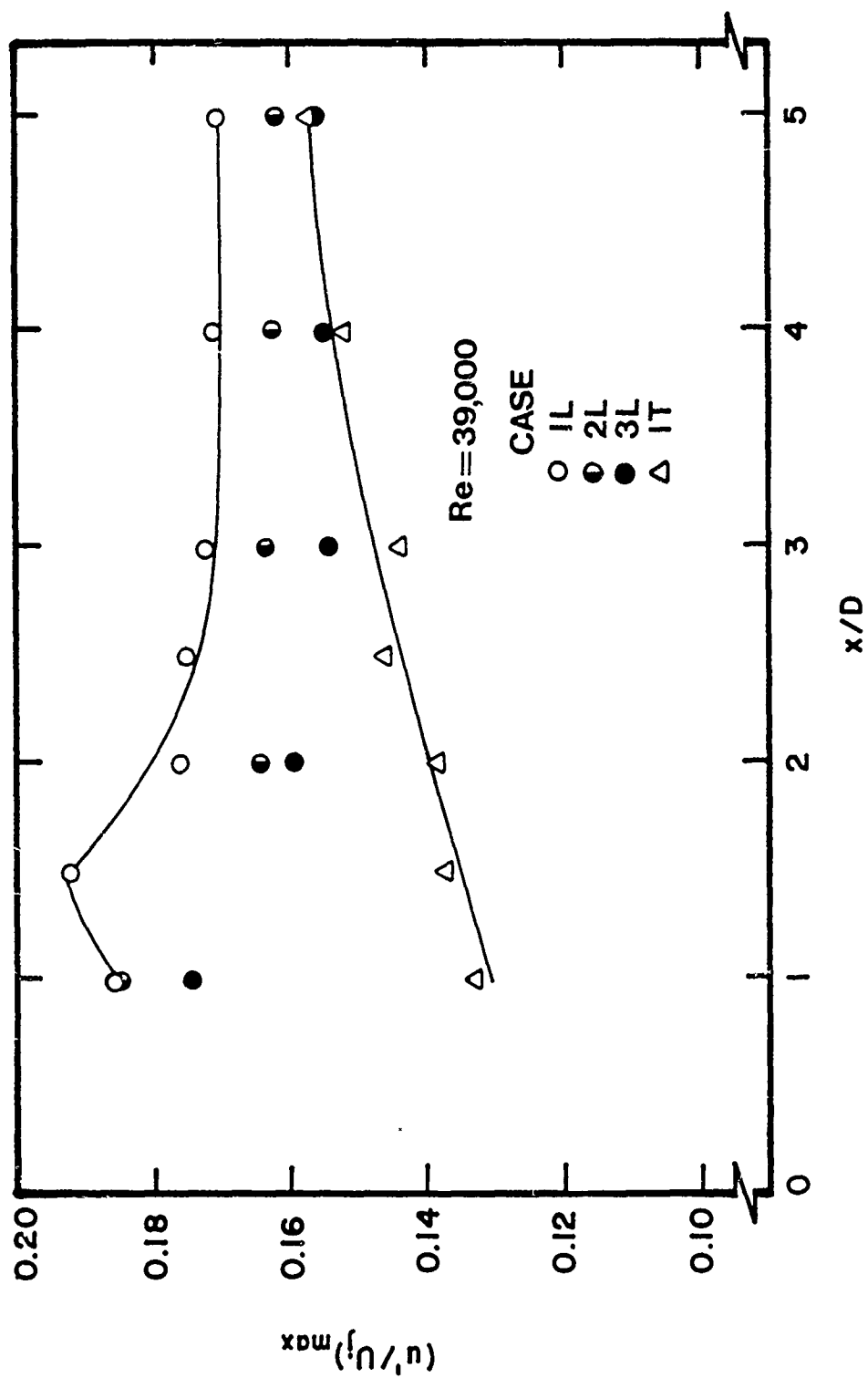
Figure 28. Effect of Initial Disturbance Level on Development of Peak Streamwise Turbulence Intensity
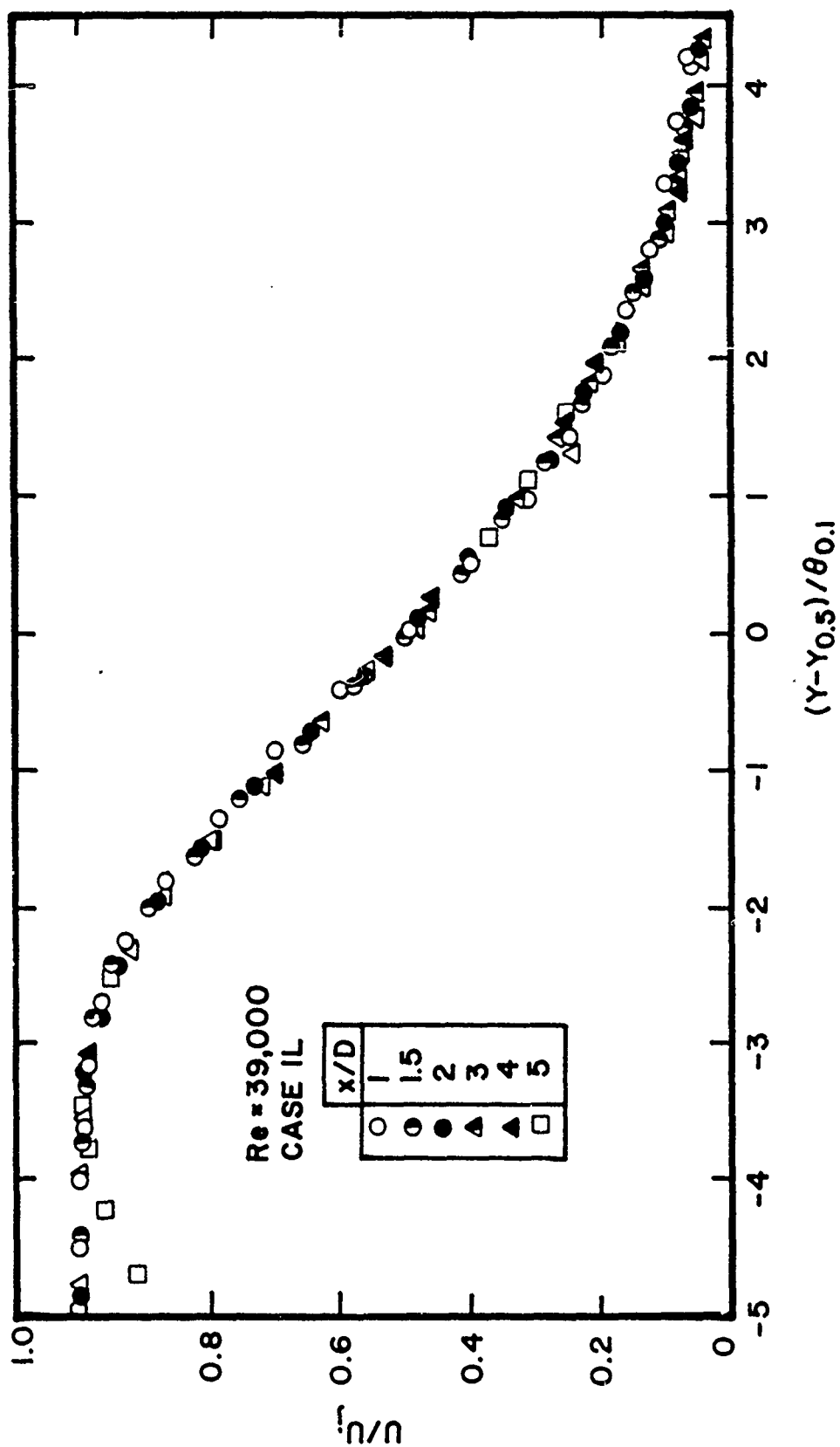
Figure 29. Normalized Mean Streamwise Velocity Profiles for Case 1L at Re = 39,000
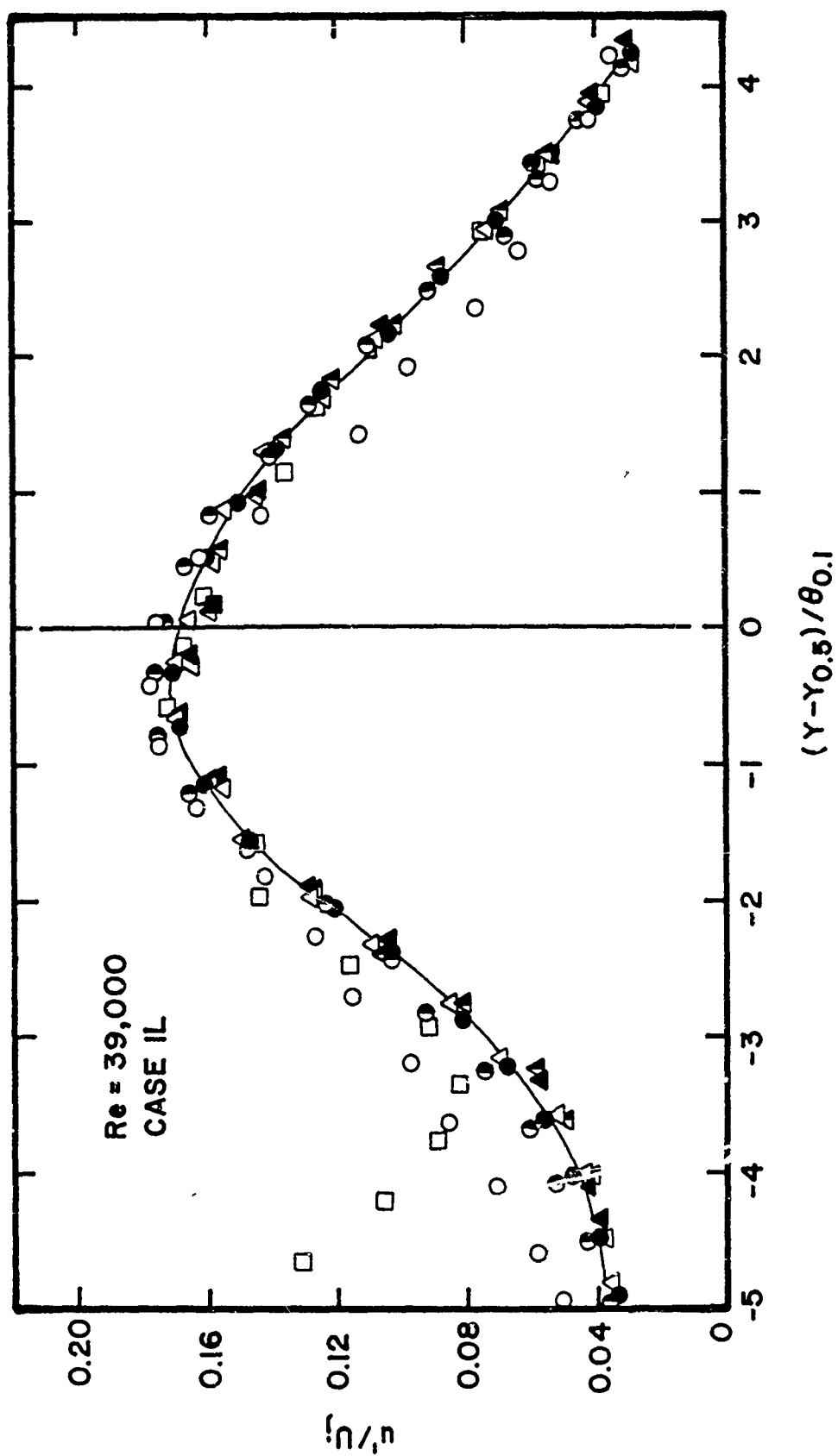
Figure 30. Normalized Streamwise Turbulence Intensity Profiles for Case 1L
at Re = 39,000
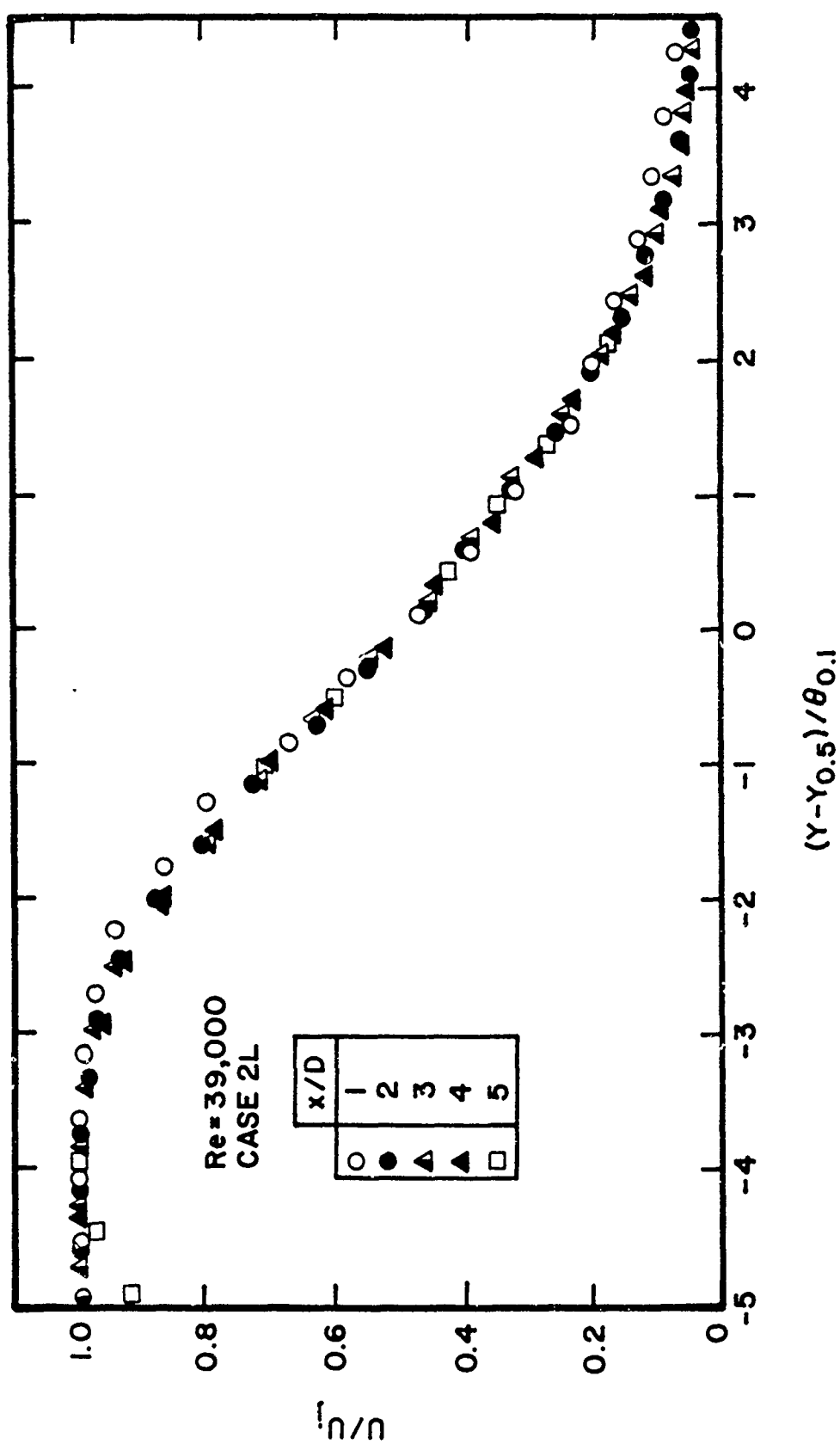
Figure 31. Normalized Mean Streamwise Velocity Profiles for Case 2L at Re = 39,000
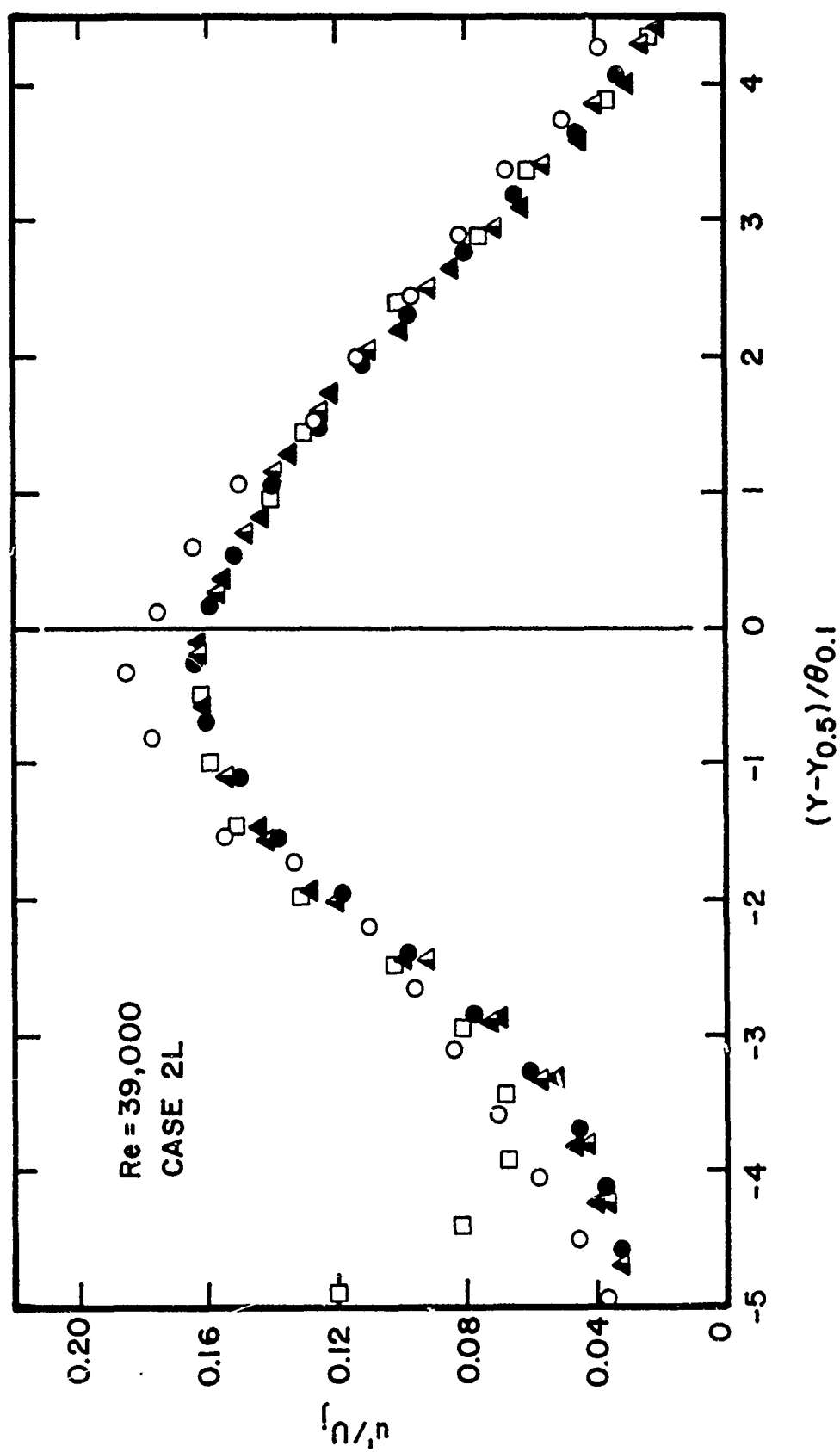
Figure 32. Normalized Streamwise Turbulence Intensity Profiles for Case 2L
at Re = 39,000
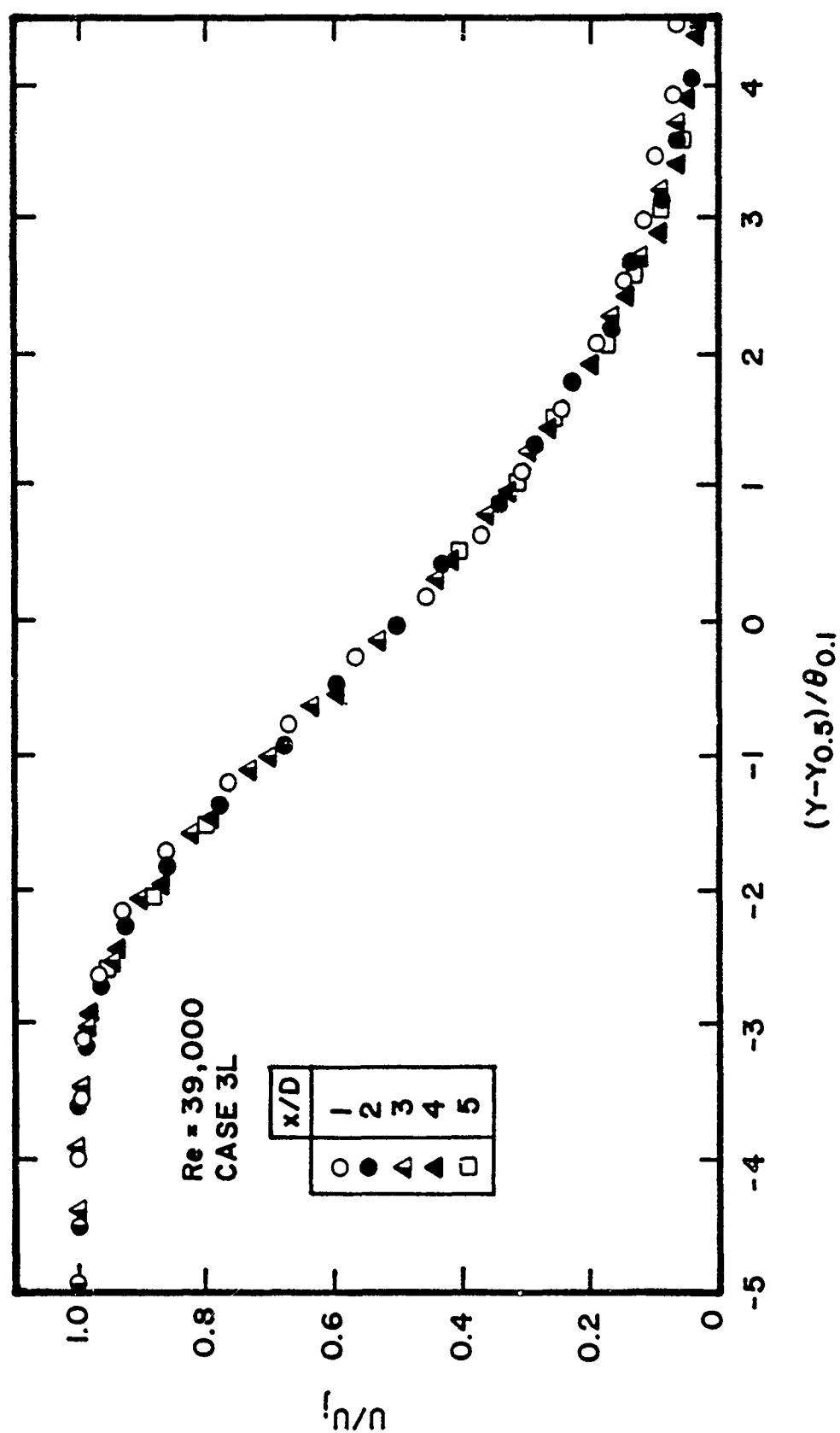
Figure 33. Normalized Mean Streamwise Velocity Profiles for Case 3L at Re = 39,000
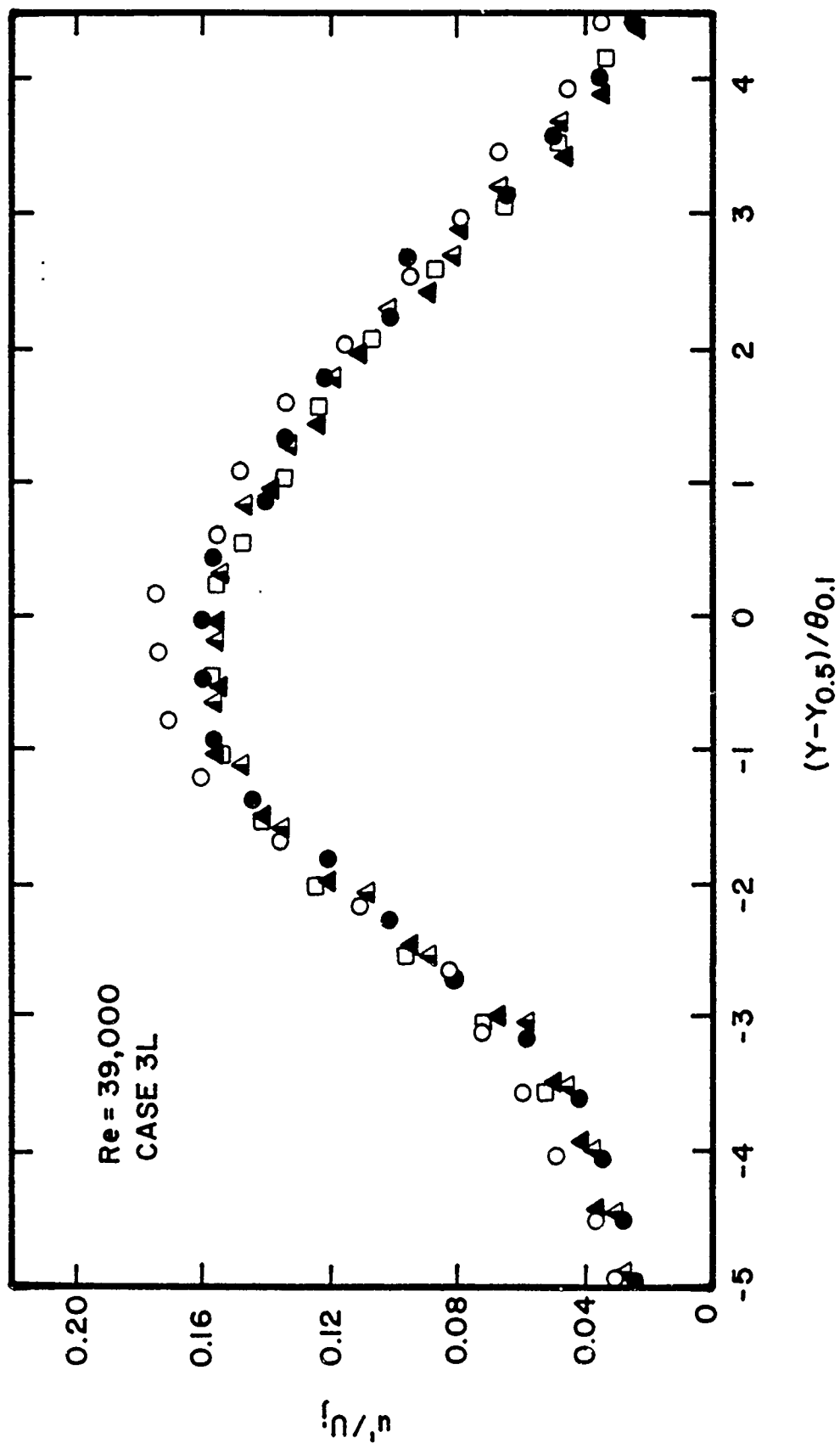
Figure 34. Normalized Streamwise Turbulence Intensity Profiles for Case 3L
at $Re = 39,000$

225
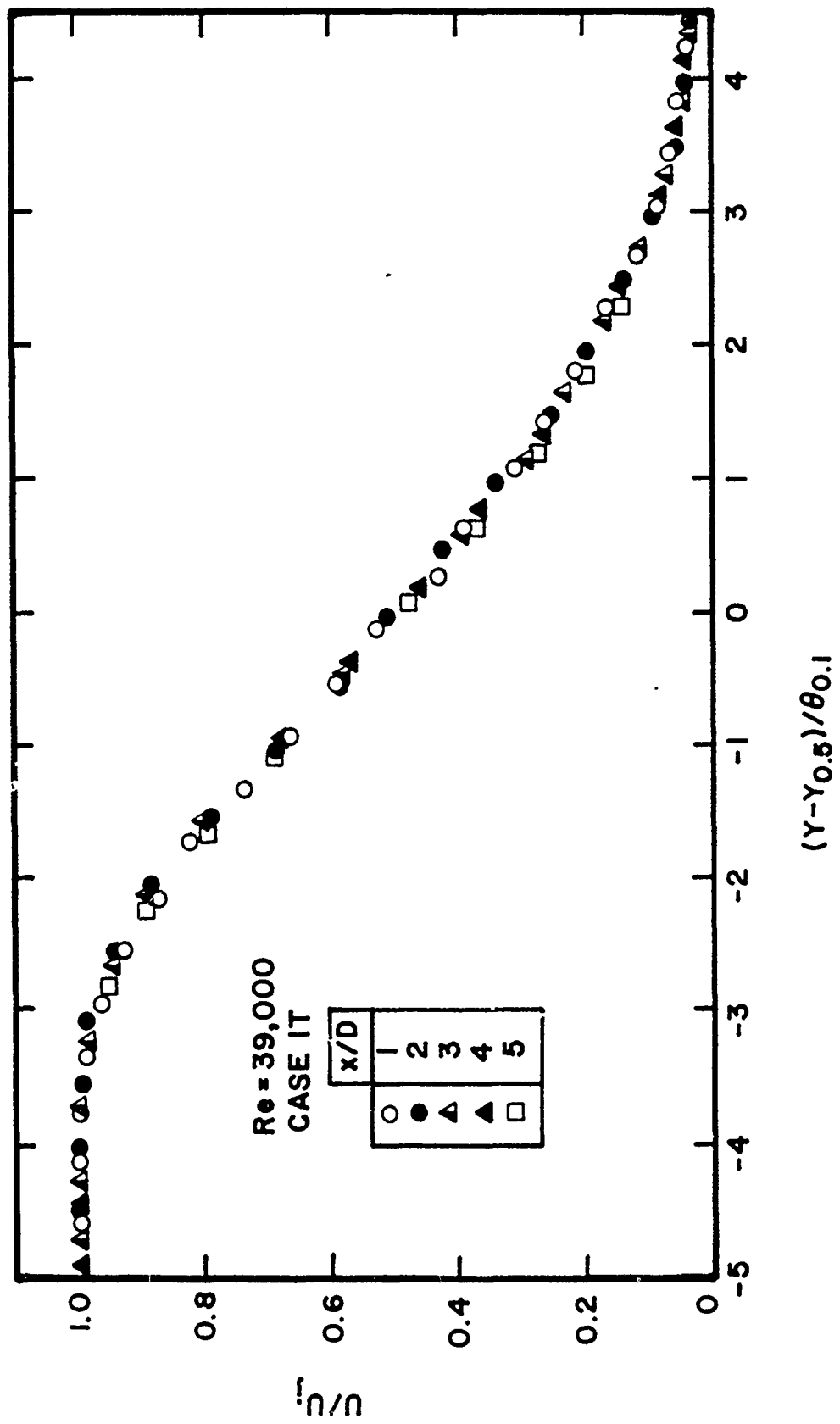
Figure 35. Normalized Mean Streamwise Velocity Profiles for Case 1T with
L/D = 0.75 at Re = 39,000
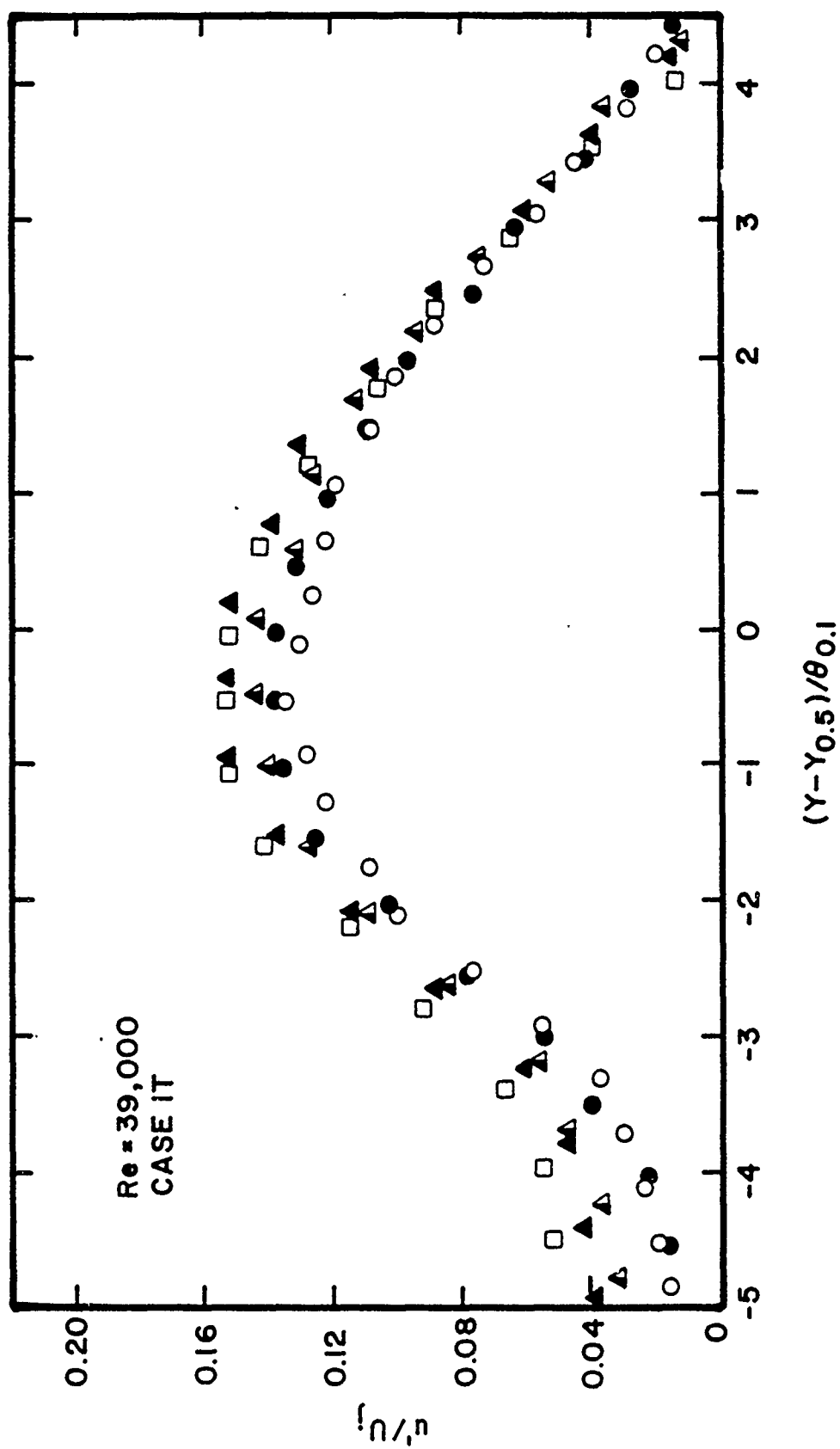
Figure 36. Normalized Streamwise Turbulence Intensity Profiles for Case 1T with
L/D = 0.75 at Re = 39,000
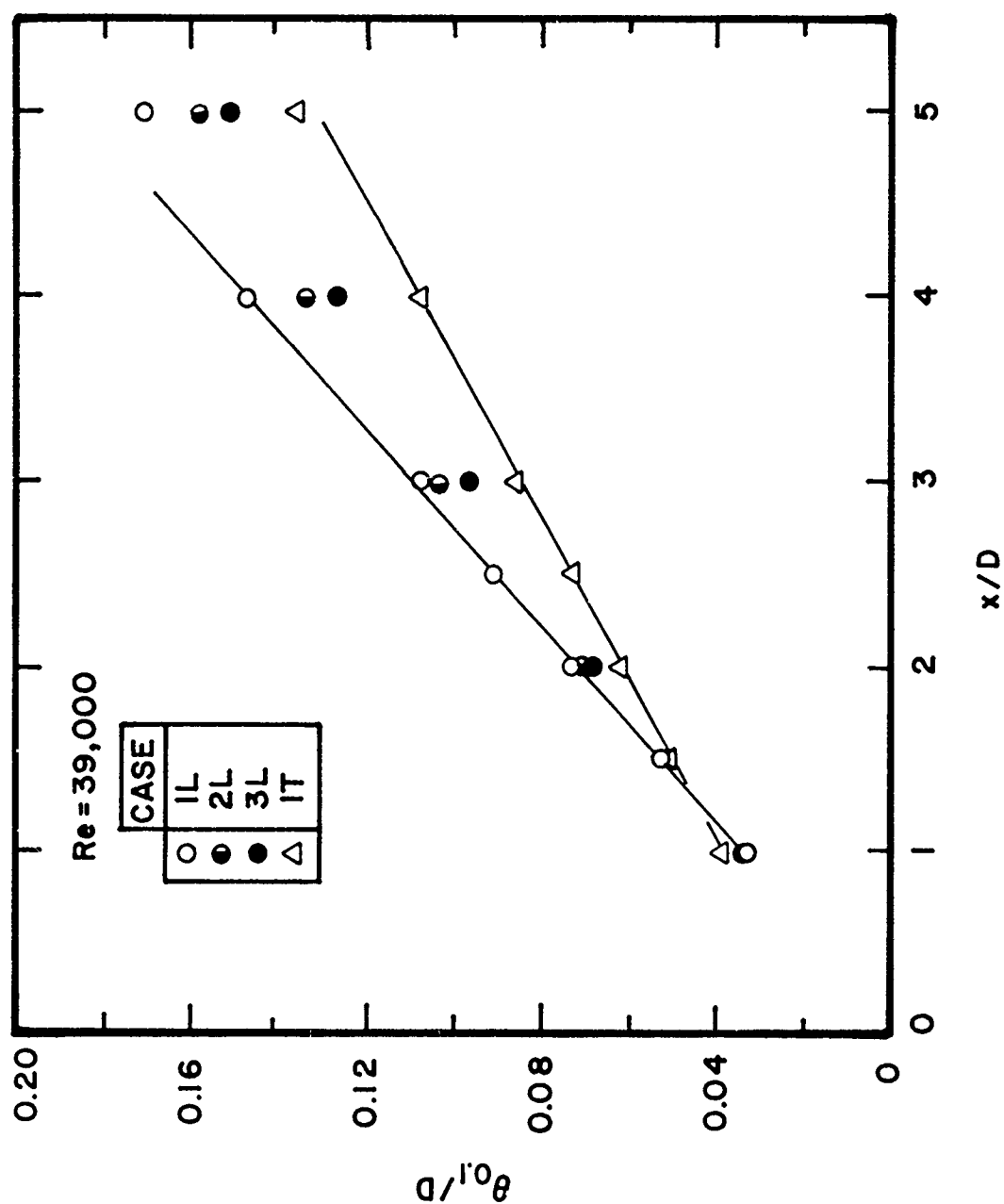
Figure 37. Effect of Initial Conditions on Jet Growth at Re = 39,000

228
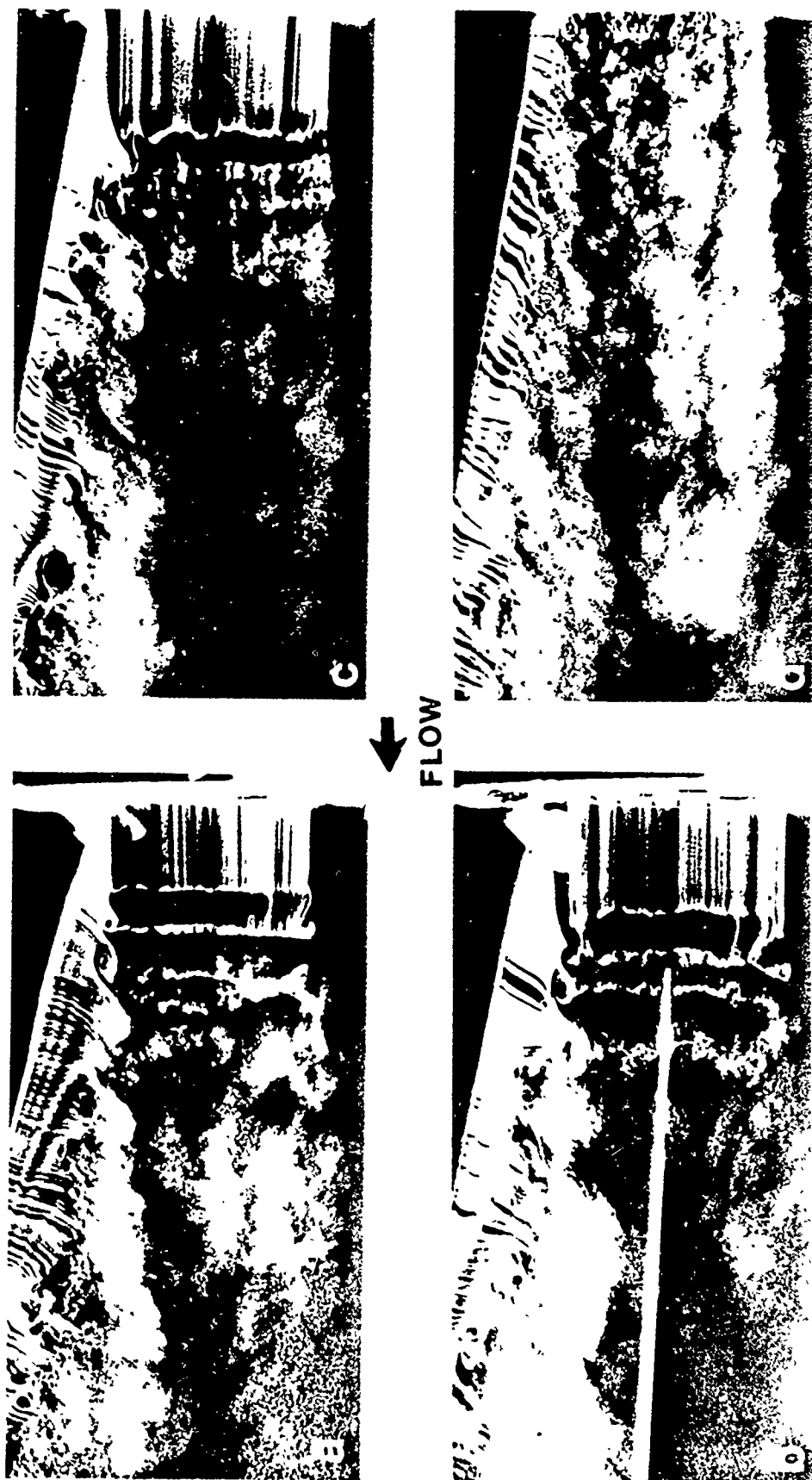
Figure 38. Flow Visualization at Re = 40,000 Showing Azimuthal Development of and Entrainment into the Jet and Illustrating the Effect of Initial Conditions on its Growth: (a) Case 1L, (b) Case 2L, (c) Case 3L, (d) Case 1T with L/D = 0.75
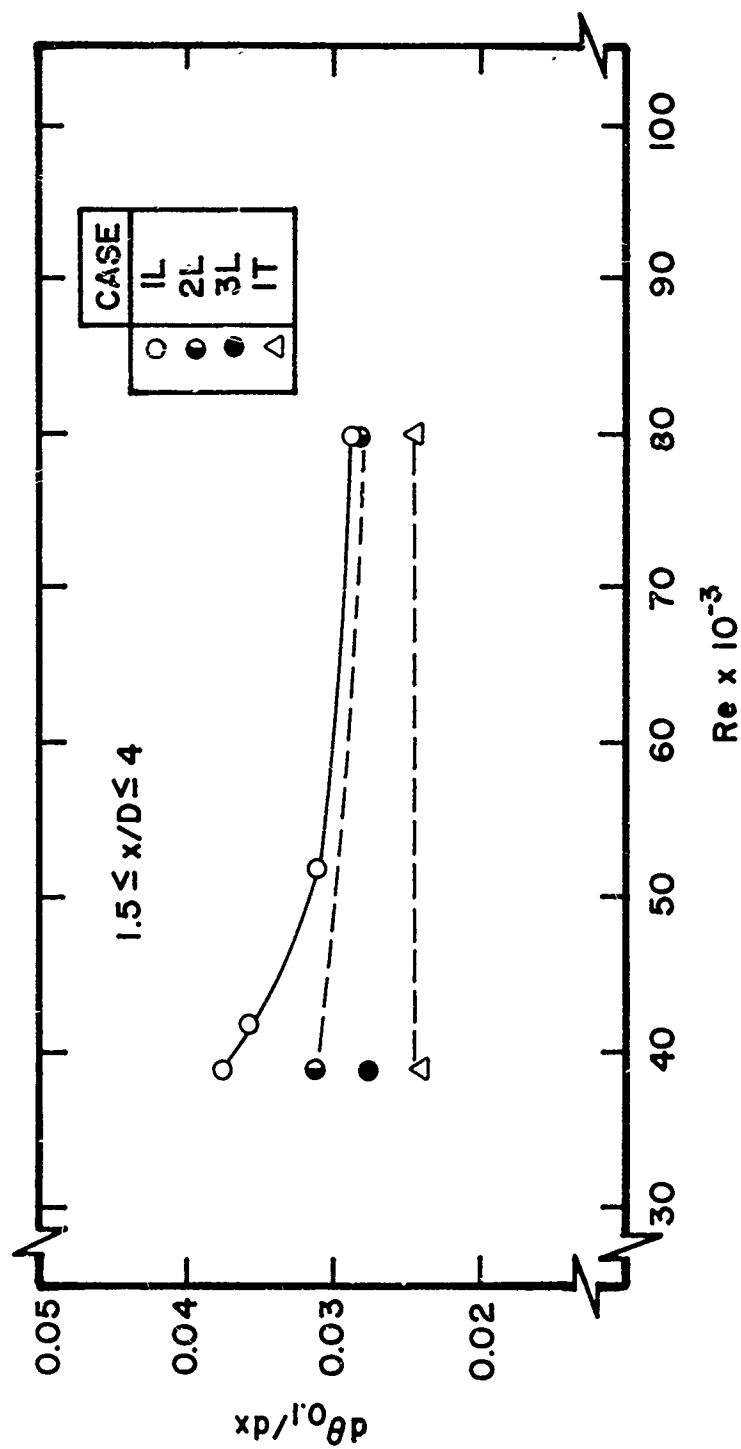
Figure 39. Effect of Reynolds Number and Initial Conditions on Jet Growth Rate
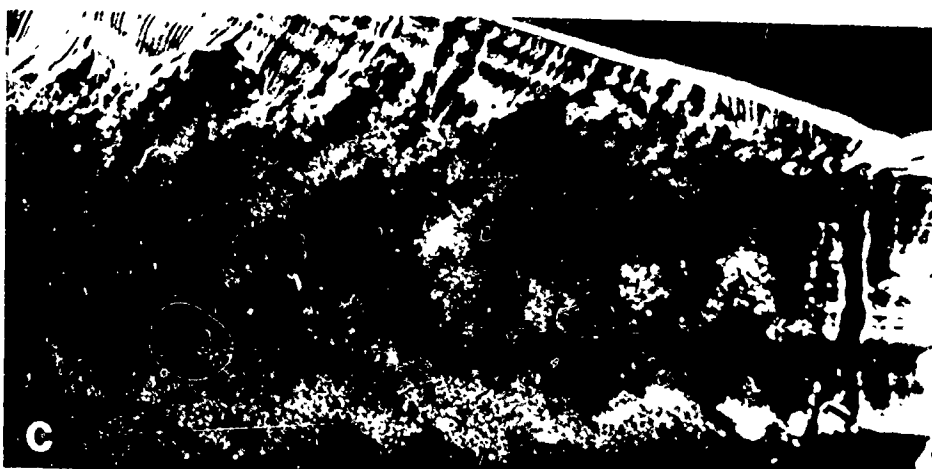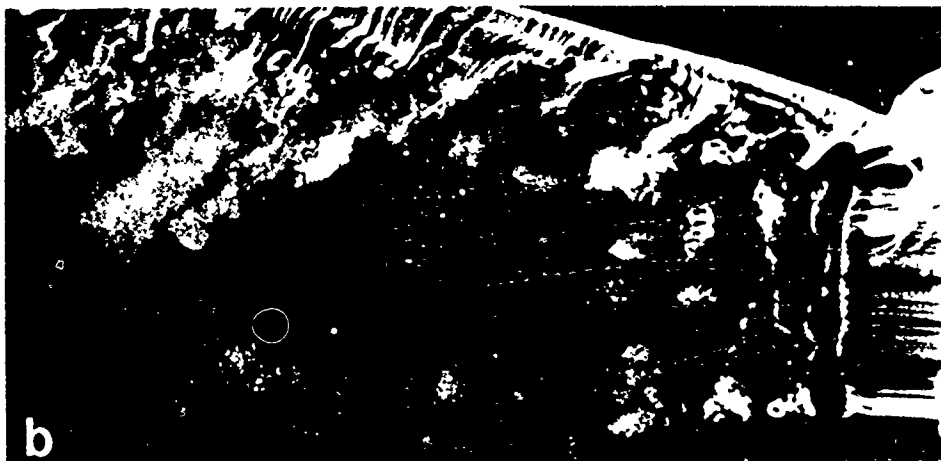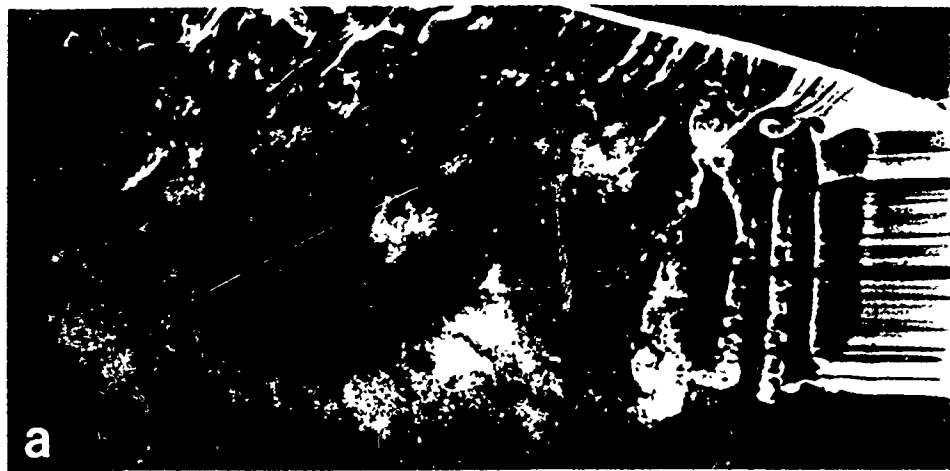
FLOW

Figure 40. Flow Visualization Illustrating Effect of
Reynolds Number on Entrainment into Jet for Case 1L:
(a) Re = 42,000, (b) Re = 52,000, (c) Re = 80,000
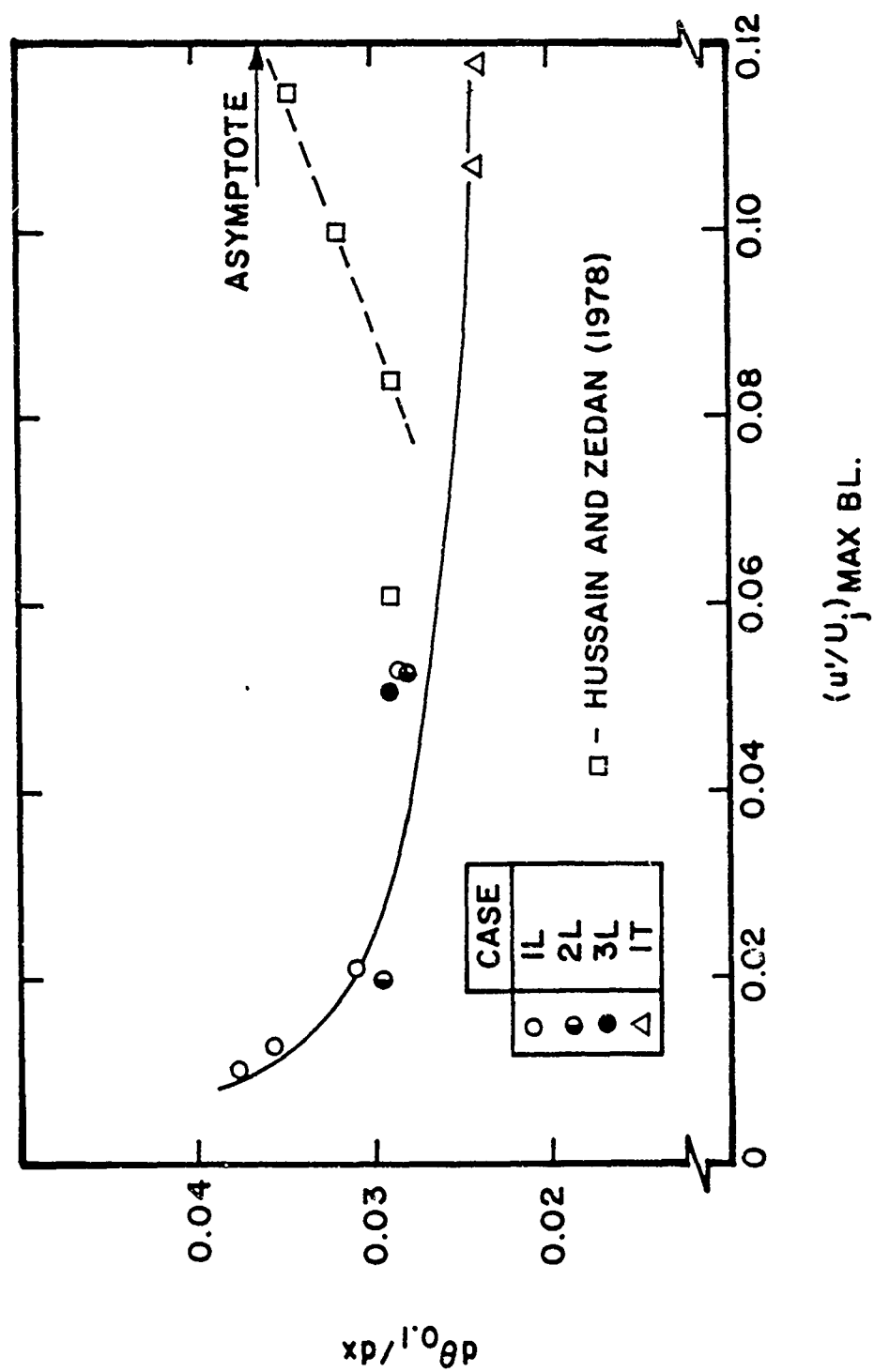
Figure 41. Effect of Peak Turbulence Intensity Level in Exit Boundary Layer on Jet Growth Rate
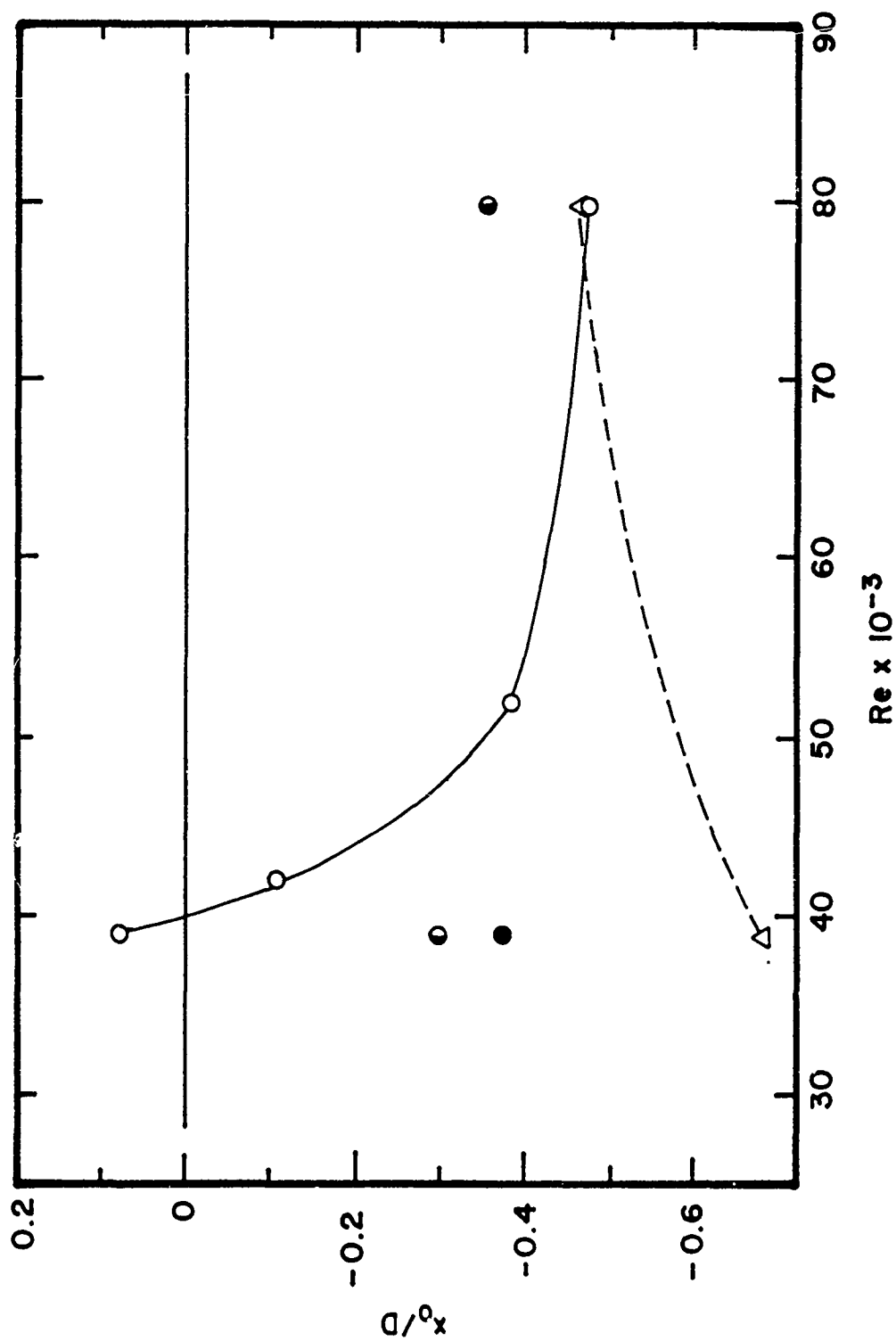
Figure 42. Variation of Jet Virtual Origin with Reynolds Number and Initial Conditions
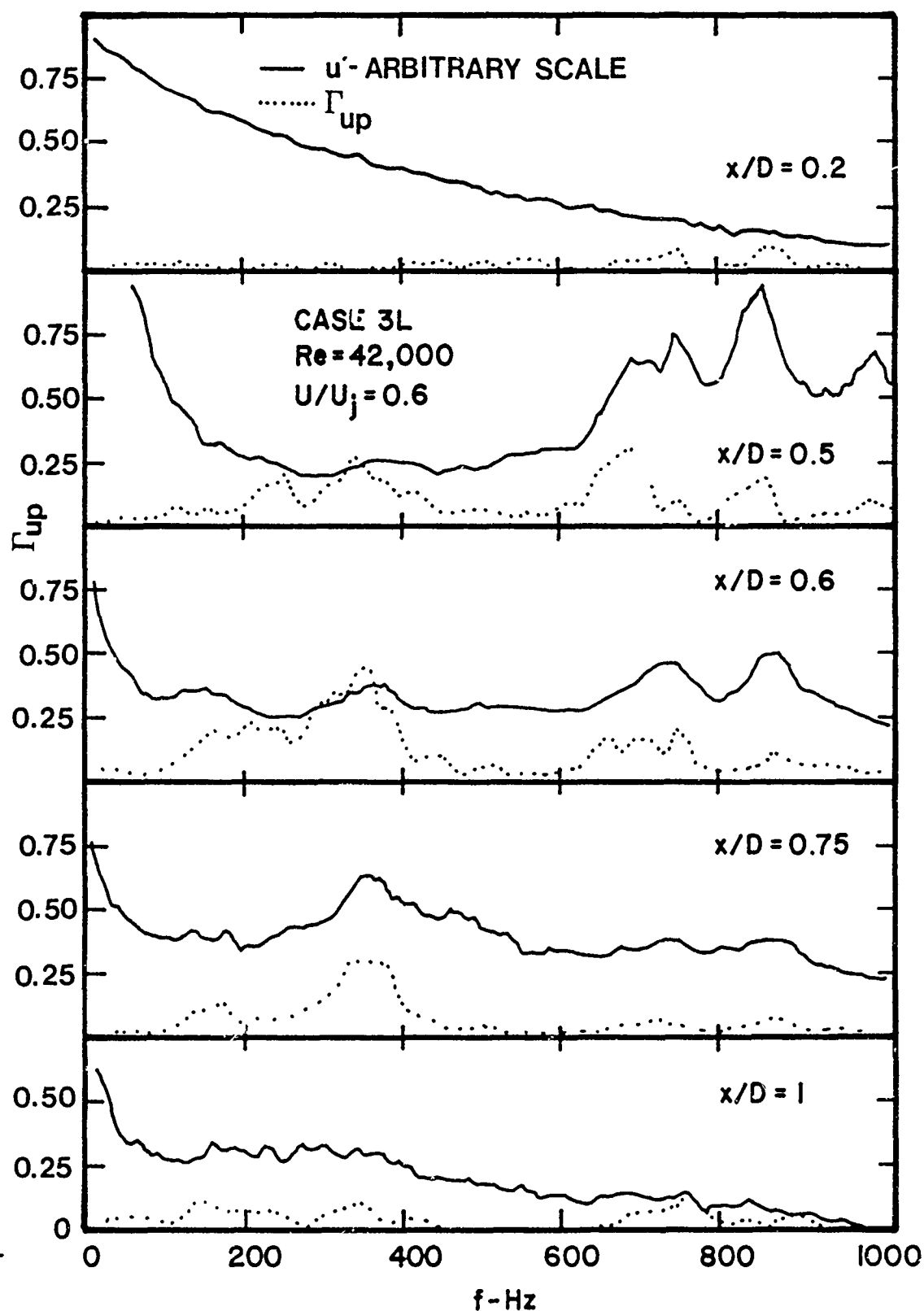
Figure 43. Development of Streamwise Velocity Spectrum
and Coherence Between Velocity and Near-Field Pressure;
Case 3L, Re = 42,000, U/U$_j$ = 0.6
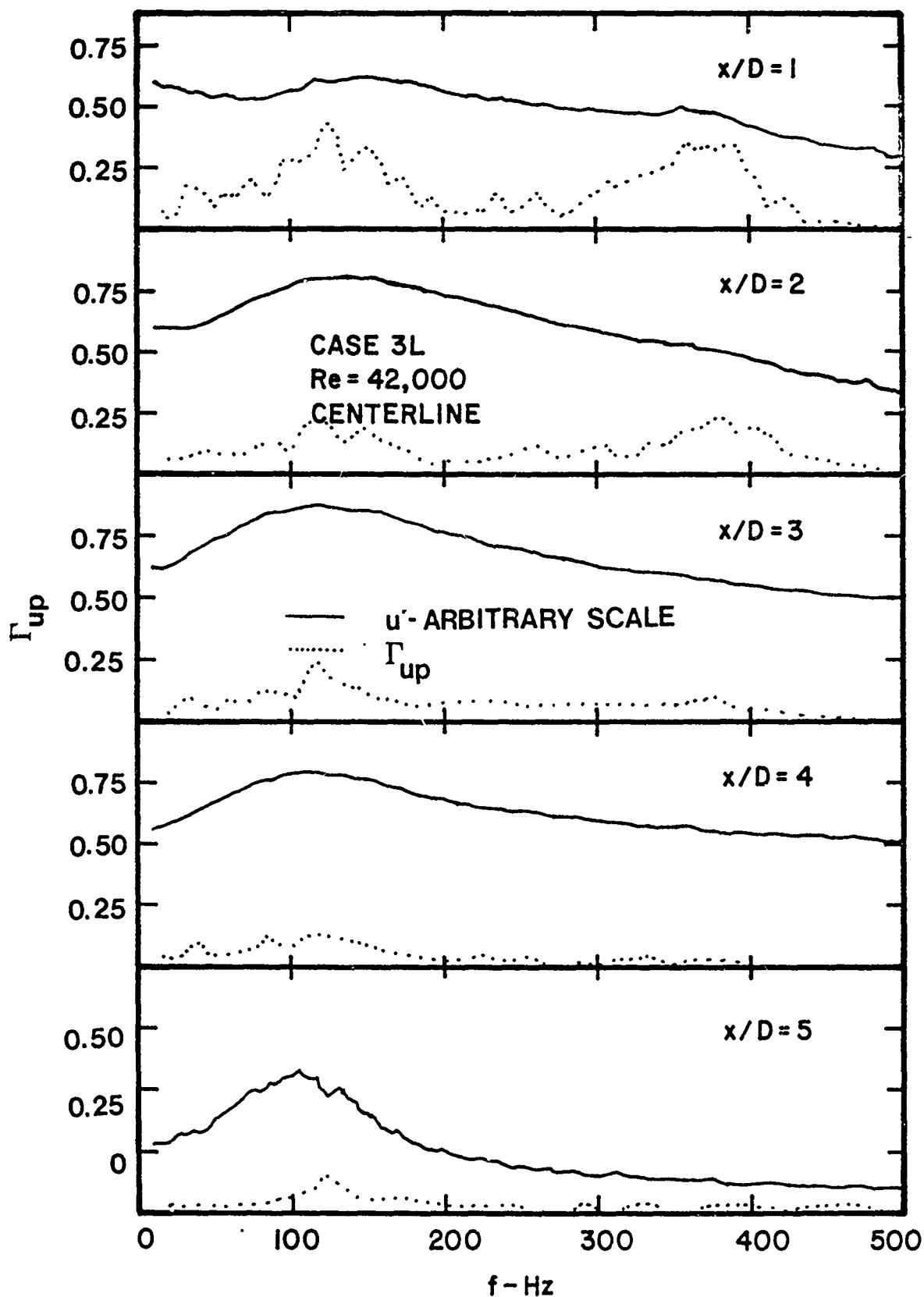
Figure 44. Development of Streamwise Velocity Spectrum
and Coherence Between Velocity and Near-Field Pressure;
Case 3L, Re = 42,000, Jet Centerline
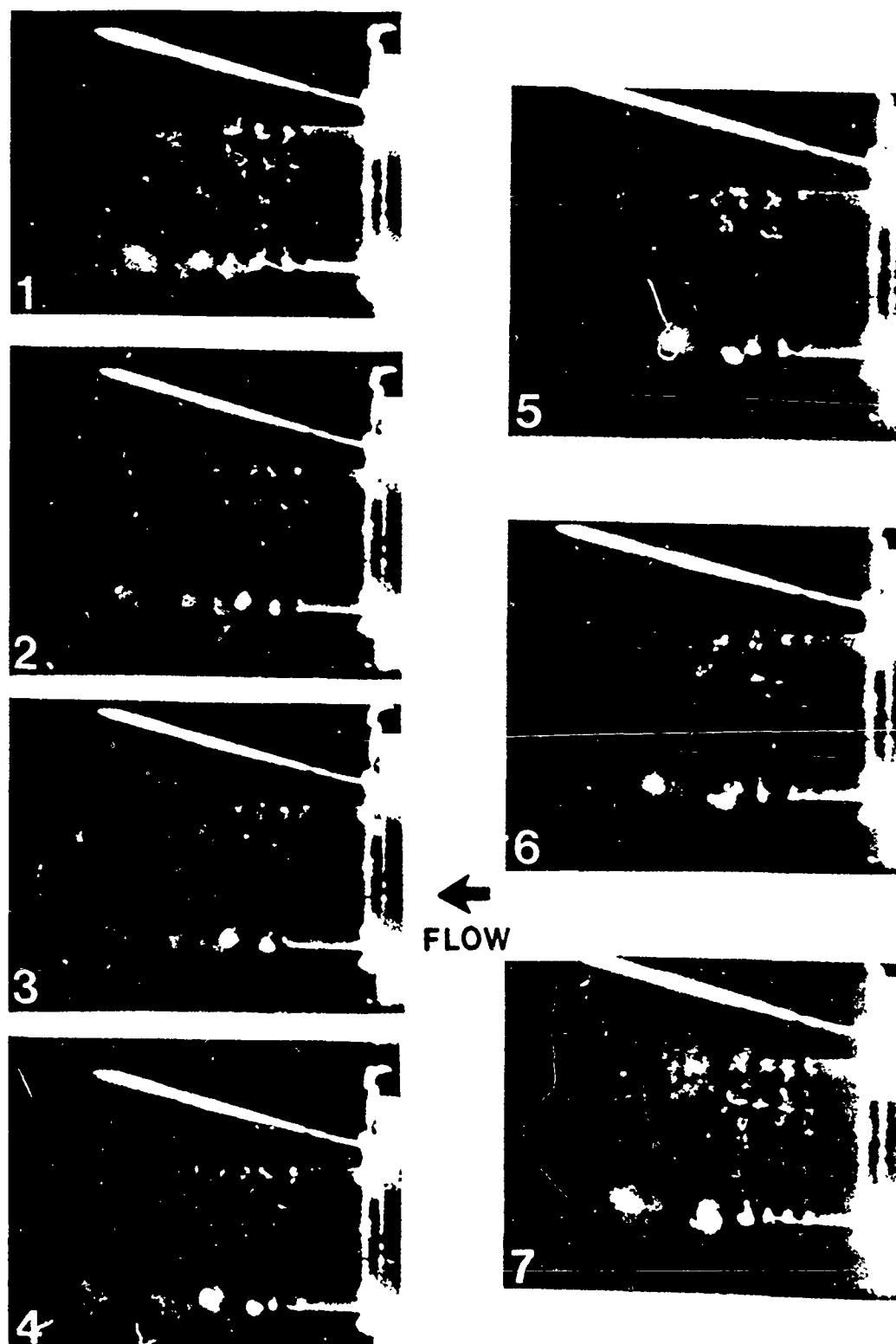
FLOW

Figure 45. Flow Visualization Sequence Taken from a
High Speed Movie for Case 3L at Re = 39,000
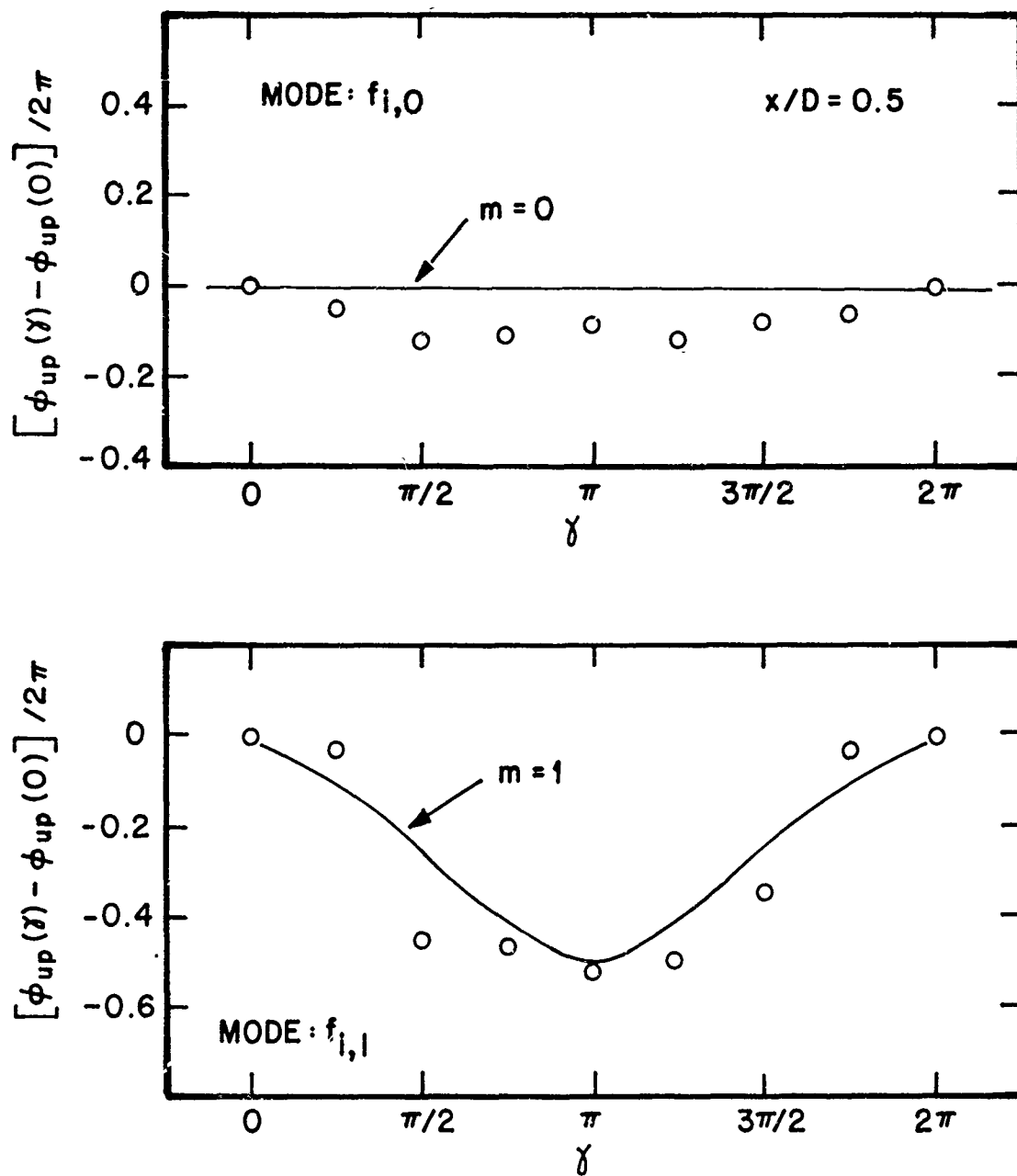
Figure 46. Azimuthal Phase Variation of Initial
Axisymmetric and Helical Modes
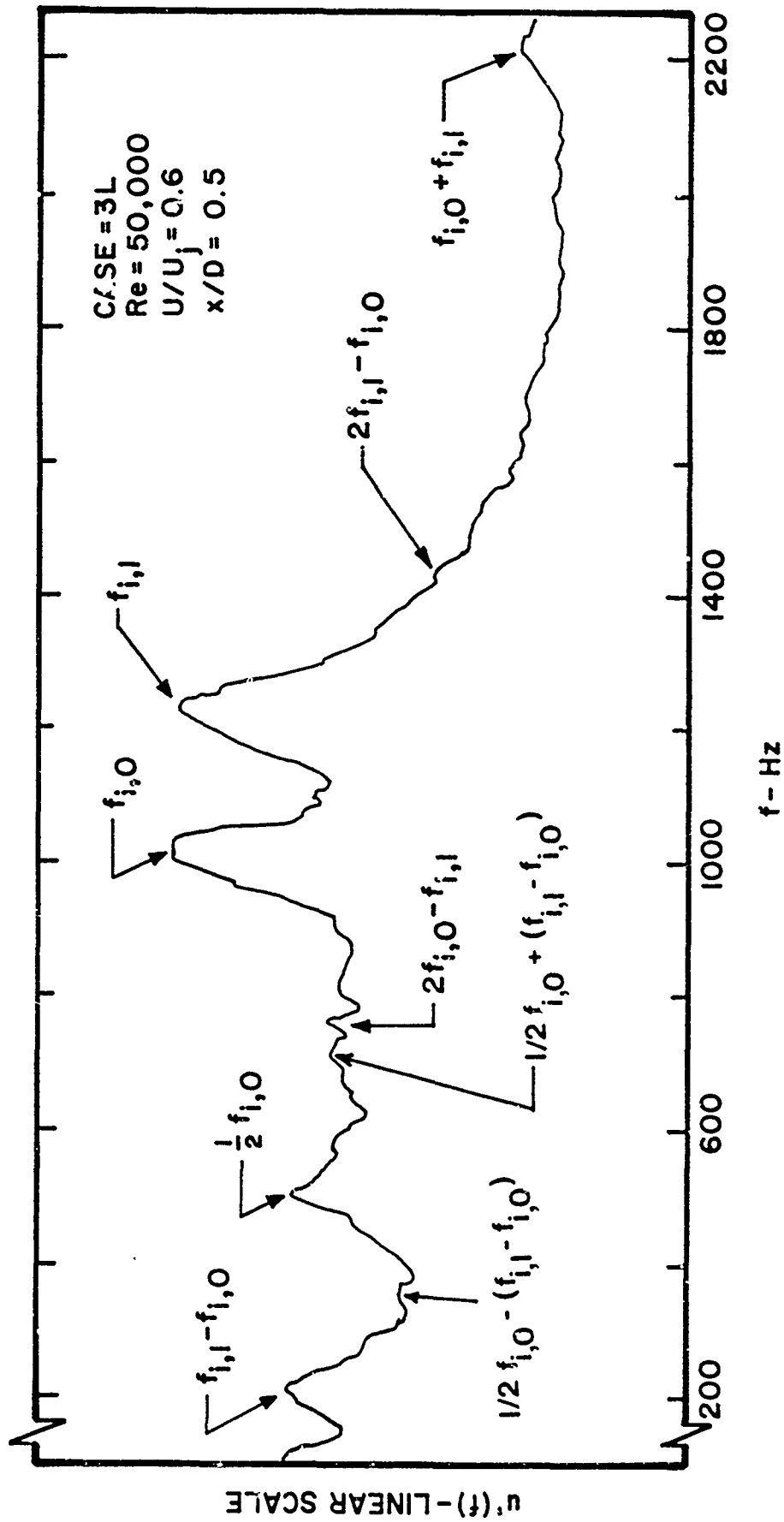
Figure 47. Velocity Spectrum for Case 3L at Re = 50,000 and U/U_j= 0.6 Detailing Nonlinear Interactions Between m = 0, m = 1 and Subharmonic Modes
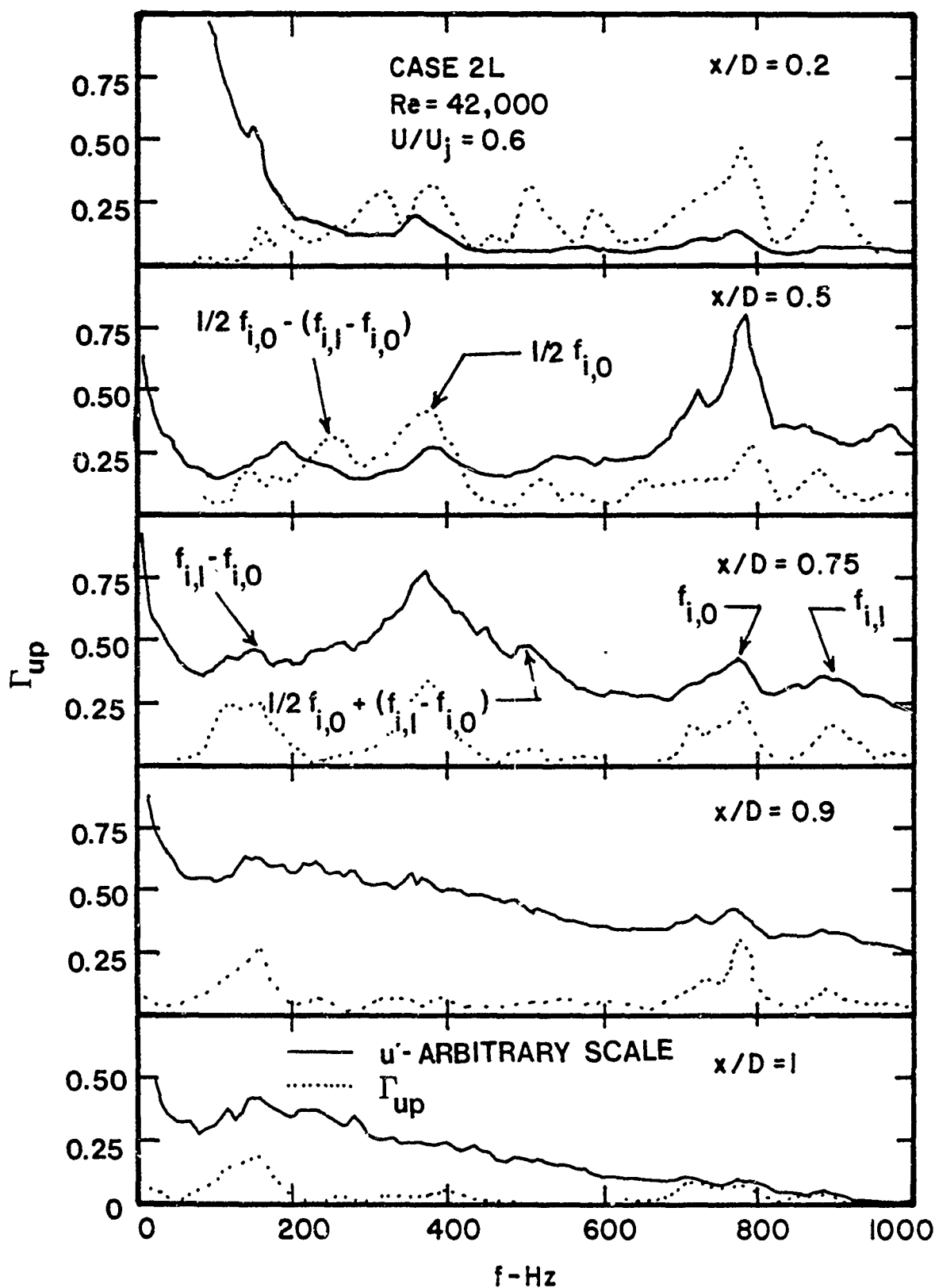
Figure 48. Development of Streamwise Velocity Spectrum and Coherence Between Velocity and Near-Field Pressure; Case 2L, Re = 42,000, $U/U_j = 0.6$
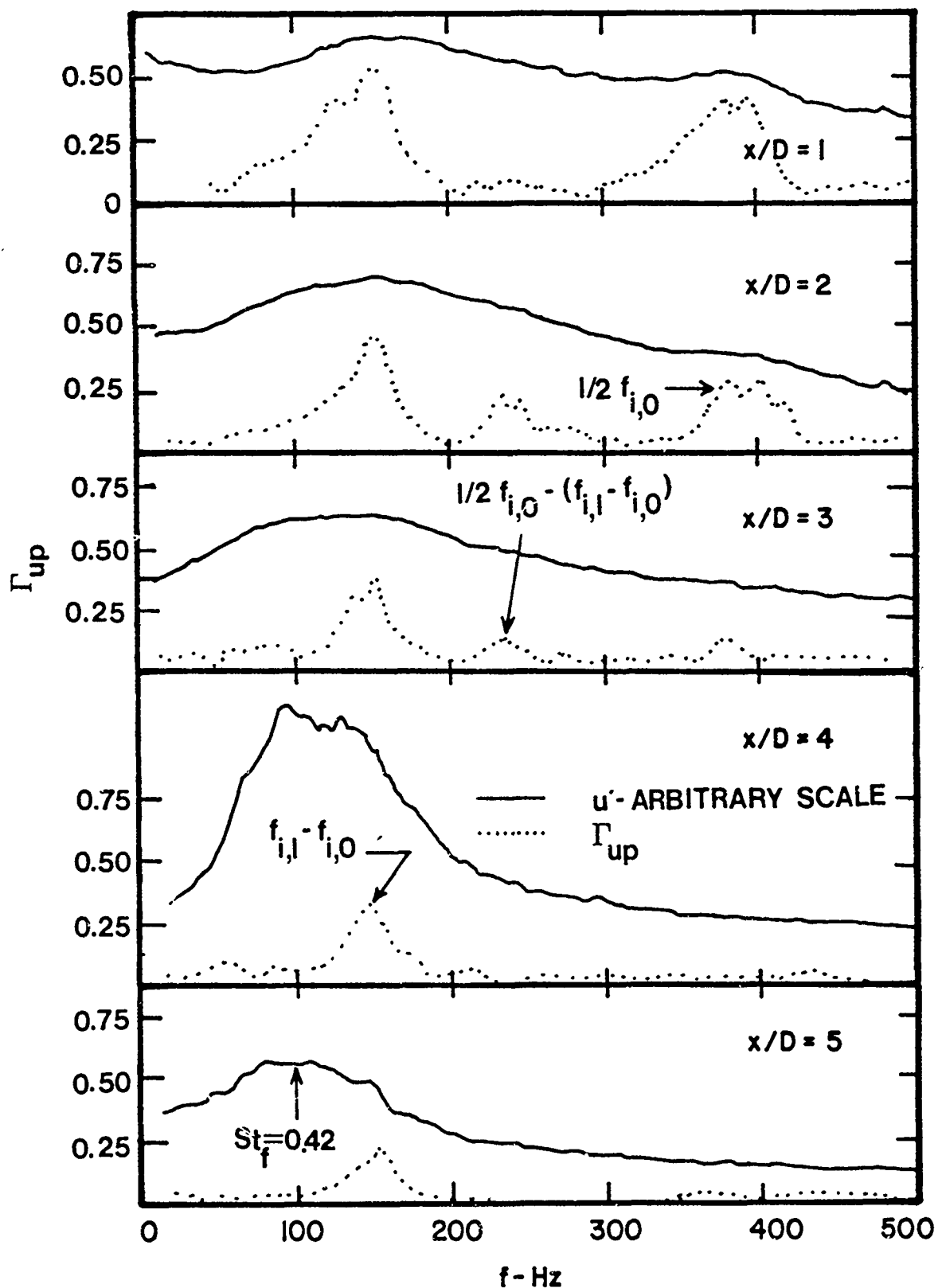
Figure 49. Development of Streamwise Velocity Spectrum
   and Coherence Between Velocity and Near-Field Pressure;
   Case 2L, Re = 42,000, Jet Centerline
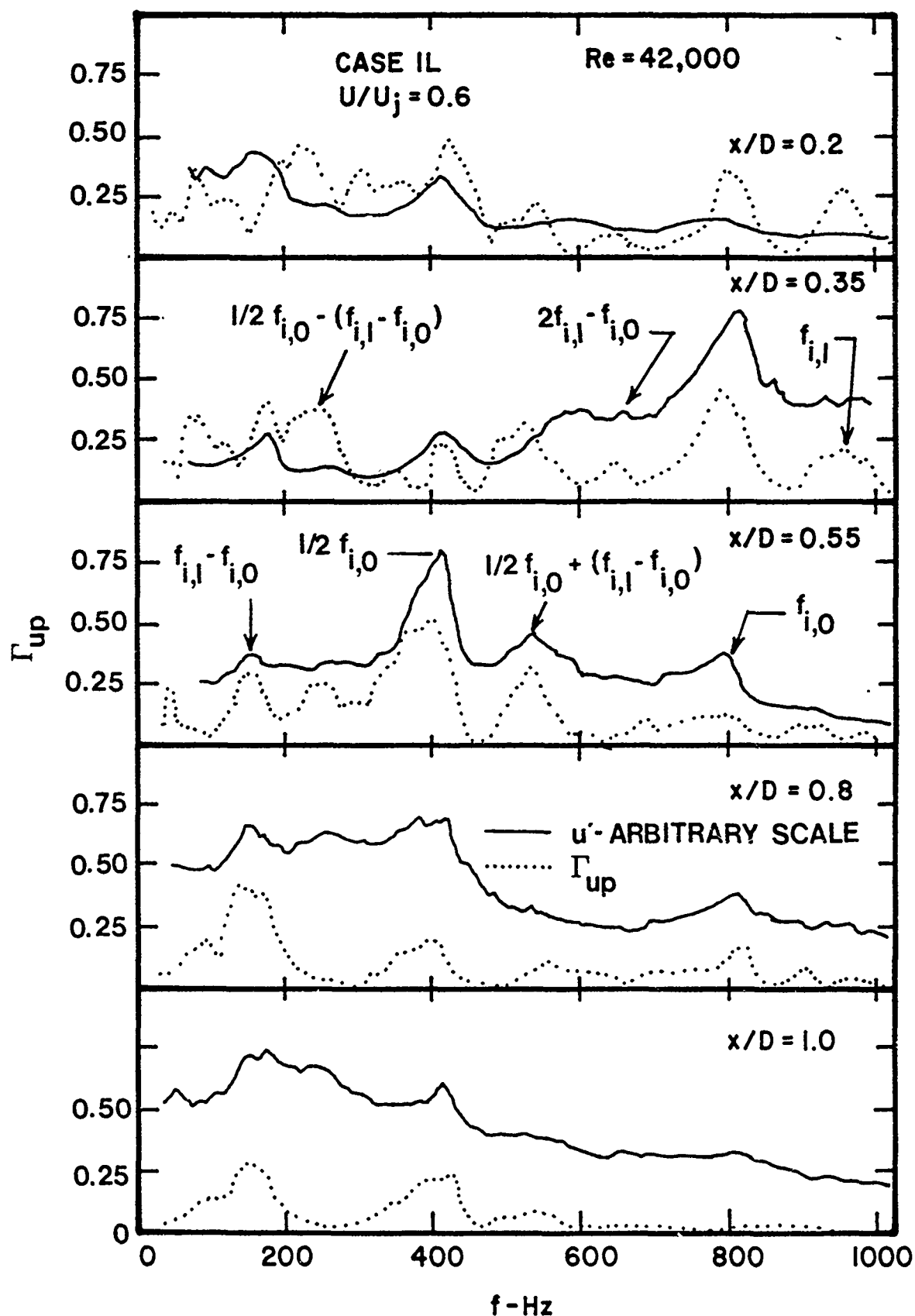
Figure 50. Development of Streamwise Velocity Spectrum
and Coherence Between Velocity and Near-Field Pressure;
Case 1L, Re = 42,000, $U/U_j = 0.6$
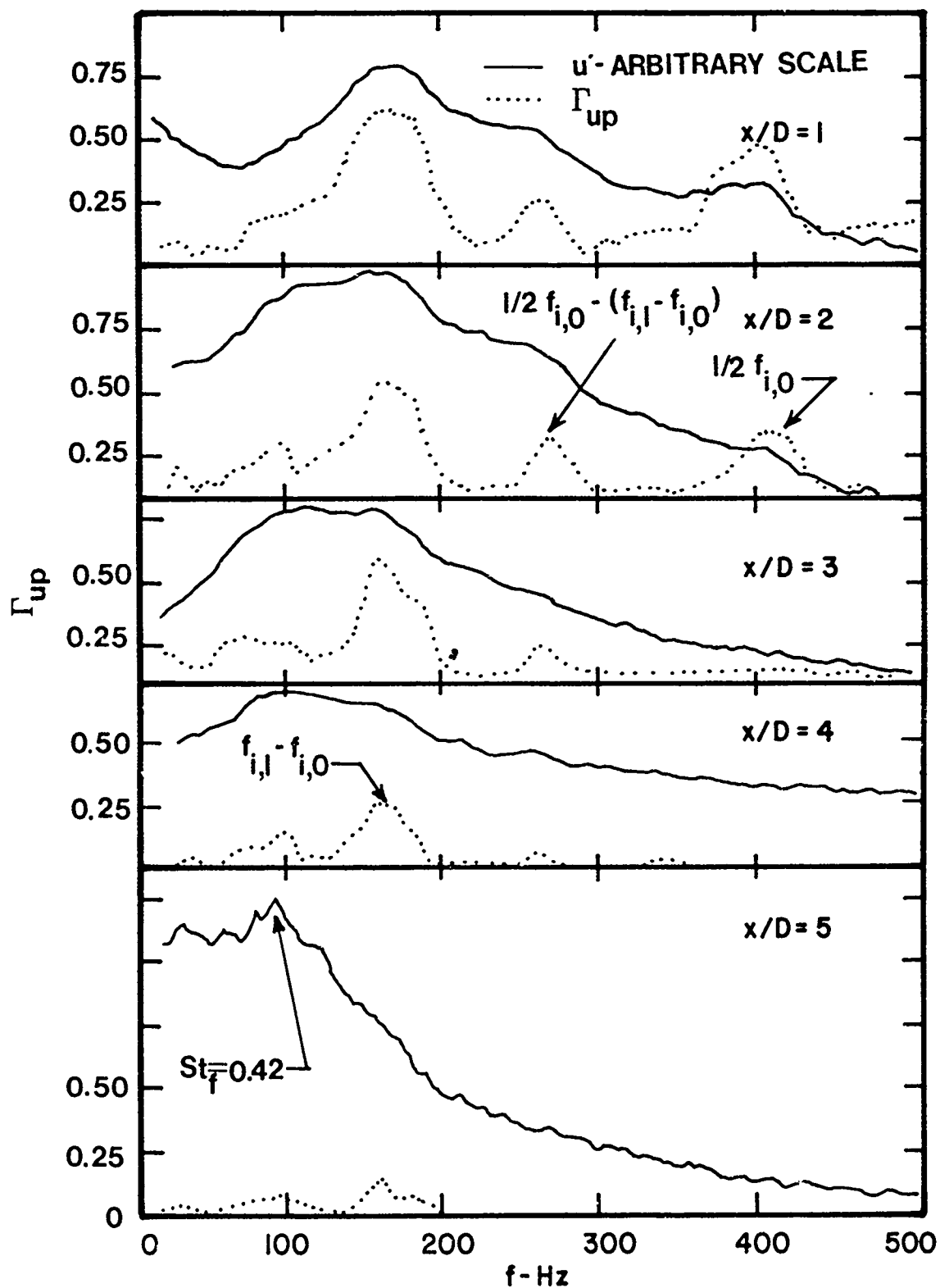
Figure 51. Development of Streamwise Velocity Spectrum
and Coherence Between Velocity and Near-Field Pressure;
Case 1L, Re = 42,000, U/U$_j$= 0.6
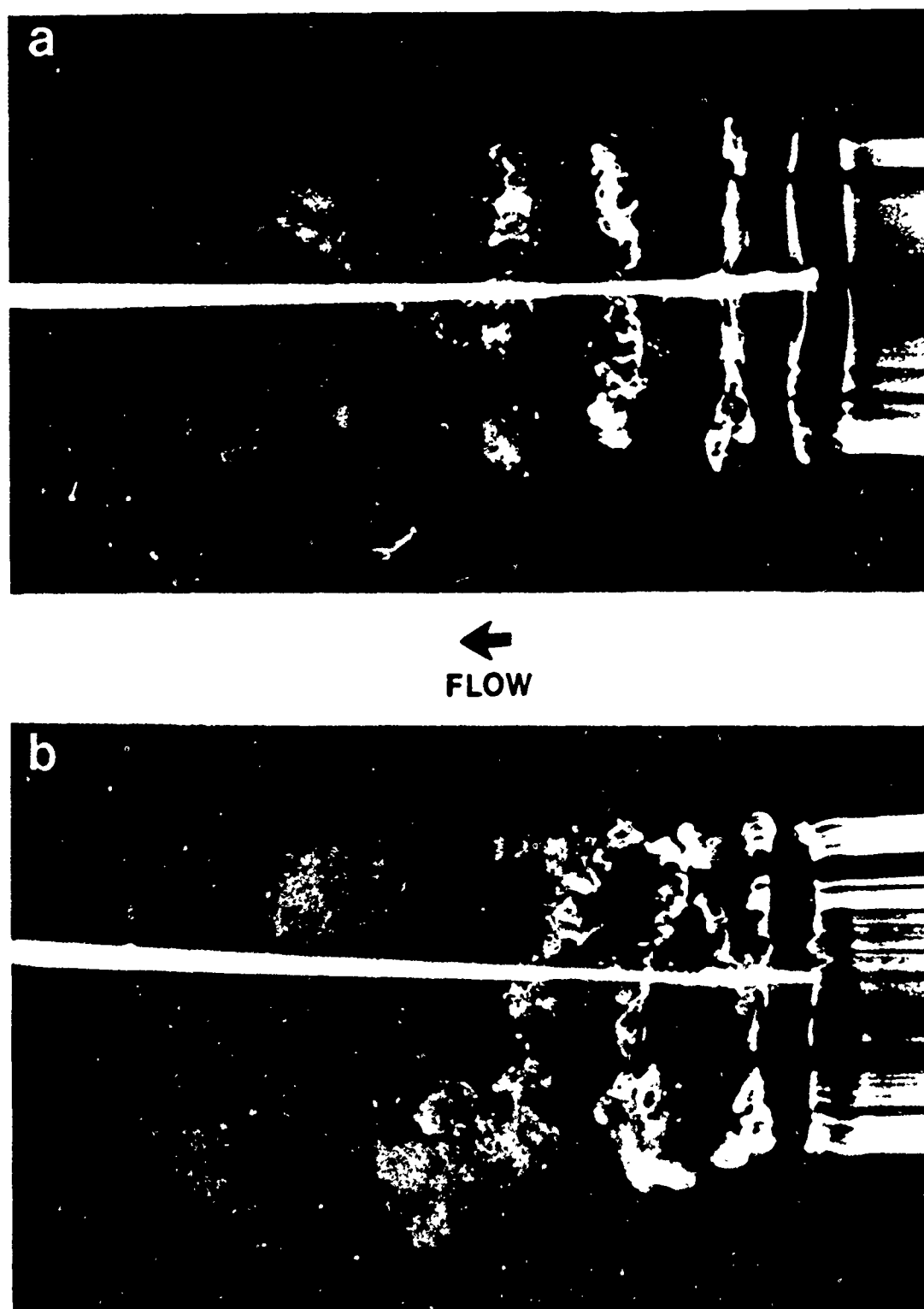
FLOW

Figure 52. Flow Visualization of Case 1L at Re = 42,000 Highlighting Both Axisymmetric and Non-Axisymmetric Modes
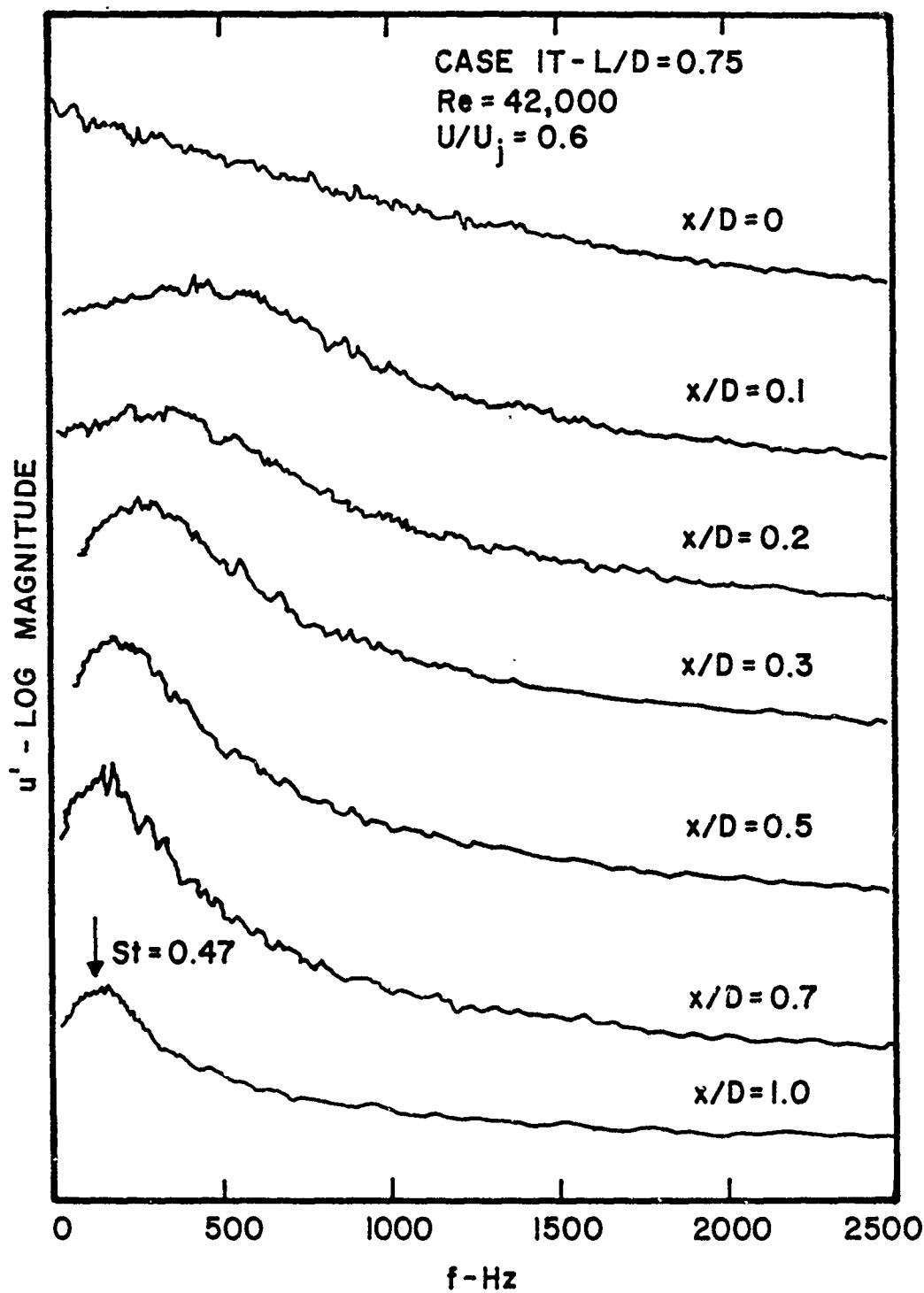
Figure 53. Development of Streamwise Velocity Spectrum
for Case 1T with L/D = 0.75; U/U$_j$ = 0.6 at Re = 42,000
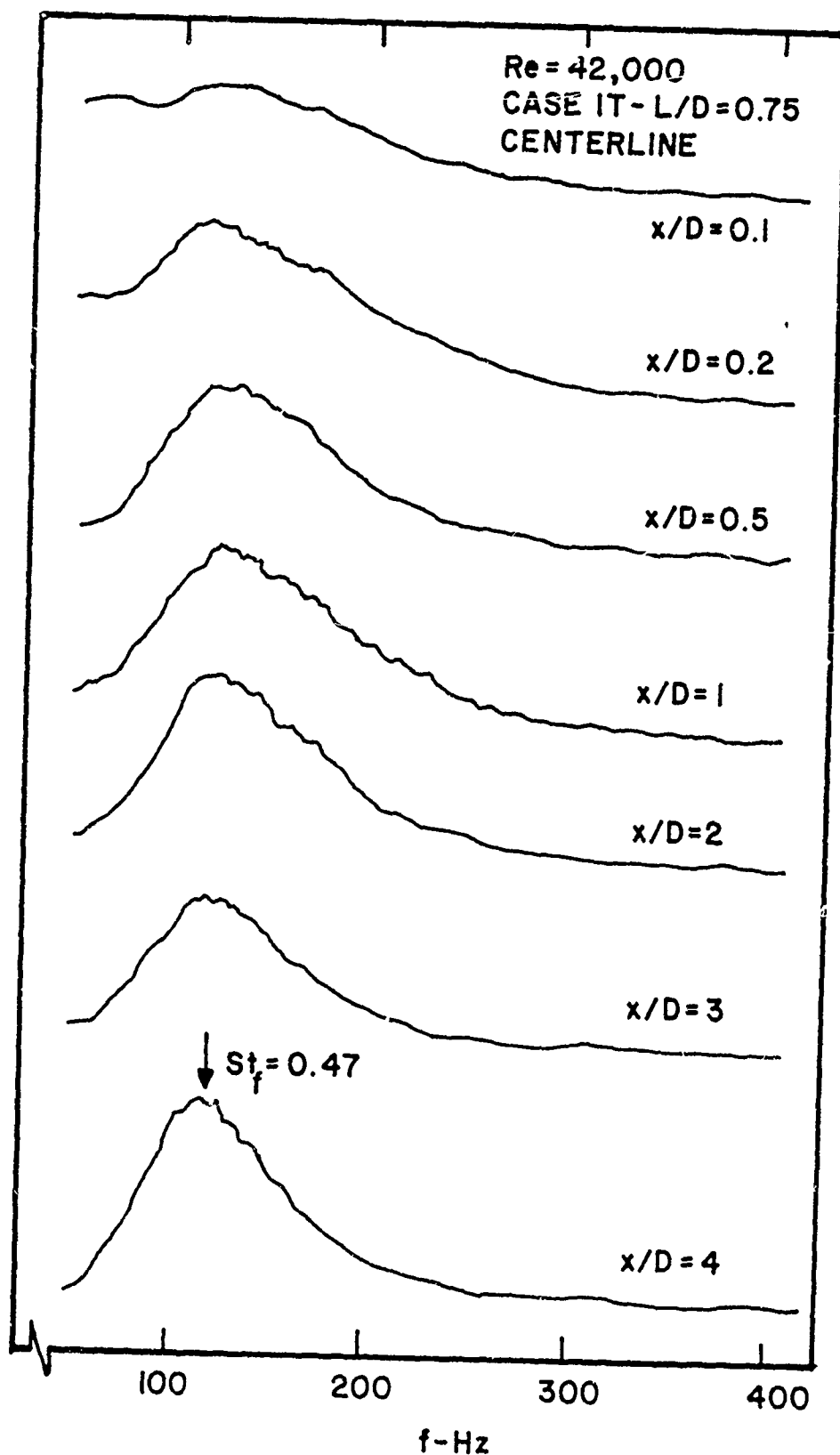
Figure 54. Development of Streamwise Velocity Spectrum for Case 1T with L/D = 0.75 on Jet Centerline for Re = 42,000
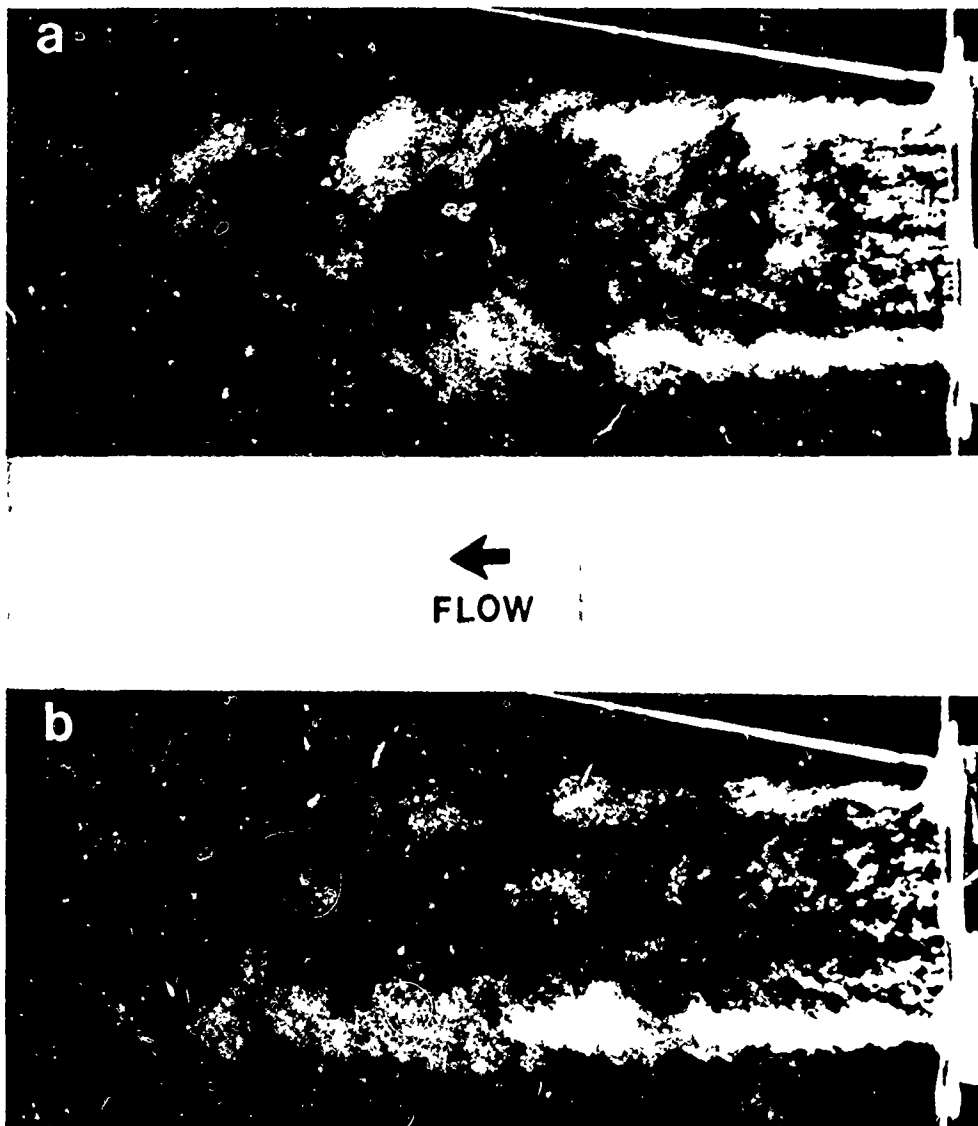
FLOW

Figure 55. Flow Visualization of Case 1T with
L/D = 0.75 at Re = 100,000 Highlighting Both
Axisymmetric and Non-Axisymmetric Modes
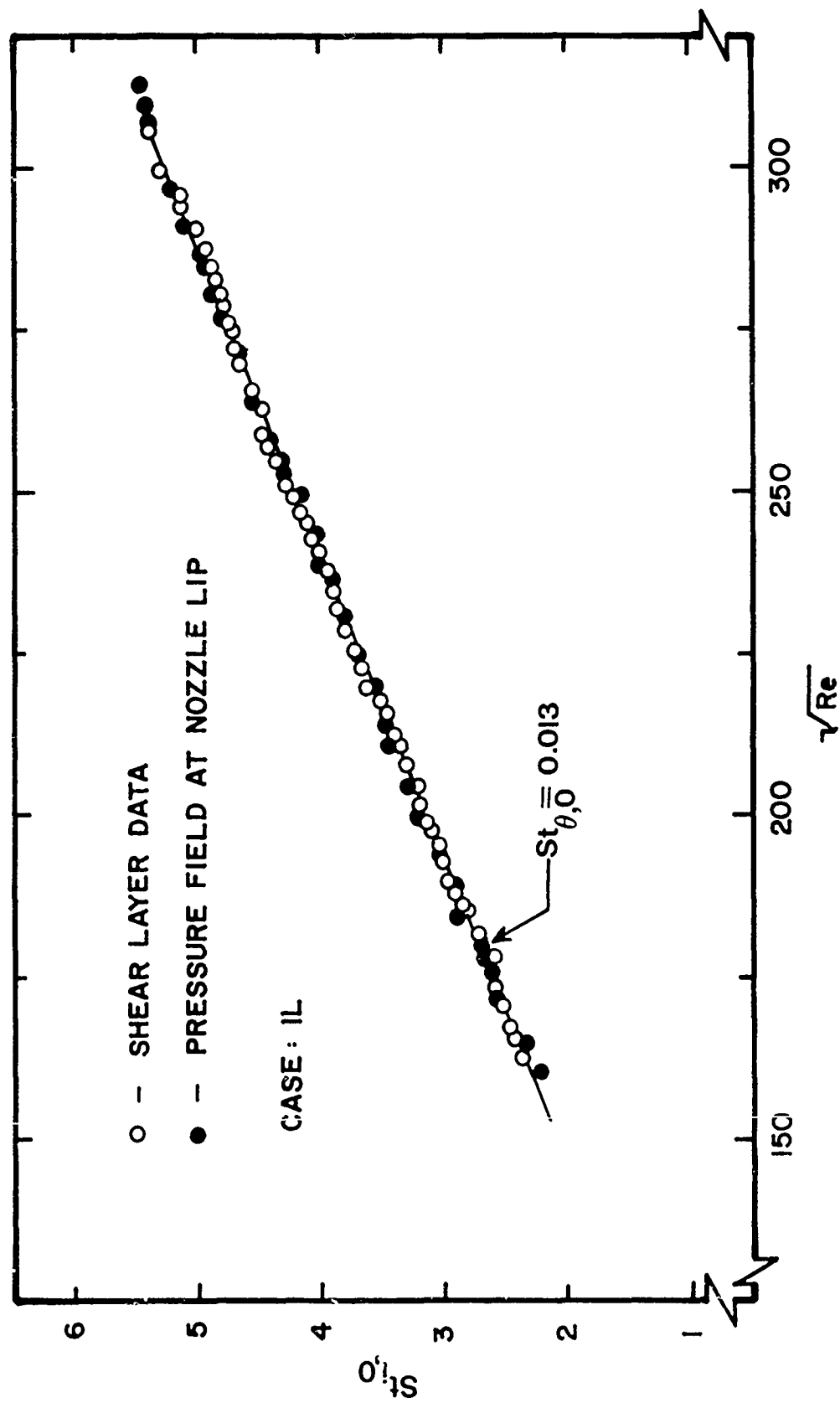
Figure 56. Variation of Initial Axisymmetric Strouhal Frequency with Reynolds
Number for Case 1L
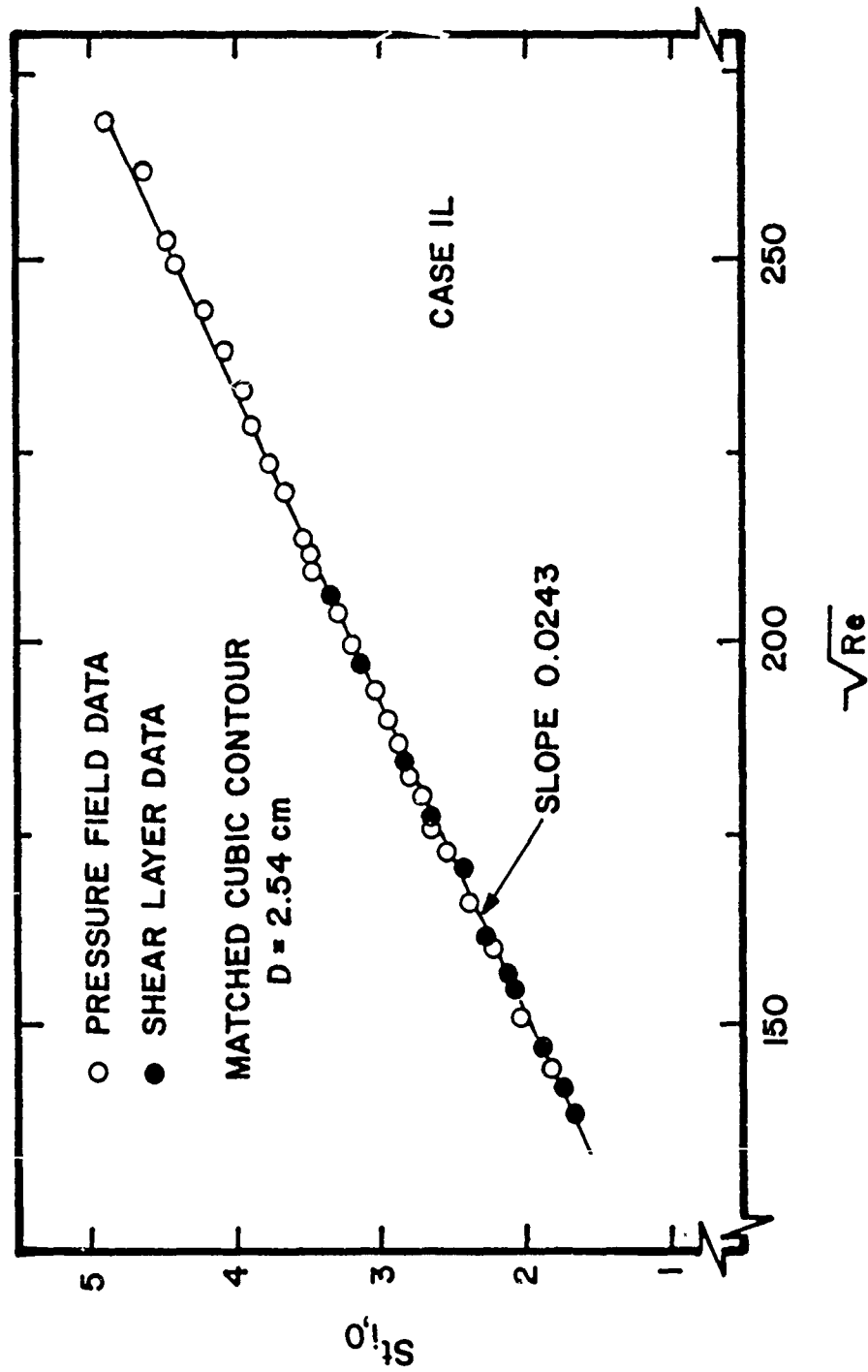
Figure 57. Variation of Initial Axisymmetric Strouhal Frequency with Reynolds Number for Case 1L Utilizing a Matched Cubic Nozzle with a 2.54 cm Diameter
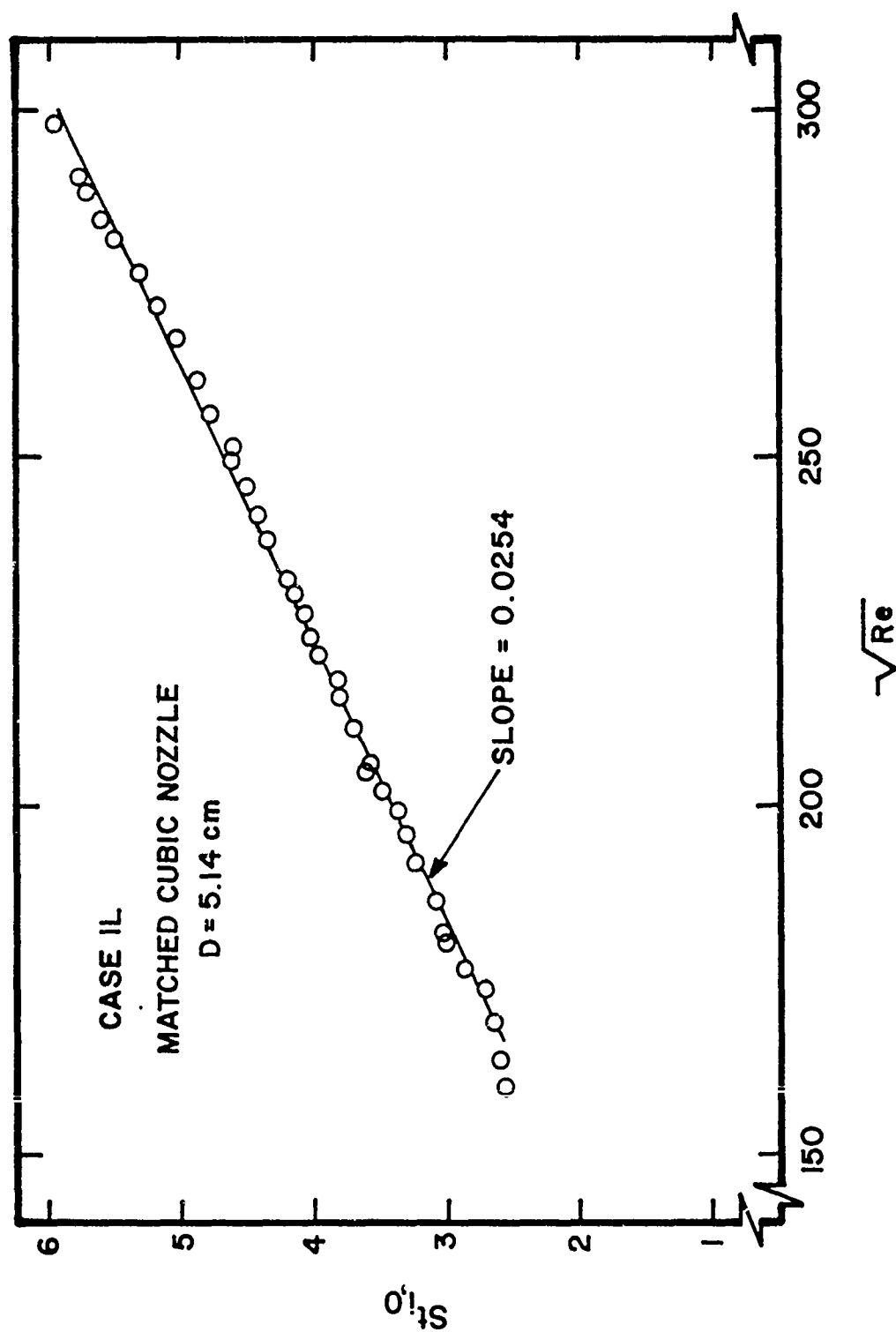
Figure 58. Variation of Initial Axisymmetric Strouhal Frequency with Reynolds Number for Case 1L Utilizing a Matched Cubic Nozzle with a 5.14 cm Diameter
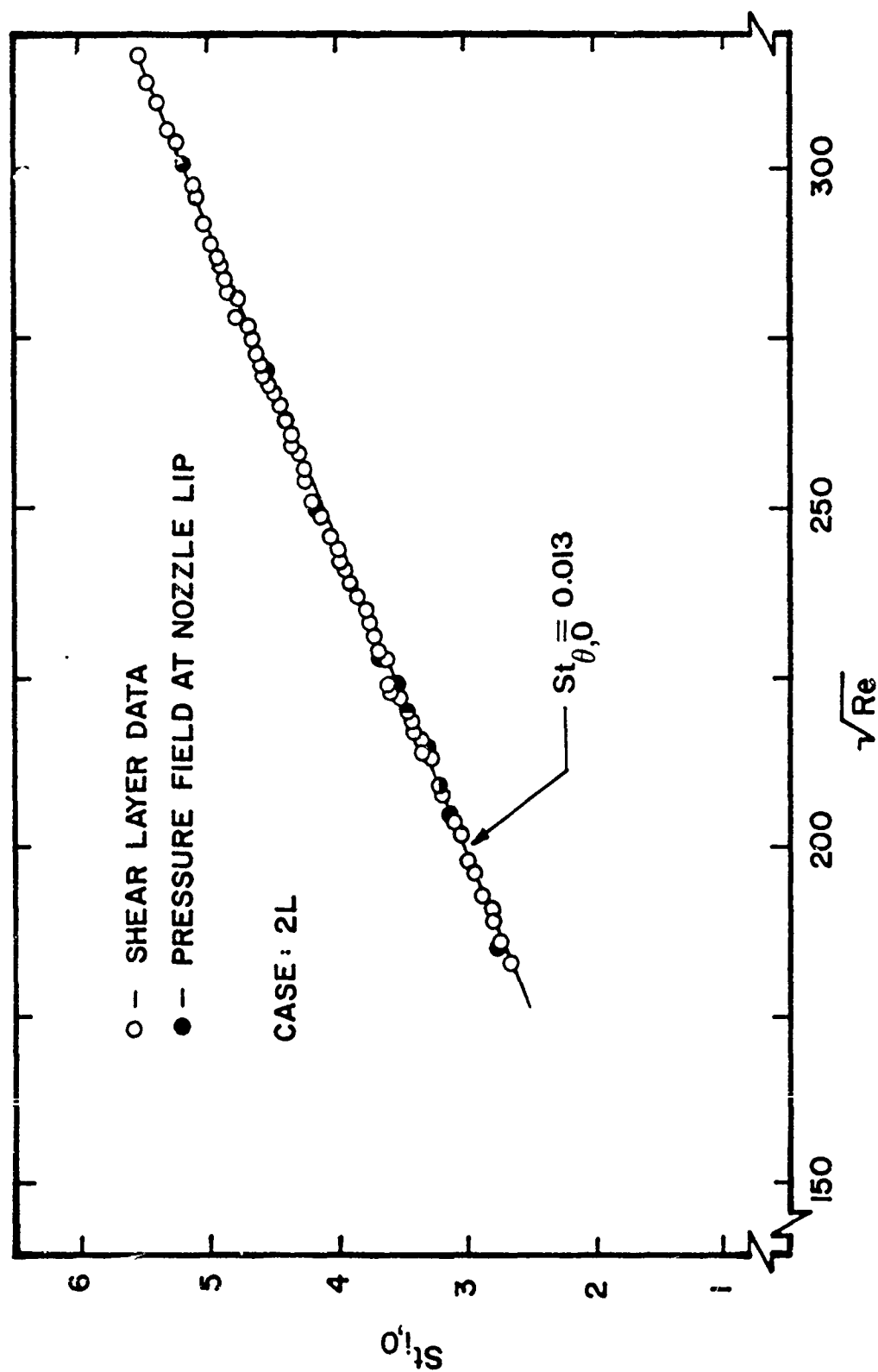
Figure 59. Variation of Initial Axisymmetric Strouhal Frequency with Reynolds Number for Case 2L
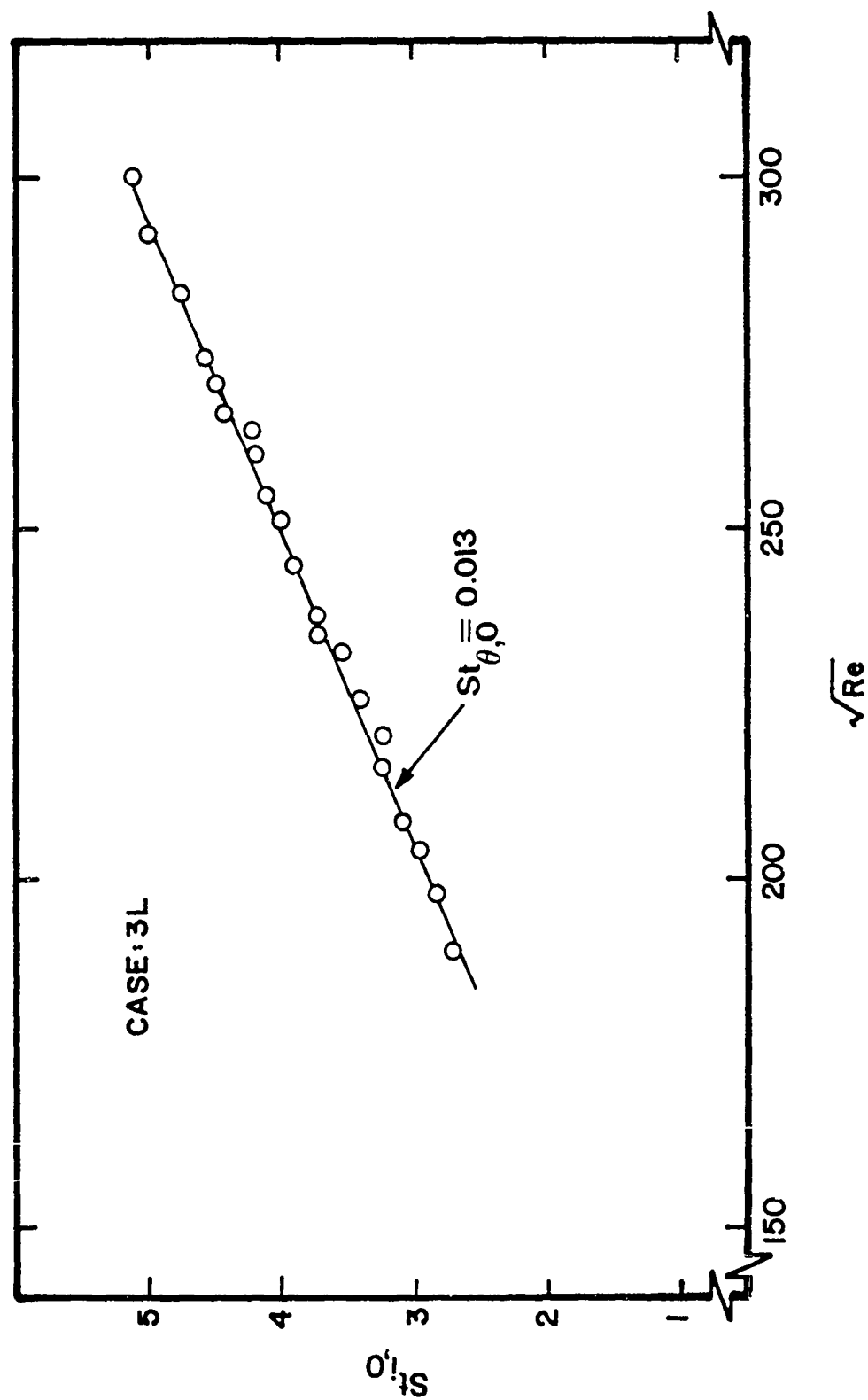
Figure 60. Variation of Initial Axisymmetric Strouhal Frequency with Reynolds Number for Case 3L
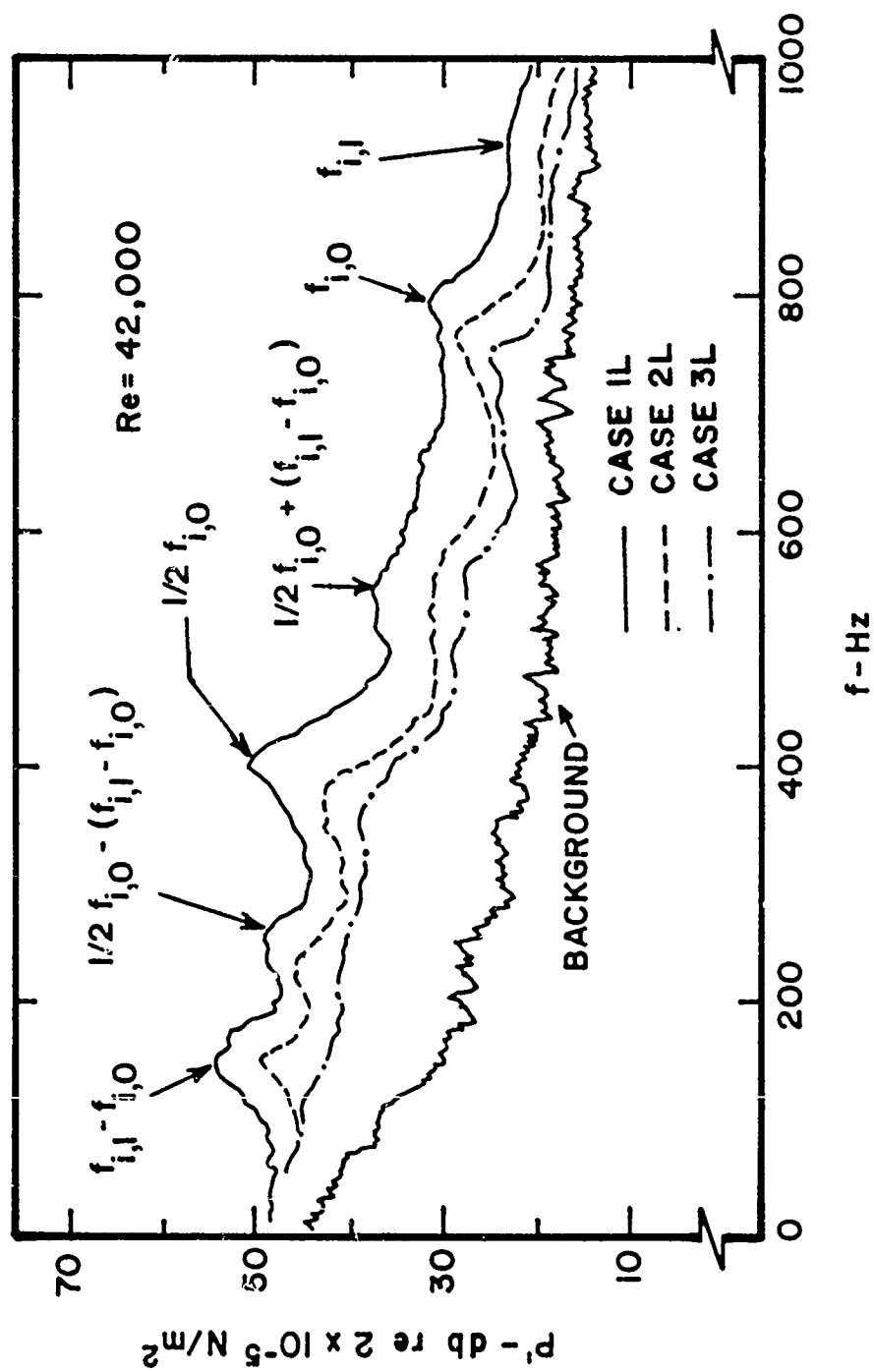
Figure 61. Effect of Initial Disturbance Level on Near-Field Pressure Spectrum;
Re = 42,000
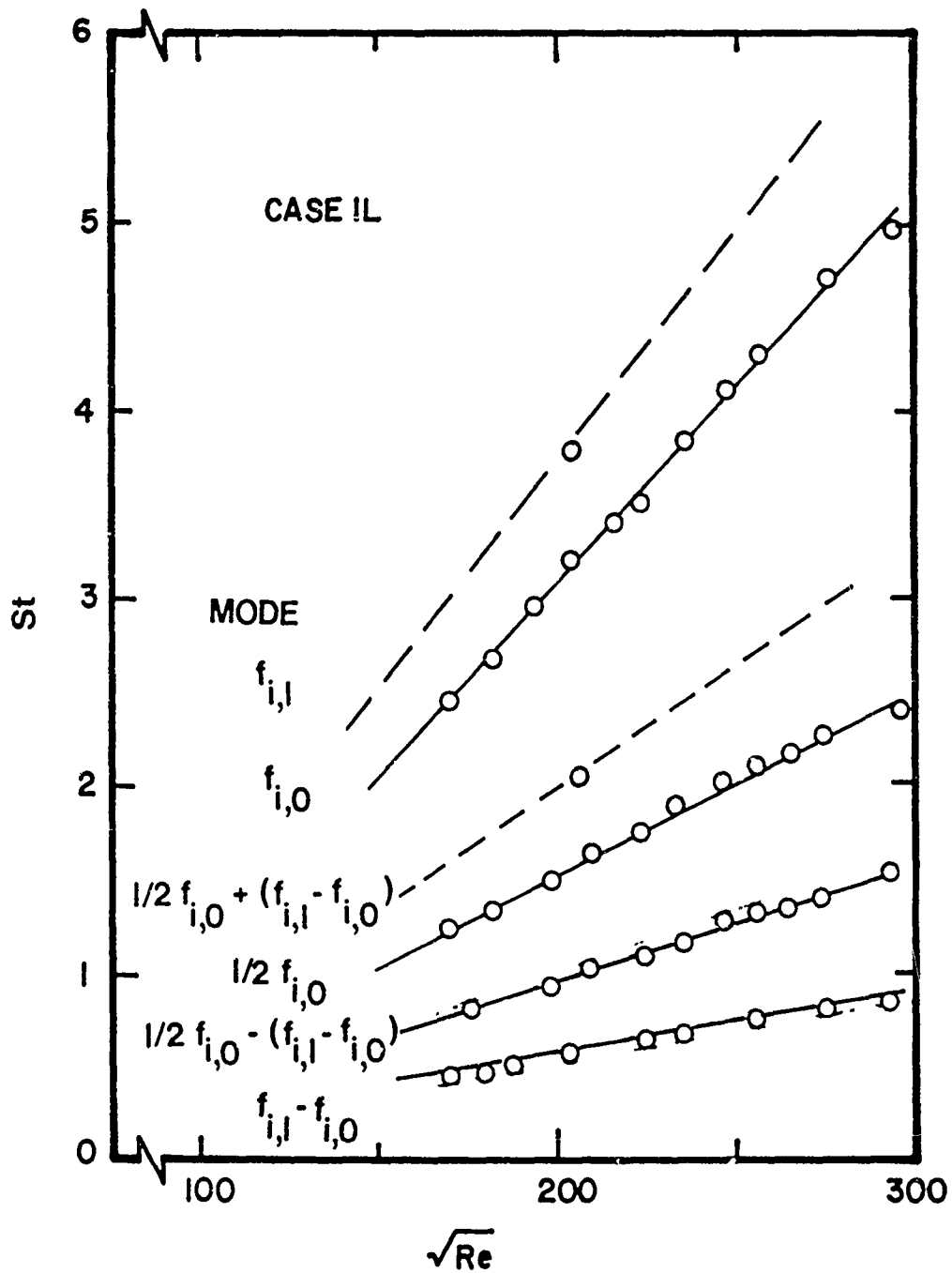
Figure 62. Variation of Strouhal Frequency of Observed Instability Modes with Reynolds Number for Case 1L
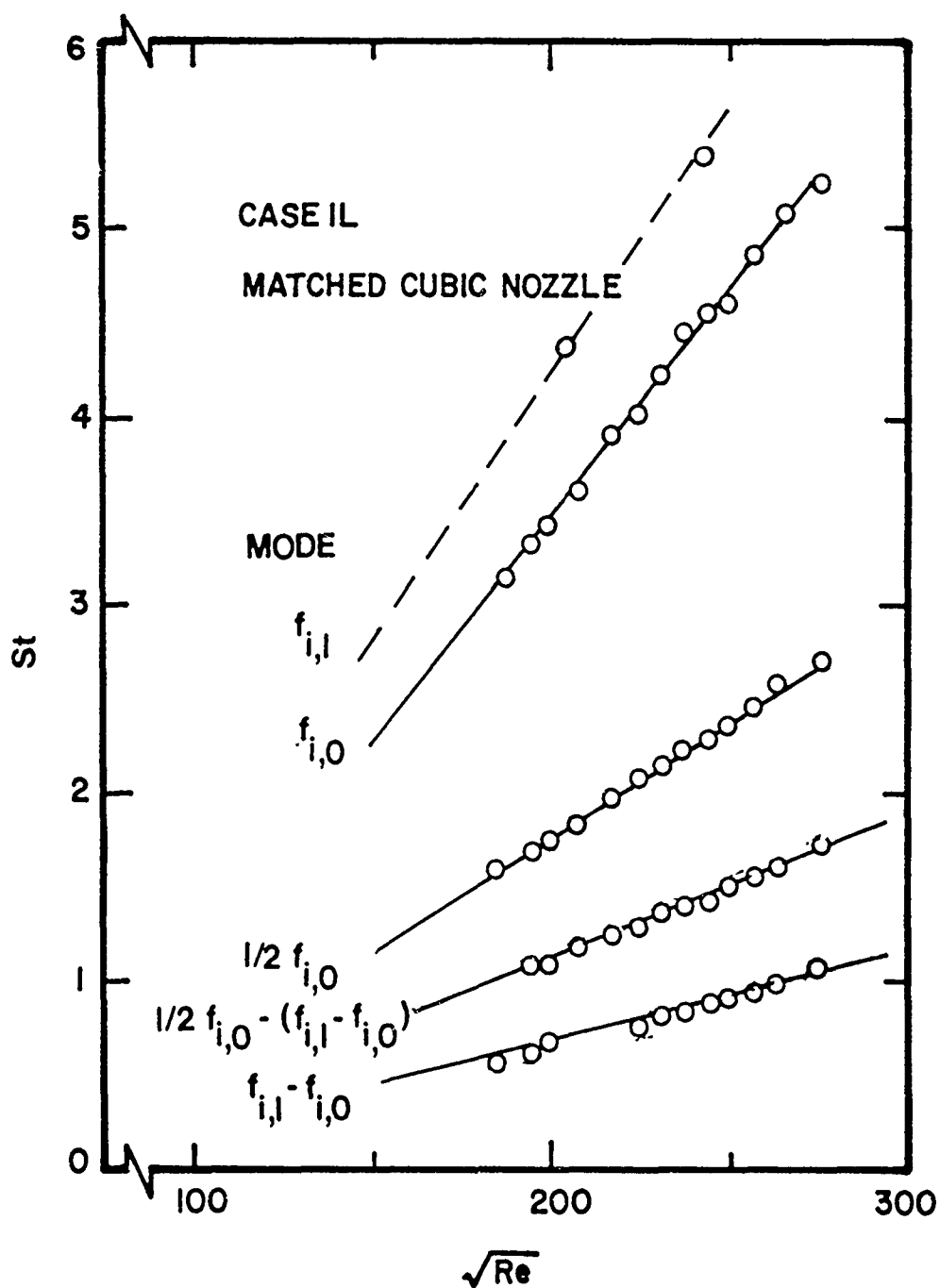
Figure 63. Variation of Strouhal Frequency of Observed
Instability Modes with Reynolds Number for Case 1L
Using a Matched Cubic Nozzle with a 5.14 cm Diameter
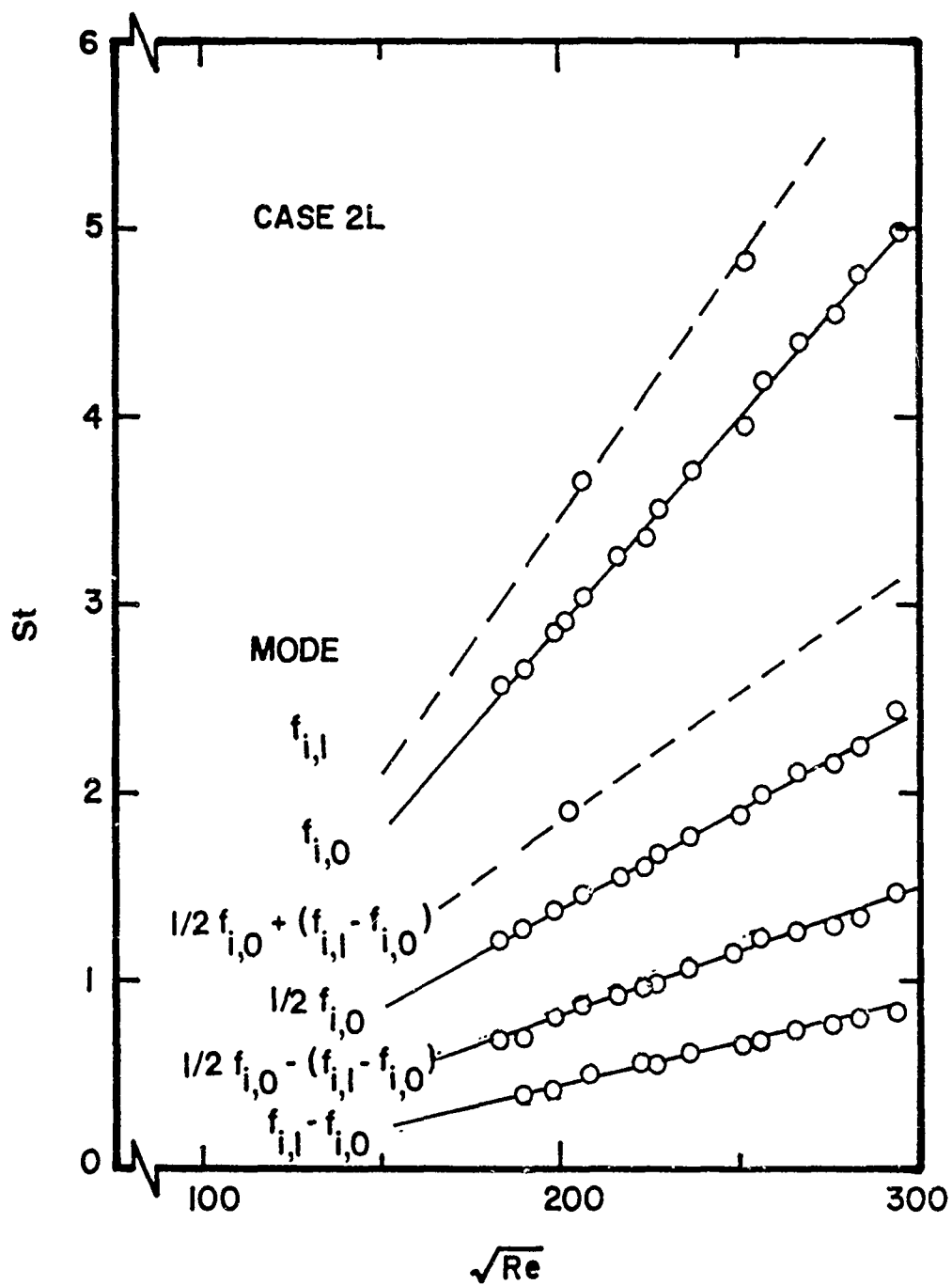
Figure 64. Variation of Strouhal Frequency of Observed Instability Modes with Reynolds Number for Case 2L
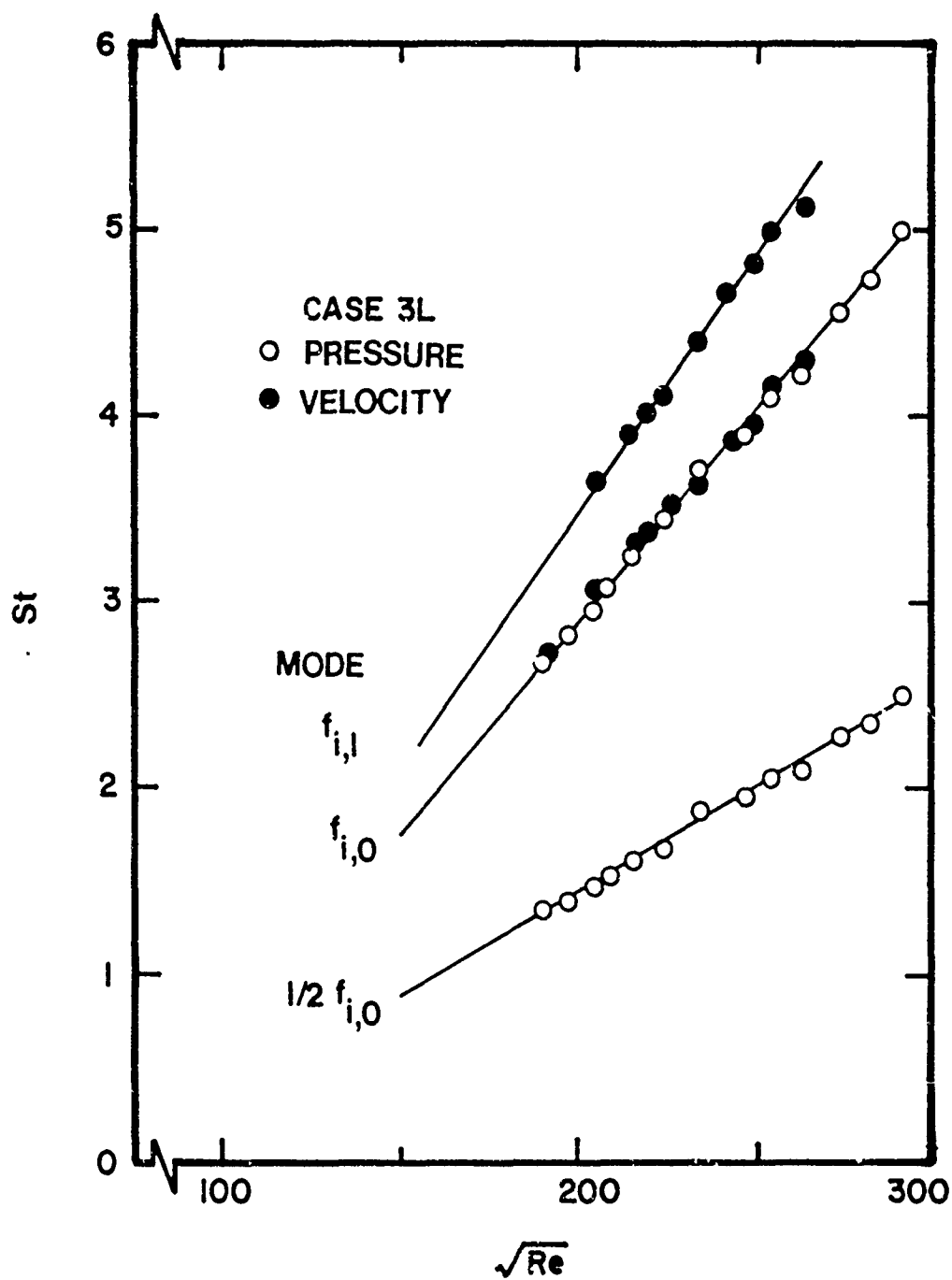
Figure 65. Variation of Strouhal Frequency of
Axisymmetric, Helical and Subharmonic Modes with
Reynolds Number for Case 3L
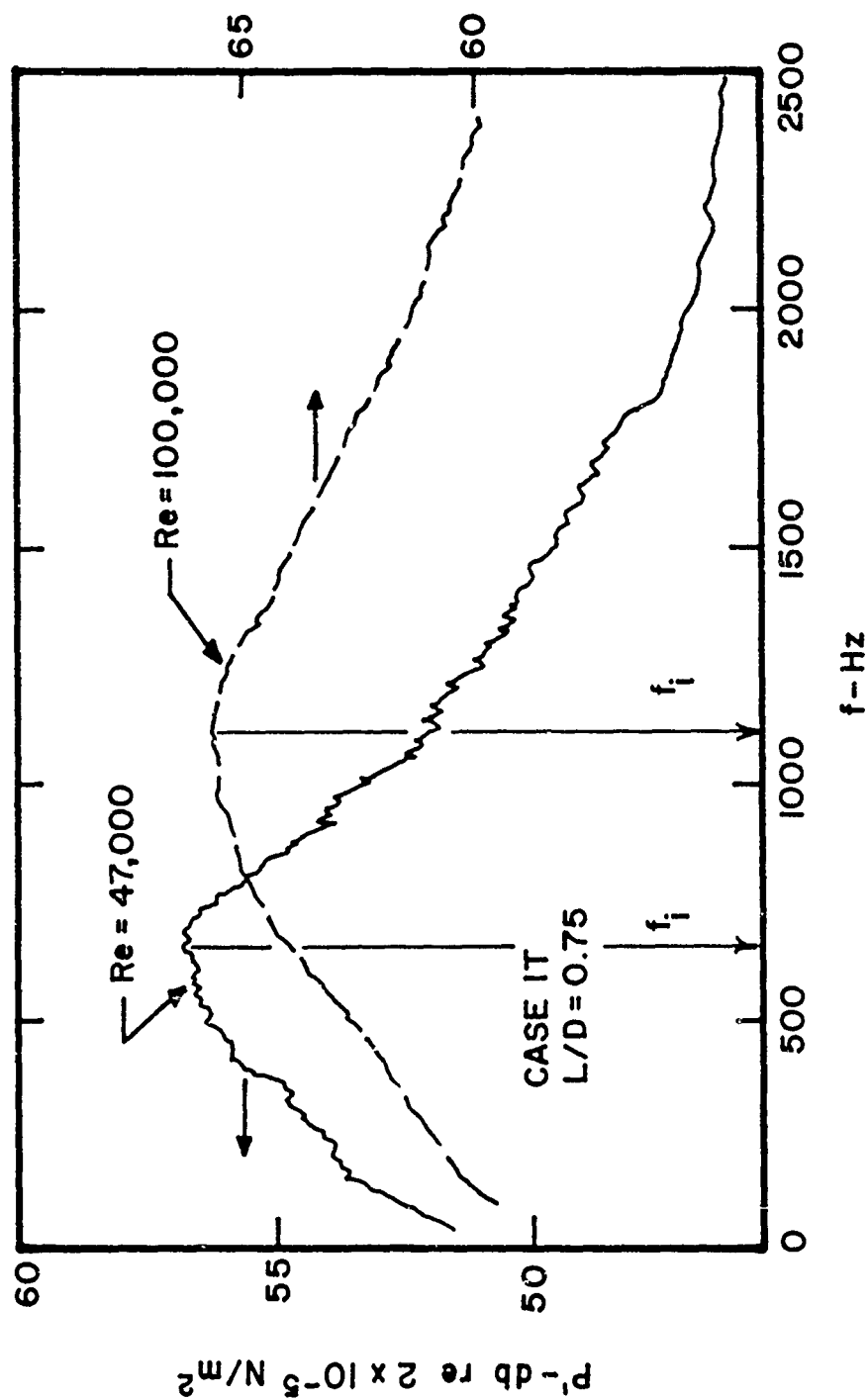
Figure 66. Typical Near-Field Pressure Spectra for Case 1T with L/D = 0.75
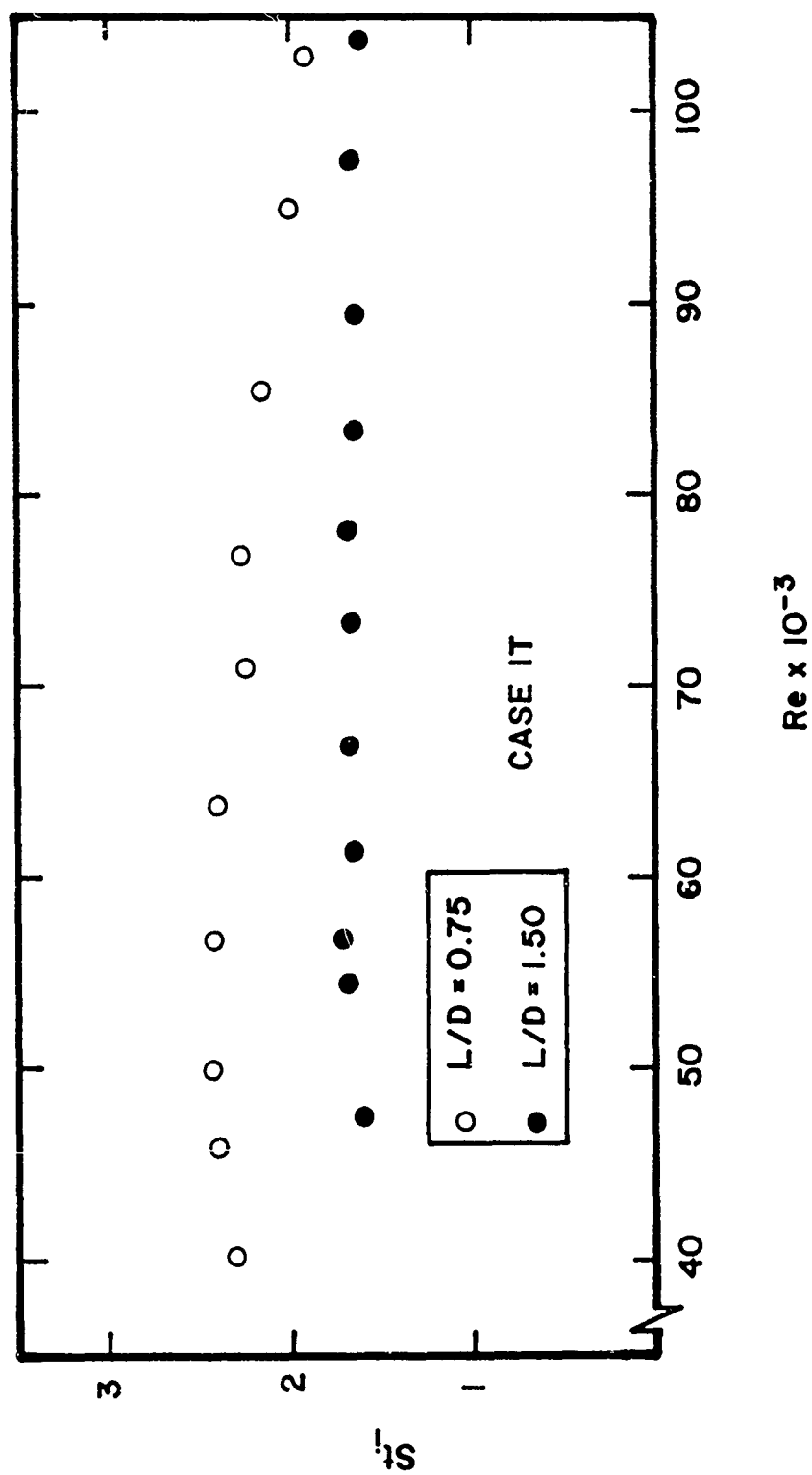
Figure 67. Variation of Initial Strouhal Frequency with Reynolds Number for Case 1T
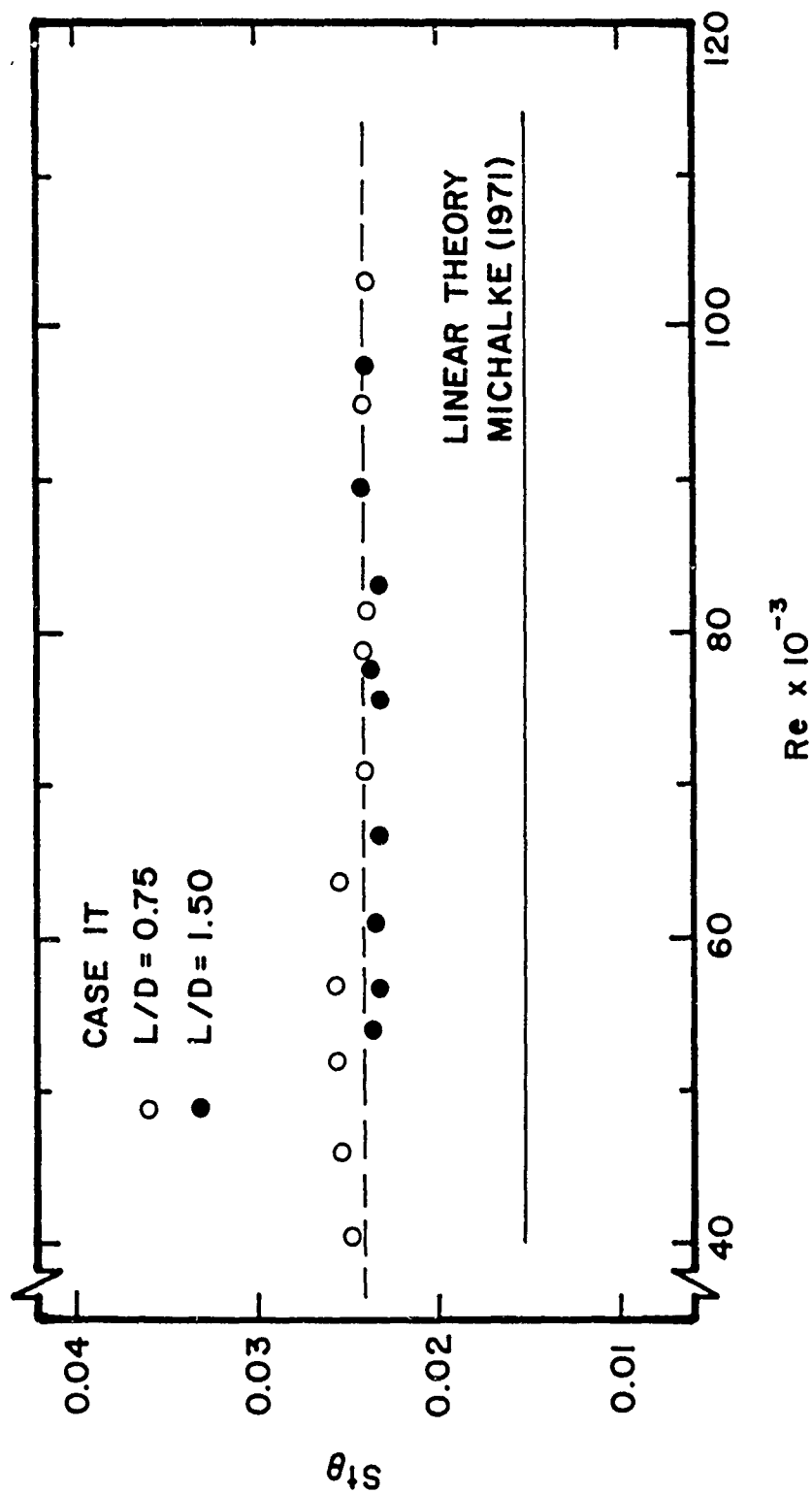
Figure 68. Variation of Initial Strouhal Number, Based on Exit Momentum Thickness
with Reynolds Number for Case 1T .
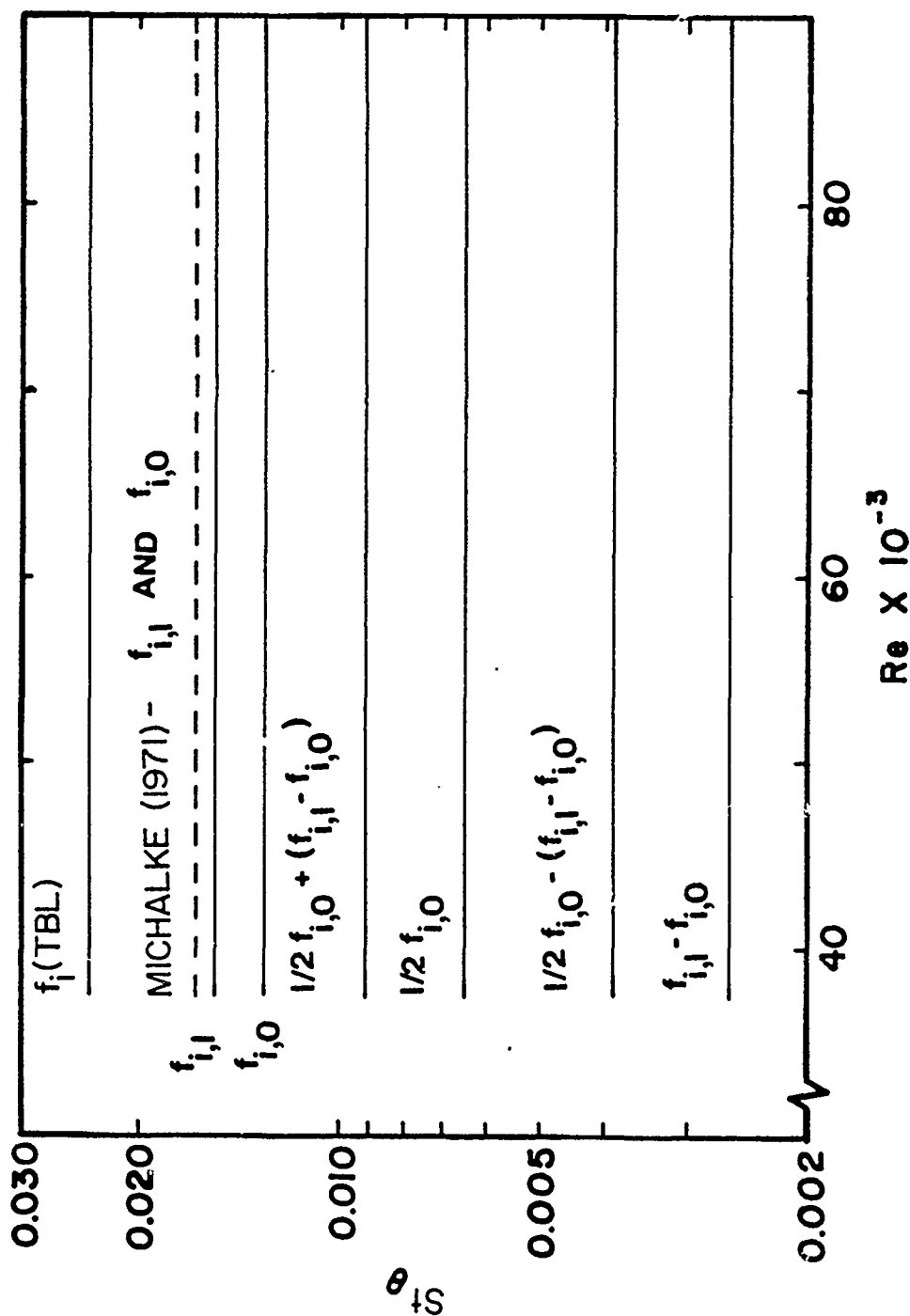
Figure 69. Variation of Initial Strouhal Number, Based on Exit Momentum Thickness and Various Observed Frequencies, with Reynolds Number for All Test Flow Conditions
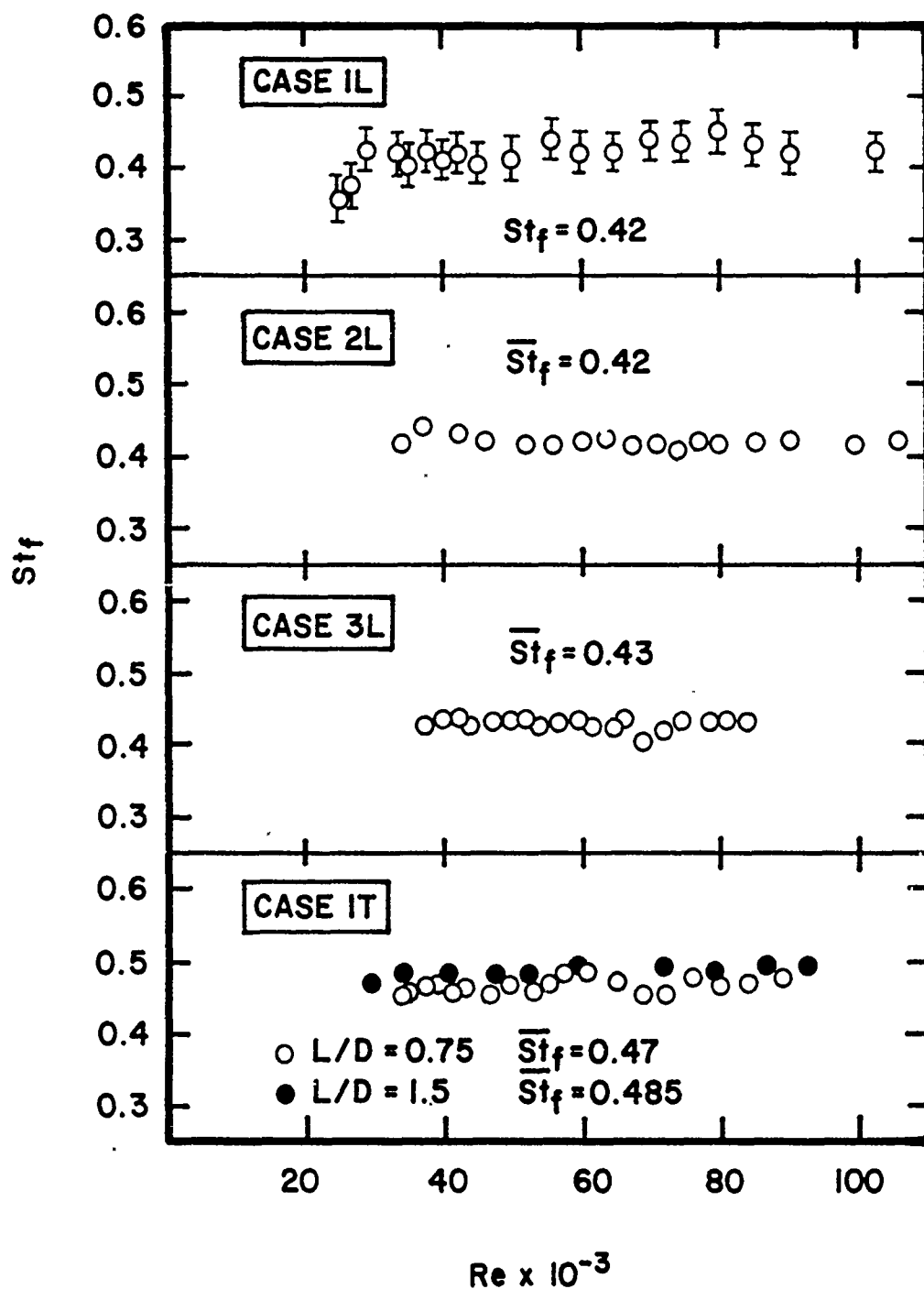
Figure 70. Variation of Final Strouhal Frequency with
Reynolds Number for All Test Flow Conditions
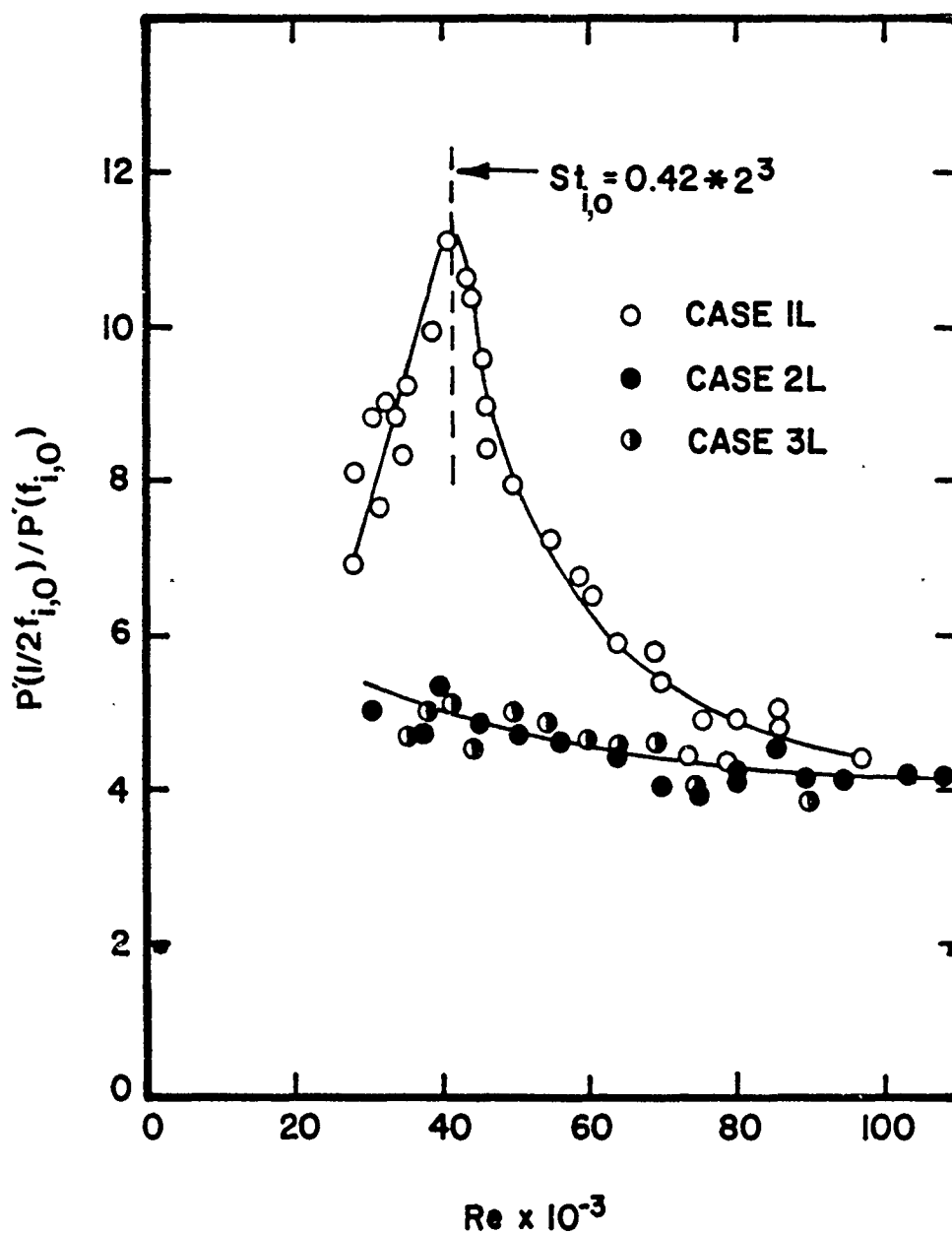
Figure 71. Reynolds Number Dependence for Normalized
Amplitude of Near-Field Pressure from Subharmonic Mode
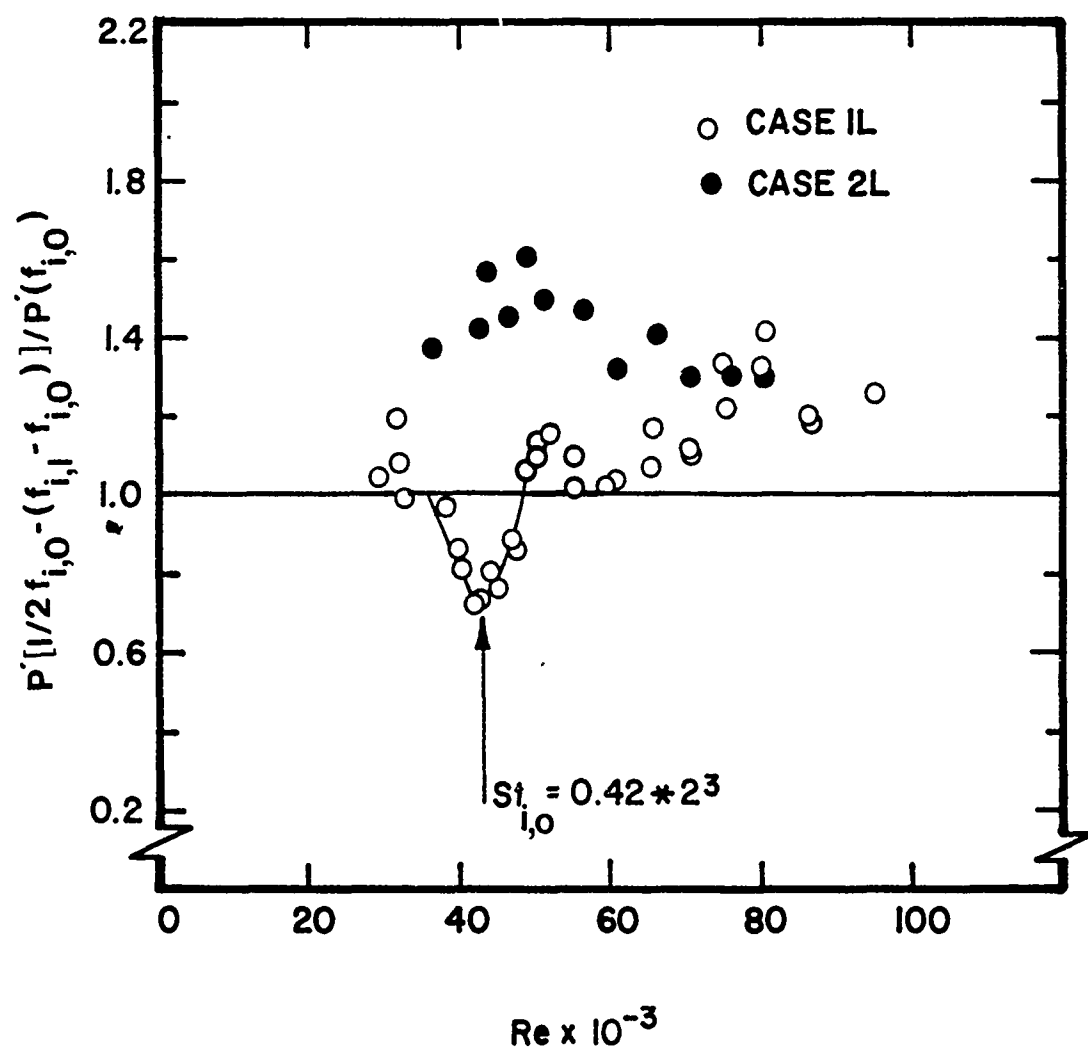
Figure 72. Reynolds Number Dependence for Normalized
Amplitude of Near-Field Pressure from Nonlinear Mode
Based on Interaction Between Initial Helical and
Axisymmetric Disturbances
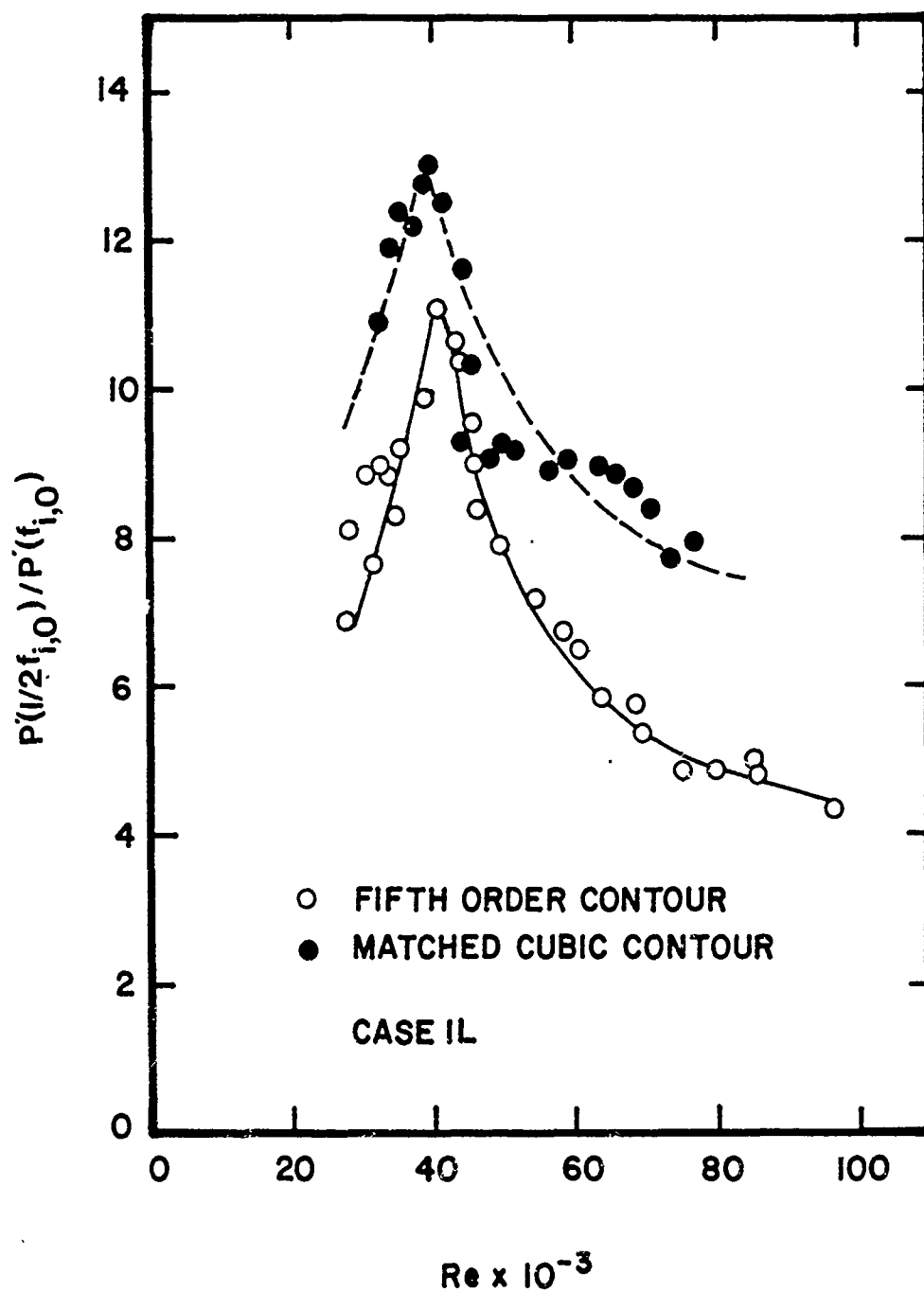
Figure 73. Effect of Nozzle Shape on Reynolds Number
Dependence for Normalized Amplitude of Near-Field
Pressure from Subharmonic Mode
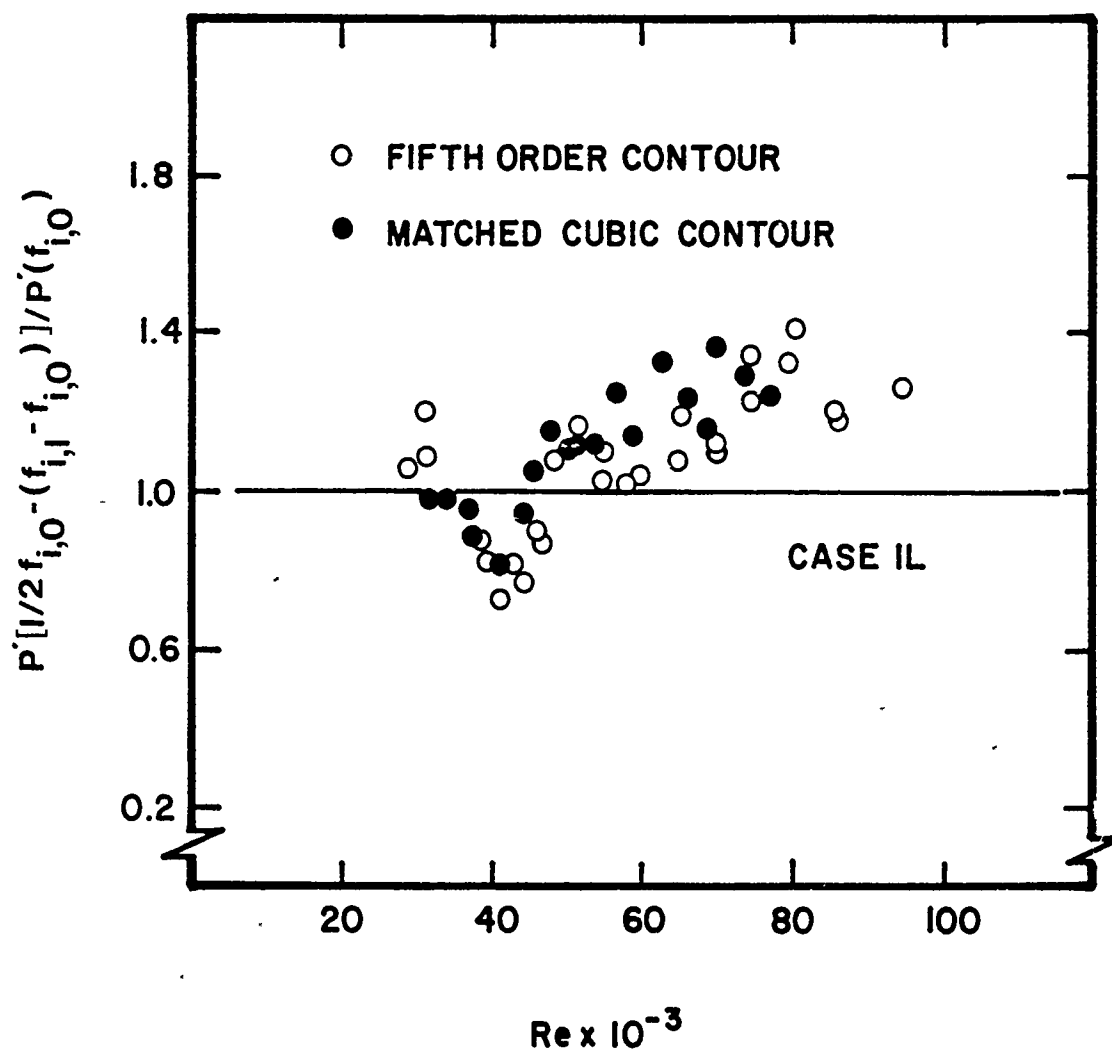
Figure 74. Effect of Nozzle Shape on Reynolds Number
Dependence of Normalized Amplitude of Near-Field
Pressure from Nonlinear Mode Based on Interaction
Between Initial Helical and Axisymmetric Disturbances
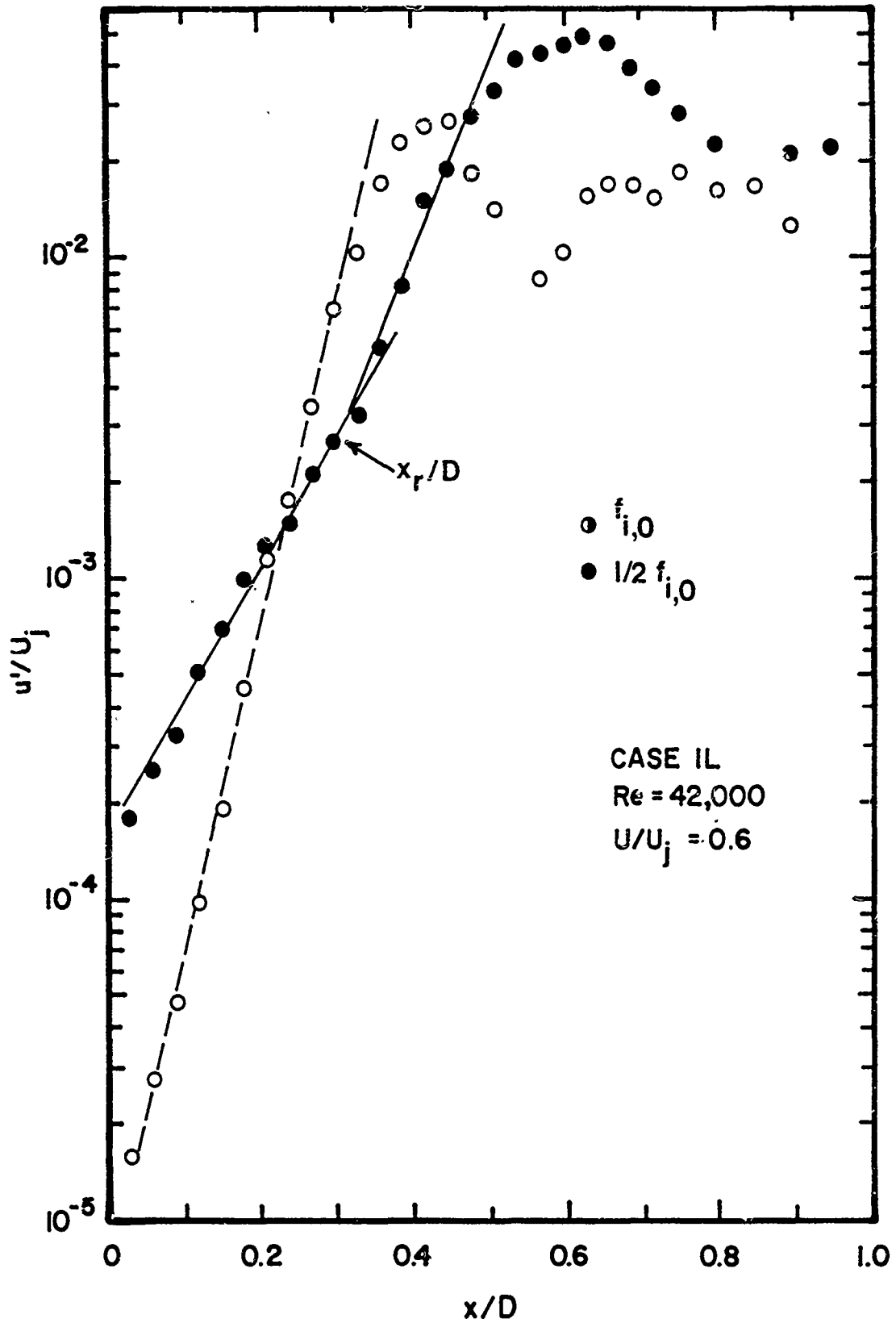
Figure 75. Development of Initial Axisymmetric Mode
and its Subharmonic along $U/U_j = 0.6$ at Re = 42,000
for Case 1L
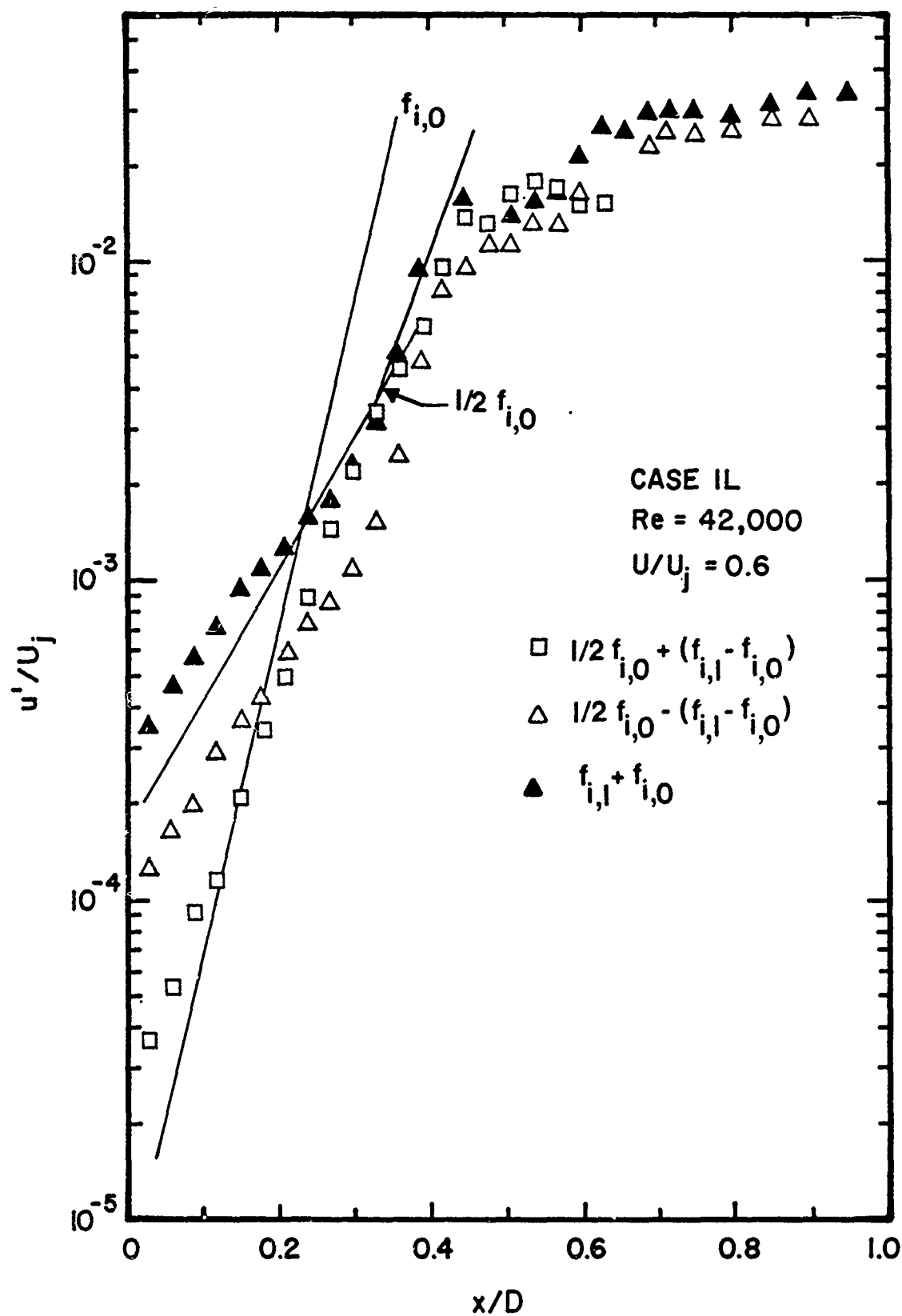
Figure 76. Development of Nonlinearly Generated Modes along $U/U_j = 0.6$ at Re = 42,000 for Case 1L
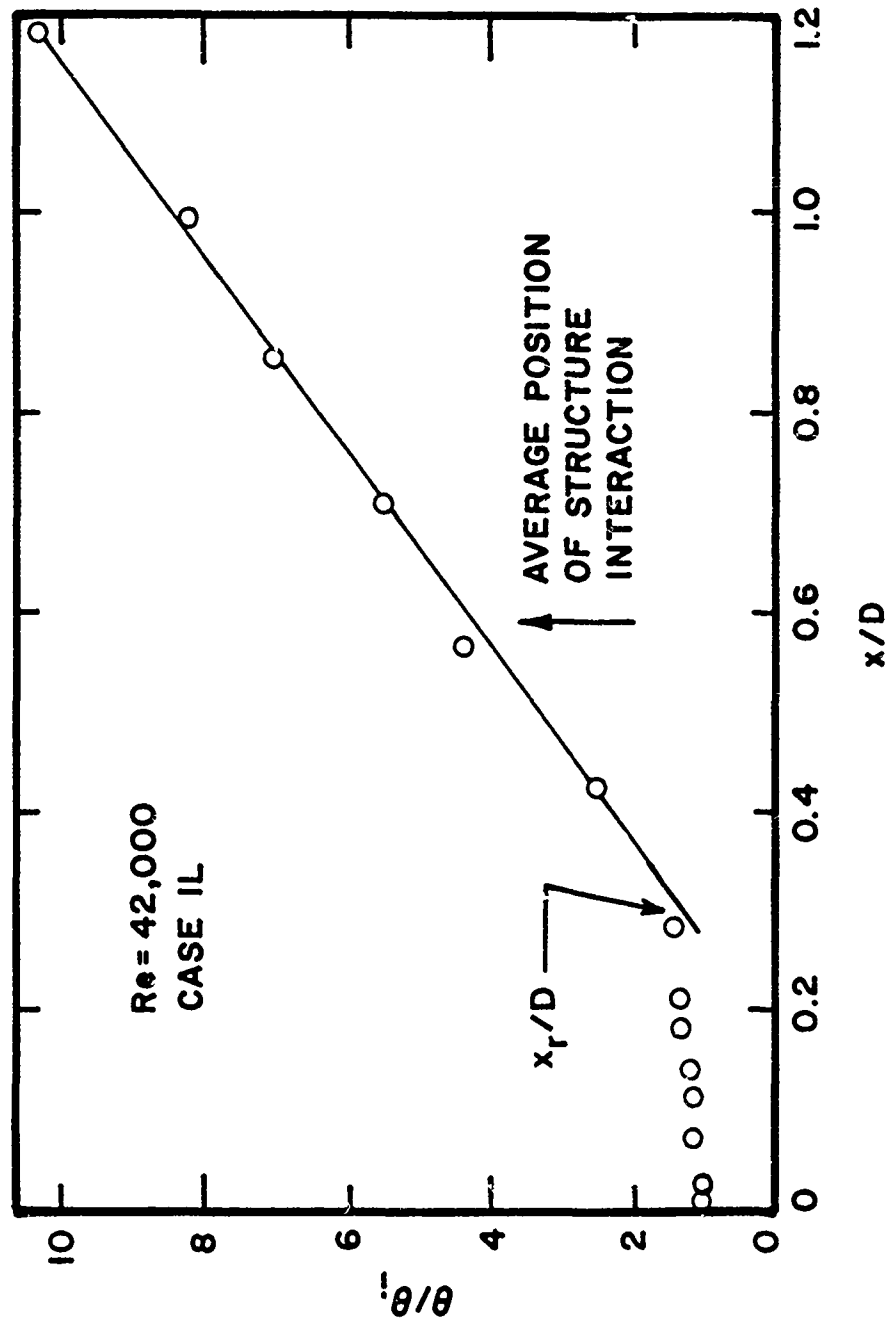
Figure 77. Development of Jet Momentum Thickness at Re = 42,000 for Case 1L
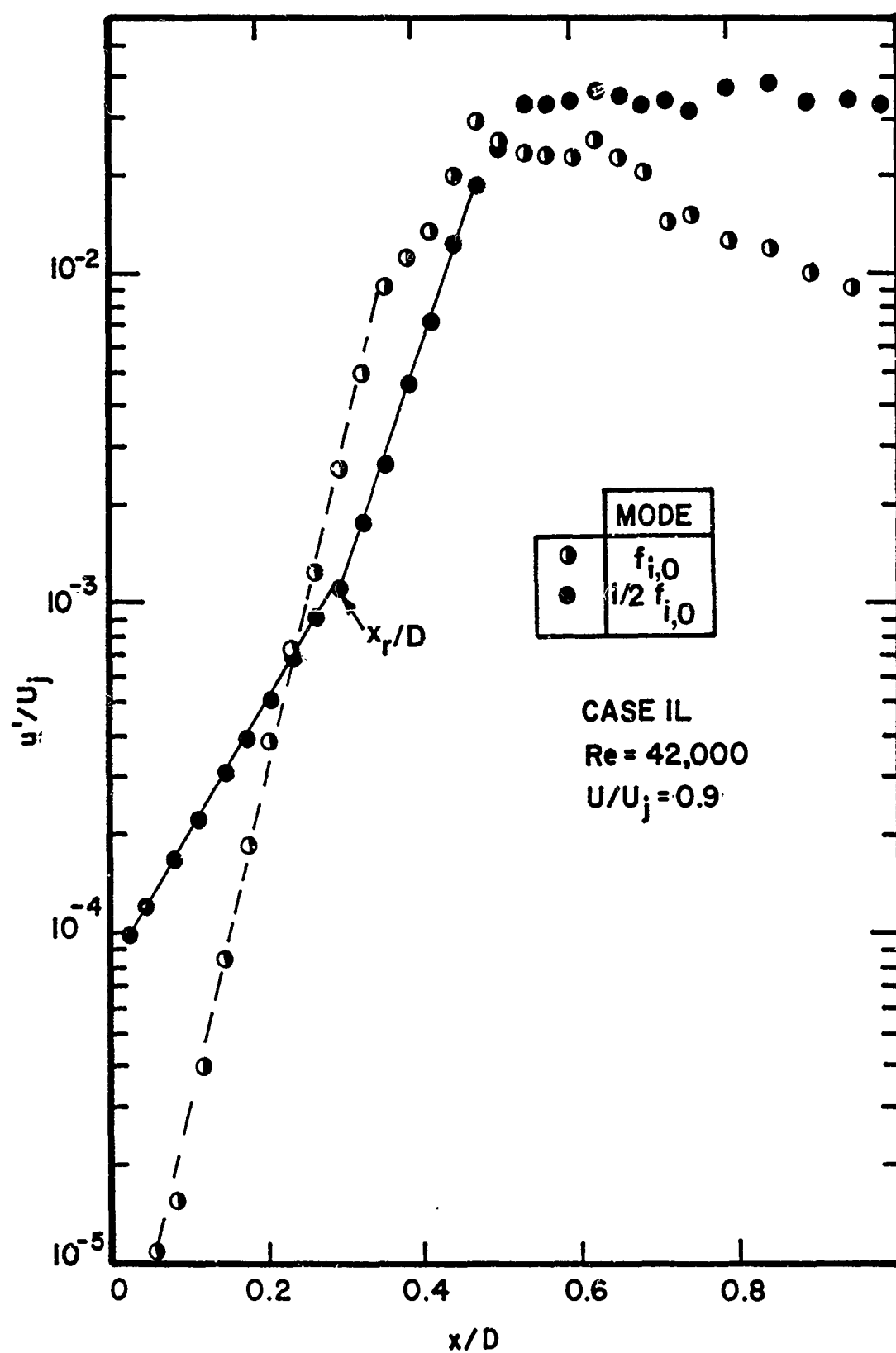
Figure 78. Development of Initial Axisymmetric Mode and its Subharmonic along $U/U_j = 0.9$ at Re = 42,000 for Case 1L
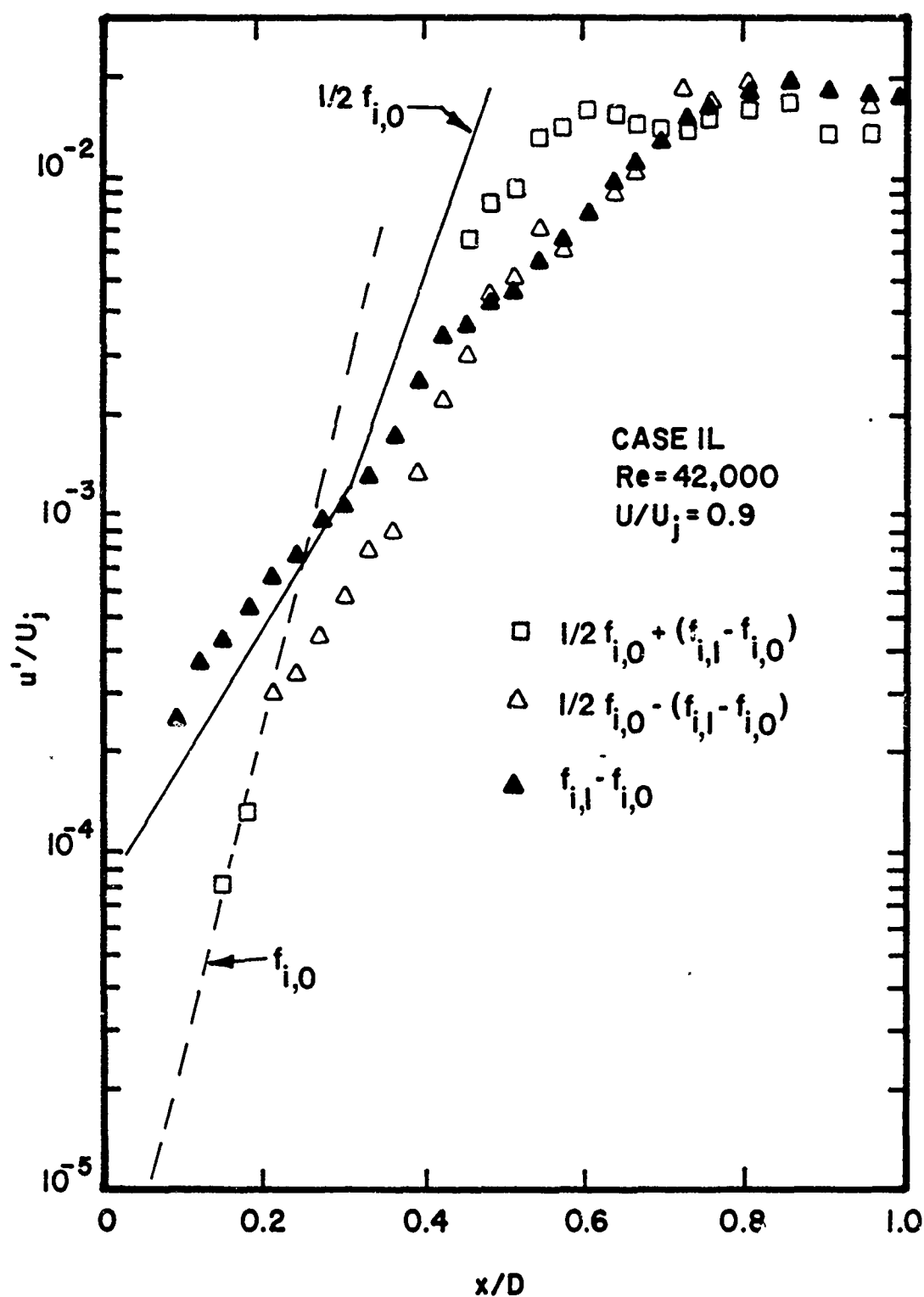
Figure 79. Development of Nonlinearly Generated Modes along $U/U_j = 0.9$ at Re = 42,000 for Case 1L
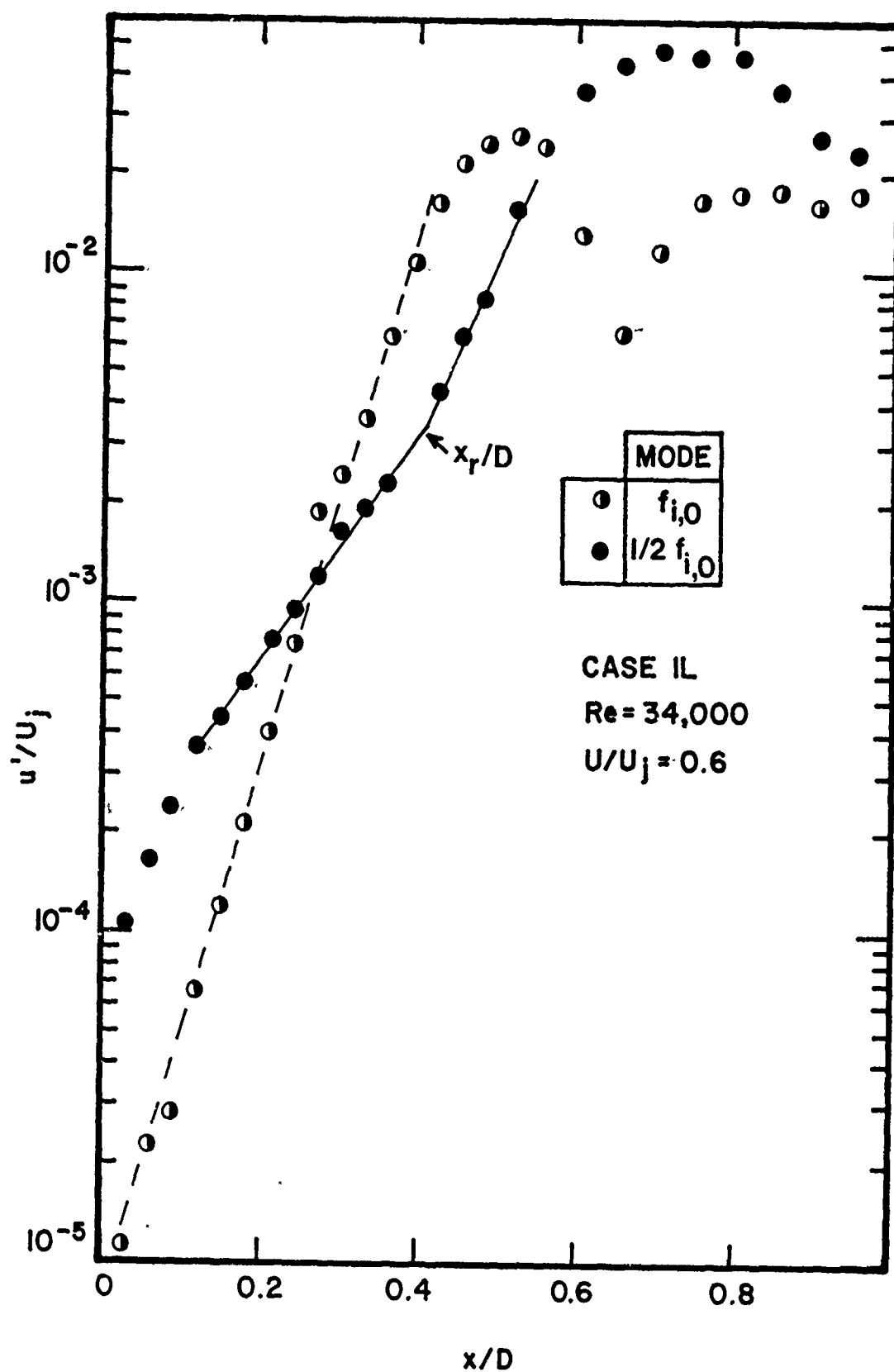
Figure 80. Development of Initial Axisymmetric Mode
and its Subharmonic along $U/U_j= 0.6$ at Re = 42,000
for Case 1L
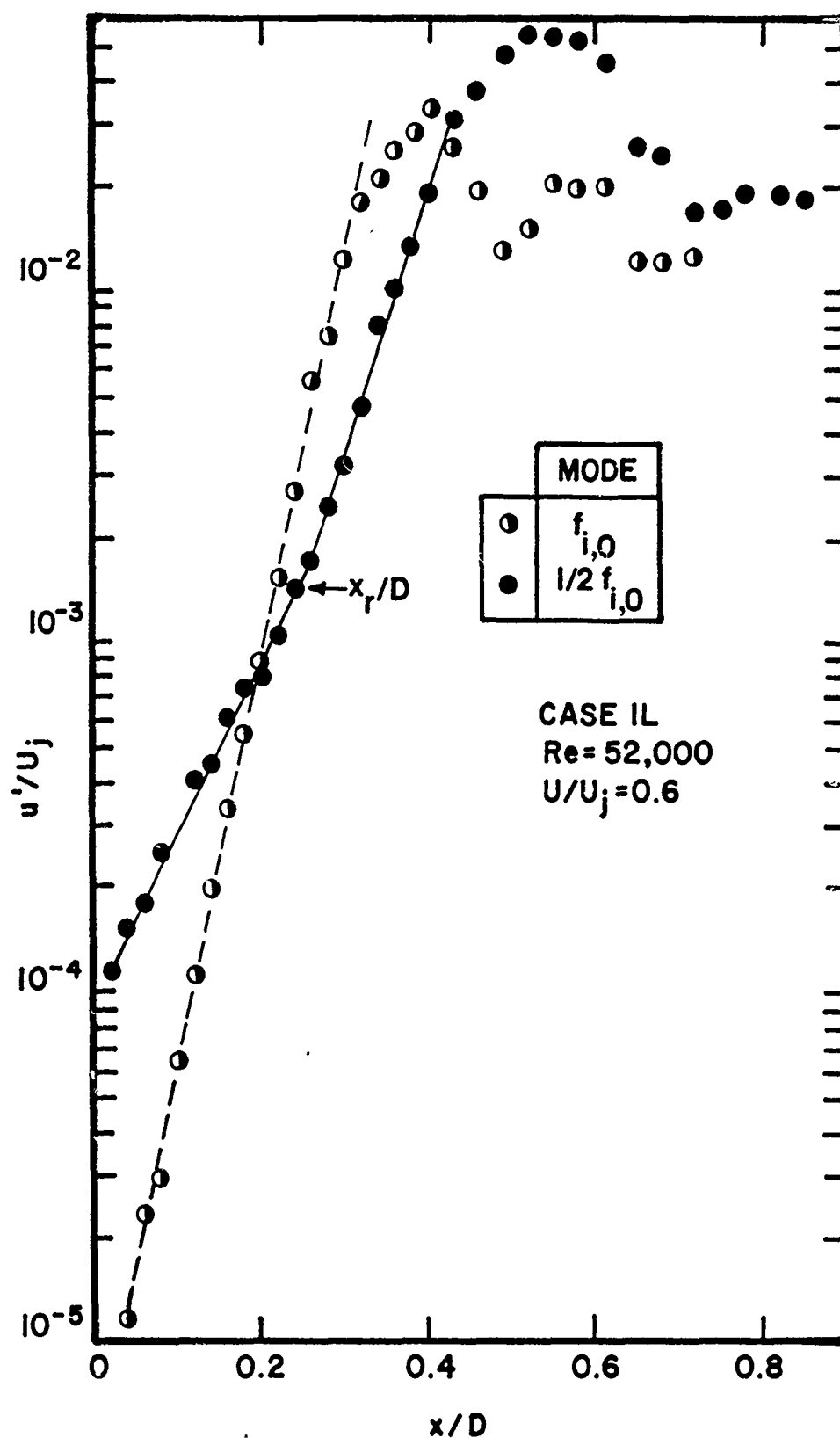
Figure 81. Development of Initial Axisymmetric Mode and its Subharmonic along $U/U_j = 0.6$ at Re $= 52,000$ for Case 1L
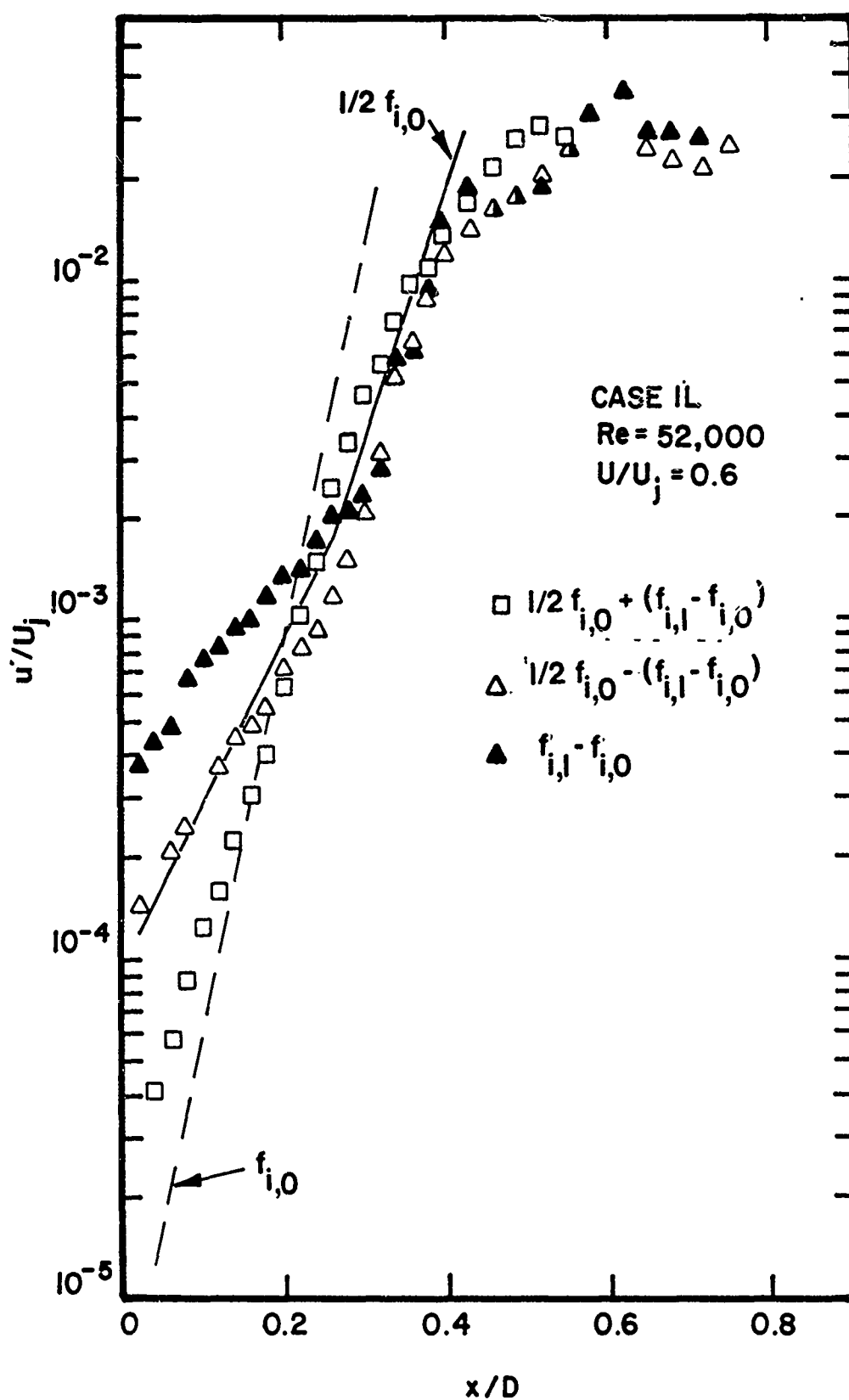
Figure 82. Development of Nonlinearly Generated Modes along $U/U_j = 0.6$ at $Re = 52,000$ for Case 1L
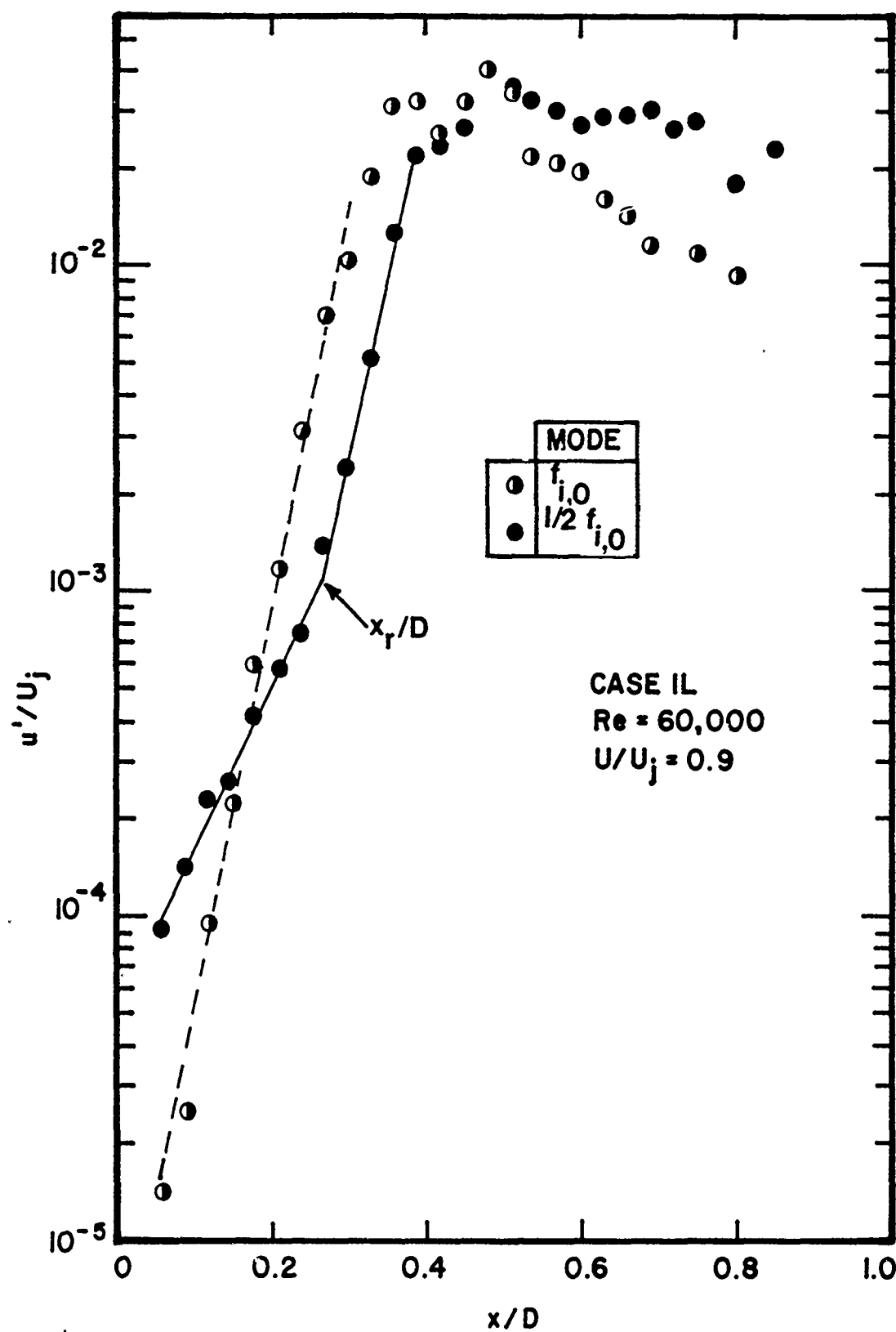
Figure 83. Development of Initial Axisymmetric Mode
and its Subharmonic along $U/U_j = 0.9$ at $Re = 60,000$
for Case 1L
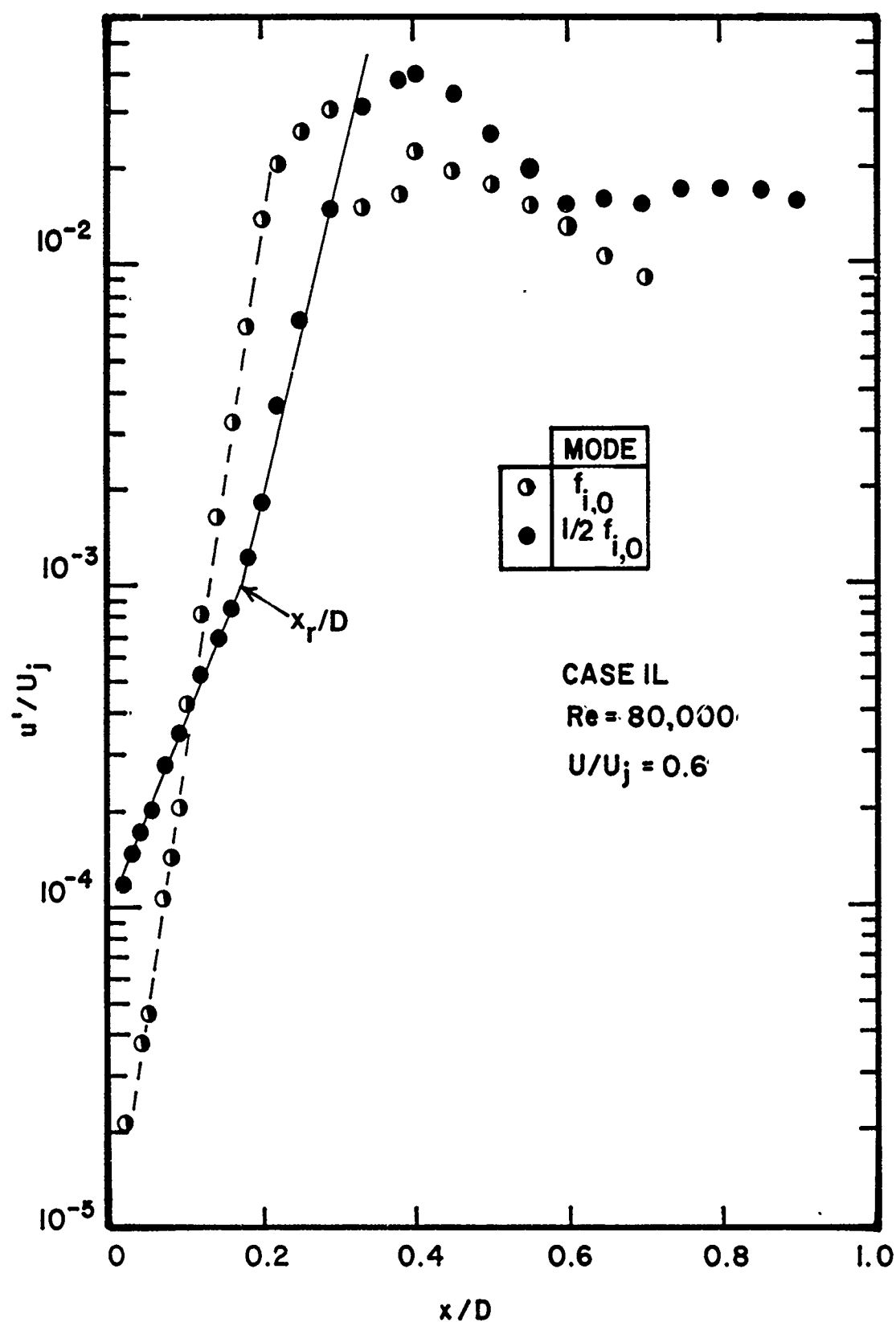
Figure 84. Development of Initial Axisymmetric Mode
and its Subharmonic along $U/U_j = 0.6$ at Re = 80,000
for Case 1L
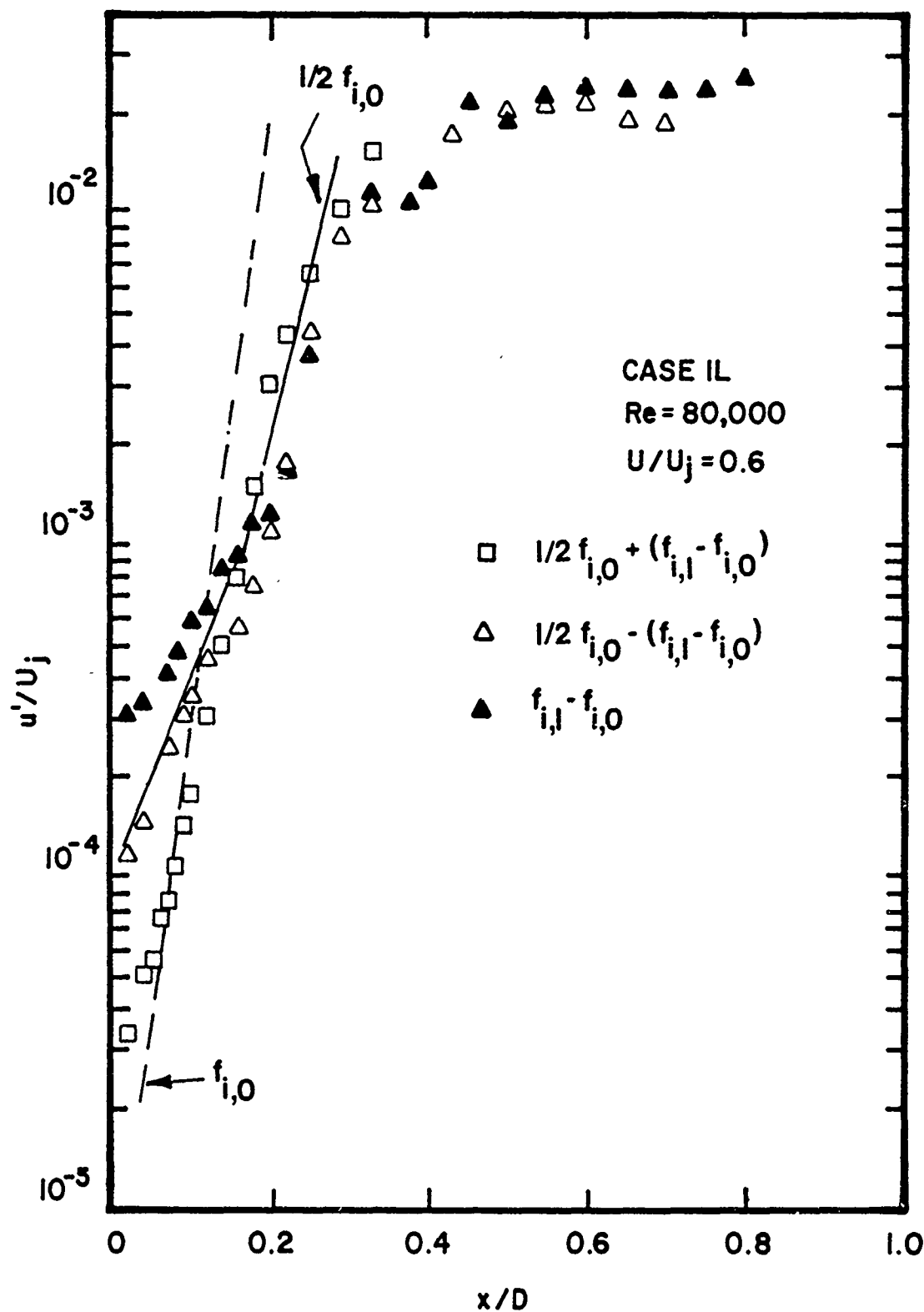
Figure 85. Development of Nonlinearly Generated Modes along $U/U_j = 0.6$ at Re = 80,000 for Case 1L
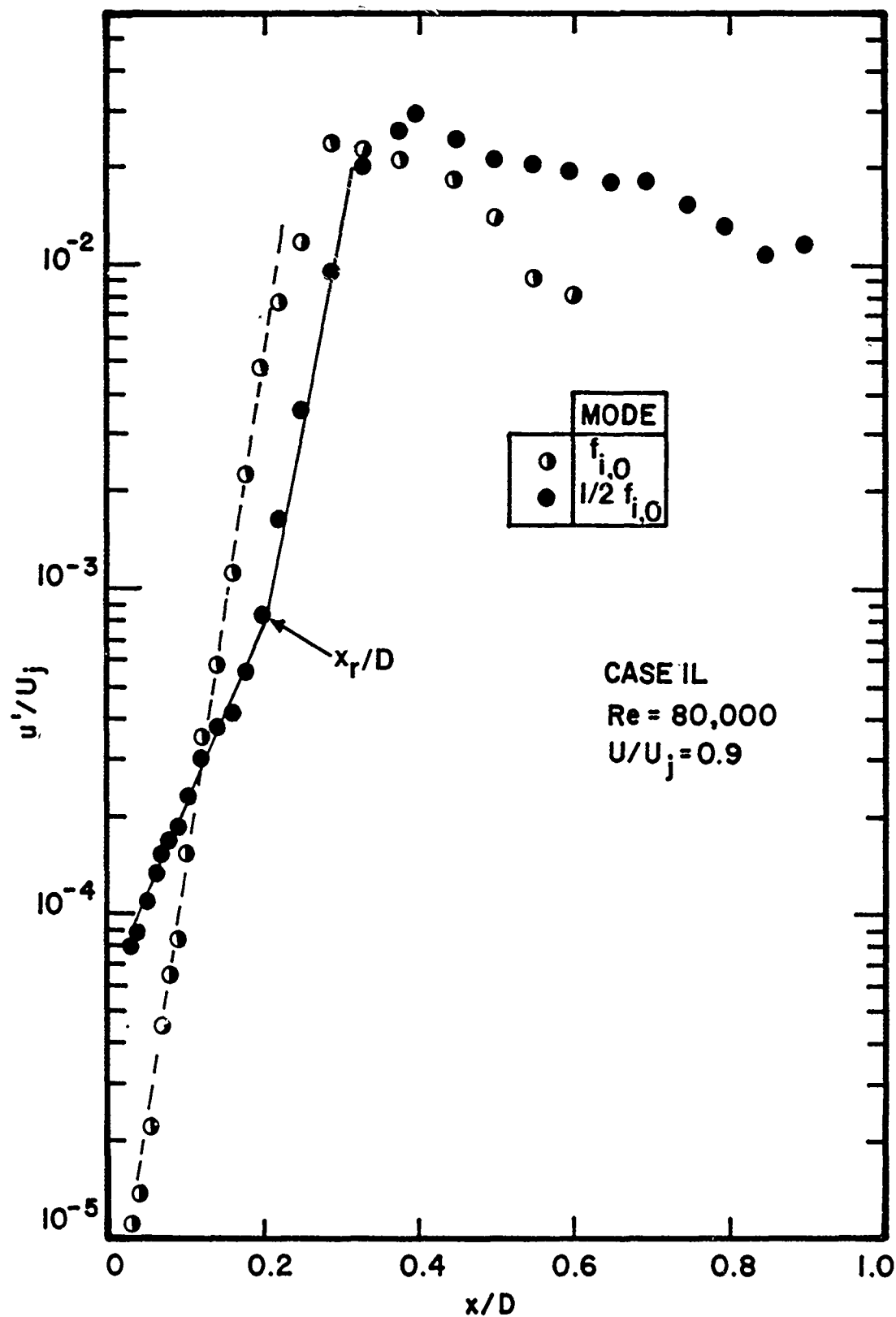
Figure 86. Development of Initial Axisymmetric Mode
and its Subharmonic along $U/U_j = 0.9$ at $Re = 80,000$
for Case 1L
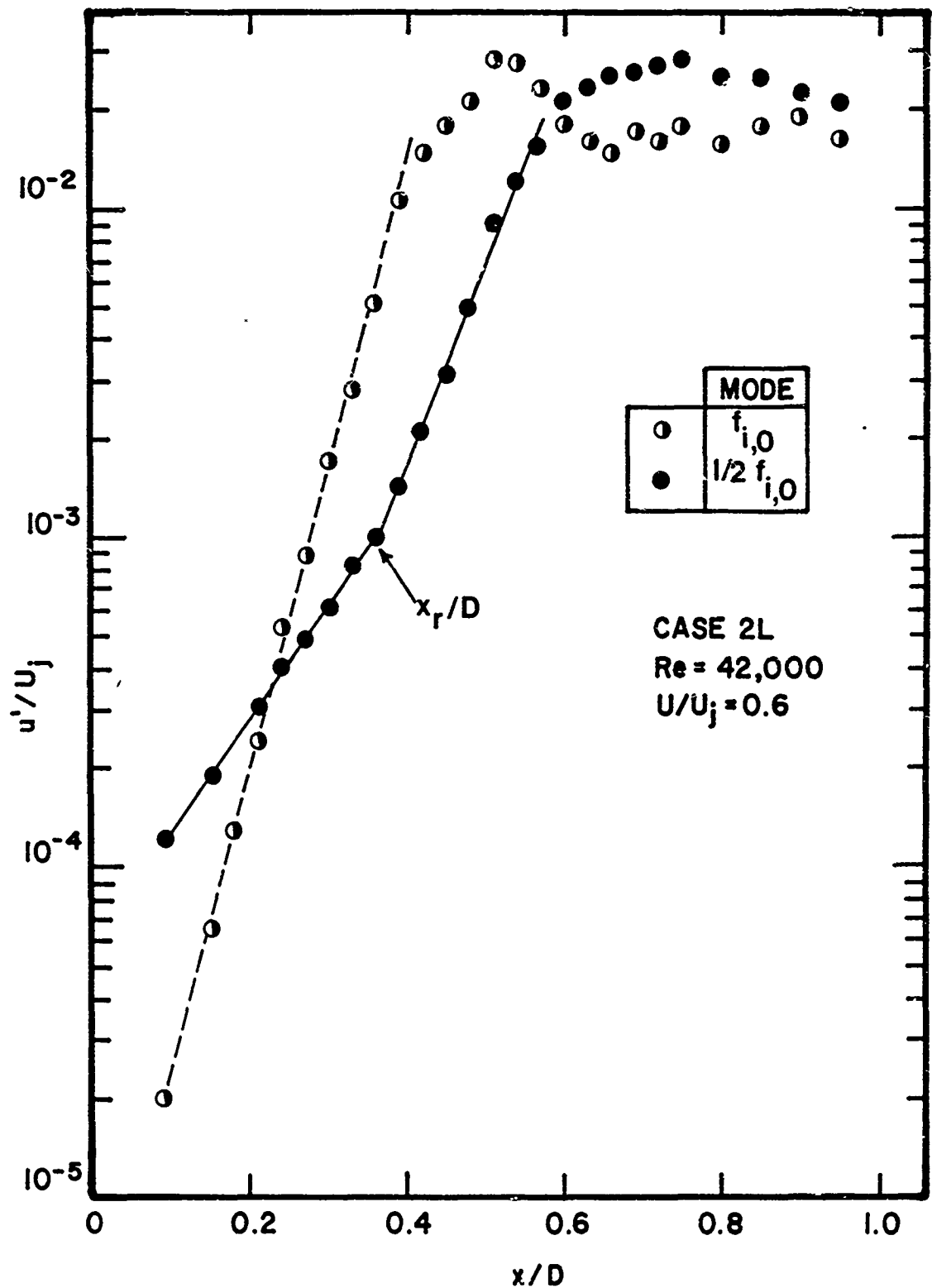
Figure 87. Development of Initial Axisymmetric Mode and its Subharmonic along $U/U_j = 0.6$ at Re = 42,000 for Case 2L
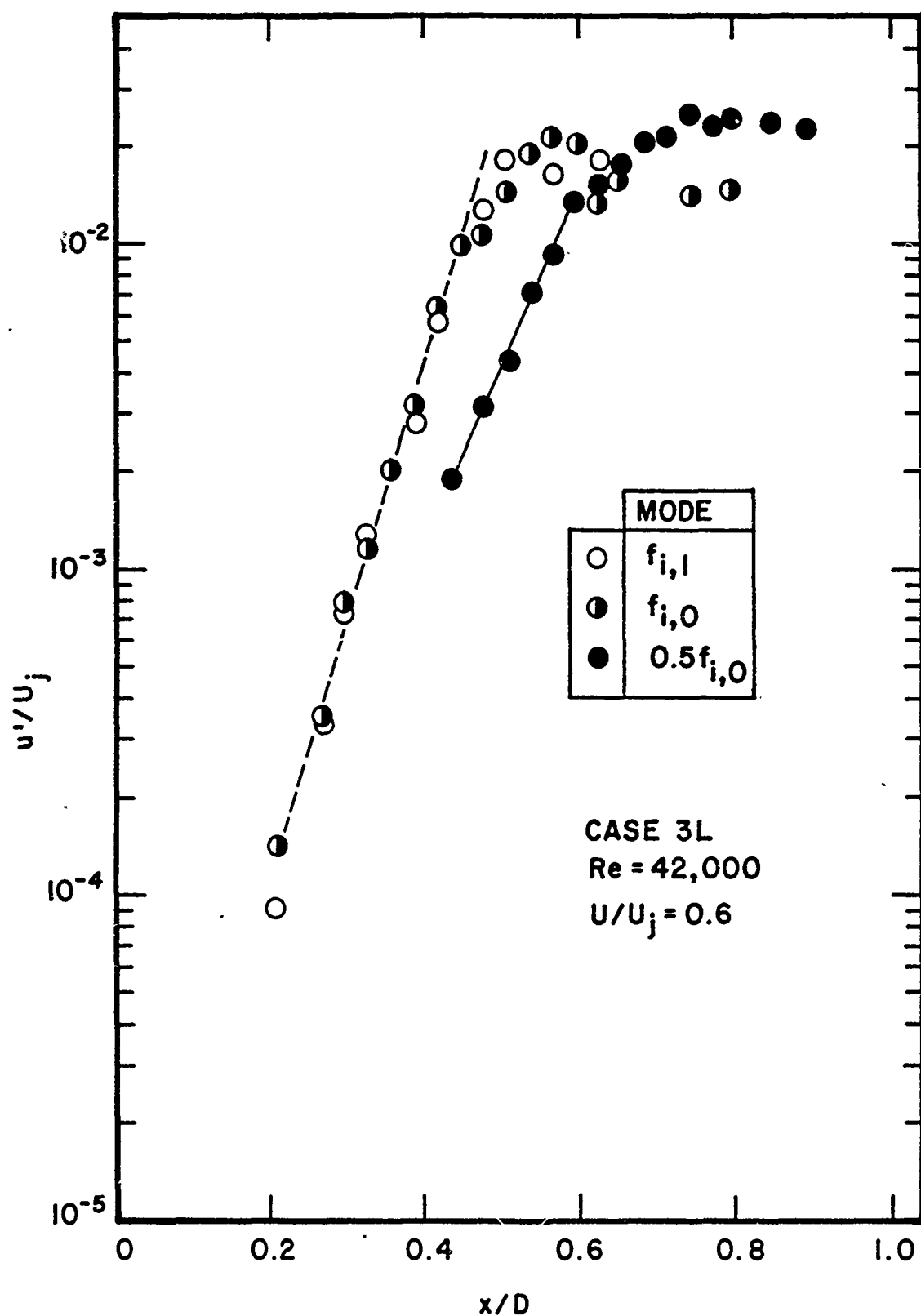
Figure 88. Development of Initial Axisymmetric Mode, its Subharmonic and Initial Helical Mode along $U/U_j = 0.6$ at Re = 42,000 for Case 3L
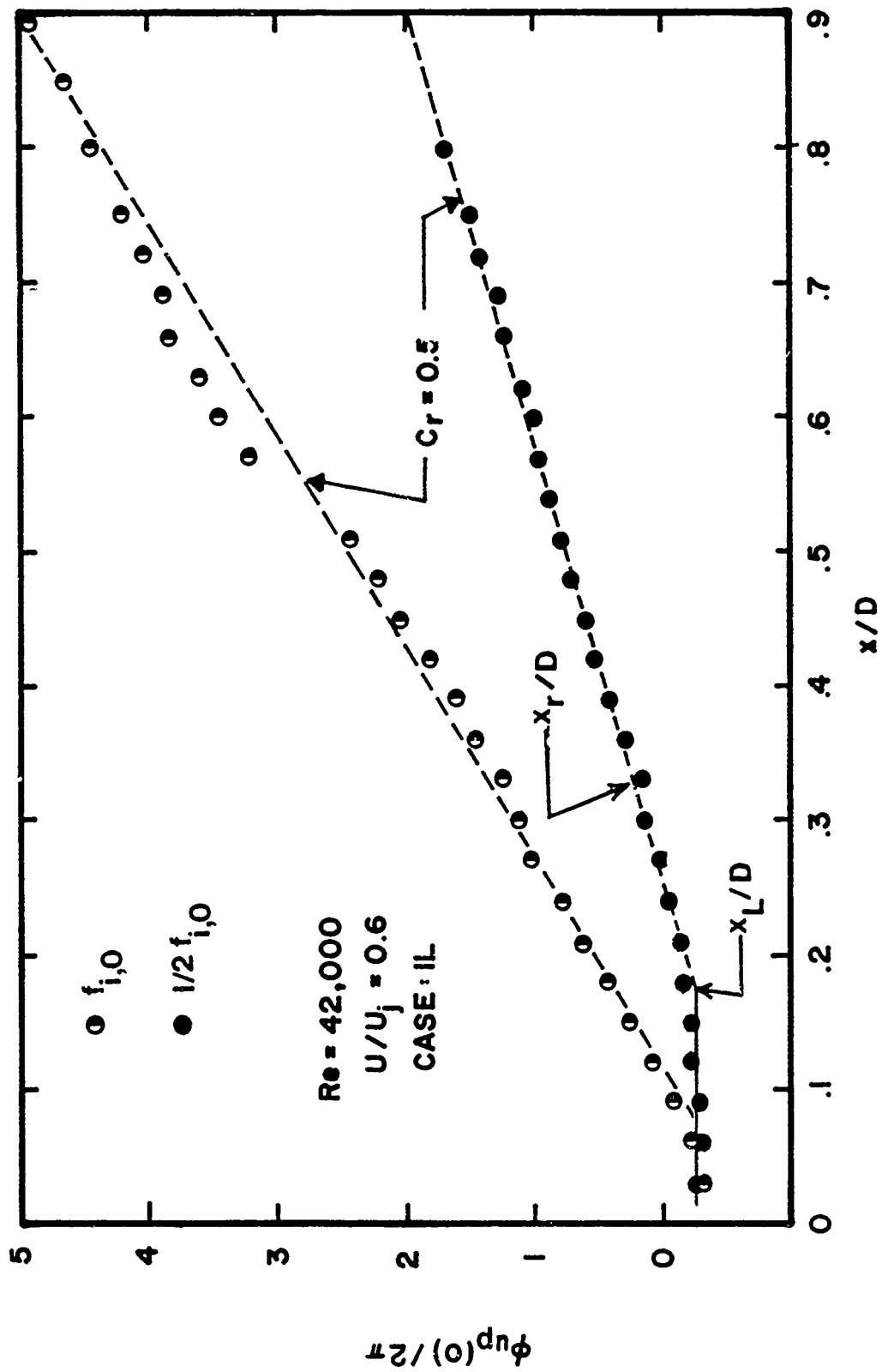
Figure 89. Streamwise Phase Variation of Initial Axisymmetric Mode and its Subharmonic along $U/U_j = 0.6$ at Re = 42,000 for Case 1L
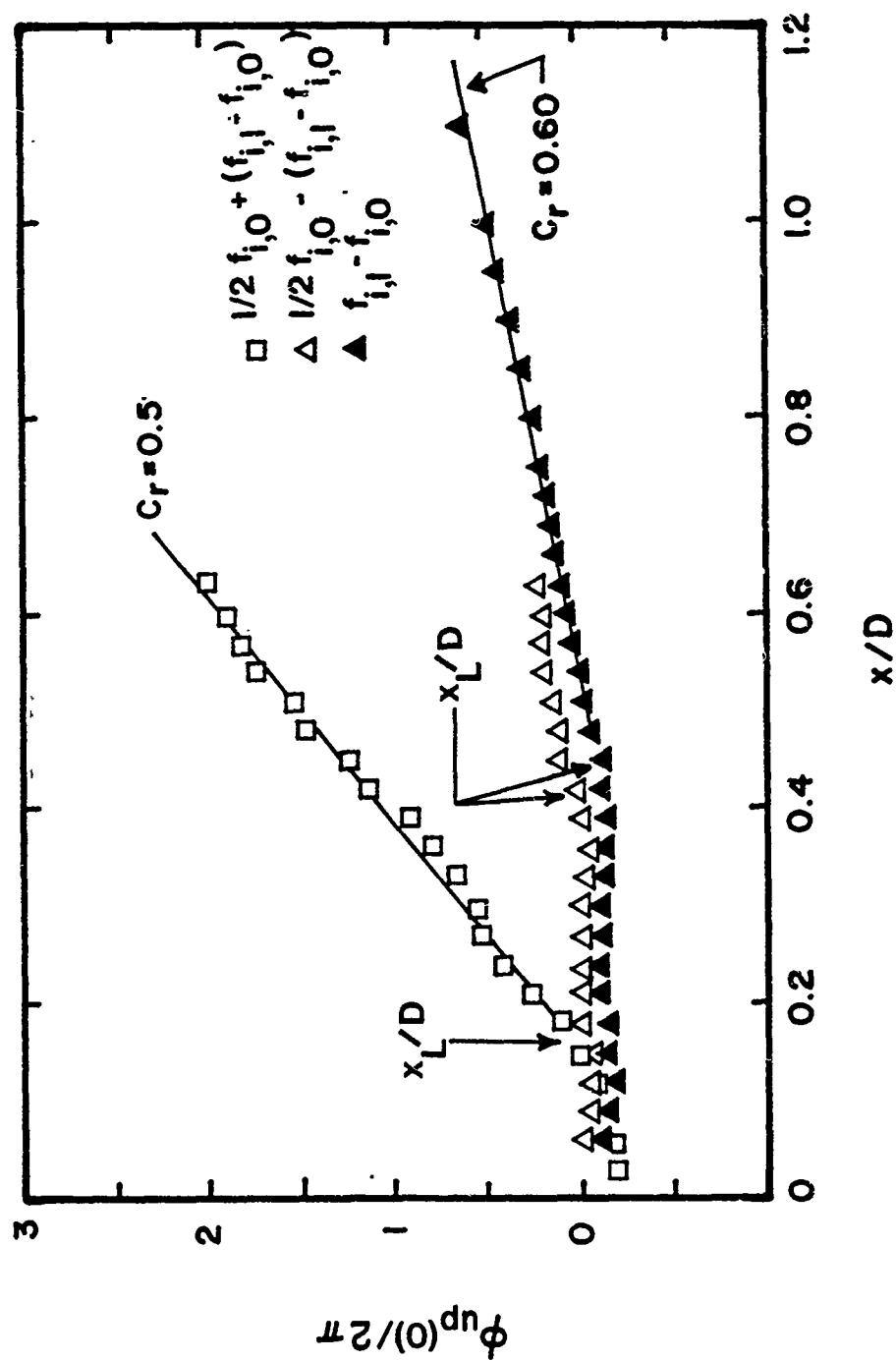
Figure 90. Streamwise Phase Variation of Nonlinearly Developed Modes Along $U/U_j = 0.6$ at Re = 42,000 for Case 1L
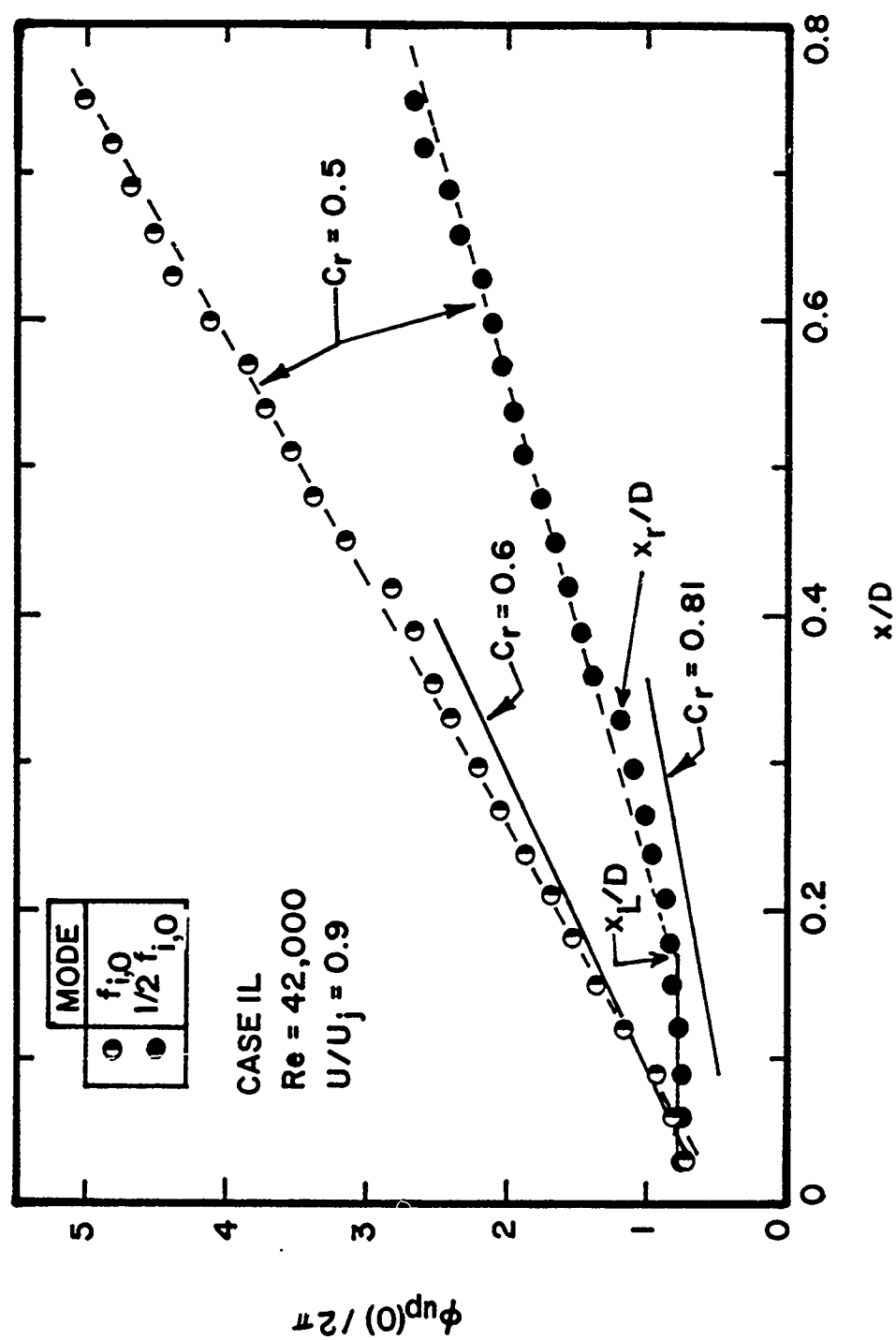
Figure 91. Streamwise Phase Variation of Initial Axisymmetric Mode and its Subharmonic along $U/U_j = 0.9$ at $Re = 42,000$ for Case 1L
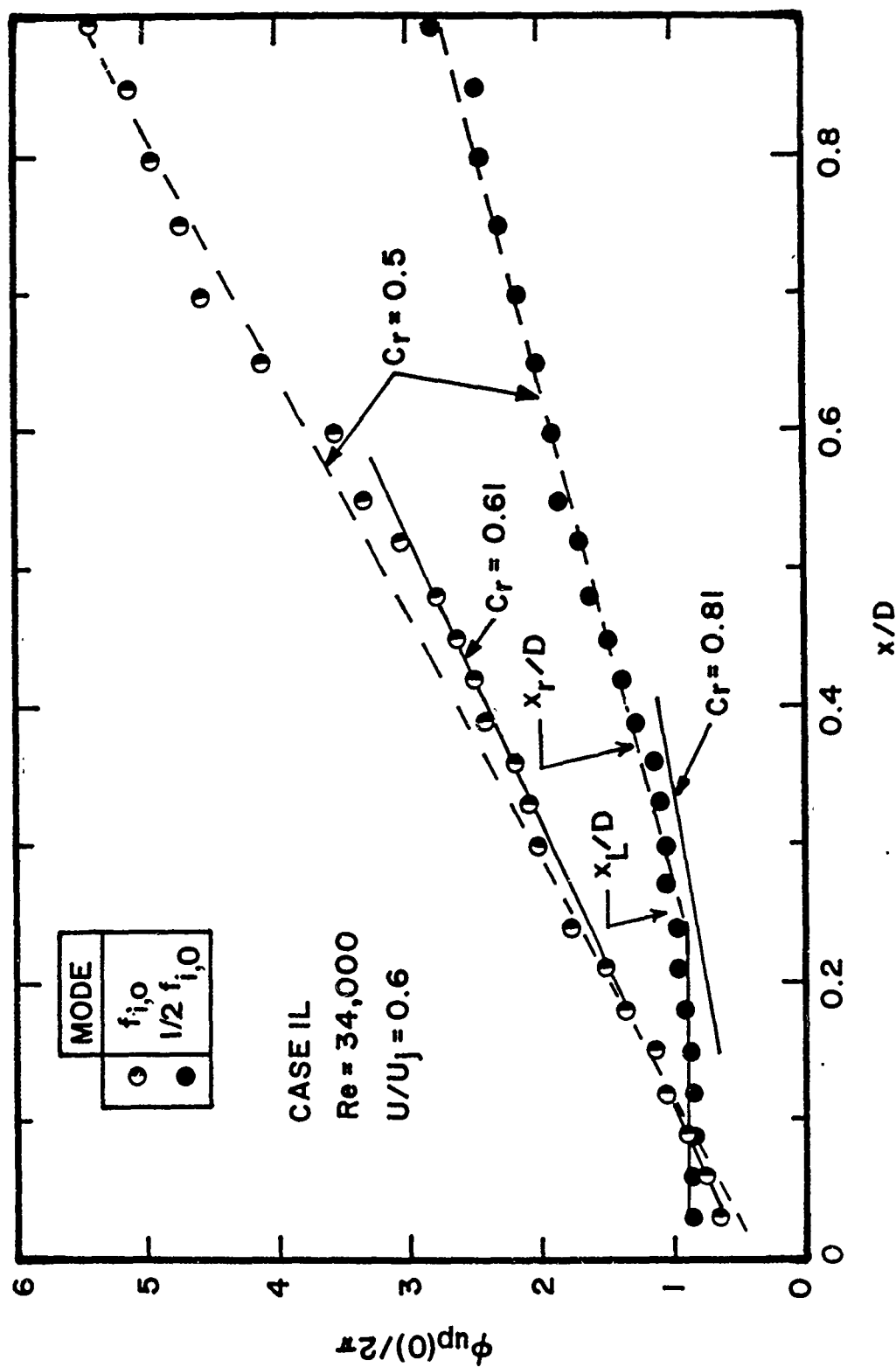
Figure 92. Streamwise Phase Variation of Initial Axisymmetric Mode and its Subharmonic along $U/U_j = 0.6$ at Re = 42,000 for Case 1L
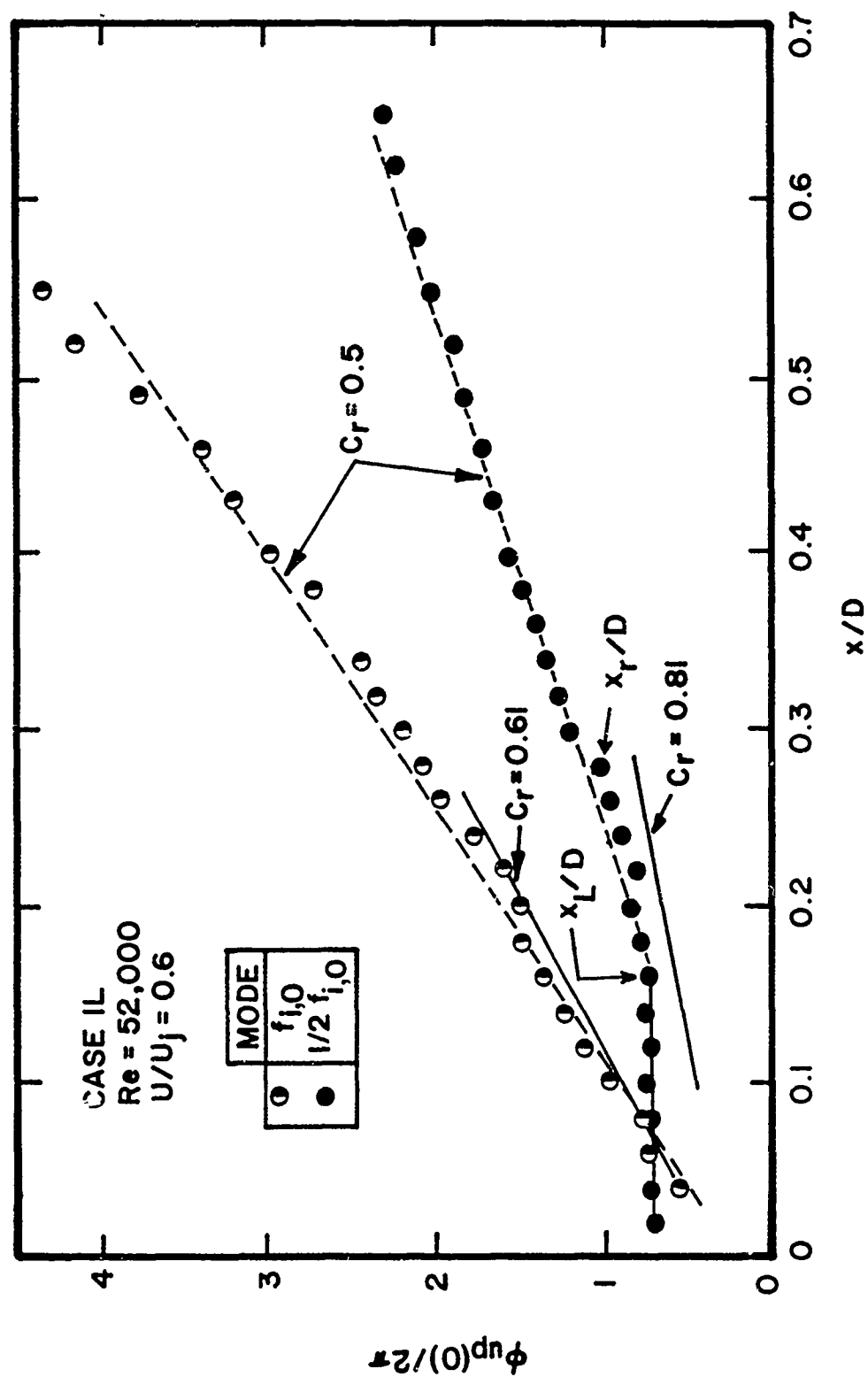
Figure 93. Streamwise Phase Variation of Initial Axisymmetric Mode and its Subharmonic along $U/U_j = 0.6$ at Re = 52,000 for Case 1L
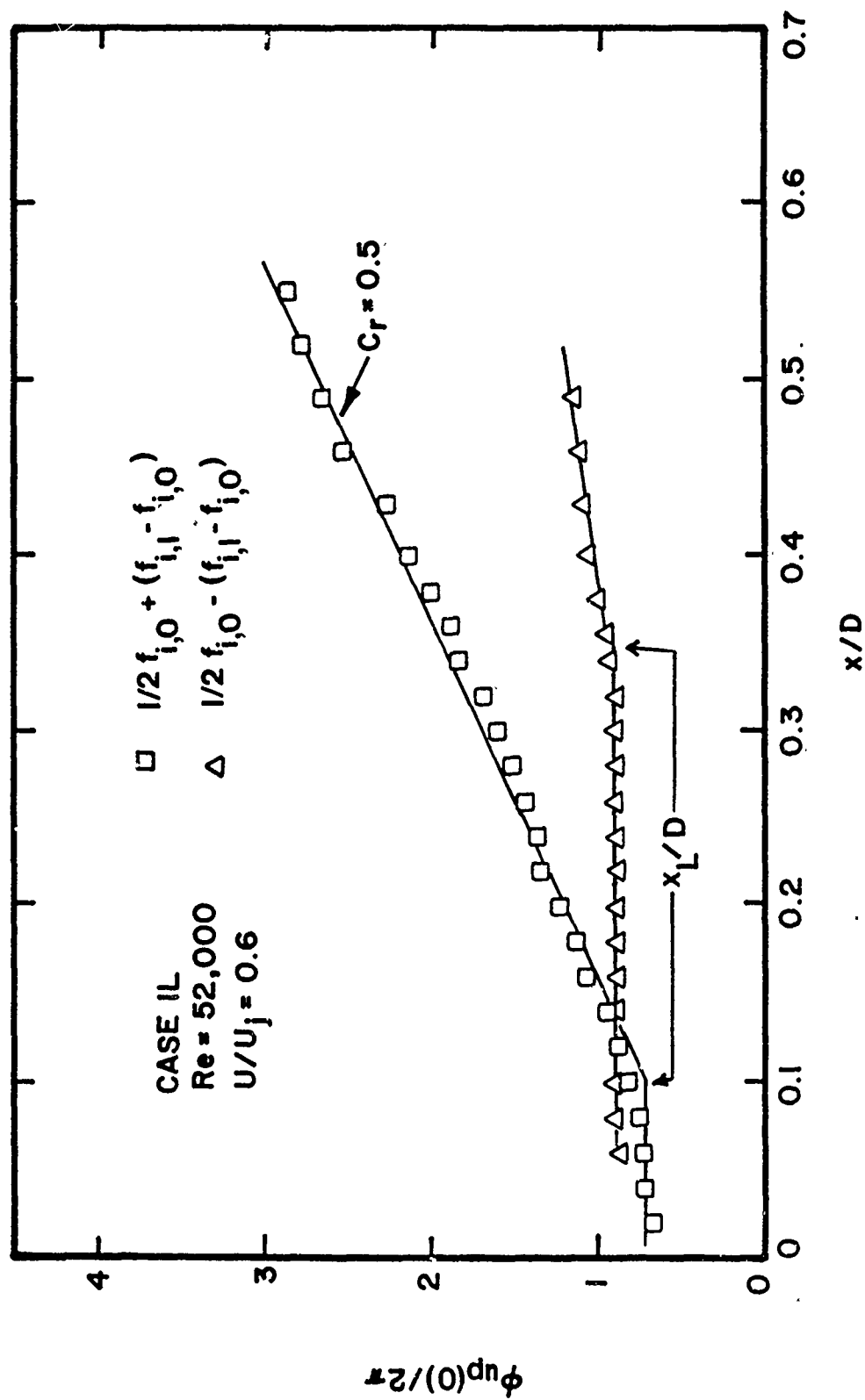
Figure 94. Streamwise Phase Variation of Nonlinearly Developed Modes Along
$U/U_j = 0.6$ at Re = 52,000 for Case 1L
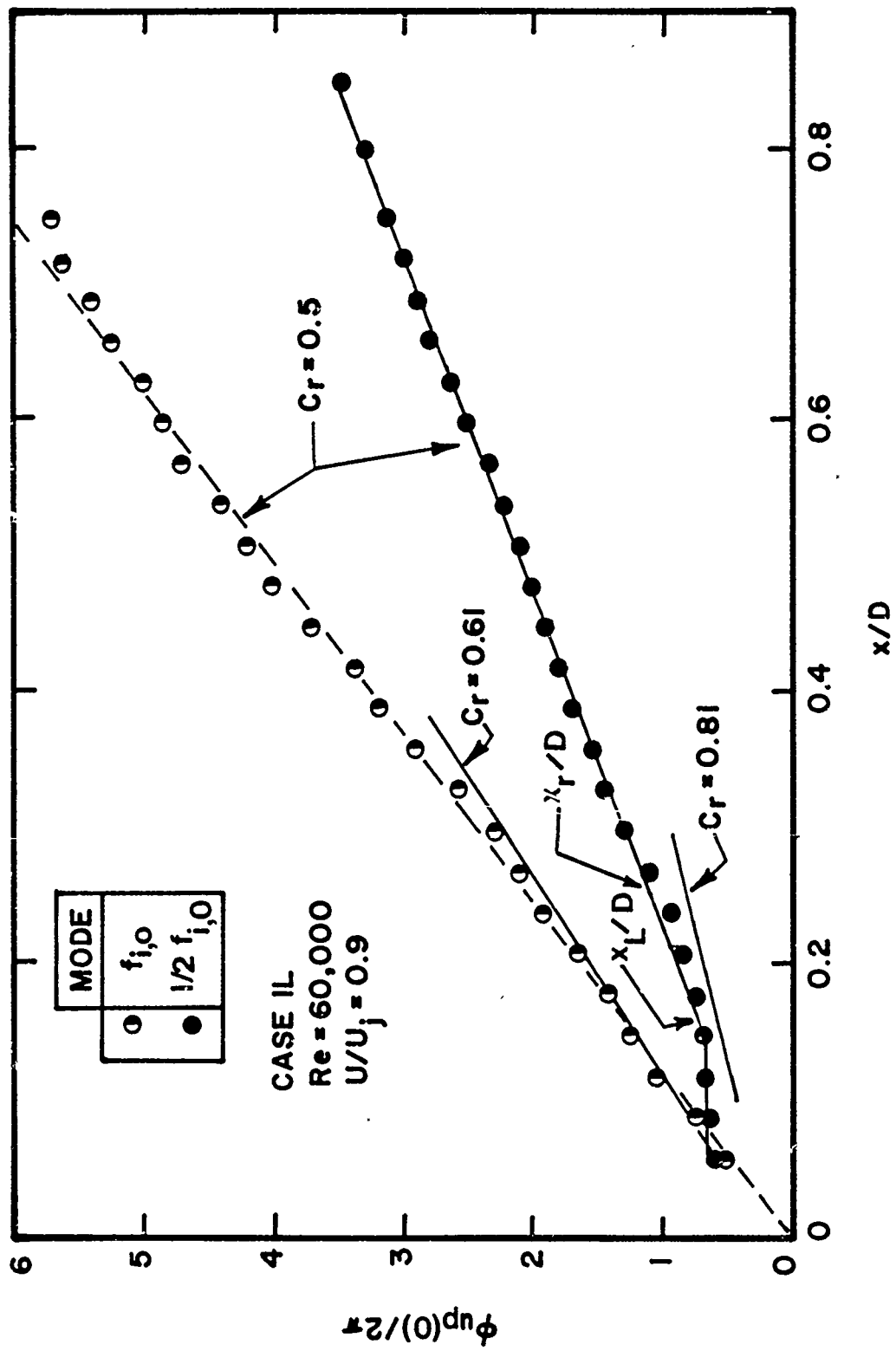
Figure 95. Streamwise Phase Variation of Initial Axisymmetric Mode and its Subharmonic along $U/U_j = 0.9$ at $Re = 60,000$ for Case 1L
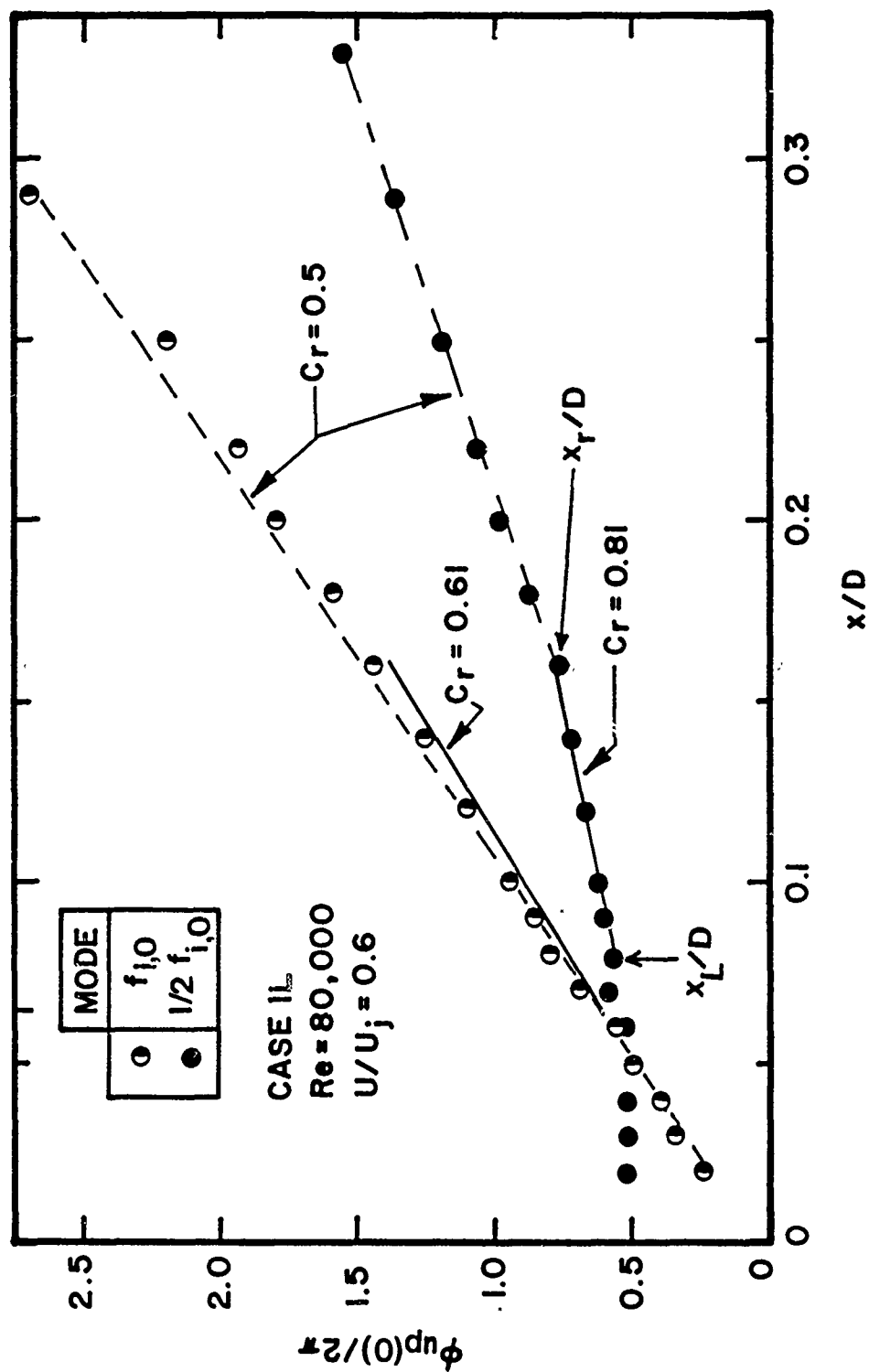
Figure 96. Streamwise Phase Variation of Initial Axisymmetric Mode and its Subharmonic along $U/U_j = 0.6$ at $Re = 80,000$ for Case 1L
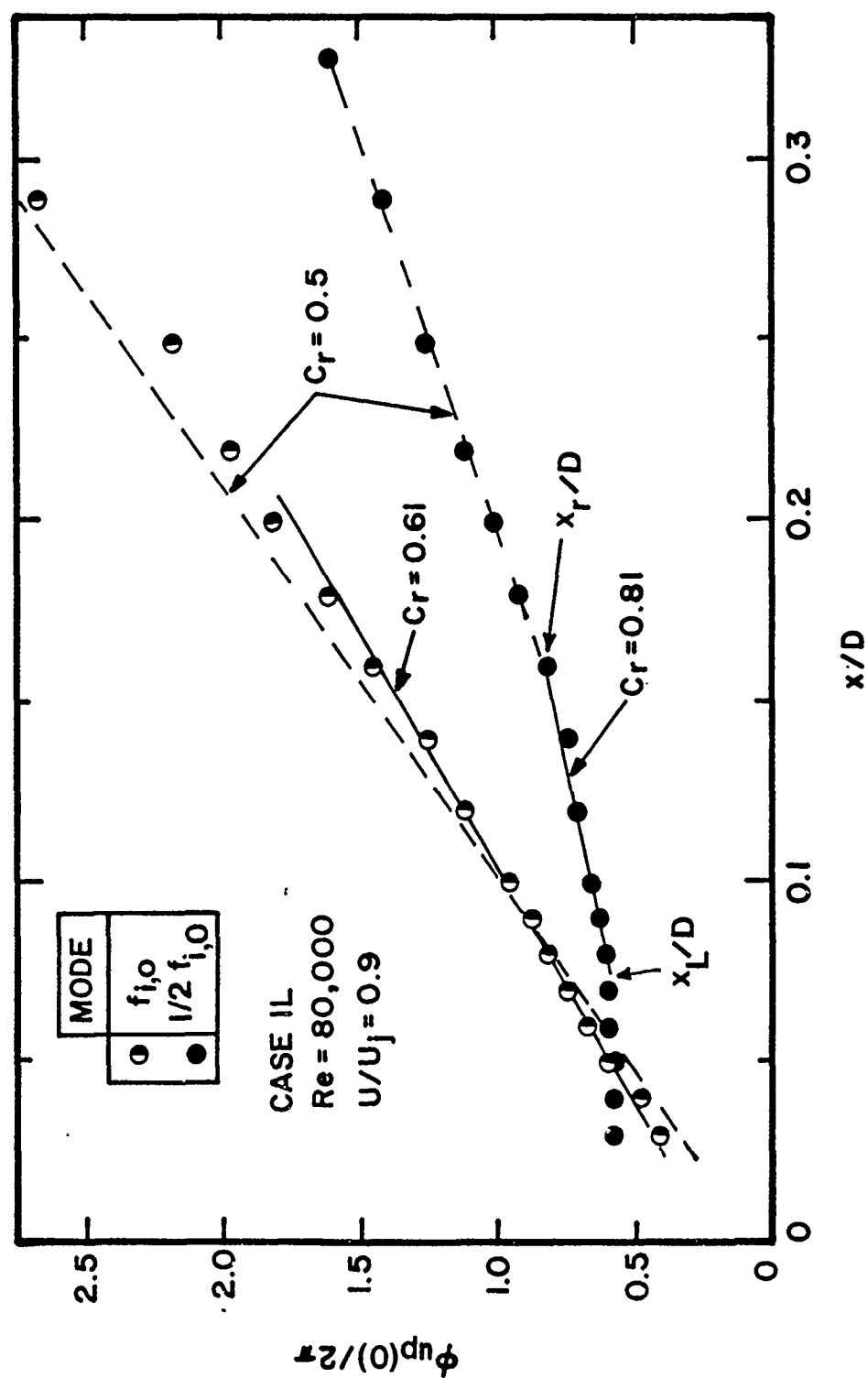
Figure 97. Streamwise Phase Variation of Initial Axisymmetric Mode and its Subharmonic along $U/U_j = 0.9$ at Re = 80,000 for Case 1L.
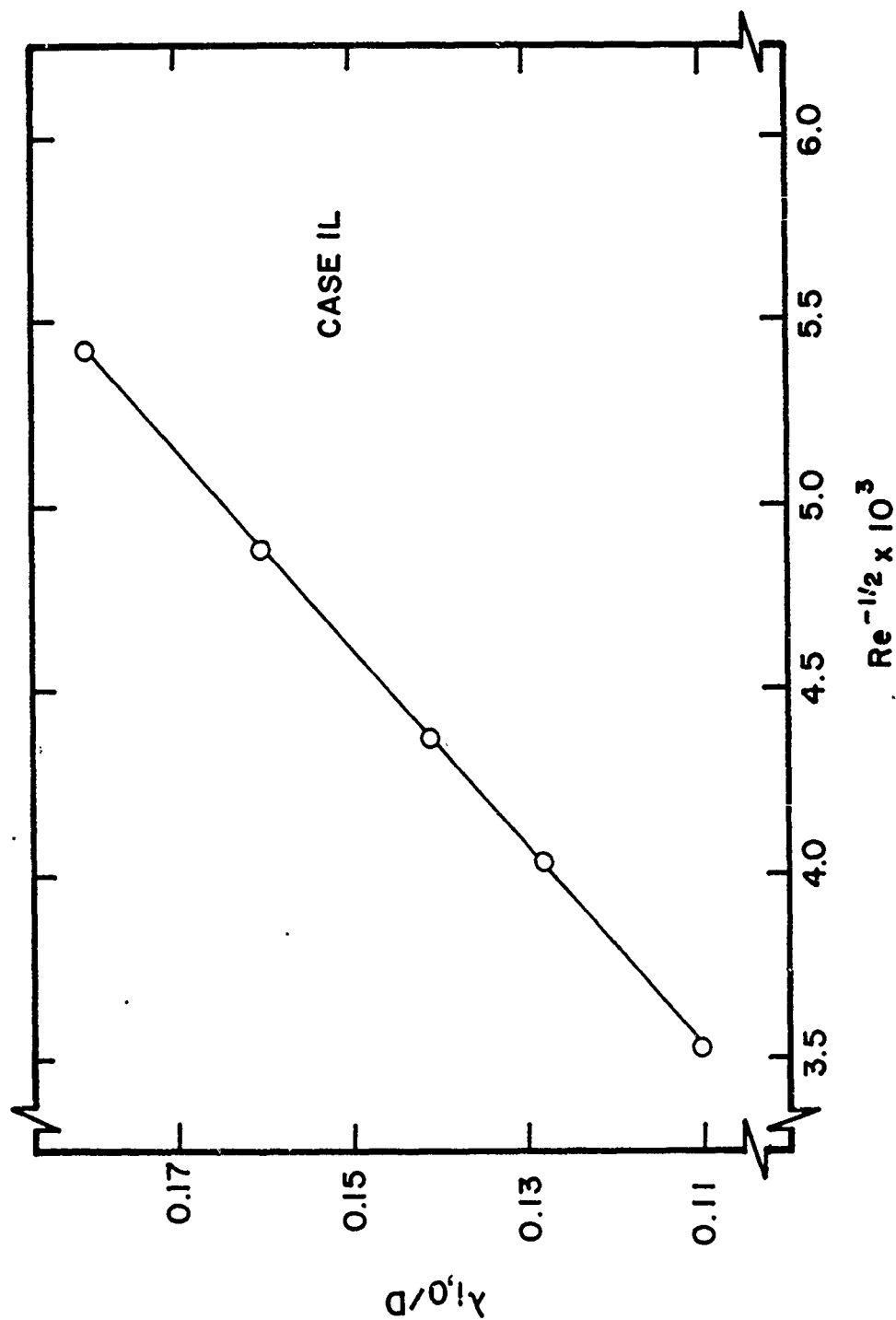
Figure 98. Dependence of Wave Length of Initial Axisymmetric Mode
on Reynolds Number
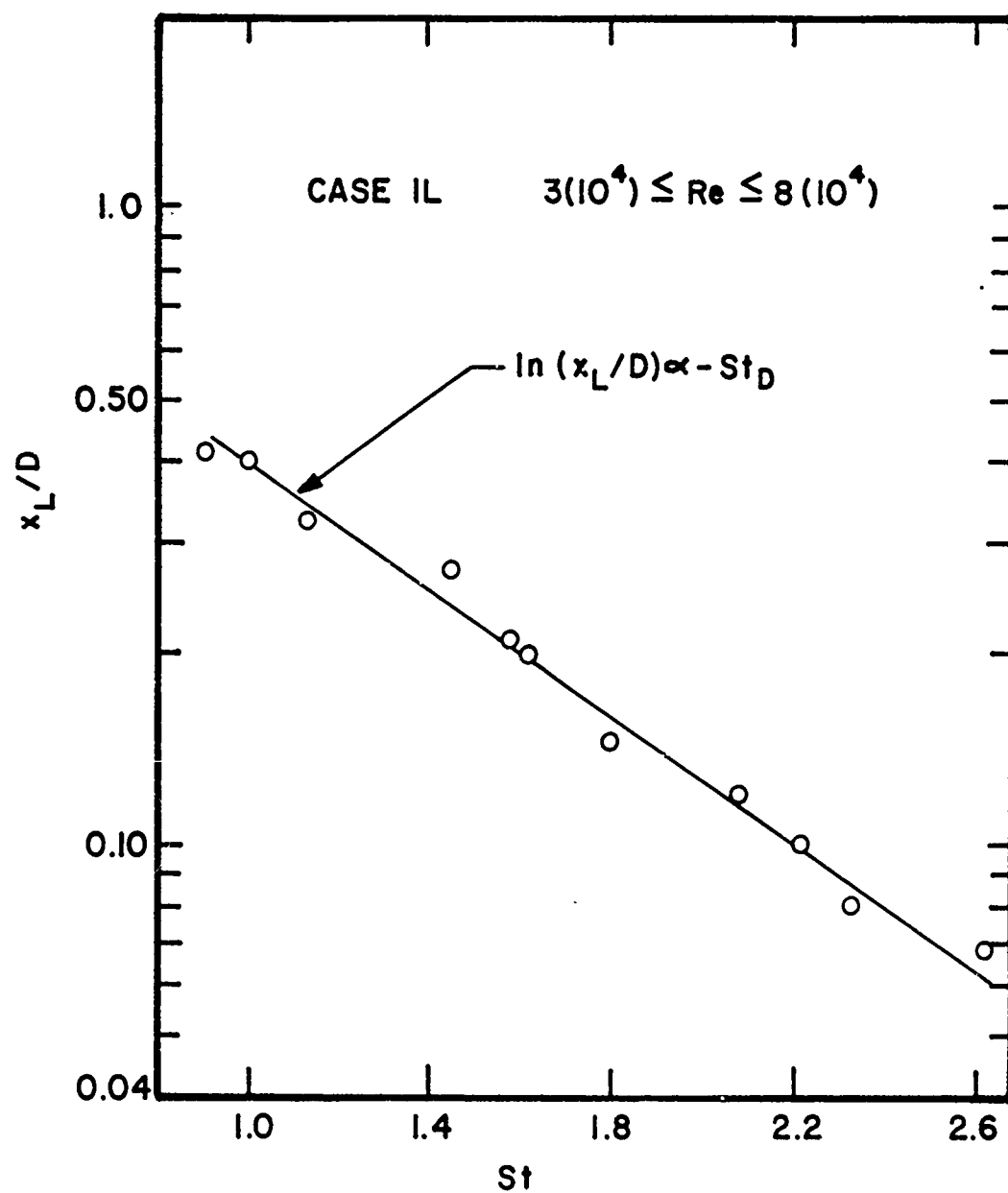
Figure 99. Dependence of Nozzle-Lip Influence Region on Mode Strouhal Frequency
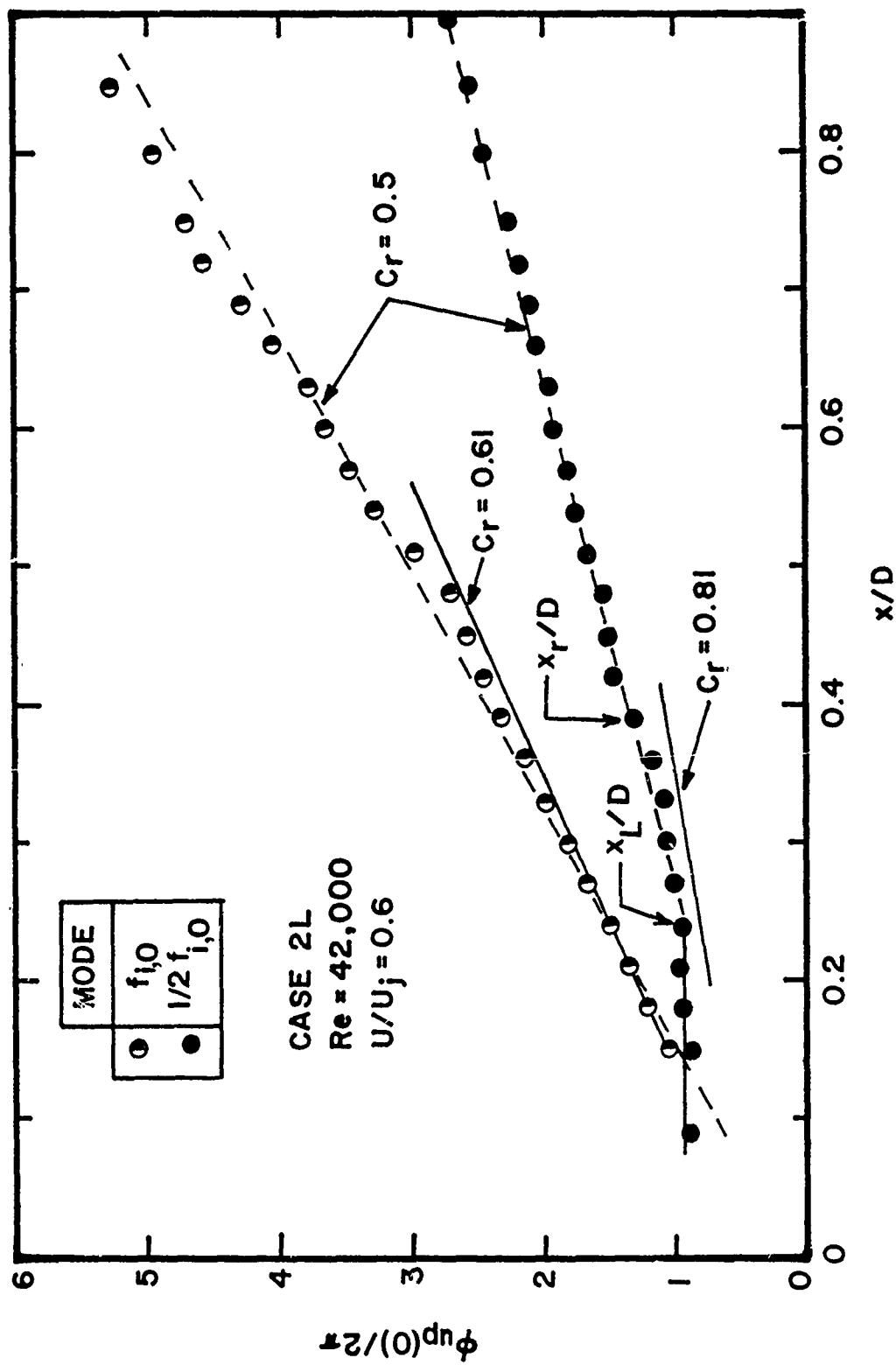
Figure 100. Streamwise Phase Variation of Initial Axisymmetric Mode and its Subharmonic along $U/U_j = 0.6$ at $Re = 42,000$ for Case 2L
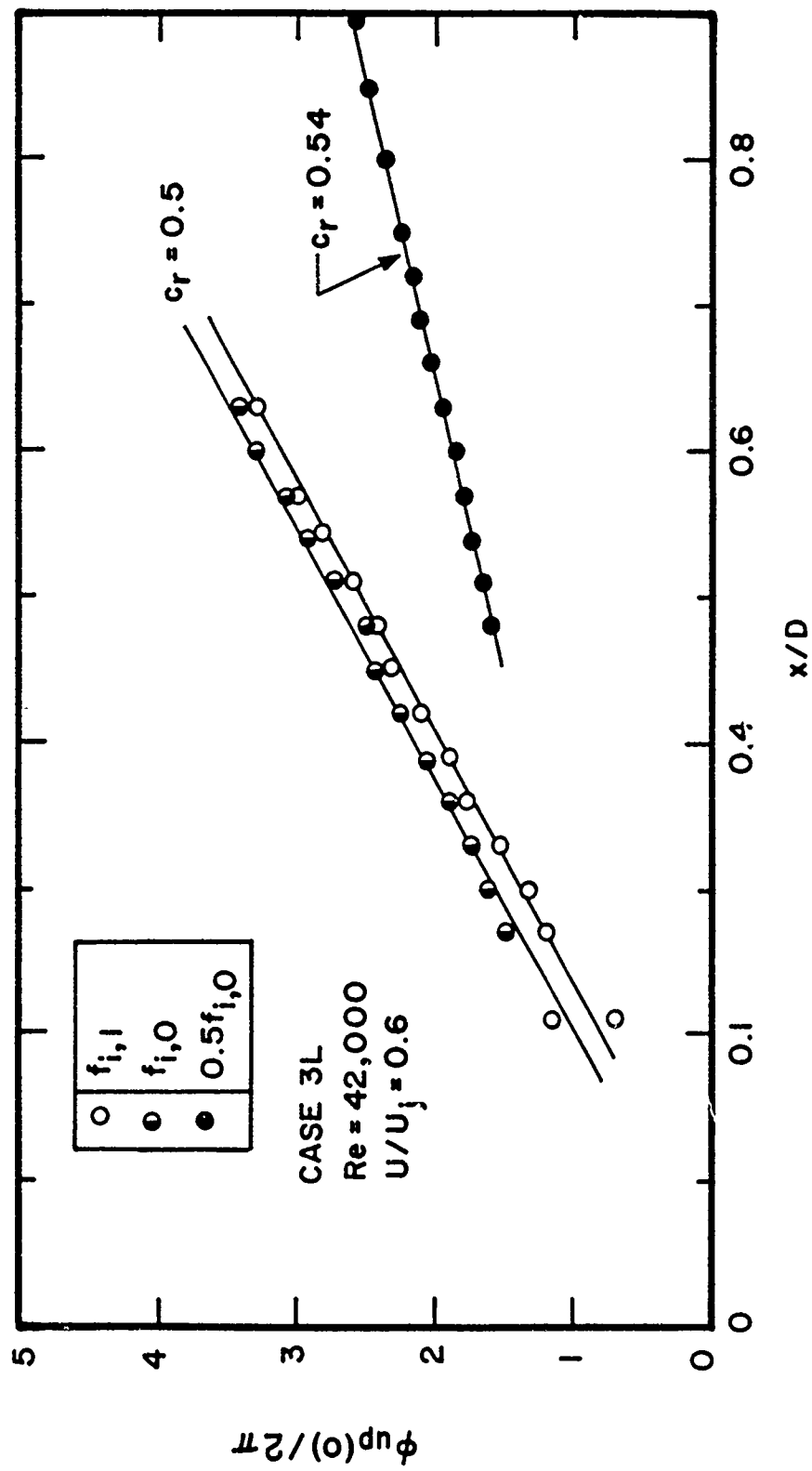
Figure 101. Streamwise Phase Variation of Initial Axisymmetric Mode, its Subharmonic and Initial Helical Mode along $U/U_j = 0.6$ at $Re = 42,000$ for Case 3L
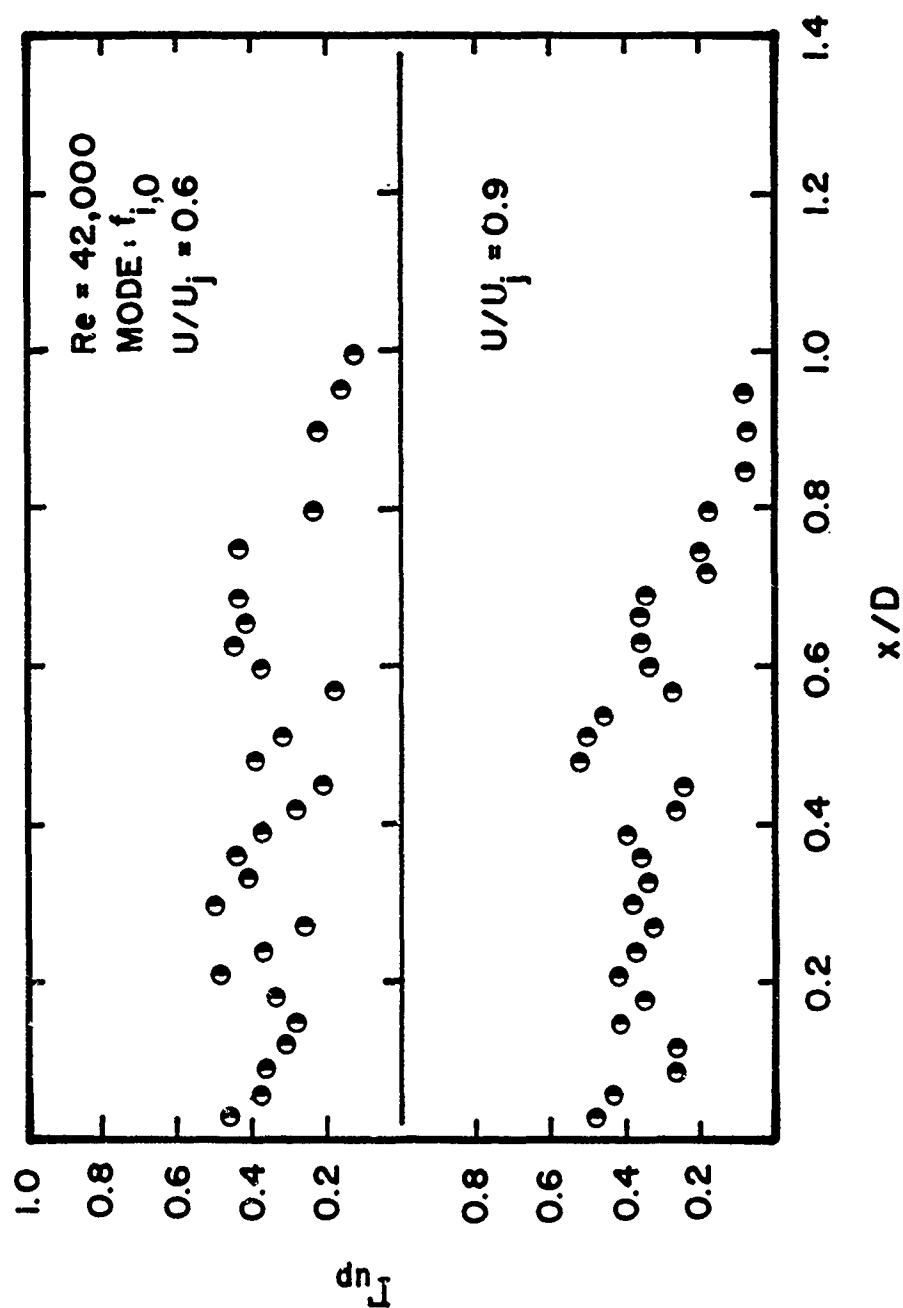
Figure 102. Streamwise Variation of Coherence Between Velocity and Near-Field Pressure for Initial Axisymmetric Mode at Re = 42,000 for Case 1L
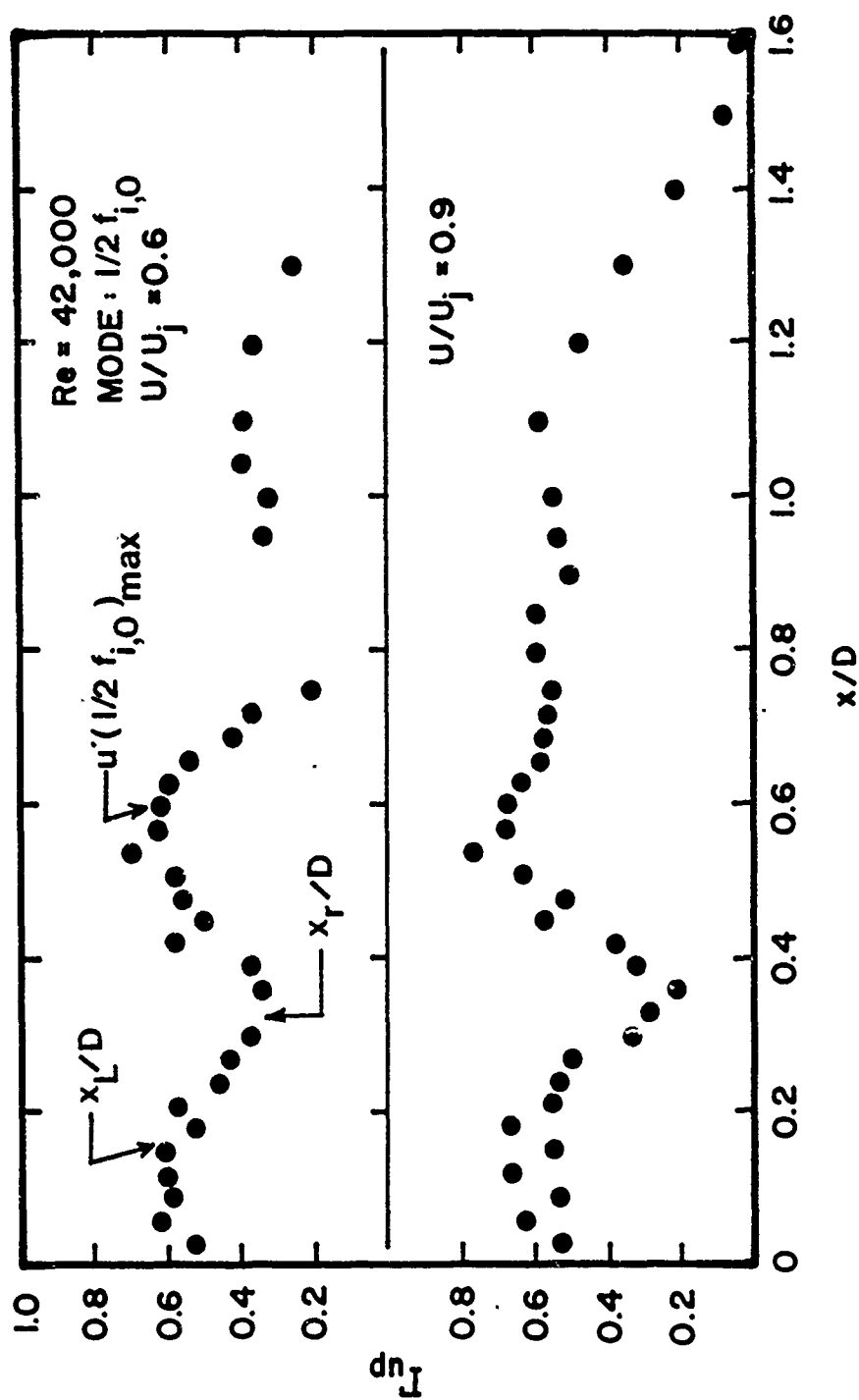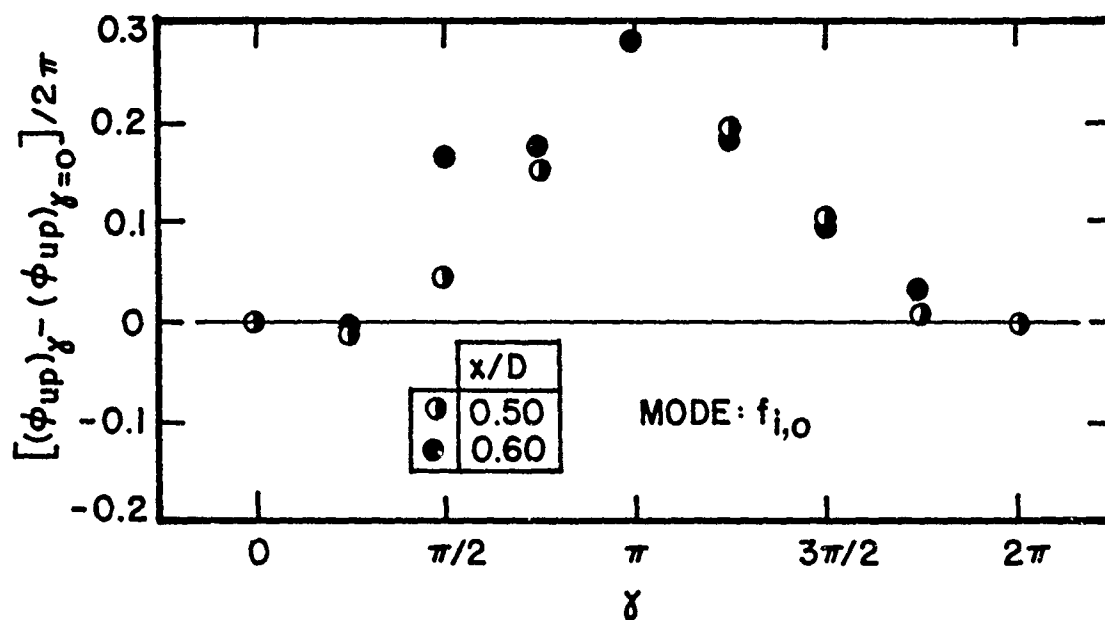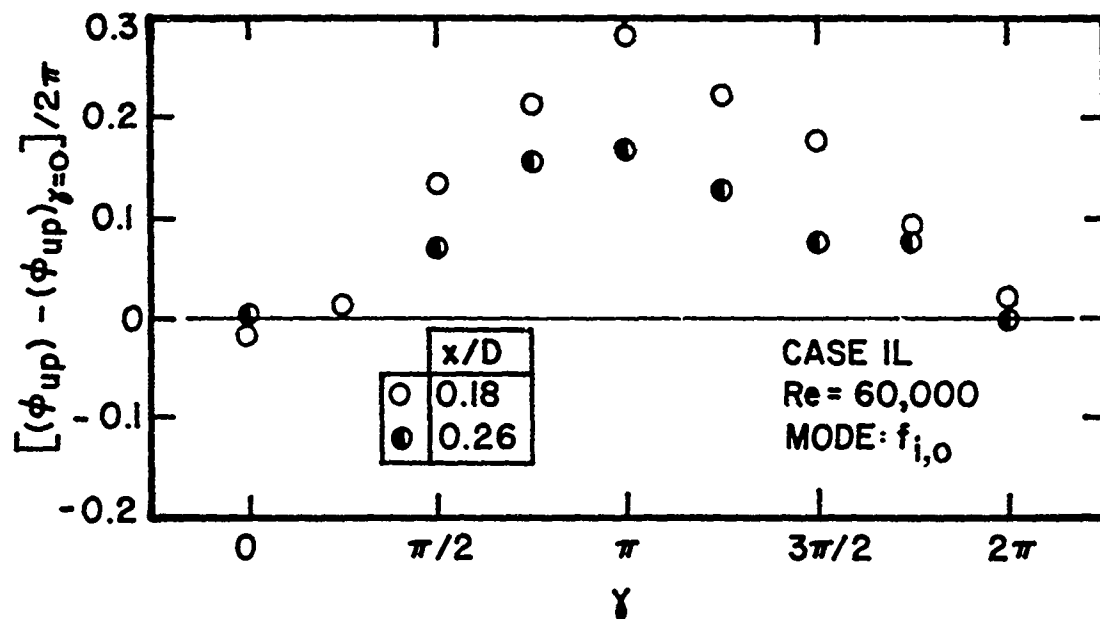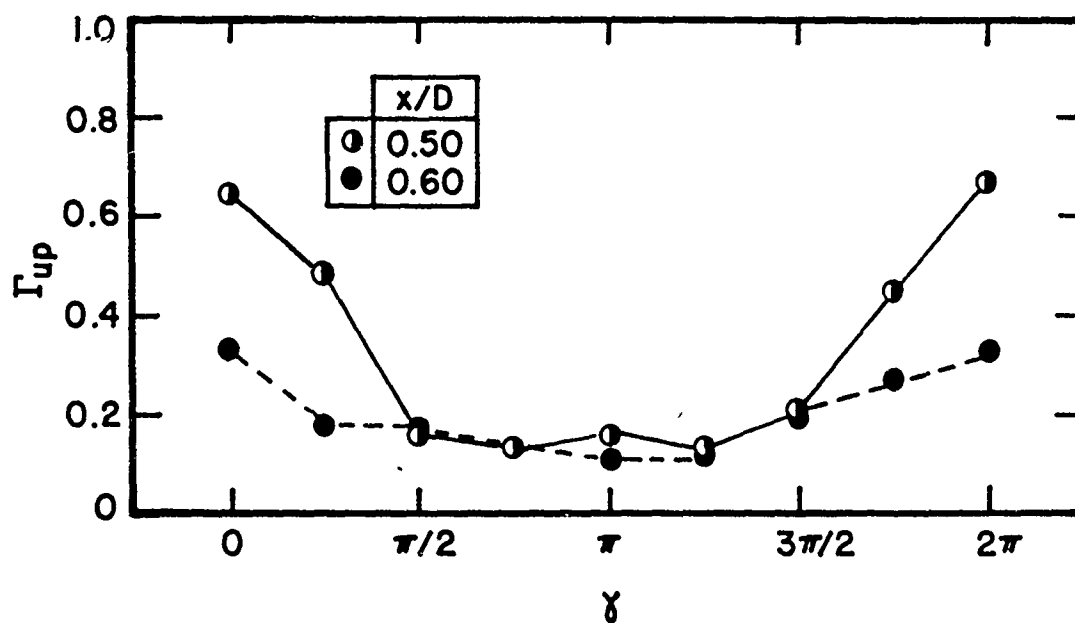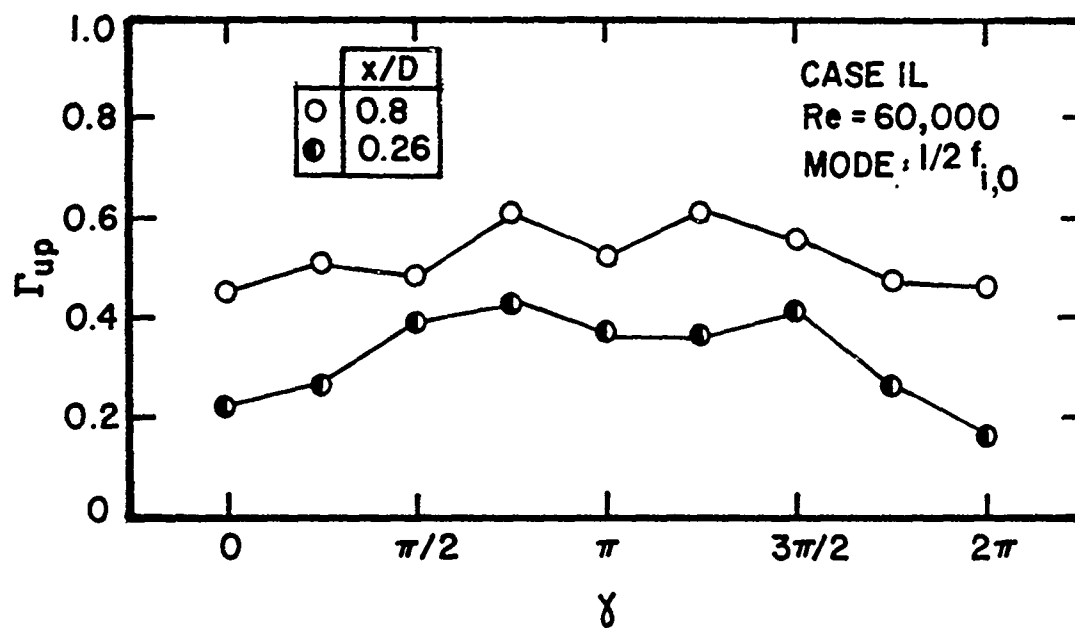
Figure 103. Streamwise Variation of Coherence Between Velocity and Near-Field
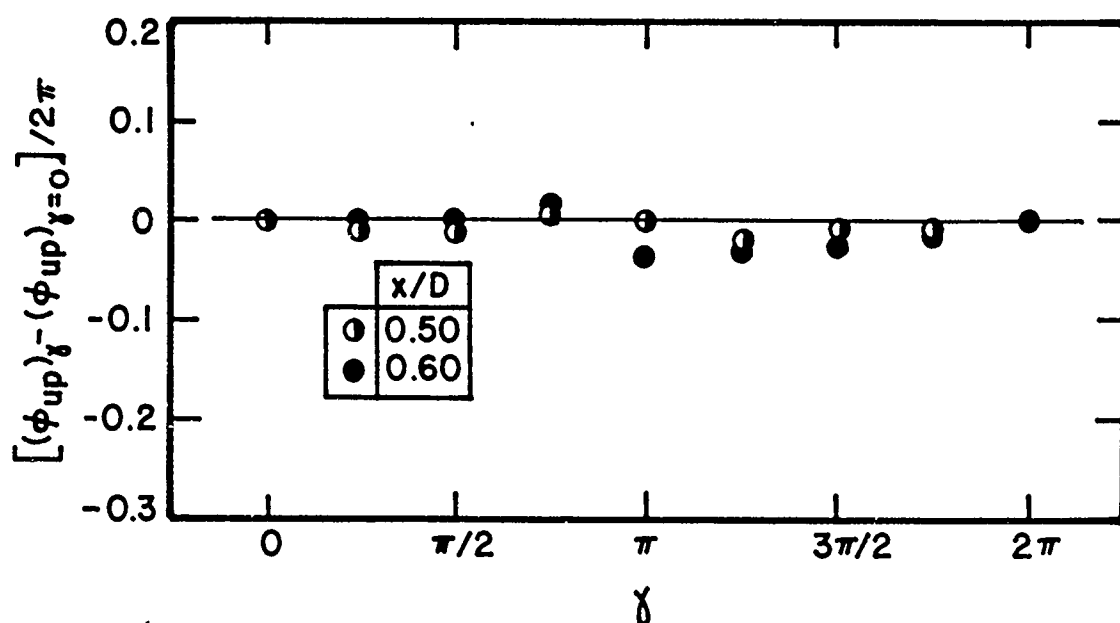Pressure for Subharmonic Mode at Re = 42,000 for Case 1L
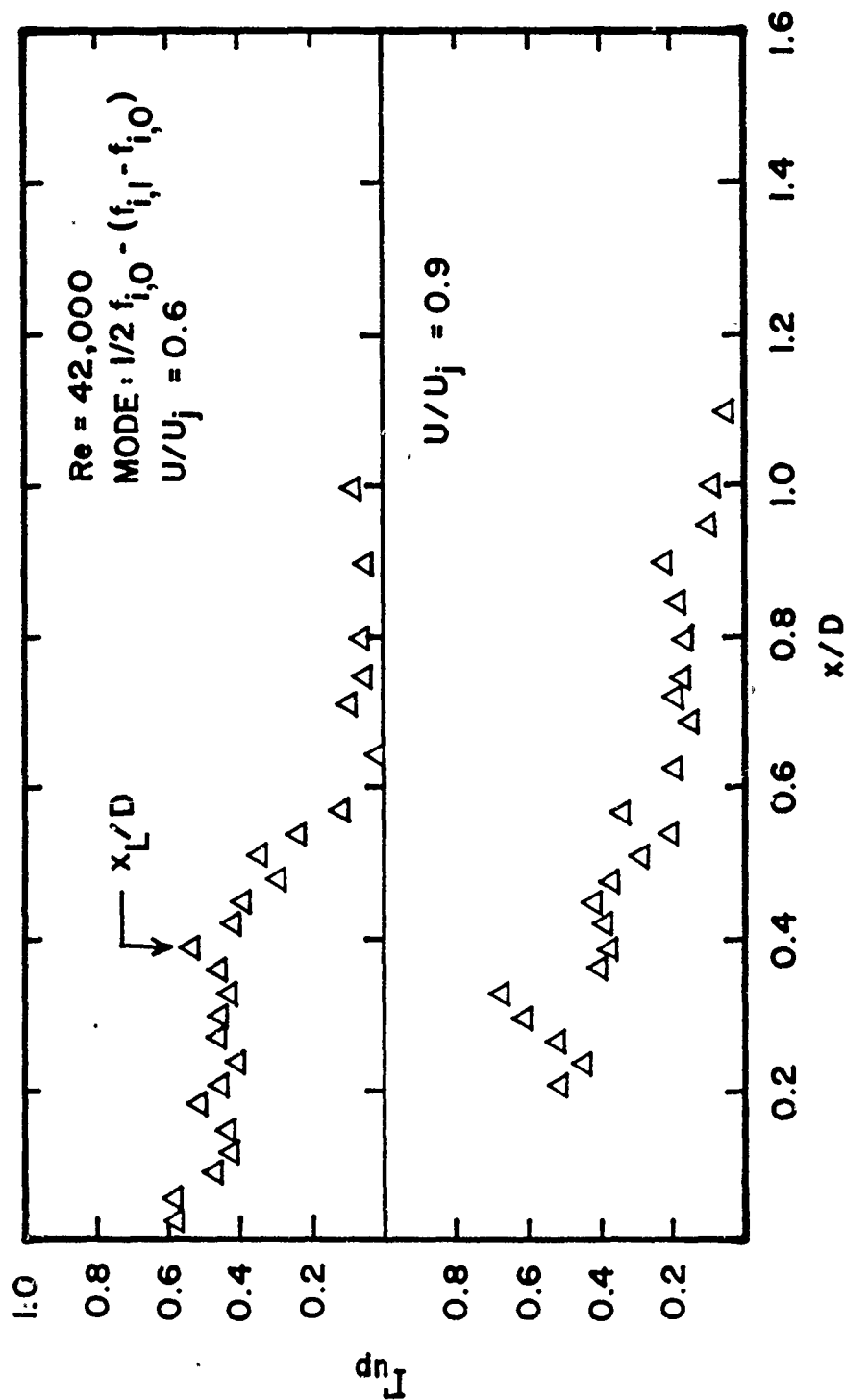
Figure 104. Streamwise Variation of Coherence Between Velocity and Near-Field Pressure for a Three-Wave Nonlinear Interactive Mode at Re = 42,000 for Case 1L
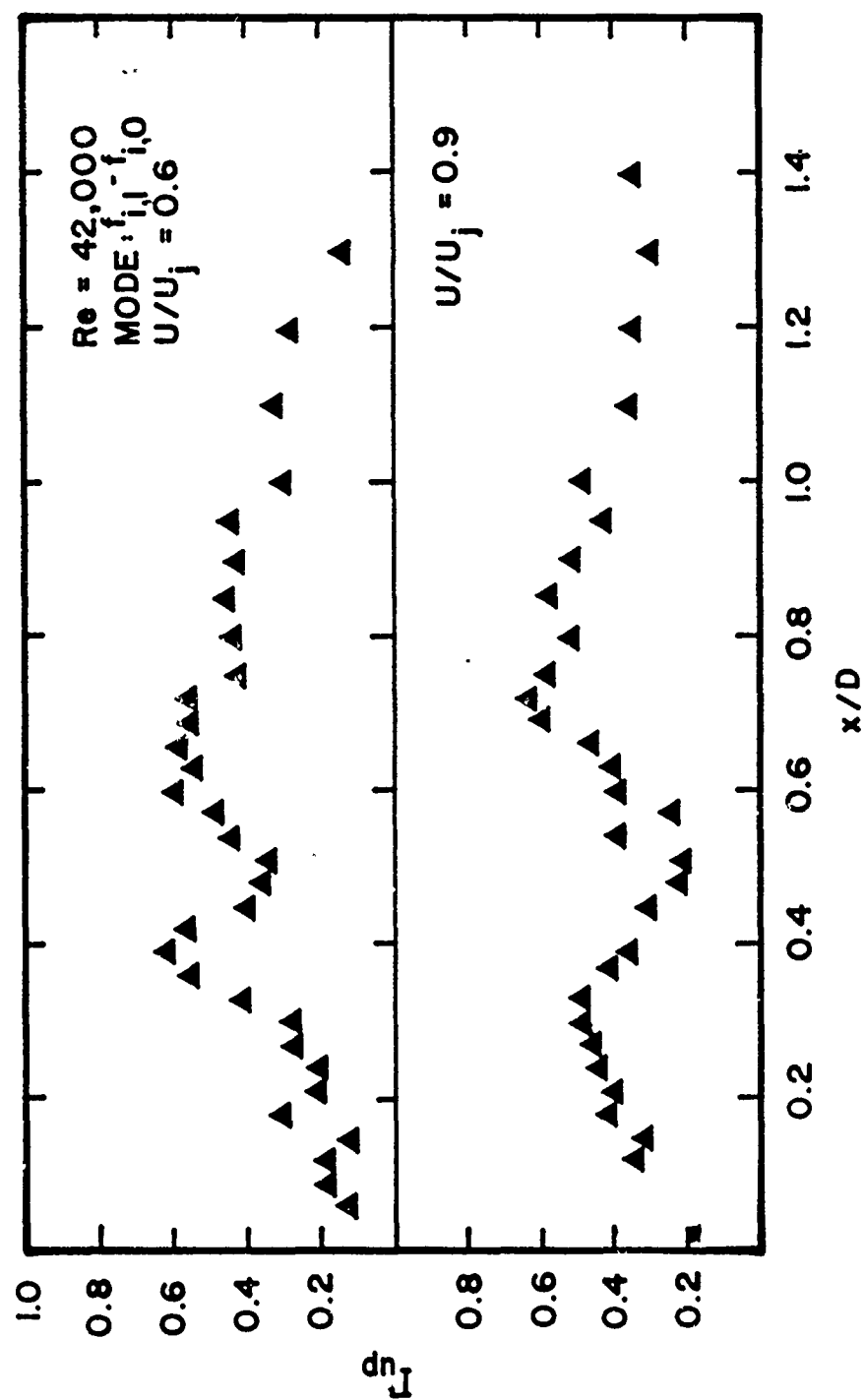
Figure 105. Streamwise Variation of Coherence Between Velocity and Near-Field Pressure for Axisymmetric-Helical Difference Mode at Re = 42,000 for Case 1L
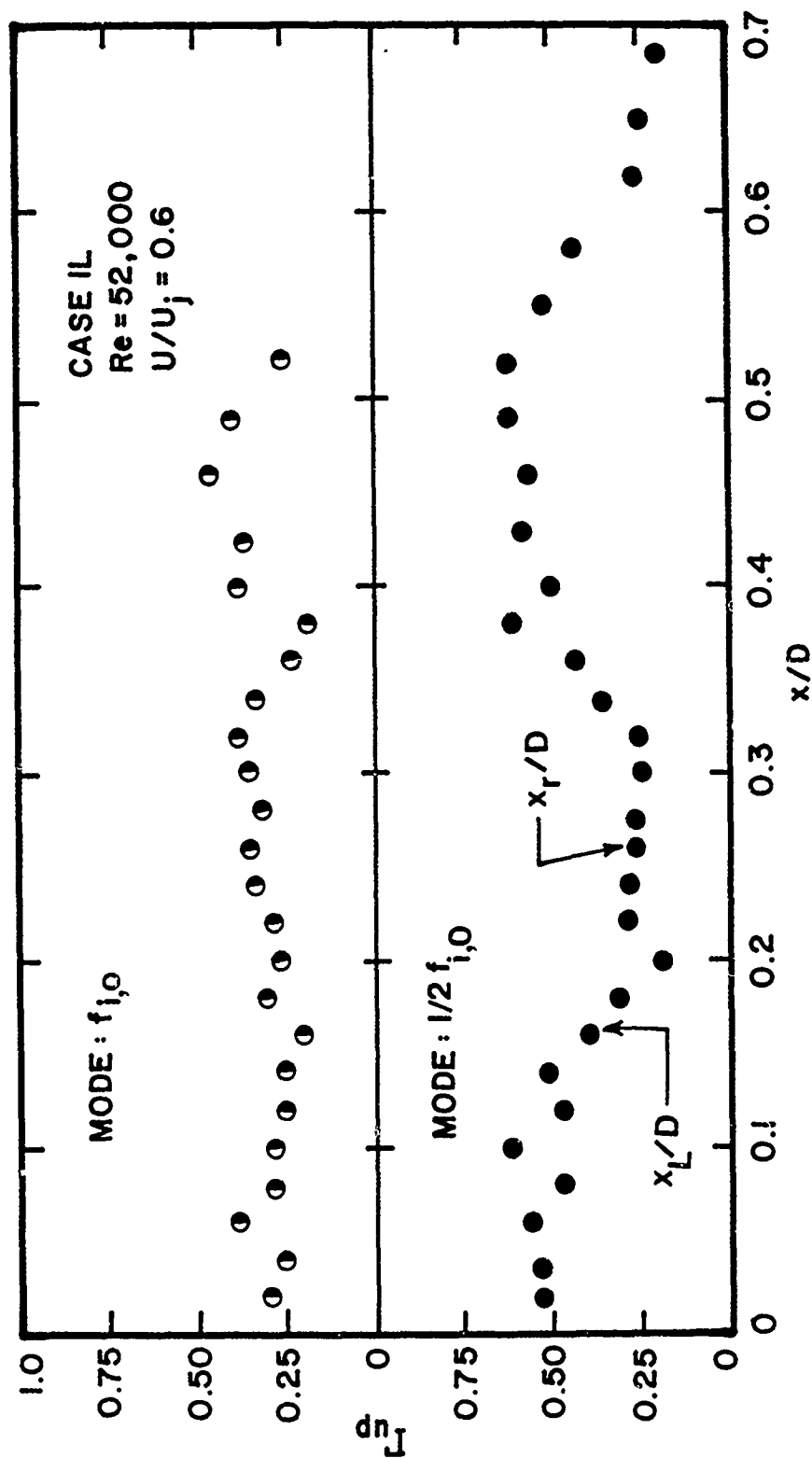
Figure 106. Streamwise Variation of Coherence Between Velocity and Near-Field
Pressure for Initial Axisymmetric Mode and its Subharmonic at Re = 52,000
for Case 1L
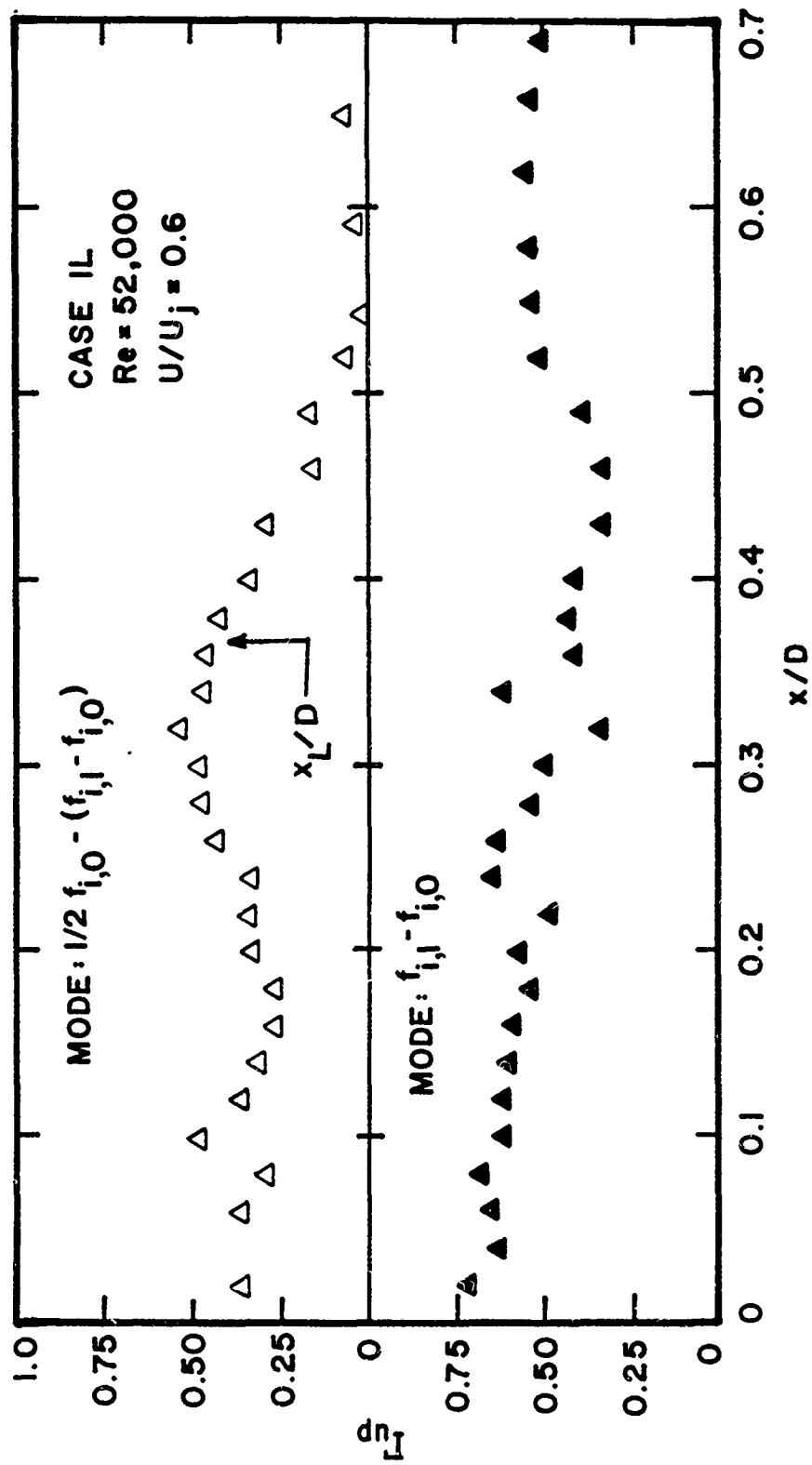
Figure 107. Streamwise Variation of Coherence Between Velocity and Near-Field Pressure for Nonlinearly Developing Modes at Re = 52,000 for Case 1L
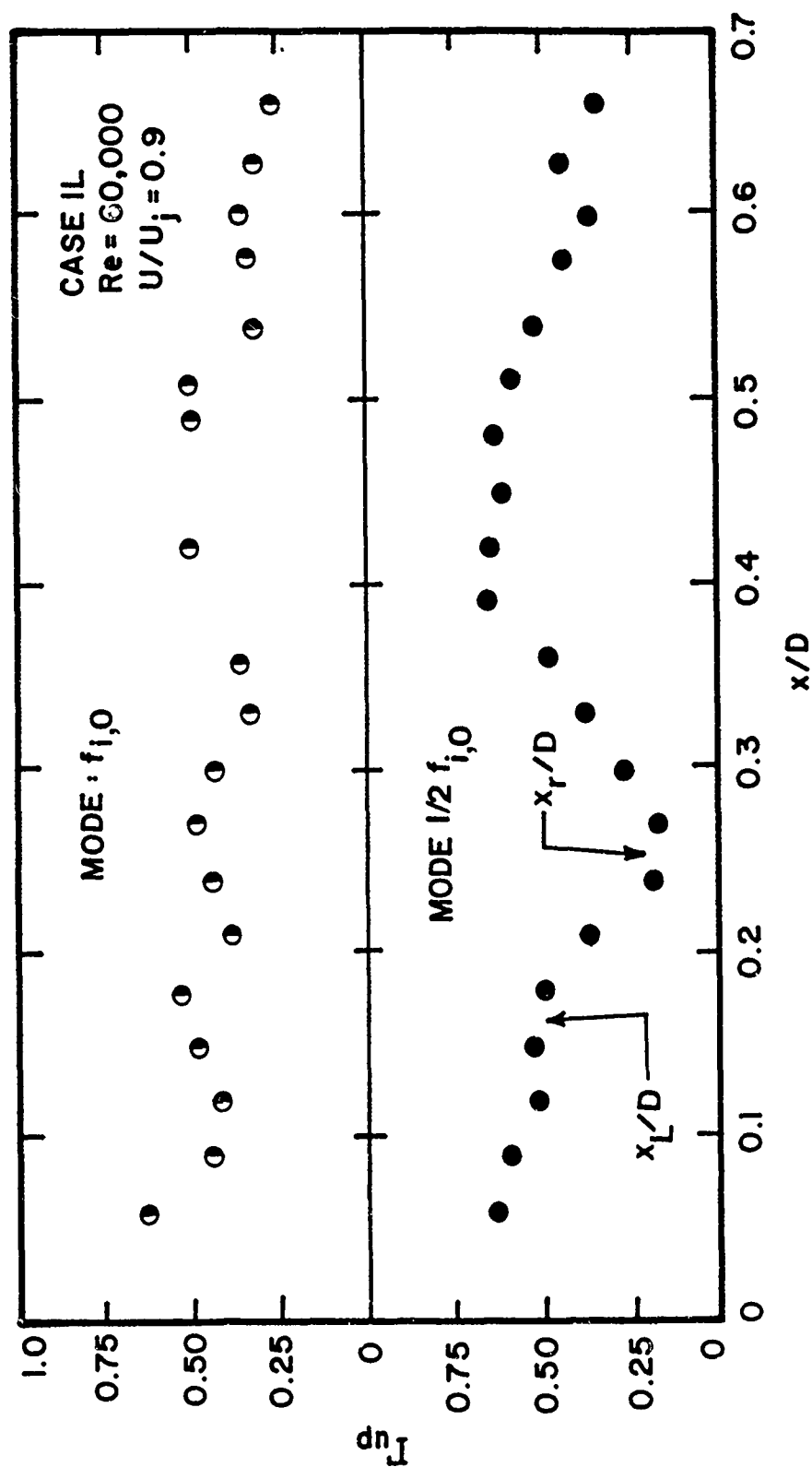
Figure 108. Streamwise Variation of Coherence Between Velocity and Near-Field Pressure for Axisymmetric Mode and its Subharmonic at Re = 60,000 for Case 1L
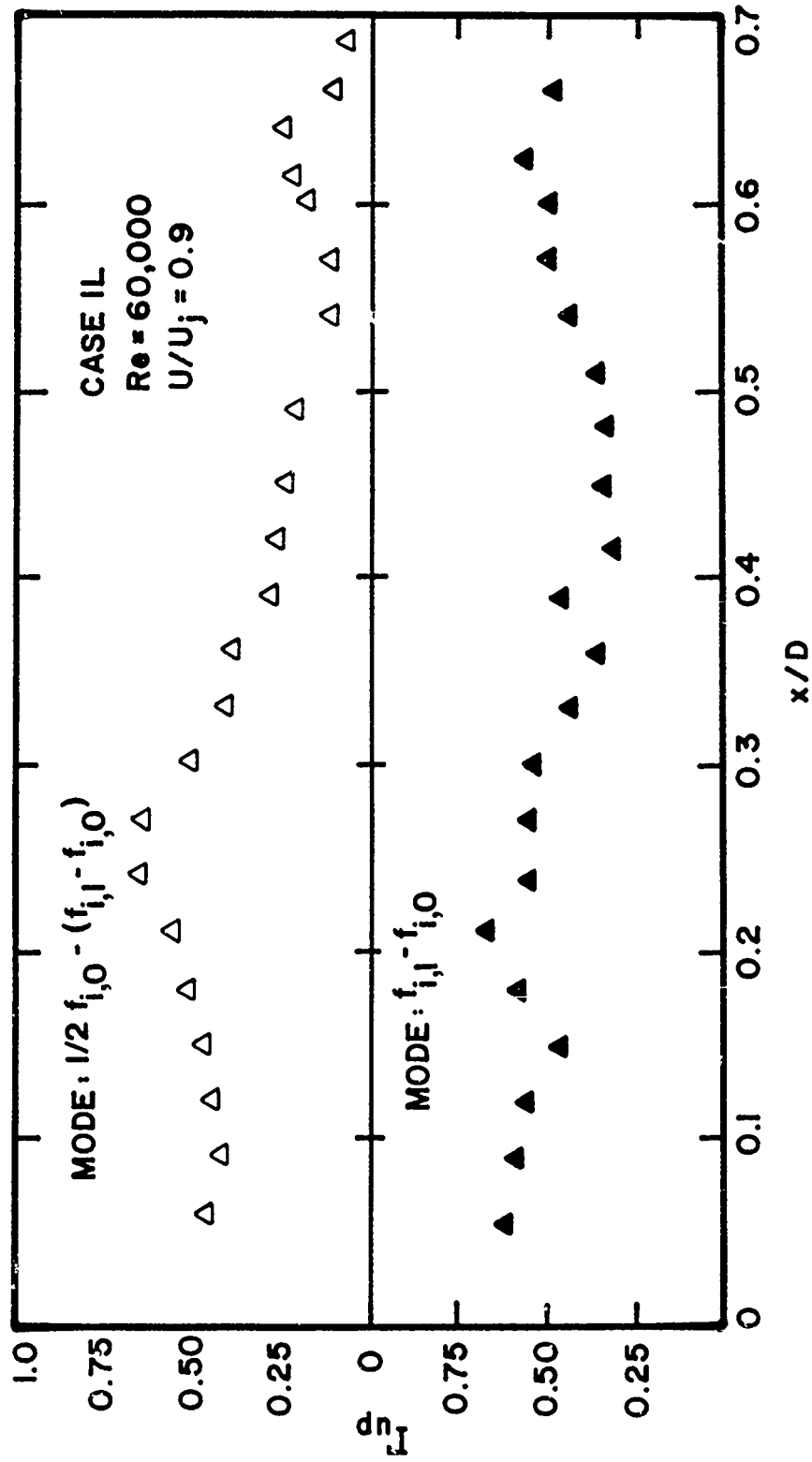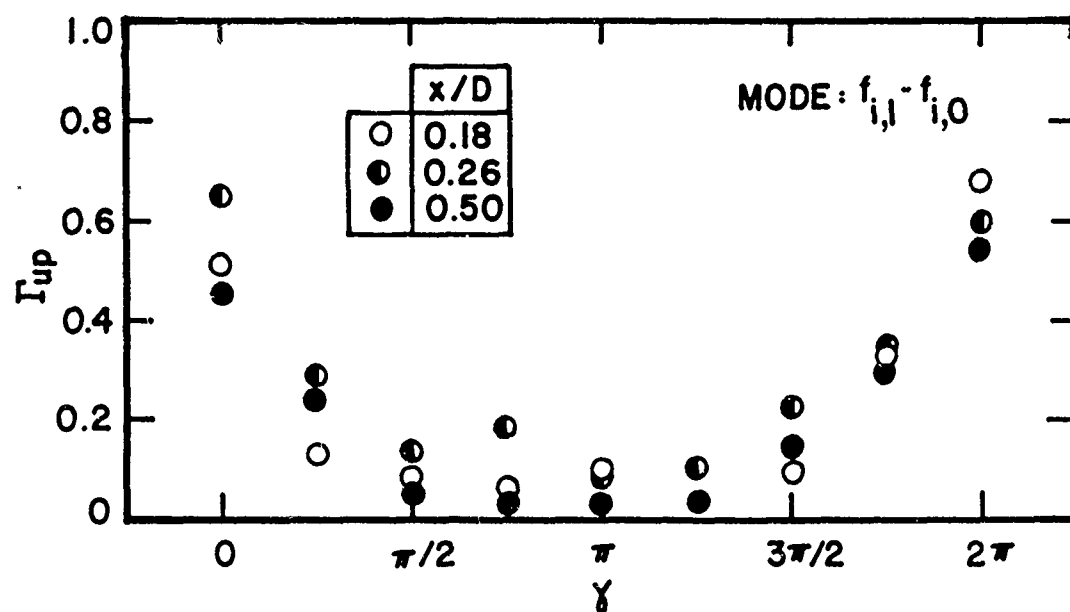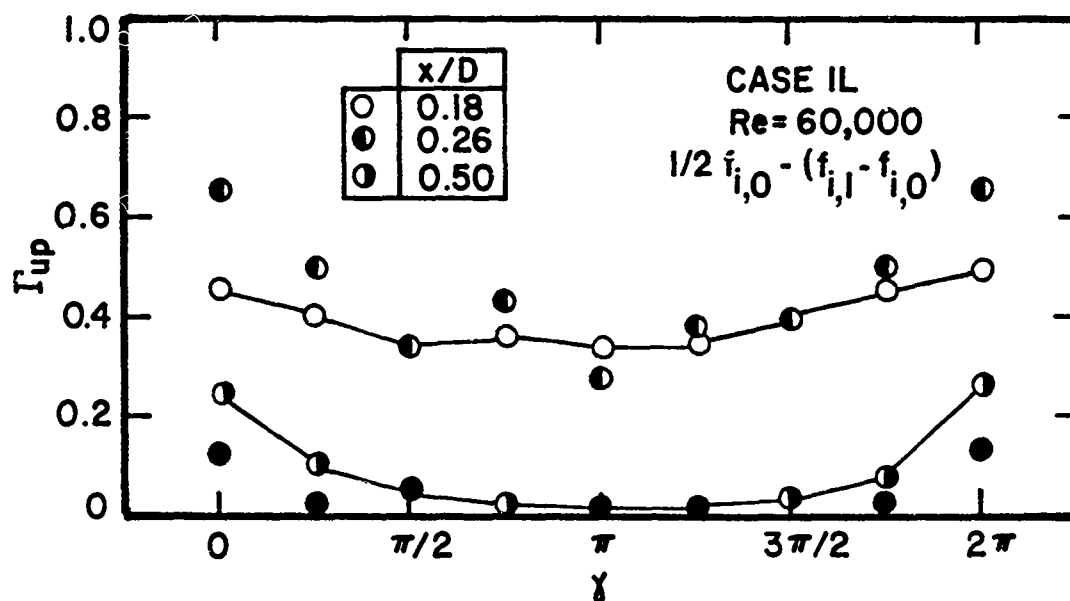
Figure 109. Streamwise Variation of Coherence Between Velocity and Near-Field Pressure for Nonlinearly Developing Modes at Re = 60,000 for Case 1L
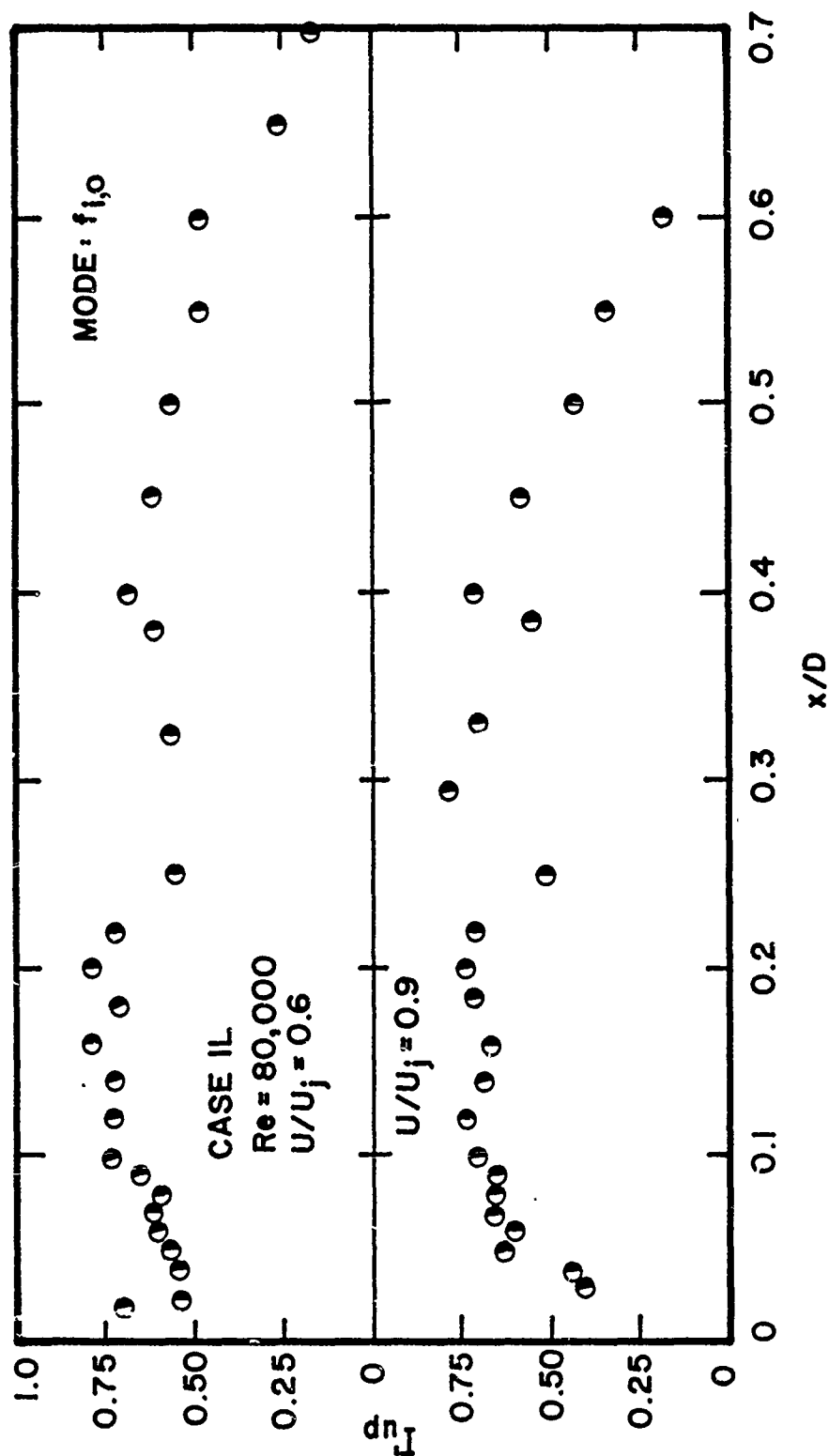
Figure 110. Streamwise Variation of Coherence Between Velocity and Near-Field
Pressure for Initial Axisymmetric Mode at Re = 80,000 for Case 1L
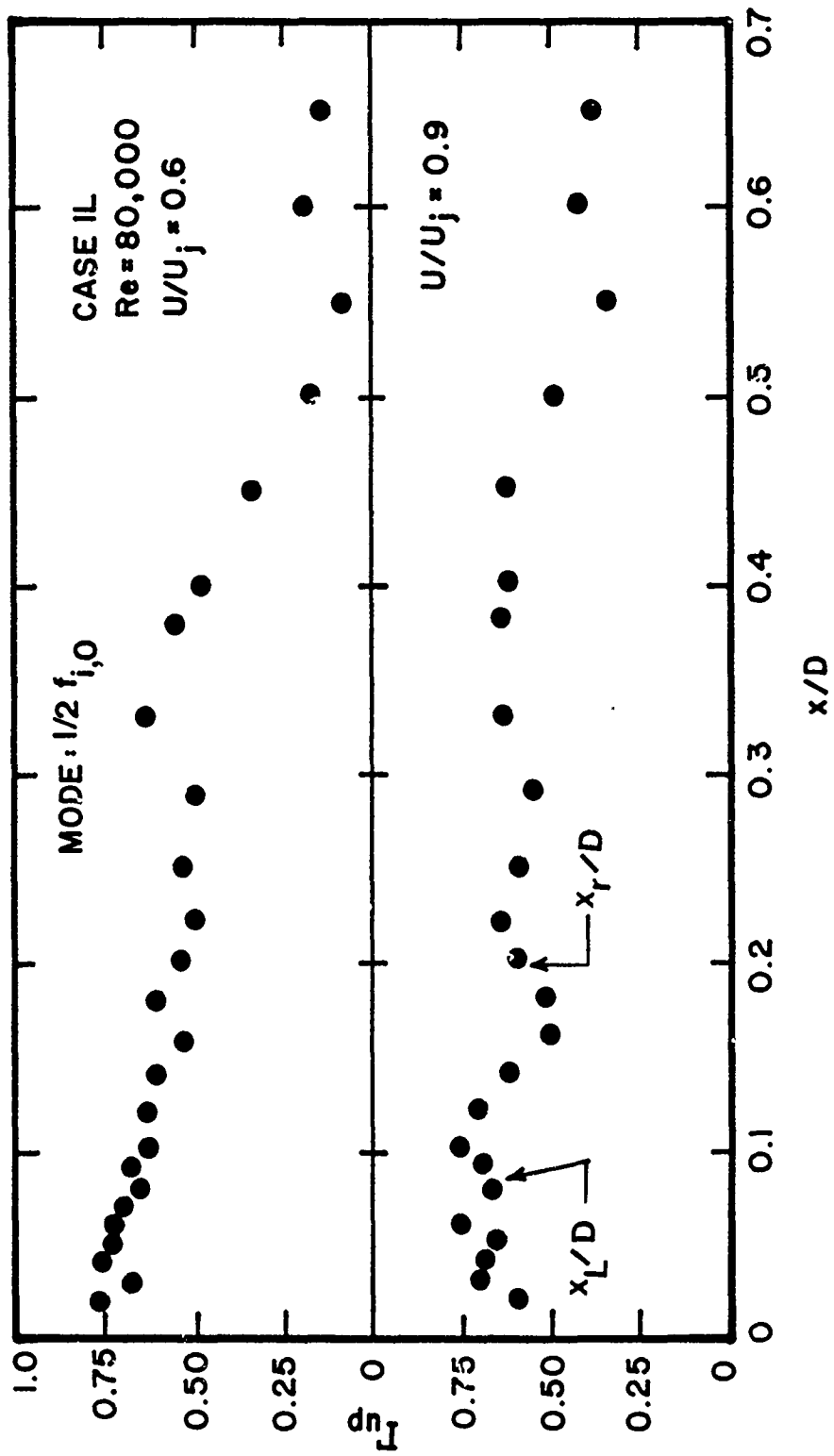
Figure 111. Streamwise Variation of Coherence Between Velocity and Near-Field Pressure for Subharmonic Mode at Re = 80,000 for Case 1L
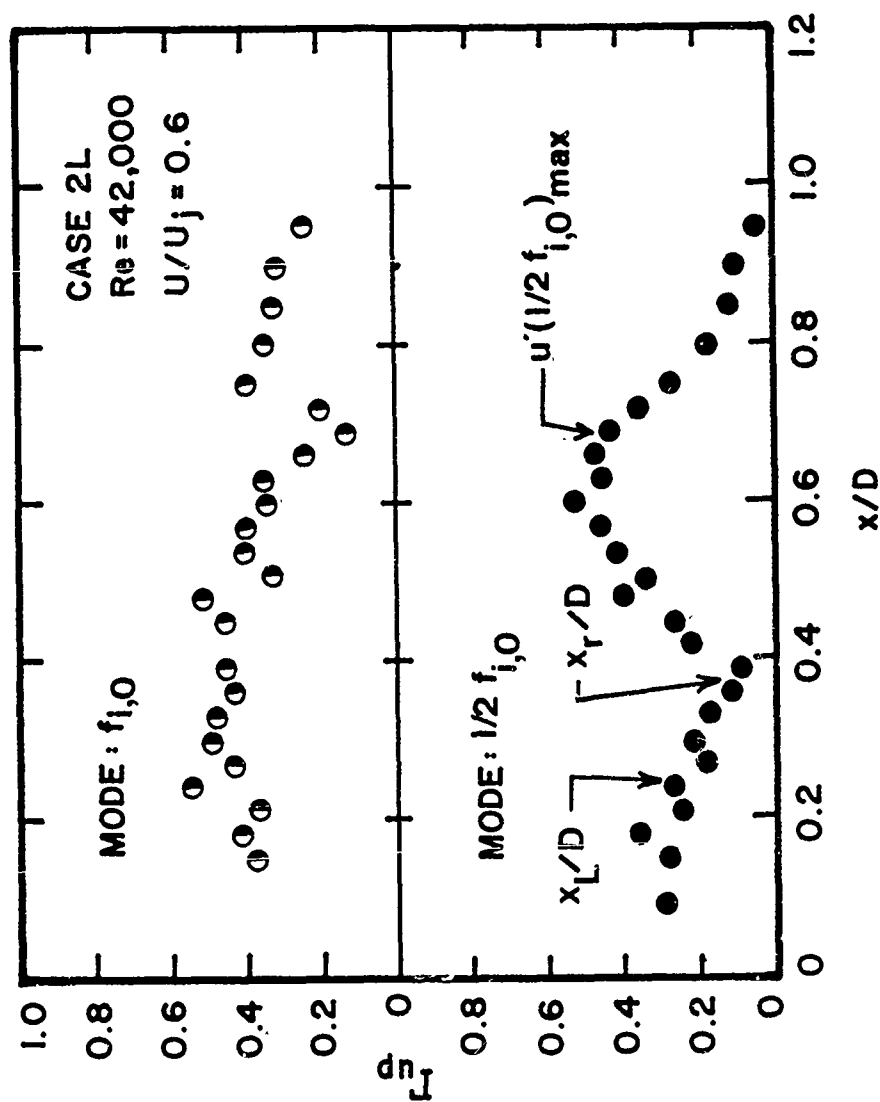
Figure 112. Streamwise Variation of Coherence Between Velocity and Near-Field Pressure for Initial Axisymmetric Mode and its Subharmonic at Re = 42,000 for Case 2L
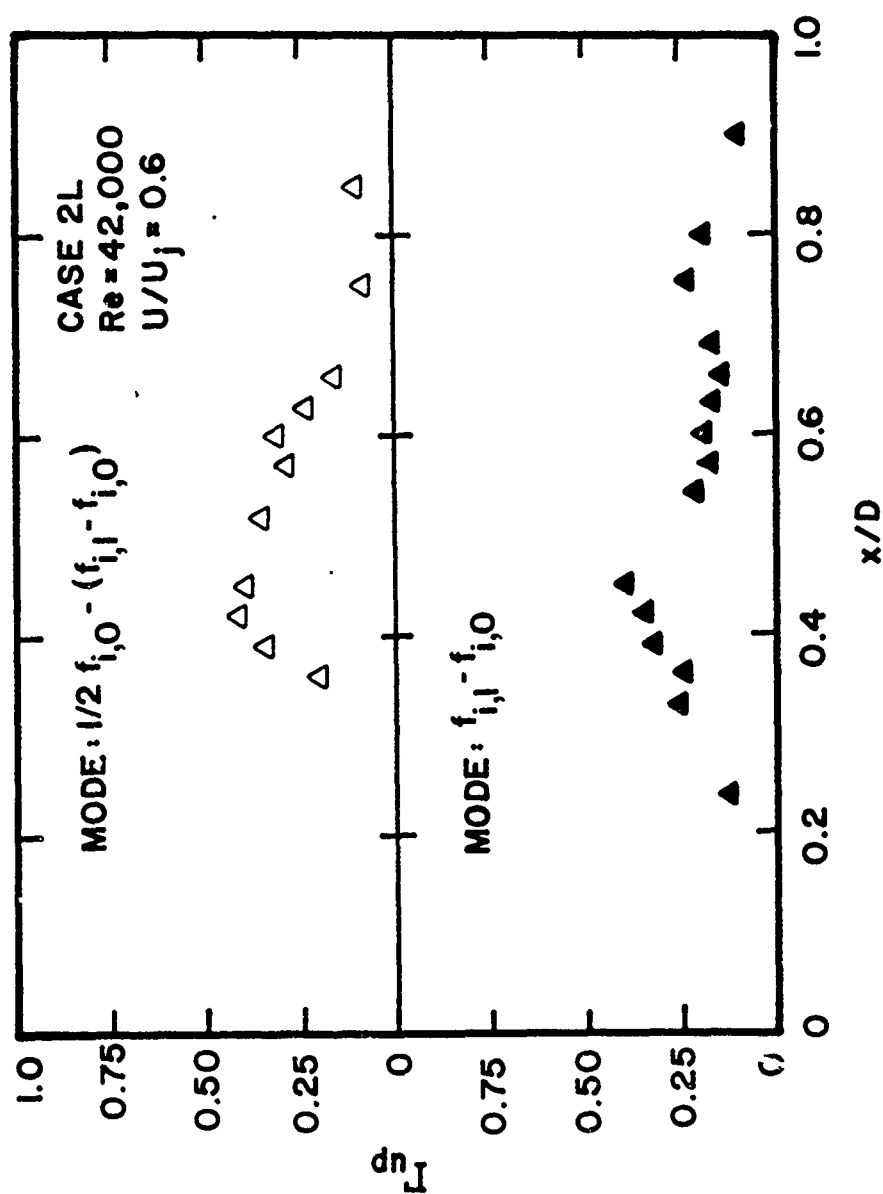
Figure 113. Streamwise Variation of Coherence Between Velocity and Near-Field
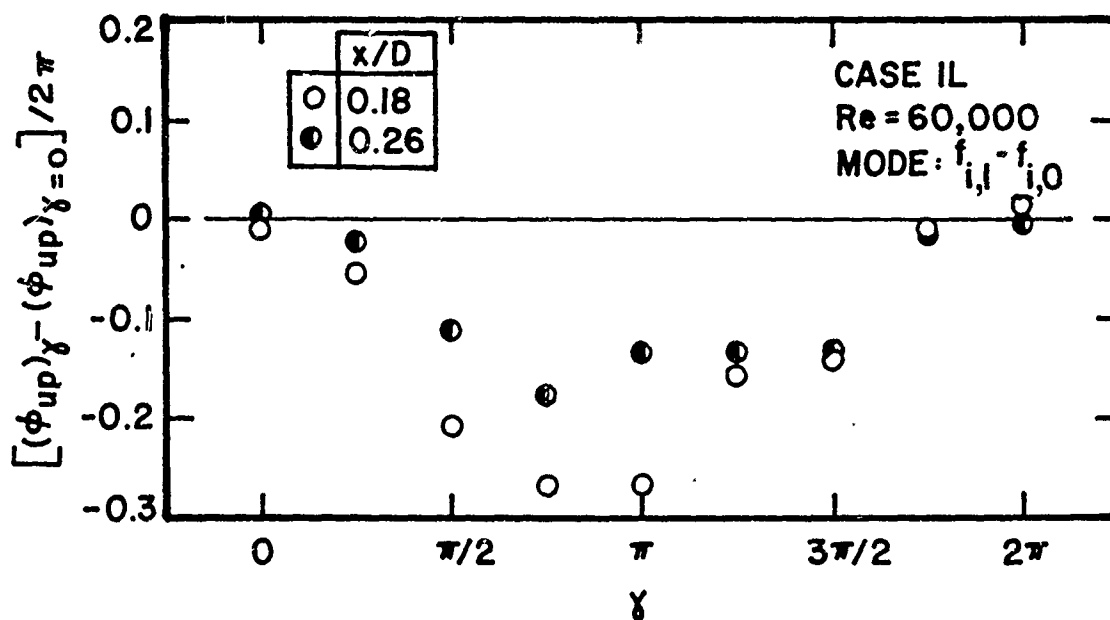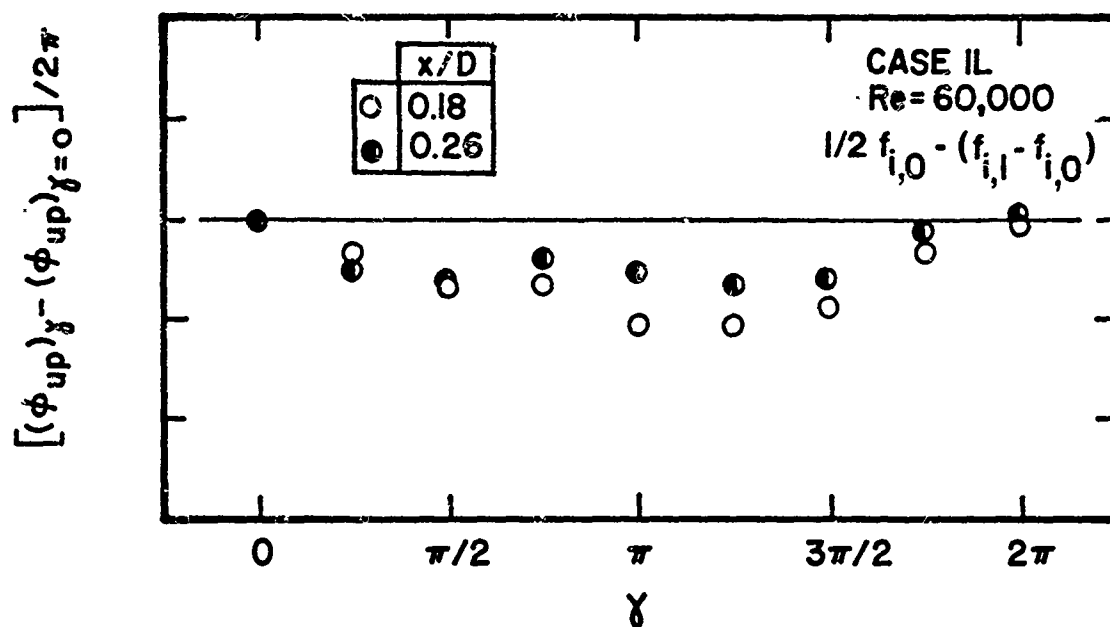Pressure for Nonlinearly Developing Modes at Re = 42,000
for Case 2L
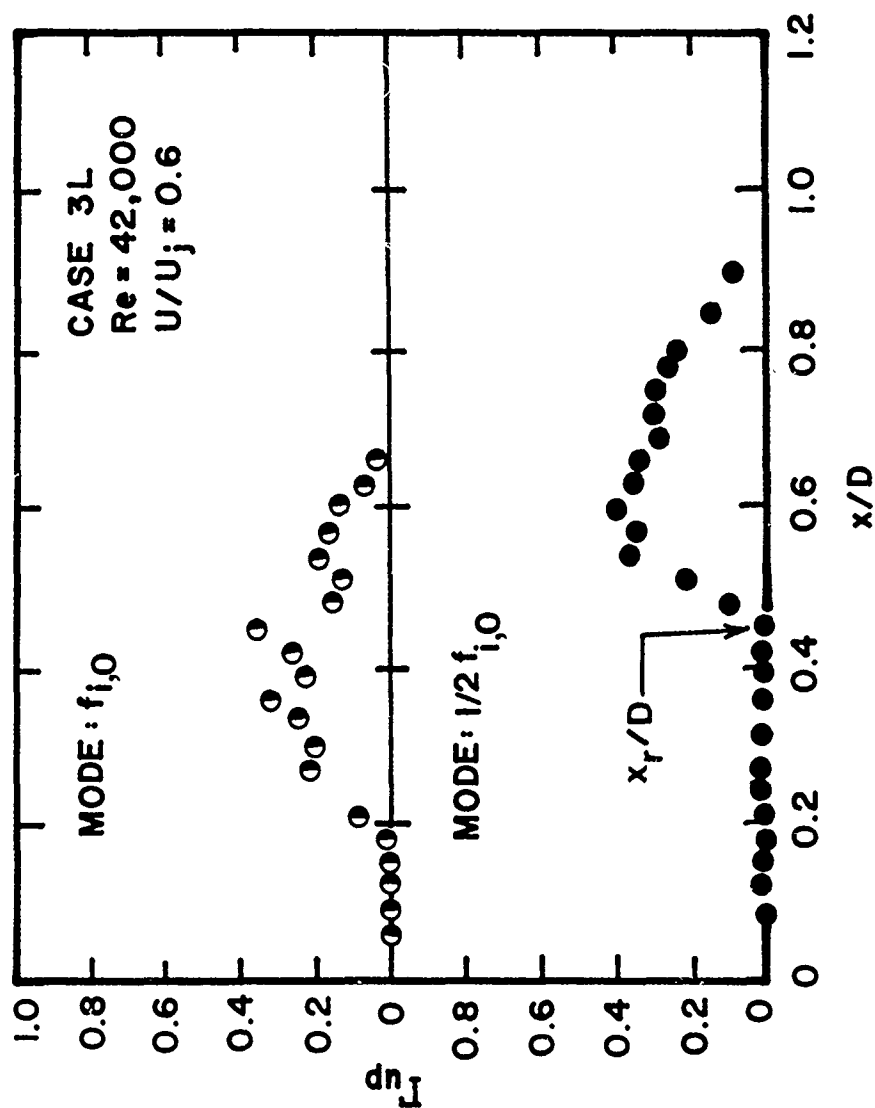
Figure 114. Streamwise Variation of Coherence Between Velocity and Near-Field Pressure for Initial Axisymmetric Mode and its Subharmonic at Re = 42,000 for Case 3L
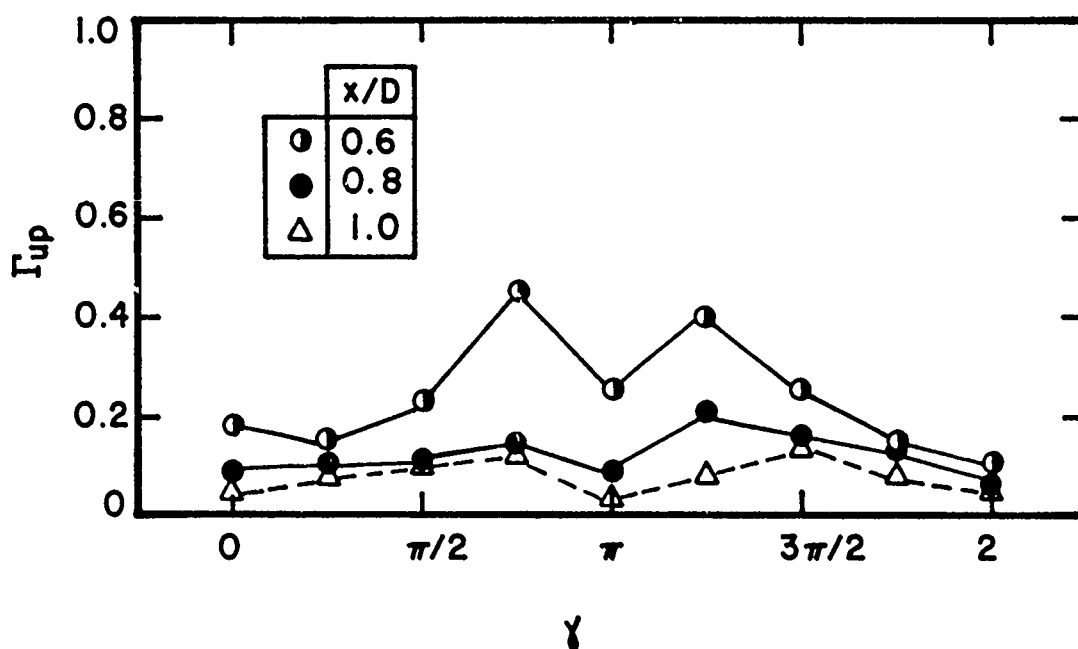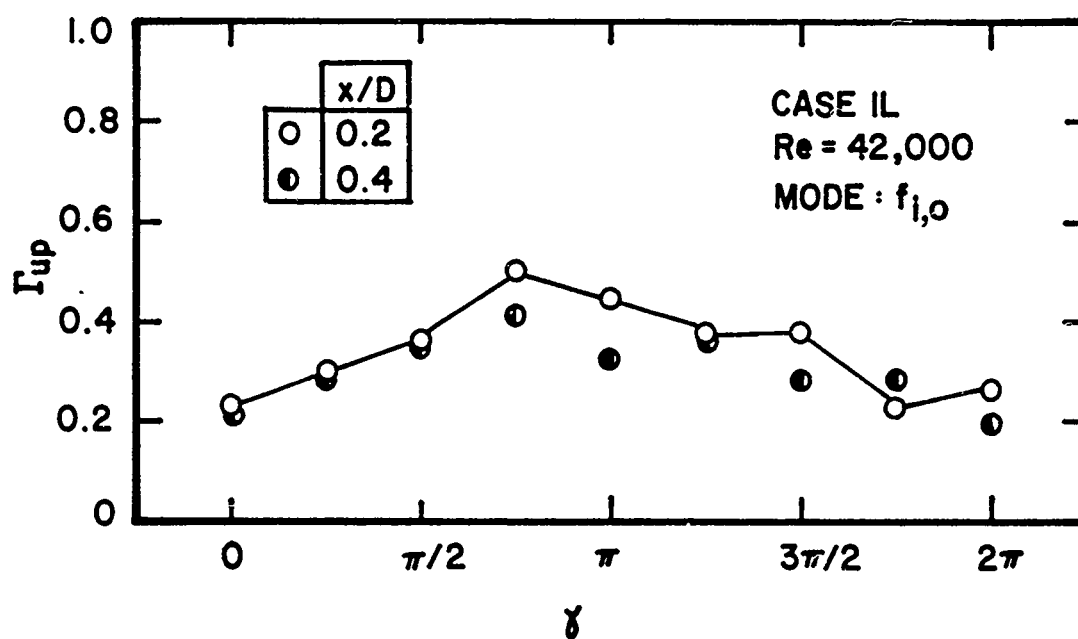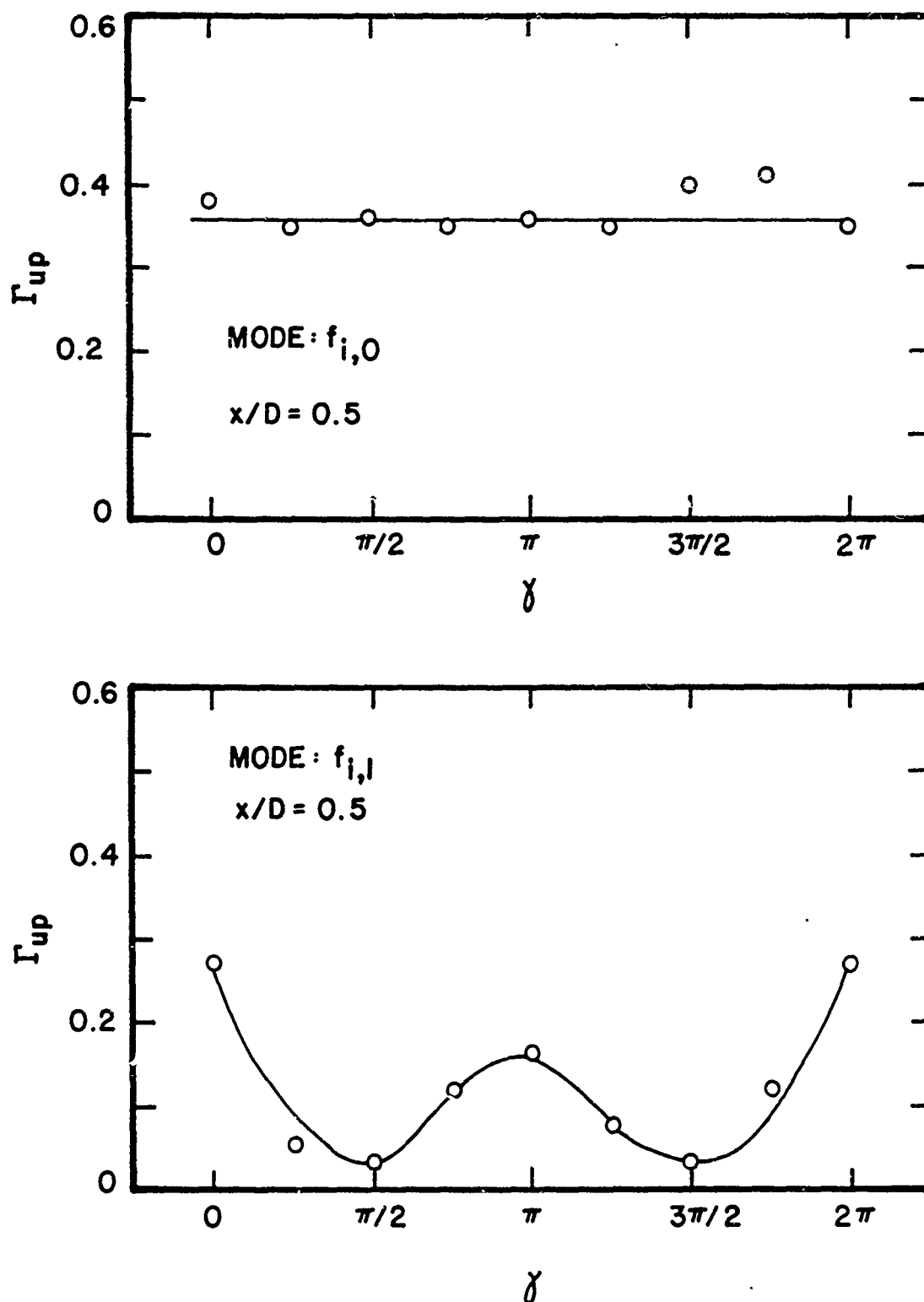
Figure 115. Azimuthal Variation of Coherence Between
Velocity and Near-Field Pressure for Initial
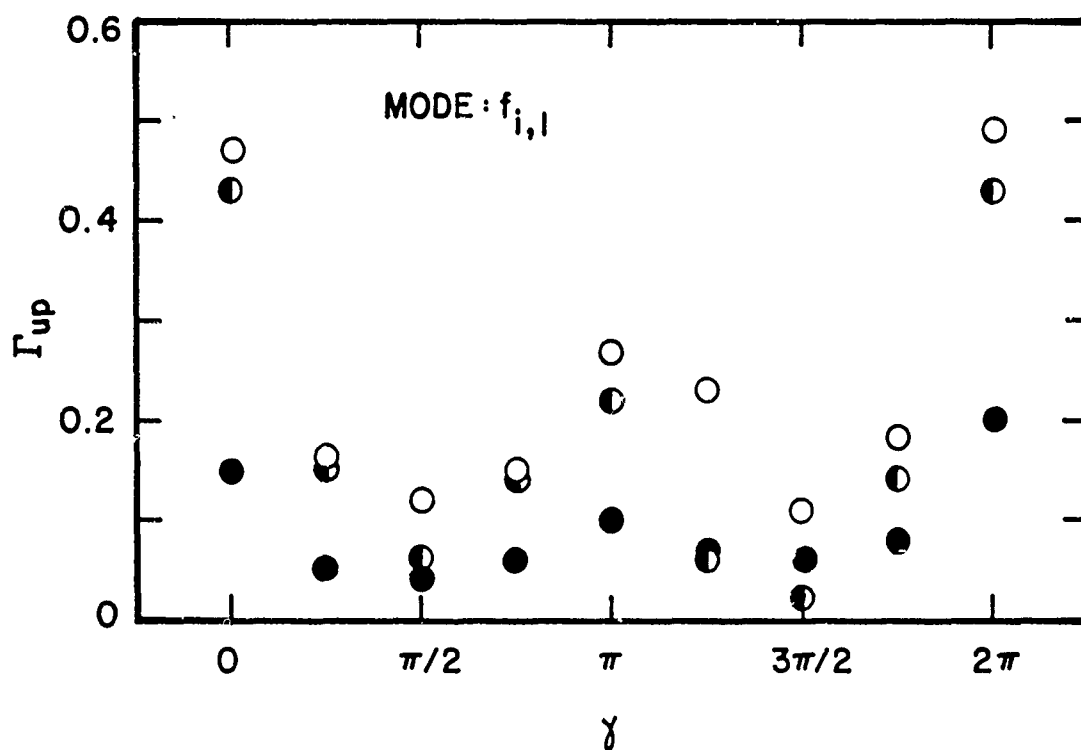Axisymmetric Mode at Re = 42,000 for Case 1L
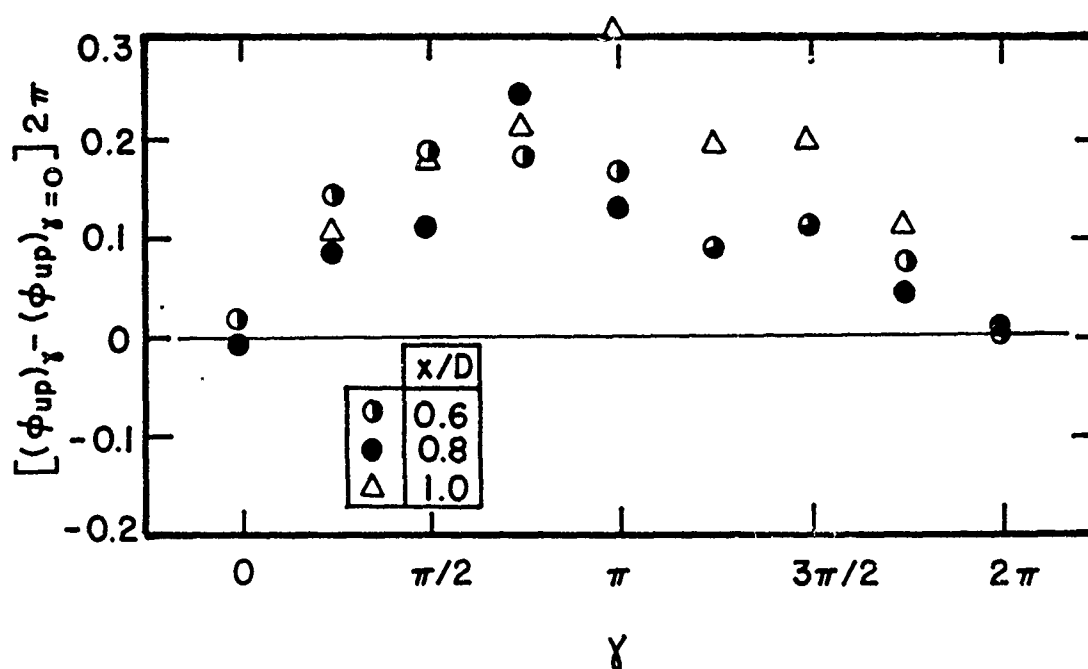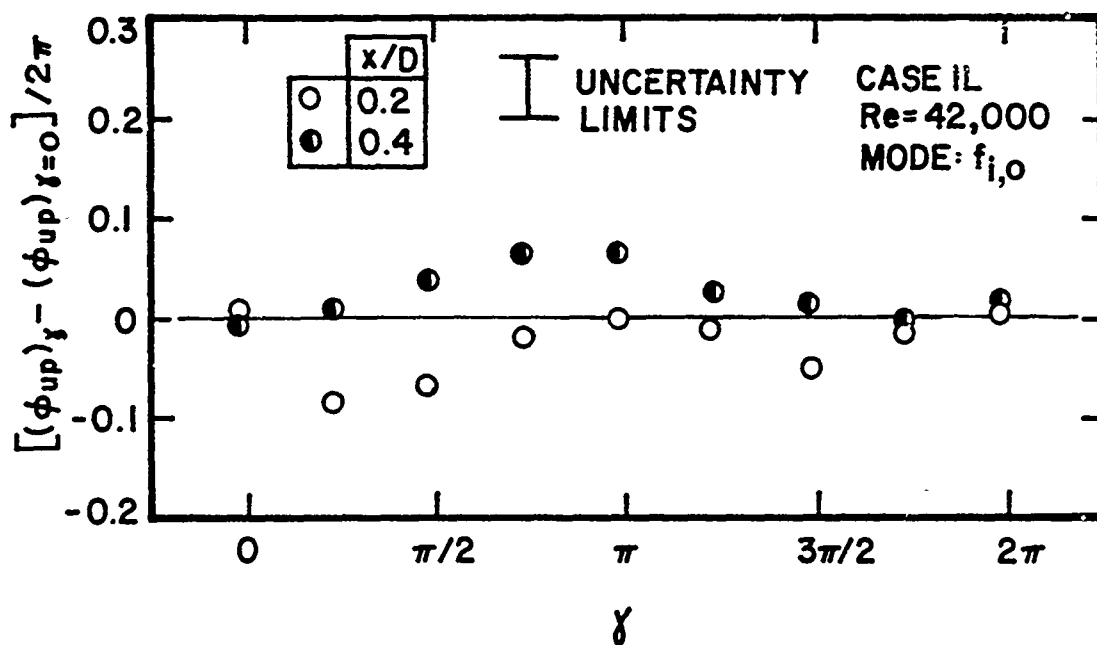
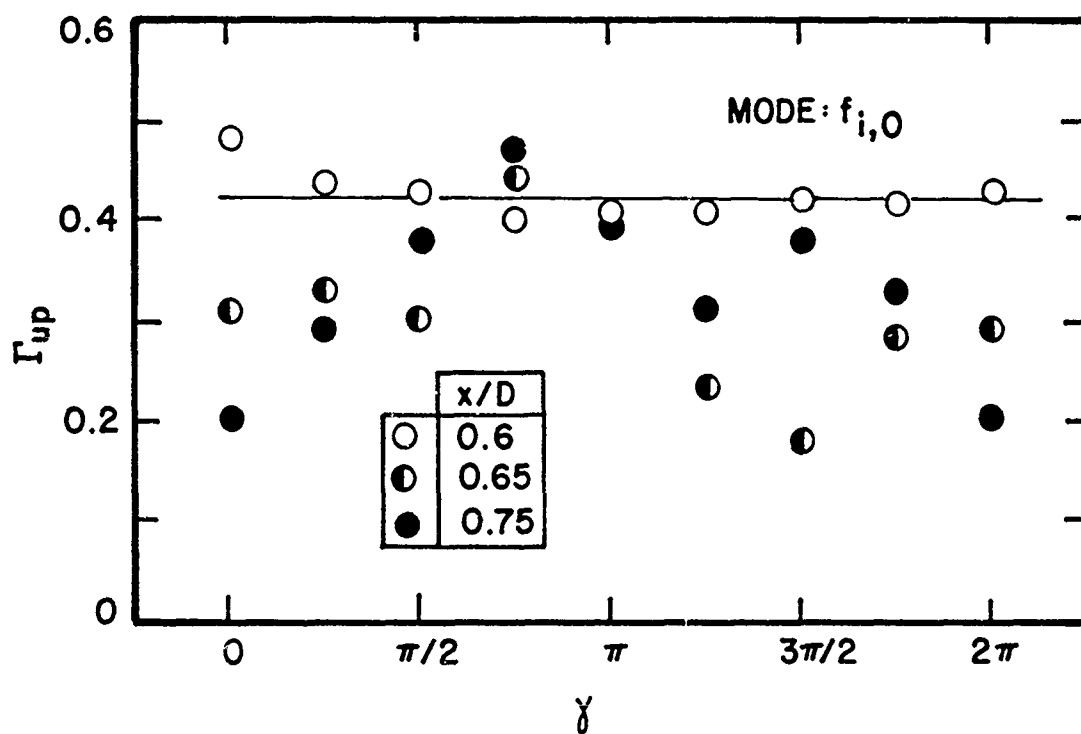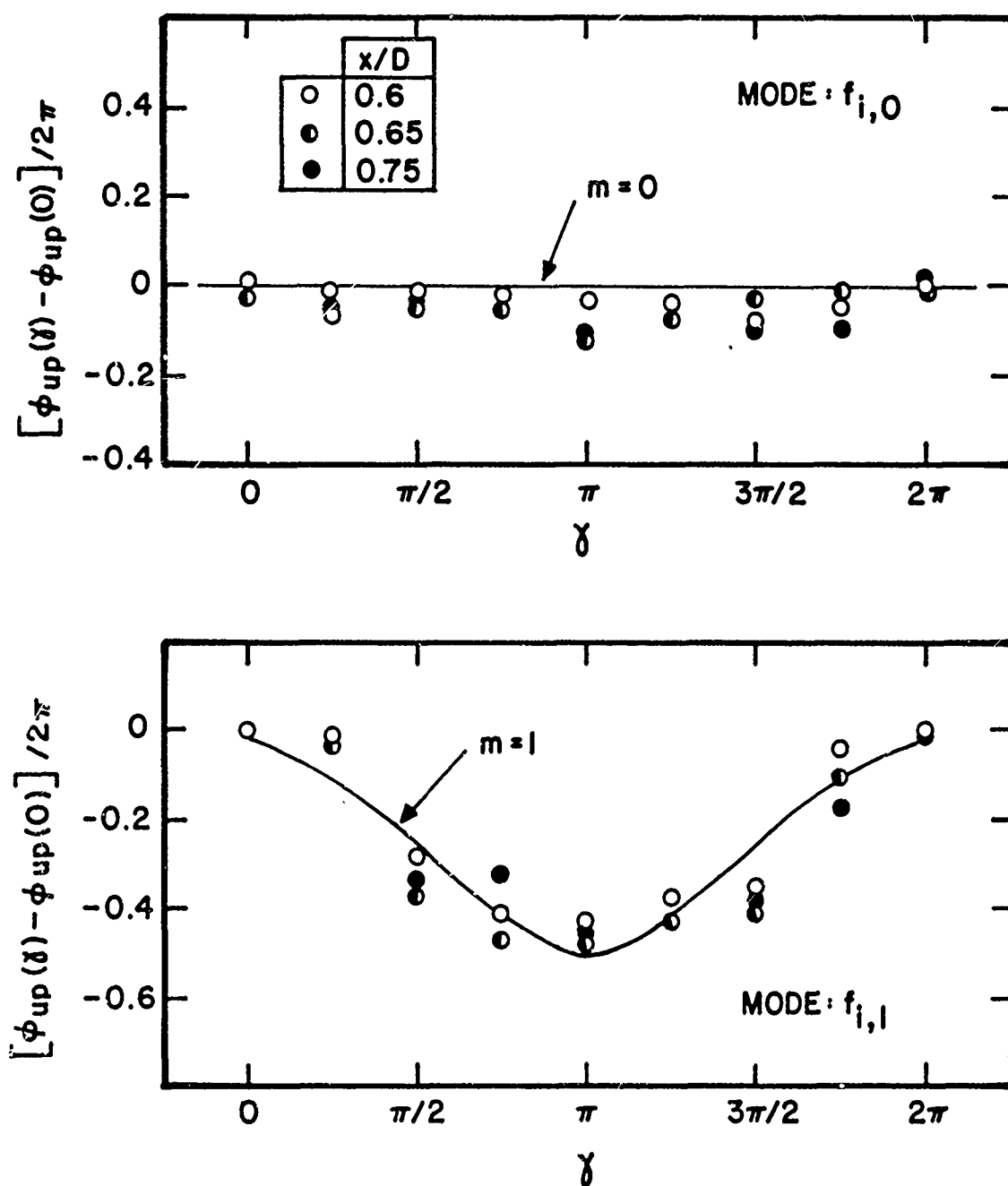Figure 116. Azimuthal Variation of Phase Difference Between
Velocity and Near-Field Pressure for Initial Axisymmetric
Mode at Re = 42,000 for Case 1L
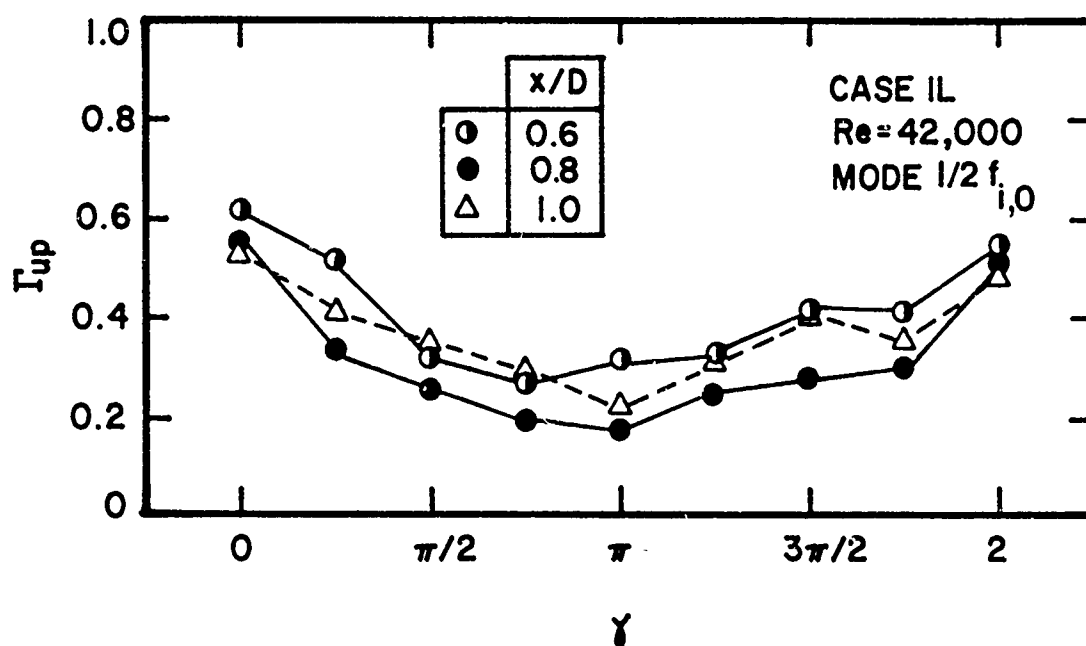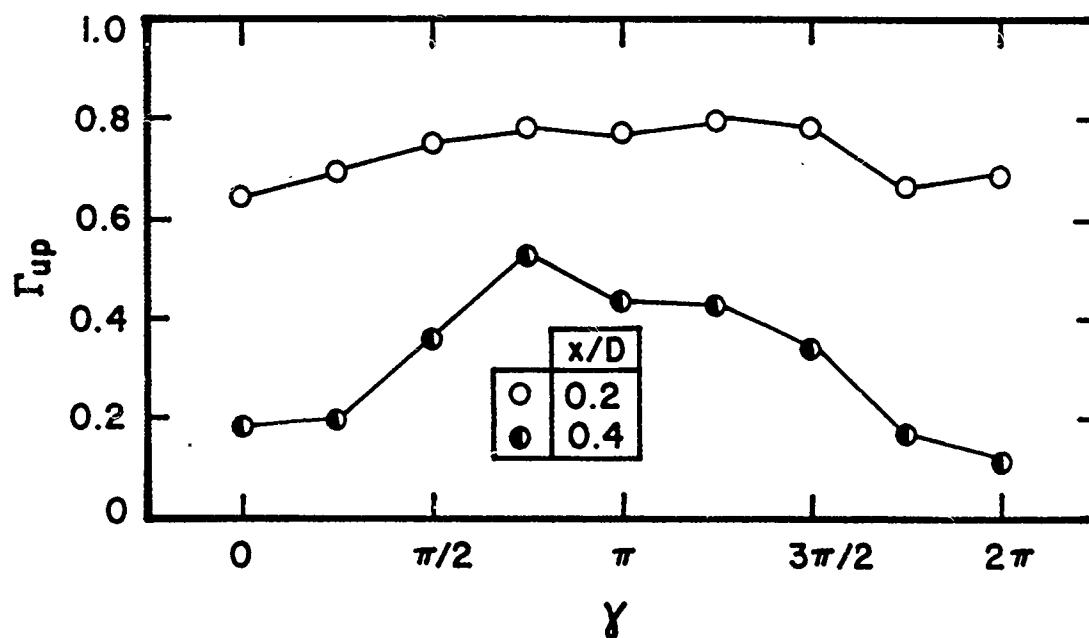
Figure 117. Azimuthal Variation of Coherence Between
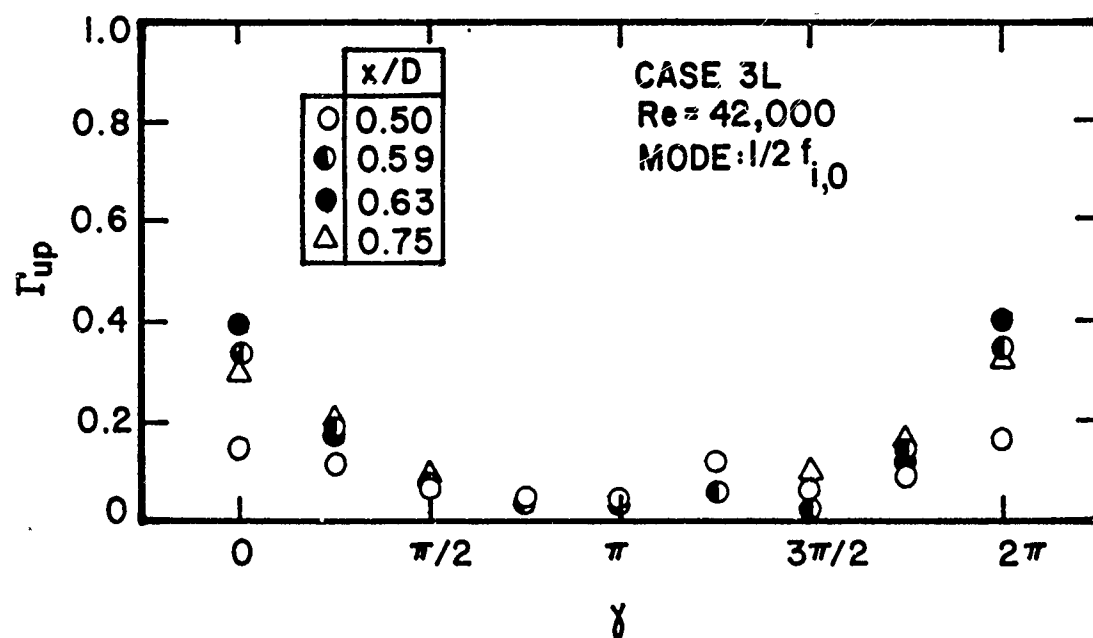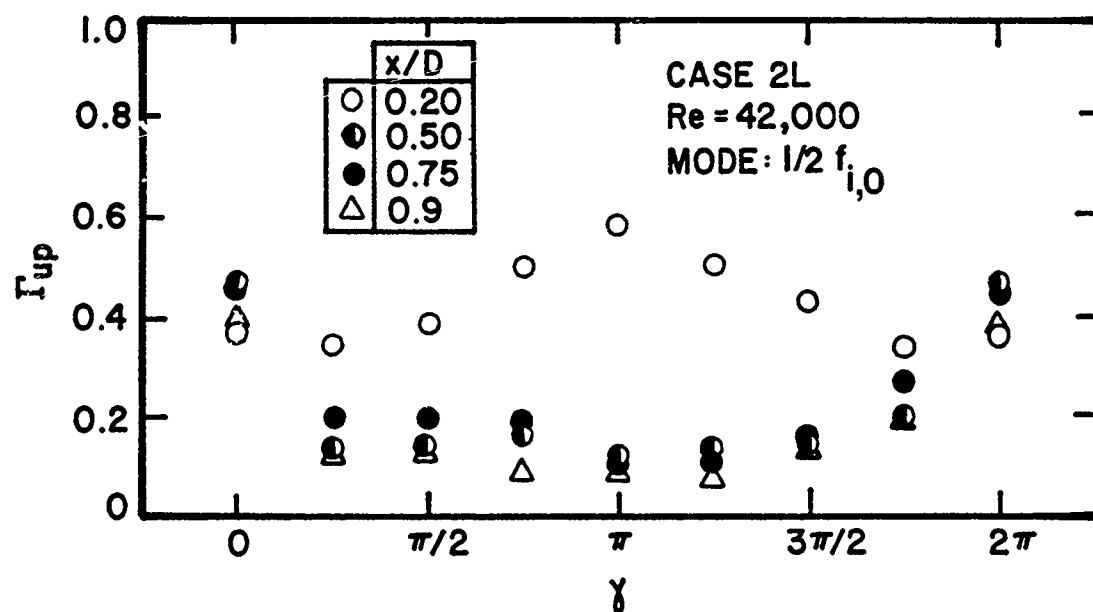Velocity and Near-Field Pressure for Subharmonic
Mode at Re = 42,000 for Case 1L
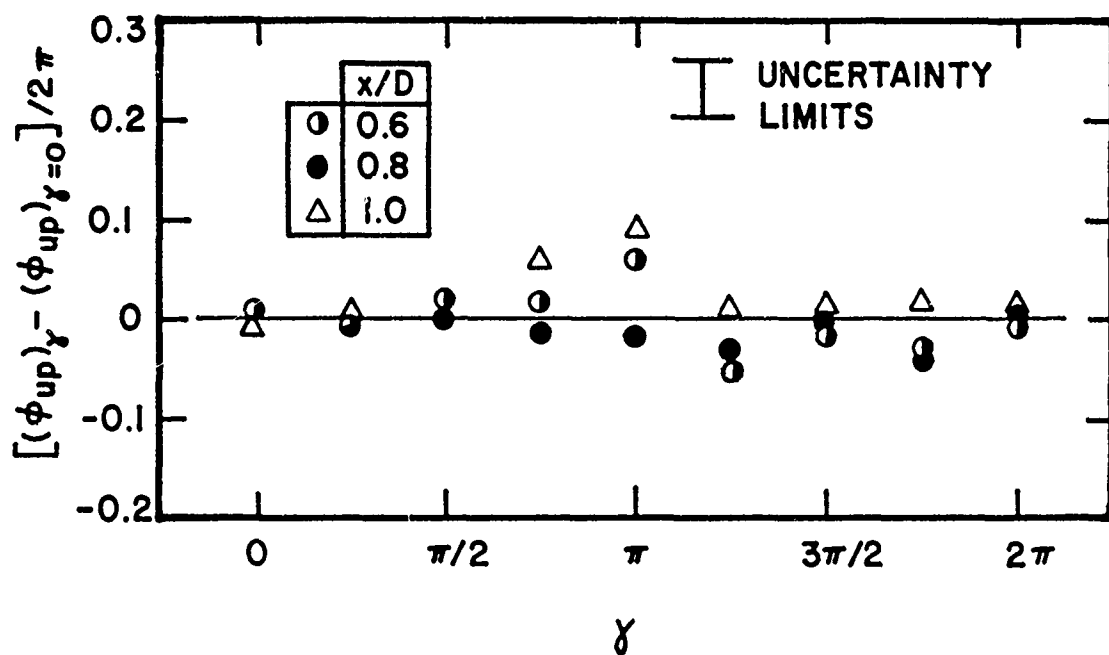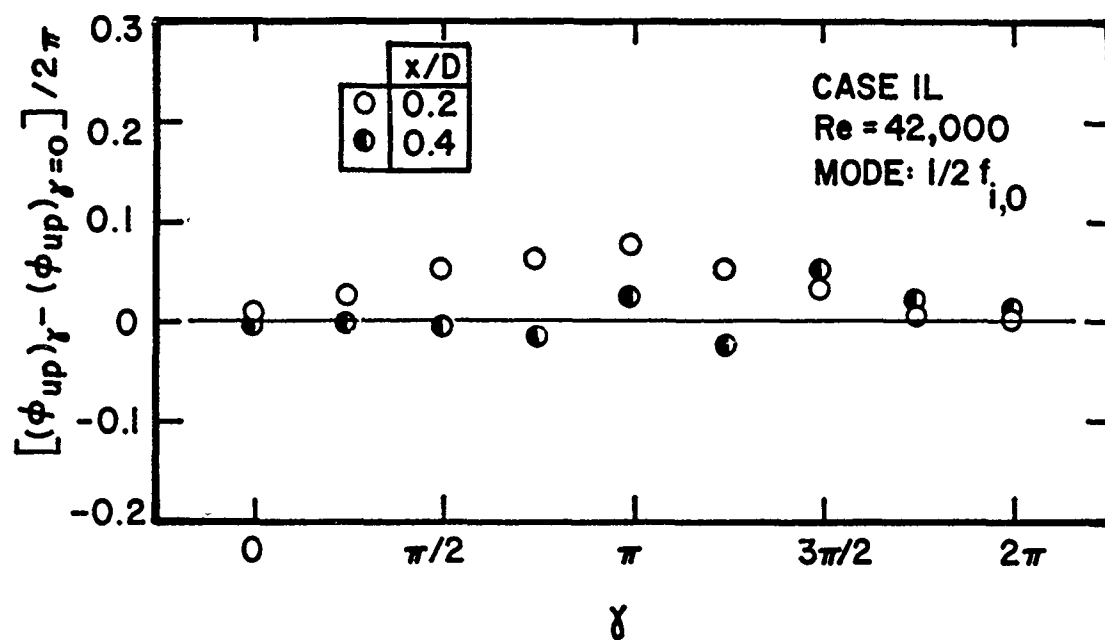
Figure 118. Azimuthal Variation of Phase Difference
Between Velocity and Near-Field Pressure for
Subharmonic Mode at Re = 42,000 for Case 1L
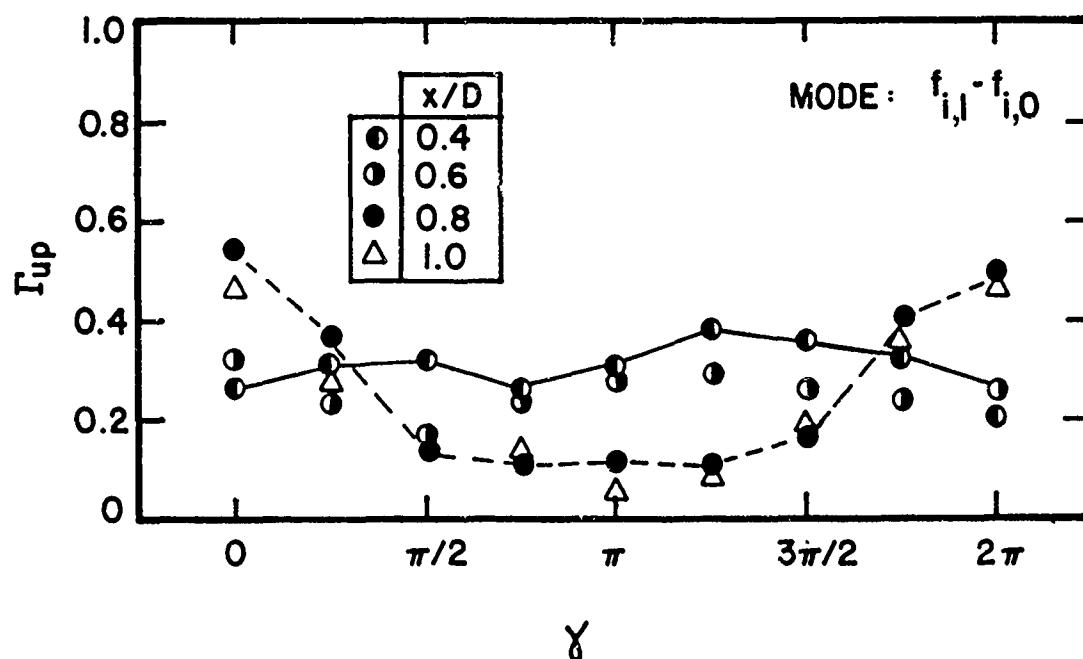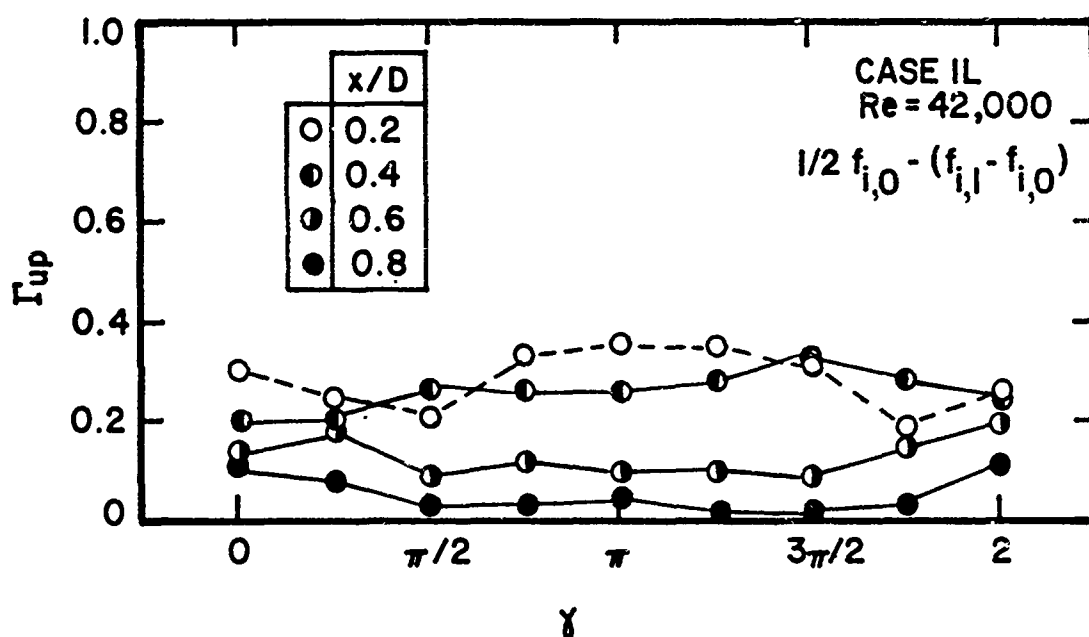
Figure 119. Azimuthal Variation of Coherence Between
Velocity and Near-Field Pressure for Nonlinearly
Developing Modes at Re = 42,000 for Case 1L
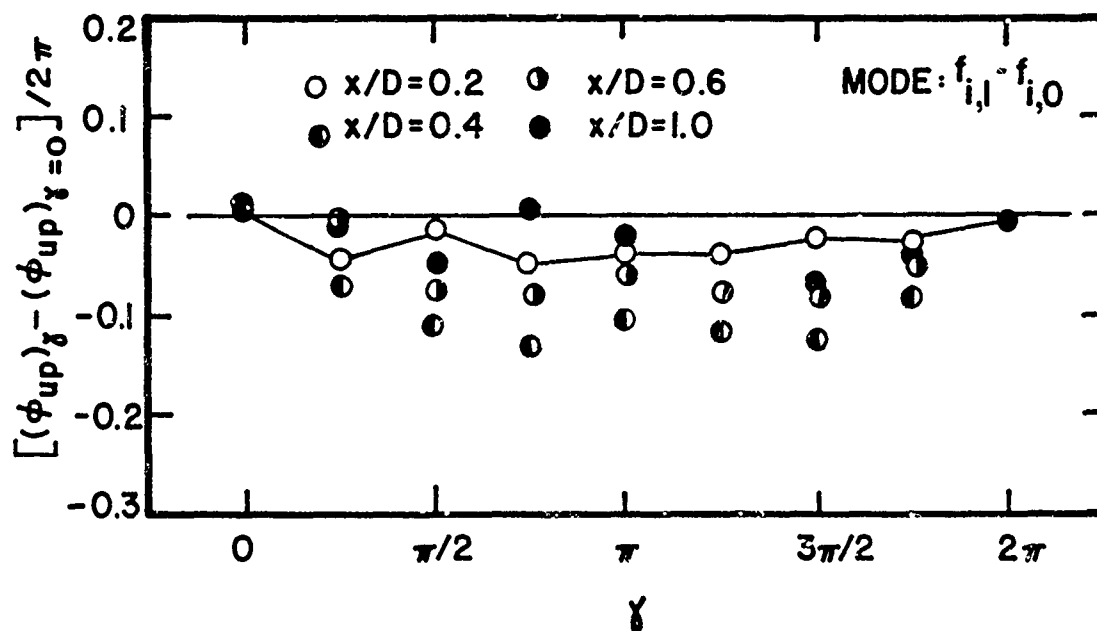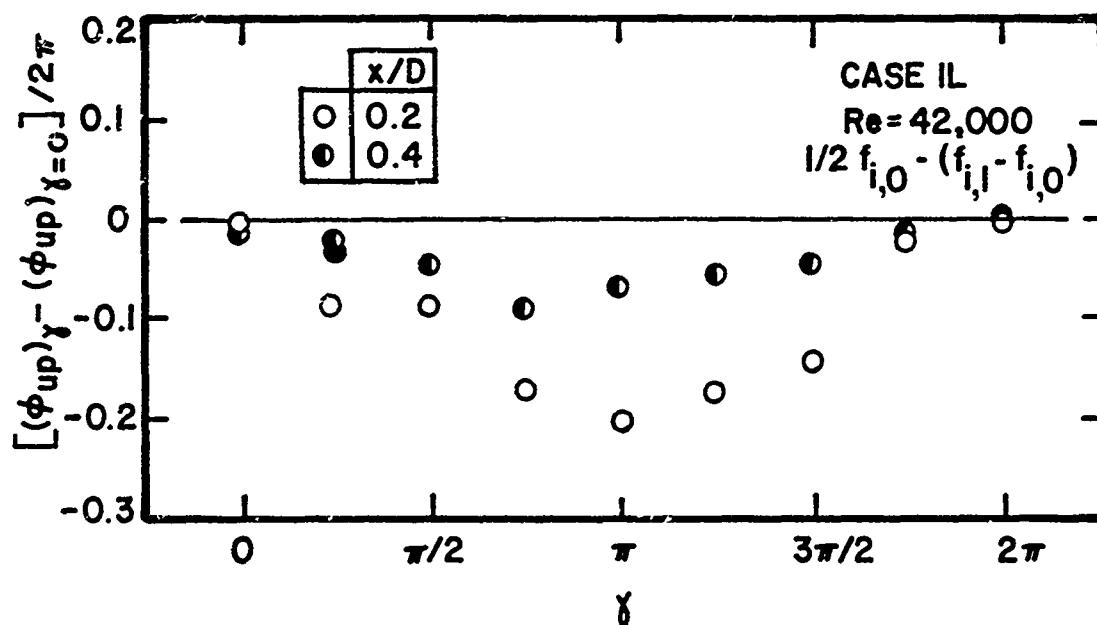
Figure 120. Azimuthal Variation of Phase Difference Between Velocity and Near-Field Pressure for Nonlinearly Developing Modes at Re = 42,000 for Case 1L
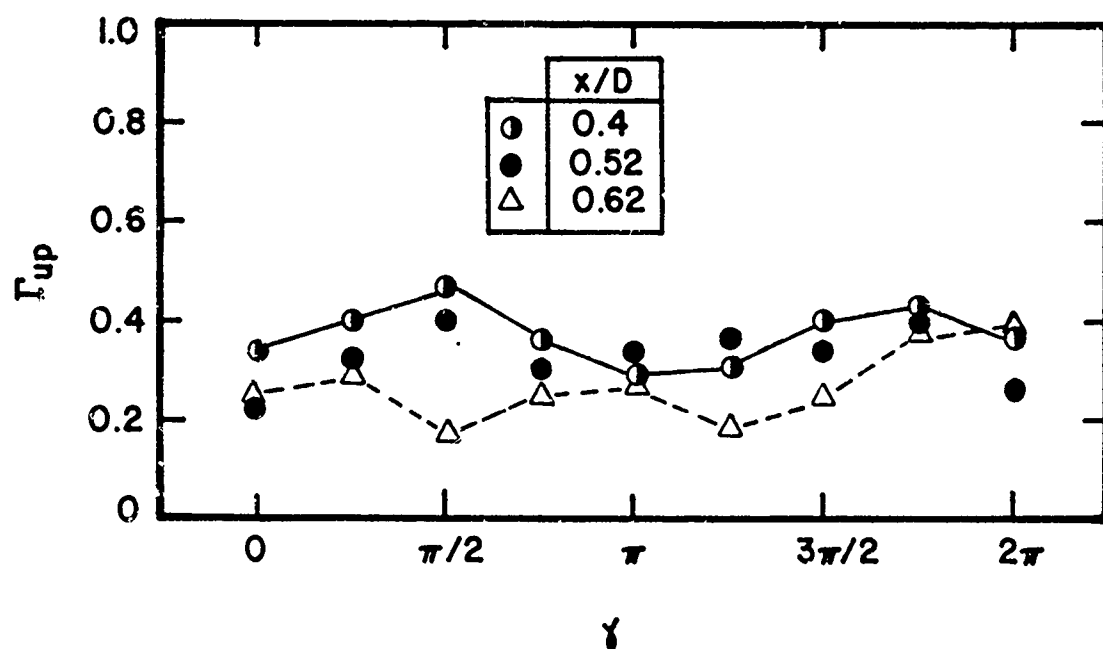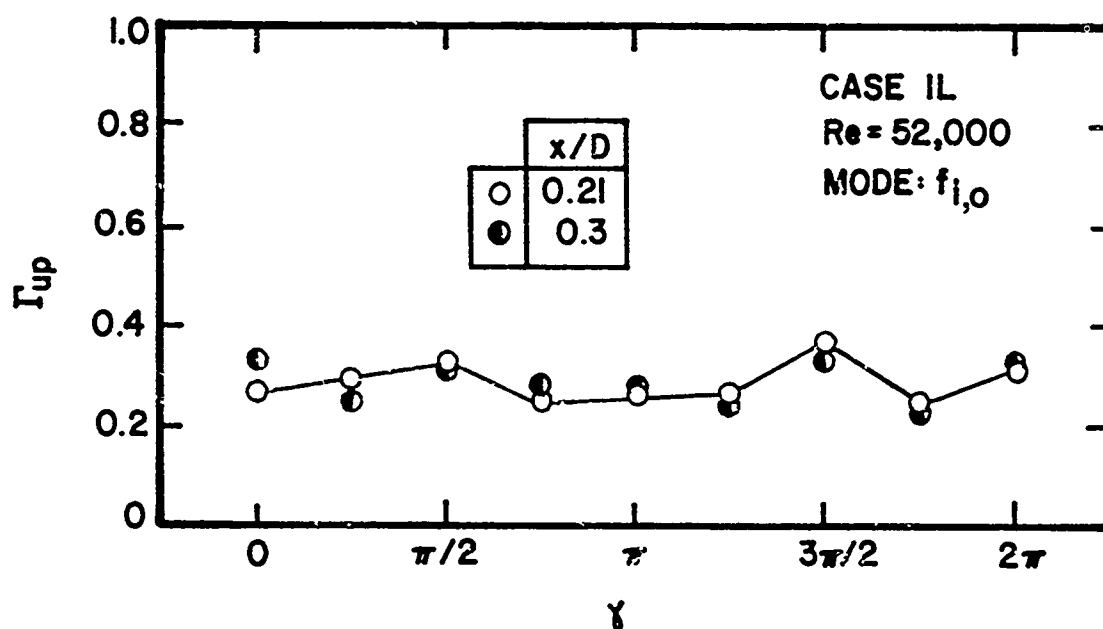
Figure 121. Azimuthal Variation of Coherence Between
Velocity and Near-Field Pressure for Initial
Axisymmetric Mode at Re = 52,000 for Case 1L
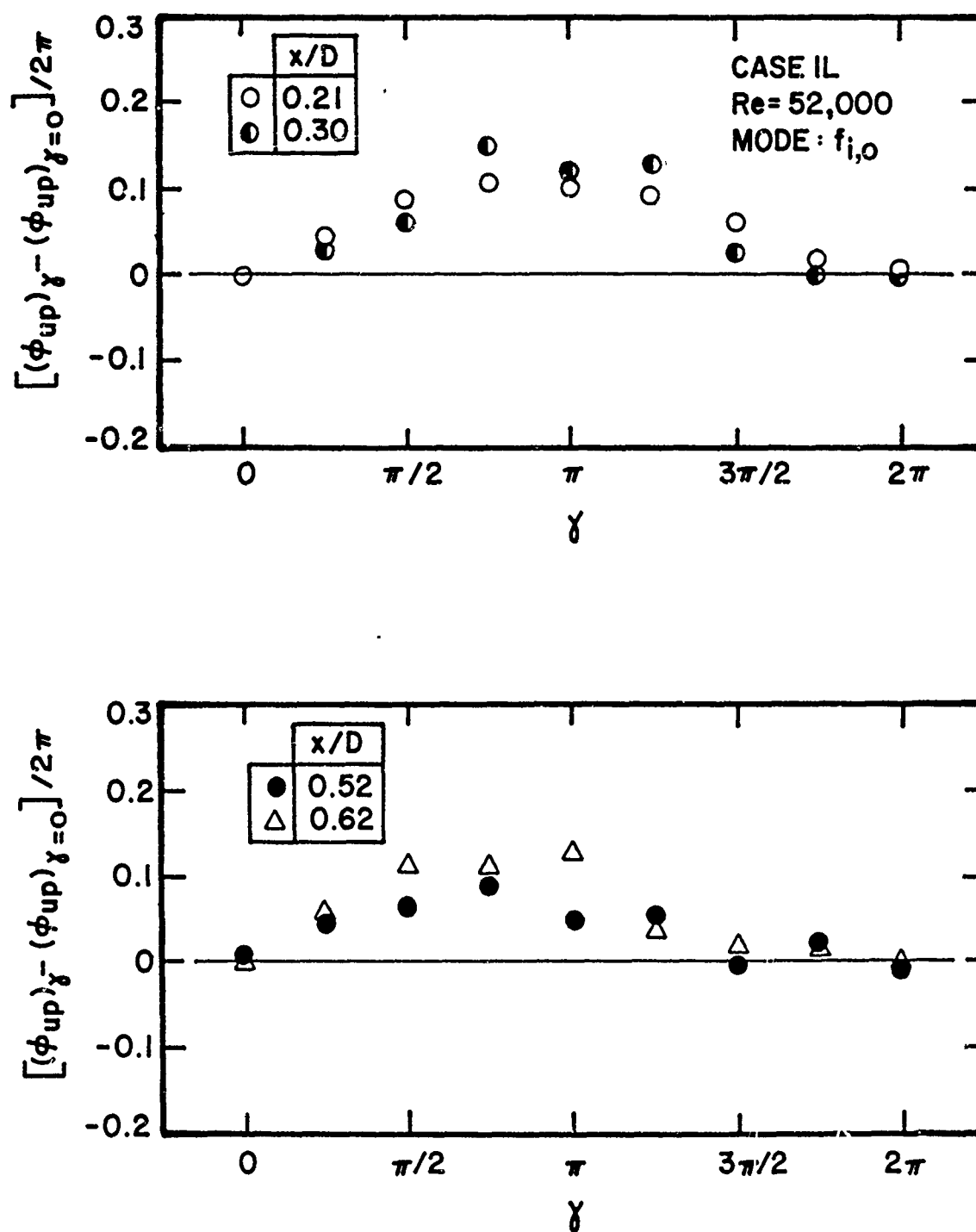
Figure 122. Azimuthal Variation of Phase Difference
Between Velocity and Near-Field Pressure for
Initial Axisymmetric Mode at Re = 52,000 for Case 1L
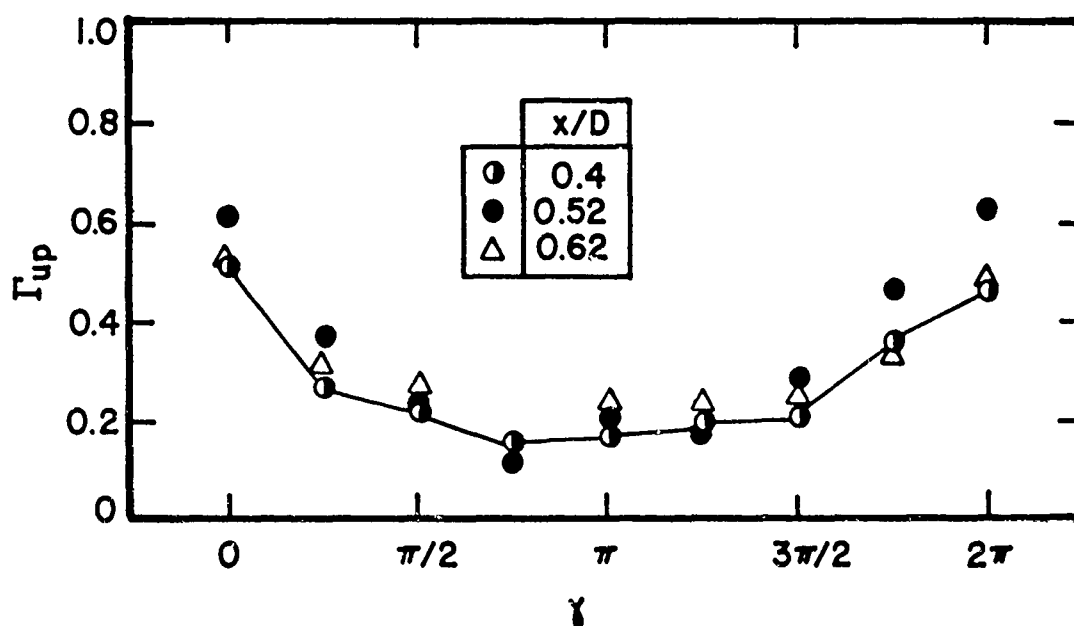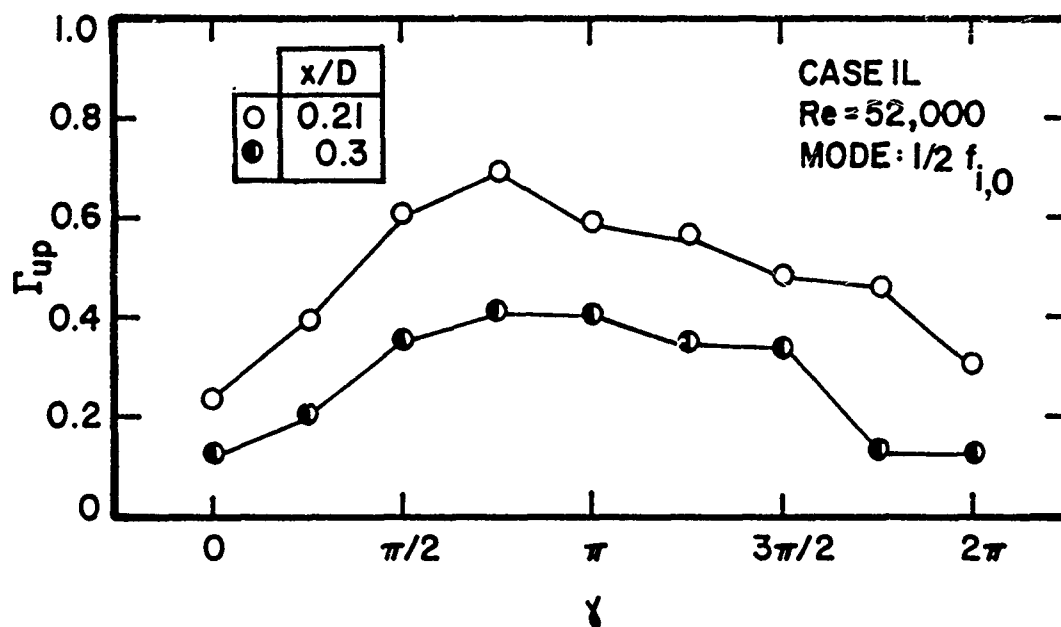
Figure 123. Azimuthal Variation of Coherence Between
Velocity and Near-Field for Subharmonic Mode at
Re = 52,000 for Case 1L
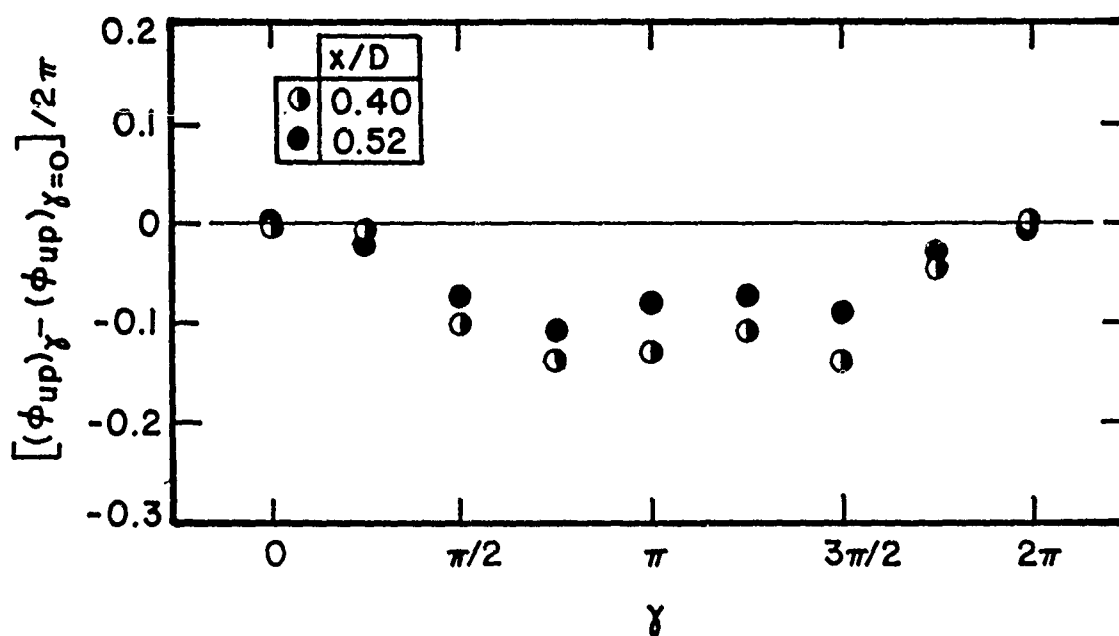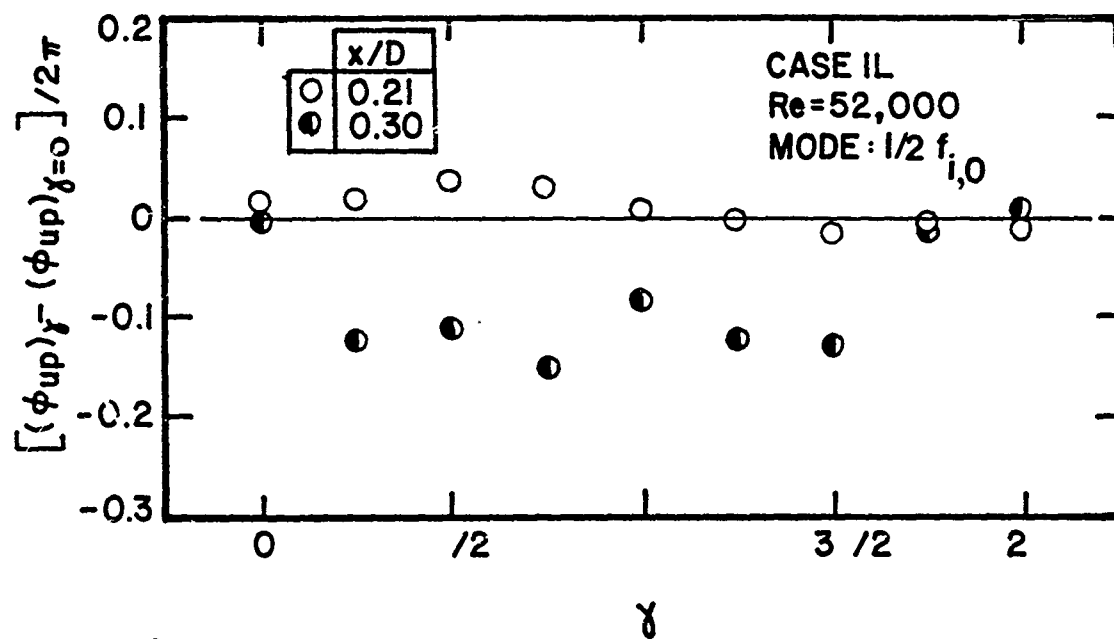
Figure 124. Azimuthal Variation of Phase Difference Between Velocity and Near-Field Pressure for Subharmonic Mode at Re = 52,000 for Case 1L
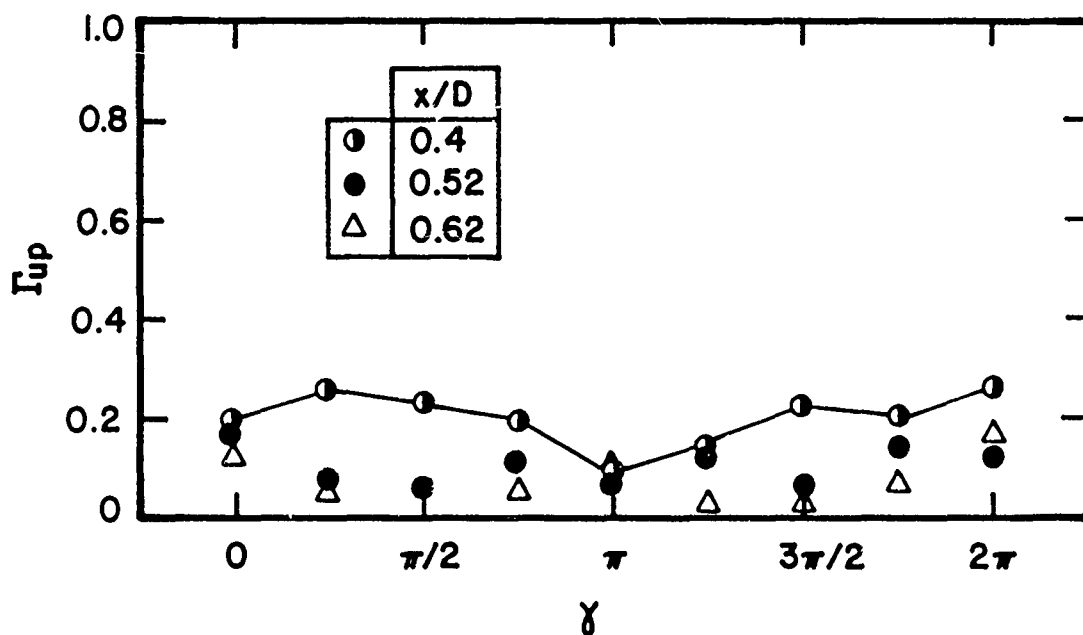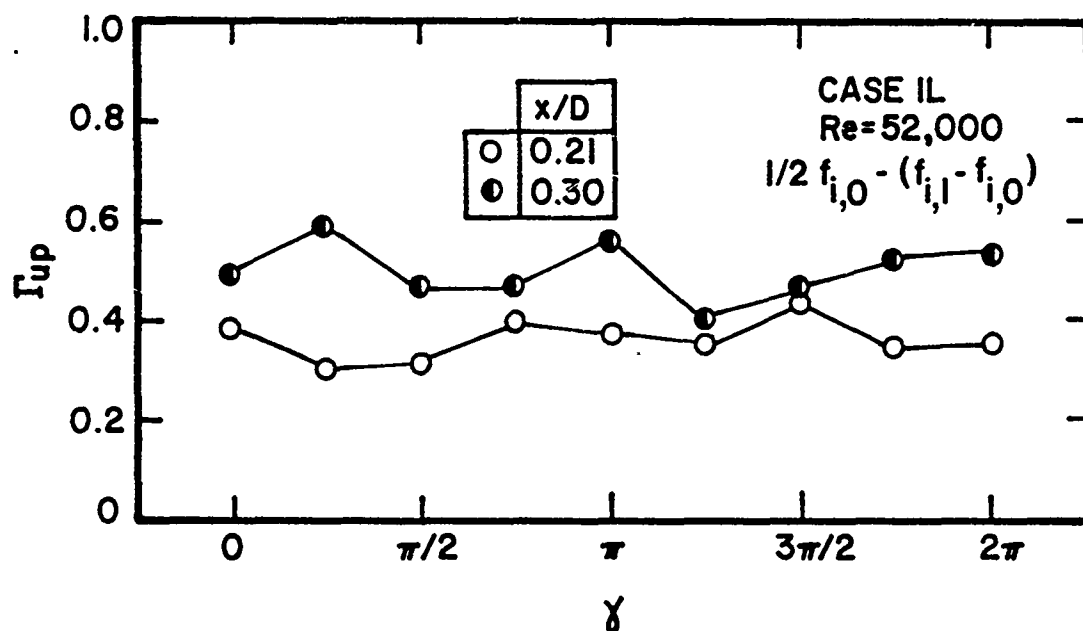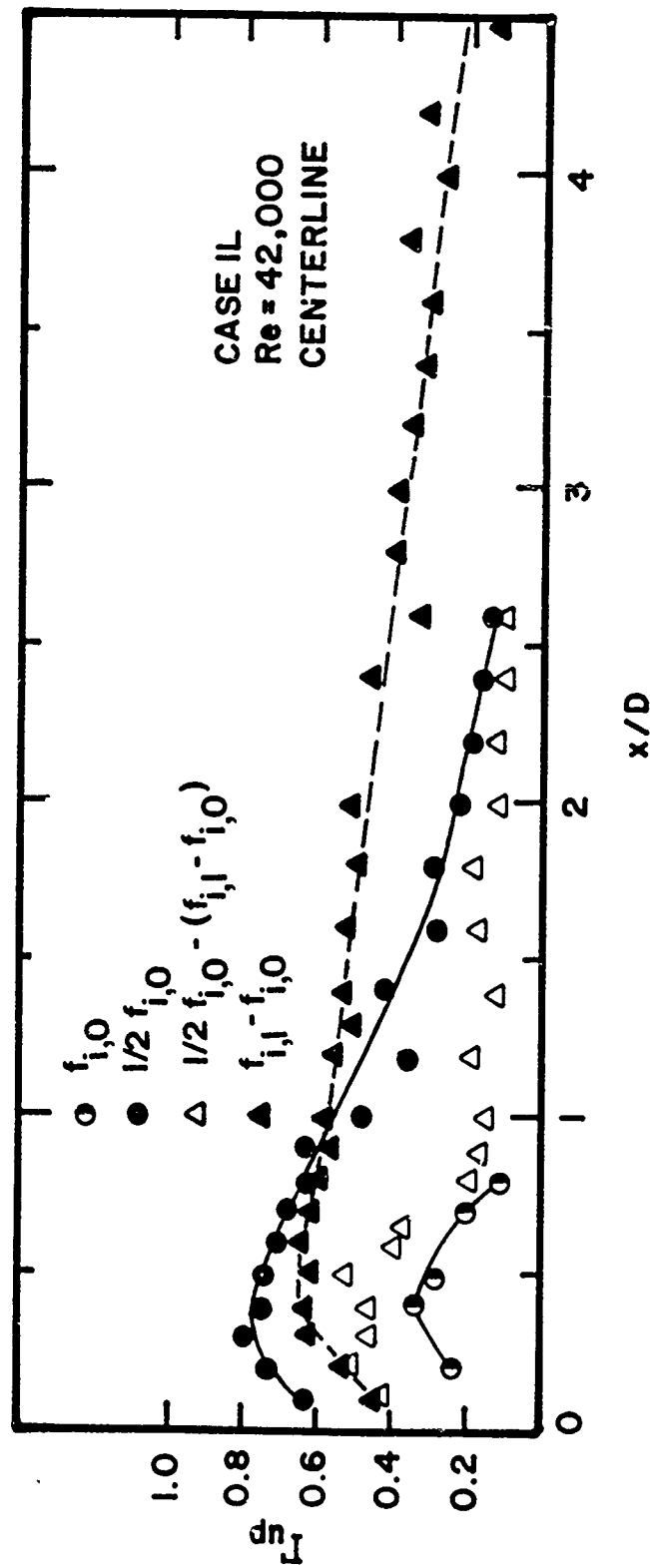
Figure 125. Azimuthal Variation of Coherence Between
Velocity and Near-Field Pressure for Three-Wave
Nonlinear Interaction at Re = 52,000 for case 1L
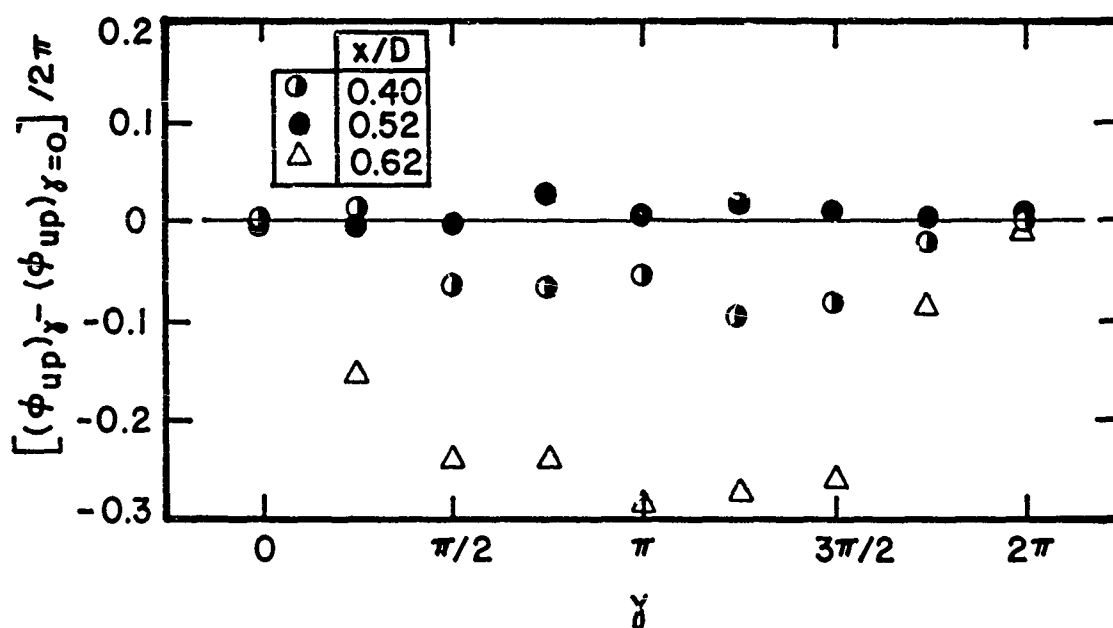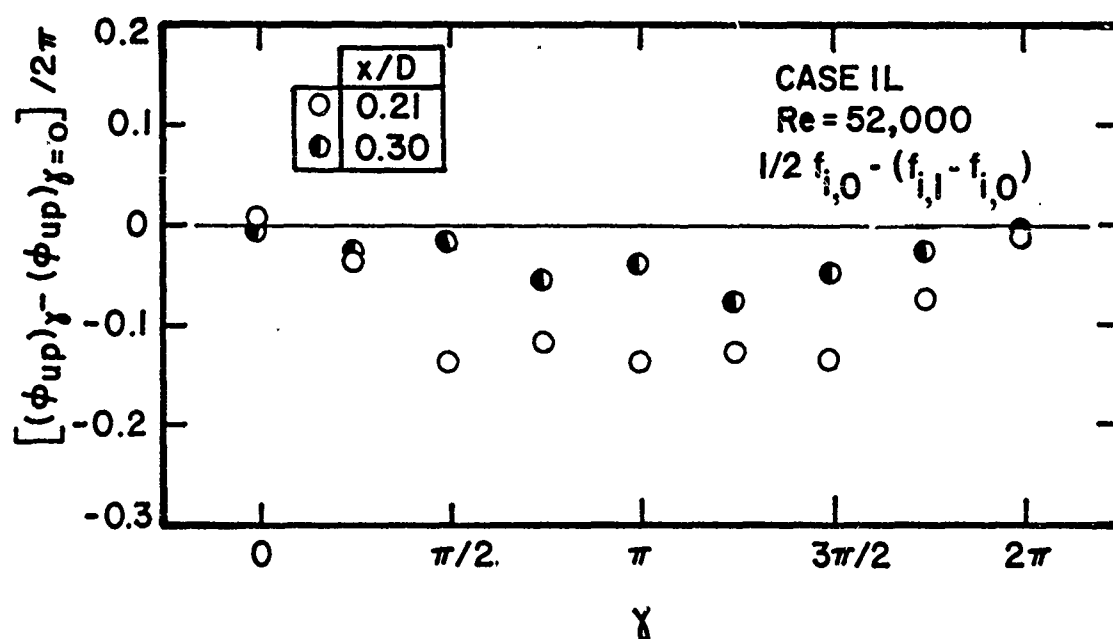
Figure 126. Azimuthal Variation of Phase Difference
Between Velocity and Near-Field Pressure for Three-Wave
Nonlinear Interaction at Re = 52,000 for Case 1L
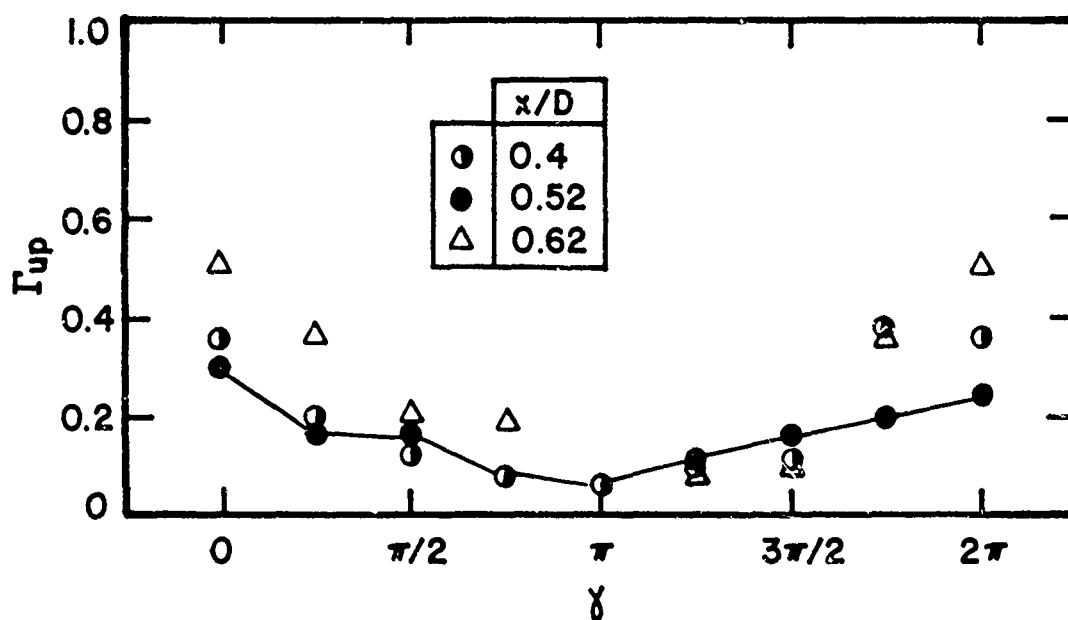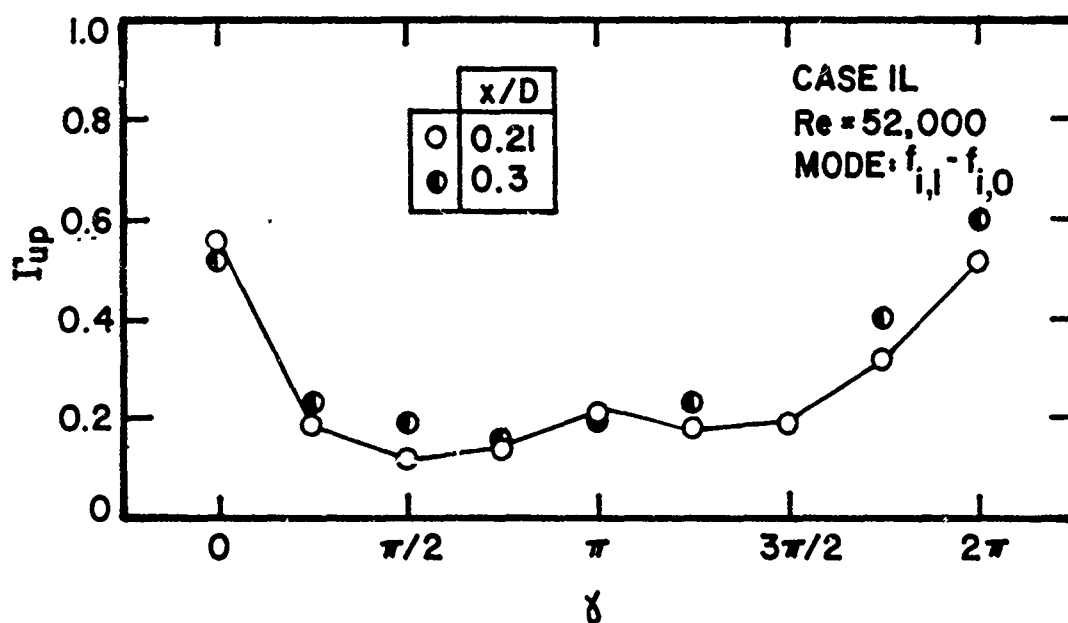
Figure 127. Azimuthal Variation of Coherence Between
Velocity and Near-Field Pressure for Initial Axisymmetric-
Helical Difference Mode at Re = 52,000 for Case 1L
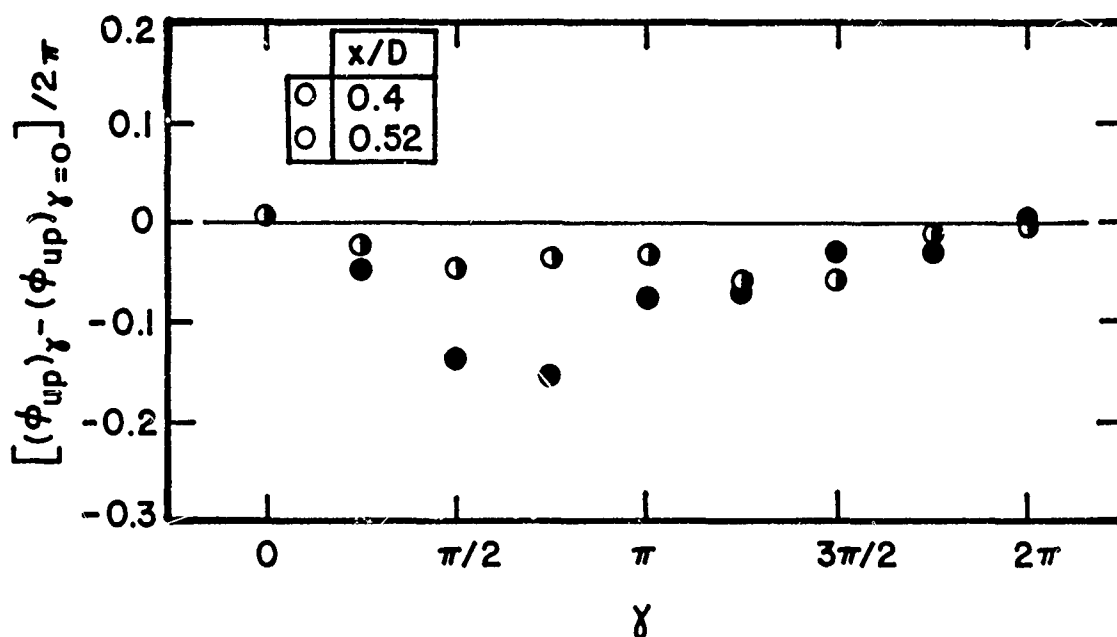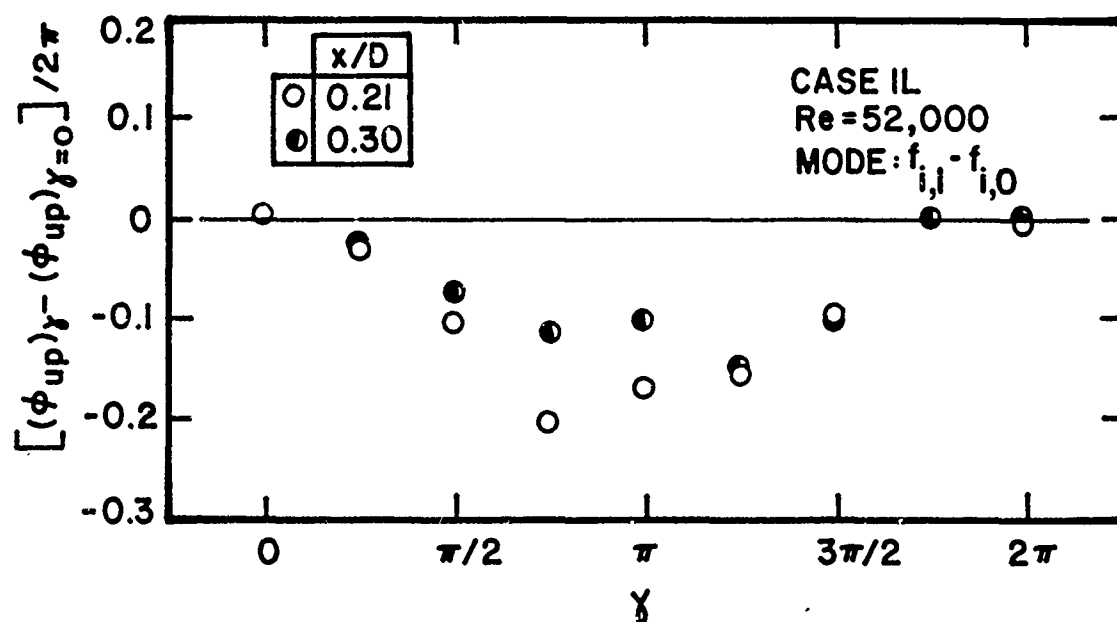
Figure 128. Azimuthal Variation of Phase Difference Between Velocity and Near-Field Pressure for Initial Axisymmetric-Helical Difference Mode at Re = 52,000 for Case 1L
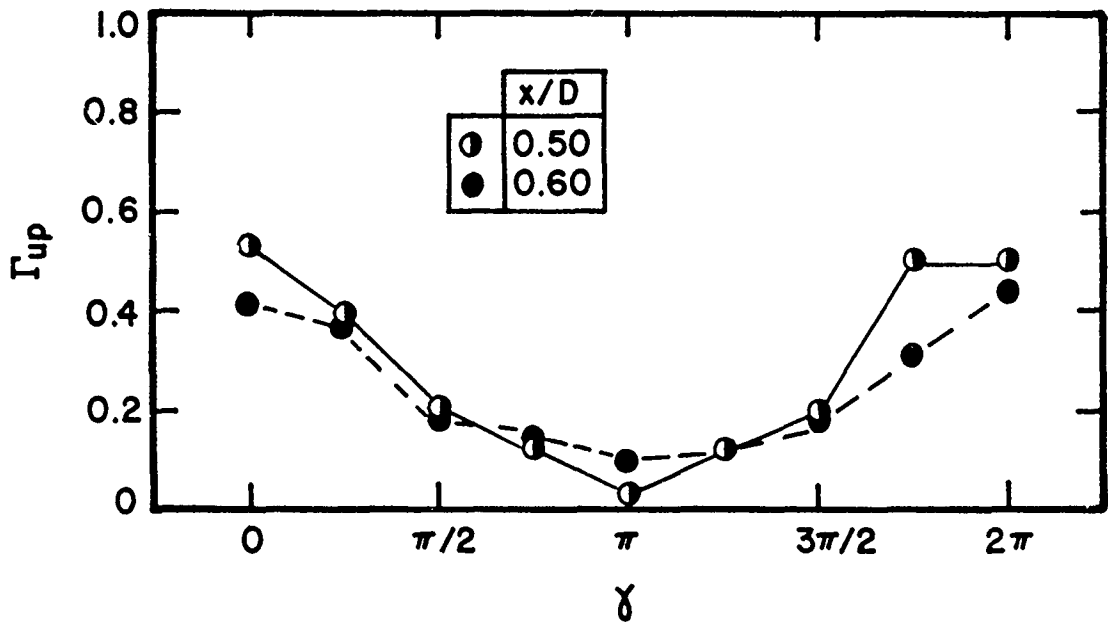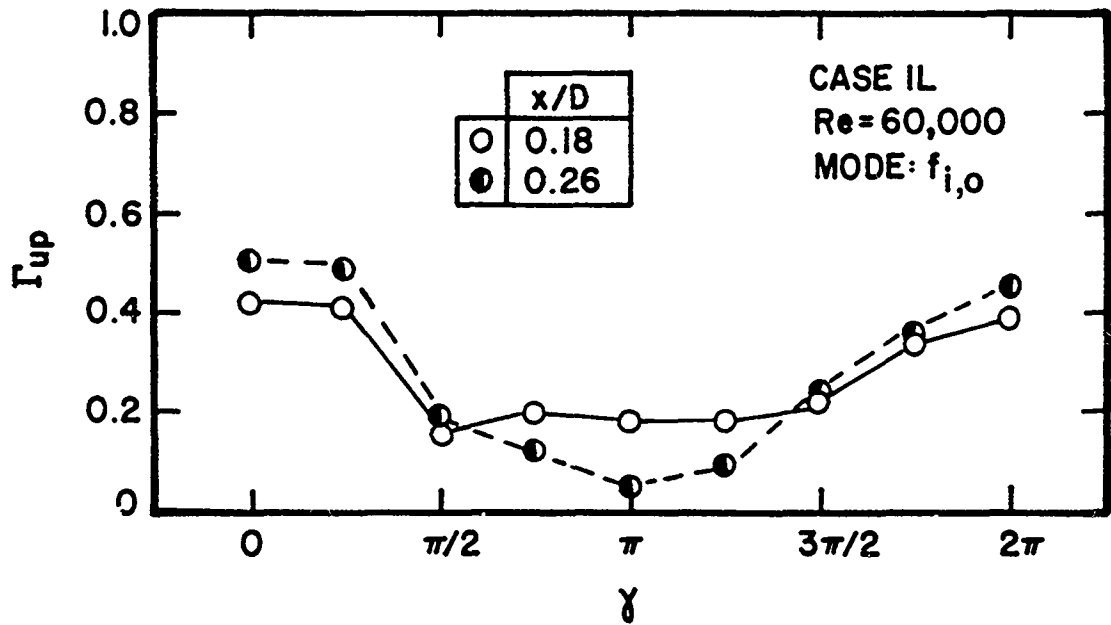
Figure 129. Azimuthal Variation of Coherence Between
Velocity and Near-Field Pressure for Initial
Axisymmetric Mode at Re = 60,000 for Case 1L

Figure 130. Azimuthal Variation of Phase Difference
Between Velocity and Near-Field Pressure for
Initial Axisymmetric Mode at Re = 60,000 for Case 1L

Figure 131. Azimuthal Variation of Coherence Between
Velocity and Near-Field Pressure for Subharmonic
Mode at Re = 60,000 for Case 1L
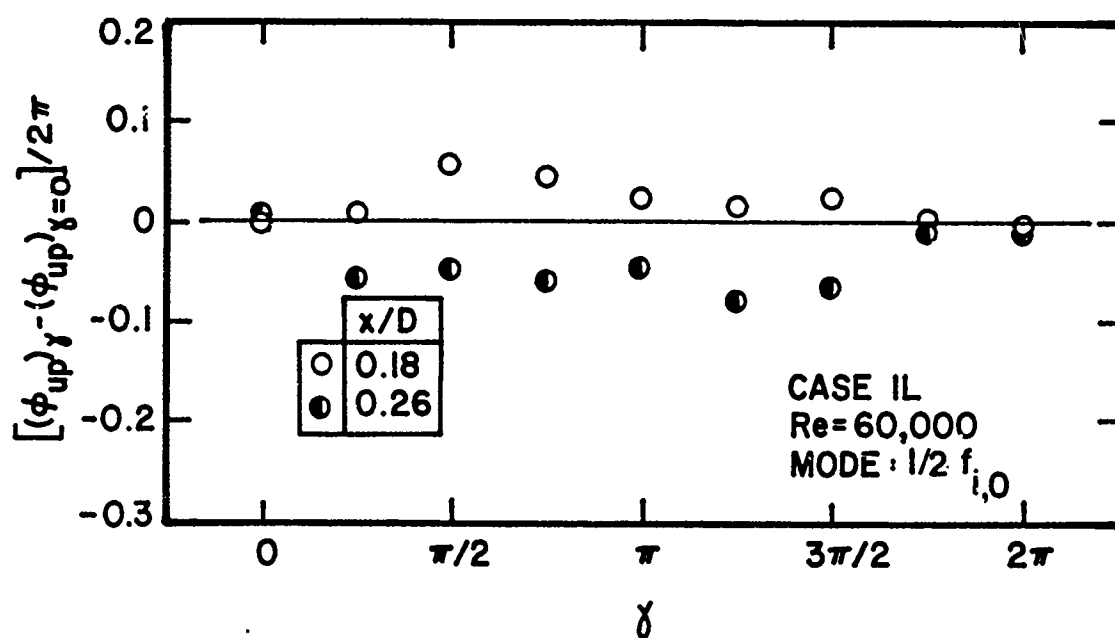
Figure 132. Azimuthal Variation of Phase Difference
Between Velocity and Near-Field Pressure for
Subharmonic Mode at Re = 60,000 for Case 1L

Figure 133. Azimuthal Variation of Coherence Between
Velocity and Near-Field Pressure for Nonlinearly
Developing Modes at Re = 60,000 for Case 1L

Figure 134. Azimuthal Variation of Phase Difference Between Velocity and Near-Field Pressure for Nonlinearly Developing Modes at Re = 60,000 for Case 1L

Figure 135. Azimuthal Variation of Coherence Between
Velocity and Near-Field Pressure for Initial Axisymmetric
and Helical Modes at Re = 42,000 for Case 3L

Figure 136. Azimuthal Variation of Coherence Between
Velocity and Near-Field Pressure for Initial Axisymmetric
and Helical Modes at Re = 42,000 for Case 3L

Figure 137. Azimuthal Variation of Phase Difference
Between Velocity and Near-Field Pressure for Initial
Axisymmetric and Helical Modes at Re = 42,000 for Case 3L

Figure 138. Azimuthal Variation of Phase Difference
Between Velocity and Near-Field Pressure for
Subharmonic Mode at Re = 42,000 for Cases 2L and 3L

Figure 139. Streamwise Variation of Coherence Between Velocity and Near-Field Pressure for Observed Instability Modes on Jet Centerline at Re = 42,000 for Case 1L
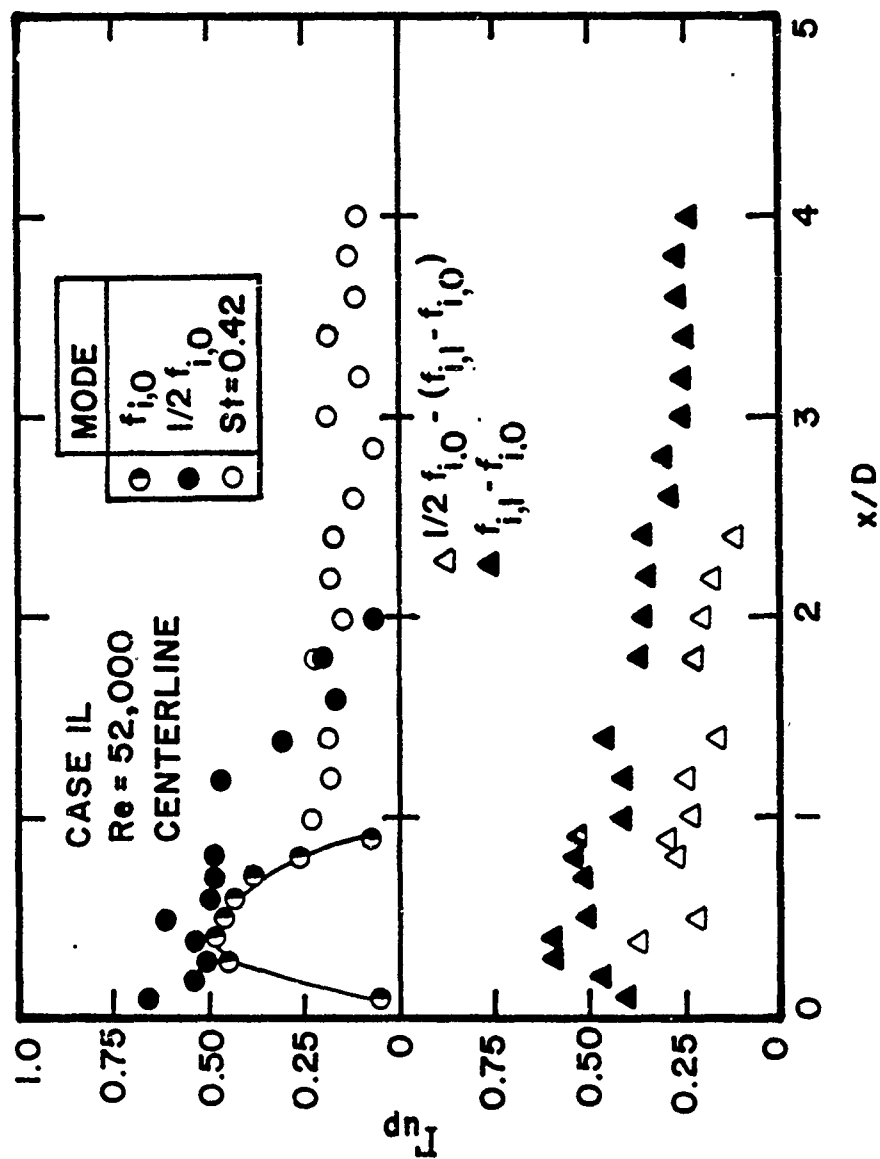
Figure 140. Streamwise Variation of Coherence Between Velocity and Near-Field
Pressure for Observed Instability Modes on Jet Centerline at Re = 52,000
for Case 1L
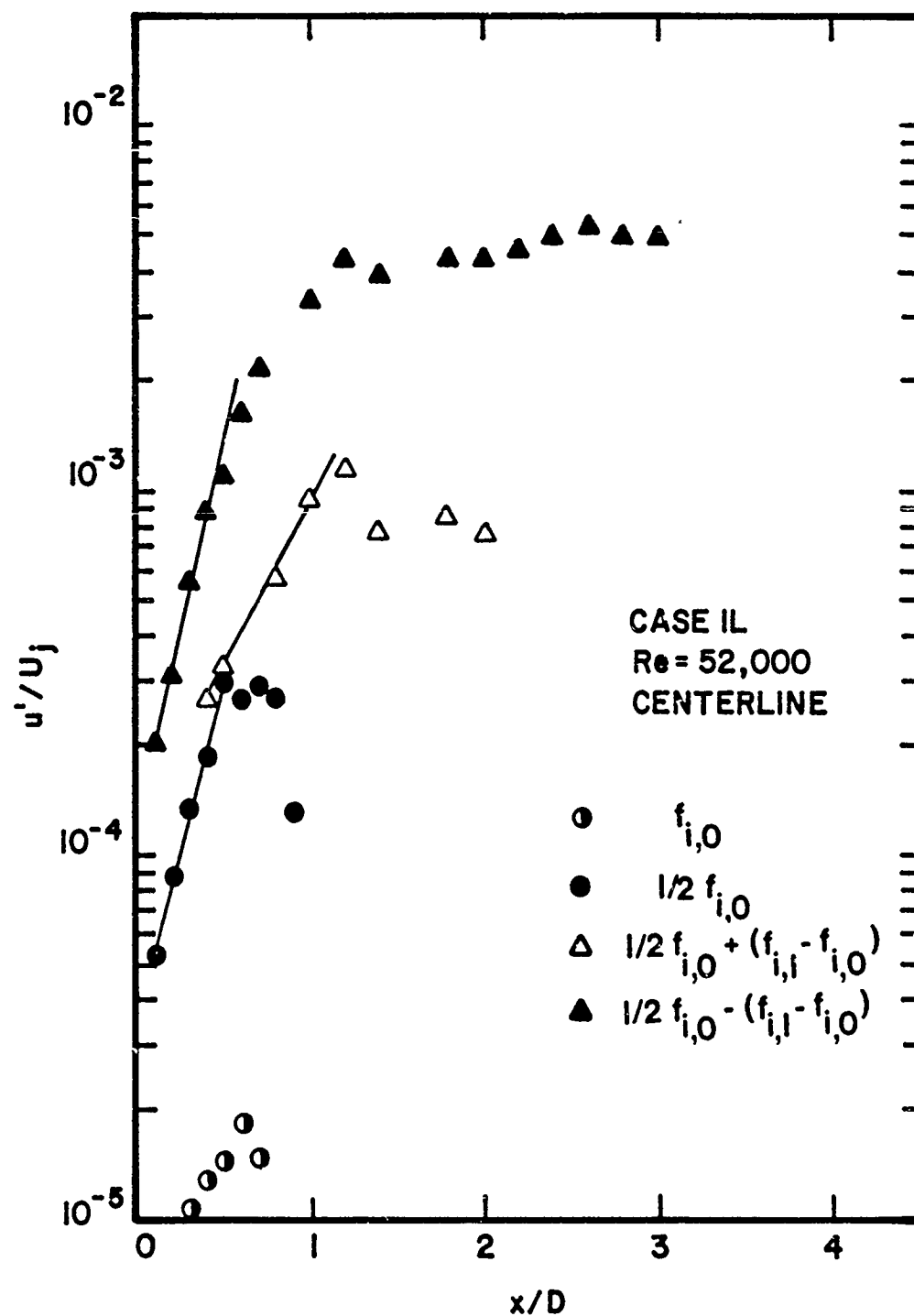
Figure 141. Streamwise Development of Amplitude of Observed Instability Modes on Jet Centerline at Re = 52,000 for Case 1L
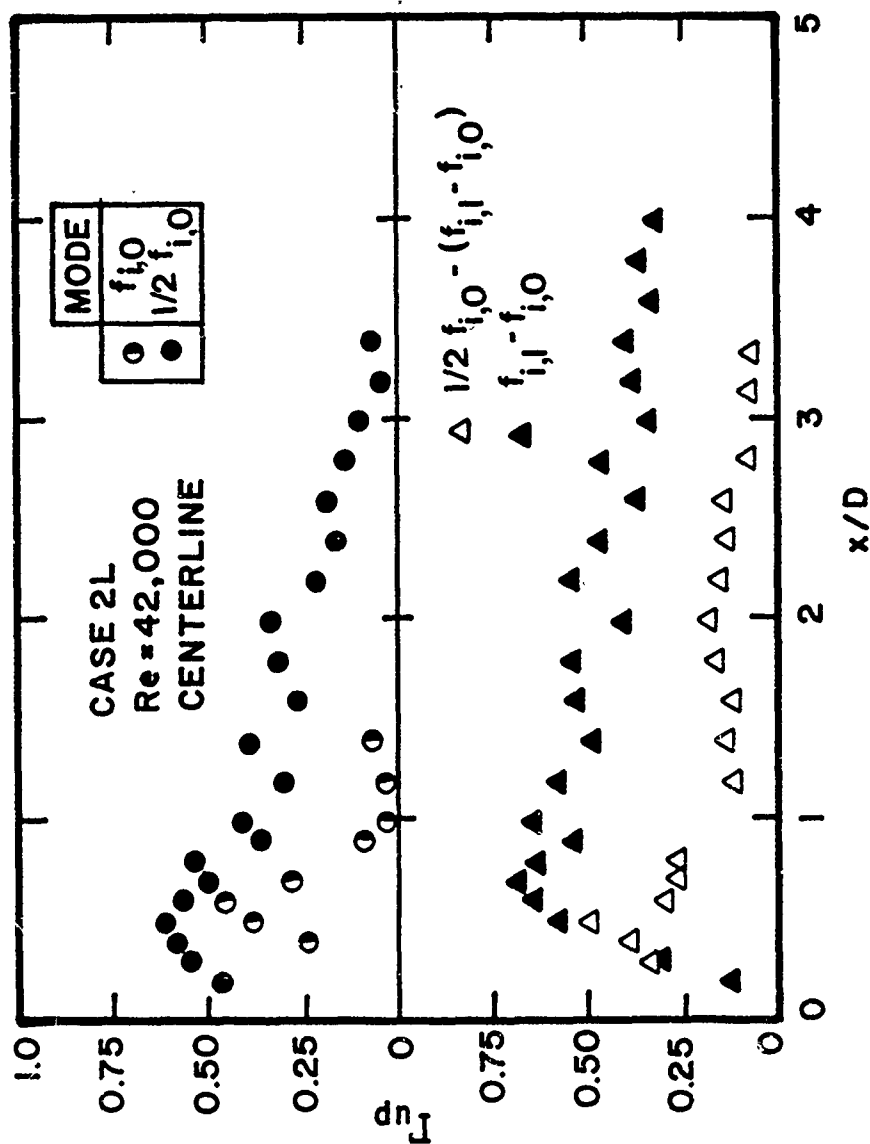
Figure 142. Streamwise Variation of Coherence Between Velocity and Near-Field Pressure for Observed Instability Modes on Jet Centerline at Re = 42,000 for Case 2L
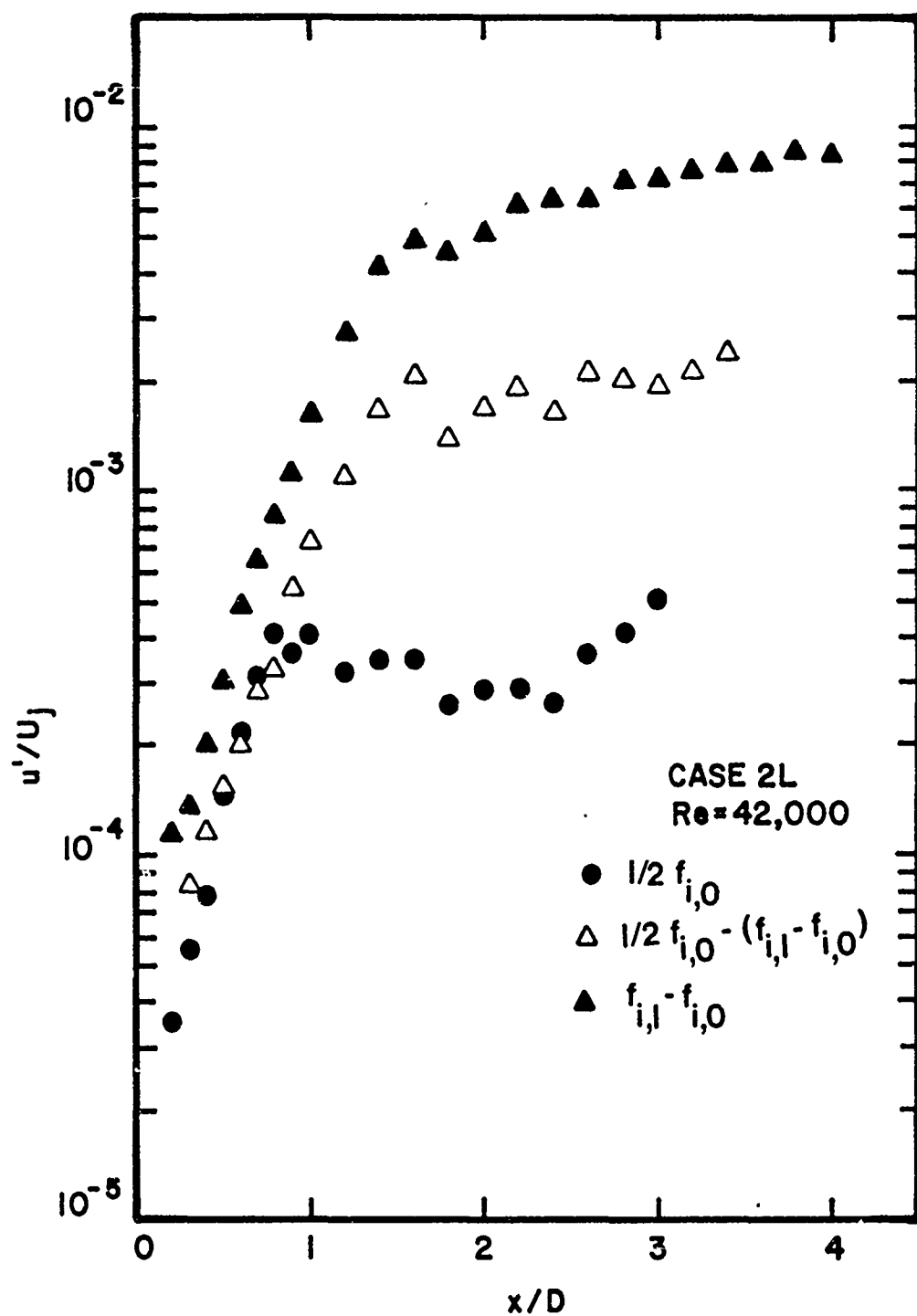
Figure 143. Streamwise Development of Amplitude of
Some Observed Instability Modes on Jet Centerline
at Re = 42,000 for Case 2L
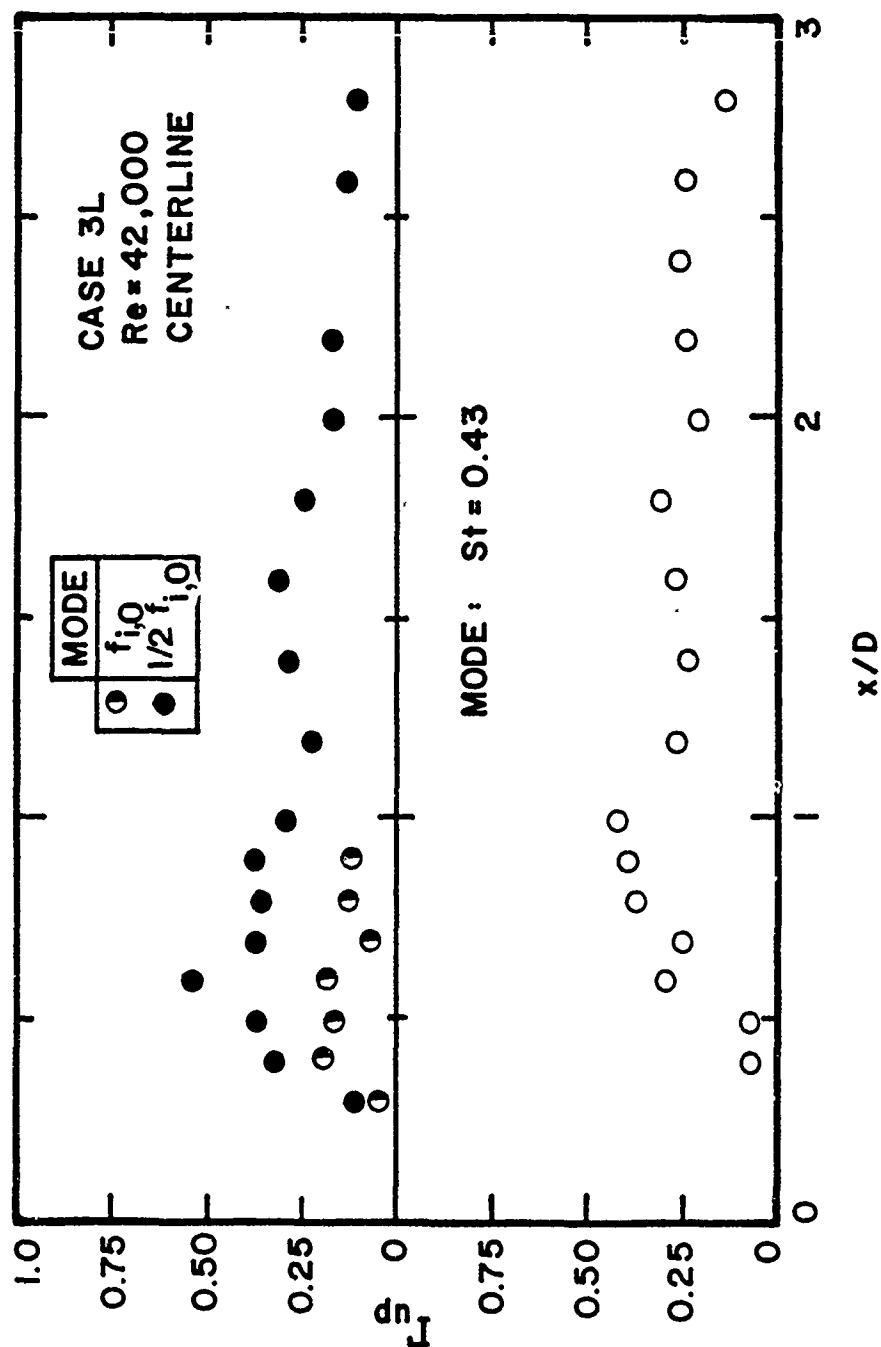
Figure 144. Streamwise Variation of Coherence Between Velocity and Near-Field Pressure for Some of the Observed Instability Modes on Jet Centerline at Re = 42,000 for Case 3L
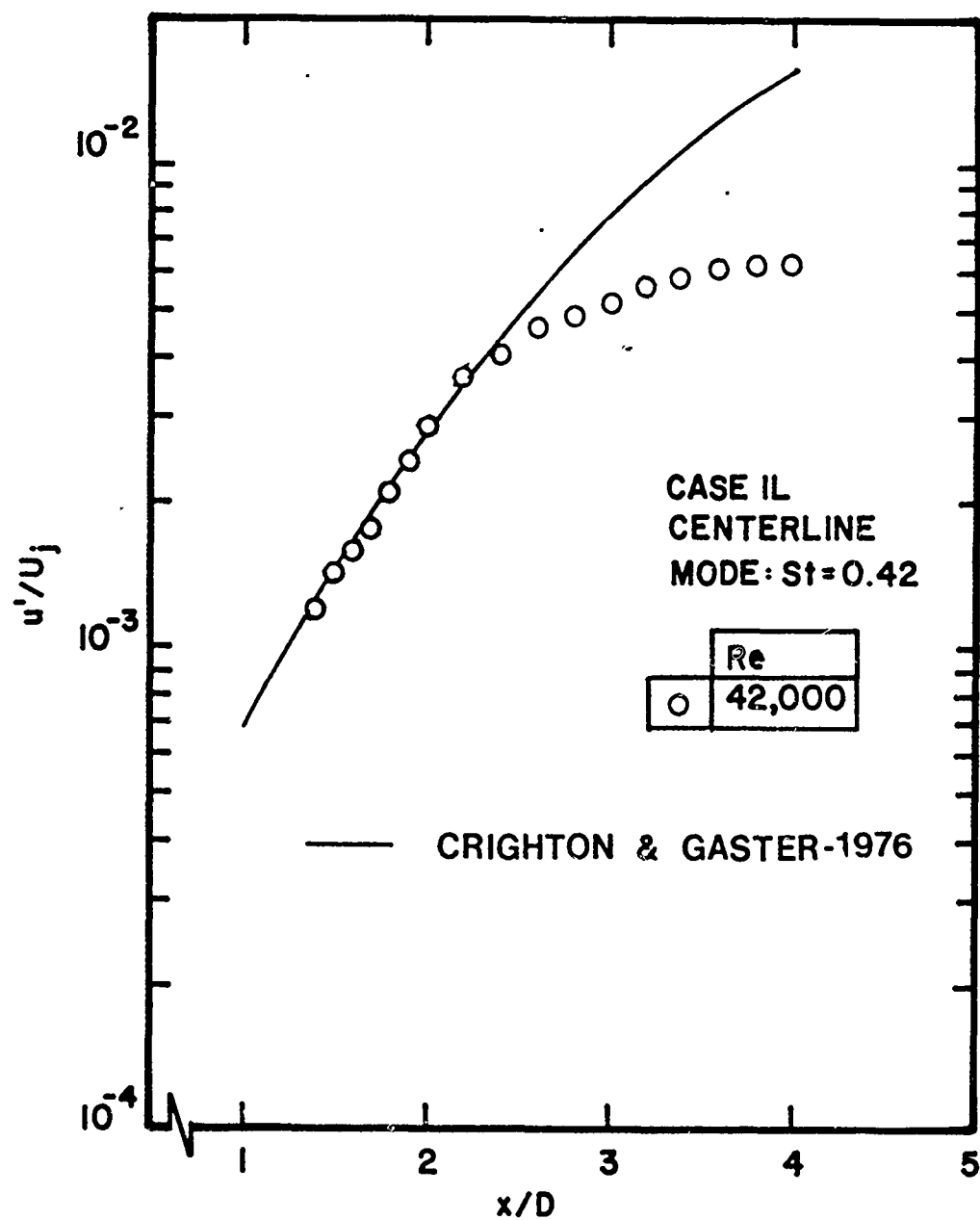
Figure 145. Streamwise Development along Jet
Centerline of Amplitude of Final Strouhal
Frequency for Case 1L at Re = 42,000
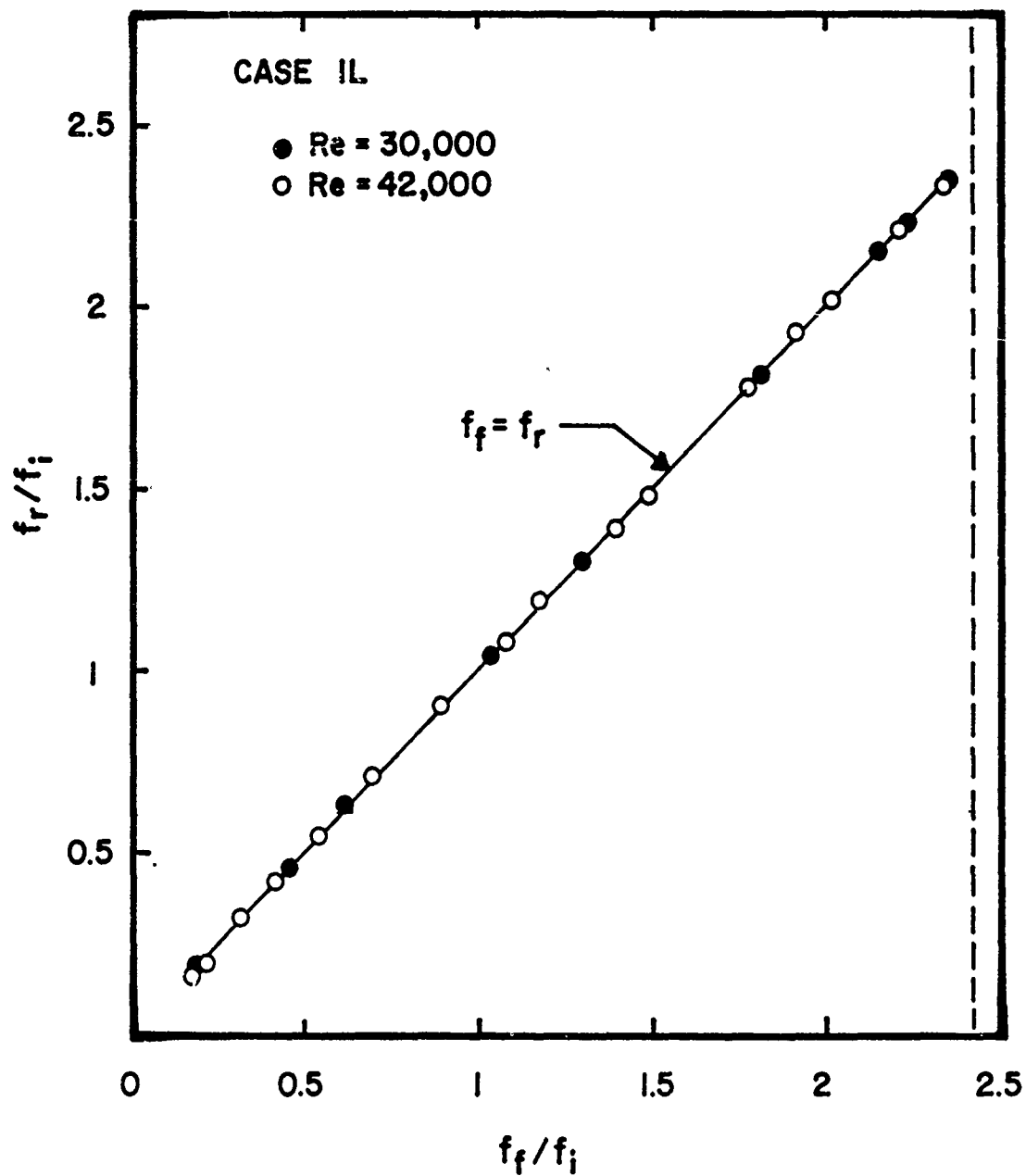
Figure 146. Variation of Response Frequency of
Initial Jet to External Excitation Frequency
for Case 1L
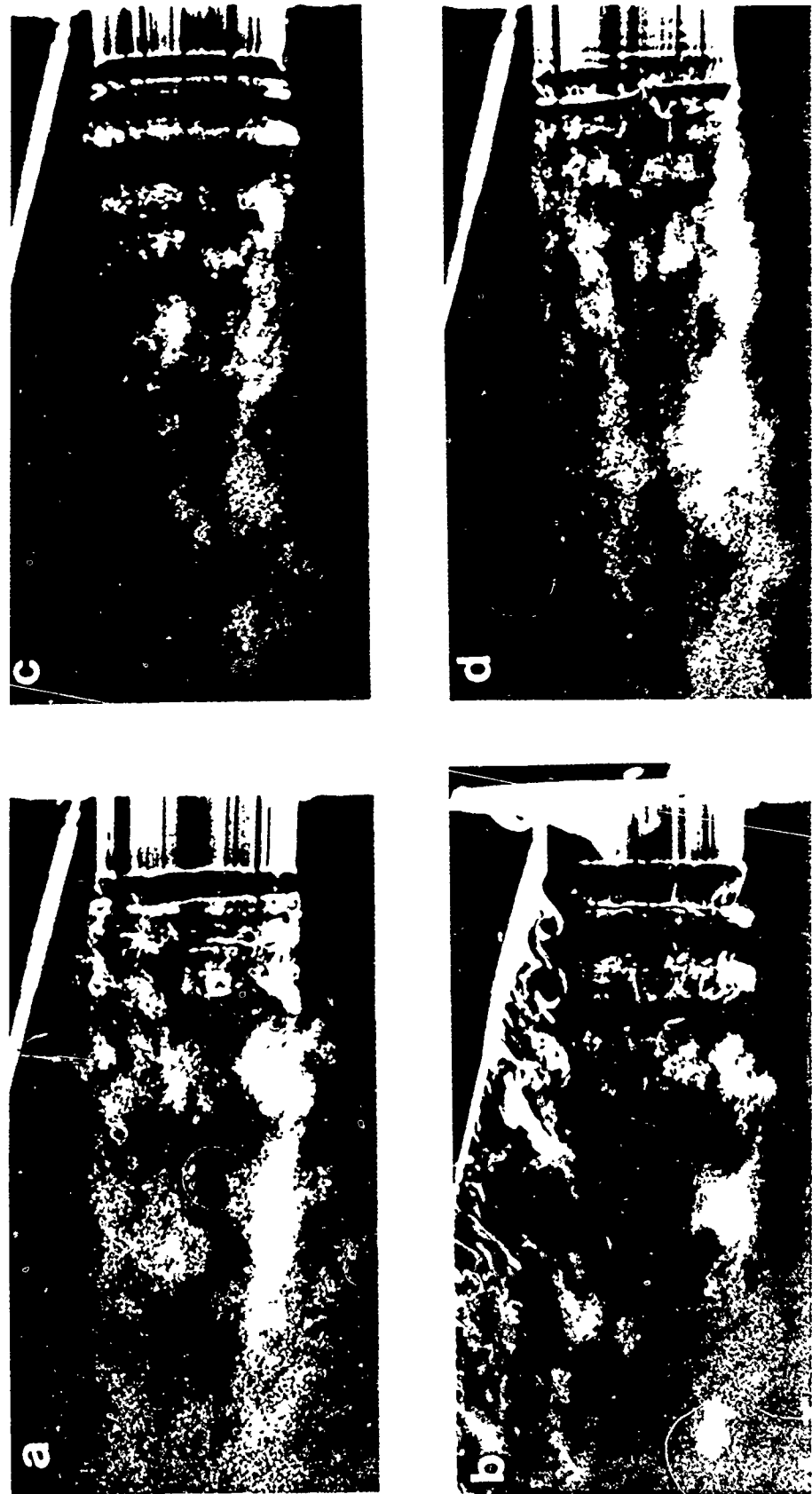
FLOW

Figure 147. Flow Visualization Illustrating Effect of Forcing Frequency on Initial Jet Development: (a) unforced, (b) $St_\theta = 0.013$, (c) $St_\theta = 0.0065$, (d) $St_\theta = 0.003$; Re = 42,000, Case 1L
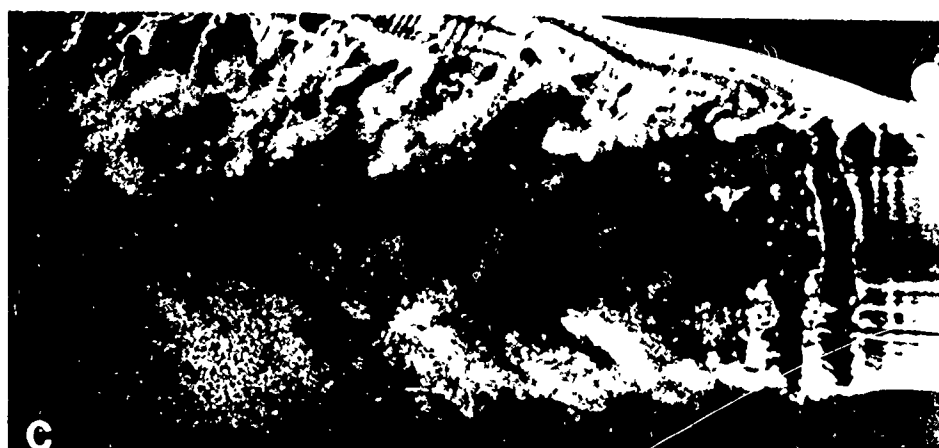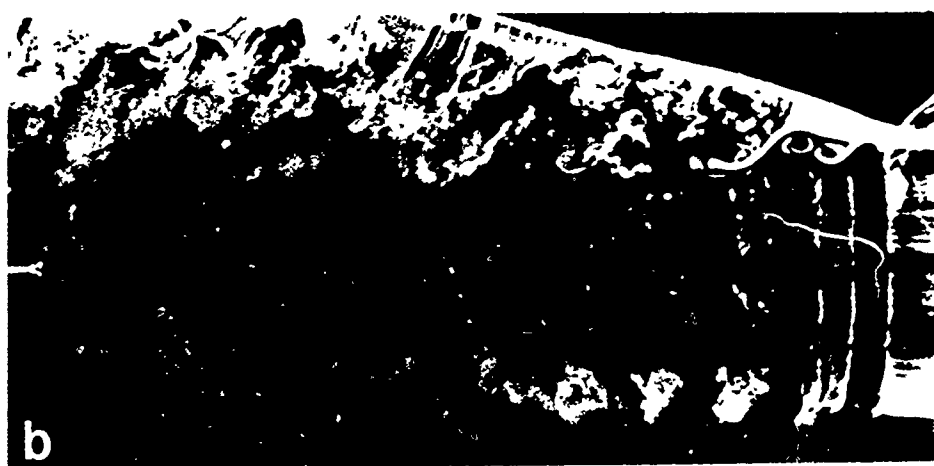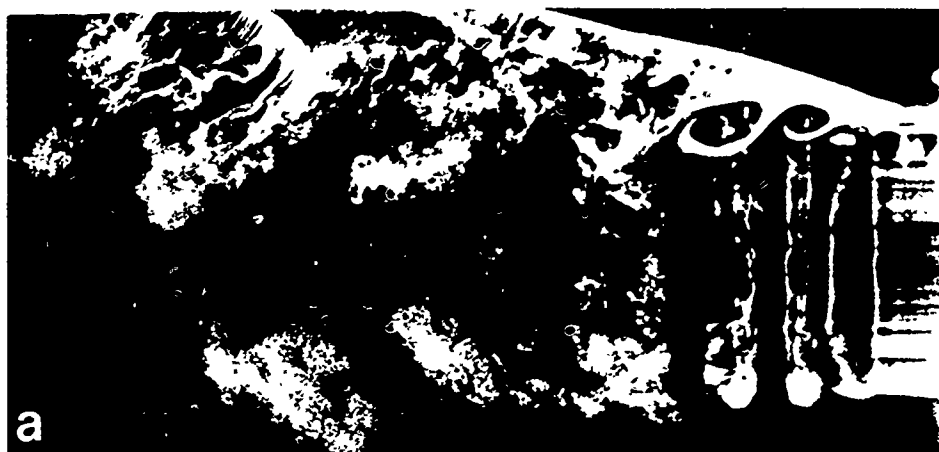
FLOW

Figure 148. Flow Visualization Illustrating Effect
of Forcing Frequency on Entrainment into Jet:
(a) St_θ= 0.0065, (b) St_θ= 0.013, (c) St_θ = 0.03;
Re = 42,000, Case 1L
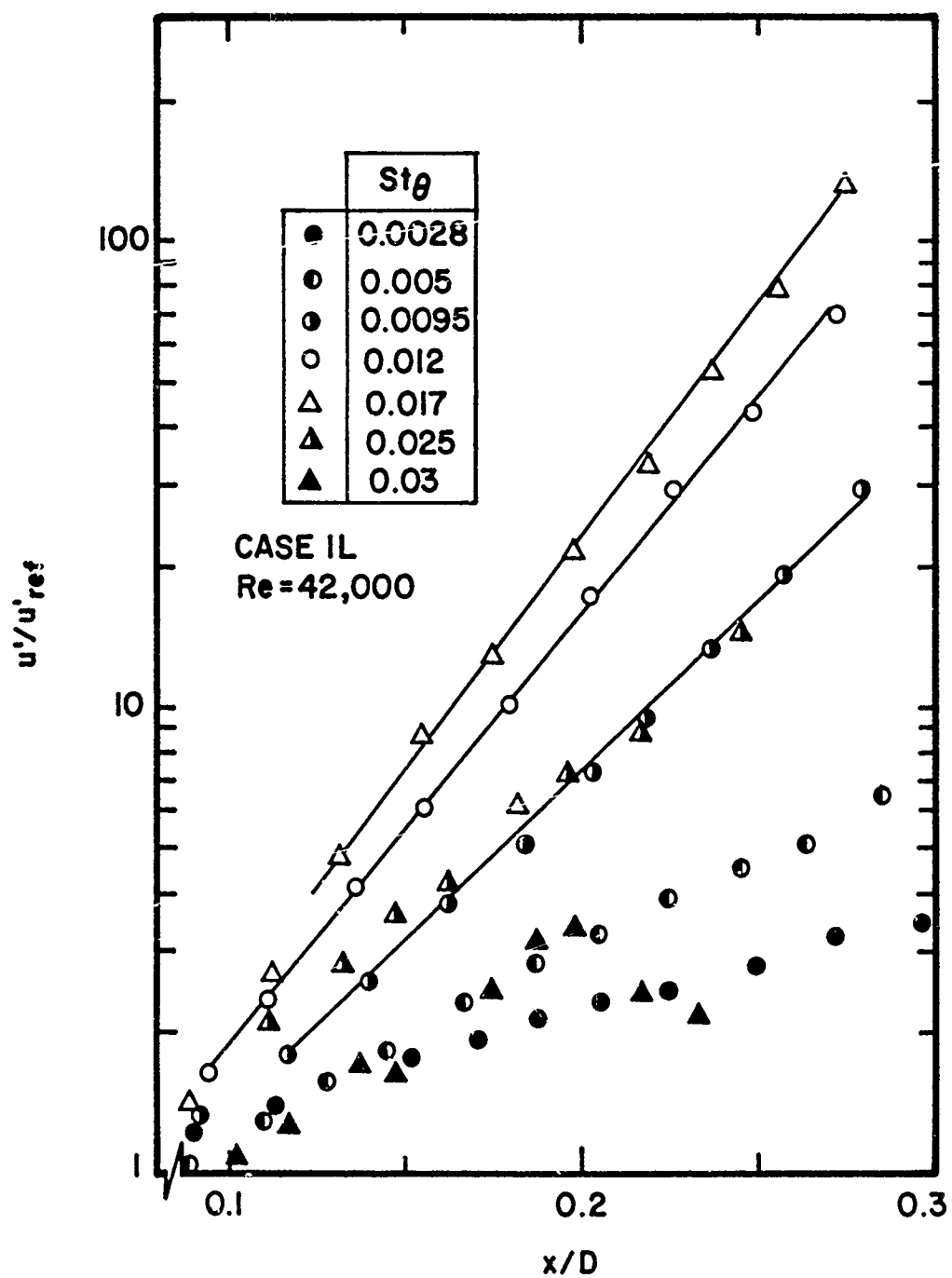
Figure 149. Streamwise Development of Amplitude of
Forced Mode as a Function of Excitation Frequency;
$U/U_j = 0.6$, Re = 42,000, Case 1L
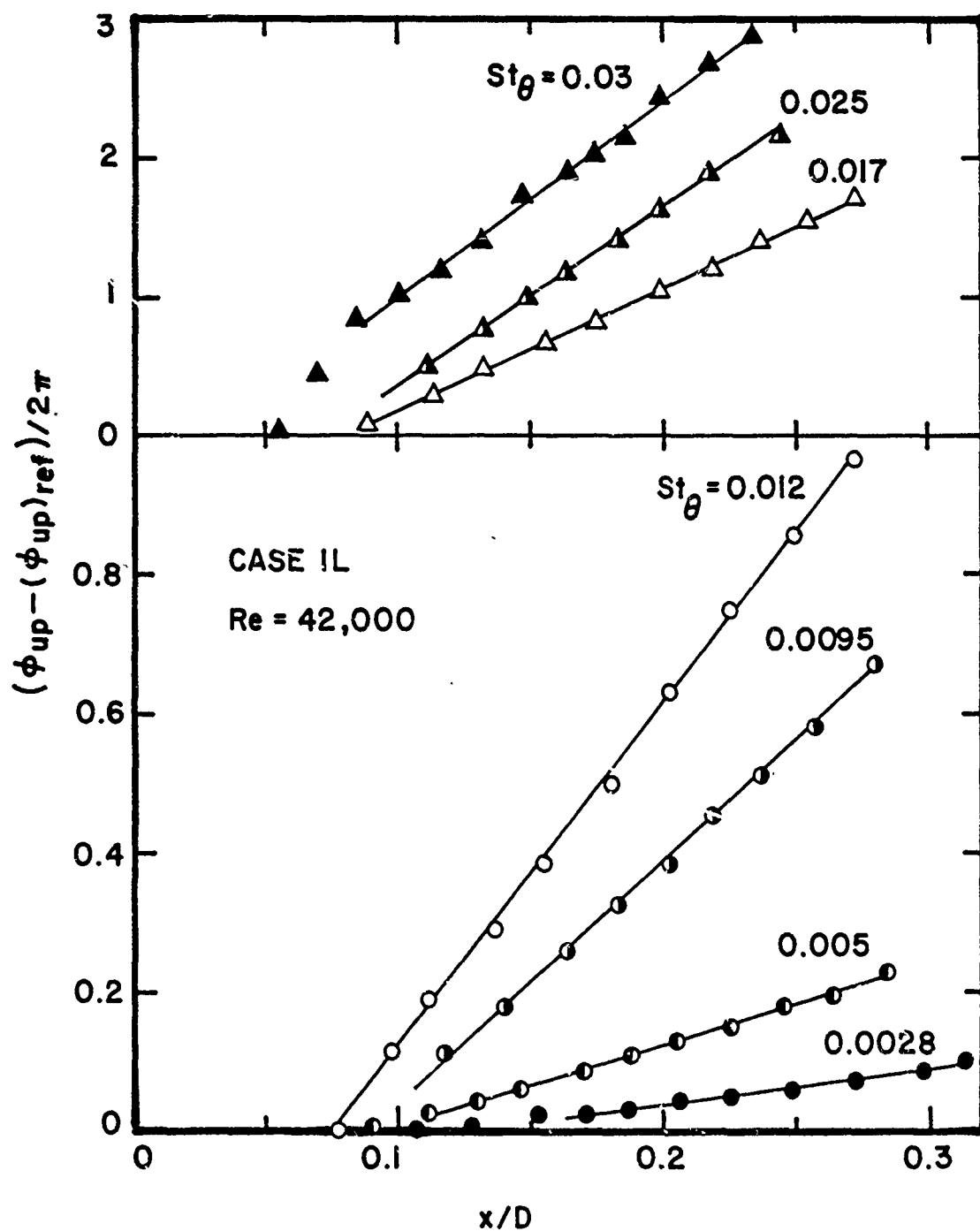
Figure 150. Streamwise Phase Variation of Forced
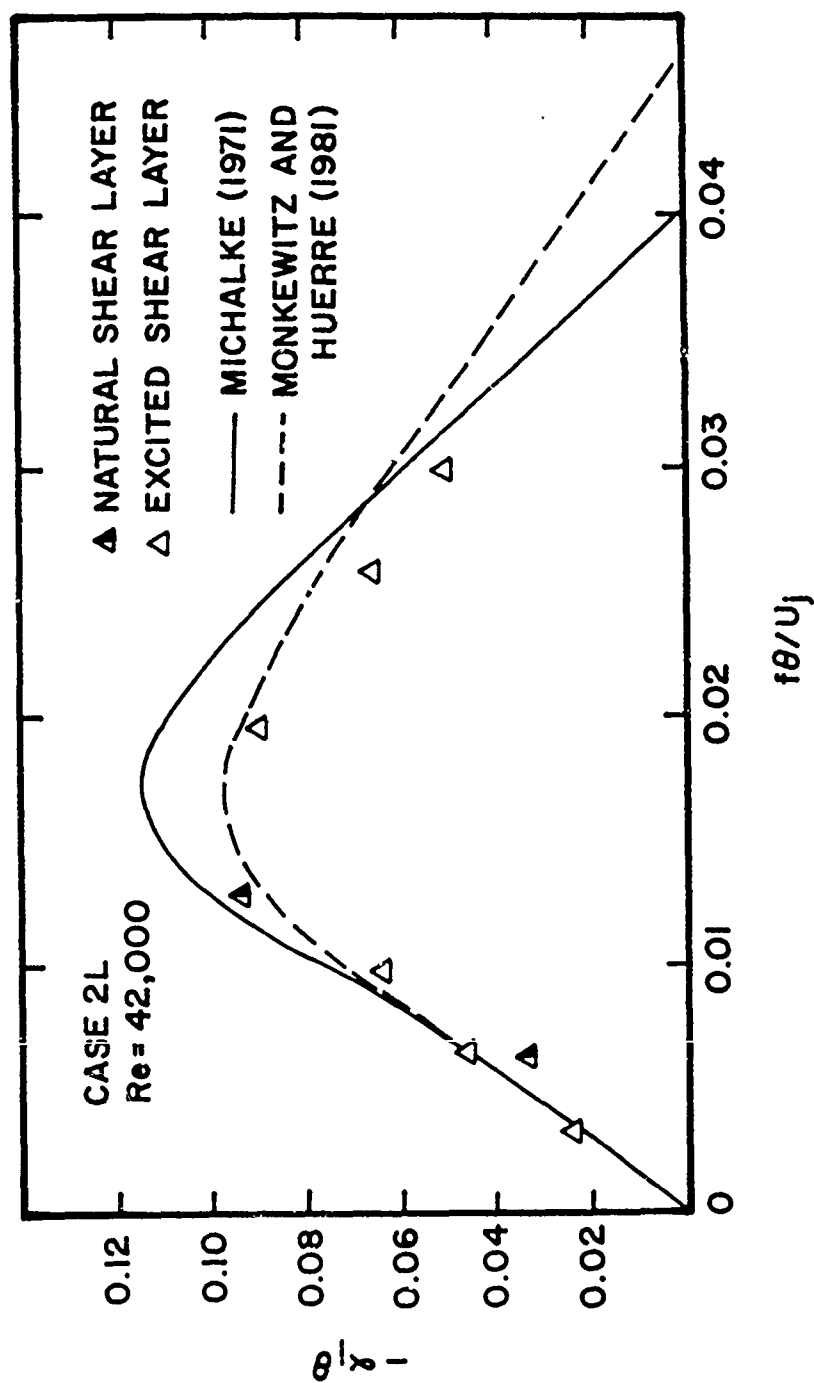Mode as a Function of Excitation Frequency;
$U/U_j = 0.6$, Re = 42,000, Case 1L
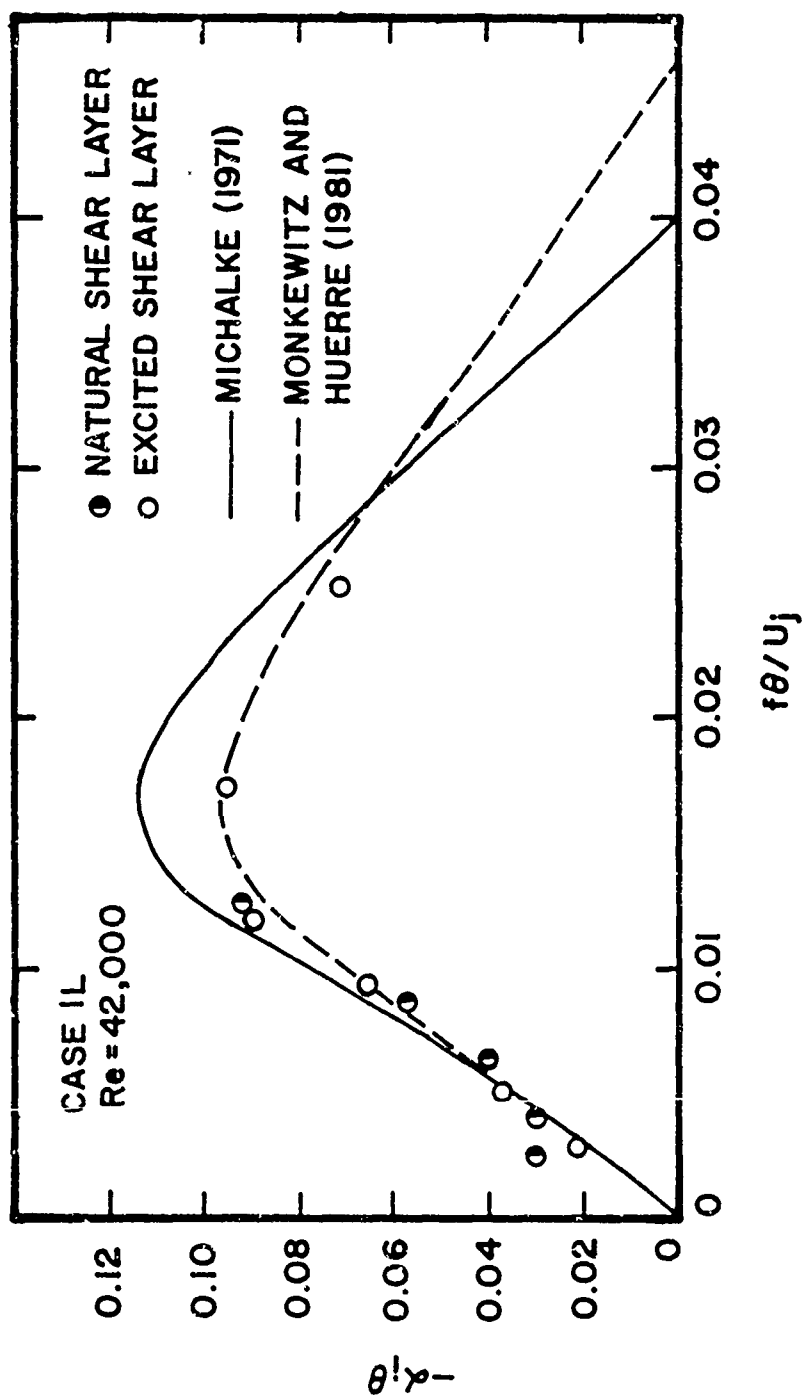
Figure 151. Variation of Mode Growth Rate with External-Excitation Strouhal Number
for Case 1L at Re = 42,000
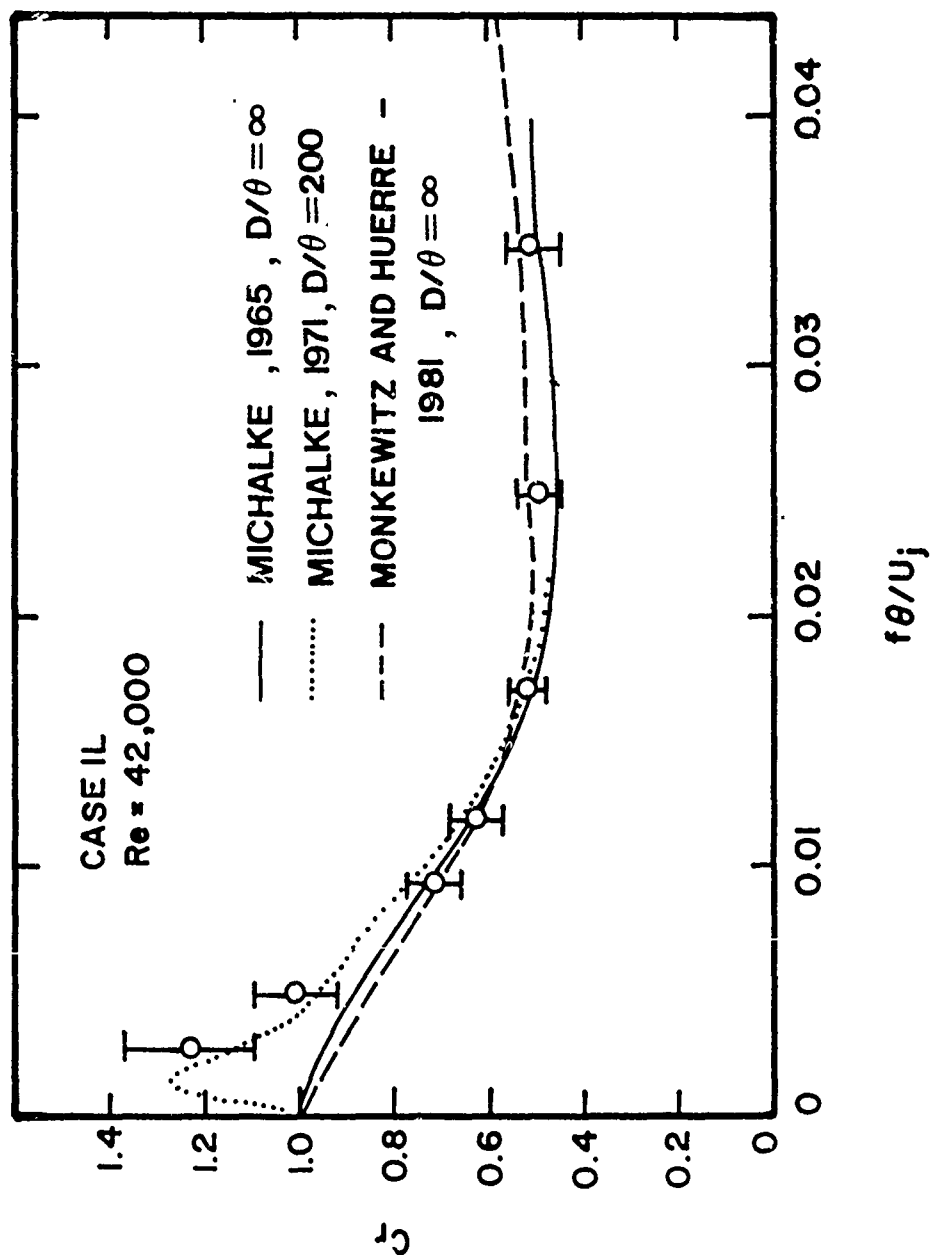
Figure 152. Variation of Mode Phase Speed with External-Excitation Strouhal Number
for Case 1L at Re = 42,000

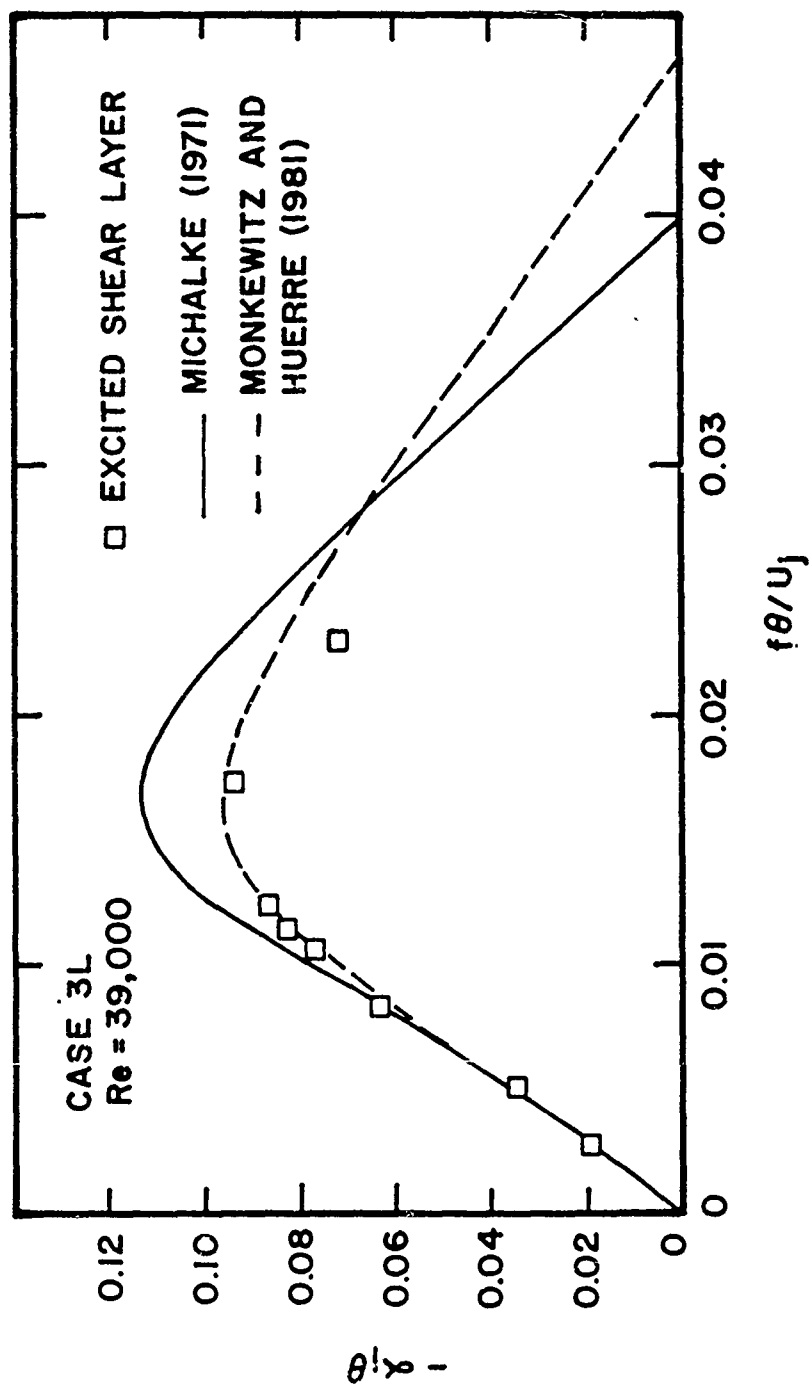Figure 153. Variation of Mode Growth Rate with External-Excitation Strouhal Number for Case 2L at Re = 42,000

Figure 154. Variation of Mode Growth Rate with External-Excitation Strouhal Number for Case 3L at Re = 39,000
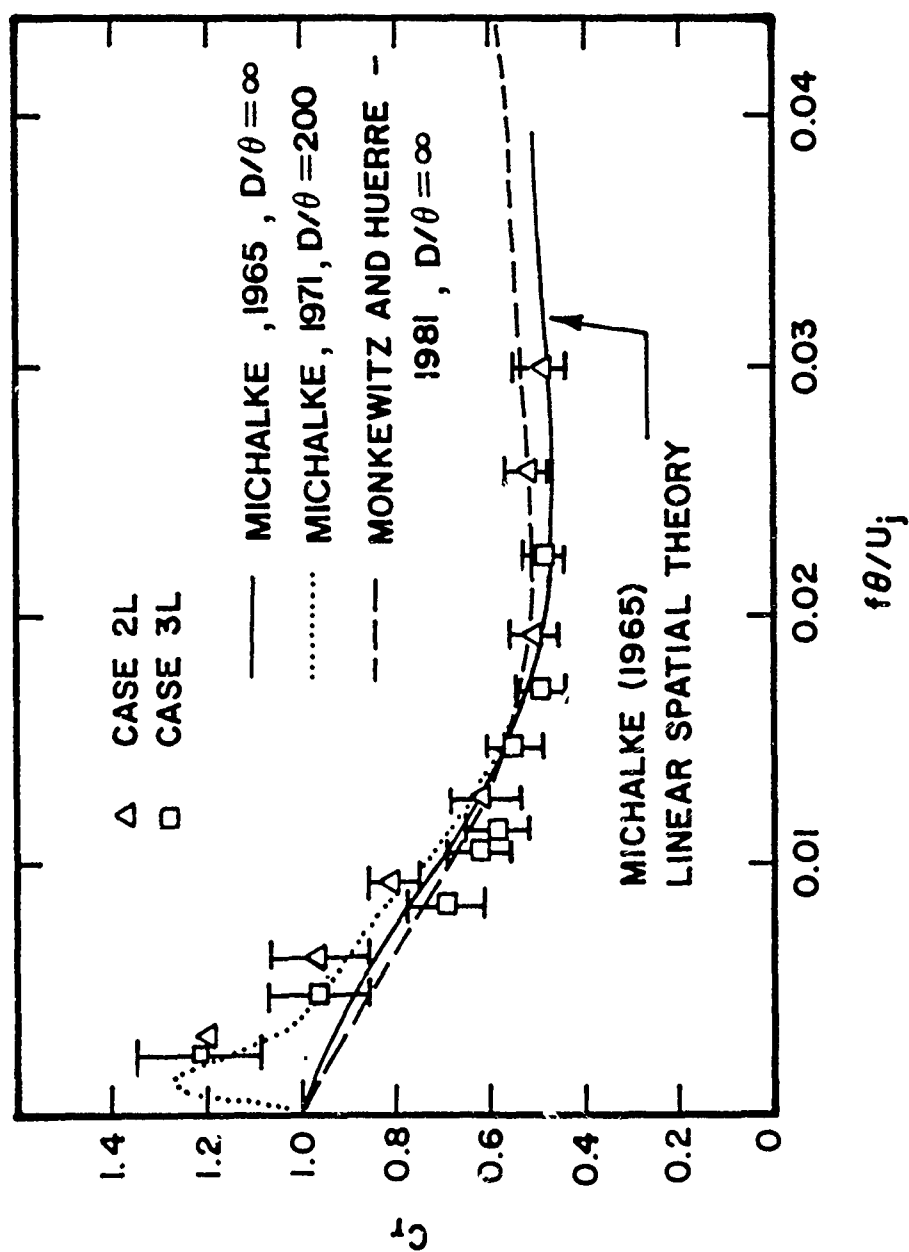
Figure 155. Variation of Mode Phase Speed with External-Excitation Strouhal Number for Cases 2L and 3L
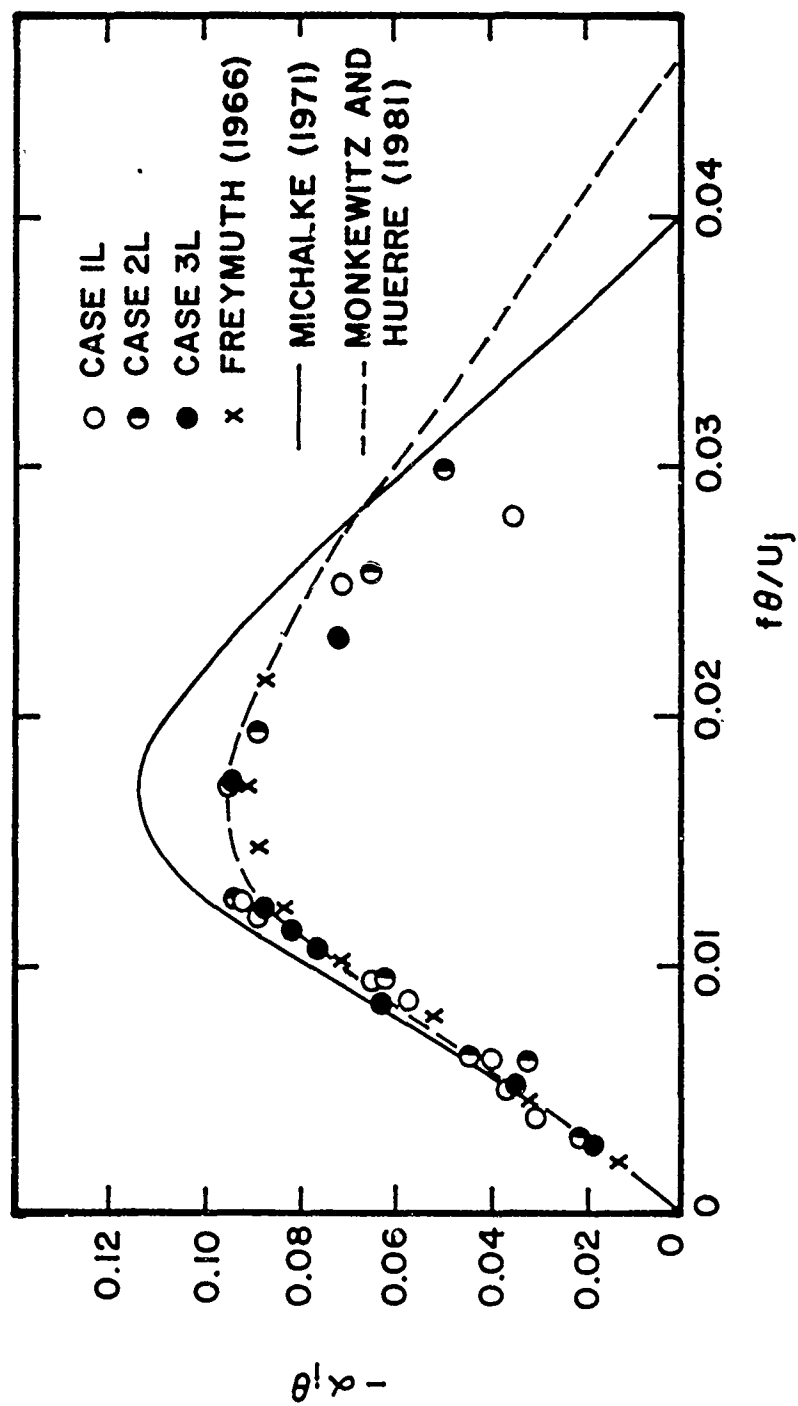
Figure 156. Summary of Mode Growth Rates with External-Excitation Strouhal Number for all Laminar Boundary Layer Cases
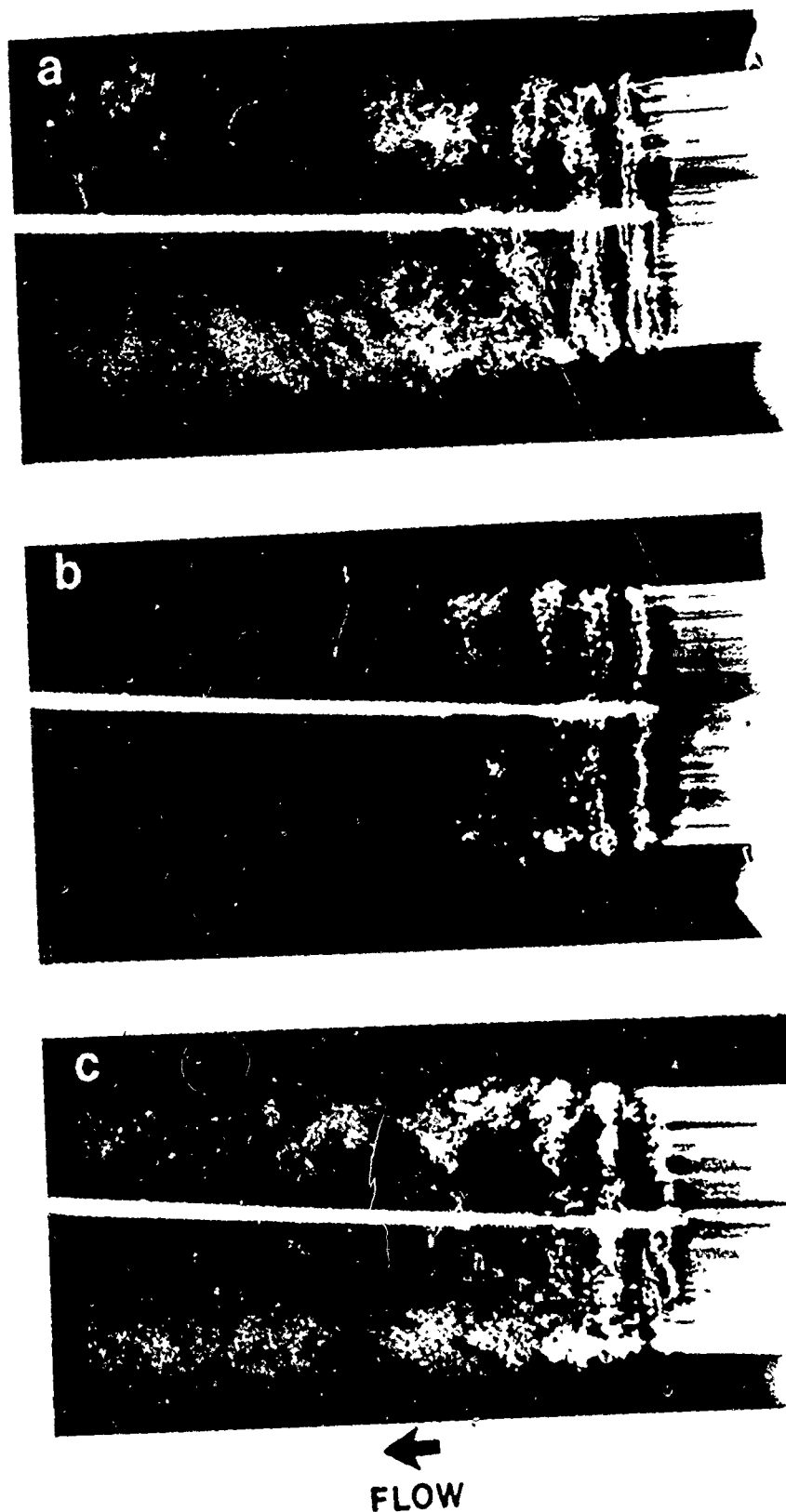
FLOW

Figure 157. Effect of Initial Flow Conditions on Jet
Development as Highlighted by Multiple-Exposure Flow
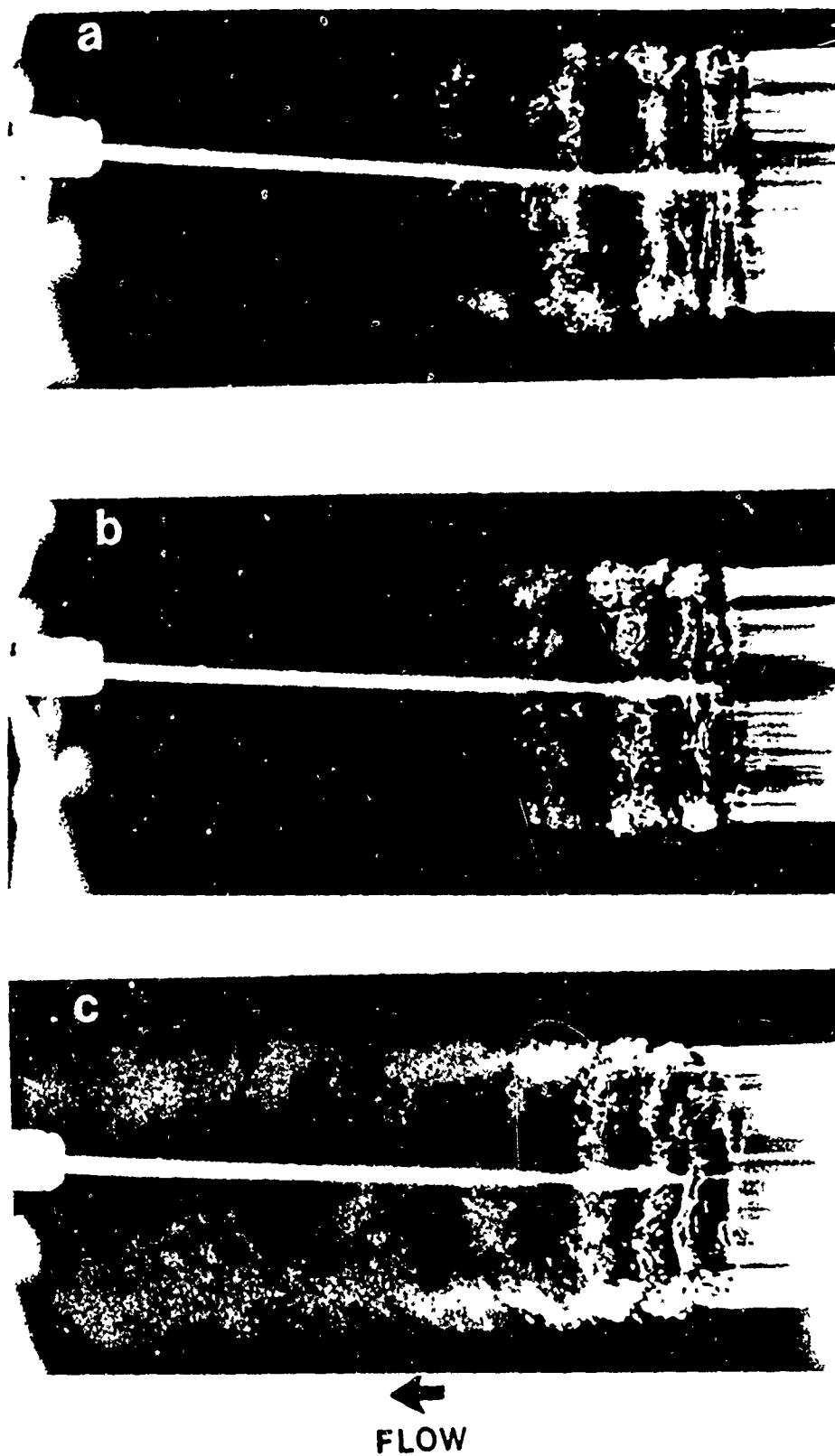Visualization Conditioned on Initial Axisymmetric Mode

FLOW

Figure 158. Effect of Initial Flow Conditions on Jet
Development as Highlighted by Multiple-Exposure
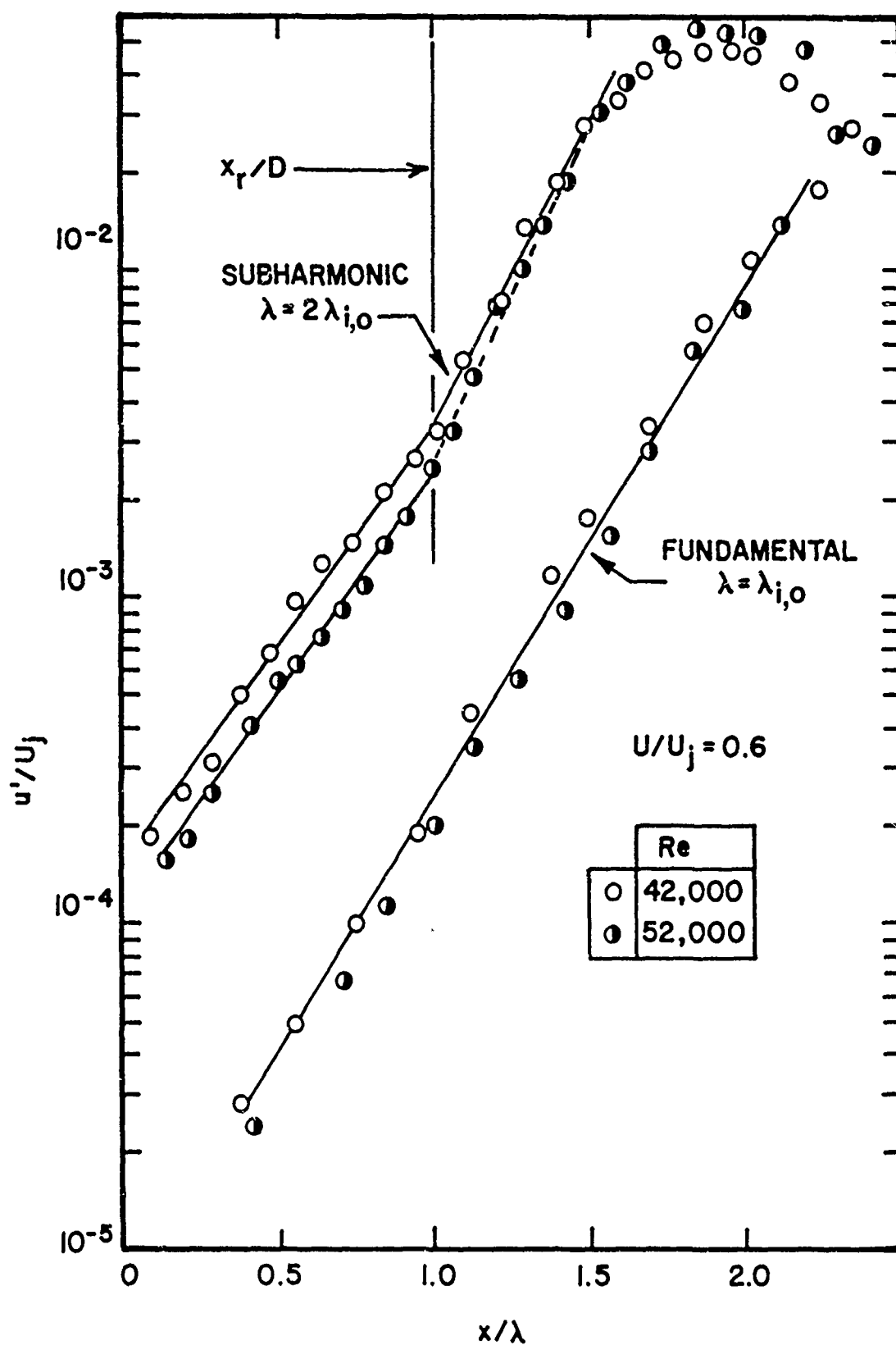Flow Visualization Conditioned on Subharmonic Mode.

Figure 159. Streamwise Development of Normalized Amplitude of Initial Axisymmetric Mode and its Subharmonic along $U/U_j = 0.6$ for Case 1L
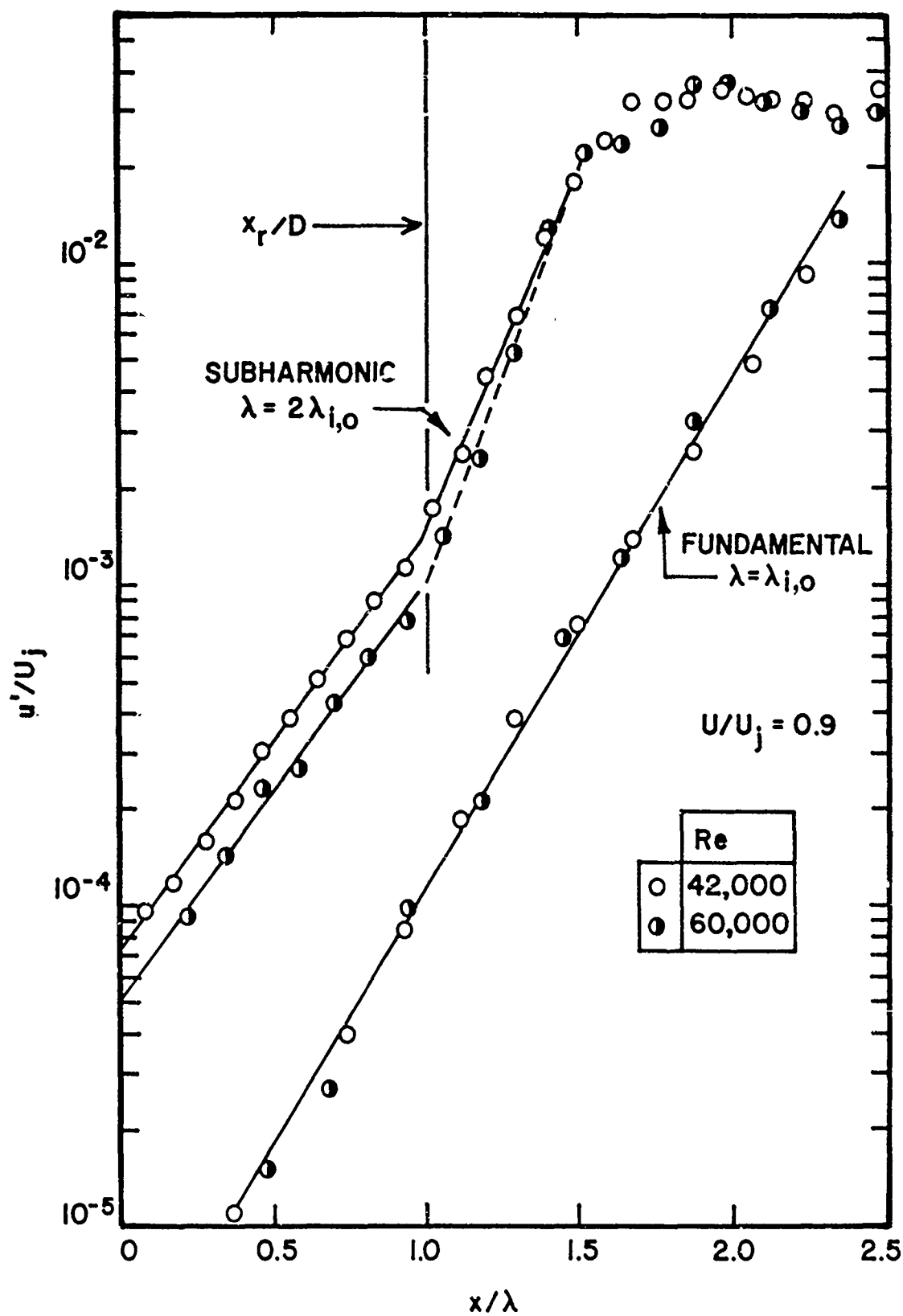
Figure 160. Streamwise Development of Normalized
Amplitude of Initial Axisymmetric Mode and its
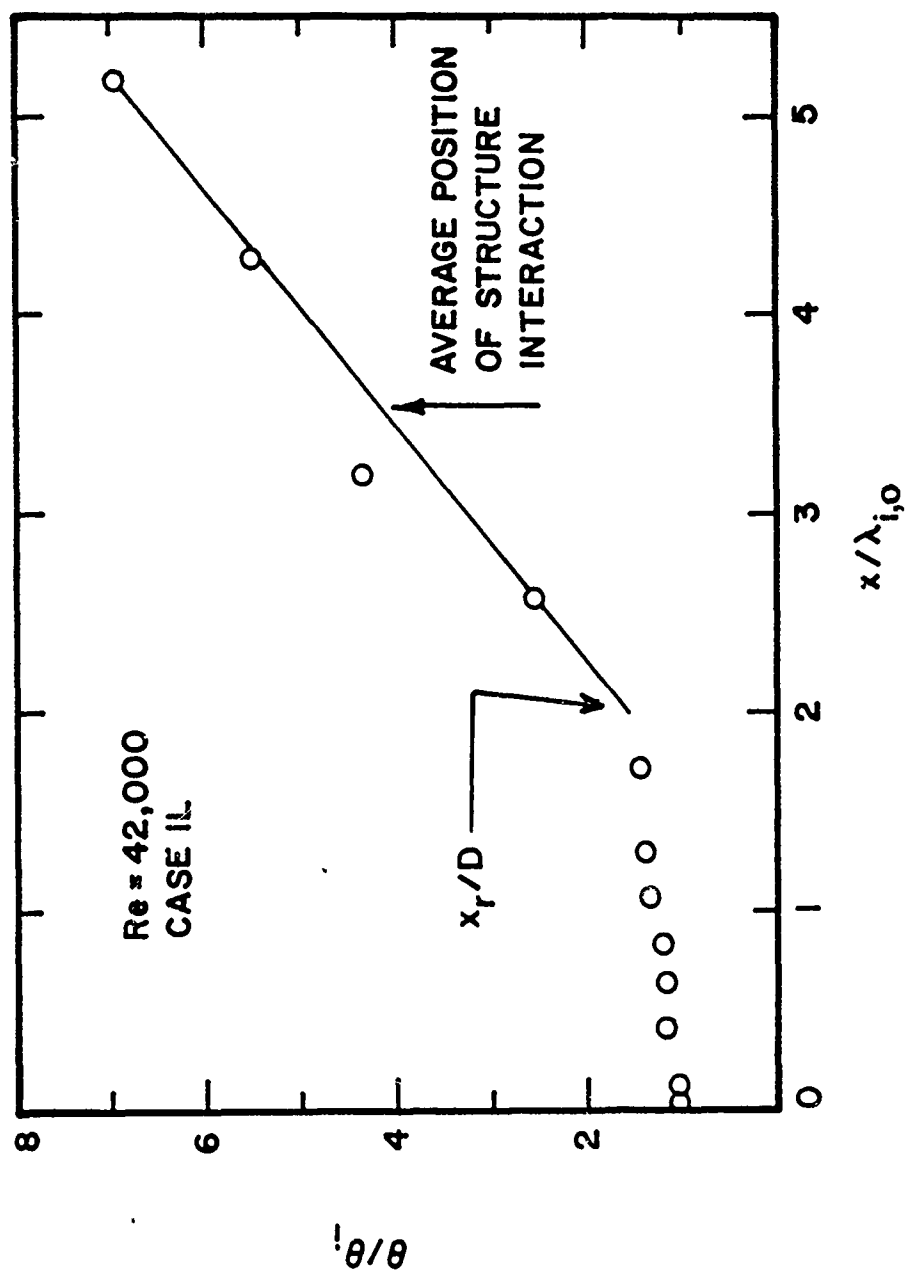Subharmonic along $U/U_j = 0.9$ for Case 1L

Figure 161. Streamwise Development of Normalized Jet Momentum Thickness for Case 1L at Re = 42,000
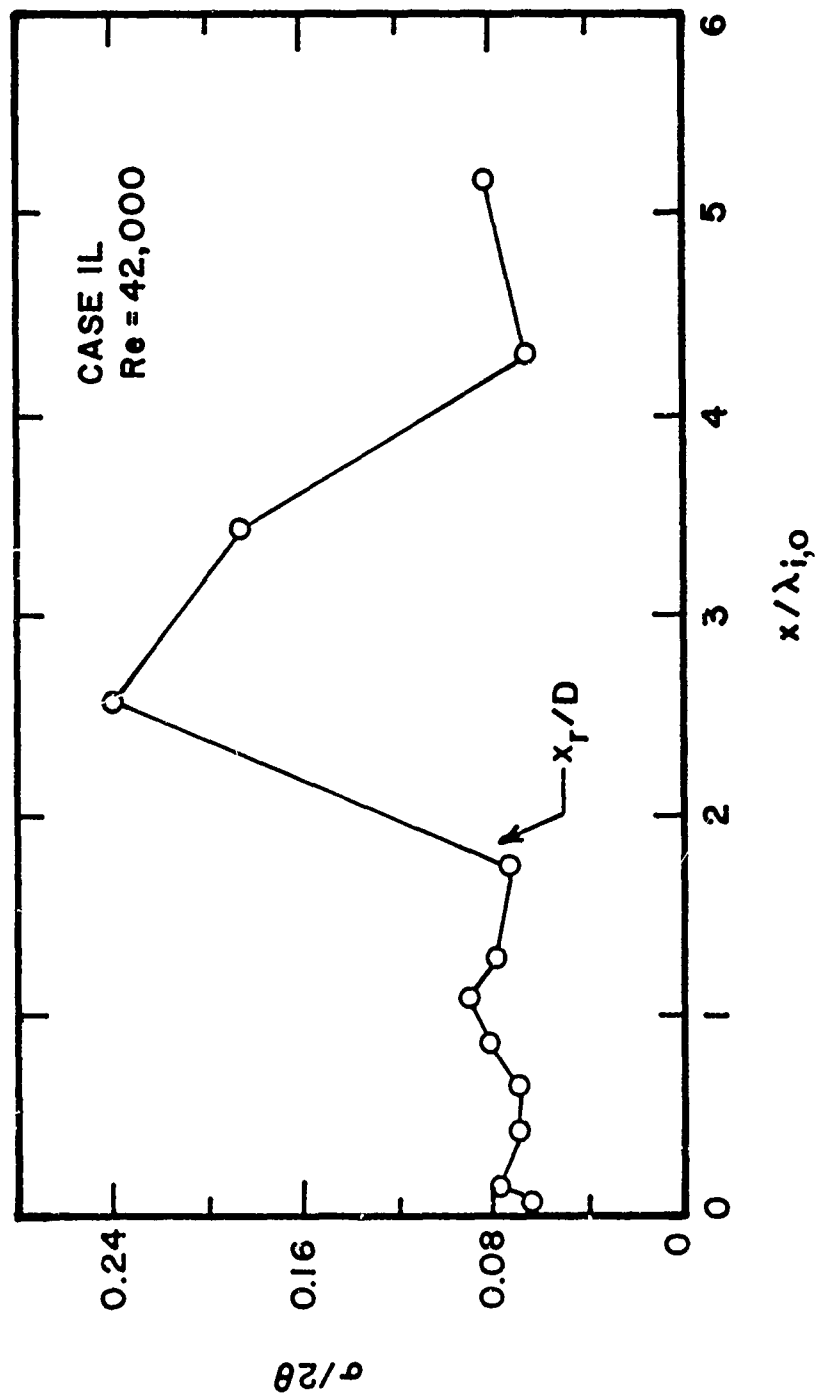
Figure 162. Deviation of Measured Jet Velocity Profiles from Hyperbolic Tangent
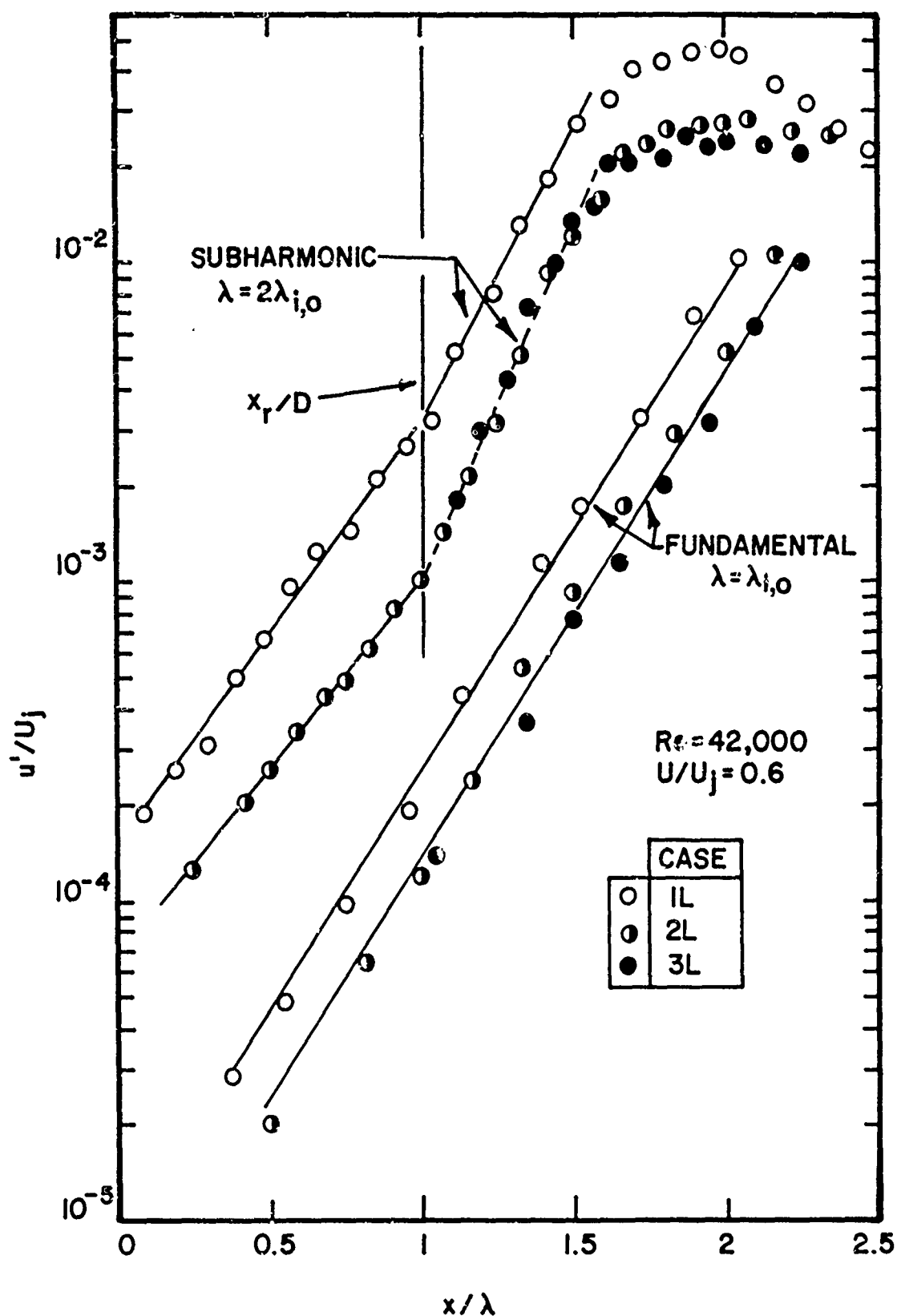Function as Function of Normalized Axial Position

Figure 163. Streamwise Development of Normalized Amplitude of Initial Axisymmetric Mode and its Subharmonic along $U/U_j = 0.6$ at Re = 42,000 for Cases 1L, 2L and 3L
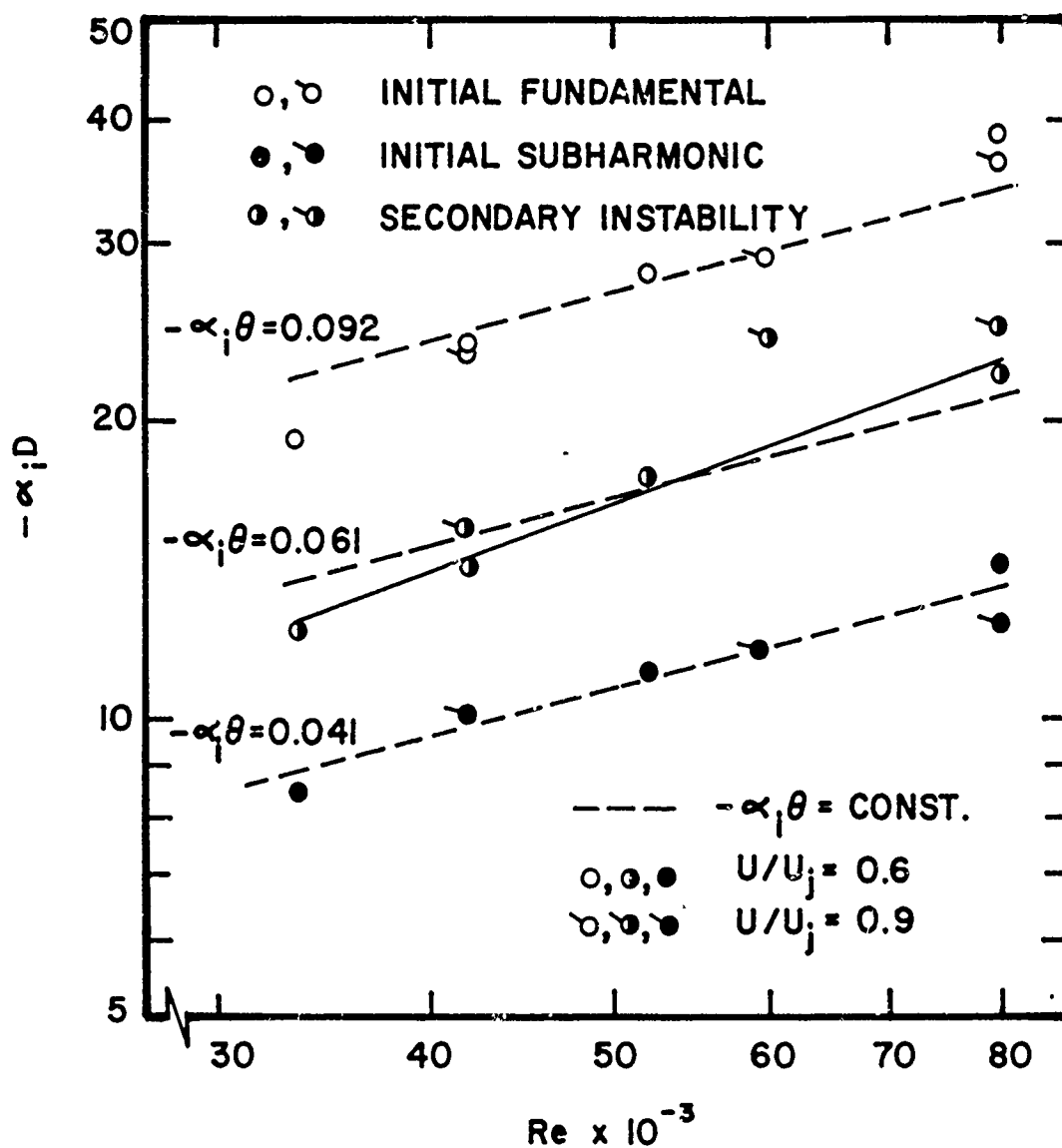
Figure 164. Variation of Measured Growth Rates with Reynolds Number
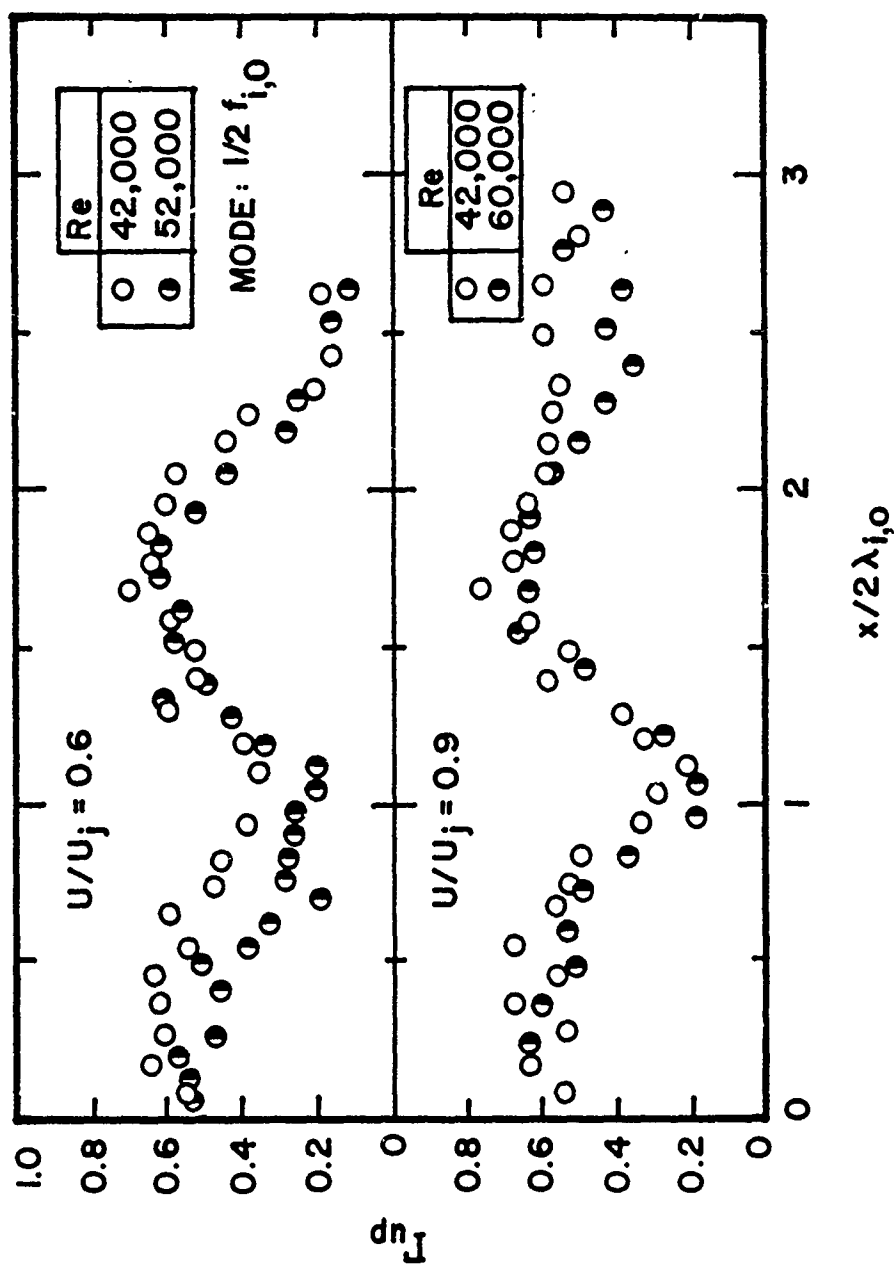
Figure 165. Streamwise Development of Coherence Between Velocity and Near-Field
Pressure for Subharmonic Mode in Case 1L
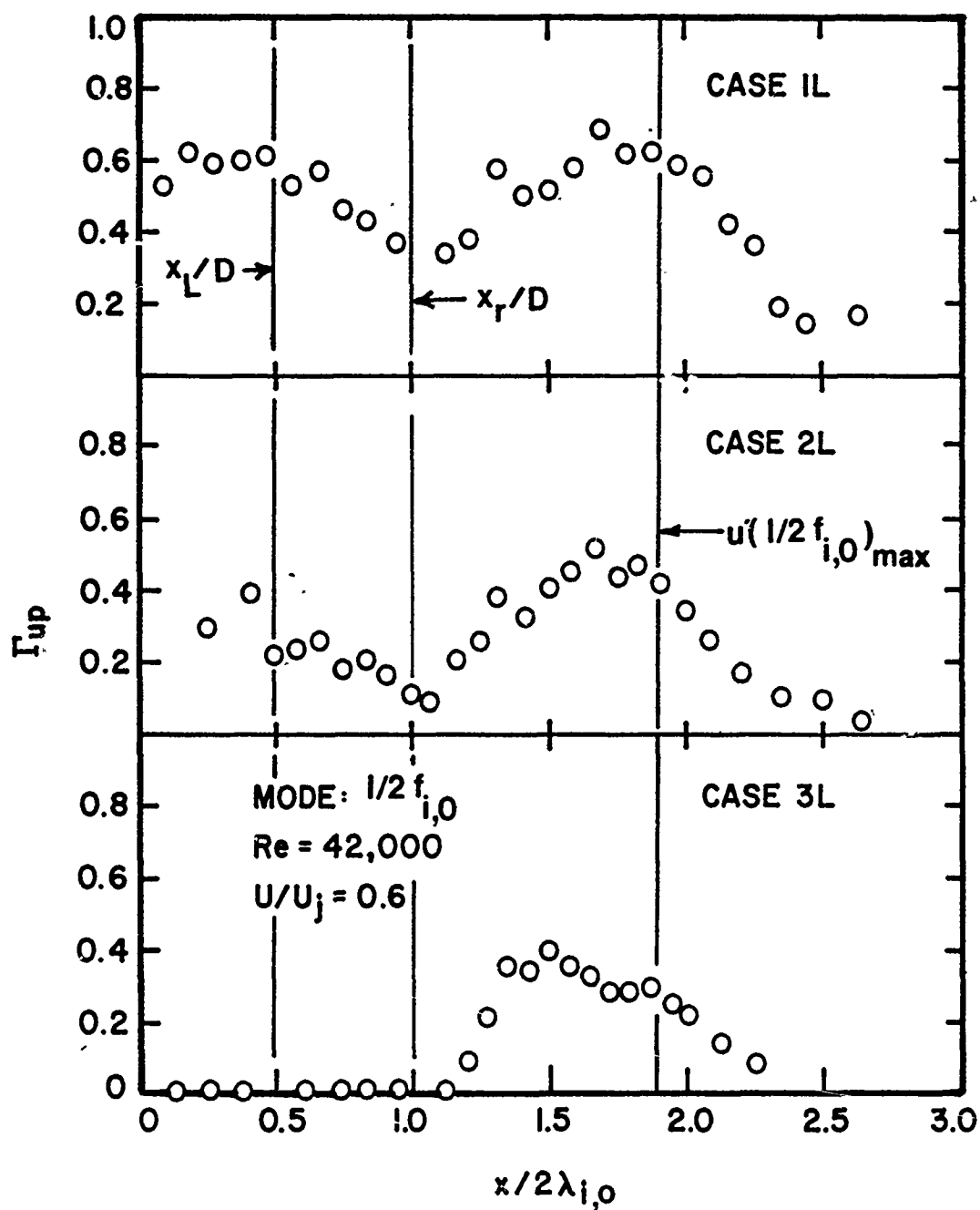
Figure 166. Influence of Initial Disturbance Level
on Streamwise Development of Coherence Between
Velocity and Near-Field Pressure for Subharmonic
Mode along $U/U_j = 0.6$ at Re = 42,000
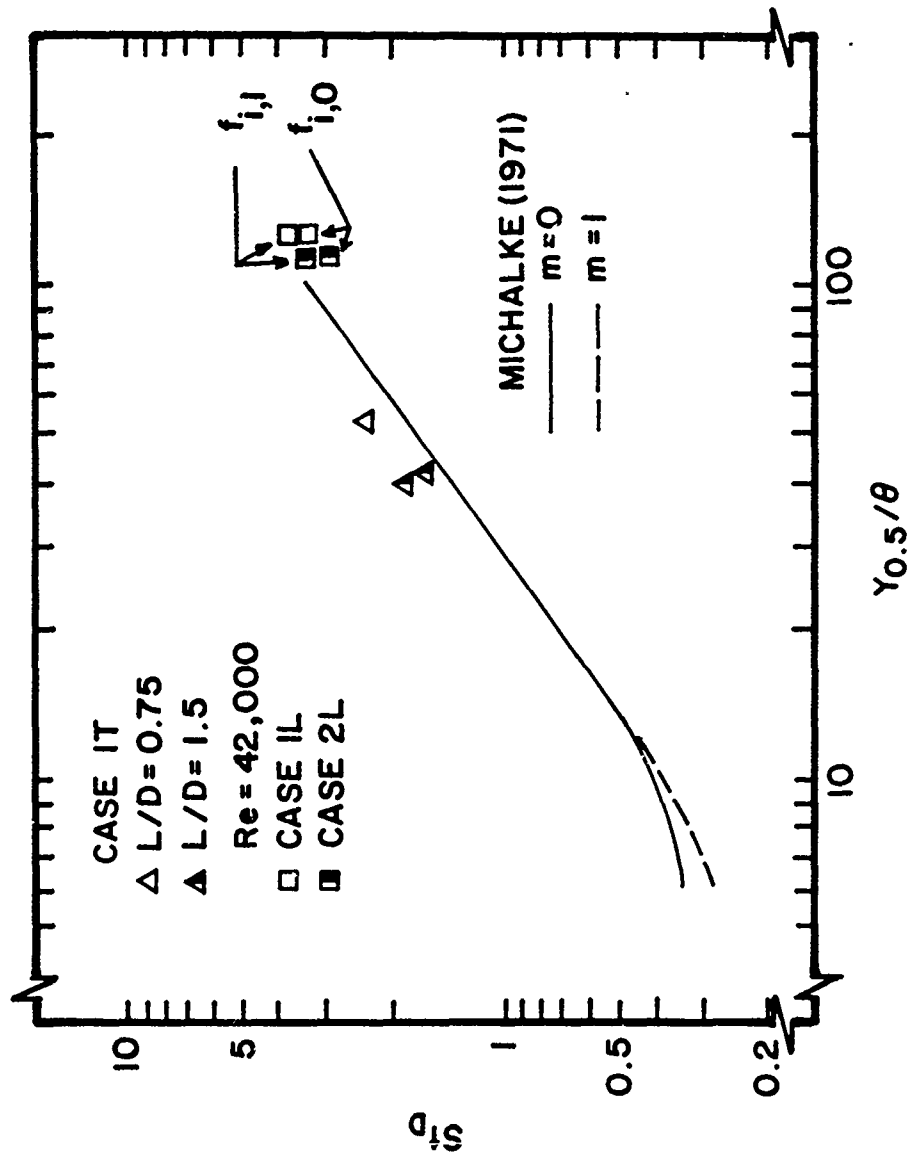
Figure 167. Variation of Initial Axisymmetric and Helical Strouhal Frequencies with Momentum Thickness of Jet-Exit Boundary Layer
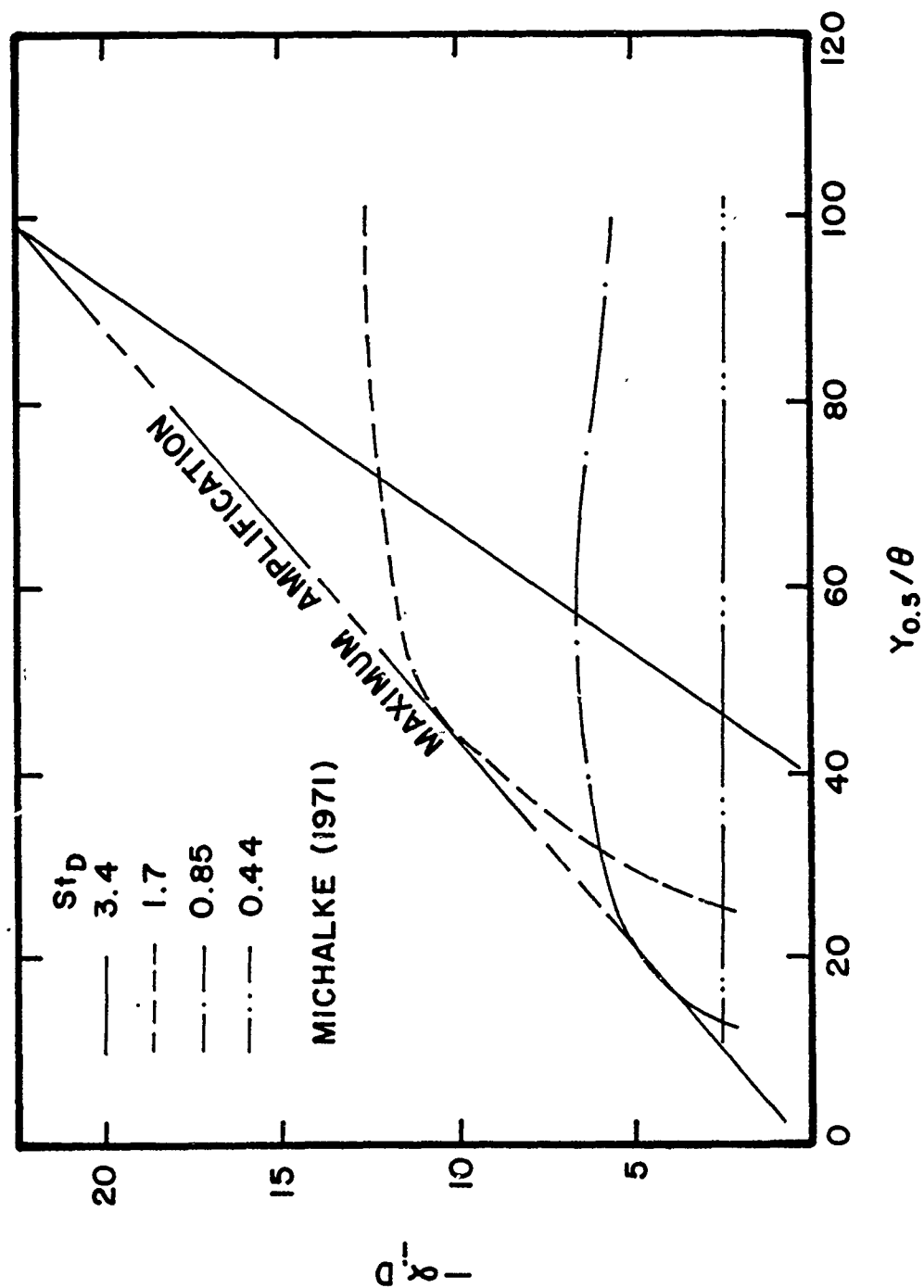
Figure 168. Variation of Mode Amplification Rates with Momentum Thickness of Developing Jet, according to Michalke (1971)
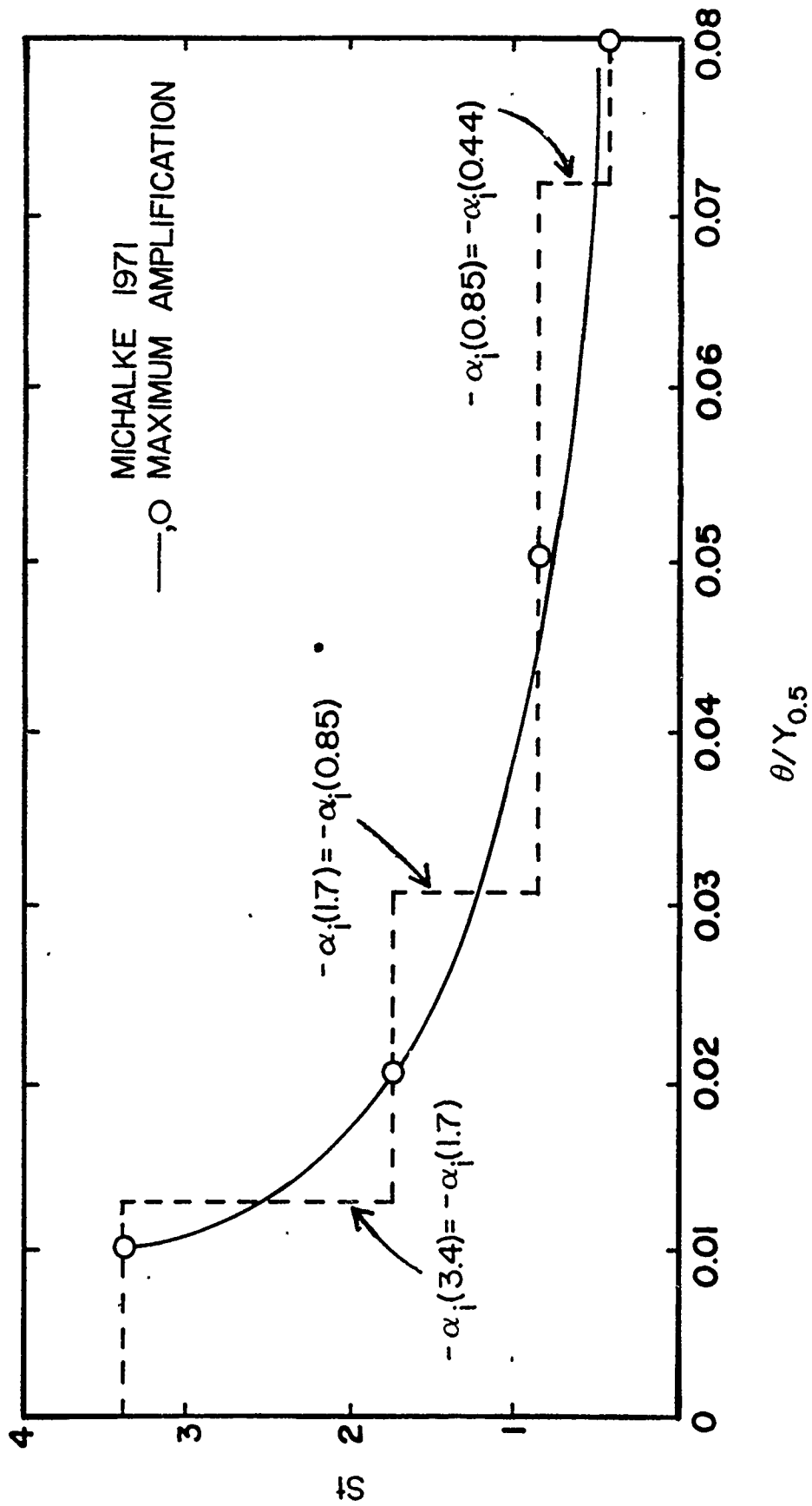
Figure 169. Variation of Maximum Amplified Strouhal Frequency with Momentum Thickness of Developing Jets, according to Michalke (1971)
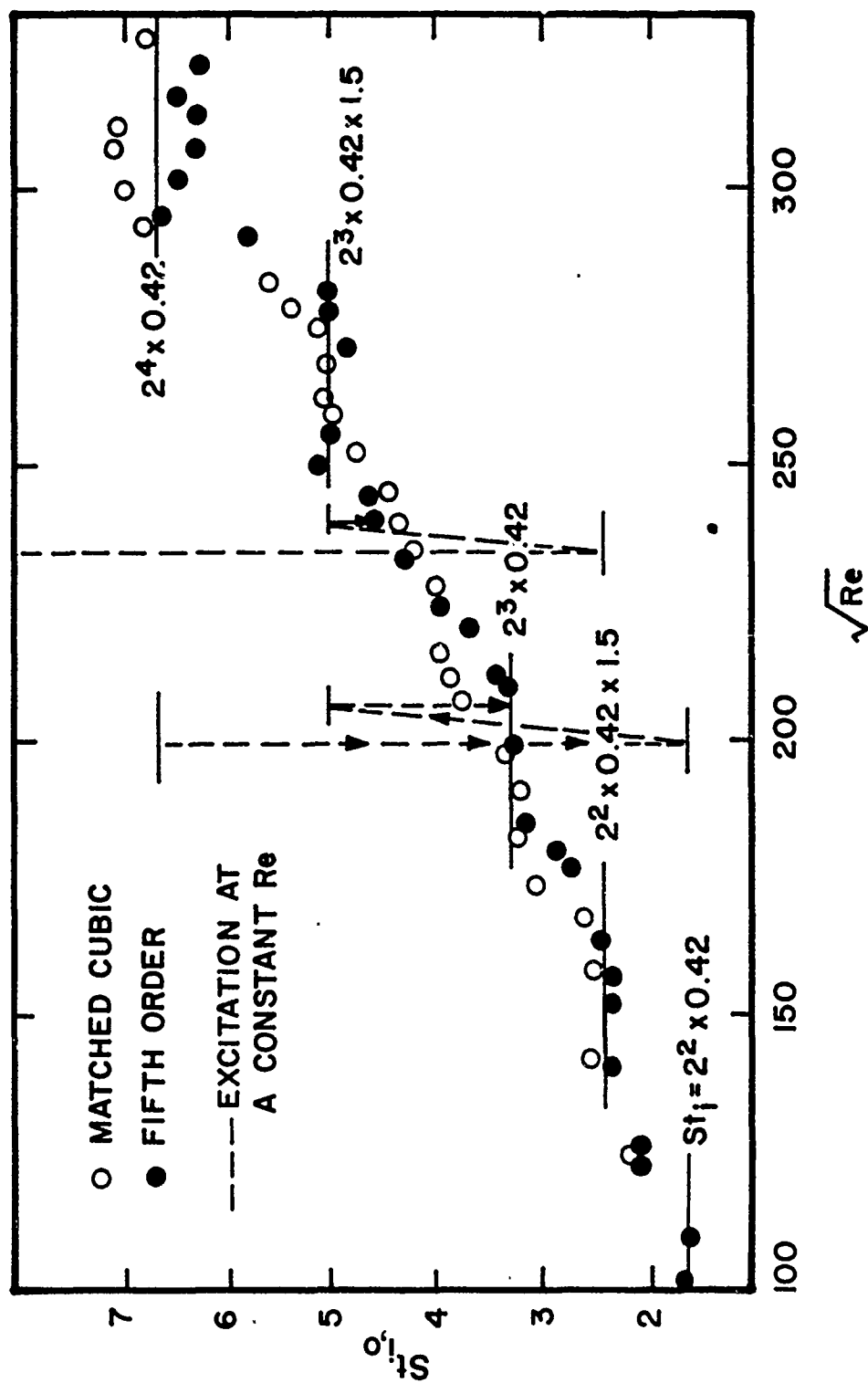
Figure 170. Variation of Initial Axisymmetric Strouhal Frequency with Reynolds Number Before Sound Insulation was Added
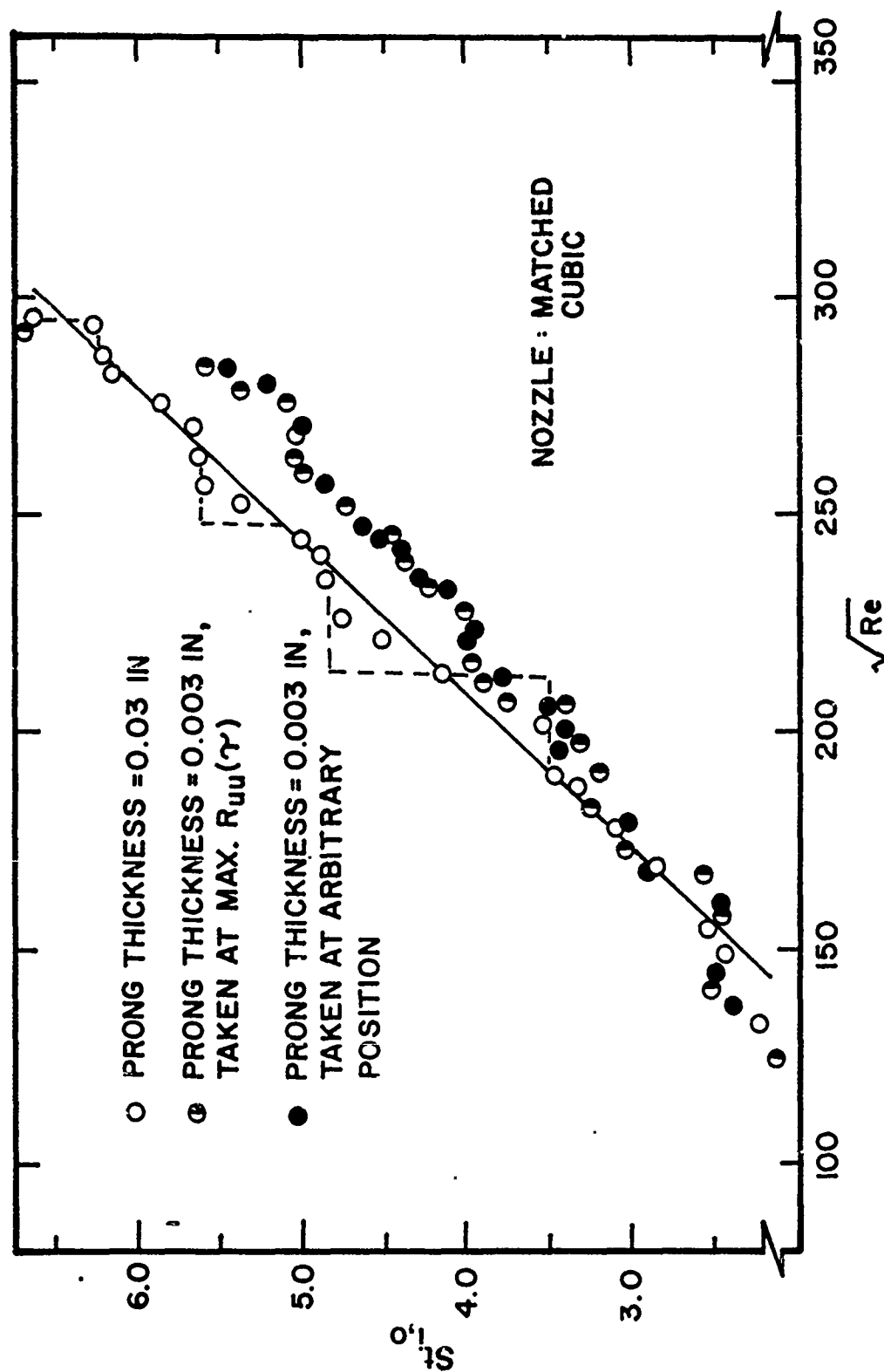
Figure 171. Effect of Hot-wire Prong Size on Variation of Initial Axisymmetric Strouhal Frequency with Reynolds Number Before Sound Insulation was Added
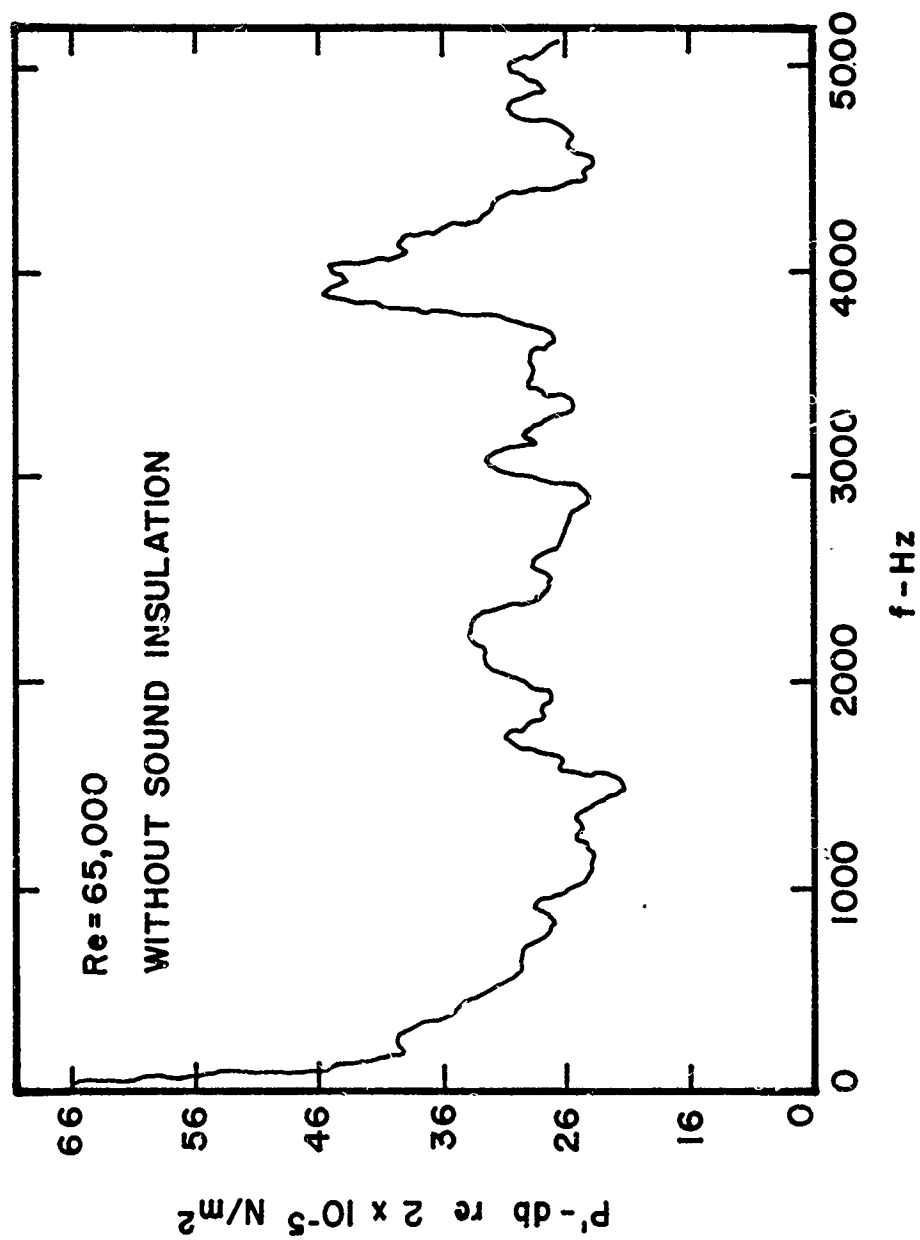
Figure 172. Background Pressure Spectrum Near Nozzle Before External Duct Sound
Insulation was Added
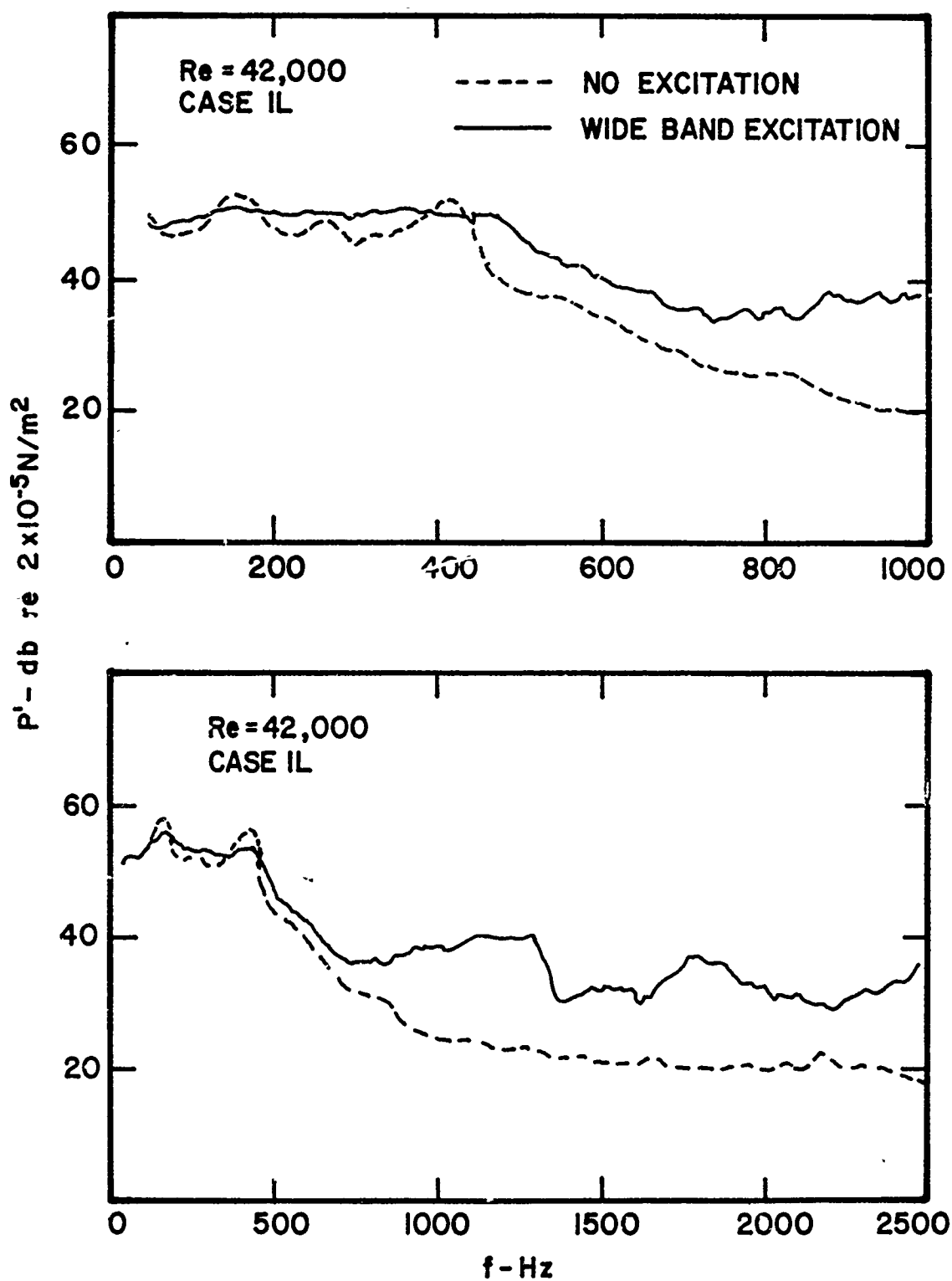
Figure 173. Pressure Spectrum Near Nozzle Lip With and Without Wide Band Excitation
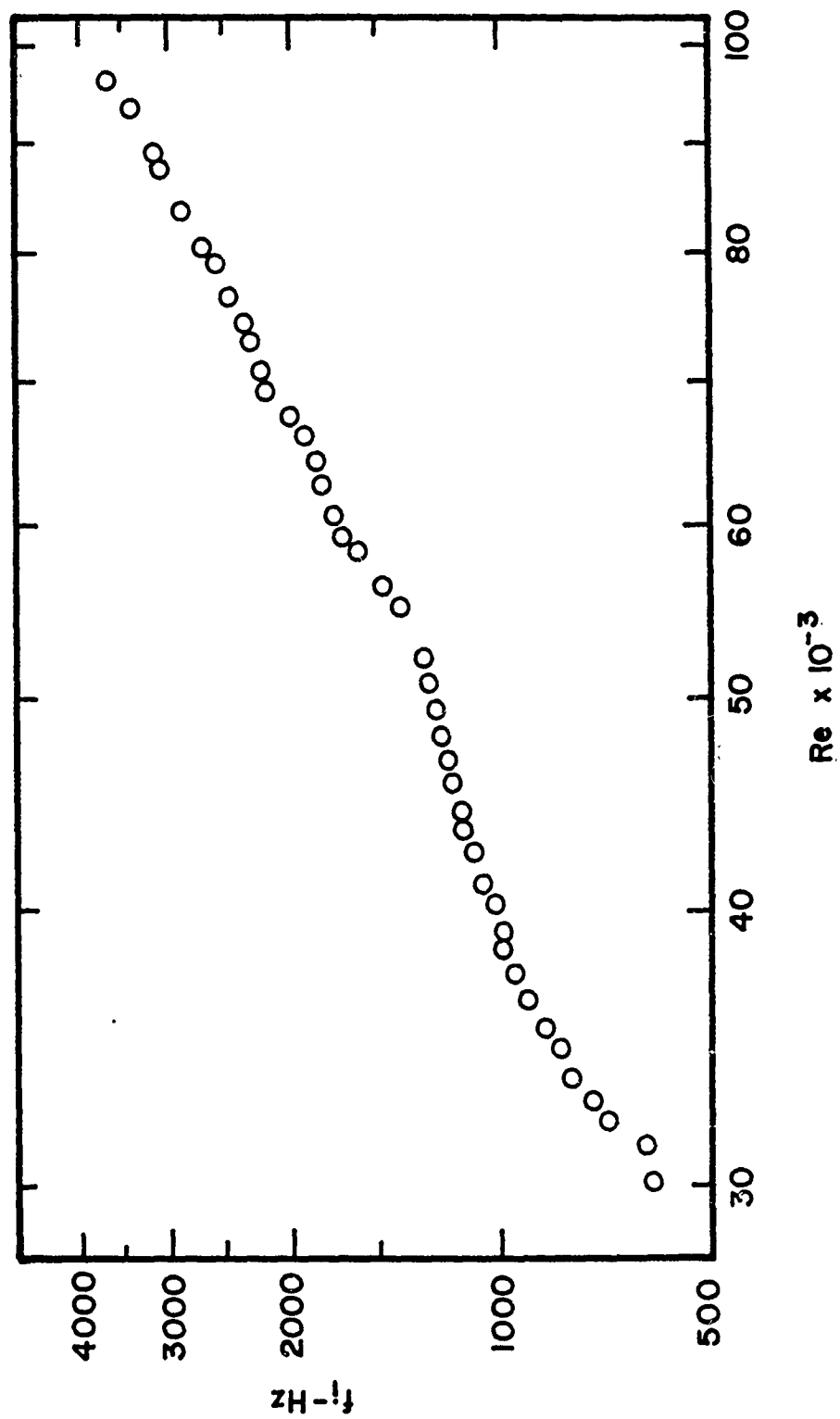
Figure 174. Variation of Initial Instability Frequency with Reynolds Number Using Wide Band Excitation

Figure 175. Variation of Initial Strouhal Frequency with Reynolds Number Using Wide Band Excitation

BIBLIOGRAPHY

Acton, E. 1976. The Modelling of Large Eddies in a Two-Dimensional Shear Layer. J. Fluid Mech., 76, p. 561.

Acton, E. 1980. A Modelling of Large Eddies in an Axisymmetric Jet. J. Fluid Mech., 98, p. 1.

Ahmed, M., Wigeland, R. A. and Nagib, H. M. 1976. Generation and Management of Swirling Flows in Confined Streams. I.I.T. Fluids and Heat Transfer Report R76-2, ARO-ITR-76-1.
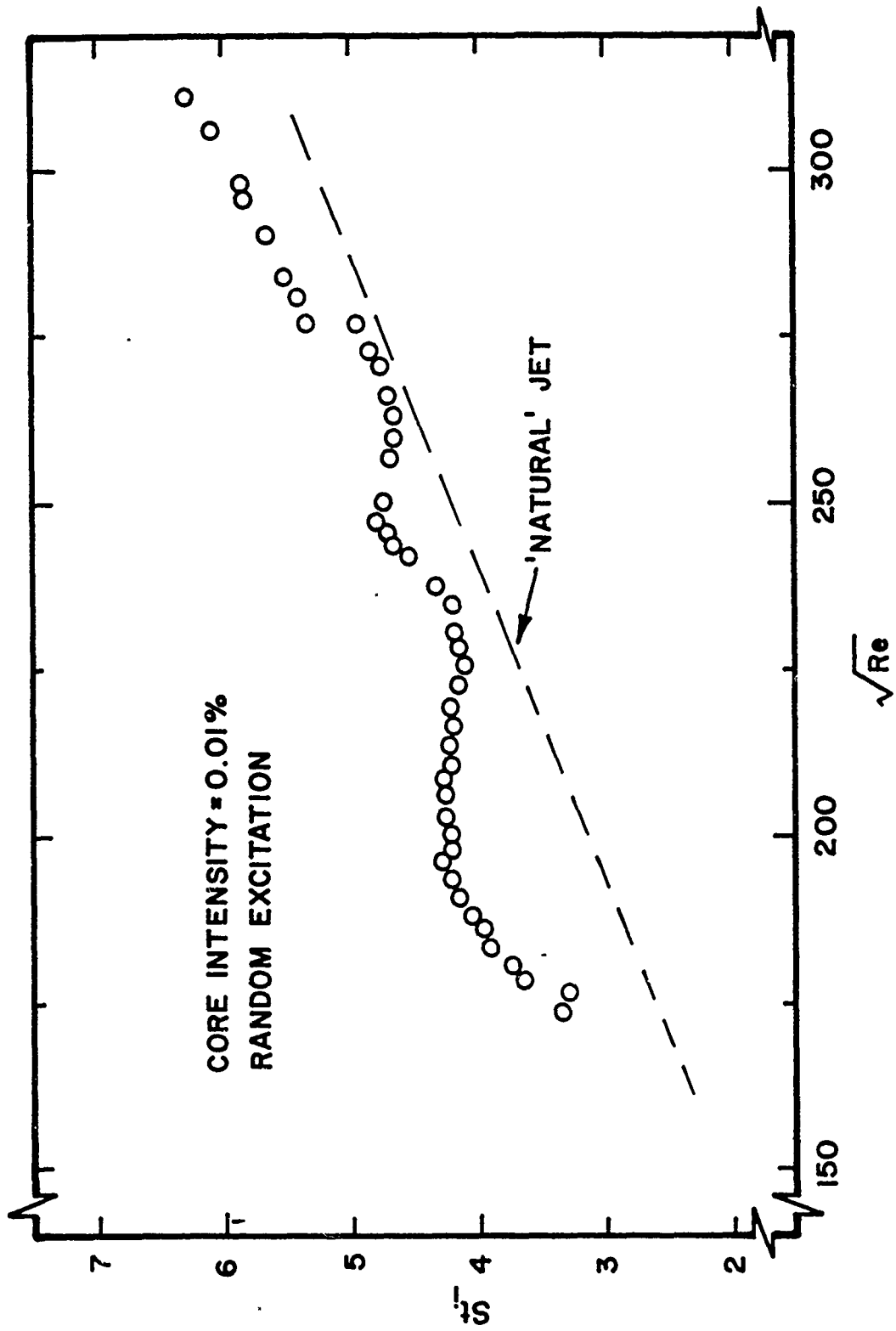
Batchelor, G. and Gill, A. 1962. Analysis of the Stability of Axisymmetric Jets. J. Fluid Mech., 14, p. 529.

Bechert, D. and Pfizenmaier, E. 1975. On Wavelike Pertubations in a Free Jet Travelling Faster than the Mean Flow in the Jet. J. Fluid Mech., 72, p. 341.

Bendat, J. S. and Piersol, A. G. 1980. Engineering Applications of Correlation and Spectral Analysis. John Wiley & Sons, New York.

Billingsley, J. and Kinns, R. 1976. The Acoustic Telescope. J. Sound Vib., 48, p. 485.

Bonnet, C.M.T. and Fisher, M. J. 1979. Correlation Techniques and Modal Decomposition Analysis for the Detection of Azimuthally Coherent Structures in Jet Flows. J. Sound and Vibration, 66, p. 545.

Bouchard, E. E. 1981. The Growth and Structure of the Mixing Layer Region of a Forced Jet. Ph.D. Dissertation. Dept. of Mechanical Engineering, Stanford University.

Bradshaw, P. 1966. The Effect of Initial Conditions on the Development of a Free Shear Layer. J. Fluid Mech., 26, p. 255.

Bradshaw, P., Ferriss, D. H. and Johnson, S. 1964. Turbulence in the Noise Producing Region of a Circular Jet. J. Fluid Mech., 19, p. 591.

Broward, F. K. and Latigo, B. O. 1979. Growth of the Two-Dimensional Mixing Layer From a Turbulent and Non-Turbulent Boundary Layer. Phys. Fluids, 22, p. 1011.

Brown, G.L. and Roshko, A. 1974. On Density Effects and Large Structures in Turbulent Mixing Layers. J. Fluid Mech., 64, p.775.

Bruun, H. H. 1977. A Time-Domain Analysis of the Large Scale Flow Structure in a Circular Jet: Moderate Re. J. Fluid Mech., 83, p. 641.

Cantwell, B. 1981. Organized Motion in Turbulent Flow. Ann. Rev. Fluid Mech.

Chan, Y. Y. 1974. Spatial Waves in Turbulent Jets. Phys. of Fluids, 17, p. 46.

Chan, Y. Y. 1974. Spatial Waves in Turbulent Jets Part II. Phys. of Fluids, 17, p. 1667.

Chan, W. T. and Ko, N.W.M. 1978. Coherent Structures in the Outer Mixing Region of Annular Jets. J. Fluid Mech., 89, p. 515.

Chandrsuda, C., Mehta, R. D., Weir, A. D. and Bradshaw, P. 1978. Effect of Free-Stream Turbulence on Large Structure in Turbulent Mixing Layers. J. Fluid Mech., 85, p. 693.

Corcos, G. M. and Sherman, F. S. 1976. Vorticity Concentration and the Dynamics of Unstable Shear Layers. J. Fluid Mech., 73, p. 241.

Corke, T. C. 1981. A New View on Origin, Role and Manipulation of Large Scales in Turbulent Boundary Layers. Ph.D. Thesis, Illinois Institute of Technology.

Corke, T., Koga, D., Drubka, R. and Nagib, H. 1977. A New Technique for Introducing Controlled Sheets of Smoke Streaklines in Wind Tunnels. Proc. ICIASF, IEEE Publication 77CH1251-8 AES, p. 74.

Crighton, D. G. 1972. The Excess Noise Field of Subsonic Jets. J. Fluid Mech., 56, p. 683.

Crighton, D. G. 1981. Acoustics as a Branch of Fluid Mechanics. J. Fluid Mech., 106, p. 261

Crighton, D. G. and Gaster, M. 1976. Stability of Slowly Diverging Jet Flow. J. Fluid Mech., 77, p. 397.

Crow, S. C. and Champagne, F. H. 1971. Orderly Structure in Jet Turbulence. J. Fluid Mech., 48, p. 547.

Davis, M. R. and Davies, P.O.A.L. 1979. Shear Fluctuations in a Turbulent Jet Shear Layer. J. Fluid Mech., 93, p. 281

Dimotakis, P. E. and Brown, G. L. 1976. Mixing Layer at High Reynolds Number: Large Structure Dynamics and Entrainment. J. Fluid Mech., 78, p. 535.

Drubka, R. E. and Wlezien, R. W. 1979. Efficient Velocity Calibration and Yaw-Relation Truncation Errors in Hot-Wire Measurements of Turbulence. Abstract Published in the Bulletin of the American Physical Society, Fluid Dynamics Division, 24, p. 1142.

Fflowcs Williams, J. E. and Kempton, A. J. 1978. The Noise from the Large Scale Structure of a Jet. J. Fluid Mech., 84, p. 673.

Freymuth, P. 1966. On Transition in a Separated Laminar Boundary Layer. J. Fluid Mech., 25, p. 683.

Gatski, J. B. 1979. Sound Production Due to Large Scale Coherent Structures. AIAA J., 17, p. 614.

Grant, A. J. 1974. A Numerical Model of Instability in Axisymmetric Jets. J. Fluid Mech., 66, p. 707.

Gutmark, E. and Ho, Chih-Ming. 1980. Feedback Mechanism in a Free Jet. Bulletin of the Amer. Phys. Soc. Ser. II.

Heavens, S. N. 1980. Visualization of the Acoustic Excitation of a Subsonic Jet. J. Fluid Mech., 100, p. 185.

Ho, Chih-Ming. 1981. Private Communication.

Ho, Chih-Ming. 1981. Local and Global Dynamics of Free Shear Layers. Proc of Symp. on Numerical and Physical Aspects of Aerodynamic Flows, Long Beach, CA.

Ho, Chih-Ming and Huang, L. 1981. Subharmonics and Vortex Merging in Mixing Layers. Submitted to J. Fluid Mech.

Ho, Chih-Ming and Nosseir, N. 1981. Dynamics of an Impinging Jet. Part 1. The Feedback Phenomenon. J. Fluid Mech., 105, p. 119.

Husain, Z. D. and Hussain, A.K.M.F. 1979. Axisymmetric Mixing Layer: Influence of Initial and Boundary Conditions. AIAA J., 17, p. 48.

Hussain, A.K.M.F. and Clark, A. R. 1981. On the Coherent Structure of the Axisymmetric Mixing Layer: A Flow Visualization Study. J. Fluid Mech., 104, p. 263.

Hussain, A.K.M.F. and Husain, Z. D. 1980. Turbulence Structure in the Axisymmetric Free Mixing Layer. AIAA J., 18, p. 1462.

Hussain, A.K.M.F. and Zaman, K.B.M.Q. 1978. The Free Shear Layer Tone Phenomenon and Probe Interference. J. Fluid Mech., 87, p. 349.

Hussain, A.K.M.F. and Zaman, K.B.M.Q. 1980. Vortex Pairing in a Circular Jet Under Controlled Excitation. Part 2. Coherent Structure Dynamics. J. Fluid Mech., 101, p. 493.

Hussain, A.K.M.F. and Zaman, K.B.M.Q. 1981. The Preferred Mode of the Axisymmetric Jet. J. Fluid Mech., 110, p. 39.

Hussain, A.K.M.F. and Zaman, K.B.M.Q. 1981. The Natural Large-Scale Coherent Structure on Initially Turbulent Plane Mixing Layer. Abstract Published in the Bulletin of the American Physical Society, Fluid Dynamics Division, 26, p. 1273.

Hussain, A.K.M.F. and Zedan, M. F. 1978. Effects of Initial Conditions on the Axisymmetric Free Shear Layer: Effects of Initial Momentum Thickness. Phys. of Fluids, 21, p. 1100.

Hussain, A.K.M.F. and Zedan, M. F. 1978. Effects of Initial Conditions on the Axisymmetric Free Shear Layer: Effects of the Initial Fluctuation Level. Phys. of Fluids, 21, p. 1475.

Jung, W. G. 1977. IC Timer Cookbook. Howard W. Sams & Co. Indianapolis, Indiana.

Kelly, R. E. 1967. On the Stability of an Invised Shear Layer Which is Periodic in Space and Time. J. Fluid Mech., 27, p. 657.

Kibens, V. 1980. Discrete Noise Spectrum Generated by an Acoustically Excited Jet. AIAA J., 18, p. 343.

Kibens, V. 1980. Interaction of Jet Flowfield Instabilities With Flow System Resonances. McDonnel Douglas Research Laboratory Report.

Kibens, V. 1980. Instability Interactions in Axisymmetric Jets. McDonnel Douglas Research Laboratory Report.

Knisley, C. and Rockwell, D. 1981. Self-Sustaining Low Frequency Amplitude Modulation of a Cavity Shear Layer. Submitted to J. Fluid Mech.

Ko, N.W.M. and Davies, P.O.A.L. 1971. The Near Field Within the Potential Cone of Subsonic Cold Jets. J. Fluid Mech., 50, p. 49.

Lau, J. C. 1979. The Vortex Street Structure of Turbulent Jets - Part 2. Proc. R. Soc. Lond., A368, p. 547.

Lau, J. C. and Fisher, M. J. 1975. The Vortex Street Structure of Turbulent Jets - Part 1. J. Fluid Mech., 67, p. 299.

Laufer, J. 1981. Instability and Turbulence in Jets. Transition and Turbulence. Academic Press, Inc.

Loehrke, R. I. and Nagib, H. M. 1976. Control of Free Stream Turbulence by Means of Honeycombs: A Balance Between Suppression and Generation. J. Fluid Eng., Trans. ASME, 98, p. 342.

Long, D., Van Lent, T. and Arndt, R.E.A. 1981. Jet Noise at Low Reynolds Numbers. AIAA Paper No. 81-1962.

Mattingly, G. E. and Chang, C. C. 1974. Unstable Waves on an Axisymmetric Jet Column. J. Fluid Mech., 65, p. 541.

Michalke, A. 1965. On Spatially Growing Disturbances in an Inviscid Shear Layer. J. Fluid Mech., 23, p. 521.

Michalke, A. 1971. Instabilitat eines Kompressiblen Ruden Friestrahls unter Berucksichtingung des Einflusses der Strahlgrenzschichtdicke, Z. Fluzwiss. 9, p. 319.

Michalke, A. and Fuchs, H. V. 1975. On Turbulence and Noise of an Axisymmetric Shear Flow. J. Fluid Mech., 70, p. 179.

Miksad, R. W. 1972. Experiments on the Non-linear Stages of Free Shear Layer Transition. J. Fluid Mech., 56, p. 695.

Miksad, R. W. 1973. Experiments on Non-linear Interactions in Transition of a Free Shear Layer. J. Fluid Mech., 59, p. 1.

Moallemi, M. K. and Goldschmidt. V. 1981. Smoke Wire Visualization of the External Region of a Two-Dimensional Jet. Proc. Turbulence in Liquids, Rolla, MO.

Monkewitz, P. A. and Huerre, P. 1981. The Influence of the Velocity Ratio on the Spatial Instability of Mixing Layers. Submitted to J. Fluid Mech.

Moore, C. J. 1977. The Role of Shear-Layer Instability Waves in Jet Exhaust Noise. J. Fluid Mech., 80, p. 321.

Morkovin, M. and Paranjape, S. V. 1971. Acoustic Excitiation of Shear Layers. Z. Flugwiss, 9, p. 329.

Mungur, P. 1977. On the Sensitivity of Shear Layers to Sound. AIAA Paper Number 77-1369.

Patnaik, P. C., Sherman, F. S. and Corcos, G. M. 1976. A Numerical Simulation of Kelvin-Helmboltz Waves of Finite Amplitude. J. Fluid Mech., 73, p. 215.

Peterson, R. A. 1978. Influence of Wave Dispersion on Vortex Pairing in a Jet. J. Fluid Mech., 89, p. 469.

Pfizenmaier, E. 1974. On the Structure of Velocity and Pressure Fluctuations in a Sound Influenced Free Jet. Proc. Colloquium on Coherent Structures in Turbulence, Southampton, England.

Pierrehumbert, R. T. 1980. The Structure and Stability of Large Vortices in a Inviscid Flow. Ph.D. Thesis, Massachusetts Institute of Technology.

Plaschko, P. 1979. Helical Instabilities of Slowly Divergent Jets. J. Fluid Mech., 92, p. 209.

Pui, N. K. and Gartshore, I. S. 1979. Measurements of the Growth Rate and Structure in Plane Turbulent Mixing Layers. J. Fluid Mech., 91, p. 111.

Riley, J. J. and Metcalfe, R. W. 1980. Direct Numerical Simulation of a Perturbed, Turbulent Mixing Layer. AIAA Paper No. 80-0274.

Sarohia, V. and Massier, P. F. 1978. Experimental Results of Large Scale Structure in Jet Flows and its Relation to Jet Noise Production. AIAA J., 16, p. 831.

Schaffar, M. 1979. Direct Measurements of the Correlation Between Axial In-Jet Velocity Fluctuations and Far Field Noise Near the Axis of a Cold Jet. J. Sound and Vib., 64, p. 73.

Tan-atichat, J. 1980. Effects of Axisymmetric
    Contractions of Various Scales. Ph.D. Thesis, Illinois
    Institute of Technology.

Wille,R. 1963. Beitrage Zur Phanomenologie der Freistrahlen.
    Z. Flugwiss.,11,p.222.

Winant,C.D. and Browand,F.K. 1974. Vortex Pairing: The
    Mechanism of Turbulent Mixing Layer Growth at
    Moderate Reynolds Number. J. Fluid Mech.,63,p.237.

Wlezien, R. W. 1981. The Evolution of the Low Wavenumber
    Structure in a Turbulent Wake. Ph.D. Thesis, Illinois
    Institute of Technology.

Wygnanski, I., Fiedler, H., Oster, D. and Dziomba, B.
    1979. On the Perseverance of a Quasi Two-Dimensional
    Eddy Structure in a Turbulent Mixing Layer. J. Fluid
    Mech., p. 325.

Yule, A. J. 1978. Large-Scale Structure in the Mixing
    Layer of a Round Jet. J. Fluid Mech., 89, p. 413

Zaman, K.B.M.Q. and Hussain, A.K.M.F. 1979. Vortex
    Pairing in a Circular Jet Under Controlled Excitation.
    Part 1. General Jet Response. J. Fluid Mech., 101,
    p. 449.

Zaman, K.B.M.Q. and Hussain, A.K.M.F. 1981. Turbulence
    Suppression in Free Shear Flows by Controlled
    Excitation. J. Fluid Mech., 103, p. 133.

END

FILMED

12-82

DTIC